Pathophysiological mechanisms involved in amyotrophic lateral sclerosis caused by mutations in the FUS gene

Inmaculada Sanjuan Ruiz

UNIVERSITÉ DE STRASBOURG

ÉCOLE DOCTORALE DES SCIENCES DE LA VIE ET DE LA SANTÉ

U1118

THÈSE présentée par :

Inmaculada SANJUAN RUIZ

soutenue le : **27 Septembre 2019**

pour obtenir le grade de : **Docteur de l'université de Strasbourg**

Discipline/ Spécialité : Neurosciences

Pathophysiological mechanisms involved in amyotrophic lateral sclerosis caused by mutations in the *FUS* gene

THÈSE dirigée par :

Mr. DUPUIS Luc	Directeur de recherches Inserm Université de Strasbourg, Strasbourg

RAPPORTEURS :

Mme. BUÉE-SCHERRER Valérie	Maître de conférences Université d'Artois, Arras
Mr. KABASHI Edor	Directeur de recherches Inserm Institut Imagine, Paris

---

AUTRES MEMBRES DU JURY :

Mme. MATHIS Chantal	Directeur de recherches CNRS Université de Strasbourg, Strasbourg
Mme. LATOUCHE Morwena	Maître de conférences EPHE, Paris

“I am among those who think that science has a great beauty”

Marie Curie

Acknowledgments

The accomplishment of finishing a thesis is a long journey, through which you evolve as a scientist but also as a person. This work would not have been possible without the help and support of the following people:

I would like to thank **Luc Dupuis**, my thesis director, who trusted me since the first day with this project. I remember the first day I stepped into the laboratory you told me "it is going to be hard". Well, I couldn't imagine how right you were at that moment. It has been hard, but it has also been a wonderful experience in which you have helped, advised and supported me in every step of the way. Thank you for being so open to any crazy scientific ideas I may have presented you and foremost for reminding me when I needed it the most that I was capable of doing it.

I would like to thank **Valérie Buée-Scherrer**, **Edor Kabashi**, **Chantal Mathis** and **Morwena Latouche** for having accepted and taken the time to read my manuscript and assist as jury for my thesis.

During these three years of PhD I have had the pleasure to be involved in collaborations that have immensely contributed with the work we have done. For that I would like to thank people in **Don Cleveland's** lab, **Sandrine Da Cruz**, **Clotilde Lagier-Tourenne**, **Dorothée Dormann**, **Sabine Liebscher, Anne-Laurette Boutillier** and **Valérie Demais** who has always accepted our projects with a smile on her face even though she knew she was doing to spend weeks on it.

I would like to thank all members of the laboratory who have helped in any way giving scientific advice of dealing with administrative tasks, **Jean-Philippe Loeffler**, **Frédérique René**, **Caroline Rouaux**, **Brigitte Kuenemann**, **Annie Picchianena**, **Jérôme Sinniger**, **Marc De Tapia**, **Marie-Jo Ruivo** who totally understood me when every time I said how bad the weather was in Strasbourg and **José-Luis Gonzalez De Aguilar** for his advice and conversations in Spanish.

Sylvie Grosch and **Pascal Kessler** for having helped me with the acquisition and analyses of the many samples of many genotypes we have studied.

I would also like to thank all the post-docs in the lab. They have always been available for any technical or theoretical doubts. **Raphaelle**, you are always willing to help people at the professional level but also at the personal level and I simply love your sarcasm/sense of humour Thank you for your support and advice, I have really appreciated it. **Jelena**, you taught me a lot when I arrived to the lab and you have always given technical advice. **Matei**, even though you have arrived at the end of my thesis you will always be the funny guy with a big moustache and weird socks.

This person wanted a full paragraph on his own, so here you have, not just because you wanted it, but because you deserve it. **Steph**, thank you so much for all the help you have given me since the first day I arrived at the lab. For always willing to be involved in the projects we have worked together, all the dissections you have helped with me with, all the biochemical processing and analysis, all the hours you have spent in front of the computer measuring mice behaviour. But still, I think your favourite one has been the western blots, specially Nrxn1. However, I want you to know that without your help I would have never been able to manage these projects in the time we have done.

Claudia, you have been of great support by the end of my thesis, handling like a boss all the nicotine tests, injections, implantations, the hours and hours you have spent in the animal house doing behaviour tests. Thank you for your patience, your help and your good mood.

To all the "young" people (it's not like if I were old), thank you for creating such a good environment in the lab and during meals and allowing me to mentally evade from the work. Petit **Marco**, thank you for your good mood and loud sneezes. **Alizée**, even though we barely see you its always great to have you around. **Laura**, although you have just landed in our lab you always have a smile on your face. **Haoyi** thank you for always thinking about us when you go to China and bring us weird Chinese food.

To all those that left the lab but were here at the beginning of my adventure. **Christine**, you were my first neighbour, helped me with finding an apartment, all the administrative things but also, we had great moments together, doing sport programs or running the weekends. Thank you for your support. **Mathieu**, you are such a sweet person, always willing to help with a great sense of humour. I loved teaching you veggies and fruits in Spanish even though the next day you couldn't remember a thing. **Robin**, thank you for always being in a good mood, you really cheered us all up when we all needed it. You were also one of my victims with Spanish lessons, although you are not able of making the difference between Spanish and Mexican people.

Alex and Cyril, my second neighbours but not only. **Alex**, we started this adventure together and you have become such an important person for me during these years. We have been through a lot, good and funny moments but also bad ones when we have been there for each other to listen, advice and hug when we needed it the most. You are a great person and greater scientist, which I think you sometime need to be reminded because you easily forgot. **Cyril**, you first arrived to the lab during your masters' degree where you were a little bit cocky, but you have proved me wrong by showing how such a caring and supportive person you are and I am glad you have found each other. Thank you both for everything you have done for me during these years.

Gina and Aurore, you two have also been crucial persons during my thesis who have also been there for the good and the bad moments. **Gina**, you have witnessed my entire journey during the last three years. You have always been such a good listener and have given good advice in every situation, personal or professional. Thank you for all the help and support during these years, I means a lot to me. You are a good friend, with whom I have spent really funny moments, basically because the weirdest things always happen to you. **Aurore**, petite Aurore, you have become my desk neighbour in the last year and even though you speak more or less as much as Gina or Marco when you're not in the mood of doing your bibliography, it's always funny to sing songs with you like "Oh my god, look at her…" (you know how it ends). I was amazed how such a fan of Harry Potter you are and I loved watching all over the saga at your place with the girls, making fun of each dramatic situation, which you hated by the way. What I am trying to say is thank you girls, you rock!

At last but not least, **Thibaut**. We have spent the first two and a half years without barely speaking to each other. Then we went to Oxford where I got a glimpse of your personality and after we went to Ulm where you discovered my natural gift for speaking German. Since then I have got the chance to get to know you better, to discover a completely different person, kind and sweet, willing to support and listen to me. I am glad we have had the chance to shared one of the toughest parts of this process, writing the thesis, during which we have helped and encouraged each other. Things are always better with a partner in crime. Thank you for everything sweet blueberry-man.

To my **parents** and my sister **Victoria**, you three are the biggest support I have in my entire life. You all have always supported me in every decision I have made during these last years. Whenever I wanted to do my masters' abroad, when the opportunity of doing a PhD came up, you were always there. If today I am the person in which I have become it is thanks to you. Your precious advice and support have allowed me to dream big and accomplish every goal I have had. Despite the bad moments, in which you have always been there, we always get to overcome the difficulties. I am the luckiest person to have you in my life and even though I really don't say it often, I love you so much.

Amélie, **Claire** and **Sarah**, we know each other from a long time ago, when we were young and beautiful (which we still are, of course). The three of you have such an important place in my life, we have shared so many moments in different periods of our life, impossible to mention them all. You have always been here to support me, to say the things I needed to hear whether I liked it or not. Even though each one of you have chosen to live in far and remote places, Amelie, in the center of France surrounded by cows, Claire in Oslo surrounded by penguins and Sarah in the mountains surrounded by goats, I love that we always get to see each other and spend time as things had never changed. I love you girls.

Marc and **Marta**, we also know each other from a while now, since the faculty. Thank you for all the good times, the parties, the studying sessions at the library, the trips, the chiringuito drinks and so many other moments. But foremost, thank you for having followed me every where I have been, for the laughs and the love. Having you by my side during all these years is something I will never be able to thank you enough. I can tell you one thing for sure, I am so lucky to have you.

Table of contents

Table of figures

Abbreviations

ACh: Acetylcholine

AChE: Acetylcholine esterase

AD: Alzheimer's disease

ALS: Amyotrophic lateral sclerosis

ChAT: Choline acetyltransferase

CSF: Cerebrospinal fluid

EMG: electromyography

FF: fast fatigable

FTD: Frontotemporal dementia

FUS: Fused in sarcoma

LCD: Low complexity domain

LLPS: Liquid-liquid phase separation

LMN: Lower motor neurons

MND: Motor neuron disease

NES: Nuclear export signal

NLS: Nuclear localisation signal

NMD: Non-sense mRNA mediated decay

NMJ: Neuromuscular junction

PD: Parkinson's disease

RBP: RNA binding protein

RNP: Ribonucleoprotein

UMN: Upper motor neurons

Preface

Amyotrophic lateral sclerosis (ALS) is a fatal neurodegenerative disease of the motor neuron, affecting simultaneously upper motor neurons localized in the cortex and lower motor neurons in the spinal cord. ALS patients characteristically present muscular weakness that progresses until affecting respiratory muscles, principal cause of patients' death within 3 to 5 years after diagnosis. The aetiology of ALS remains unknown even though a series of mutations in genes have been identified causing the disease.

Frontotemporal lobar degeneration (FTLD) is a neurodegenerative disease characterized by the atrophy and neuronal degeneration of brain structures. Frontotemporal dementia (FTD) is a type of FTLD and the second most common type of dementia worldwide after Alzheimer's disease. Many subtypes of FTD have been described, affecting different brain regions and carrying different symptoms such as behaviour, emotional or linguistic deficits, all of them presenting alterations of frontal and temporal lobes.

Recently a continuum between ALS and FTD, known as ALS-FTD continuum, has been proposed arising from scientific evidence linking these two diseases although they present their specific hallmarks. Clinically, about 15% of ALS patients develop during the disease course FTD symptoms and vice versa. Furthermore, genetic mutations in *C9ORF72*, *TDP-43* or *FUS* genes among others and histopathological hallmarks have been identified in both diseases reinforcing the existence of an ALS-FTD continuum.

Despite the efforts of the scientific community to decipher the mechanisms of ALS-FTD and develop novel diagnostic tools, little success has been reached in terms of treatments efficacy for the onset and delay progression of the disease as well as improve patients' life quality.

Mutations of *FUS* are causative of ALS in adult and juvenile patients with rapid and aggressive disease progression. FUS is a protein which localization is mainly nuclear, where it exerts many functions but is also found in the cytoplasm at lesser concentrations where it plays important cytoplasmic roles. Alterations of FUS have been observed in ALS as well as FTD patients, where FUS cytoplasmic aggregates have been found. Several animal models have tried to elucidate the pathophysiological mechanisms underlying the pathology but have only succeeded to partially recapitulate the histological and behavioural features.

This manuscript is composed by an introduction in two parts, with first a description of ALS and FTD diseases with their clinical aspects, second a description focused on FUS physiological and pathological implications in the ALS-FTD continuum, followed by the results obtained during my thesis presented as three articles and finally a discussion of the scientific interest and contribution to the characterization and understanding of FUS alterations in an ALS-FTD mouse model.

Introduction

Part 1: The amyotrophic lateral sclerosis – Fronto-temporal dementia (ALS-FTD) continuum

Amyotrophic lateral sclerosis (ALS), also known as Charcot's disease was first described in 1869 by Jean-Martin Charcot. ALS is a fatal neurodegenerative disease of the motor neuron affecting the functioning and viability of upper and lower motor neurons resulting in a general loss of muscular function. It mainly affects mid-life and elderly people from 50 to 70 years of age. Patient's life expectancy after being diagnosed is between 3 to 5 years. Fronto-temporal dementia (FTD) is the second most common type of dementia, affecting mid-life to elderly people characterized by an atrophy of the frontal and temporal lobes accompanied by cognitive and behavioural impairments. Even though these two diseases are characterized by very different symptoms, they share key pathophysiological features, and overlap clinically and genetically, thus defining a continuum between them.

1. Epidemiology: a worldwide disease

a. ALS

i. Incidence and prevalence

The incidence of ALS in European populations has been extensively analysed by several studies in Europe and is of 2 to 3 people per year per 100.000 general population. It has also been shown that lifetime risk is higher in men by 1:350 that in women by 1:400 (Johnston *et al.*, 2006). Some evidence suggests that the incidence and prevalence of ALS are lower in populations with elevated mixed ancestry (Zaldivar *et al.*, 2009). Contrarily to Alzheimer's disease, ALS peaks around 50 to 75 years and decreases afterwards. Patient's survival is very variable but generally death overcomes by respiratory insufficiency within 3 to 5 years after onset (Logroscino *et al.*, 2010; Huisman *et al.*, 2011; Wittie *et al.*, 2013).

ii. Geographic distribution

ALS cases are detected worldwide but it would seem that there are some specific clusters where the frequency of the disease is higher. This is the case in the Pacific island of Guam, in the Chamorro tribe where many cases of ALS with dementia and parkinsonism were described in 1945 (Koerner, 1952; Arnold *et al.*, 1953; Mulder *et al.*, 1954). Another cluster with high frequency of ALS cases was detected in two different areas of the Kii Peninsula in Japan and has been recently linked to mutations in the *C9ORF72* expanded repeat expansion mutation (Ishiura *et al.*, 2012). Other genetic mutations have been found to have founder effects on clustered populations such as in North Africa, where there is a higher recessive disease frequency; in the Italian island of Sardinia, where ALS cases are vastly due to mutations in the *TARDBP* gene; in Finland with mainly mutations in the *C9ORF72* expanded repeat expansion, in Sweden with the recessive mutation Asp90Ala of the superoxide dismutase 1 (*SOD1*) gene (Andersen e Al-Chalabi, 2011).

iii. Aetiology: from genetics to environment

The majority of patients with ALS have no other relatives affected by the disease, representing 90% of the cases and classified as sporadic ALS (sALS). Nevertheless, there is a 10% of cases with a positive family history that are collectively termed as familial ALS (fALS). The inheritance in fALS generally follows a Mendelian pattern with high penetrance (Couratier *et al.*, 2016). Mutations in many genes are responsible for 70% of fALS, namely *C9ORF72* located in chromosome 9 involved in 40% fALS and up to 5 – 11% of sALS (Byrne *et al.*, 2012); *TARDBP* located in chromosome 1 involved in 5% of fALS and 1% of sALS (Sreedharan *et al.*, 2008); *SOD1* located in chromosome 21 found in 10 – 20% of fALS and 1 – 5% of sALS; *FUS* located in chromosome 16 found in 5% of fALS and 0,5% in sALS; and *TBK1* located in chromosome 12 accounting for 1% of ALS cases (Cudkowicz *et al.*, 1997; Cirulli *et al.*, 2015).

Besides genetic variants, a number of other factors are also considered as risk factors for the disease, even though with less scientific ascertainment. These are very diverse, from occupation (athletes, military personnel), to environmental factors such as electric shocks and magnetic fields, metals, pesticides or viruses. Like in many other diseases the lifestyle and medical conditions might be considered important risk factors. Smoking, low body mass, diet and intense physical exercise as well as chronic traumatic encephalopathy and head trauma are considered as lifestyle risk factors in ALS. Moreover, physiological states such as hypermetabolism or neuroinflammation have also been linked to increase the risk of developing the disease (Al-Chalabi e Hardiman, 2013; Couratier *et al.*, 2016).

b. FTD

i. Incidence and prevalence

FTD is the second most common type of dementia with a broad level of incidence due to heterogenous studies from 1 to 17 per year per 100.000 people. The average age of onset is in mid-50's, but some cases have been reported at earlier ages, some as early as in their 20's (Stone *et al.*, 2003; Onyike e Diehl-Schmid, 2013). FTD prevalence is accounted to range from 1 to 461 people per 100.000 and there is no evidence of higher frequency of the disease regarding the gender (Hogan *et al.*, 2016). Survival in FTD patients varies widely depending on the subtype as much as 3 to 14 years, with FTD-MND having the poorest survival rates (Onyike e Diehl-Schmid, 2013).

ii. Geographic distribution

To determine the geographic distribution of FTD is complicated due to the limited number of studies that have collected this information and partial since most of current studies have focused on populations of Europe and North America. Therefore, the available data rarely include non-Caucasian populations (Onyike e Diehl-Schmid, 2013). Although some recent preliminary studies start emerging in India (Alladi *et al.*, 2011) and Asia (Ren *et al.*, 2012). As previously mentioned, clusters caused by founder effects of genetic mutations in the

C9ORF72 expanded repeat expression are found in isolated populations in the Kii Peninsula in Japan as well as in Finland, presenting dementia.

iii. Aetiology

The major risk factor in FTD is genetic inheritance of mutations. Five main mutations have been described, namely *C9ORF72*, Progranulin (*GRN*), microtubule-associated protein tau (*MAPT*), valosin-containing protein (*VCP*) and chromatin-modifying protein 2B (*CHMP2B*). Mutations in *C9ORF72*, *GRN* and *MAPT* have been shown to be fully penetrant and represent about 80% of the hereditary FTDs, whereas *VCP* and *CHMP2B* mutations account for less than 1%. Patients with *C9ORF72*, *GRN* or *VCP* mutations present intraneuronal inclusions with different characteristics according to the specific mutation. *C9ORF72* and *GRN* inclusions are TDP-43 positive and Tau negative, whereas *VCP* inclusions in *VCP* mutants are TDP-43 positive, *MAPT* inclusions are both TDP-43 and Tau positive and finally, CHMP2B inclusions are negative for TDP-43 staining. Most *C9ORF72* mutations are linked to FTD-MND cases. Mutations in TDP-43, Fused in Sarcoma (FUS) and ubiquilin-2 genes have been linked to MND (Onyike e Diehl-Schmid, 2013). Other risk factors have been described in a study realized in the Netherlands, where head trauma and thyroid disease where found to increase the risk in developing FTD (Rosso *et al.*, 2003).

2. CLINICAL FEATURES: A MULTIFACTORIAL DISEASE

a. ALS

ALS is a progressive relentless neurodegenerative disease characterized by a wide heterogeneity of forms. Three key neuropathological features define the disease. First, the presence of TDP-43 inclusions (Neumann *et al.*, 2006; Saberi *et al.*, 2015). Second, the loss of lower motor neurons (LMN) in the ventral horns of the spinal cord and brainstem (Hughes, 1982; Ghatak *et al.*, 1986). Third, the loss of cortical upper motor neurons (UMN), affecting initially Betz cells (large pyramidal neurons in layer V) in the primary cortex and the degeneration of lateral corticospinal tracts including axonal projections from the primary motor cortex to motor neurons (Hammer *et al.*, 1979; Udaka *et al.*, 1986; Maekawa *et al.*, 2004). In all, accompanied by the presence of reactive gliosis characterized by the hypertrophy of glial cells in motor cortex and the spinal cord (Kawamata *et al.*, 1992; Schiffer *et al.*, 1996).

i. Forms of ALS

Many forms have been described depending on the location or age of onset, disease progression and origin sporadic or familial. There are three major location onset sites of the disease, each one presenting different spectrum of symptoms and therefore the differential involvement of upper or lower motor neurons at a higher or lesser extent. Spinal-ALS forms, with a spinal onset are the most frequent, starting asymmetrically with painless weakness in a limb (Rowland e Shneider, 2001). The main clinical symptoms are an atrophy and weakness of muscles, fasciculations, hyperreflexia, hypertonia, usually with the absence of Babinski sign. The bulbar onset form of ALS represents up to 20% of the cases and is characterized by an initial weakness in the

bulbar muscles, dysarthria, dysphagia and tongue fasciculations. Patients also present jaw jerk reflexes, indicating alterations in the vagus nerve and in some cases pseudobulbar alterations. Clinical manifestations of limb hyperreflexia are indicative of the spreading of the disease (Swinnen e Robberecht, 2014). This form of ALS can be misdiagnosed with other diseases with similar clinical symptoms such as Kennedy's disease characterized by bulbar and spinal muscular atrophy and has been found to be predominant in females. Bulbar-ALS is frequently associated with mutations in *C9ORF72* and has a very poor prognosis, with a mean of only 2 years and 3% of long-term survival (Chiò *et al.*, 2011; Swinnen e Robberecht, 2014). Finally, the respiratory onset form of ALS is clinically characterized with orthopnoea or dyspnoea symptoms and in some cases spinal or bulbar signs (Chiò *et al.*, 2011). This form of ALS has the worse prognosis with a mean survival of 1.4 years, no long-term survival and male predominance (Shoesmith *et al.*, 2007; Chiò *et al.*, 2011).

Two atypical forms of ALS have been described affecting predominantly upper or lower motor neuron populations. Primary lateral sclerosis (PLS) affects predominantly UMN, with onset symptoms in the legs and symmetrical ascension to the arms and bulbar muscles. Studies have shown that PLS patients without electromyography (EMG) alterations within 4 years after onset disease have a higher survival (Gordon *et al.*, 2006; Tartaglia *et al.*, 2007). Whereas PLS patients with EMG alterations and LMN involvement have a lower survival and poor prognosis (Gordon *et al.*, 2009), and are considered nowadays as ALS patients with UMN isolated symptoms. PLS patients also commonly present symptoms related to FTD, with cognitive impairment and behavioural alterations (Grace *et al.*, 2011). Progressive muscular atrophy (PMA) is the second atypical form of ALS and affects predominantly LMN. In PMA patients, disease onset can occur in any body region and affects predominantly men over women. About 30% of PMA patients develop UMN symptoms usually 18 months after disease onset and can also develop FTD symptoms (Visser *et al.*, 2007; Kim *et al.*, 2009; Raaphorst *et al.*, 2011). Some studies have also shown that 50% to 63% of PMA patients present transcranial magnetic stimulation (TMS) abnormalities of the central motor conduction (Kaufmann *et al.*, 2004; Floyd *et al.*, 2009), suggesting that they are rather ALS patients with a predominant LMN presentation.

ALS forms can also be classified depending on their origin, sporadic or familial. Around 90% of ALS cases do not have an affected relative and are therefore considered as sporadic cases, but the other 10% present an affected relative and are thus considered as familial ALS cases (Renton *et al.*, 2014). Causes of sporadic ALS remain unknown and as previously described could be due to many different factors in the environment or lifestyle. However, many cases of sALS are misclassified because of lack of familial history but are later identified as carriers of *C9ORF72* mutations (Swinnen e Robberecht, 2014). Familial ALS cases defined by the presence of a mutation of a gene or a variant. Because of the update in the actual scientific techniques, an increasing number of genes carrying mutations linked to ALS are identified. But some constitute the vast majority of familial cases such as *C9ORF72*, *SOD1*, *TARDBP* and *FUS*, which will be latter explained in detail.

The age and the rate of progression of the disease are also used to classify or correlate the disease to a specific form or mutation. Most ALS cases develop around the fifth or sixth decade of life, but many cases have also been described with younger ages at onset. Those affecting patients younger than 25 years of age are considered as juvenile ALS cases and linked to mutations in mainly of *FUS* and in rare cases of *ALS2*, *SEXT* and *FUS* genes. Exceptionally mutations *FUS*Pro525Leu and *FUS*R495X have a very aggressive progression and patients carrying them have a dramatic decrease in survival (Bäumer *et al.*, 2010; Belzil *et al.*, 2012; Yamashita *et al.*, 2012; Waibel *et al.*, 2013). At elderly stages upper motor neurons are not involved in the development of the disease and patients present bulbar-ALS with poor prognosis, especially when disease onset is beyond the age of 80 years (Pupillo *et al.*, 2014; Swinnen e Robberecht, 2014). Disease progression varies very importantly among the different forms of onset and only 10% survive more than 10 years (Pupillo *et al.*, 2014). However, familial forms of ALS have been associated with increased or diminished survival such as *SOD1* Asp90Ala (longer survival) or *SOD1* Ala4Val (shorter survival) (Rowland e Shneider, 2001) (Figure 1).

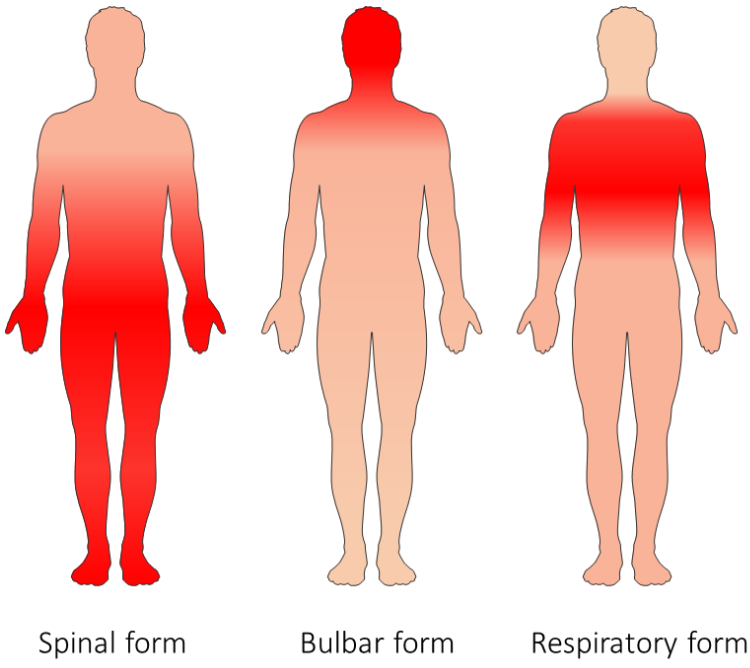

Figure 1: Typical forms of ALS.
The most represented forms of ALS are the spinal form with symptoms onset at upper and lower limbs, the bulbar form initially affecting bulbar muscles involved in swallowing and mastication and finally the respiratory form characterized by very early respiratory deficits.

ii. Neuronal components

1. Upper motor neurons (UMN)

UMN represent less than 1% of all cells and neurons in the motor cortex located in layer V of the cerebral cortex, which project to spinal motor neurons through the corticospinal tract and are responsible of most

descending motor commands for voluntary movement (Lemon, 2008). In patients, they are affected at early stages of the disease, even before the disease onset. The disintegration of Betz cells apical dendrites has been characterized in cases of sALS, fALS and ALS-FTD and present electrophysiological alterations such as hyperexcitability (Genç *et al.*, 2017) (Vucic *et al.*, 2008; Geevasinga *et al.*, 2016). Betz cells receive most inputs from long-distance projections such as thalamocortical and callosal projections, local circuitry neurons and inhibitory neurons located in layers II/III and V of the cortex. The consequences of the degeneration of these cells have a major impact on LMN and the overall motor circuitry (Dervishi e Ozdinler, 2018) (Figure 2). Clinical signs due to the degeneration of these cells are initially absent in about 7-10% of MND (Rocha e Maia Júnior, 2012). Symptoms progress typically with an early involvement of upper limb muscles and late impairment of respiratory muscles (Sabatelli *et al.*, 2011) and are identified by hyperreflexia with pathological reflex spread, spasticity, clonus, preserved reflexes in weak wasted limbs, Babinski sign (Brooks *et al.*, 2000) as well as paucity, impairment in motor control and clumsiness. Several studies in mouse models with ALS mutations such as mSOD1, (Jara *et al.*, 2012; Fogarty *et al.*, 2015), absence of alsin (Gautam *et al.*, 2016) or mutations in profilin-1 (Fil *et al.*, 2017) have shown similar patterns of the disease, inducing alterations in corticospinal motor neurons (Betz cells in humans) with vacuolization and spine loss (Fogarty *et al.*, 2015; Handley *et al.*, 2017) and corresponding UMN symptoms (Dentel *et al.*, 2013). Therefore, UMN seem to play a critical role in ALS development.

2. Lower Motor Neurons (LMN)

LMNs are composed by bulbar and spinal motor neurons which project through peripheral nerves to innervate skeletal muscle fibers (Burke *et al.*, 1981). Distal limb muscles are innervated by LMN located laterally in the cervical or lumbar enlargements of the spinal cord (Ravits e La Spada, 2009). They are modulated by corticospinal tracts and polysynaptic tracts (Burke *et al.*, 1981). Different types of LMN can be found, but a specific subtype is particularly vulnerable in ALS, the alpha-motor neurons (αMN). These are responsible for the innervation of skeletal muscle fibers and are classified in categories according to their contractile properties (Figure 2). In ALS αMN innervating fast-twitching and fast-fatigue (FF) fibers are the first to degenerate (Roselli e Caroni, 2014). Many hypotheses have arisen to clarify the vulnerability of this subpopulation of LMN that will be discussed below. The loss of LMN has been clinically easier to detect than for UMN by the distinctiveness of the symptoms. Typically, clinical manifestations of LMN loss consist in muscular atrophy, muscle weakness, fasciculations and hyporeflexia or areflexia (Swinnen e Robberecht, 2014).

3. Disease propagation

Three different hypotheses have been proposed to explain the course and propagation of ALS, though there is not yet clear evidence for any of them and could be variable depending on the type of the disease. First, the “Dying-back” hypothesis which supports the idea that the degeneration would begin in the periphery at the

distal axon of LMN where axonal transport defects would result in motor neurons death leading to a disconnection of the muscles at the neuromuscular junction level (NMJ) culminating in a series of clinical symptoms at the muscular level (Dadon-Nachum *et al.*, 2011). Then, it would follow with a progressive ascending neuronal degeneration until the degeneration of UMN, all in all accompanied by neuroinflammatory processes and gliosis. A recent study by Cheng AJ and collaborators in a SOD1 mouse model have shown that mice muscular strength and muscle fibers integrity remain intact, whereas the neuromuscular junction is already altered (Cheng *et al.*, 2019), thus supporting the hypothesis of contiguous spread. Second, the "Dying-forward" hypothesis claims the opposite as the previous one, where the disease onset would start at the cerebral motor cortex, with an initial first lesion of pyramidal motor neurons. Secondary lesions resulting from the first ones would arise in subcortical regions in a corticofugal axonal pathway manner, auto-propagating the lesions cell-to-cell (Braak *et al.*, 2013). The disease would then propagate to the periphery descending by the corticospinal tract until LMN with at the long-term the same end, skeletal muscles alterations (Figure 2). This hypothesis is based in a network dysfunction dependent on synapses connections (Brooks, 1991; Seeley *et al.*, 2009). Indeed, Fogarty and collaborators observed defects in cortical neurons' dendrites and spines before motor symptoms (Fogarty *et al.*, 2016). Furthermore, clinical evidence supports this hypothesis since cortical hyperexcitability is one of the earliest hallmarks that can be identified in ALS patients before any motor symptom (Vucic *et al.*, 2008; Bae *et al.*, 2013; Williams *et al.*, 2013). Finally, a third intermediate hypothesis was proposed, stating that the onset would initiate at both ends in UMN and LMN and would progressively spread surrounding region of onset and affecting the neuronal network ending by a complete dysfunction at the central and peripheral levels (Ravits, 2014; Vucic *et al.*, 2014; Geevasinga *et al.*, 2016).

4. Vulnerability of other neuronal populations

The Raphe nuclei are serotoninergic nuclei that project throughout the brain and are implicated in a wide variety of functions such as appetite, emotions and movement. Several studies have now shown that the serotoninergic system is altered in ALS, with decreased binding of specific receptors in cortex and the Raphe nucleus (Turner *et al.*, 2005), a decrease in CSF, plasma and/or spinal cord of serotonin (5-HT), 5-HIAA (5-HT main metabolite) and tryptophan, 5-HT precursor (Monaco *et al.*, 1979; Ohsugi *et al.*, 1987; Bertel *et al.*, 1991; Sofic *et al.*, 1991). Furthermore, platelet levels of 5-HT are positively correlated with survival in ALS patients (Dupuis *et al.*, 2010) and serotonin neurons degenerate in ALS patients and models (Dentel *et al.*, 2013). Increasing interest in the serotoninergic system and its pharmacological modulation have identified specific receptor subtypes such as the 5-HT2B receptor expressed in microglia which can limit degeneration of spinal cord microglia and slow the disease progression or clarified the role of the degeneration of 5-HT neurons in the Raphe nuclei inducing spasticity (El Oussini *et al.*, 2016; El Oussini *et al.*, 2017). Thus, clinical symptoms previously attributed to UMN degeneration like spasticity could arise from the dysfunction of the serotoninergic system (Figure 2).

Besides, other neuronal populations have been observed to be affected in ALS namely interneurons. Renshaw cells (RC) are glycinergic inhibitory cells that degenerate early in the disease (Chang e Martin, 2009). These interneuron populations located in the spinal cord receive direct input from motor axon collaterals and synapse motor neurons inhibiting them (Alvarez e Fyffe, 2007). Moreover, they receive inputs from spinocerebellar and corticospinal tracts (Mazzocchio *et al.*, 1994; Pierrot-Deseilligny *et al.*, 2005). RC are thought to play key roles in motor control, more precisely during postural tasks or muscle contraction, regulating movement stability and smoothness. Two clinical studies with ALS patients support RC impairment, where they recorded electrophysiological abnormalities (Raynor e Shefner, 1994; Shefner e Logigian, 1998). Hypothetically, RC deficits could be preceded by corticospinal tract degeneration, which all together could result in increased motor neurons excitability and increased glutamate toxicity (Pasquali *et al.*, 2009), resulting in potentially an initial trigger for motor neurons death (Figure 2). Recent studies have focused in the implications of cortical interneurons in ALS. Apart from the clinical evidence where patients present cortical hyperexcitability suggesting defects in the excitatory-inhibitory balance, Nihei K and collaborators observed decreased levels of cortical parvalbumin positive cells and decreased mRNA of the subunit α of GABAergic receptors (Nihei e Kowall, 1993). Several studies with ALS animal models have also shown to present defects in cortical interneurons. A study with zebrafish detected decreased inhibitory currents before the detection of motor neurons defects (Mcgown *et al.*, 2013). In rodent animal models, Clark RM and collaborators observed in a SOD1 mouse model alterations in interneurons as well as intrinsic reduced excitability and increased neurite complexity (Clark *et al.*, 2017; Clark *et al.*, 2018). A decrease of up to 72% of GABA inhibitory currents at the layer V of motor cortex was described in the Wobbler mouse model (Moser *et al.*, 2013) and a TDP-43 mouse model showed deficits in GABAergic signalling which resulted in cortical hyperexcitability (Sreedharan *et al.*, 2008; Zhang *et al.*, 2016). Overall this data suggests that inhibitory populations are also affected in ALS, but further studies are needed to elucidate their role in the disease.

It is well known that specific cell types are particularly vulnerable in ALS, the reasons of this cellular selectivity remain still unknown. Sensory and autonomic as well as cerebellar neurons remain unaffected or mildly affected during the disease course while motor neurons and frontotemporal neurons are the most affected cellular types in ALS. However, there are differences within subpopulations of motor neurons that are affected at a higher or lower extent such as oculomotor neurons and Onuf's nucleus containing sacral motor neurons responsible for the innervation of sphincter muscles that remain unaffected (Kanning *et al.*, 2010) (Figure 2). Moreover, differences in vulnerability of motor neurons within the spinal cord are well known, where larger motor neurons degenerate in higher proportions than small motor neurons. Many hypotheses have been proposed to explain this cell-type specific vulnerability from intrinsic cellular features to non-autonomous cellular effects. Large motor neurons reach large fields of innervation, have a limited sprouting capacity and are mainly FF units. Contrarily, slow tonic motor neurons are smaller in size, innervate small neuromuscular

fields and have a higher sprouting capacity. Therefore, the cellular stress-coping linked to the cell physiology has been proposed as a potential factor for motor neurons survival (Robberecht e Philips, 2013). Intrinsic cellular factor at the molecular level have also been proposed as critical survival factors such as the ephrin system, where large motor neurons strongly express the ephrin receptor EPHA4 and studies showing a deletion or blockade of this one have shown to have beneficial effects for motor neurons survival (Van Hoecke *et al.*, 2012). Glutamate induced excitotoxicity is a process well known to induce cell death in many pathophysiological conditions. In ALS patients and mouse models, it has been shown that a loss in the excitatory amino acid transporter 2 (EEAT2), thus leading to a decrease clearance of glutamate by this receptor in motor neurons result in an increased glutamatergic stimulation and cell death (Rothstein *et al.*, 1992; Bruijn *et al.*, 1997). Other excitotoxic mechanisms leading to motor neurons death have been suggested to be mediated by calcium entry though AMPA-type glutamate receptors, where motor neurons express GluR2 prone to glutamatergic excitotoxicity by lethal calcium overload (Van Damme *et al.*, 2007). Importantly, motor neurons capacity to buffer calcium is limited compared to oculomotor neurons, which reinforces their vulnerability to excitotoxicity processes (Robberecht e Philips, 2013).

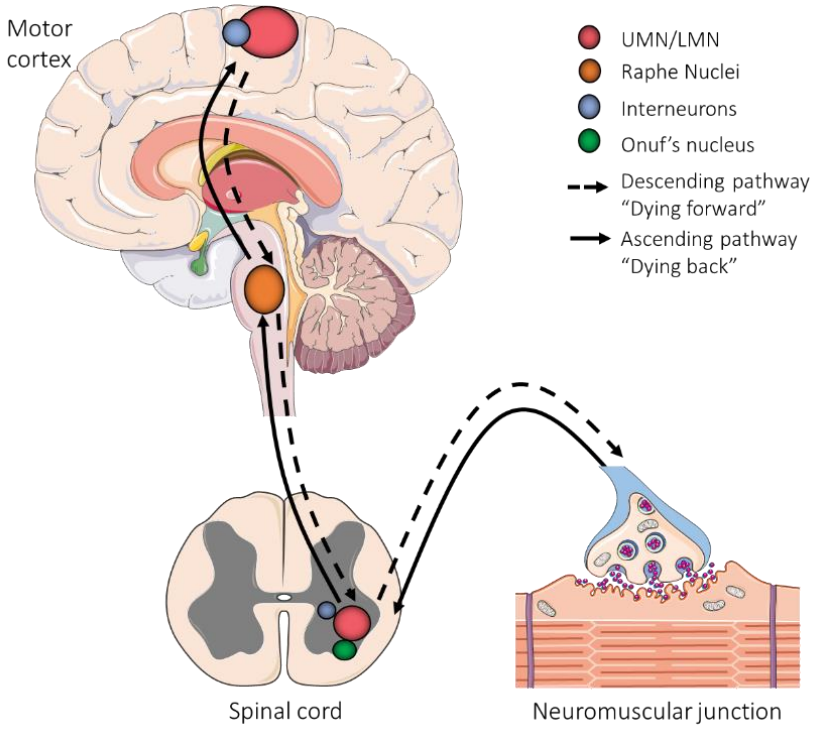

Figure 2: Neuronal components affected in ALS.
ALS is characterized by the degeneration of upper and lower motor neurons (red circles), neurons in the Raphe nuclei (orange circle) and cortical and Renshaw interneurons (bleu circles). Only motor neurons in Onuf's nucleus survive during the disease. Evidence suggests the disease progresses in different ways: (1) initiating in the cortex, descending to the spinal cord and finally reaching the neuromuscular junction (descending pathway; dotted arrows), (2) initiating at the periphery, ascending from the neuromuscular junction, spinal cord until reaching the brain (ascending pathway; full arrows), (3) initiating at both upper and lower motor neurons at the same time.

iii. Non-neuronal components

1. Glial alterations

The central nervous system (CNS) has its own specialized immune system cells that intervene in case of acute or chronic damage. These are divided into macroglial cells composed by astrocytes, oligodendrocytes and NG2-positive progenitors, derived from the ectoderm and microglial cells, derived from the mesoderm and described as the resident macrophages of the CNS (Pehar *et al.*, 2017). These cellular components have specific properties to maintain neurons homeostasis and can adopt completely different morphologies and molecular patterns in cases of injury. However, in pathological conditions like neurodegenerative diseases such as ALS, alterations in these immune cells can interfere with their functions and molecular patterns becoming noxious to surrounding neurons environment, contributing to neuronal degeneration in a non-cell autonomous manner.

Astrocytes contribute to neurons homeostasis by providing neurotrophic factors, controlling synaptic functions and formation and regulating the concentration of neurotransmitters at the synapses, importantly glutamate (Burda *et al.*, 2016). In neurodegenerative diseases astrocytes change their shape and molecular expression patterns, turning into reactive astrocytes (Maragakis e Rothstein, 2006; Heneka *et al.*, 2010; Sofroniew, 2015). Non-cell autonomous pathomechanisms by astrocytes have been shown to contribute to neurodegeneration in ALS (Ilieva *et al.*, 2009), and their selective ablation can slow disease progression and increase survival in rodent models (Boillée *et al.*, 2006; Yamanaka *et al.*, 2008). ALS genetic mutations have shown to have effects on astrocytes functioning with mutated proteins inclusions. In physiological conditions astrocytes control and reduce extracellular levels of glutamate, which found in excess in the synaptic cleft leads to an excessive firing of neurons resulting in an increase of calcium influx that can be toxic. Astrocytes in ALS present some pathological features leading to excitotoxicity discussed above such as a decrease in glutamate re-uptake *via* EEAT2 due to a loss of this transporter or a loss in AMPA-like GluR2 receptors. But also changes in the endogenous co-agonist of NMDA D-serine, that induces glutamate release and that is increased in sALS and fALS patients (Sasabe *et al.*, 2012), mitochondrial abnormalities with increased levels of reactive oxygen species strongly linked to neurodegenerative processes (Cassina *et al.*, 2008) and a wide variety of pro-inflammatory cytokines and inflammatory mediators such as IFN, PDG2 and TGF-β. Moreover, astrocytes play a critical role in the survival and maintenance of motor neurons by secreting neurotrophic factors (GDNF, BDNF, CNF). Deletion of the major promoter of GDNF release and synthesis by astrocytes, TNFR1, result in accelerated neurodegeneration (Brambilla *et al.*, 2016) reaffirming the importance of astrocytes neurotrophic functions. The functioning of astrocytes intrinsic organelles seem to be altered in ALS, particularly mitochondrial functions responsible for lactate production, which are decreased in response to defects in cellular shuttling of lactate between motor neurons and astrocytes (Cassina *et al.*, 2008; Madji Hounoum *et al.*, 2017), increased calcium release from the endoplasmic reticulum (Kawamata *et al.*, 2014)

and increased number of connexin-43 contributing to motor neurons toxicity by calcium excitotoxicity (Almad *et al.*, 2016) (Figure 3). The role and implications of astrocytes in ALS have nevertheless permitted to try new therapeutic strategies to try to slow disease progression by targeting the anti-inflammatory and/or antioxidant systems and stem cell transplantation methods.

Microglia are the resident macrophages of the CNS and can be found in two different states, resting or activated (Cherry *et al.*, 2014). At their resting state they are screening or "surveilling" the environment, also known as homeostatic microglia. Its many functions include ensuring synaptic plasticity and synaptogenesis by shaping neuronal circuits (Schafer *et al.*, 2013), acting as trophic support by the secretion of neurotrophic factors such as BDNF, NGF or IGF1 controlling the PI3K signalling pathway (Shi *et al.*, 2003) or playing a key role in neurogenesis by phagocyting debris of excessive newborn neurons and the secretion of cytokines (Butovsky e Weiner, 2018). Homeostatic microglia are characterized by expressing P2Y purinoceptor 12 (P2ry12), transmembrane protein 119 (Tmem119) and β-hexosaminidase subunit β (Hexb). Some of these receptors have also been identified in human microglial cells such as P2RY12 and TMEM119 (Butovsky *et al.*, 2014). Recently, the pattern of surface markers of homeostatic microglia has been deeply studied and has been characterized by the expression of CD11b, CD200R1, CX3CR1, IBA1. Homeostatic microglia expression is regulated by the activation of transcription factors such as MEF2A or MAFB (Butovsky e Weiner, 2018). However, a specific surface marker has been identified and is not expressed by all CNS microglial cells. Triggering receptor expressed on myeloid cells 2 (TREM2) is expressed on the surface of brain microglia in cases of immune responses and has also been linked to Alzheimer's disease and ALS and/or FTD when mutated (Giraldo *et al.*, 2013; Cady *et al.*, 2014; Colonna e Wang, 2016) (Figure 3). TREM2 recognizes damaged cells exposing phosphatidylserine groups on their surface and initiate microglial activation *via* ApoE signalling (Krasemann *et al.*, 2017). Keren-Shaul H and collaborators have recently described the activation process of microglia in neurodegenerative states such as Alzheimer's disease or ALS (Keren-Shaul *et al.*, 2017). Homeostatic microglia seem to be activated in a two steps process characterized by an initial activation TREM2-independent and a full activation TREM2-dependent. The initial activation by TREM2-independent mechanism involves the downregulation of homeostatic microglia checkpoint genes such as P2ry12 or CX3CR1 and the upregulation of B2m, ApoE and Tyrdop genes, the last one encoding for TREM2 adaptor protein (Castellano *et al.*, 2011). Whereas full activation of microglia which is TREM2-dependent consists in the upregulation of phagocytic and lipid metabolic genes such as Cst7 and Lpl. The activation of homeostatic microglia seems to require a first TREM2-independent activation in order to acquire its full activation state *via* TREM2 signalling (Keren-Shaul *et al.*, 2017). Recent studies have shown evidence of homeostatic microglial activation *via* TREM2 signalling in ALS mouse models. Keren-Shaul and collaborators showed in $SOD1^{G93A}$ mice two different populations of microglia, ones expressing Hexb and Cx3CR1, corresponding to homeostatic microglia, whereas the other one showed upregulated TREM2 and Tyrobp with downregulated Cx3CR1

corresponding to activated microglia. Moreover, ApoE is a ligand of TREM2 in microglia (Atagi *et al.*, 2015). SOD1 mice present activated TREM2-ApoE signalling pathway with the subsequent increased expression of miR-155, a pro-inflammatory marker, and loss of the homeostatic signature (O'connell *et al.*, 2010; Butovsky *et al.*, 2015; Krasemann *et al.*, 2017). The knock down of ApoE or miR-155 in SOD1 mice resulted in restored homeostatic microglia and increased mice survival (Butovsky *et al.*, 2015; Krasemann *et al.*, 2017). Thus, the microglial TREM2-ApoE signalling pathway seems to be of great relevance in the ALS-FTD pathogenesis and requires further investigations.

Oligodendrocytes interact closely with neurons axons by recovering them with a multi-layered myelin sheath (Nave, 2010). Myelin is composed of lipids and proteins, the most abundant being PLP and MBP, and allows the propagation of action potentials in a very fast and efficient manner across long distances, by saltatory conduction at nodes of Ranvier. Oligodendrocytes also contribute to neurons homeostasis by providing energy support through lactate and pyruvate (Nonneman *et al.*, 2014). In ALS sporadic and familial cases present TDP-43 (Philips *et al.*, 2013) and FUS (Mackenzie, Ansorge*, et al.*, 2011) inclusions in oligodendrocytes, indicating that ALS alters this cell type with myelin abnormalities, demyelination, and their degeneration in grey matter of ventral spinal cord patients (Kang *et al.*, 2013) (Figure 3). Studies in mouse models have described mutated proteins inclusions in the spinal cord (Stieber *et al.*, 2000), oligodendrocytes degeneration before alterations of surrounding motor neurons entering apoptotic states so called dysmorphic. Dysmorphic oligodendrocytes present irregular shape, enlarged cytoplasm, elongated reactive processes and are very present in number before disease onset and increase with disease progression (Philips *et al.*, 2013). Moreover, the presence of clusters of activated microglia have been described surrounding dystrophic oligodendrocytes (Kang *et al.*, 2013), indicative of cellular degeneration as well as increased number of oligodendrocytes and myelination defects (Scekic-Zahirovic *et al.*, 2017). Nevertheless, oligodendrocytes are very sensitive cells rapidly affected by the extracellular environment and prone to degenerate by glutamate mediated toxicity, oxidative damage, inclusions from genetic mutations and reactive astrocytes of activated microglial cells.

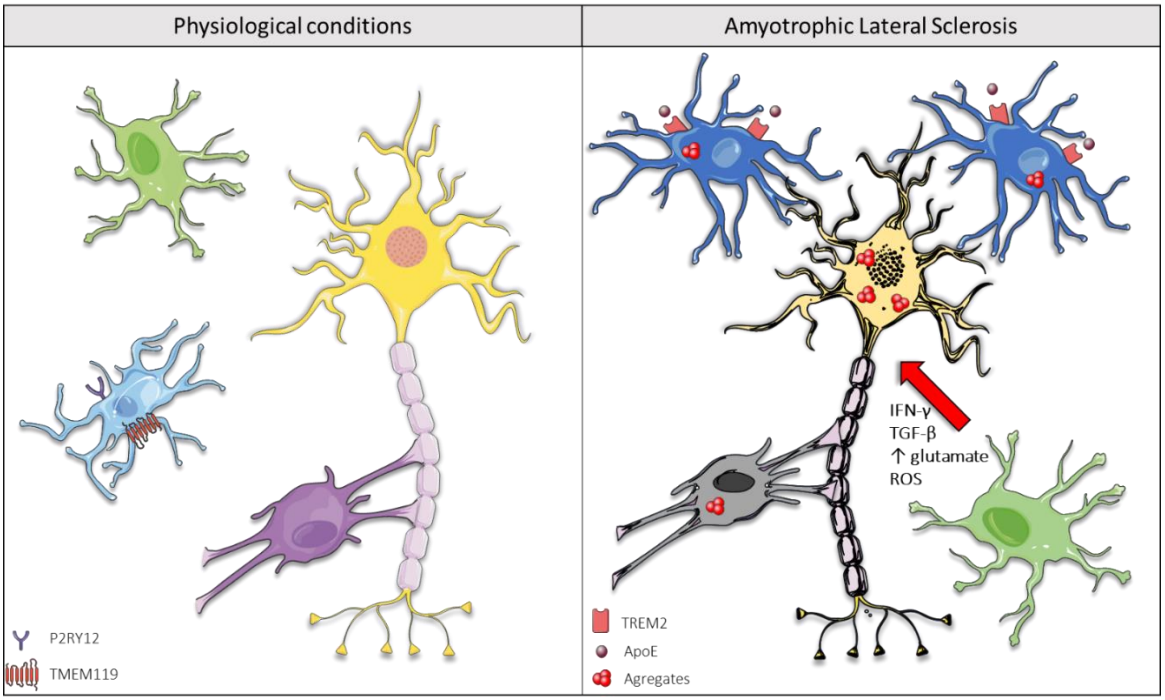

Figure 3: Glial alterations in ALS.
Glial cells in physiological conditions (left panel) contribute to the maintenance of neurons homeostasis. Homeostatic microglia express P2RY12 and TMEM119 surface receptors. In ALS (right panel), oligodendrocytes present mutant protein aggregates and become dystrophic, astrocytes release pro-inflammatory mediators and activated microglia express TREM2 receptors activated by ApoE as well as cytoplasmic aggregates.

2. Muscular involvement

ALS affects mainly skeletal muscles that get progressively denervated, resulting in muscular weakness and atrophy, but not all skeletal muscles are affected at the same extent, depending on disease progression and site of onset, as well as on their fiber composition. As previously mentioned, some cell types are more vulnerable than others in ALS, FF fibers being the earlier and most affected, but even depending on the types of fibers composing the muscles, they can be affected at a higher or lesser extent during the disease. Skeletal muscles displaying oxidative stress metabolism more affected in ALS (Leclerc *et al.*, 2001), and a switch from oxidative to glycolytic metabolism in muscles occurs with disease progression (Staunton *et al.*, 2011). The role of skeletal muscles in ALS remains controversial in regards of the disease onset and progression as studies on the SOD1 model have shown it can have a toxic effect on motor neurons causing their degeneration with associated ALS symptoms (muscle weakness, abnormal neuromuscular junctions, axonopathy) (Wong e Martin, 2010), but also that it has no effect on motor neurons fate, although presenting as well ALS typical symptoms (reduced muscle strength, atrophy and mitochondrial dysfunction) (Dobrowolny *et al.*, 2011). What is certain is that the muscle and its functional mechanisms are altered in ALS with oxidative stress, mitochondrial dysfunctions, bioenergetic disturbances and dismantlement of the neuromuscular junction (NMJ) even before motor neurons degeneration (Moloney *et al.*, 2014). From a molecular point of view many studies have highlighted abnormalities in animal models such as the aggregation of mutated proteins (Turner

et al., 2003), the decrease of heat shock proteins in myofibrils (Bhattacharya *et al.*, 2014), an increase in reactive oxygen species resulting in exacerbated oxidative metabolism, altered expression of PGC1-α and metabolic perturbations in TDP-43 and VAPB (Loeffler *et al.*, 2016). All these data are indicative of major alterations in oxidative stress and bioenergetic processes in skeletal muscles in ALS pathogenesis.

The NMJ is constituted by a peripheral tripartite of cellular components, (1) the motor neuron nerve ending, (2) the post-synaptic membrane on skeletal muscle and (3) terminal Schwann cells (predominant glial cells of the peripheral nervous system). The MNJ is the relay site of transmission of information between nervous and muscular inputs. In ALS the nerve terminals, which are sensitive to increases in reactive oxygen species and calcium influxes lead to an accelerated decline of the NMJ as well as an alteration in neurotransmitters (NTs) release machinery at the pre-synaptic terminals (Pollari *et al.*, 2014). Furthermore, pre-synaptic terminals contain altered mitochondria, a decrease in synaptic vesicle density (Cappello *et al.*, 2012) and a decrease in the size of synaptic vesicle pools as a consequence of impaired vesicular axonal transport (Pun *et al.*, 2006). In patients, decreased levels of ACh at the pre-synaptic level contribute to motor neurons degeneration, accompanied by a decrease in choline-acetyl transferase (ChAT), acetylcholine esterase (AChE) and vesicular acetylcholine transferase (VAChT) enzymes (Campanari *et al.*, 2016). Acetylcholine receptors (AChRs) at the NMJ are organized in clusters stabilized by Schwann cells. Interestingly, in ALS these receptors present a decrease in affinity for their endogenous ligand, acetylcholine (Ach), but are not altered in number nor distribution (Tsujihata *et al.*, 1984). Schwann cells can be classified in two categories, myelinating Schwann cells, that form a myelin sheath around LMN axons and non-myelinating or perisynaptic Schwann cells, charged of support, development, maturation, maintenance and regeneration of NMJs. In presence of denervation events, Schwann cells switch from resting state to activated (repair) state, usually triggered by a sudden interruption of Ach signalling *via* muscarinic AChRs on Schwann cells membrane. They adopt a macrophage-like behaviour and phagocyte axonal and cellular debris from degenerating axons (Duregotti *et al.*, 2015). Moreover, activated Schwann cells have functions of axonal guidance, sprouting and reinnervation of the previously occupied synaptic clefts as well as remodelling post-synaptic clusters of AChRs and stabilization of NMJs (Kang *et al.*, 2013). In ALS, Schwann cells are deficient in reinnervation processes (Kang *et al.*, 2003), in muscarinic activation towards the repairing phenotype leading to defects in NMJ architecture and function, and are decreased in number potentially due to alterations in the neuregulin-ErbB pathway implicated in the maintenance and stability of NMJs resulting in a loss of synapses (Arbour *et al.*, 2017).

Overall, in ALS the NMJ present deficits in morphology, complexity (Clark *et al.*, 2016) and functioning but it remains unknown if these are the first to occur or are secondary to other cellular toxicity propagation. Recent studies are trying to clarify the exact role and its potential toxicity and implications in ALS onset and

progression by elucidating the role and contribution of the muscle and its potential toxicity to disease onset and propagation (Picchiarelli 2019, in press), therefore leading to potential new therapeutic targets.

3. Metabolic alterations

ALS is a multifactorial disease as different systems appear to be altered. Metabolic alterations have been clearly defined in ALS patients and reproduced in different mouse models. Patients present some metabolic clinical features as increased energy consumption at rest in about 60% of patients (Desport *et al.*, 2006; Bouteloup *et al.*, 2009; Vaisman *et al.*, 2009). Moreover, ALS patients have hyperlipidaemia (Dupuis *et al.*, 2008) and glucose intolerance with or without insulin resistance (Dupuis *et al.*, 2011). The body mass index (BMI), determined by weight, decreased in ALS patients before onset of motor symptoms and lower BMI is a risk factor (O'reilly *et al.*, 2013) and is negatively correlated with survival. Weight loss is due to muscle and adipose tissue loss and likely caused by a combination of hypermetabolism and eating disturbances, loss of appetite and depressive symptoms (Ferri e Coccurello, 2017). At the muscular level, mutated protein aggregates (Krasnianski *et al.*, 2005) and mitochondria abnormalities in their volume and morphology (Loeffler *et al.*, 2016) have been described in muscular biopsies. Alterations of the metabolism in humans and animal models affecting mitochondria oxidative capacity, calcium signalling, mitochondrial complexes of electrons transport chain have been linked with alterations in adaptation of muscular fibers to substrates therefore resulting in defects of skeletal muscles. Alteration in the AMPK pathway, responsible for the regulation of autophagy flux and promoter of PGC1-α, which is implicated in mitochondrial biogenesis, oxidative metabolism among other functions are also present in ALS patients and animal models (Handschin e Spiegelman, 2006; Perera *et al.*, 2014; Liu *et al.*, 2015), contributing to the overall metabolic failure.

In the CNS, the hypothalamus integrates energy homeostasis. The hypothalamus contains distinct cellular regions with several functions as regulators of energy homeostasis. Several studies have shown that the hypothalamus is altered in ALS patients, presenting an atrophy correlated with their BMI (Gorges *et al.*, 2017), and defects in the melanocortin system accompanied by loss of cellular populations such as POMC, essential in feeding behaviour (Vercruysse *et al.*, 2016).FTD patients also present eating disturbances and hypothalamic defects (Piguet, 2011; Ahmed *et al.*, 2014; Ahmed, Iodice*, et al.*, 2015), indicating it is a common feature in the ALS-FTD continuum.

Clinical treatments have since then focused on treating patient's weight loss and metabolic imbalance with high-caloric nutritional strategies with gastrostomy (Wills *et al.*, 2014), to rebalance the energetic deficit in ALS. This approach has also been used in a mouse models with the administration of a high fat diet (Dupuis *et al.*, 2004) and has demonstrated very promising results in patients (Wills *et al.*, 2014)(Ludolph submitted). Thus, the regulation of ALS patient's nutrition seems to be crucial for disease progression.

b. FTD

FTD is the second most common type of dementia after Alzheimer's disease. It is characterised by the atrophy of the frontal and temporal lobes and depending on the site of initiation and the brain regions affected, patients will present with a specific subtype of FTD. Patients with a right hemisphere predominance atrophy will show strong behaviour impairments whereas language impairments are the key feature associated with predominant left hemisphere atrophy. Apart from the clinical evidence suggesting FTD contains different phenotypes, molecular pathology and genetics play a major role in the classification and identification of each one of them, with a notorious overlap with motor neuron diseases.

i. Types of FTD

According to the clinical classification, two major FTD phenotypes exist those being the behavioural variant (bvFTD) and progressive paralysis aphasia (PPA), where the latter is subdivided into 3 other phenotypes; semantic variant (svPPA), non-fluent variant (nfvPPA) and logopenic variant (lvPPA).

The svPPA phenotype is characterized by the degradation of semantic knowledge, single-word comprehension and impaired speech sound production (Gorno-Tempini *et al.*, 2011). These symptoms are related to abnormalities in the left anterior temporal lobe and its connections. The nfvPPA phenotype is more variable between individuals but generally presents slow and effortful speech with errors and difficulty in understanding complex sentences. Anatomically, these symptoms have been linked with dysfunctions of the underlying regions responsible for motor speech planning such as the left inferior frontal gyrus, insula, premotor and superior motor areas (Gorno-Tempini *et al.*, 2004). Finally, the lvPPA phenotype is characterised by phonologic errors and slower speech and is associated with left fronto-parietal junction abnormalities (Erkkinen *et al.*, 2018). The lvPPA phenotype is also considered as an Alzheimer's disease variant.

FTD patients can over time develop motor neuron diseases such as ALS, progressive supranuclear palsy (PSP) or corticobasal syndrome (CBS). The nfvPPA phenotype is associated with the development of PSP or CBS, whereas the lvPPA phenotype has been more linked to developing underlying Alzheimer's disease. Aside from their clinical features, protein inclusions are found in post-mortem FTD patients of microtubule associated protein Tau (FTD-Tau), TDP-43 (FTD-TDP) or FUS (FTD-FUS). Rarer cases of positive ubiquitin inclusions without TDP-43 or FUS immunoreactivity have been described and are known as FTD-UPS. The correlation between clinics and pathophysiology are poor in bvFTD cases contrarily to svPPA and FTD-MND where it is highly associated with TDP-43 pathology (Josephs *et al.*, 2011) or to PSP and CBS where it is highly correlated to FTD-tau. Finally, FTDs have an important genetic factor, with 10% to 20% of familial forms with mutations in most cases in 3 different genes, *MAPT*, *GRN* or *C9ORF72*. Other mutations identified and related to FTD are *CHMP2B*, *VCP*, *SQSTM1*, *TARDBP* and *TBK1* (Meeter *et al.*, 2017)(Figure 4).

FTD-MND are considered as another category, where there is an overlap between FTD and MND symptoms and pathological features. About 15% of bvFTD cases end up by developing ALS symptoms (Rascovsky *et al.*, 2011), with its characteristic upper and lower motor neurons and skeletal muscle deficits and around 30% of ALS patients' present FTD symptoms over disease course (Lomen-Hoerth, 2011), with cognitive impairment and behaviour deficits. These patients are characterised by a shorter survival of approximately 2,4 years after disease onset and widespread frontal and temporal lobes atrophy. Typically, FTD-MND are associated with mutations in TDP-43, FUS and C9ORF72, the latter accounting for more than half of all FTD-MND cases (Mackenzie *et al.*, 2006; Mackenzie, Munoz*, et al.*, 2011; Cooper-Knock *et al.*, 2015).

Because of the relevance of FUS in bvFTD cases and the upcoming studies presented in this manuscript, this phenotype will be more extensively considered. bvFTD is the most common type of FTD (Hogan *et al.*, 2016). Clinically it is characterised by the dysfunction of the non-dominant prefrontal cortex, anterior lobe, paralimbic structures, hippocampus and subcortical structures.

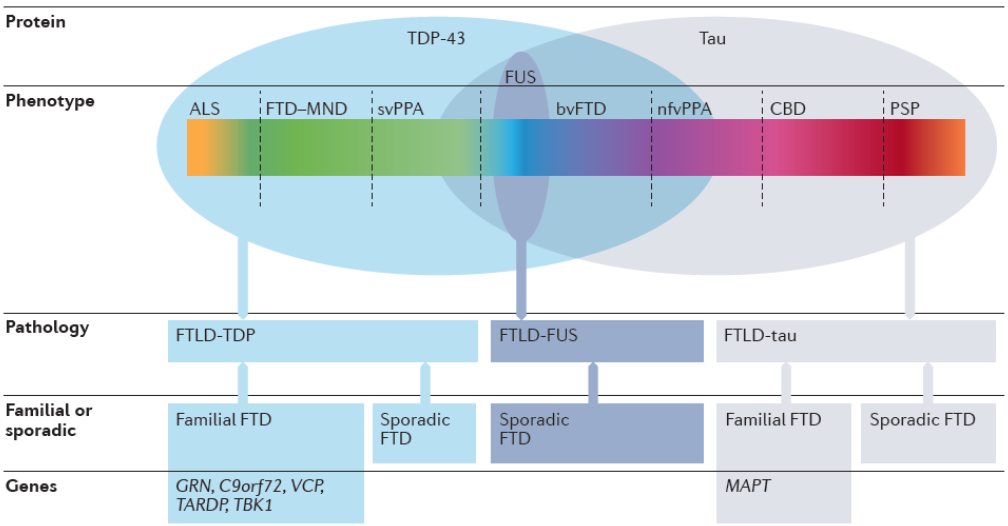

Figure 4: The FTD spectrum.
The FTD spectrum is mainly characterized by hallmark inclusions of different proteins (TDP-43, FUS, Tau), resulting in widely varied phenotypes that underly different pathologies and/or origins. Image from Meeter et al., 2017.

ii. Cognitive and behaviour impairments in bvFTD

Patients present early in the disease course a series of symptoms that are clinically identifiable altering their cognitive capacities and behaviour such as alteration in patient's behaviour, personality, emotions and executive control. The main identifiable symptoms consist in lack of empathy or sympathy for people surrounding them, including family members and animals. General disinhibition is another key feature in bvFTD, affecting their daily lives not being able to normally communicate with others because of atypical attitudes as hugging strangers, performing inappropriate sexual acts or even criminal behaviours. These symptoms are linked to the neurodegeneration of the orbitofrontal cortex. Another specific feature is changes

in their dietary habits which is due to alterations in insular cortex, striatal and hypothalamic regions. Repetitive movements, stereotypies and impulsivity are also present in bvFTD patients and arise from fronto-subcortical dysfunctions. Finally, at the cognitive level, patients have problems in multitasking, present poor working memory, mental rigidity and environmental dependency (Lanata e Miller, 2016).

iii. Eating disturbances in bvFTD

Apart from cognitive and behavioural changes in FTD patients, other alterations related to nutrition have been observed that are also used as clinical features for diagnosis. Particularly in bvFTD patients, three criteria have been established those being, sweet food preference (sweet tooth), increase in food consumption as well as tobacco and alcohol, and consumption of inedible objects (Piguet, 2011). Recent studies, many of them carried out by Ahmed et al. have allowed to identify brain structures altered that could originate such alterations, as well as metabolic changes like those found in ALS, thus endorsing the ALS-FTD continuum. Due to the increase in food consumption bvFTD patients present a higher BMI and increased levels of AgrP, a neurohormone responsible for promoting food consumption, accompanied by an atrophy of the hypothalamus (Ahmed, Latheef*, et al.*, 2015), core regulating region in the CNS for food consumption. Moreover, bvFTD patients as ALS patients are hypermetabolic, with increased resting energy expenditure, atrophy of several brain regions linked to autonomic body functions regulation (Ahmed *et al.*, 2017) and insulin-resistant (Ahmed *et al.*, 2016). However, no changes in peripheral hormone levels and hypothalamic neuropeptides alterations have been found (Ahmed, Iodice*, et al.*, 2015).

iv. Neurotransmitter alterations in FTD

The underlying molecular mechanisms in FTD remain unclear. However, studies in the integrity of neurotransmitter (NT) systems and transmission have revealed several alterations. Deficits in the dopaminergic system resulting in extrapyramidal symptoms as parkinsonism, observed in up to 70% of FTD patients (Gil-Navarro *et al.*, 2013) or behaviour changes (aggressivity, agitation, psychosis), have been linked to alterations in the nigrostriatal (motor) and mesocortical (behaviour) pathways (Murley e Rowe, 2018) subsequent to the loss of dopaminergic neurons, dopamine transporter binding and decreased levels of dopamine (Nagaoka *et al.*, 1995; Rinne *et al.*, 2002). The noradrenergic system in the frame of FTD has not received much attention, but although paucity of studies, this system seems to be overall preserved in the disease (Murley e Rowe, 2018). In terms of behaviour regulation, the serotoninergic system is the prevalent one in charge. Several studies have shown that alterations importantly contribute to bvFTD cognitive symptoms with a decrease in the serotoninergic transmission and receptors density in frontal and temporal lobes, resulting in aggression, impulsivity, increased appetite and depression (Huey *et al.*, 2006; Bowen *et al.*, 2008; Hughes *et al.*, 2015). Furthermore, tau depositions in the Raphe nuclei have been observed (Irwin *et al.*, 2016) and alterations in the gene promoter of serotonin transporter have been linked with brain atrophy (Premi *et al.*, 2015). The cholinergic system is mostly known for its deterioration in Alzheimer's disease, with

its characteristic loss of cholinergic neurons sin the nucleus basalis of Meynert (NbM), projecting to cortex and hippocampus, and decreased levels of choline acetyl transferase (ChAT). Studies in FTD patients have found some alterations in the cholinergic system mainly involving loss of cholinergic neurons and decreased levels of ChAT and of acetylcholine esterase (AChE) in the NbM (Wood *et al.*, 1983; Sparks e Markesbery, 1991; Procter *et al.*, 1999). Some controversial studies have also observed alterations in muscarinic ACh receptors (Weinberger *et al.*, 1991; Procter *et al.*, 1999), but without clear conclusions from it. Finally, the glutamate-GABA systems are highly communicated in regards of general brain functioning as they represent the balance of excitation and inhibition. Alterations in both of them have also been observed in FTD, where patients present decreased number of glutamatergic pyramidal neurons and GABAergic neurons in layers II/III of frontal and temporal lobes (Ferrer, 1999). Decreased concentrations in glutamate/glutamine (Murley e Rowe, 2018) and GABA levels (Kanazawa *et al.*, 1988), and decrease in glutamatergic receptors (Procter *et al.*, 1999; Bowen *et al.*, 2008) and their composition (Gascon *et al.*, 2014). Overall these findings indicate that alterations in many neurological systems contribute to FTD symptomatology, thus potentially requiring combined neuromodulation in order to treat or attenuate them.

3. DIAGNOSIS: LACK OF TOOLS

a. ALS

i. Scales

The establishment of an accurate diagnostic criteria is fundamental in ALS due to the disease short life expectancy in order to include patients in clinical therapies. In 1994 was published the first scale to diagnose ALS, the El Escorial (Brooks, 1994). It consists in the identification of upper and lower motor neurons signs, defined in a 4 stages scale from suspected ALS to definite ALS, depending on the clinical assessment, the extent and distribution of motor signs and neurophysiological (electromyography) and imaging data (MRI, PET). In 2008, a revision of the El Escorial method was published known as the Awaji-Shima criteria which includes some recommendations for the diagnosis of ALS such as electrophysiological data, revealing LMN dysfunctions by the presence of fibrillation potentials and unstable motor units as well as active denervation by the presence of fasciculations (Al-Chalabi *et al.*, 2016). The major flaw of these diagnostic scales is the lack of extra-motor features that are present in ALS-FTD patients, which need to be assessed clinically and will be further discussed.

In order to determine the progression of ALS, the ALS Functional Rating Scale (ALSFRS) was the first scale established, evaluating general daily life actions ranging from 0 to 4, meaning a total loss or unaffected capacities respectively. This scale was revised in 1999 currently known as the ALSFRS-R, including further parameters to evaluate in patients such as dyspnoea, orthopnoea and respiratory insufficiency (Cedarbaum *et al.*, 1999). However, other scales to evaluate ALS progression have been recently proposed such as the King's College (KC) scale or the Milan Torino Staging (MiToS) system. The KC is based in the evaluation of the

affection of the bulbar region, upper or lower limbs, weight and respiratory symptoms, whereas the MiToS evaluates 12 daily life aspects ranging from 4 as not affected to 0 as severely affected (Corcia *et al.*, 2019).

The use of diagnostic and progression scales varies depending on the clinician, patients' symptomatology and hospital facilities. Nevertheless, complementary studies are required to ascertain ALS patient's diagnosis.

ii. Imaging

1. Brain

Imaging studies have observed alterations in ALS patients' brains. Qualitative studies using magnetic resonance 2T have shown a hyperintensity at the corticospinal tract level (Agosta *et al.*, 2010), indicating reduced axonal and myelin density, linked to UMN signs and bulbar onset (Vázquez-Costa *et al.*, 2018). Furthermore, a low signal intensity rim in pre-central cortex has been observed (Petri *et al.*, 2012), corresponding to iron depositions resulting in abnormal iron homeostasis in motor neurons. ALS patients' brain alterations have been quantified by structural and functional MRI as well as diffusion tensor imaging (DTI). Structural studies have observed atrophy of the pre-central gyri (Agosta *et al.*, 2007; Zhang *et al.*, 2014; Devine *et al.*, 2015) and extra-motor regions (Kassubek *et al.*, 2005; Christidi *et al.*, 2018). Thinning of the cortex in primary motor cortex regions (Agosta *et al.*, 2007; Al-Chalabi *et al.*, 2016) and extra-motor regions (Verstraete, Veldink*, et al.*, 2012; Walhout *et al.*, 2015) has also been observed. Functionally, ALS patients present cerebral alterations during motor (Cosottini *et al.*, 2012; Mohammadi *et al.*, 2015) and other tasks accompanied by a decrease in connectivity with the sensorimotor network (Zhou, F. *et al.*, 2013). Finally, DTI studies have observed alterations in corpus callosum (Agosta *et al.*, 2007), extra-motor regions (Agosta *et al.*, 2007; Rosskopf *et al.*, 2015) and the corticospinal tract (Rosskopf *et al.*, 2015).

2. Spinal cord

Alterations in the spinal cord of ALS patients have been characterized, those affecting motor, sensory and metabolic (Carew *et al.*, 2011) pathways. The motor system is affected by the degeneration of the corticospinal tract and the anterior horns, which has been shown to predominantly drive the atrophy (Paquin *et al.*, 2018) and has been correlated with patients' functional disability (Rasoanandrianina *et al.*, 2017). Spinal cord atrophy is linked to muscle weakness (Rasoanandrianina *et al.*, 2017) and electrophysiological markers such as TMS or motor evoked potentials (Cohen-Adad, El Mendili*, et al.*, 2013). Gray and white matter have been observed to equally contribute to spinal cord atrophy (Rasoanandrianina *et al.*, 2017; Paquin *et al.*, 2018). Even though the sensory system does not seem to be impacted in ALS, imaging studies have revealed degeneration of the dorsal column (Cohen-Adad, Zhao*, et al.*, 2013; Rasoanandrianina *et al.*, 2017), implying an early involvement of the sensory system characterized by DTI combined with neurophysiology studies (Iglesias *et al.*, 2015). Contrarily to brain imaging studies, very few data has been collected regarding longitudinal spinal cord changes. However, it has been observed a progressive cord atrophy in presymptomatic

patients carrying genetic mutations (El Mendili *et al.*, 2014; De Albuquerque *et al.*, 2017; Paquin *et al.*, 2018), affecting early the cervical cord, allowing to predict respiratory dysfunctions (Gil *et al.*, 2008; Grolez *et al.*, 2018).

iii. Peripheral markers

1. CSF and blood

The biomarker that is the most used in clinics to corroborate ALS diagnosis is through the measurement of levels of neurofilaments (NfL). NfLs are a major structural component of axons, which are released first in CSF then diffuse to blood after an axonal injury. It is now well known that ALS patients have increased levels of a subunit of NfL, NfL heavy chain in CSF (Ganesalingam *et al.*, 2011; Tortelli *et al.*, 2012) which furthermore correlates with rate of disease progression and survival (Ganesalingam *et al.*, 2011; Lehnert *et al.*, 2014). Increased levels of NfL heavy chain in plasma, serum or CSF are correlated with faster ALSFRS-R rate of decline and reduced survival (Bakkar *et al.*, 2015).

Other biomarkers are such as tau or TDP-43 levels, although there are mixed results for tau with some studies showing an increase in total levels in CSF or blood (Süssmuth *et al.*, 2010) and others no difference (Lehnert *et al.*, 2014) between ALS patients and healthy controls. TDP-43 is a promising biomarker for ALS as it is a key feature of ALS pathophysiology by its cytoplasmic inclusions. It has been found to be increased in CSF (Noto *et al.*, 2011) and plasma (Verstraete, Kuiperij*, et al.*, 2012) but further studies need to be undertaken to validate its use in clinics.

Finally, neuroinflammatory biomarkers have been shown to be altered with activation of microglia and other immune cells (Robelin e Gonzalez De Aguilar, 2014) in patients' blood samples. Levels of inflammatory mediators such as IL-8 (Mitchell *et al.*, 2009) and wide-range C-reactive protein (Keizman *et al.*, 2009) have been observed to be increased in patients CSF. Moreover, a study by Su and collaborators correlated increased levels of IL-8 in CSF with shorter lifespan (Su *et al.*, 2013). Neuroinflammatory biomarkers can be useful to modulate the immune system of patients during therapies but are not sufficient to establish a robust diagnose of the disease on their own.

2. Muscular functions

The neurite outgrowth inhibitor, Nogo-A, which is expressed in skeletal muscle (Dupuis *et al.*, 2002) was also proposed as a muscular biomarker, although some further studies have questioned its specificity (Askanas *et al.*, 2007). Nogo-A expression has been found to be increased in ALS patients' muscles and is correlated with disease severity and muscle atrophy (Dupuis *et al.*, 2002; Jokic *et al.*, 2005; Jokic *et al.*, 2006; Pradat *et al.*, 2007). There is currently an ongoing clinical trial with Ozanezumab, a Nogo-A monoclonal antibody that has been reported to show negative results (Meininger *et al.*, 2014). The principal limitation of using Nogo-A as a muscular biomarker is the obtention of tissue by muscular biopsy.

The assessment of muscular functions can also be studies by electrophysiological techniques such as motor unit number estimation (MUNE) or electrical impedance myography (EIM). MUNE consists in the evaluation of intact motor units that innervate a single muscle by monitoring its maximal response action potentials and estimating the number of individual units. Increased changes in MUNE have been linked with rate of disease progression and survival (Ahn *et al.*, 2010; Shefner *et al.*, 2011). EIM in ALS patients has been shown to decline over time (Rutkove, 2009; Rutkove *et al.*, 2012) and is partially correlated with ALSFRS-R. EIM of single muscles is also correlated with MUNE (Rutkove *et al.*, 2014).

b. FTD

i. Clinical diagnosis

The variability among FTD patients and the overlapping symptomatology between the different subtypes results often in misdiagnoses. In 2011, Rascovsky et al and Gorno-Tempini et al described new diagnostic criteria for FTDs.

bvFTD and PPAs can be diagnosed as "possible", "probable" or with definite FTD pathology. Cases of "possible" bvFTD are characterised by at least three of the following behavioural or cognitive symptoms: early behavioural disinhibition; early apathy; early loss of sympathy or empathy; early perseverative, stereotyped or compulsive behaviour; hyperphagia or dietary changes; and neuropsychological profile such as executive deficits, sparing of memory or visuospatial skills. svPPA "possible" diagnosis is characterised by impaired confrontation naming, impaired single-word comprehension and at least three of the following criteria: impaired object knowledge; dyslexia or dysphagia, spared repetition; and spared speech production. To diagnose a "possible" nfvPPA criteria to be met are the following: at least agrammatism or effortful halting speech; accompanied by at least two of the following features; impaired comprehension, spared single-word comprehension and spared object recognition.

The diagnosis for "probable" bvFTD and PPAs implies patients meet criteria for "possible" diagnosis as well as significant cognitive decline and brain imagining alterations. Patients with bvFTD or PPAs and definite FTD pathology must meet criteria for "possible" or "probable" diagnosis, accompanied by histopathological evidence or presence of a known mutation. Exclusion criteria in bvFTD patients are behaviour deficits or altered biomarkers related to other neurodegenerative or neuropsychiatric diseases.

ii. Neuroimaging

1. Structural changes

a. Grey matter

With techniques such as magnetic resonance imagining (MRI), the measurement of brain volume, rate of atrophy and volume of specific regions, it is possible to evaluate changes in grey matter. Decreased volume in grey matter are usually correlated with neuronal loss and brain atrophy. It is a non-invasive technique allowing

a good discrimination between FTD and AD cases. Several studies have observed that grey matter atrophy occurs in all FTD types, with different regions and degrees of affectation (Meeter *et al.*, 2017). bvFTD patients present an atrophy of frontal and temporal lobes, insula and anterior cingulate cortex and subcortical areas such as hippocampus, amygdala, basal ganglia or thalamus (Schroeter *et al.*, 2007; Seeley *et al.*, 2009; Pan *et al.*, 2012; Schroeter *et al.*, 2015). PPA grey matter atrophy depends on the subtype even though there are predominant alterations on the left hemisphere. All PPA forms extend overtime within the left hemisphere and progress to the opposite hemisphere. Genetic mutations related FTDs also present specific altered regions depending on the mutation with an asymmetrical fronto-temporo-parietal atrophy in *GRN* patients, an almost symmetrical anteromedial-temporal and orbitofrontal atrophy in *MAPT* patients and in *C9ORF72* a symmetrical atrophy of thalamus and superior cerebellum (Meeter *et al.*, 2017) (Figure 5). FTD-FUS patients characteristically present an atrophy of the caudate and orbitofrontal cortices, anteromedial temporal, anterior cingulate and insula (Josephs *et al.*, 2010; Seelaar *et al.*, 2010). However, MRI presents its limitations as it is not possible to distinguish FTD-tau from FTD-TDP (Whitwell e Josephs, 2012). The use of only MRI is not sufficient to determine a diagnosis and complementary tests are required.

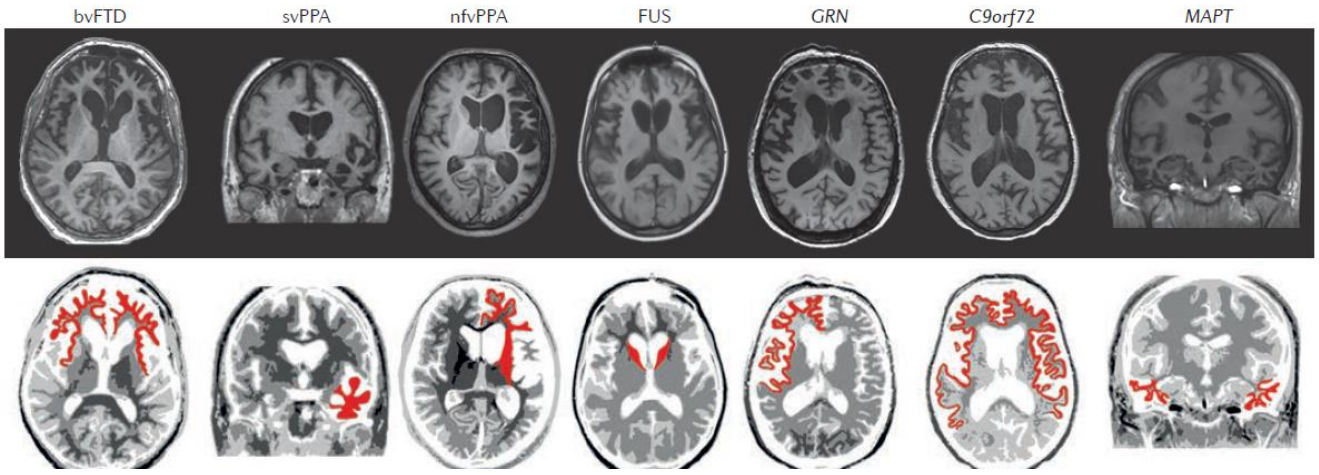

Figure 5: FTLDs differential brain atrophy.
MRI brain scans reveal differential grey matter region atrophy patterns among the different subtypes of FTLD (in red): bvFTD with prominent frontal atrophy, svPPA with asymmetrical temporal atrophy, nfvPPA with asymmetrical frontal and insular atrophy, FUS-FTD with nucleus caudatus atrophy, GRN-FTD with asymmetrical frontotemporoparietal atrophy, C9orf72-FTD with general symmetrical atrophy and MAPT-FTD with symmetrical temporal atrophy. Image from Meeter et al., 2017.

b. White matter

Changes in white matter composition are commonly measured by diffusion tensor imaging (DTI), allowing the study of the microstructural integrity of the white matter correlated to potential axonal degeneration, myelin breakdown and global loss of white matter integrity (Lu *et al.*, 2014). In FTD patients white matter abnormalities have been observed before grey matter atrophy, and these seem to be widespread throughout

the entire brain (Mahoney *et al.*, 2014). DTI allows to differentiate FTD cases from other types of dementia, individuals without dementia and among different subtypes of FTD. Thus, permitting disease monitoring and detection of early changes before disease onset. White matter alterations have been found to co-occur during frontal, temporal and insular atrophy, due to axonal degeneration associated with grey matter neuronal loss (Meeter *et al.*, 2017). Studies have revealed that the major regions affected in FTD are the anterior corpus callosum, the bilateral anterior and descending cingulum and the uncinate fasciculus tracts, tightly related to motor, executive and language networks (Zhang *et al.*, 2013). As it occurs with grey matter, depending on the different type of FTD and related or not with a genetic mutation, the regions affected vary. For instance, the uncinate fasciculus, cingulum bundle and genu of corpus callosum are the regions most affected in bvFTD. Contrarily to MRI, DTI can potentially differentiate FTD-tau from FTD-TPD cases as an increased loss in white matter has been observed in FTD-tau individuals (Mcmillan *et al.*, 2013; Agosta *et al.*, 2015).

2. Functional changes

a. PET

PET studies allow the visualization of differential alterations in brain metabolism that precede grey matter atrophy. FTD individuals present brain regional hypometabolism with asymmetric low glucose metabolism in orbitofrontal, dorsolateral and medial prefrontal cortices as well as anterior temporal poles and basal ganglia. These are key regions that have been shown to be hypometabolic in the bvFTD type and are considered as an early feature of "possible" bvFTD. PPA patients, as previously described, can have other underlying pathologies that overcome with time. PET studies can be used as an evolution predictor as a bilateral tempoparietal hypofunction is indicative of potential conversion in Alzheimer's disease, parietal hypometabolism into CBS and basal ganglia, midbrain and cerebellum hypometabolism into PSP (Cerami *et al.*, 2017). As with structural techniques presented above, regions altered depend on the type or genetic mutation of FTD. Amyloid and tau PET tracers are used to differentiate the different types of FTD and from other neurodegenerative diseases like Alzheimer's disease. Their potential diagnostic use resides in svPPA patients that tend to convert in Alzheimer's cases and FTD-MAPT patients that are associated with tau pathology.

b. Arterial spin labelling (ASL)

ASL is a type of MRI measuring brain perfusion in a non-invasive manner by magnetic labelled water protons in arterial blood, resulting in an endogenous tracer of cerebral blood. ASL has a good correlation with PET metabolism studies and has the advantage that can be combined with other MRI techniques. The main features detected in FTD patients with this technique is an hypoperfusion in the insula, the amygdala and several medial frontal lobe regions. Pre-symptomatic GRN or MAPT individuals present an even more important decrease in blood flow, which can be used as an early biomarker. There is an important overlap in the altered regions detected by ASL and PET, which permits to differentiate FTD subtypes from other neurodegenerative diseases such as bvFTD from AD patients.

c. *Resting-state functional MRI (RS-fMRI)*

This technique measures the functional connectivity between different brain regions. In FTD a decreased connectivity between the fronto-insular and anterior cingulate cortices has been observed (Filippi *et al.*, 2013). Although it is quite controversial as other studies have not observed any differences or others an increase in connectivity (Farb *et al.*, 2013). The high variability in these results studies may be probably due to differences in the studied cohorts, equipment or brain regions of interest. However, svPPA, C9orf72-bvFTD and GRN studies seem to confirm a decrease in connectivity in patients with FTD (Meeter *et al.*, 2017).

iii. *CSF biomarkers*

1. CSF amyloid and β-tau

In Alzheimer's disease, three different biomarkers are used namely, phosphor-tau$_{181}$ (p-tau), total-tau (t-tau) and amyloid $\beta_{1\text{-}42}$ ($A\beta_{1\text{-}42}$). Typical cases of Alzheimer's biomarkers are an increase in p-tau and t-tau and a decrease in $A\beta_{1\text{-}42}$, whereas in FTD the ratios of p-tau: $A\beta_{1\text{-}42}$ or t-tau: $A\beta_{1\text{-}42}$ are increased. Because of the wide variety of FTD types, once more each one presents different levels in the CSF. lvPPA have a more Alzheimer's-like CSF composition and C9orf72 a decrease in $A\beta_{1\text{-}42}$ levels. The most significant application of this biomarker, aside from differentiating Alzheimer's disease cases is it allows to differentiate between FTD-TDP patients that present a lower ratio of p-tau:t-tau than FTD-tau patients (Meeter *et al.*, 2017).

2. Neurofilament proteins

As in ALS, NfL is found increased in blood and CSF of FTD patients, correlating with disease severity, progression, survival and atrophy. The increase of the levels of NfL have been found to increase equally among the different types of FTD, but more particularly in FTD-MND cases (Scherling *et al.*, 2014; Skillbäck *et al.*, 2014; Pijnenburg *et al.*, 2015; Rohrer *et al.*, 2016), where it would seem that the FTD component added to the MND dramatically increases this biomarker levels. Thus, NfL remains one the most promising non-invasive biomarkers for the disease staging, prognosis and monitoring.

3. Gene specific biomarkers

Progranulin is implicated in neurite outgrowth and inflammation. Mutations in the *GRN* gene are linked to decreased levels of progranulin in blood and CSF. Therefore, difference in progranulin levels in these two body compartments allow to discriminate between pre-symptomatic and symptomatic *GRN* mutation carriers and non-carriers. The major flawless of this biomarker is that there is no indication of the neurodegeneration extent.

Cases of *C9ORF72* account for an important percentage of FTD cases, thus biomarkers to identify them are of high interest. Increased levels of glycine-proline-repeating protein (poly(GP)), one of the dipeptide-repeat proteins have been observed. Despite the fact that CSF levels do not correlate with disease onset, progression, severity or survival, poly(GP)s can be of great use as a pharmacodynamic marker (Meeter *et al.*, 2017).

4. TREATMENTS: A MULTIDISCIPLINARY CHALLENGE

a. ALS

i. Pharmacological treatments

Many different drugs have been tested in animal models but there are only three that currently used to ALS patients and all of them have shown limited effects in clinical trials. The first drug to be accepted in use for patients was riluzole in the early 90's, a glutamate antagonist, nowadays approved for its use worldwide. Riluzole's mechanism of action resides in its influence on glutamate metabolism by increasing extracellular glutamate reuptake, inhibiting its release from presynaptic terminals and as an NMDA antagonist limiting glutamatergic transmission. Besides, riluzole stabilizes voltage-dependent sodium channels (Dorst *et al.*, 2018), reducing neuronal hyperexcitability. Clinical trials have shown positive effects of riluzole treatment by prolongating median survival by about 6 months (Zoccolella *et al.*, 2007) and increasing survival rate (Bensimon *et al.*, 1994; Lacomblez *et al.*, 1996). However, its effects seem to be the most effective at the last stage of the disease (Fang *et al.*, 2018). Riluzole is a drug with a safe profile, with a recommended dosage of 100 mg/day in two single doses of 50 mg (Miller *et al.*, 2012). No major side effects have been observed except for some cases with interstitial lung disease, asthenia, nausea, headache and hypertension.

Edavarone is the second available drug in clinics that was recently approved in May 2017 but only in the US and Japan. Its main use was as an antioxidant to treat patients with cerebrovascular injuries such as strokes in Japan. Edavarone's mechanism of action remains completely unknown. The recommended dosage is of 60 mg by intravenous administration during 6 cycles, where the first cycle consists in a daily administration for 14 days followed by 14 days edavarone-free. Because of the mode of administration edavarone treatment is exclusively undertaken in clinical centers (Dorst *et al.*, 2018). However, edavarone's efficacy has been recently questioned in a clinical trial, since patients receiving placebo or edavarone treatment did worse than patients receiving no treatment at all (Turnbull, 2018).

Rasagiline is the latest drug that has been proposed to treat ALS and very limited studies are currently available. Rasagiline is a drug used to treat Parkinson's disease with a safe profile. Its mechanism of action is the inhibition of monoamine oxidase-B having thus antioxidative (Abu-Raya *et al.*, 1999) and antiapoptotic (Maruyama *et al.*, 2001) effects. In ALS animal models, rasagiline alone or in combination with riluzole has shown to prolong mice survival of about 20% (Waibel *et al.*, 2004). However, its effects in the available clinical trials remains still controversial as few studies have shown rasagiline beneficial effects. A trial where patients were administered with 2 mg/day for 12 months observed no effects in the disease progression but noticed differences in patients' symptoms accompanied by changes in some biomarkers (Macchi *et al.*, 2015). Recently, a clinical trial where patients were administered 1 mg/day of rasagiline alone or in combination with riluzole at a dose of 100 mg/day observed differences in disease progression in patients with a specific ALSFRS-R slope (Ludolph *et al.*, 2018), whereas another clinical trial, less powered, found no effect at all (Statland *et*

al., 2019). Further clinical trials need to be done with standardized procedures to evaluate rasagiline's potential effects to treat ALS.

Antisense nucleotides (ASO) have also been considered as a treatment for ALS, particularly with the objective to be used as a gene-silencing therapy. In SOD1 animal models it has shown promising results by decreasing mRNA (Evers *et al.*, 2015) and protein levels in brain and CSF (Winer *et al.*, 2013). Miller and collaborators carried the first ASO clinical trial in SOD1 patients and showed that the administration was well tolerated (Miller *et al.*, 2013). Thus, human application of ASO seem to present great potential for therapeutic approaches despite its administration pathway (intrathecally).

ii. Non-pharmacological treatments

1. Nutritional treatments

Weight loss in ALS patients is a clear negative prognosis factor thus therapies targeting their diet is of major relevance. Nonetheless, results from clinical trials remain still elusive because of the discrepancies found. Clinical research carried on French and German cohorts observed higher patient's survival, with increased ratios of LDL/HDL (12 months survival advantage) (Dupuis *et al.*, 2008) or with higher triglycerides (21,6 months advantage) (Dorst *et al.*, 2011). Contrarily, studies in US (Paganoni *et al.*, 2011) and Italian (Chiò *et al.*, 2009) cohorts found no beneficial effects of BMI in ALS patients. Further studies have tried high caloric diets either with high fat or high carbohydrate content (Dorst *et al.*, 2013). A critical step in ALS patients requires the application of gastrostomy procedures when patients are no longer capable to swallow or masticate in order to stabilize their body weight and reduce the risk of aspiration (Andersen *et al.*, 2012; Wills *et al.*, 2014). This stage requires previous discussion with the patient to evaluate their personal wishes and implement the procedure as soon as the first symptoms of dysphagia arise. In patients with gastrostomy, hypercaloric diet was able to increase survival as compared to isocaloric diet, confirming that nutritional approaches might be efficient in slowing disease progression (Wills *et al.*, 2014).

2. Respiratory support

Respiratory support in ALS patients is highly recommended due to progressive weakness of the diaphragm and denervation of auxiliary respiratory muscles. It can be provided either by non-invasive ventilation or invasive ventilation. Non-invasive ventilation consists in ventilatory support through the upper ways with a nasal or full-mask and is recommended to be implemented as soon as the first symptoms of respiratory difficulty are observed such as hypercapnia, sleep disturbances or cognitive impairment (Dorst *et al.*, 2018). Clinical studies have observed a prolongation of patient's life by about 7 months or even 13 months (Berlowitz *et al.*, 2016). The main adverse effects of ventilatory support are patients discomfort eventually causing anxiety or panic attacks which can be overcome with time and habituation. Invasive ventilation consists in performing a tracheotomy to support the lower ways and is considered as an option late in the disease course

if the patient does not tolerate non-invasive ventilation or cannot be stabilized. This method can considerably improve patients' survival until very advanced stages of the disease when they present complete paralysis (Spataro *et al.*, 2012).

3. Physiotherapy

Many physiotherapy strategies are used to alleviate and compensate patients' motor deficits. Muscular activity in order to preserve and strengthen residual motor function as well as preserve muscles from atrophy, contractions, lymphatic oedemas, thrombosis or musculoskeletal pain are recommended. Physical activity is also thought to generally improve ALS patient's quality of life and their physical and mental integrity. Exercise programs are however of controversy as regular muscle activity could lead to increased motor neurons excitation therefore accelerating their degeneration and disease progression (Dorst *et al.*, 2018). Indeed, diaphragm pacing has been shown to exacerbate disease progression in two independent clinical trials (Committee e Collaborators, 2015; Gonzalez-Bermejo *et al.*, 2016).

b. FTD

i. Pharmacological treatments

1. Cognitive symptoms

Different pharmacological approaches to treat cognitive symptoms in FTD have been used but with mixed results. First, AChE inhibitors have been used in order to try to up-regulate neurotransmission in the cholinergic system and its related cognitive deficits. Studies have shown a complete lack of effect and even worsened behaviour in FTD patients in clinical trials where donepezil (Mendez *et al.*, 2007), rivastigmine (Moretti *et al.*, 2004) or galantamine (Kertesz *et al.*, 2008) were used. Clinical trials with donepezil (Fabbrini *et al.*, 2001) or rivastigmine (Liepelt *et al.*, 2010) were also used in patients with PSP where cognitive symptoms seemed to be mildly improved, but worsened motor symptoms. Second, neuromodulation of the glutamatergic system with the NMDA antagonist memantine, widely used in Alzheimer's disease for cognitive dysfunctions (Tariot *et al.*, 2004) were used in FTD patients. Its effects are inconclusive as two clinical trials (Swanberg, 2007; Boxer *et al.*, 2009) showed cognitive functions improvement but had no positive effects on two other clinical trials (Vercelletto *et al.*, 2011; Boxer *et al.*, 2013). In all, FTD cognitive symptoms remain an important factor with no efficient treatment.

2. Behavioural symptoms

As previously mentioned, the serotoninergic system is one the key components in behaviour regulation which appears altered in FTD. Several pharmacological approaches have been tried to alleviate those symptoms. Selective serotonin re-uptake inhibitors (SSRIs) are commonly used to treat major neuropsychiatric disorders such as schizophrenia or depression. Clinical trials have shown that FTD patients treated with SSRIs such as sertraline (Prodan *et al.*, 2009), citalopram (Herrmann *et al.*, 2012) or trazodone (Lebert *et al.*, 2004) generally improve behaviour symptoms and are well tolerated. Only paroxetine effects seem to be controversial as two

studies (Chow e Mendez, 2002; Moretti *et al.*, 2003) showed an improvement in behaviour symptoms, whereas another study showed no positive effects (Deakin *et al.*, 2004). Another therapeutic strategy that has been used in clinics to treat behavioural symptoms have been antipsychotics, where there is an increased risk in appearance of extrapyramidal side effects. Once again, overall effects of antipsychotics seemed to have beneficial effects in FTD patients carried by multiple clinical trials with risperidone, aripiprazole or olanzapine except for quetiapine, which showed lesser clear effects. Finally, anti-epileptics have also been used as mood stabilizers (Tsai e Boxer, 2016).

3. Motor symptoms

An important percentage of FTD patients present motor symptoms as parkinsonism, therefore treatments used in Parkinson's disease (PD) have been used to try to modulate the dopaminergic system and alleviate symptoms. Surprisingly, FTD patients do not respond to classic drugs used in PD such as levodopa/carbidopa possibly because of the implication and alteration of other brain regions that remain unaffected in PD (Tsai e Boxer, 2016).

ii. Non-pharmacological treatments

FTD patients' treatments also include physical therapy aiming to improve and alleviate gait disturbances and to train balance. A study carried out by Cheng and collaborators, (Cheng *et al.*, 2014) observed that exercise is beneficial for FTD patients, improving their cognition, mood and general health. FTD varieties affecting speech such as PPA include speech therapy (Tippett *et al.*, 2015) to help facilitate patients communication. Patients daily lives can also be improved by making them participate to educational conferences, support groups, educate caregivers and family members as well as neurorehabilitation and community-based activities (Kortte e Rogalski, 2013).

5. Genetics and Pathophysiology in the ALS-FTD continuum: an expanding field

a. Genetic mutations

Advances in the detection of genetic mutations and variants have allowed to identify many genes related to ALS and FTD, implicated in different molecular pathways and with varied physiological functions (Figure 6). Here, we will discuss the most represented and relevant mutations linked to ALS, FTD and the ALS-FTD continuum.

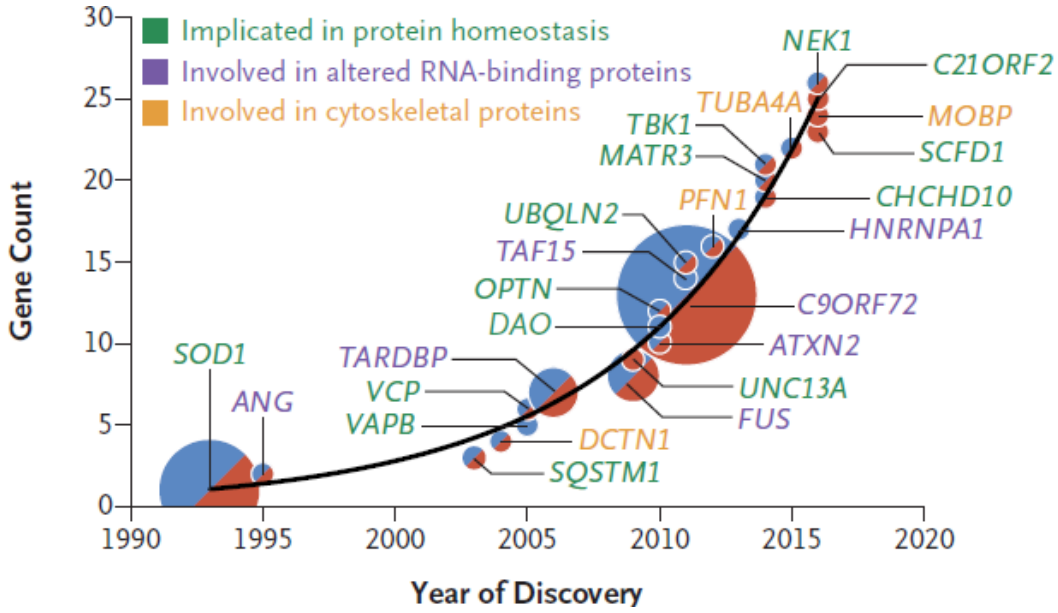

Figure 6: Genetics in ALS-FTD.
The discovery of genetic mutations linked to ALS-FTD have exponentially increased since SOD1 in 1993. Since then mutations have been classified according to their function in three major categories: protein homeostasis (green), RBPs (violet), cytoskeleton (yellow). Circles represent the percentage of familial (in blue) and sporadic (in red) cases. Image from Brown et al., 2017.

i. SOD1

Mutations in the gene encoding Cu/Zn superoxide dismutase 1 (SOD1) were the first to be identified in 1994 (Rosen *et al.*, 1994) causing ALS in a dominantly inherited manner. *SOD1* mutations are only found in ALS patients and account for approximately 10% of fALS and 3% of sALS (Andersen, 2006). Most fALS cases of *SOD1* present deposits of mutant SOD1 (Valentine *et al.*, 2005), whereas sALS cases can present wild-type SOD1 protein in inclusions (Rotunno e Bosco, 2013). *SOD1* chromosomal locus is 21q22.11 and encodes for an enzyme whose main function is to scavenge free radicals. SOD1 is found ubiquitously and is mainly located in the cytosol. More than 180 mutations have been currently identified, from which initially it was thought to lead to a loss of function of the protein. However, it has been shown that the ablation of *Sod1* does not lead to motor neurons degeneration (Reaume *et al.*, 1996). Indeed, *SOD1* mutations have been linked to a toxic gain of function, where mice models carrying *SOD1* mutations have mimicked ALS patients' symptoms such as SOD1 inclusions, motor neurons loss, paralysis and death (Gurney *et al.*, 1994; Wang *et al.*, 2009). Importantly,

knocking out the endogenous *Sod1* gene did not modify disease progression in the models (Bruijn *et al.*, 1997) arguing for a gain of toxic function. The first SOD1 transgenic mouse model was carrying the G93A mutation and presented spinal motor neurons degeneration, progressive paralysis motor deficits, paralysis and death at 5-6 months of age (Gurney *et al.*, 1994; Chiu *et al.*, 1995). All SOD1 mutations that have been characterized so far affect the protein in different domains, but they all seem to alter the protein function in two specific ways, either by impairing its metal binding capacity (mutation G85R) or by rendering the protein more sensitive to disulphide reducing agents (mutations A4V and G93A), both of them resulting in an alteration of the enzymes' hydrophobic properties (Tiwari *et al.*, 2005). Furthermore, studies have shown how mutant SOD1 presents an aberrant misfolding resulting in the proteins' aggregation (Nordlund e Oliveberg, 2008) and prion-like behaviour spreading from cell to cell in *in vitro* studies *via* macropinocitosis (Münch *et al.*, 2011) or *in vivo* by the injection of mutant SOD^{G93A} protein in mice SOD^{G85R} (Ayers *et al.*, 2014). Finally, SOD1 mutations alter its physiological functions interfering at multiple cellular levels such as gene transcription (Sau *et al.*, 2007) or mitochondrial deficits (Israelson *et al.*, 2010), ER stress (Nishitoh *et al.*, 2008), neurofilaments RNA stability (Volkening *et al.*, 2009), and axonal transport defects (Zhang *et al.*, 2007). Despite more than 25 years of research on SOD1 mutations, the understanding of its toxic gain of function in ALS remain elusive.

ii. TDP-43

TDP-43 is a protein encoded by the gene TAR DNA binding protein (*TARDBP*), which is localised in the chromosomal locus 1p36.22. Mutations in *TARDBP* account for approximately 4% of all fALS cases and 1% of sALS cases (Volk *et al.*, 2018) and have been described in sALS and fALS cases (Kabashi *et al.*, 2008), and mainly affect the C-terminal region (Sreedharan *et al.*, 2008). TDP-43 is ubiquitously expressed (Wang *et al.*, 2008; Zhang *et al.*, 2008) and is composed by two RNA-recognition motifs, a nuclear localisation signal and a nuclear export signal (Winton *et al.*, 2008). This allows the protein to shuttle between the nucleus, its predominant localisation, and the cytoplasm (Buratti e Baralle, 2008). Some of TDP-43 functions include mRNA splicing, nucleocytoplasmic transport of RNAs and cytosolic mRNA transport to dendrites (Barmada *et al.*, 2010; Kabashi *et al.*, 2010). Furthermore, TDP-43 is capable of regulating its own RNA therefore autoregulating its levels (Ayala *et al.*, 2011; Polymenidou *et al.*, 2011). In pathological conditions, TDP-43 depositions have been linked with several neurodegenerative diseases, described as TDP-43 proteinopathies (Kwong *et al.*, 2007). TDP-43 ubiquitinated cytoplasmic inclusions can be found in ALS patients' spinal motor neurons and FTD patients' cortical neurons. These depositions are composed by full-length or fragmented TDP-43, ubiquitinated and phosphorylated cytoplasmic aggregates accompanied by decreased levels of nuclear TDP-43 (Neumann *et al.*, 2006). The remaining question in TDP-43 pathologies is whether its toxicity is due to a loss or gain of function. In order to assess TDP-43 loss of function, Sephton and collaborators developed a TDP-43 knock-out mouse model, which resulted in embryos dead (Sephton *et al.*, 2010), showing a crucial role of TDP-43 in development. Further studies using conditional or partial knock-out models showed that loss of TDP-43

function mimics ALS symptoms with motor neuron defects, progressive motor phenotypes and TDP-43 proteinopathy (Kabashi *et al.*, 2010; Wu, L. S. *et al.*, 2012). Conversely, many studies have supported the implication of TDP-43 gain of function in the disease (Ash *et al.*, 2010; Kabashi *et al.*, 2010; Li *et al.*, 2010; Wils *et al.*, 2010). Besides, the selective induction of TDP-43 loss or gain of function in glial cells have revealed an important role in the disease (Diaper *et al.*, 2013; Yang, C. *et al.*, 2014). Common TDP-43 proteinopathy hallmarks are found in ALS and FTD with cytosolic mislocalization of the protein and C-terminal fragments mostly in brain inclusions (Neumann *et al.*, 2006; Igaz *et al.*, 2008), with prone aggregating properties (Fuentealba *et al.*, 2010). Since TDP-43 mutations mainly affect the C-terminal region, mutated proteins tend to misfold resulting in decreased RNA transport (Johnson *et al.*, 2009; Alami *et al.*, 2014). Finally, an ALS and FTD hallmark of TDP-43 proteinopathy is the hyperphosphorylation and ubiquitination fragmented, aggregated and detergent-resistant TDP-43, also linked to misfolding and aggregation (Hasegawa *et al.*, 2008; Neumann, Kwong, *et al.*, 2009). Very recent studies have observed that mutations in the low complexity domain of TDP-43 result in a gain of splicing function, where TDP-43 impairs its own autoregulation mechanisms by increasing the production of variants including intron7-exon7 resulting in a stable form of its mRNA, thus increasing protein levels contributing to TDP-43 pathology (Fratta *et al.*, 2018; White *et al.*, 2018).

iii. FUS

Fused in Sarcoma (FUS) is an RNA binding protein involved in many physiological functions and has a predominant nuclear localisation. In 2009, the first FUS mutations linked to ALS were identified (Kwiatkowski *et al.*, 2009). FUS physiological functions and implications in the ALS-FTD pathogenesis will be further discussed below.

iv. C9ORF72

The recent discovery of mutations in the hexanucleotide GGGGCC repeat expansion in the first intron of C9ORF72 gene, has been revealed to be the most frequent genetic mutation in ALS and FTD patients (Dejesus-Hernandez *et al.*, 2011) being the first genetic evidence of the ALS-FTD continuum. *C9ORF72* chromosomal location is 9p21.2 and in healthy individuals is found in 11 or less hexanucleotide repeats (Rutherford *et al.*, 2012). Conversely, ALS and FTD patients present an extensive number of hexanucleotide repeats ranging from hundreds to thousands. Determining the cut-off of pathogenic expansion repeats is controversial, but most studies have established it above 30 repeats (Rutherford *et al.*, 2012; Simón-Sánchez *et al.*, 2012). Besides, *C9ORF72* ALS and FTD patients present TDP-43 inclusions, which corroborates a common pathological pathway between these two diseases (Ling *et al.*, 2013). *C9ORF72* expanded GGGGCC repeats are bidirectionally transcribed into repetitive RNA resulting in sense and antisense RNA foci (Lagier-Tourenne *et al.*, 2013; Mizielinska *et al.*, 2013). These repetitive RNAs can be translated in every reading frame, arising five different dipeptide repeat proteins (DPRs) namely, poly-GA, poly-GP, poly-GR, poly-PA and poly-PR. DPRs are obtained *via* a non-canonical mechanism, the repeat-associated non-ATG (RAN) translation (Zu *et al.*, 2013).

RNA foci are composed by sense and antisense *C9ORF72* repeat RNA and have been observed in several regions of the CNS such as in frontal and motor cortices, hippocampus, spinal cord, motor neurons and occasionally in interneurons, but less frequently in glial cells (Mahoney *et al.*, 2012; Gendron *et al.*, 2013; Lagier-Tourenne *et al.*, 2013; Mizielinska *et al.*, 2013; Zu *et al.*, 2013). DPR inclusions are p62 positive and TDP-43 negative and can be constituted by more than one DPR (Gendron *et al.*, 2013; Zu *et al.*, 2013). They have been observed as neuronal cytoplasmic or neuritic inclusions as well as pre-inclusion diffusely in cytoplasm and sometimes as intranuclear inclusions (Gendron *et al.*, 2013; Mackenzie *et al.*, 2013; Saberi *et al.*, 2018). Nonetheless, the different types of DPRs are not equally found in inclusions where poly-GA are predominantly found, followed by poly-GP and poly-GR sense derived, being poly-PA and poly-PR antisense the less frequent poly-GA (Mori *et al.*, 2013; Mackenzie *et al.*, 2015). Mutations in C9ORF72 lead to 3 different mechanisms, (1) *C9ORF72* loss of function, C9ORF72 gain of function of sense and antisense (2) repeat RNAs or (3) repeat DPRs. *C9ORF72* mutations inducing loss of function have been characterized by decreased levels of one or more transcript variants, particularly variants 1 and 2 (Todd e Paulson, 2013; Van Blitterswijk e Rademakers, 2015), accompanied by decreased levels of mature spliced C9ORF72 and increased levels of sense and antisense transcripts containing intron 1 (Mori *et al.*, 2013; Zu *et al.*, 2013). Furthermore, *C9ORF72* loss of function has been linked to cellular trafficking and autophagy defects (Amick *et al.*, 2016; Shi *et al.*, 2018). Gain of toxic function resulting from C9ORF72 mutations remain controversial as the origin is not clear yet. On one hand, studies have shown how repeat RNA forms *in vitro* and *in vivo* secondary structures that sequestrate RNA-binding proteins, thus contributing to RNA toxicity (Haeusler *et al.*, 2014). On the other hand, DPRs have been shown to induce neurodegeneration in a *Drosophila* model (Mizielinska *et al.*, 2014). Wether alone or in combination they are responsible for C9ORF72 gain of toxic functions needs to be further investigated.

v. GRN

Granulin precursor (GRN) gene chromosomal location is 17q21.31 and encodes for the progranulin (PGRN) protein. In 2006, mutations in GRN were identified to be linked with FTD patients (Baker *et al.*, 2006; Cruts *et al.*, 2006) and account nowadays for approximately 11,2% of all patients (Abella *et al.*, 2017). Carriers of *GRN* mutations present ubiquitin and TDP-43 positive inclusions (Baker *et al.*, 2006; Cruts *et al.*, 2006). Most *GRN* mutations result in an haploinsufficiency du to mutant mRNA degradation leading to a decrease in progranulin protein levels (Cruts e Van Broeckhoven, 2008). Other GRN mutations have been linked with neurite outgrowth defects and proinflammatory responses (Kleinberger *et al.*, 2013).

vi. TBK1

TANK-binding kinase 1 (*TBK1*) is a gene located in chromosome 12q14.2 and encodes for a kinase involved in the phosphorylation of substrate in cellular signalling pathways (Helgason *et al.*, 2013), inflammatory responses (Yu *et al.*, 2012), innate immunity (Clément *et al.*, 2008) and cellular growth and proliferation (Ou *et al.*, 2011). Two of TBK1 major substrates are optineurin (OPTN) and p62, which play a very important role

in autophagy (Wild *et al.*, 2011; Pilli *et al.*, 2012) and have been linked to ALS-FTD pathology (Edens *et al.*, 2016). Mutations in *TBK1* result in a loss of function or missense mutations leading to decreased protein expression or loss of interaction with its adaptor molecules (Edens *et al.*, 2016). The identification of *TBK1* mutations have been linked with ALS-FTD (Cirulli *et al.*, 2015; Pottier *et al.*, 2015).

b. Nucleocytoplasmic transport defects

Nucleocytoplasmic transport is essential for the import of proteins and the export of RNAs. However, there is evidence that this mechanism is altered in ALS-FTD (Figure 7). For instance, mutations in *SOD1, FUS*, *TARDBP* and *C9ORF72* result in nucleocytoplasmic transport defects. In pathological conditions, cytosolic aggregated proteins can sequester and mislocalize proteins involved in the nucleocytoplasmic transport (Woerner *et al.*, 2016). In the ALS mouse model $SOD1^{G93A}$, importins α and β, necessary for nuclear import are mislocalized (Zhang *et al.*, 2006). Furthermore, *SOD1* mutations lead to discontinuous localization of nuclear pore complexes on the nuclear membrane (Kinoshita *et al.*, 2009). Mutations in TDP-43 or FUS have been characterized by the formation of toxic protein aggregates in the cytosol. Several studies have revealed a blockade of nuclear import, with alteration of nuclear import factors such as transportin1/karyopherin-β2 (TnPO1/Kβ2), also known as importins α and β (Winton *et al.*, 2008; Dormann *et al.*, 2010; Nishimura *et al.*, 2010) likely originating the observed accumulation of proteins in the cytosol. Moreover, similar alterations have been observed in ALS-FTD patients' brains, with altered levels and distribution of TNPO (Nishimura *et al.*, 2010; Neumann *et al.*, 2012). Nucleocytoplasmic transport defects have also been characterized in C9ORF72 mutations, where RNA repeats bind to RBPs and nuclear pore complex proteins (Zhang *et al.*, 2015) and DPRs block the central channel of nuclear pores (Shi *et al.*, 2017). Nucleocytoplasmic transport defects majorly contribute to the accumulation of proteins in the cytosol potentially leading to aggregates formation, which play a critical role in cellular homeostasis.

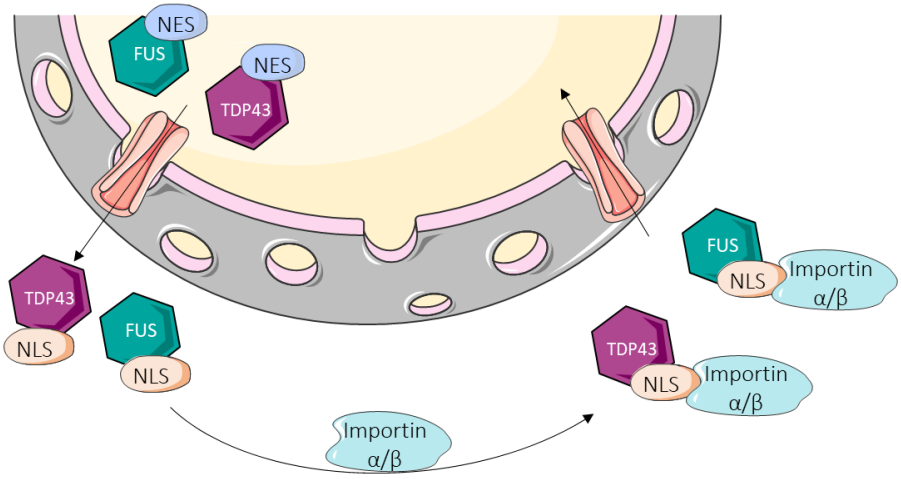

Figure 7: RBPs nucleocytoplasmic transport.
RBPs are exported from the nucleus *via* their nuclear export signal (NES). In the cytosol, importins α/β recognize the nuclear localisation signal and bind to them, allowing RBPs import to the nucleus.

c. *Disturbed RNA metabolism*

RBPs are known to play a critical role in many steps of cellular RNA metabolism. TDP-43 and FUS are RBPs sharing similar structure and functions (Lagier-Tourenne *et al.*, 2010) involved in nuclear transcription and splicing and cytosolic transport, localisation and translation. In the nucleus, TDP-43 and FUS can bind to their own mRNAs, induce their splicing in a dose-dependent manner and produce transcripts that may undergo non-mediated decay as a mechanism of autoregulation (Polymenidou *et al.*, 2011; Lagier-Tourenne *et al.*, 2012; Zhou, Y. *et al.*, 2013). FUS RNA metabolism and autoregulation mechanisms will be further detailed in the next chapter. TDP-43 has been characterized to bind to more than 6.000 RNA targets in the brain and can regulate the transcription of its targets which are genes with long intron (>100 kb) encoding proteins for neuronal functions (Polymenidou *et al.*, 2011; Lagier-Tourenne *et al.*, 2012). RBPs levels are critical as they influence the expression of their targets and other RBPs. TDP-43 knock-down has been observed to result in decreased levels of FUS transcript as well as altered levels of other targets such as EAAT2, APP, progranulin or tau (Polymenidou *et al.*, 2011; Sephton *et al.*, 2011). Moreover, several studies have shown how decreased levels of RBPs result in more than 600 splicing product alterations (Polymenidou *et al.*, 2011; Tollervey *et al.*, 2011; Lagier-Tourenne *et al.*, 2012). Furthermore, TDP-43 has been shown to bind pre-mRNAs at different sites, implying a role in mRNAs maturation as well as to non-coding RNAs (ncRNA), which have regulatory roles in chromatin remodelling, transcription regulation and post-transcriptional processing. Some of these ncRNAs are NEAT1 or MALAT1, which expression has been observed increased in ALS-FTD patients (Tollervey *et al.*, 2011). Recently the most affected transcript by TDP-43 in pathological conditions has been characterized. Human stathmin-2 is aberrantly spliced and prematurely polyadenylated (Melamed *et al.*, 2019), where TDP-43 and FUS seem to influence the use of alternative polyadenylation sites (Masuda *et al.*, 2015; Rot *et al.*, 2017). Finally, RBPs such as TDP-43, FUS or hnRNAP1 bind to microRNAs and modulate their biogenesis (Alarcón *et al.*, 2015; Eitan e Hornstein, 2016). Other ALS causing mutations have been identified to cause alterations in the RNA metabolism such as senataxin or angiogenin. Senataxin is an RNA/DNA helicase which in physiological conditions regulates gene expression by inducing transcriptional termination (Skourti-Stathaki *et al.*, 2011). Mutations in senataxin result in premature protein termination that interfere with helicases function or affects the N-terminal protein interactions (Chen *et al.*, 2014). Angiogenin mutations result in impaired angiogenesis due to deficient ribonucleases activity and defects in nuclear import and localisation (Wu *et al.*, 2007). RBPs role at the cytoplasmic level include transport, localisation and traduction of mRNAs (Lagier-Tourenne *et al.*, 2010; Alami *et al.*, 2014). Alami and collaborators observed that ALS-FTD carriers of mutant TDP-43 presented protein disrupted capacities to transport and deliver mRNAs to distal compartments (Alami *et al.*, 2014). Whereas FUS mutant proteins bind more cytoplasmic targets (Hoell *et al.*, 2011) and present defects in mitochondria and lysosomes (Guo *et al.*, 2017; Naumann *et al.*, 2018) (Figure 8).

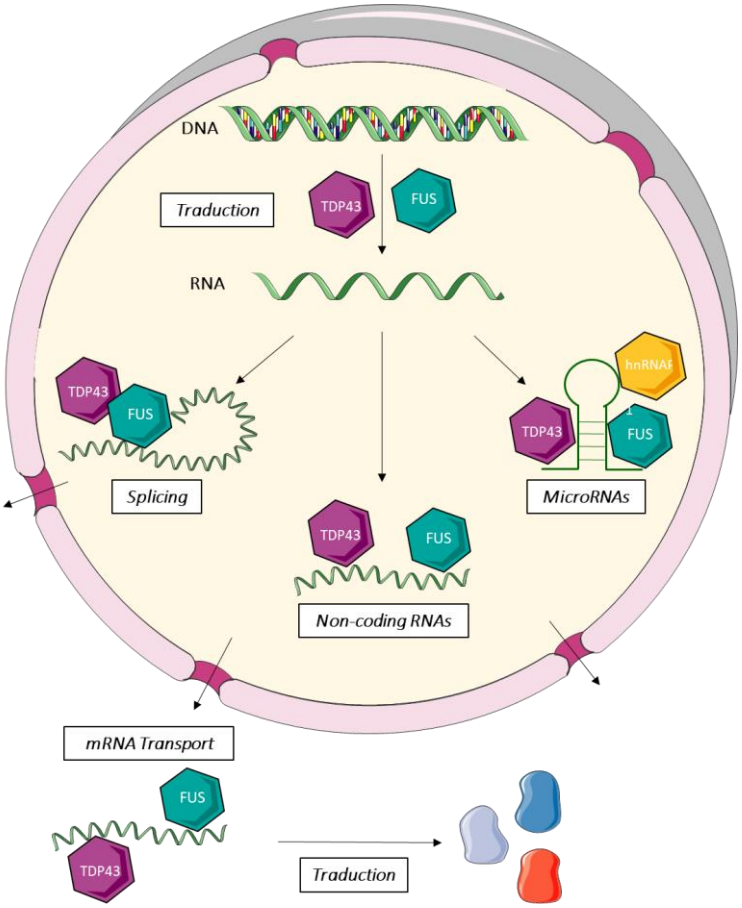

Figure 8: RBPs role in RNA metabolism.
RBPs play different roles at different steps of RNA metabolism. In the nucleus they are involved in RNAs' traduction, splicing of RNAs and ncRNAs and miRNAs biogenesis. In the cytosol they are responsible for mRNA transport and traduction.

d. Impaired proteostasis

Protein homeostasis is affected in many different aspects in ALS-FTD and several linked mutations to the disease have shown to impair correct proteostasis mechanisms. One of the key pathways of protein homeostasis is autophagy, allowing the degradation of misfolded or unfunctional proteins. Autophagy is a process in which many components intervene such as endosomes, lysosomes and autophagosomes. Two key molecules in autophagy are p62/SQSTM1 (sequestrosome 1; also known as ubiquitin-binding protein 1) and optineurin (OPTN) and participate as autophagic adaptor proteins. P62/SQSTM1 binds to different substrate for selective autophagy and play a key role against oxidative stress *via* Nrf2 transcription factor activation that has been shown to be compromised in ALS-FTD (Goode *et al.*, 2016). Furthermore, p62/SQSTM1 has been observed to colocalise with TDP-43 aggregates (Hiji *et al.*, 2008) and increased levels in C9ORF72 mutation carriers (Cooper-Knock *et al.*, 2012) overall indicating impaired autophagic processes. OPTN binds ubiquitin and acts also as an autophagy receptor (Wild *et al.*, 2011). Decreased clearance of protein aggregates and defective mitochondria were found in studies where OPTN levels were decreased (Korac *et al.*, 2013; Wong e Holzbaur, 2014). OPTN and valosin containing protein (VCP) have been observed to colocalize with TDP-43,

p62/SQSTM1 and ubiquitin inclusions in sALS and fALS cases. ALS-FTD mutations in OPTN mainly affect the ubiquitin-binding domain, resulting in impaired interaction with LIR domains and dysfunctional autophagy (Shen *et al.*, 2015). More precisely, mutation OPTN E696K disrupts the OPTN/TBK1 complex (Li *et al.*, 2016), where TBK1 phosphorylates OPTN in order to bind to damaged mitochondria (Heo *et al.*, 2015; Matsumoto *et al.*, 2015). As previously mentioned, mutations in *TBK1* have been linked to ALS-FTD. TBK1 functions consist in phosphorylating proteins such as OPTN and p62/SQSTM1 to be rapidly recruited to damaged mitochondria. However, mutations in *TBK1* have been linked with a loss of function of the protein, resulting in decreased phosphorylation of OPTN and p62/SQSTM1 (Gijselinck *et al.*, 2015) thus, impairing autophagy. TBK1 has been identified to also play a role in the NFkB pathway, tightly related to cellular survival *via* TrkB activation (Arumugam *et al.*, 2018) leading to a potential role of TBK1 in cellular survival. Mutations in *SOD1, TARDBP, FUS or C9ORF72* have also been linked with defective autophagy. SOD1 has been found to block vesicles nucleation through abnormal interactions (Lee *et al.*, 2015); TDP-43 carriers present increased autophagy (Wang *et al.*, 2015); *FUS* mutations lead to protein concentration in stress granules accompanied by decreased autophagy, probably by interfering with early autophagosomes (Ryu *et al.*, 2014); and C9ORF72 mutations result in increased levels of p62/SQSTM1 (Cooper-Knock *et al.*, 2012). CHMP2B is a subunit of the endosomal sorting complex for transport (ESCORT III). Mutations in CHMP2B have been linked to FTD (Skibinski *et al.*, 2005) and ALS (Parkinson *et al.*, 2006; Cox *et al.*, 2010). Specifically models of $CHMP2B^{intron5}$ mutations show important alterations in the autophagy process, with abnormal accumulation of autophagosomes and multilamellar bodies (Lee *et al.*, 2007), lysosomal pathology (Clayton *et al.*, 2015) and FTD hallmarks such as p62 and ubiquitin positive aggregates and behavioural deficits (Gascon e Gao, 2014; Vernay *et al.*, 2016; Clayton *et al.*, 2017). VCP is a multifunctional ATPase with a key role in ubiquitin-dependent degradation by proteasome, autophagy, endosomal sorting and intracellular signalling pathways such as NFkB (Meyer *et al.*, 2012). Mutations in this gene have shown to interfere with autophagic clearance of damaged mitochondria, stress granules and ruptured lysosomes as well as TDP-43 pathology (Tresse *et al.*, 2010; Buchan *et al.*, 2013; Kim *et al.*, 2013; Papadopoulos *et al.*, 2017). Many other genetic mutations identified in ALS-FTD have been linked with protein homeostasis defects. GRN and PGRN are proteins localised inside lysosomes and mutations resulting in PGRN haploinsufficiency have been linked with lysosomal defects (Kao *et al.*, 2017). Ubiquilin-2 (*UBQLN2*) mutations result in defective protein degradation by ineffective cargo delivery to the proteasome (Chang e Monteiro, 2015) and Alsin-2 (*ALS2*) mutations lead to defective endosomal trafficking (Chandran *et al.*, 2007). Finally, another key pathway in protein homeostasis is the proper transport or proteins between the endoplasmic reticulum (ER) and the Golgi apparatus, which also seems to be altered in the ALS-FTD pathology. C9ORF72 tightly interacts with different Rab proteins involved in the endocytic trafficking or recycling of proteins between the plasmatic membrane and the Golgi, thus mutations in C9ORF72 interfere with this process (Farg *et al.*, 2014; Aoki *et al.*, 2017). VAPB has a major role in recycling proteins between the

ER and the Golgi (Kuijpers *et al.*, 2013). The VAPB mutation P56S has been linked with fALS (Nishimura *et al.*, 2004) and results in the accumulation of inclusions including disrupted ER (Papiani *et al.*, 2012) along with the recruitment of wild-type VAPB (Teuling *et al.*, 2007). Further evidence of disruptions in the ER-Golgi pathway have been observed with several SOD1 mice models, where the secretory pathway seems to be altered showing increased levels of BDNF (Atkin *et al.*, 2014). Overall, these data indicate clear defect processes in protein homeostasis in the ALS-FTD continuum (Figure 9).

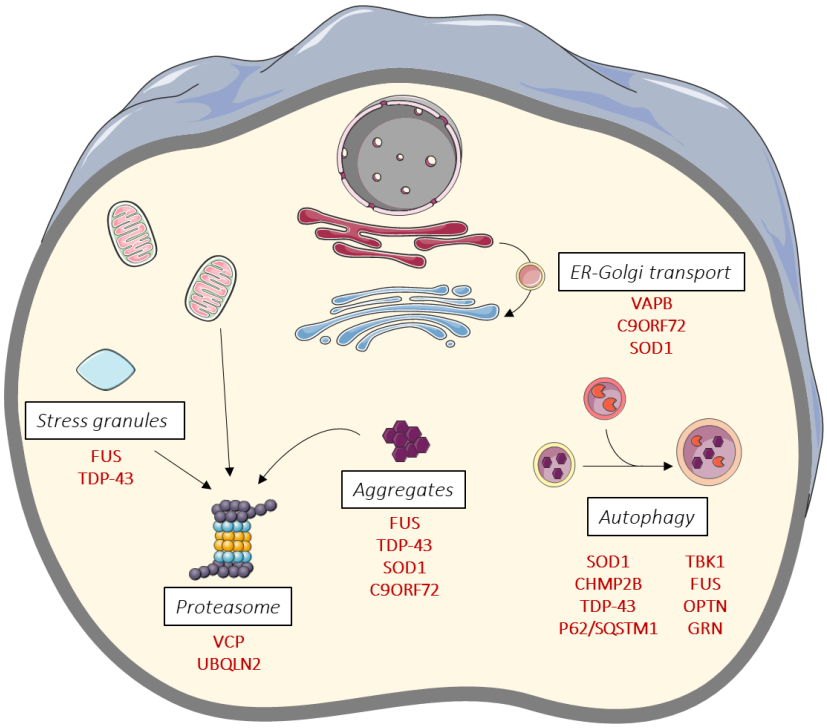

Figure 9: Protein homeostasis dysregulations in ALS-FTD.
Mutations in ALS-FTD linked genes have revealed important deficits in several protein homeostasis pathways. Alterations in the recycling of vesicles from the ER to the Golgi, defects in autophagy and stress granules formation accompanied by dysfunctional proteasome properties contribute to defective protein degradation.

e. Cytoskeletal and axon transport defects

Cellular cytoskeleton and axonal transport are key features for the proper functioning of cells, but in ALS-FTD both components seem to be severely impacted. Axonal transport is ensured by two different motor proteins, kinesins and dyneins, responsible for the anterograde and retrograde transport respectively of mitochondria, endosomes and proteins. Mutations in kinesin-5A (*KIF5A*) have been linked with ALS (Brenner *et al.*, 2018) and mostly affect the C-terminal region of the protein where the cargo is bonded (Nakajima *et al.*, 2012), resulting in impaired transport. Furthermore, *SOD1* and *FUS* mutations have been shown to alter the fast axonal transport (Morfini *et al.*, 2013; Sama *et al.*, 2017), where mutant FUS dysregulates mRNAs of several kinesins (Hoell *et al.*, 2011). Mutations in another gene, *DCTN1* encoding for $p150^{Glued}$, a dynactin complex protein, have been identified in sALS and fALS (Münch *et al.*, 2007), which block the binding of $p150^{Glued}$ to

microtubules, leading to dysfunctional cargos transport (Ikenaka *et al.*, 2012). Neurofilaments also play a major role in axonal transport and have been directly linked with disease severity. Their accumulation results toxic for motor neurons as was shown in a SOD1 mouse model, where neurofilament removal was beneficial for mice and decreased disease progression (Williamson *et al.*, 1998). However, neurofilaments accumulation could be due to defective functioning of kinesis and dyneins (Sunil *et al.*, 2012).

Mutations in cytoskeletal proteins have also been linked with ALS-FTD. Mutations in the neurofilament heavy chain (*NFH*) result in the accumulation of phosphorylated neurofilament proteins, leading to axonal transport defects (Munoz *et al.*, 1988; Mizusawa *et al.*, 1989). Peripherin (PRPH) is a neuronal intermediate filament protein and mutations have shown to disrupt neurofilaments network assembly (Gros-Louis *et al.*, 2004). Mutations in tubulinβ-4A (*TUB4A*) lead to microtubule destabilization and decreased re-polymerization (Smith *et al.*, 2014), whereas mutations in profilin (*PFN1*) or cofilin (*CFL1*) alter actin dynamics by inhibiting axon outgrowth (Wu, C. H. *et al.*, 2012) or interacting with C9ORF72 (Sivadasan *et al.*, 2016) respectively 5figure 10).

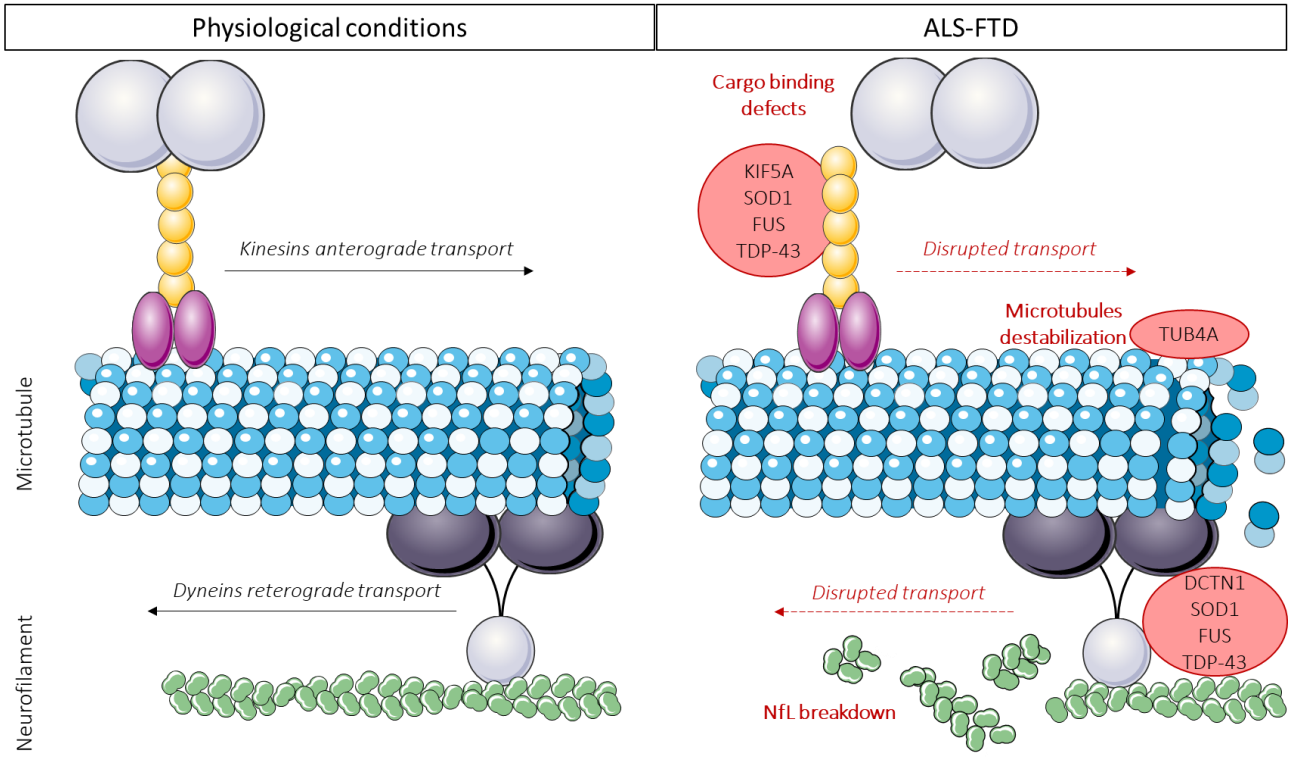

Figure 10: ALS-FTD alterations in axonal and cytoskeletal transport.
In physiological conditions (left panel) motor proteins kinesis and dyneins assure the proper transport of cargos along microtubules and/or neurofilaments within neurons. In ALS (right panel), mutations affect the binding cargo regions and the integrity of neurofilaments, resulting in general disruption of cargos transport.

f. Liquid phase separation and protein aggregation

Recent findings have shown that the cytoplasm is organised in membrane-less organelles formed by phase separation and are thought to be part of a cellular stress survival strategy (Alberti, 2017; Franzmann e Alberti, 2019). In normal physiological conditions, RBPs and mRNAs interact to form messenger ribonucleoprotein particles (mRNPs) (Singh *et al.*, 2015) and their fate will depend on their composition. RBPs contain a region in their structure known as low complexity domain (LCD), allowing their assembly into mRNPs (Murray *et al.*, 2017) and at inactive states, mRNPs assemble into larger membrane-less structures such as stress granules (Erickson e Lykke-Andersen, 2011). Novel studies have elucidated that RBPs LCD are intrinsically disordered, with prone self-aggregating properties to form liquid droplets and can enter into a liquid-liquid phase separation (LLPS) (Burke *et al.*, 2015; Molliex *et al.*, 2015; Patel *et al.*, 2015). RBPs are tightly linked to ALS and FTD pathogenesis characterized by the presence of aberrant proteinic inclusions (Neumann *et al.*, 2006; Neumann, Roeber*, et al.*, 2009) containing other RBPs or TIA1 granule stress marker (Dormann *et al.*, 2010). Mutations in TDP-43, FUS or hnRNAP1 have shown to interfere with the LCD, resulting in an accelerated phase transition from liquid to solid structures promoted by increased concentrations of mutated protein and highly resembling the pathological aggregates or inclusions observed in ALS-FTD (Murakami *et al.*, 2015; Patel *et al.*, 2015). In the specific case of FUS, Patel and collaborators showed *in vitro* how FUS separates into liquid droplets with the capacity of fusion, whereas mutant FUS formed aggregate-like structures (Patel *et al.*, 2015). Murakami and collaborators showed in *C. elegans in vivo* how FUS forms membrane-free liquid droplets with hydrogel properties, whereas mutant FUS whether carrying mutations in the LCD or not, resulted in neurotoxic fibrillar hydrogels that sequestered other RNPs (Murakami *et al.*, 2015). Fewer studies have been carried for TDP-43 but Conicella and collaborators observed that TDP-43 also undergoes phase separation into liquid droplets and its mutant forms enhance their conversion into aggregates over time (Conicella *et al.*, 2016). Similarly, studies on hnRNAP1 have observed the formation of liquid droplets in a concentration dependent manner, but the induction of aggregates with the mutation D262V (Molliex *et al.*, 2015). In physiological conditions, these liquid-phase transitions are reversible but in pathological conditions there seem to be alterations impeding this demixing. Hofweber and Dormann have recently reviewed how a series of post-translation modifications (PTM) can influence or reverse LLPS transition, more precisely *via* two typical PTMs namely methylation and phosphorylation (Hofweber *et al.*, 2018). Two studies have demonstrated that the arginine residue in RGG/RG is required for phase separation for FUS (Hofweber *et al.*, 2018; Qamar *et al.*, 2018). FUS methylation decreases its aggregating-prone properties with increased droplets dynamics (Hofweber *et al.*, 2018), whereas FUS hypomethylation results in increased number of droplets, decreased sphericity and decreased fusion properties (Qamar *et al.*, 2018). Hofweber and Dormann hypothesize that the loss of FUS arginine methylation leads to pathogenic states promoting LLPS and liquid to solid transitions resulting in the formation of aggregates. Besides they propose how the methylation of arginine could regulate RNP granules assembly by (1) altering protein-protein or protein-RNA interactions or (2) interfering with

nucleocytoplasmic transport of RBPs thus, altering their nuclear and cytoplasmic concentrations. Furthermore, Monahan and collaborators evaluated *in vitro* the effects of phosphorylation in the LLPS process and observed that FUS was phosphorylated at many Ser/Thr residues by DNA-dependent protein kinases, which interfered with phase separation of LCD and prevented liquid to solid phase formation (Monahan *et al.*, 2017). Wang and collaborators showed similar effects with the phosphorylation of TDP-43, reducing LLPS transition (Wang *et al.*, 2018). In all, data suggests that liquid-phase transition is perturbed in ALS-FTD which could originate the formation of aggregates and PTMs could be a potential target to avoid neuronal pathogenic depositions (Figure 11).

Many different mechanisms aforementioned could lead to the formation of aggregates. Disrupted protein homeostasis with impaired autophagy resulting in cytoplasmic accumulation of mutated proteins or debris could lead to the formation of aggregates. Nucleocytoplasmic transport defects resulting in the accumulation of toxic mutated proteins in the cytosol with prion-like aggregating properties such as TDP-43 or FUS. Cytoskeleton and axonal transport defects, resulting in abnormal cargos transport and cytoskeletal disruptions, which can lead to the formation of aggregates. Finally, the just mentioned liquid-phase transition where mutations in RBPs clearly show enhanced LLPS and liquid to solid phase transitions resulting in aggregates formation. Nevertheless, genetic mutations leading to protein variants with increased prone aggregating properties have also been identified as for microtubule-associated protein tau (MAPT) mutations (Combs e Gamblin, 2012) or C9ORF72 RNA foci and DPRs (Edbauer e Haass, 2016). Most MAPT mutations affect neurons microtubule-binding and stabilization properties and some increase tau aggregation properties (Combs e Gamblin, 2012). It is still not clear and of great controversy the protective or pathological role of aggregates (Ross e Poirier, 2005), since in some cases it is correlated with neurodegeneration as for tau (Van Swieten e Spillantini, 2007), whether in C9ORF72 aggregates can be found in brain regions where no degenerative processes occur (Mackenzie *et al.*, 2013). However, a very recent study by Gill and collaborators in a SOD1 mouse model indicates that aggregates would rather have neuroprotective effects by increasing mice lifespan (Gill *et al.*, 2019).

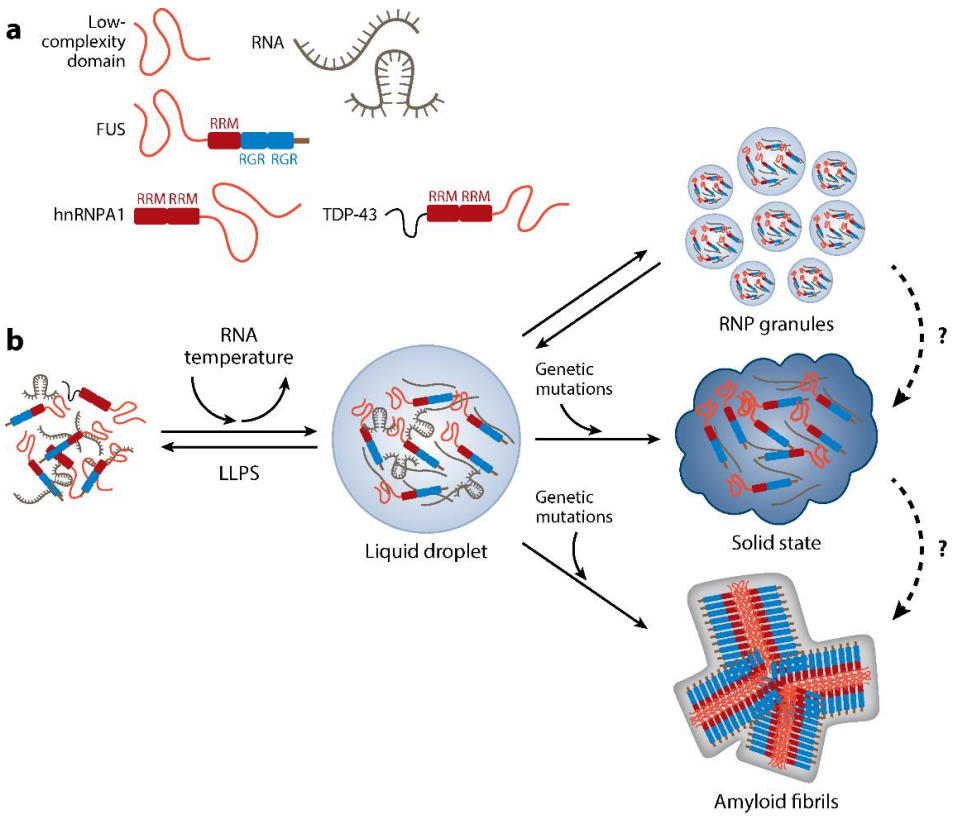

Figure 11: Formation of pathogenic liquid-phase RBP aggregates.
RBPs containing LCD include TDP-43, FUS and hnRNPA1, which together with RNAs form organelles *via* LLPS (a). The assembly of RBPs and mRNAs in droplet-like particles such as SGs undergo dynamic phase transitions with changes of RNA concentrations or temperature in a reversible fashion from liquid droplet to hydrogels. In pathological conditions liquid-to-solid phases become irreversible leading to more stable solid states resulting in the formation of aggregates. Image from Hofmann JW et al., 2019.

Part 2: FUS involvement in the ALS-FTD continuum

Fused in sarcoma (FUS) also known as Translocated liposarcoma (TLS) was first identified as an oncogene in myxoid liposarcomas (Rabbitts *et al.*, 1993). FUS is a protein member of the FET family, comprising FUS, EWSR1 and TAF15, which have similar structure and functions (Morohoshi *et al.*, 1998), and have been linked to neurodegenerative diseases such as ALS and FTD (Couthouis *et al.*, 2012). Mutations in the FUS gene were identified causing fALS and sALS cases containing FUS depositions (Vance *et al.*, 2009). Whereas FTD patients without carrying any FUS mutation where observed to have FUS brain inclusions (Munoz *et al.*, 2009; Neumann, Rademakers*, et al.*, 2009; Neumann, Roeber*, et al.*, 2009). Thus, defects in FUS seem to contribute to the ALS-FTD continuum but its specific role in both diseases needs further elucidation.

1. FUS PROPERTIES AND LOCALIZATION

a. Structure

FUS is a 526 amino acid multidomain protein composed by an N-terminal transcriptional activation domain, several nucleic acid binding domains and a C-terminal domain with a nuclear localisation signal (NLS). The N-terminal region contains a SYGQ-rich domain from amino acids 1 to 165, which is a transcriptional activation domain when it fuses with the DNA binding domain of other transcription factors (Prasad *et al.*, 1994) such as CHOP in liposarcomas (Rabbitts *et al.*, 1993). This region also has prion-like properties (Cushman *et al.*, 2010; King *et al.*, 2012) and has been shown to be required for FUS aggregation (Sun *et al.*, 2011). The nucleic acid binding domains are composed by three arginine-Glycine-Glycine (RGG1, 2 and 3) boxes crucial for protein-protein interactions (Doi *et al.*, 2010) and FUS DNA damage recruitment by RGG2 (Mastrocola *et al.*, 2013). This domain is also composed by a RNA recognition motif (RRM) from amino acids 285 to 371 a nuclear export signal (NES) and a Cys2-Cys2 zinc finger (ZnF) (Burd e Dreyfuss, 1994). Experimental evidence has shown that the RGG2-ZnF-RGG3 sequence is the major RNA binding domain and has preference for GGUG motifs (Lerga *et al.*, 2001; Bentmann *et al.*, 2012). Finally, the C-terminal region contains a non-classical NLS domain composed of proline-tyrosine NLS (PY-NLS) and the RGG3 domain (Dormann *et al.*, 2010; Dormann *et al.*, 2012). This region is recognized by TNPO1/Karyopherin-β2, responsible of transporting PY-NLS protein from the cytoplasm to the nucleus (Lee *et al.*, 2006). Moreover, FUS contains two prion-like domains from amino acids 1 to 239 and from 391 to 407 conferring the protein aggregating properties (Chen *et al.*, 2019) (Figure 12).

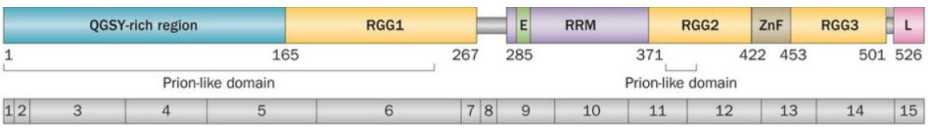

Figure 12: FUS structure and domains.
FUS is composed by a QGST-rich region, three RGG domains (RGG1, RGG2 and RGG3), a RRM containing a NES (E), a ZnF and a NLS (L) regions. Besides, FUS contains two prion-like domains and encodes for a 15 exons protein. Adapted from Deng et al., 2014.

b. *Nuclear transport*

FUS main localization is nuclear, however tiny amounts of protein are also found in the cytoplasm since FUS is implicated in the stabilization, transport and traduction of mRNAs. Thus, FUS localization is subjected to nuclear import and export mechanisms allowing the proteins shuttle between compartments and proper homeostatic levels. FUS contains a NES sequence for nuclear export and a NLS for nuclear import. FUS export is thought to occur in three different ways but further investigations are required for better comprehension of FUS export mechanism. First, exportins are known to bind to leucin-rich sequences at the NES domain. FUS contains a leucine-rich sequence at its NES domain in the RRM region, thus FUS export could be mediated by exportins (Lorenzo-Betancor *et al.*, 2014). Second, FUS plays a major role in mRNAs metabolism and could remain attached to them and their export complex during mRNAs nuclear export (Sugiura *et al.*, 2007). Third, FUS molecular mass is below the limit size of nuclear pore complexes passive diffusion, though FUS could shuttle to the cytoplasm simply by passive diffusion (Ederle e Dormann, 2017). FUS import mechanism is better understood and how alterations in ALS-FTD interfere with the protein relocalization to the nucleus. For instance, there is a correlation between the levels of nuclear import blockade and the disease onset and progression (Bosco e Landers, 2010; Dejesus-Hernandez *et al.*, 2010; Dormann *et al.*, 2010). *FUS*^{P525L} is a severe form of ALS-FUS and has been shown to present important levels of mutant protein import blockade (Dormann *et al.*, 2010). Several studies have shown that TNPO1/Kβ2 are responsible for nuclear import of FUS by binding the RGG3 domain, next to the NLS sequence (Bosco e Landers, 2010; Dormann *et al.*, 2010; Dormann *et al.*, 2012). However, it has been shown that cargo transport can be altered by PTMs such as arginine methylation (Bedford e Clarke, 2009). PRMT1 is a methyltransferase responsible for 90% of asymmetrical arginine dimethylation modifications (ADMA) (Tang *et al.*, 2000), and several studies have shown that FUS is asymmetrically demethylated at the RGG domains (Du *et al.*, 2011) by PRMT1, leading to FUS-ADMA species. Nevertheless, FUS-ADMA has been observed to alter FUS nucleocytoplasmic localization, leading to accumulated protein in the cytoplasm due to decreased binding affinity with TnPO1/Kβ2 as a result of its methylation interfering with its protein-protein binding properties (Dormann *et al.*, 2012; Tradewell *et al.*, 2012; Jäckel *et al.*, 2015; Suarez-Calvet *et al.*, 2016). Interestingly, Suárez-Calvet and collaborators observed differential FUS methylation in ALS-FUS and FTD-FUS inclusions from brain samples, where ALS-FUS inclusions contained exclusively FUS-ADMA forms, whereas FTD-FUS inclusions contained mono- or unmethylated forms of FUS (Suarez-Calvet *et al.*, 2016), suggesting differential pathogenic mechanisms for these two diseases.

c. *Autoregulation*

In 2012 Lagier-Tourenne and collaborators were the first to observe a potential autoregulatory capacity of FUS as it has been shown for other RBPs (Lagier-Tourenne *et al.*, 2012). They described how they detected a variant of FUS containing intron 7 but not intron 8 in mouse and human brain that seemed to be degraded by NMD. Furthermore, they showed that FUS specifically interacts at exon7-intron7 junction of its own pre-mRNA. Based on this evidence, Zhou and collaborators went one step further and elucidated FUS autoregulation

mechanism more in detail. FUS has the capacity to bind to the sequence intron6-exon7-intron7 of FUS pre-mRNA, which is a highly conserved region among species. The skipping of exon7 generates in an open reading frame shift where is introduced a premature codon stop in exon 8, which results in the degradation of the transcript by NMD. Besides, they showed that FUS acts as a repressor of its own exon7, where reduced levels of FUS protein results in less exon 7 repression (Zhou, Y. *et al.*, 2013). Thus, FUS is capable to autoregulate its own protein levels as it was shown in a mouse model where overexpression of human wild-type FUS led to decreased levels of endogenous FUS protein (Mitchell *et al.*, 2013). Furthermore, Zhou and collaborators studied the effects of FUS autoregulation when the protein was mutated with three different mutations, all of them affecting the NLS but with dose-dependent levels of accumulated mutated protein. They observed that the more FUS mutated protein was accumulated in the cytosol, the less FUS exon 7 was repressed resulting in a positive feedback for toxic protein accumulation (Figure 13). In fact, they observed wild-type FUS in cytoplasmic FUS inclusions, suggesting that mutant FUS is capable to sequester wild-type FUS, contributing to their formation. Nevertheless, other studies have shown that FUS autoregulation can be impaired by other ways and its impairment has major repercussions for cells homeostasis. Dini Modigliani and collaborators identified how mutations in the 3'-UTR of FUS (G48A) affect the binding site of FUS and repression to two miRNAs, miR-141 and miR-200a from whom FUS is involved in their biogenesis, but in turn impact FUS protein synthesis by increasing its mRNA and protein levels (Dini Modigliani *et al.*, 2014). Furthermore, a recent study links FUS mutations to disrupted protein homeostasis and RNA processing due to overexpression of FUS possibly resulting in a saturation of FUS autoregulatory mechanisms (Ling *et al.*, 2019). Therefore, FUS levels autoregulation of mRNA and protein are fundamental for proper cell homeostasis.

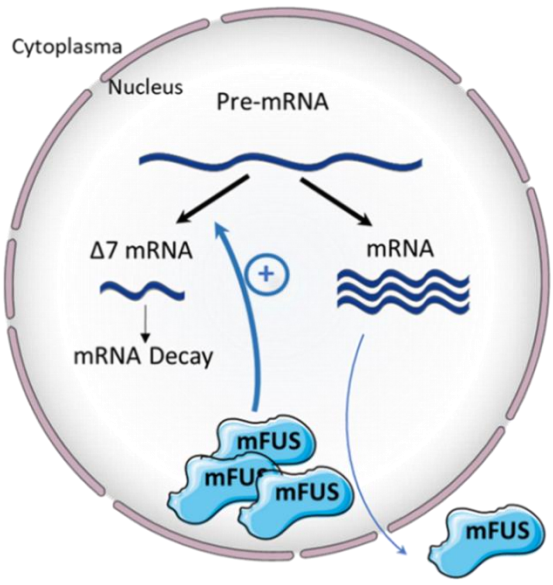

Figure 13: FUS autoregulation mechanism.
The autoregulation of FUS is controlled by the splicing of its own pre-mRNA into a variant skipping the exon 7, leading to mRNA NMD decay. Elevated nuclear protein levels activate this autoregulatory loop.

2. FUS FUNCTIONS

a. Nuclear FUS

i. DNA repair

DNA damage in neurons is usually due to reactive oxygen species leading to single strand breaks (SSB) or double strand breaks (DSB) (Madabhushi *et al.*, 2014). FUS plays a major role in DNA repair being recruited within seconds (Patel *et al.*, 2015) to DNA damage sites *via* its RGG2 domain and poly (ADP-ribose) polymerase (Rulten *et al.*, 2014). Once FUS binds to the damaged DNA, it participates in the formation of a D-loop stabilizing the genome (Baechtold *et al.*, 1999) and interacting with the enzyme histone deacetylase 1 (HDAC1) to repair the DNA (Wang *et al.*, 2013). Studies have shown that FUS can repair DSB *via* homologous recombination or non-homologous end joining. One of the earliest indicators of DNA DSB is the phosphorylation of H2AX by ATM into γH2AX, where γH2AX is thought to regulate the formation of DNA repair foci (Fillingham *et al.*, 2006). Interestingly, FUS is recruited to the damaged sites while γH2AX is still accumulating, proving the early implication of FUS in DNA repair (Wang *et al.*, 2013). Animal models with FUS defects (knock-out or mutated) have shown decreased interaction with HDAC1, decreased DSB repair and increased chromosome abnormalities with increased DNA damage (Hicks *et al.*, 2000; Mastrocola *et al.*, 2013; Wang *et al.*, 2013; Hill *et al.*, 2016). DNA damage has also been found increased in ALS carriers of FUS mutations or FTD patients where FUS is phosphorylated and mislocalized to the cytoplasm (Wang *et al.*, 2013; Deng *et al.*, 2014; Higelin *et al.*, 2016).

ii. Transcription

FUS participates in RNAs transcription in many different ways. Its SYGQ-rich domain at the N-terminal region, which is a LCD involved in FUS self-assembly, is responsible for FUS dimerization and binding to chromatin for its transcriptional regulation (Yang, L. *et al.*, 2014). FUS can furthermore bind to ssDNA elements in gene promotors and regulate their transcription (Tan *et al.*, 2012). Moreover, studies have shown that FUS can associate with transcription factor D II (TFIID) complex (Bertolotti *et al.*, 1996) or RNA polymerase II (RNA pol II) and regulate its phosphorylation during transcription (Schwartz *et al.*, 2012). Masuda and collaborators showed that FUS can also regulate the alternative polyadenylation (polyA) signals and depending on its position of binding in the nascent pre-mRNA it can have different effects. When FUS binds downstream an alternative polyA sequence, it recruits polyA factors to induce the polyA of alternative short transcripts, whether its binding upstream the polyA sequence results in downregulation of the RNA (Masuda *et al.*, 2015). Studies of FUS mutations linked to ALS-FTD have observed a decrease in FUS binding interactions with RNA pol II (Schwartz *et al.*, 2014) and active chromatin (Yang, L. *et al.*, 2014), resulting in deficient regulation of the transcription of FUS gene targets.

iii. Splicing

FUS has been described to bind to several hundreds of RNAs which expression results to be altered when FUS splicing activity is deficient (Hoell *et al.*, 2011; Lagier-Tourenne *et al.*, 2012; Ishigaki *et al.*, 2017). As previously mentioned, FUS has also been found to regulate its own mRNA with the exon 7 skipping variant resulting in NMD (Zhou, Y. *et al.*, 2013). FUS splicing activity is mediated by its interaction with many components of the spliceosome such as SMN protein, U1, U11 and U12 small ribonucleoproteins (snRNP) and Sm-snRNP complex (Yamazaki *et al.*, 2012; Gerbino *et al.*, 2013). It is though that FUS acts as a mediator between mRNAs transcription and splicing as it controls RNA pol II activity during transcription, but it also binds to nascent pre-mRNAs and mediates U1 splicing activity (Yu e Reed, 2015). Many of FUS targets are long introns in neuronal cells (Rogelj *et al.*, 2012), histones (Raczynska *et al.*, 2015) or *MAPT* exonic and intronic sites (Orozco *et al.*, 2012). Several studies carried on FUS splicing functions have observed splicing defects due to the loss of nuclear FUS splicing activity and regulation as it is the case for MAPT, where it leads to variants with exons 3 and 10 skipped promoting the 4 repeat variant expression linked with FTD (Hutton *et al.*, 1998). Besides, FUS splicing activity plays an important role in regulating miRNAs. FUS interacts with Drosha, a complex involved in early steps of miRNAs processing (Gregory *et al.*, 2004), by recruiting it to active transcription sites, which in turn facilitates miRNAs biogenesis (Morlando *et al.*, 2012). Some of FUS miRNAs' control of biogenesis contribute to regulate FUS levels in an autoregulatory loop manner (Dini Modigliani *et al.*, 2014). Mutations of FUS have shown to impact the expression of many miRNAs involved in neuronal functions and synaptogenesis (Hoell *et al.*, 2011). FUS role with long ncRNAs is less clear but two specific targets have been identified namely MALAT1 and NEAT1 both of them being transcriptional regulators for many genes (Lagier-Tourenne *et al.*, 2012).

b. Cytoplasmic FUS

i. mRNA stabilization

FUS mRNA stabilizing functions have been recently been investigated and it has been found that it controls the stability of many neuronal mRNA transcripts (Colombrita *et al.*, 2012). Udagawa and collaborators idientified one of FUS main mRNAs stabilizing activity with GluA1, which encodes for an AMPA receptor subunit and is importantly involved in the regulation of dendritic spines maturation and behaviour. The mechanism through which FUS stabilized GluA1 mRNA is by binding its 3'UTR site and recruiting a poly-specific ribonucleoprotein PAN2 to control and maintain the polyA tail in the cytoplasm (Udagawa *et al.*, 2015). Therefore, it could be possible to speculate that mutations in FUS could lead to defects in GluA1 mRNA stabilization, resulting in dendritic spines alterations and behaviour defects as it is observed in ALS-FTD.

ii. mRNA transport and traduction

mRNP particles containing FUS and mRNAs are transported from the soma to neurons dendrites and axon terminals where FUS regulates local translation of the corresponding mRNAs at the synapse (Belly *et al.*, 2005;

Fujii e Takumi, 2005). In *in vitro* studies FUS has been found to be relocated to dendrites and dendritic spines *via* mGluR5 activation, along with β-actin and NdL-1 mRNAs, the latest being an actin stabilizing protein. Thus, FUS could play a role in the transport of factors allowing spine remodelling (Fujii *et al.*, 2005). Furthermore, Zhang and collaborators showed that FUS is enriched at post-synaptic densities after neuronal stimulation, showing its transport at the synapses is of crucial importance for proper cellular responses (Zhang *et al.*, 2006). However, a recent study suggests that FUS could be transported by an alternative mechanism involving ER tubules and neurofilament cytoskeleton (Muresan e Ladescu Muresan, 2016). Regarding the role of FUS in mRNAs translation little is known, but Yasuda and collaborators observed in mouse fibroblasts that FUS is present in mRNP granules in cell protrusions, colocalizing with the APC protein of ribonucleoprotein complexes, promoting the translation of associated mRNAs (Yasuda *et al.*, 2013) (Figure 14).

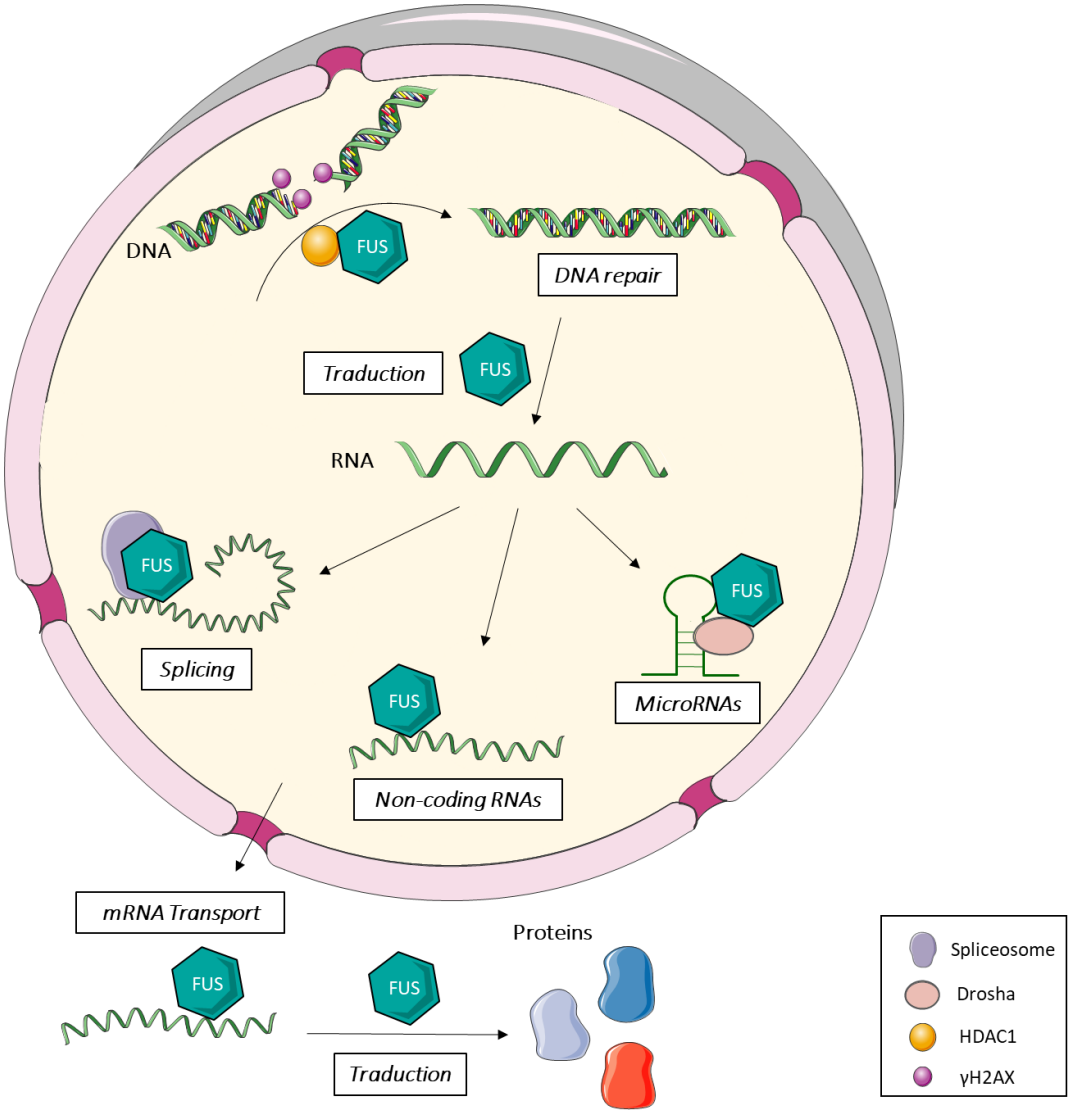

Figure 14: Nuclear and cytoplasmic functions of FUS.
FUS is involved in many physiological functions at the nucleus and the cytoplasm. At the nuclear level, FUS intervenes in DNA repair, mRNAs translation and splicing, ncRNAs splicing and miRNAs biogenesis. At the cytoplasmic level FUS plays important roles in the stabilization, transport and translation of mRNAs.

3. FUS PATHOPHYSIOLOGY

a. FUS mutations

The main histological hallmark in FUS disorders is the presence of FUS immunoreactive positive inclusions in the cytoplasm and less frequently in the nucleus, which have been found in both, ALS and FTD patients (Neumann, Roeber*, et al.*, 2009; Vance *et al.*, 2009). In 2009, mutations in the *FUS* gene were linked for the first time to ALS patients, presenting motor neurons loss and FUS positive cytoplasmic inclusions in motor neurons accompanied by dystrophic neurites (Kwiatkowski *et al.*, 2009; Vance *et al.*, 2009). About more than 60% of *FUS* mutation carriers present disease onset in their late teens or early 20's (Bäumer *et al.*, 2010; Huang *et al.*, 2010). However, very rare mutations in *FUS* linked to FTD cases have been found (Deng *et al.*, 2014). Since the identification of the first *FUS* mutations related to ALS, over more than 50 other mutations in *FUS* have been discovered. Most of them present an autosomal dominant inheritance and are missense mutations with few exceptions. FUS mutations have been found to be concentrated in two specific regions, with the majority of them affecting exons 12 to 15 (encoding ZnF, RGG2 and RGG3 regions) and other at a lesser frequency affecting exons 3 to 6 (encoding for QGSY-rich and RGG1 regions). Mutations located at the C-terminal part of FUS have been mainly found in fALS cases, whereas mutations in the N-terminal have been mostly found in sALS cases (Deng *et al.*, 2014) (Figure 15). Furthermore, among the different types of *FUS* mutations, studies have revealed that FUS positive inclusions composition might differ one to another, suggesting different underlying mechanisms for each variant. For instance, FUS pP521C inclusions have a prominent tangle-like shape and are found in neurons and oligodendrocytes; whereas FUS pP525L besides FUS positive inclusions, have round basophilic inclusions which are have also been detected in some FTD cases; and FUS pR521G, pR521H, pR524W or pG507N present neuronal and glial FUS positive inclusions without basophilic inclusions (Mackenzie, Munoz*, et al.*, 2011). More recently, FUS mutations have also been linked with other neurodegenerative diseases such as essential tremor (Rajput *et al.*, 2014) suggesting its implication in the regulation of motor pathways.

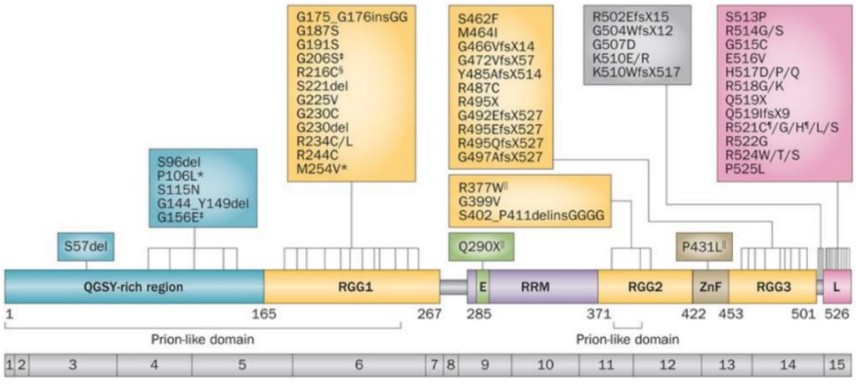

Figure 15: FUS genetic mutations.
Mutations of FUS are mainly localized at the C-terminal region of the protein, affecting the RGG3 and NLS domain ant at a lesser extent the QGSY-rich region and RGG1 domain. Image from Deng et al., 2014.

b. *Dendrite and synaptic defects*

The interest of the role of FUS in dendrites and at the axon synapses has increased over the last few years. It is well established that FUS is transported to dendrites *via* kinesins and dyneins motor proteins (Kanai *et al.*, 2004), and transports RNA granules (Fujii e Takumi, 2005). Several studies have shown that FUS travels along the axons in *in vivo* and *in vitro* models (Groen *et al.*, 2013; Machamer *et al.*, 2018) and mutations of FUS can impair axonal transport in motor neurons (Guo *et al.*, 2017). Besides, FUS can move to dendritic spines upon glutamate activation (Fujii *et al.*, 2005) *via* actin-based motor protein myosin-Va (Yoshimura *et al.*, 2006). Several studies with FUS mutations have shown defects in dendritic spines formation with defects in dendrites morphology, arborization and functions (Fujii *et al.*, 2005; Qiu *et al.*, 2014; Udagawa *et al.*, 2015; Shiihashi *et al.*, 2017) that could be restored by the reintroduction of crucial elements for dendrites homeostasis such as BDNF, Ndl-1, Gria1 or SynGAP α2 that closely interact with FUS functions (Fujii *et al.*, 2005; Qiu *et al.*, 2014; Udagawa *et al.*, 2015; Yokoi *et al.*, 2017). Schoen and collaborators showed by super-resolution microscopy that FUS localization is pre-synaptic at glutamatergic synapses, near Bassoon proteins and very close to synaptic vesicles. FUS was also found to colocalize with gephyrin, even though at a lesser extent, which could suggest that FUS plays also a role in inhibitory synapses (Schoen *et al.*, 2015). Nevertheless, Deshpande and collaborators recently observed that FUS localization seems to be preferentially at post-synapses in immature neurons within dendrites, whereas it is preferentially found at pre-synapses in mature neurons within axons. Furthermore, they observed in ALS patients derived motor neurons an increase in positive cluster of FUS in neurites, an accumulation of FUS at the synapses and increased Bassoon (pre-synaptic marker) and Homer1 (post-synaptic marker) proteins at motor neurons synapses. Overall their data suggest that FUS could interfere with local mRNA translation and sequester synaptic proteins into aggregates (Deshpande *et al.*, 2019). Other studies have corroborated that mutated FUS seems to sequester mRNAs and proteins, impeding proper proteins homeostasis at the synapses, where FUS is found to accumulate (Shiihashi *et al.*, 2017; Lopez-Erauskin *et al.*, 2018). Furthermore, there is increasing evidence that synaptic and dendrites deficits due to FUS mutations lead to FTD symptoms such as hyperactivity, disinhibition, impaired memory and social interactions deficits (Udagawa *et al.*, 2015; Lopez-Erauskin *et al.*, 2018). Further studies are needed to have a better comprehension of FUS role at the synapse and its pathological mechanisms.

c. *Stress granules*

Under stress conditions cells have developed protective mechanisms. Stress granules (SGs) are membrane-less organelles formed upon stress conditions such as oxidative stress. They are composed by mRNAs, polyA binding protein 1 (PABP-1), G3BP, TIA-1, translation initiation factors (eIF4α, eIF4GE, eIF4G), RBPs and small ribosomal subunits (Anderson e Kedersha, 2009). Besides, SGs participate in promoting cell survival by increasing the translation of mRNAs encoding for stress response factors such as heat shock proteins and, sequestering apoptotic signalling pathway components and silencing the transcription of housekeeping mRNAs (Kim *et al.*, 2005; Anderson e Kedersha, 2008; Arimoto *et al.*, 2008). SGs are dynamic structures that

can assemble because of increased concentrations of protein-protein or protein-RNA interactions (Tourrière *et al.*, 2003; Gilks *et al.*, 2004) and disassemble when cellular stress is overcome upon Hsp70 activity (Ganassi *et al.*, 2016). Cytoplasmic FUS has been observed to be recruited in SGs (Bosco e Landers, 2010; Dormann *et al.*, 2010; Bentmann *et al.*, 2012) and to colocalize with SG markers PABP-1 and eIF4G in FUS cytoplasmic inclusions of ALS and FTD patients (Bäumer *et al.*, 2010; Dormann *et al.*, 2010). Whether mutations of FUS leading to its cytoplasmic mislocalization and accumulation lead into SGs formation resulting in aggregates or SGs sequester mutant FUS as a cellular protective mechanism remains yet to be elucidated. Nevertheless, several studies have observed defective stress granules formation upon pathogenic cytoplasmic FUS mutants. FUS recruitment to SGs has been observed to be dependent of its RGG2-ZnF-RGG3 domain (Bentmann *et al.*, 2012), whereas the N-ter LCD mediates transition of LLPS processes that can occur during SGs formation (Burke *et al.*, 2015; Patel *et al.*, 2015), thus FUS mutations might result in impaired SGs formation and function. Models using the R521G mutation observed that cytoplasmic mutant FUS promoted the formation of SGs without observing further cellular damage (Bosco e Landers, 2010; Sun *et al.*, 2011). Other studies observed that mutant FUS delayed the formation of SGs, but once initiated they became bigger in size and number (Baron *et al.*, 2013). Ryu and collaborators showed in mouse cortical neurons that mutant FUS increases the concentration of FUS in SGs and impairs their clearance upon arsenite stress induction (Ryu *et al.*, 2014). Finally, mutant FUS degree of mislocalization would seem to correlate with its localization in SGs in a dose-dependent manner (Vance *et al.*, 2013; Ryu *et al.*, 2014; Lenzi *et al.*, 2015). Currently many authors hypothesise that the formation of SGs and their impairments due to FUS mutations could be the first step of FUS pathological inclusions embodiment (Dormann *et al.*, 2010; Dormann e Haass, 2011; Wolozin, 2012).

d. Aggregates

Neurodegenerative diseases generally share a common hallmark, the deposition of misfolded proteins forming aggregates. As previously described, FUS contains two prion-like domains in its structure that confers self-assembling properties to the protein (Gitler e Shorter, 2011). FUS proteins can assemble *via* their prion-like domain, forming amyloid-like fibrils and can reversely solubilize by regulation mechanisms such as FUS protein concentration, DNA or RNA levels and the phosphorylation of the GQSY-rich domain (Sun *et al.*, 2011; Han *et al.*, 2012; Kato *et al.*, 2012). Therefore, FUS undergoes LLPS processes at physiological concentrations (Burke *et al.*, 2015), where increased local concentrations of FUS spontaneously induce the formation of liquid droplets. This event has been observed in situations of DNA damage, where FUS is rapidly recruited at the damage site where its concentration increases forming liquid-droplets and potentially promoting DNA repair (Dutertre *et al.*, 2014). FUS can be found in three different forms, dispersed, liquid-droplets and hydrogels where the last two are closed compartments and it can dynamically switch from one form to another in a reversible manner (Patel *et al.*, 2015). Nevertheless, alterations in FUS concentrations with overexpressed levels of FUS have shown to induce transitions of FUS from liquid-droplets and hydrogels into aggregates (Patel

et al., 2015) or by increased FUS levels in SGs possibly also resulting in aggregates (Dormann e Haass, 2011). Mutations in the LCD/prion-like domain of FUS are thought to be the main cause of FUS aberrant self-aggregating properties resulting in the formation of irreversible amyloid-like aggregates. Studies have shown that mutations affecting the LCD domain result in the formation of less soluble and stable FUS hydrogels (Shang e Huang, 2016), whereas Murakami and collaborators showed that mutations in the prion-like domain result in a decrease in phase transition, where liquid to solid transition is accelerated and the repeat of gelation-degelation cycles result in irreversible hydrogels (Murakami *et al.*, 2015). However, a very recent study by Hofweber and collaborators elucidate the mechanisms regulating FUS phase separation (Hofweber *et al.*, 2018). First, the RGG3-PY domain can itself lead FUS to undergo phase transition from diffuse forms to droplet-like forms, more precisely, the arginines in this domain are responsible for FUS phase separation. Second, TnPO acts as a chaperone by regulating FUS cytoplasmic levels *via* nuclear import thus, preventing FUS from undergoing phase transition and its accumulation in SGs. Mechanistically TnPO blocks FUS phase transition by binding to the C-terminal RGG3-PY domain arginines, interfering with their phase transition inducing properties. Finally, they observed that arginines methylation of the C-terminal RGG3-PY domain reduced FUS LLPS and accumulation in SGs (Hofweber *et al.*, 2018), which correlates with the observations in FTD-FUS patients' inclusion where FUS is unmethylated (Dormann *et al.*, 2012; Suarez-Calvet *et al.*, 2016). Moreover, mutations in the C-terminal region alter the binding sensitivity of TnPO with FUS (Hofweber *et al.*, 2018) (Figure 16).

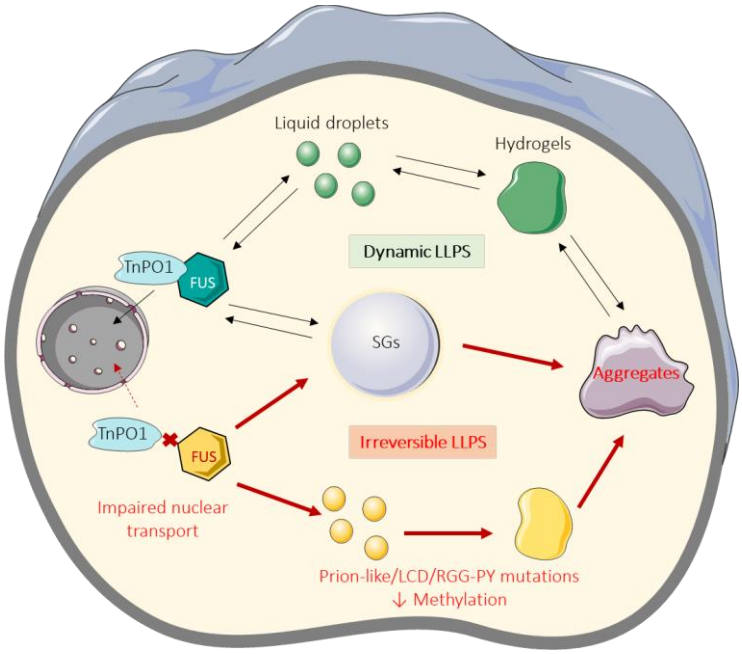

Figure 16: Pathogenic FUS LLPS transitions into aggregates.
FUS undergoes dynamic LLPS from soluble states to liquid-to-solid transitions and is regulated by its own levels and TnPO1 chaperone activity. ALS and FTD aggregates are issued from TnPO defective activity, mutations in several FUS domains or loss of arginines-methylation resulting in irreversible LLPS transitions. Adapted from Chen et al., 2019.

e. *Animal models*

The understanding of FUS physiological and pathological functions has been studied for the last 10 years in many different in vitro and in vivo models with invertebrate and vertebrate animals. Here we will only detail the advances in the field obtained with mouse models.

i. *Loss of function models*

Studies of *Fus* depletion in mouse models were carried before FUS mutations were linked with ALS, mainly because of its known oncogenic properties. Hicks and collaborators created a knockout ($Fus^{-/-}$) mouse model disrupting the protein at the exon 12. The first observation they made was that $Fus^{-/-}$ died few hours after birth. Phenotypically they were smaller but present a normal overall development. However, the size of the thymus was decreased, and they presented lymphopenia and chromosomal abnormalities (Hicks *et al.*, 2000). The same year, Kuroda and collaborators developed another $Fus^{-/-}$ mouse model, this time disrupting the protein at the exon 8. Similarly, they observed decreased size and weight but an overall normal development. They particularly focused on the reproductive capacities of these mice and found that males were sterile, whereas females had decreased fertility. Furthermore, males presented decreased reproductive organs size and genetic abnormalities such as defective homologous recombination in sperm cells and enhanced radiation sensitivity (Kuroda *et al.*, 2000). These two studies presented evidence of DNA damage in the absence of *Fus*. It is unknown whether these two models could still present residual, truncated FUS protein.

In 2015, Kino and collaborators aimed to study Hicks $Fus^{-/-}$ mouse model at later stages in life. For that they bred these mice with a mixed background, indicating that $Fus^{-/-}$ perinatal lethality is dependent on the genetic background. In this study they found that mice had smaller size but not ALS-like phenotypes. Mice had no motor deficits, nor ChAT+ spinal cord neurons degeneration, nor muscle atrophy, nor tremor-like phenotypes. However, they presented abnormal behaviours such as hyperactivity measured by home cage and open field tests and decreased anxiety evaluated by elevated-plus maze and light/dark box. Histologically they presented hippocampal vacuolations, accompanied by alterations in gene expression profiles such as upregulated *Taf15* or *Hnrnpa1* (Kino *et al.*, 2015). Kino and collaborators showed evidence that $Fus^{-/-}$ leads to FTD-like behaviour deficits. More recently, two studies silencing *Fus in vivo* by injecting shRNA-expressing AAVs have further investigated the effects of $Fus^{-/-}$ in the hippocampus. Udagawa and collaborators observed similar behaviour deficits observed by Kino and collaborators, where mice showed deficits in social behaviour interactions in the resident-intruder test, novelty-induced hyperactivity in the open-field and novel object recognition tests, decreased anxiety in the elevated-plus maze, but no alterations in learning or memory. These behavioural phenotypes were partially rescued by the administration of GluA1 mRNA, thus proving that $Fus^{-/-}$ has an impact on its RNA targets, resulting in disinhibition as it is observed in FTD patients (Udagawa *et al.*, 2015). Similarly, Ishigaki and collaborators silenced *Fus* in the hippocampus and recapitulated the same behaviour deficits. Nevertheless, they also observed an atrophy of the hippocampus, accompanied by cellular loss of 3R-Tau

positive cells, considered to participate in neurogenesis, as well as altered ratios of 4R/3R-Tau protein and phosphorylated-Tau inclusions (Ishigaki *et al.*, 2017). Overall, these data suggest that *Fus*$^{-/-}$ mice models can recapitulate DNA damage, FTD-like behaviour deficits and tau alterations which are proof-of-concept of the crucial roles of FUS in DNA repair and RNAs metabolism as it controls GluA1 mRNA stabilization (Udagawa *et al.*, 2015) and tau splicing (Orozco *et al.*, 2012; Ishigaki *et al.*, 2017). However, loss of nuclear FUS does not seem to have direct implications in ALS-like phenotypes as several studies showed that *Fus*$^{-/-}$ did not present spinal motor neurons loss (Kino *et al.*, 2015; Scekic-Zahirovic *et al.*, 2016).

ii. Gain of function models

Most mutations in FUS affect the C-terminal part where the NLS is located, resulting in a mislocalization of FUS in the cytoplasm. Thus, the idea that cytoplasmic FUS might acquire toxic functions became quickly appealing and several studies were carried to clarify FUS cytoplasmic pathogenic functions. Verbeeck and collaborators approached this question by overexpressing 3 different forms of FUS with somatic brain transgenesis or recombinant AAVs in neurons. They used human wild-type FUS, FUS^{R521C} and FUS$^{\Delta 14}$, where humans' carriers of FUS^{R521C} mutations have disease onset at 40 years old and FUS$^{\Delta 14}$ around 20 years old. Mice did not present any motor behaviour deficit signs nor neuronal loss or glial activation. However, FUS^{R521C} and FUS$^{\Delta 14}$ mice presented cellular alterations linked to the degree of FUS cytoplasmic mislocalization. FUS^{R521C} mice presented increased levels of cytoplasmic FUS in soma, dendrites and axons mainly in hippocampus neurons, but without the presence of inclusions or aggregates. Whereas FUS$^{\Delta 14}$ mice, presenting a more aggressive mutation presented higher FUS cytoplasmic levels and cytoplasmic inclusions that were found to be basophilic, ubiquitin, PABP-1 and P62 positive. Moreover, nucleocytoplasmic fractionation showed increased FUS cytoplasmic levels in a dose-dependent manner according to the severity of the mutation (Verbeeck *et al.*, 2012). Therefore, mutated FUS in the cytoplasm induces the formation of inclusions containing pathological hallmarks observed in ALS-FTD patients.

Mitchell and collaborators created a mouse model overexpressing wild-type human FUS under control of the mouse prion protein promoter and focused in the characterization of homozygous mice phenotype expressing 1.7-fold increase of total FUS versus their wild-type littermates. Homozygous mice developed motor symptoms such as hindlimb paralysis and impaired gait at early ages that worsened in an age-dependent fashion as well as the inability of weight gain. Histological analysis of homozygous mice revealed FUS positive inclusions in layer V of neurons in motor and somatosensory cortices along with other brain structures involved in ALS-FTD pathology in humans. Similarly to Verbeeck and collaborators, immunohistochemistry techniques revealed increased cytoplasmic staining without nuclear FUS signal decrease, whereas nucleocytoplasmic fractionation showed increased nuclear levels of FUS and even higher levels in cytoplasm showing that FUS localization depends on its level of expression. Cortical FUS inclusions were ubiquitin positive with a ring-like shape, which was not always the case in spinal cord inclusions. Finally, homozygous mice

presented significant loss of spinal cord motor neurons compared to their wild-type and heterozygous littermates, the latter showing a decrease but not significant, increased glial cells activation and decreased neuromuscular functions with loss of fast twitching fibers and motor units (Mitchell *et al.*, 2013). Therefore, these two studies showed that FUS mislocalization to the cytoplasm not only induces the formation of inclusions in a dose-dependent manner, but also impacts motor neurons survival and motor function as it is observed in ALS patients.

In 2014, Qiu and collaborators studied another mouse model overexpressing the mutation FUS^{R521C} under control of the mouse prion promoter, replicating motor behaviour deficits as impaired gait, decreased muscular mass and decrease motor coordination. Nevertheless, they observed that mutant FUS^{R521C} can form complexes with endogenous wild-type FUS, thus altering its distribution at nerve terminals of spinal cord axons, astrocytes and oligodendrocytes. Moreover, FUS^{R521C} shows less interaction with HDAC1 and seems likewise to interfere in the interaction of HDAC1 with wild-type FUS. Interestingly, increased levels of DNA damage markers such as γH2AX and ATF3 are also found, particularly in spinal cord motor neurons. Quantifications in the number of spinal motor neurons in these animals revealed a significant loss, neuromuscular denervation and active glial cells, suggesting FUS cytoplasmic intrinsic toxicity. Furthermore, they observed defects in dendrites branching in spinal motor neurons as well as in pyramidal neurons in layers IV-V of the cortex, with decreased synaptic densities, preceding motor neurons loss and potentially contributing to their degeneration. Dendritic defects were partially explained by mutated FUS^{R521C} interfering with *Bdnf* DNA damage markers and splicing defects of its mRNA at the 5' exon, where FUS^{R521C} was found to form complexes with *Bdnf* RNA resulting in decreased levels of BDNF protein, crucial for the proper dendritic growth and synapse formation. Besides, they observed decreased activation of its receptor TrkB in brain and spinal cord that worsened in an age-dependent manner without altering the receptor protein levels. Importantly, the TrkB-BDNF pathway plays a major role in synaptic plasticity. Finally, *via* RNA-seq analysis they confirmed that FUS^{R521C} alters the expression of splicing products and synaptic functions (Qiu *et al.*, 2014). The evaluation of behavioural deficits in this mouse model would have been of great interest as per their dendritic and synaptic deficits in order to evaluate the implications FUS gain of function in FTD-like behaviours. In all, data obtained from overexpressing FUS in mouse models has allowed to observe pathological functions of cytoplasmic FUS such as the formation of cytoplasmic inclusions, deregulation of synaptic functions and development of motor deficits, all of them recapitulated in human ALS-FTD pathology.

iii. Loss vs. Gain of function models

Studies of loss or gain of FUS functions alone have elucidated some of the pathological mechanisms in ALS-FTD, but it is necessary to consider simultaneously the effects of the nuclear loss of functions and the cytoplasmic gain of functions of FUS in animal models, therefore resulting in the generation of mouse models considering loss *vs* gain of function.

Robinson and collaborators generated a mouse model containing a cDNA encoding for human FUS without the RRM domain ($FUS^{\Delta RRM}$) under the control of the Thy1 neuronal promoter. These mice presented reduced weight and early lethality around 20 days of age with the development of tremor signs few days prior death. Biochemical and histological analysis revealed an increase in brain and spinal cord of total FUS RNA expression. Further brain analyses showed an increase in mutant FUS and wild-type FUS protein redistribution in the cytoplasm of cortical neurons with inclusions positive for $FUS^{\Delta RRM}$, the stress granule marker TIAR and in some cases ubiquitin accumulation. However, these mice did not display motor neuron loss nor gliosis in the brain (Robinson *et al.*, 2015). Later, Sharma and collaborators created a conditional mouse lines expressing wild-type human FUS ($hFUS^{WT}$) and human FUS mutations R521C ($hFUS^{R521C}$) related to adult-onset or P525L ($hFUS^{P525L}$) related to juvenile-onset ALS, all of them in the *MAPT* locus, inducible with Cre-recombination activity. FUS expression levels were 4 times higher in mice containing mutated forms of FUS compared to $hFUS^{WT}$, due to an increase of mutated protein translation. Spinal cord motor neurons of wild-type FUS and $hFUS^{WT}$ mice models showed FUS localization mainly nuclear, whereas mutated FUS mice presented mislocalized mutant FUS protein in cytoplasm, dendrites and sciatic nerve, with $hFUS^{P525L}$ presenting the most severe phenotype. Nevertheless, both mice with both mutant forms maintained endogenous FUS in the nucleus, thus no endogenous FUS redistribution resulting from the presence of mutated FUS. In $hFUS^{R521C}$ and $hFUS^{P525L}$ spinal motor neurons loss was found at later ages accompanied by astrocytosis, microgliosis and muscle weakness in a dose and age-dependent manner. Muscle denervation was found to affect first muscles innervated by FF with reduced fiber diameter before motor neurons loss, accompanied by NMJ dysfunctions. They examined whether motor neurons degeneration was triggered by the mutation in a cell-autonomous manner by Cre-recombinase where $hFUS^{WT}$, $hFUS^{R521C}$ and $hFUS^{P525L}$ were only expressed in motor neurons. They recapitulated the exact same phenotypes as previously described and tested then if motor neurons degeneration was due to the loss of nuclear FUS functions or a toxic gain of cytoplasmic FUS. For that they used a conditional knock-out by tamoxifen induction, suppressing FUS in a general manner in the CNS and they found no motor neurons degeneration, thus due to a toxic gain of function of cytoplasmic FUS (Sharma *et al.*, 2016). Similarly, Scekic-Zahirovic and collaborators corroborated this statement with another mouse model, where besides they elucidated RNA alterations linked to loss or gain of function of FUS. To do so, they generated a complete knock-out $Fus^{-/-}$ mouse model, with the insertion of a trap cassette in intron 1, and a conditional knock-in by homologous recombination, inserting floxed cDNA of exons 13, 14 followed by 3 stop cassettes in intron 12 resulting in a protein lacking of NLS ($Fus^{\Delta NLS}$) with Cre-recombination activity. At birth, $Fus^{-/-}$ and homozygous $Fus^{\Delta NLS}$ ($Fus^{\Delta NLS/\Delta NLS}$) mice presented reduced size and body weight and died within few hours from respiratory deficits visible by uninflated lungs. Furthermore, $Fus^{-/-}$ were completely depleted of FUS and $FUS^{\Delta NLS/\Delta NLS}$ had total mislocalization of FUS from the nucleus to the cytoplasm. Changes in RNA expression were found in $Fus^{-/-}$ and $Fus^{\Delta NLS/\Delta NLS}$ brains with predominantly downregulation of genes and an

important overlap between both genotypes suggesting alterations in FUS target RNA expression genes due to the loss of function affecting synaptogenesis components (downregulated) and long or short isoforms of splicing including *Mapt* (increased 4R-Tau), *Atxn2* and *Sort1*. However, $Fus^{\Delta NLS/\Delta NLS}$ mice presented a unique pattern of altered transcripts. Histologically, motor neuron loss was only found in $Fus^{\Delta NLS/\Delta NLS}$ mice, accompanied by depletion of SMN1 nuclear gems, condensation of HDAC1 in nuclear foci, absence of aggregates and increased eIF2α phosphorylation, representing partially human ALS hallmarks. Reverting the mutation by Cre-recombination in ChAT+ neurons did not rescue lethality, but restored FUS mislocalization to the nucleus and rescued motor neurons loss (Scekic-Zahirovic *et al.*, 2016). Thus, mutant cytoplasmic FUS is sufficient to trigger motor neurons degeneration by acquiring toxic gain of functions. Following this study, Scekic-Zahirovic and collaborators focused in studying an intermediate model from their $Fus^{\Delta NLS}$ mice model, resembling more to human ALS pathology where mutations are only expressed in heterozygosis. Therefore, they characterized a $Fus^{\Delta NLS/+}$ mouse model which presented increased levels of FUS mRNA in the spinal cord, spinal cord motor neurons with increased cytoplasmic FUS but unchanged nuclear levels, absence of aggregates, but increased methylation (ADMA) in both nuclear and cytoplasmic compartments, p62 and ubiquitin accumulations. Besides, mice developed at advanced ages mild motor deficits with EMG alterations and spinal motor neurons degeneration. To understand if FUS loss of function was responsible for motor neurons degeneration, they parallelly studied a heterozygous mouse of wild-type FUS ($Fus^{+/-}$), which revealed decreased transcripts and protein levels in spinal cord, but no motor phenotype, EMG alterations not motor neuron loss, proving that loss of function is no sufficient to trigger motor neurons death. As they did with their previous study, they reverted *Fus* mutation in ChAT+ neurons by Cre-recombination and observed a partial rescue of mutant cytoplasmic FUS, decreased ADMA levels, rescue of motor neurons degeneration, no EMG alterations and a delay in motor deficits. Interestingly, RNA seq analysis of $Fus^{\Delta NLS/+}$ mice revealed alterations in myelin components, confirmed by histology where they observed cytoplasmic staining of FUS in oligodendrocytes and increased number of oligodendrocytes accompanied by reduced ventral roots and axons calibers with abnormal myelination that could not be rescued by Cre-recombinase activity (Scekic-Zahirovic *et al.*, 2017). The same year, Devoy and collaborators inserted a human frameshift mutation in the murine Fus gene causing skipping of the exon 14 resulting in the loss of the NLS. Even though mice expressed endogenous levels of mutant protein, they developed motor deficits and gait impairment, reduced lifespan at advanced ages (19 months), reduced motor units and defective NMJ innervation and loss of spinal motor neurons in an age-dependent manner. Endogenous nuclear levels of FUS were reduced, whereas mutant FUS was mainly localized in the cytoplasm, where it was found to be recruited in SGs. Moreover, RNAseq analysis revealed RNA expression dysregulations, predominantly genes downregulated and detected alterations of mitochondria and ribosomal components (Devoy *et al.*, 2017). Recently, Ling and collaborators have studied the influence of wild-type FUS overexpression in the loss or gain of FUS functions. They generated transgenic

mice lines expressing hFUS^{WT}, hFUS^{R514G} or hFUS^{R521C} under the mouse prion promoter, flanked by loxP sites for Cre-recombination activity. The first observation they made was that exogenous FUS levels were increased, whereas endogenous FUS levels were decreased, possibly due to FUS autoregulation mechanisms. All transgenic mice displayed abnormal posture, motor deficits, EMG alterations with motor unit loss and loss of large axon caliber, the latest only in hFUS^{WT} and hFUS^{R514G} mice. Therefore, they investigated whether increased levels of FUS could result in ALS-like pathology by producing a mouse homozygous for hFUS^{WT}. Interestingly, solely the overexpression of wild-type FUS reproduced all symptoms at earlier ages accompanied by astrogliosis and microgliosis processes, showing how variations in endogenous FUS levels can induce motor neurons disease. The analysis of the RNA expression of homozygous hFUS^{WT} mice revealed alterations in the immune system (upregulated) and metabolic components of KEEG and MAPK pathways (downregulated), as well as alterations of long introns of *neuronal intermediate filaments* and *Chat* at late stages of the disease. To understand whether RNA expression changes observed were due to a loss or gain of function, they compared the RNAseq data obtained with the one of knock down FUS mice done by Lagier-Tourenne and collaborators in 2012, and concluded that lower motor neurons degenerate in a dose dependent manner according to FUS wild-type levels *via* gain of toxic functions. Moreover, they used Hicks and collaborators mouse model and inserted the hFUS^{WT}, where they rescued lethality and partially restored RNA deficits proving thus that the regulation of FUS levels are crucial for proper functions in the CNS. Finally, homozygous hFUS^{WT} presented accumulation of p62 in motor neurons, indicative of defective autophagy processes, which was also present in hFUS^{R514G} and hFUS^{R521C} mice presenting increased p62 accumulation and decreased autophagy (Ling *et al.*, 2019).

So far, the described mice models have allowed to recapitulate many aspects of ALS-FUS in patients and have provided a better understanding of the biochemical and histological consequences of nuclear loss or cytoplasmic gain of FUS functions. However, they have not recapitulated FTD-FUS symptoms whether because the models did not present such phenotypes, whether because the studies did not focus on these characteristics. Nevertheless, recent studies have started to elucidate the link between FUS mutations and the development of FTD symptoms in ALS-FTD mice models. In 2016, Shiihashi and collaborators generated a FUS mouse model where they overexpressed exogenous FUS lacking the NLS (Fus$^{\Delta NLS}$) under Thy1 promoter where they could observe the development of typical ALS-like symptoms such as motor deficits, FUS inclusions in motor cortex and the pyramidal tract that were ubiquitin and G3BP positive, also containing endogenous wild-type Fus. Astrogliosis and microgliosis processes were present and gene expression profile was altered, particularly components of the endoplasmic reticulum (Shiihashi *et al.*, 2016). The year after, Shiihashi and collaborators published further studies carried on this same mouse model, this time enlightening symptoms related to FTD. Fus$^{\Delta NLS}$ mice expressed the mutated protein in brain regions that have been seen to be affected in FTD patients such as the frontal cortex, hippocampus and enthorinal cortex, where FUS localization was

mainly cytoplasmic. These mice exhibited behavioural symptoms before motor symptoms onset described in Shiihashi 2016, which hyperactivity related to novel environments examined by home cage and open field tests, impaired social memory at the three chambers test and impaired memory retrieval assessed by the fear-conditioning test. These behaviour deficits correlated with defects in dendrites and synapses in frontal cortex and hippocampus, where decreased dendritic spines and synapses densities were found reduced. Furthermore, electrophysiological defects were detected with decreased excitatory inputs accompanied by decreased mRNA levels of NMDA, AMPA and kainite receptors and subunits encoding for these receptors, all involved in the glutamatergic transmission. The presence of FUS aggregates was observed in frontal cortex and hippocampus, where mRNAs and RNA transporters were found to be sequestered and the transport of dendritic mRNAs transport was disrupted. Finally, they observed reduced proteins synthesis in dendrites in vitro (Shiihashi *et al.*, 2017). Lopez-Erauskin and collaborators recently published the effects of FUS mutations in a novel ALS-FTD mouse model by introducing floxed human transgenes of FUS^{WT}, FUS^{R521C}, FUS^{R521H} in different mouse lines. FUS^{R521C} and FUS^{R521H} mice showed motor deficits accompanied by loss of muscle innervation, α motor axons and motor neurons degeneration in an age-dependent manner with the presence of astrogliosis and microgliosis. However, no DNA damage nor aggregates were observed. They presented cognitive and behaviour deficits in an age-dependent manner with deficits in novel object recognition, spatial memory, sociability and anxiety. Hippocampal synapses loss was observed without neuronal degeneration in an age and mutant dependent fashion with synaptic dysfunctions. Mice depleted of endogenous *Fus* and expressing only FUS^{WT}, FUS^{R521C} or FUS^{R521H} were studied to evaluate the loss vs gain of functions of FUS, where lethality in homozygous was rescued and only mutant FUS genotypes exhibited progressive motor deficits with spinal motor neurons loss. Genes expression and splicing deficits were not caused by loss of nuclear functions and RNA expression alterations showed defects in proteins translation mediated by eIF2α, which were confirmed by *in vitro* and *in vivo* studies where proteins synthesis was found to be decreased in axons (Lopez-Erauskin *et al.*, 2018). Overall, these mouse models have brought proof-of-concept that mutations of FUS contribute to the ALS-FTD pathogenesis, recapitulating at the same time ALS as much as FTD symptoms, thus providing better and more accurate mouse models to further understand and elucidate the underlying pathophysiological mechanisms.

Objectives and summary of results

ALS and FTD are two distinctive neurodegenerative diseases characterized by their specific hallmarks, although they share genetic mutations and histopathological features implementing the concept of ALS-FTD continuum. Despite the advances in clinics and research, a major lack of understanding of the aetiology and mechanisms of the disease persist and difficult the achievement of better diagnostic tools and the development of more accurate treatments. This is partly due to the expanding genetic mutations discovered causing ALS and FTD in an increasing number of genes and their variants, which account for a minority of cases of familial inheritance whereas the majority of cases are sporadic. Furthermore, the wide physiopathology of the disease having an impact in different cellular types, from motor neurons to glial cells among others, and different physiological functions affected such as motor functions, metabolism or psychological functions make this disease even more puzzling to understand and to elucidate the connections between these alterations.

In our laboratory we have tried to elucidate the pathophysiological mechanisms involved in FUS mutations resulting in the protein mislocalization by the loss of the NLS in a knock-in mouse model (Scekic-Zahirovic *et al.*, 2016; Scekic-Zahirovic *et al.*, 2017), Picchiarelli 2019 in press). This mouse model recapitulates many pathological hallmarks observed in FUS-ALS patients. Moreover, these mice develop a FUS cytoplasmic mislocalization, an event also found in a subset of FTD cases, raising the possibility that these mice could help us in the understanding of FUS-FTD.

The objectives of my thesis have been to further characterize the heterozygous *Fus*$^{\Delta NLS}$ mouse model generated in our laboratory. Firstly, we aimed to understand the role of the loss of nuclear FUS function in the pathology of these mice via a rescue with a human wild-type *FUS* gene. Secondly, we sought to characterize whether these mice could be used as a FUS-FTD model. These two objectives led to three major results, that are presented in the results section as manuscripts in preparation.

In the first study, hereafter presented as a paper in preparation, we describe the effects of the insertion of a wild-type human *FUS* transgene in knock-in mice. The rationale behind this experiment was to rescue the loss of nuclear FUS function by reintroducing a wild type FUS protein The first observation we made is that the transgene is capable of rescuing the lethality of the mutation when expressed in homozygosis as it was described in Scekic-Zahirovic and collaborators (Scekic-Zahirovic *et al.*, 2016). Moreover, motor deficits are as well rescued restoring muscular force at wild-type littermates levels in heterozygous and homozygous mice carrying the human transgene. However, to our surprise, the transgene did not only lead to rescue of nuclear loss of function, but was able also, surprisingly to decrease the levels of cytoplasmic FUS, suggesting that it exerted indirect effects on mutant allele(s). Since FUS is known to be suject to a strong autoregulation, we

hypothesised that the observed beneficial effects could be due to the activation of this pathway by the human transgene. Indeed, we have demonstrated by biochemical and histological methods that the human transgene activates the alternative pathway of splicing skipping the exon 7, diminishing the mRNA and toxic protein levels. Furthermore, the pathological rise in FUS methylation is also reversed by the human wild-type *FUS*. Therefore, we demonstrate that motor function deficits and molecular and histological hallmarks in our *Fus*$^{\Delta NLS}$ mouse model can be rescued by the activation of FUS autoregulatory mechanisms *via* the insertion of a human wild-type *FUS* transgene. In all, while this experiment was initially designed to answer whether loss of nuclear FUS function was necessary to the toxicity of the mutation, it yielded the unexpected outcome of a potential therapeutic strategy, without answering the initial question. These results will be submitted to publication in the next months after combination with similar results obtained in parallel by colleagues in San Diego (USA).

A second objective of my thesis was to investigate whether our *Fus* knock-in mice could be considered as a model of FTD-FUS. Indeed, the FUS protein is also found accumulating in cytoplasmic aggregates in FTD FUS patients, but this occurs in the absence of germline *FUS* mutations, and several other proteins are found in these aggregates raising the question of their respective contributions to the clinical picture. Our mouse model, by isolating cytoplasmic FUS mislocalization, allows to determine whether this single event is sufficient to trigger the FTD disease. When I arrived in the laboratory, Jelena Scekic-Zahirovic had shown that *Fus* knock-in mice developed at 10-12 months of age a number of phenotypes. I performed earlier behavioural time points, histological analysis, electron microscopy and validated RNAseq results, justifying my co-first authorship of this study. Altogether, our results show that heterozygous *Fus* knock-in mice recapitulate many behavioural and cognitive deficits such as hyperactivity, disinhibition and memory deficits of FTD patients. In collaboration with Dr Liebscher, we were able to show that mice show electrophysiological alterations in cortical pyramidal neurons. However, no neuronal degeneration was detected. We further investigated potential RNA expression alterations and mainly found deficits in inhibitory synaptic components which were confirmed with structural abnormalities of cortical inhibitory synapses by TEM. In all, we show that FUS mislocalization in sufficient to induce cortical synaptic defects that could lead to FTD-like symptoms in our mouse model. These results will be complemented by several experiments ongoing and will be submitted in a collaborative manuscript on which I will be shared first author.

Finally, our previous studies showed the relevance of the expression of the mutation in cholinergic motor neurons for the development of motor symptoms (Scekic-Zahirovic *et al.*, 2017). Therefore, we questioned the potential implications of the central nervous cholinergic system in the frame of FTD, considering the importance of acetylcholine in other dementias such as Alzheimer's or Parkinson's disease. We found that our Fus$^{\Delta NLS}$ mice present a general degeneration of the central nervous cholinergic system with the loss of cholinergic neurons at the nucleus Basalis of Meynert (NbM), which also degenerate in Alzheimer's disease,

accompanied by a loss of ascending projections to the cortex. Specific Cre-recombination in cholinergic neurons allowed us to show a partial rescue of behavioural deficits, thus providing evidence that FUS mutation generally affects the central and peripheral nervous system and is partially responsible for behavioural deficits. Therefore, this study has allowed to elucidate the implications of the cholinergic system in our ALS-FTD mouse model, enlightening potential novel therapeutic strategies. We consider this last part of the thesis as more preliminary, and several experiments, in particular pharmacological, are currently being run to be able to interpret those results and submit a third publication.

Results of all three studies will be discussed at the same time in the last part of this manuscript as a global discussion.

Results

1. PART 1: PHENOTYPIC RESCUE OF A MOUSE MODEL OF FUS-ALS BY ADDITION OF AN AUTOREGULATORY COMPETENT WILD TYPE FUS TRANSGENE.

Résumé

Les études précédentes du laboratoire ont démontré que la perte de fonction de *Fus* n'est pas suffisante pour provoquer la mort du motoneurone. En effet, les souris *Fus*$^{-/-}$ ne présentent pas de perte de motoneurones. L'expression de la protéine mutée, dans notre cas, la protéine FUS$^{\Delta NLS}$ est indispensable au déclenchement de la mort du motoneurone (Scekic-Zahirovic, EMBO J2016, Acta 2017), ce qui démontre la nécessité du gain de fonction lié à la présence de la protéine mutée dans le cytoplasme, pour provoquer la maladie. Cependant, nos études ne permettaient pas de conclure quant à la nécessité de la perte de fonction. En effet, il est parfaitement envisageable, dans nos modèles, que ce soit l'action conjointe de la perte de fonction nucléaire et du gain de fonction cytoplasmique qui provoque la mort du motoneurone. Pour déterminer si la perte de fonction nucléaire est nécessaire, bien qu'insuffisante, pour la maladie, nous avons cherché à compenser la perte de fonction nucléaire dans les modèles précédents.

Pour cela, nous avons utilisé notre modèle murin knock-in hétérozygote que nous avons croisé avec une souris sauvage contenant un transgène de FUS humain sauvage (hFUS) inséré dans un chromosome artificiel bactérien. A l'issue de ces croisements nous avons caractérisé l'effet du transgène humain sauvage sur notre modèle murin knock-in. Notre hypothèse initiale était que le transgène viendrait compenser la perte de fonction nucléaire.

Nous avons observé que le transgène hFUS permet de sauver la létalité de Fus muté en homozygote, et ce jusqu'à l'âge adulte. Par la suite, nous avons observé que les troubles moteurs présents dans le modèle knock-in hétérozygote sont reversés par l'ajout du transgène hFUS, atteignant des valeurs de force musculaire similaires à celles des souris sauvages. Ces résultats indiquent que hFUS est capable de compenser les altérations physiopathologiques liées à la toxicité de Fus cytoplasmique.

Pour vérifier notre hypothèse initiale, nous avons déterminé les niveaux cytoplasmiques et nucléaires de FUS dans les différents génotypes. A notre surprise initiale, nous avons constaté que le transgène hFUS diminuait la quantité de FUS cytoplasmique, suggérant que non seulement il compensait la perte de fonction nucléaire en introduisant une protéine fonctionnelle, mais que, de plus, il permettait une diminution de la toxicité cytoplasmique.

Pour comprendre le mécanisme à travers lequel cette compensation est réalisée, nous avons fait l'hypothèse que le transgène hFUS activait l'autorégulation de FUS. De fait, il est connu que FUS à une forte capacité à s'autoréguler par activation d'une voie alternative d'épissage de l'exon 7, résultant en la dégradation de son

propre ARNm (Zhou et al 2013). Nous avons montré que l'insertion du transgène hFUS active cette voie d'épissage alternatif résultant en une diminution d'expression d'ARNm, entraînant une diminution des niveaux de protéine mutée dans le cytoplasme. L'augmentation de la méthylation de FUS dans le cytoplasme est un autre indicatif physiopathologique de la maladie présent dans notre modèle knock-in qui est également diminué par l'ajout du transgène hFUS. De la même façon, nous avons confirmé ces données par des méthodes de marquage histologiques montrant une diminution de la protéine mutée dans le cytoplasme ainsi qu'une diminution des niveaux de méthylation. Ces résultats indiquent que le transgène hFUS contrôle et renverse les niveaux de traduction de Fus muté en s'autorégulant par une voie d'épissage alternative de l'exon 7, contribuant à une diminution des effets toxiques de la mutation.

Grâce à ces données, nous concluons que l'insertion d'un transgène hFUS est capable de compenser la perte de fonction nucléaire de Fus ainsi que son gain de fonction toxique dans le cytoplasme en activant une voie d'autorégulation, prévenant la neurodégénérescence et résultant en une préservation des capacités motrices. De ce fait, des approches thérapeutiques basées dans des techniques de thérapie génique seraient de grand intérêt, permettant un ciblage plus précis des voies altérées dans la pathologie. Ces résultats sont rassemblés dans un manuscrit en préparation dont je suis premier auteur.

Phenotypic rescue of a mouse model of *FUS*-ALS by addition of an autoregulatory competent wild type *FUS* transgene.

Inmaculada Sanjuan-Ruiz et al.

Involved labs with major contributions: Dupuis, Da Cruz and Lagier-Tourenne

Abstract

Mutations in the *FUS* gene, encoding for FUS, an RNA-binding protein involved in multiple steps of RNA metabolism, are associated to the most severe forms of amyotrophic lateral sclerosis (ALS). Mutations in *FUS* lead to cytoplasmic accumulation of the physiologically nuclear FUS protein, and accumulation of cytoplasmic FUS is likely a major culprit in the toxicity of *FUS* mutations. On the other hand, deprivation in nuclear FUS leads to synaptic alterations in neurons, and might further participate in *FUS*-ALS pathogenesis. Thus, a successful therapy should aim at simultaneously preventing cytoplasmic mislocalization and nuclear deprivation of the FUS protein. FUS binds to its own pre-mRNA, leading to the skipping of exon 7 and subsequent decay of the abnormally spliced mRNA, creating an autoregulatory loop efficiently buffering FUS excess. Here, we introduced an autoregulatory competent wild-type FUS allele in $Fus^{\Delta NLS}$ mice, a knock-in mouse model of FUS-ALS that expresses a cytoplasmically retained FUS protein. Wild type FUS completely rescued the post-natal lethality of homozygous $Fus^{\Delta NLS}$ mice, and rescued mice reached adulthood without detectable motor phenotype. Consistently, wild type FUS rescued the late onset motor deficit of heterozygous $Fus^{\Delta NLS}$ mice. Mechanistically, the introduction of the wild type *FUS* allele corrected FUS cytoplasmic mislocalization in motor neurons and a number of pathological and molecular phenotypes previously observed in heterozygous $Fus^{\Delta NLS}$ mice. This was likely caused by the activation of the autoregulatory loop, leading to an overall decreased expression of the mRNA carrying the $Fus^{\Delta NLS}$ mutation. Thus, the introduction of an autoregulatory competent wild type *FUS* allele is able to correct not only loss of FUS function triggered by cytoplasmic mislocalization, but also the accumulation of the mutant protein in the cytoplasm, potentially providing a strategy for an efficient gene therapy for this devastating, currently intractable, neurodegenerative disease.

Introduction

Amyotrophic lateral sclerosis (ALS) is the major adult onset motor neuron disease, with an incidence of 2-5 new cases per 100 000 individuals per year[1,2]. ALS is characterized by a progressive paralysis, usually beginning in the 6th decade of life, and leading to death within 3 to 5 years after onset of symptoms. ALS is defined clinically by the simultaneous degeneration of upper motor neurons in the cerebral cortex and of lower, spinal and bulbar, motor neurons in the spinal cord. A subset of ALS cases is associated with family history and linked with mutations in more than 20 genes[3]. A large part of mutations causing ALS are found in genes encoding for RNA binding proteins, and more frequently in genes encoding for TDP-43 and FUS, two major RNA binding proteins involved in multiple steps of RNA metabolism[4-7]. Mutations in *FUS* cause the most severe cases of ALS, with young onset and rapid disease progression[8,9].

ALS *FUS* mutations are clustered in the C terminal region of FUS, that includes the atypical PY-nuclear localization sequence (NLS), responsible for its nuclear import through interaction with Transportin 1 and upon methylation by PRMT1[10,11]. A number of truncating mutations have been described in ALS families, leading to complete loss of the PY-NLS, and subsequent cytoplasmic aggregation of methylated FUS[11,12]. The severity of ALS is correlated with the loss of nuclear import of the FUS protein[10], suggesting that the disease is caused either by accumulation of cytoplasmic FUS, loss of nuclear FUS or both. Multiple studies in mouse models have demonstrated that cytoplasmic accumulation of FUS is necessary for triggering motor neuron degeneration[13-19]. Illustrating this, heterozygous *Fus* knock-in mouse models with ALS-like truncating mutations develop mild, late onset muscle weakness and motor neuron degeneration, while haploinsufficient *Fus* knock-out mice do not show ALS related symptoms[17-19]. However, FUS has critical role in the nucleus, as a transcriptional co-activator[20,21], a regulator of splicing in conjunction with SMN[22-26], or as a co-factor for DNA repair[27-29]. Furthermore, loss of nuclear FUS has dramatic effects on gene expression and splicing in neurons, and leads to synaptic defects[30]. Thus, while partial loss of nuclear FUS function only leads to subtle phenotypic consequences on its own if any, it might exacerbate the deleterious effects of cytoplasmic FUS accumulation. A successful therapeutic strategy for *FUS*-ALS should thus aim at both decreasing cytoplasmic FUS content, while maintaining or restoring nuclear FUS levels.

Like many other RNA-binding proteins, FUS levels are tightly controlled by autoregulatory mechanisms, and at least two of them have been documented for FUS. First, the FUS protein is able to bind to its own pre-mRNA, leading to the splicing of exon 7, and the subsequent degradation of the abnormally Δ exon 7 *FUS* mRNA[26,30]. Second, microRNA 141a and 200 expressions are stimulated by FUS and decrease FUS levels through targeting of *FUS* mRNA 3'UTR[31]. Importantly, the overriding of FUS autoregulation, through overexpression of cDNA driven, autoregulatory incompetent, FUS expression, leads to neuronal death[16,32]. Conversely, the addition of more than 20 copies of the complete human *FUS* gene, including autoregulatory

sequences, to the mouse genome only slightly increases FUS levels, and does not lead to phenotypic consequences[15], showing the efficacy of this buffering system of FUS levels.

In this study, we took advantage of the existence of this autoregulatory loop to rescue the phenotype of *Fus* knock-in mice. By crossing *Fus*$^{\Delta NLS}$ mice[18,19] with mice expressing human wild type FUS from a complete, autoregulatory competent, human gene[15], we rescued the neurological, pathological and molecular phenotypes observed in this mouse model. Importantly, the activation of the autoregulatory mechanisms also led to decreased levels of cytoplasmic FUS. This provides the proof of concept that possible gene therapies for *FUS*-ALS could take advantage of the autoregulation of FUS to target simultaneously cytoplasmic FUS accumulation and loss of nuclear FUS function.

Materials and methods

Mouse models and genotyping

Mouse experiments were approved by local ethical committee from Strasbourg University (CREMEAS) under reference number 2016111716439395.

Transgenic mice were generated as described in Scekic-Zahirovic and collaborators[18] and Lopez-Erauskin and collaborators[15], were bred in Charles River animal facility and housed in the Faculty of medicine from Strasbourg University with 12/12 hours of light/dark cycle (light on at 7:00 am) under constant conditions (21 ± 1 °C; 60% humidity) and with unrestricted access to food and water.

Mice were weaned and genotyped at 21 days by PCR from tail biopsy. The following primer sequences were used to genotype mice:

hTLS FUS-For: GAATTCGTGGACCAGGAAGGTC
hTLS FUS – Rev: CACGTGTGAACTCACCGGAGTCA
FUS-For: GAT-TTG-AAG-TGG-GTA-GAT-AGT-GCA-GG
FUS – Rev: CCT-TTC-CAC-ACT-TTA-GTT-TAG-TCA-CAG

Heterozygous Fus knock-in mice, lacking the PY-NLS, were crossed with mice expressing human wild type FUS from a complete, autoregulatory competent human gene to obtain the following genotypes: $Fus^{+/+}$, $Fus^{\Delta NLS/+}$, $Fus^{\Delta NLS/\Delta NLS}$, $Fus^{+/+}$; hFUS, $Fus^{\Delta NLS/+}$; hFUS, $Fus^{\Delta NLS/\Delta NLS}$; hFUS. The genetic background of all mice used in this study is C57Bl6/J.

Mouse behavior

Survival

Survival was studied during the first hours after birth and dead newborn mice were genotyped. Mice surviving after birth were genotyped at 21 days and were followed weekly until death or sacrifice using ketamine-xylazine if they reached any of the following endpoints: auto-mutilation, weight loss greater than 10% of the initial weight, or when they could not turn around again within 10 seconds after being laid on their side.

Inverted grid

Motor performances were weekly evaluated as previously described in Scekic-Zahirovic and collaborators[19]. The wire grid hanging time (or "hang time") was defined as the amount of time that takes the mouse to fall down from the inverted grid and was measured visually with a stopwatch. The procedure was repeated 3 times during 5min. The holding impulse corresponds to hanging time normalized with mouse weight and gravitational force.

Histological techniques

Mice were anesthetized with an intraperitoneal injection of 100 mg/kg ketamine chlorhydrate and 5mg/kg xylazine then perfused with PFA 4%. After dissection, spinal cord was included in agar 4% and serial cuts of 40µm thick were made with vibratome.

Peroxydase immunohistochemistry

For peroxidase immunohistochemistry, sections were incubated 10 min with H_2O_2 3%, rinsed 3 times with PBS 1X and incubated with rabbit anti-FUS antibody (ProteinTech 11570-1-AP; diluted 1:100) overnight at room temperature. The second day, sections were rinsed and incubated for 2h at room temperature with biotinylated donkey anti-rabbit antibody (Jackson 711-067-003; diluted 1:500). After sections were rinsed, they were incubated for 1h in horseradish peroxidase ABC kit (Vectastain ABC kit, PK-6100, Vector Laboratories Inc.), rinsed and incubated with DAB (Sigma, D5905). The enzymatic reaction was stop by adding PBS 1X, rinsed with water and sections were mounted with DPX mounting medium (Sigma, O6522).

Immunofluorescence

For immunofluorescence, sections were incubated 10 min with H_2O_2 3%, rinsed and incubated with rabbit anti-FUS antibody against the N-terminal part (ProteinTech 11570; diluted 1:100), goat anti-ChAT (Millipore AB144P; diluted 1:50), rat anti-ADMA (Homemade, Germany; diluted 1:100) or rabbit anti-ubiquitin (Abcam ab179434; diluted 1:100) overnight at room temperature. After 3 rinses, sections were incubated with Hoechst (Sigma B2261; diluted 1:50.000), Alexa-488-conjugated donkey anti-rabbit (Jackson 711-547-003; diluted 1:500) or Alexa-594-conjugated donkey anti-goat (Molecular Probes A11058; diluted 1:500) for 2h at room temperature. Sections were rinsed and mounted with Aqua/polymount (Polysciences 18606).

Electron microscopy

Mice were anesthetized with an intraperitoneal injection of 100 mg/kg ketamine chlorhydrate and 5mg/kg xylazine and transcardially perfused with glutaraldehyde (2.5% in 0.1M cacodylate buffer at pH 7.4). Brains were dissected and immersed in the same fixative overnight. After 3 rinses in Cacodylate buffer (EMS, 11650), brains were post fixed in 0.5% osmium and 0.8% potassium ferrocyanide in Cacodylate buffer 1h at room temperature. Finally, tissues were dehydrated in graded ethanol series and embedded in Embed 812 (EMS, 13940). The ultrathin sections (50 nm) were cut with an ultramicrotome (Leica, EM UC7), counterstained with uranyl acetate (1% (w/v) in 50% ethanol) and observed with a Hitachi 7500 transmission electron microscope (Hitachi High Technologies Corporation, Tokyo, Japan) equipped with an AMT Hamamatsu digital camera (Hamamatsu Photonics, Hamamatsu City, Japan).

Tissue fractionation and western blotting

Tissues were washed in PBS1x and lysed in Syn-PER Synaptic Protein Extraction (Thermo Scientific, 87793) according to the manufacturer's instructions. Protein extract were dosed by BCA Assay (Interchim, UP95424A, UP95425A). Thereafter proteins were denatured and SDS page were performed with 10 (for cytoplasmic proteins) and 30µg of protein (for nuclear proteins) on criterion TGX stain free gel 4-20% (Biorad, 5678094). Proteins were blotted on nitrocellulose membrane using semi-dry Transblot Turbo system (BioRad, France) and blocked with 10% non-fat milk during 1h. Primary antibodies Rabbit anti-hFUS (Homemade #14080; diluted 1:2000), Rabbit anti-mFUS (Homemade, #14082; diluted 1:4000), Rat anti-FUS ADMA (Homemade, Germany; diluted 1:500), Rabbit anti-FUS 293 (Bethyl A-300-293A; diluted 1:2000), Rabbit anti-FUS 294 (Bethyl A300-294A; diluted 1:2000), Sheep anti-SOD1 (Calbiochem 574597; diluted 1:1000), Rabbit anti-HDAC1 (Bethyl A300-713A; diluted 1:1000) were incubated overnight at 4°C in 3% non-fat milk. Washing were proceeded with washing buffer (Tris pH 7.4 1 M, NaCl 5M, Tween 20 100 %) and secondary antibodies anti-rabbit HRP (PARIS, BI2407; diluted 1:5000), anti-sheep HRP (Jackson 713-035-147; diluted 1:5000) were incubated 1h30 at room temperature. After successive washes, proteins were visualized with chemiluminescence using ECL Lumina Forte (Millipore, France) and chemiluminescence detector (Bio-Rad, France). Total proteins were detected with stain free gel capacity (Biorad 5678094) and used to normalize.

Antibodies:
Rabbit anti-hFUS (Custom Made[15], #14080, 1/2000),
Rabbit anti-mFUS (Custom Made[15], #14082, 1/4000)
Rat anti-FUS ADMA (Custom Made[12], Germany, 1/500)
Rabbit anti-FUS 293 (Bethyl, A-300-293A, 1/2000)

Rabbit anti-FUS 294 (Bethyl, A300-294A, 1/2000)

Sheep anti-SOD1 (Calbiochem, 574597, 1/1000)

Rabbit anti-HDAC1 (Bethyl, A300-713A, 1/1000)

Anti-rabbit HRP (PARIS, BI2407,1/5000)

Anti-sheep HRP (Jackson, 713-035-147, 1/5000)

RNA extraction and RT-qPCR

Total RNA was extracted from spinal cord and frontal cortex using TRIzol® reagent (Life Technologies). 1 µg of RNA was reverse transcribed with iScript™ reverse transcription (Biorad, 1708841). Quantitative polymerase chain reaction was performed using Sso Advanced Universal SYBR Green Supermix (Bio-Rad) and quantified with Bio-Rad software. Gene expression was normalized by calculating a normalization factor using actin, TBP and pol2 genes according to GeNorm software[33].

Primer sequences were as follows:
Actin: F- CCACCAGTTCGCCATGGAT, R-GGCTTTGCACATGCCGGAG

TBP: F-CCAATGACTCCTATGACCCCTA, R-CAGCCAAGATTCACGGTAGAT

Pol2: F-GCTGGGAGACATAG-ACCA, R-TTACTCCCCTGCATGGTCTC

hFUS: F- GCCAGAACACAGGCTATGGA, R- CGATTGGGAGCTCTGGCTAC

T-FUS: F- TTATGGACAGACCCAAAAACACA, R-TGCTGCCCATAAGAAGATTG

FUS ΔNLS: F- GCAAGATGGACTCCTAGTGTTAAT, R- ACCTCTACAAATGTGGTATGGC

Fus_exon6-8: F- CGGCATGGGGTCCTCGG, R- CCTAGGCCTTGCACGAAGAT

Statistics

All results from analysis are presented as mean ± standard error of the mean (SEM) and differences were considered significant when $p < 0.05$. Significance is presented as follows: * $p<0.05$, ** $p<0.01$, and *** $p<0.001$. For comparison of two groups, two-tailed unpaired Student's t –test was used in combination with F-test to confirm that the variances between groups were not significantly different. Comparison for more than two groups was performed using one-way ANOVA and Tukey or Bonferroni's multiple comparison post hoc tests. Data were analyzed by using the GraphPad Prism version 6.0.

Results

Human wild type FUS transgene rescues perinatal letality in homozygous Fus$^{\Delta NLS}$ mice.

Human wild type FUS transgenic mice (hFUS mice) expressing wild type FUS from a BAC have been recently generated and characterized[15]. These mice express slightly increased FUS levels, mostly of human origin, and do not show ALS-related phenotypes contrary to the human mutant FUS transgenic lines generated and characterized in parallel[15]. We crossed hFUS mice with *Fus*$^{\Delta NLS}$ mice[18], that we previously showed to develop mild, late onset motor neuron disease as heterozygous [19] while homozygous *Fus*$^{\Delta NLS}$ mice die in the perinatal period[18]. After two breeding steps, we obtained all genotypes of interest, including heterozygous and homozygous *Fus*$^{\Delta NLS}$ mice with or without the hFUS transgene (**Figure 1A**). Of note, all mice were in C57Bl/6 genetic background, and only mice from the F2 generation were analyzed here, thereby avoiding most of the possible confounding effects of genetic background heterogeneity. Importantly, these breeding steps were performed in parallel in two laboratories. 200 mice of the F2 generation were generated. Mice were genotyped at 1 month of age or at death if occurring before 1 month of age. As previously described *Fus*$^{\Delta NLS/\Delta NLS}$ mice without hFUS died within the first hours after birth[18] and we did not observe mice with this genotype at 1 month of age (**Figure 1C**). Contrastingly, the addition of the human wild type FUS transgene allowed the survival of most homozygous *Fus*$^{\Delta NLS}$ mice until adulthood (**Figure 1B, D**). We observed a slight but non-significant increased mortality of all *Fus*$^{\Delta NLS}$ groups as compared to wild type animals (**Figure 1D**).

Human wild type FUS transgene rescues late onset muscle weakness in heterozygous Fus$^{\Delta NLS}$ mice.

Fus$^{\Delta NLS/+}$ mice develop mild, late onset, muscle weakness, that can be easily followed using inverted grid test[19]. Using this test, we observed that the deficit in *Fus*$^{\Delta NLS/+}$ mice occurred after 2 months of age and was stable with age (**Figure 2A-B**). Contrastingly, *Fus*$^{\Delta NLS/+}$ mice with a human wild type FUS transgene were undistinguishable from wild type littermates in this test, suggesting that the wild type FUS transgene was sufficient to rescue the neuromuscular phenotype (**Figure 2A-B**).

Human wild type FUS transgene rescues cytoplasmic mislocalization of the FUS protein in Fus$^{\Delta NLS}$ mice.

We then asked whether human wild type FUS transgene altered subcellular localization of FUS in *Fus*$^{\Delta NLS}$ mice. As expected from previous studies[18,19], cytoplasmic fractions of cerebral cortex of *Fus*$^{\Delta NLS/+}$ mice displayed higher levels of FUS than corresponding wild type littermate fractions as assessed using western blotting (**Figure 3A-B**). This was not observed when an antibody targeting the NLS sequence, absent from the FUS$^{\Delta NLS}$ protein, was used, demonstrating that this increase is related to the mislocalization of the mutant protein. Importantly, mouse FUS, as identified using a mouse specific FUS antibody, was increased in cytoplasmic fractions of *Fus*$^{\Delta NLS/+}$ mice, and this was normalized by the human wild type FUS transgene (**Figure 3A-B**). Importantly, nuclear FUS levels were unchanged in all genotypes, irrespective of the presence of the *Fus*$^{\Delta NLS}$ mutation or of the human wild type FUS transgene. Human FUS levels were increased in *Fus*$^{\Delta NLS/\Delta NLS}$ mice carrying a human FUS transgene, likely compensating for the loss of nuclear FUS of mouse origin. To further confirm this rescuing effect of the transgene, we performed immunohistochemistry on spinal cord sections of 22 months old mice. As shown in **Figure 3C**, *Fus*$^{\Delta NLS/+}$ neurons showed lacked nuclear enrichment in FUS staining, and this was fully prevented by the human wild type FUS transgene, whether in *Fus*$^{\Delta NLS/+}$ mice or in *Fus*$^{\Delta NLS/\Delta NLS}$ mice. Double immunofluorescence using FUS and ChAT antibodies to unambiguously identify motor neurons further confirmed that the human wild type FUS transgene rescued FUS mislocalization in motor neurons (**Figure 3D**).

Human wild type FUS transgene rescues ALS-related pathology in heterozygous Fus$^{\Delta NLS}$ mice.

To further document the protective effect of the human wild type FUS transgene, we analyzed pathological hallmarks developed by these mice. Accumulation of cytoplasmic asymmetrically dimethylated (ADMA) FUS is typical of *FUS*-ALS[10-12], and has been previously observed in *Fus*$^{\Delta NLS/+}$ mice. Indeed, the large increase in ADMA-FUS in *Fus*$^{\Delta NLS/+}$ cytoplasmic fractions was largely prevented in *Fus*$^{\Delta NLS/+}$ mice with a wild type human FUS transgene (**Figure 4A-B**). This was however not true in *Fus*$^{\Delta NLS/\Delta NLS}$ mice carrying a hFUS transgene that retained high levels of cytoplasmic methylated FUS. Consistently, while ADMA-FUS immunoreactivity is diffuse in motor neurons of *Fus*$^{\Delta NLS/+}$ mice, the human wild type FUS transgene led to more localized, perinuclear immunoreactivity in *Fus*$^{\Delta NLS/+}$ mice (**Figure 4C**). Furthermore, the punctate ubiquitin pathology observed in *Fus*$^{\Delta NLS/+}$ motor neurons was also prevented by the human wild type FUS transgene (**Figure 4D**). Thus, the human wild type FUS transgene was able to rescue typical hallmarks of ALS-FUS pathology in *Fus*$^{\Delta NLS/+}$ mice.

Human wild type FUS transgene reverts overexpression of endogenous Fus and activates exon 7 skipping.

We then sought to understand how the human wild type FUS transgene could lead to decreased levels of cytoplasmic FUS, and hypothesized that the expression of the human FUS led to activation of the FUS autoregulatory loop to degrade ΔNLS mRNA. Indeed, as expected from previous studies, single human wild type FUS transgenic mice had lower expression of the endogenous *Fus* gene[15] while *Fus*$^{\Delta NLS/+}$ mice displayed a slight but significant increase in *Fus* mRNA levels at both 1 and 22 months of age in spinal cord (**Figure 5A-B**) and frontal cortex (**Supplementary Figure 2**). This overexpression of the endogenous murine gene was fully corrected by the human wild type FUS transgene. Furthermore, the expression of the human FUS transgene was accompanied by strongly increased levels of the aberrantly spliced mRNA of *Fus* devoid of exon 7, substrate to mRNA decay (**Figure 5A-B**), and by decreases in expression of the mutant ΔNLS mRNA (**Figure 5A-B**) in spinal cord and frontal cortex (**Supplementary Figure 2**). Indeed, there was a strong correlation between hFUS expression and deletion of exon 7 in endogenous mouse *Fus* mRNA (**Supplementary Figure 3**). Thus, the addition of the human wild type FUS transgene leads to decreased expression of the toxic protein through the activation of the autoregulatory loop, and subsequent alleviation of all the downstream consequences of the expression of cytoplasmically mislocalized FUS.

Figures and legends

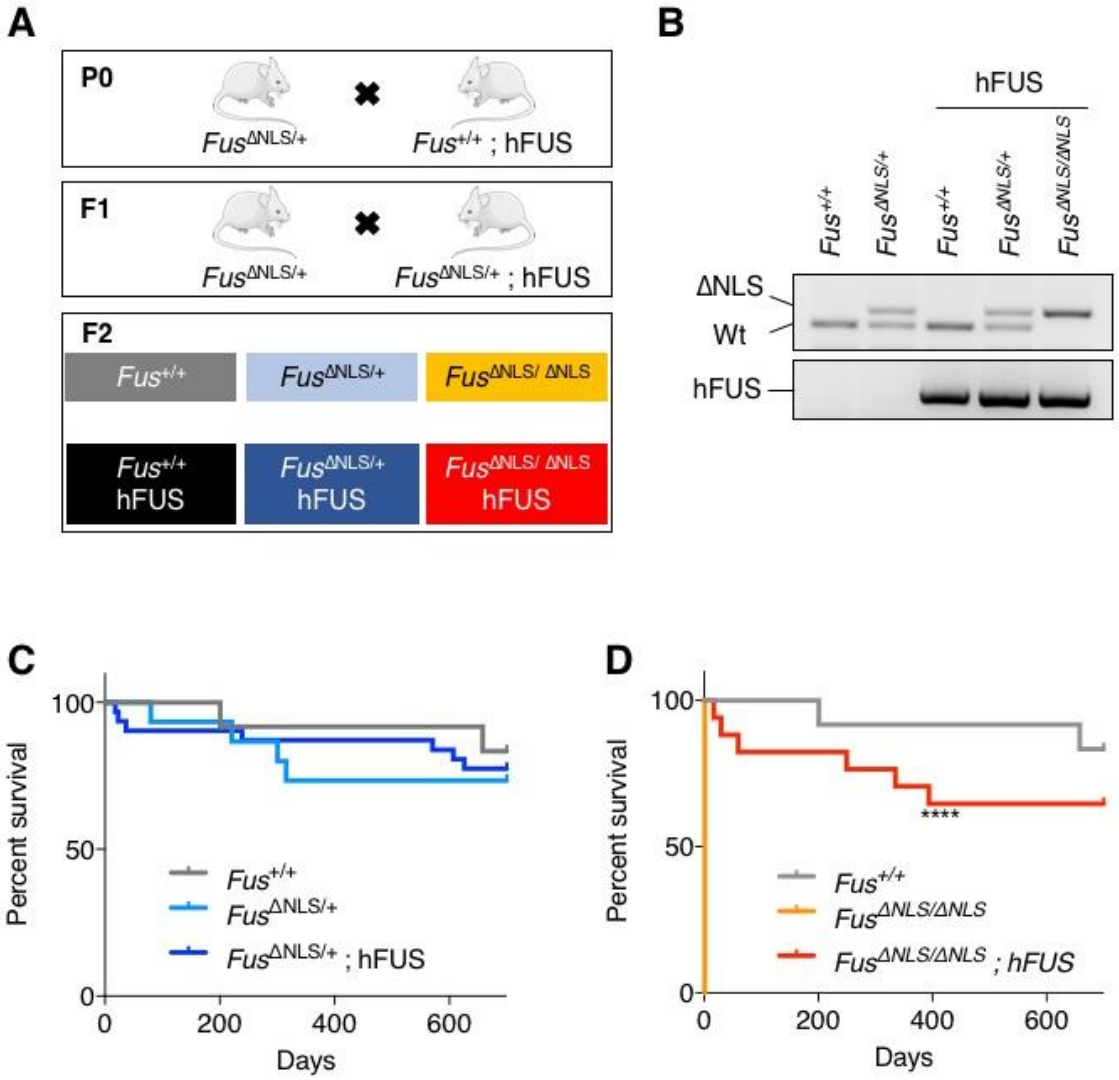

Figure 1: hFUS transgene rescues letality of homozygous ΔNLS *Fus* mutation.

A: breeding strategy

B: representative genotyping result of 5 mice of 1 month of age.

C-D: Kaplan Meier survival curve of the different genotypes either heterozygous (C) or homozygous for the ΔNLS mutation (D). Note that all homozygous ΔNLS mice die at birth, unless carrying a hFUS transgene.

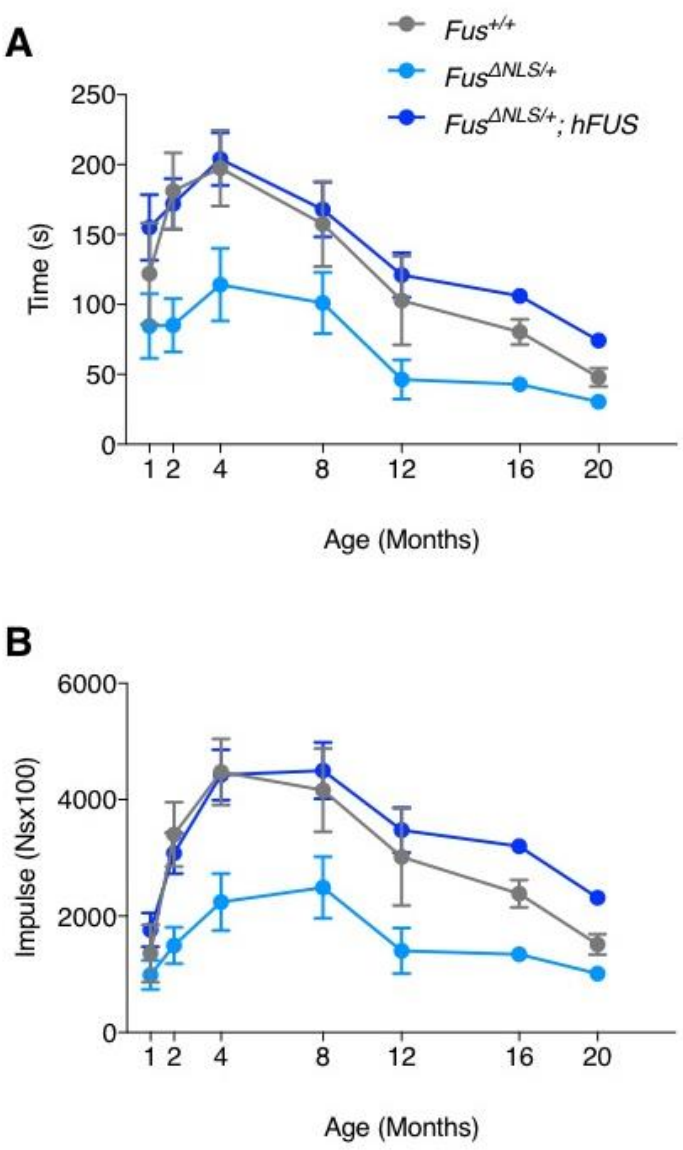

Figure 2: hFUS transgene rescues the muscle weakness of heterozygous ΔNLS *Fus* mice.

A-B: age-dependent changes in the mean hanging time (s) (A) and holding impulse (N s) (B) in the four-limb wire inverted grid test in *Fus* $^{+/+}$, and *Fus* $^{\Delta NLS/+}$ mice with or without hFUS transgene. *N* =10-28 per group. *P = 0.0002 for genotype effect between Fus* $^{+/+}$, and *Fus* $^{\Delta NLS/+}$ mice, and p<0,0001 for genotype effect between *Fus* $^{\Delta NLS/+}$ and *Fus* $^{\Delta NLS/+}$ hFUS mice. 2 way anova with age and genotype as two factors.

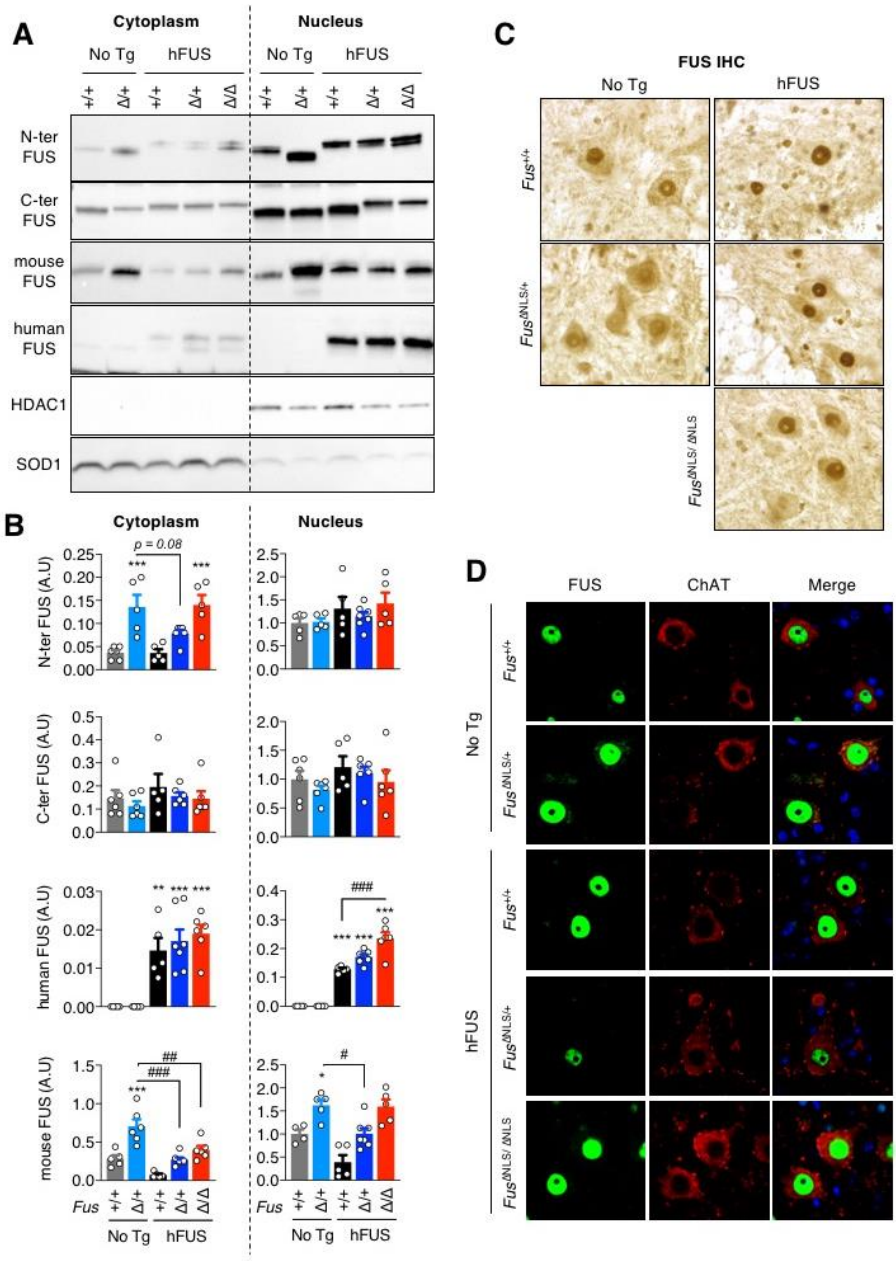

Figure 3: hFUS transgene corrects abnormal cytoplasmic accumulation of FUS protein in heterozygous *Fus*$^{\Delta NLS/+}$ mice.

A: Immunoblot analysis of FUS protein subcellular localization in cortex of *Fus* $^{+/+}$ (+/+) and *Fus* $^{\Delta NLS/+}$ (Δ/+) mice with or without hFUS transgene and of *Fus* $^{\Delta NLS/\Delta NLS}$ mice with hFUS transgene at 1 month of age. Representative results using different antibodies targeting the N-terminal part (N-ter) of FUS, the C-terminal (C-ter) NLS, mouse FUS or human FUS. SOD1 and HDAC1 are used as loading controls for cytoplasmic and nuclear protein extracts fractions, respectively. Note that these immunoblots were performed on different membranes to avoid cross reaction between different antibodies. Uncropped western blots and corresponding stain free gels are provided in supplementary data.

B: Quantification of Nter, C-ter, mouse and human FUS protein levels in cytoplasmic and nuclear fractions of the indicated genotypes. *N* = 4-8. **p* < 0.05, ****p* < 0.001vs *Fus*$^{+/+}$, #, p<0.05 and ###, p<0.001 vs indicated genotype by ANOVA followed by Tukey.

C: FUS immunohistochemistry in the spinal cord ventral horn at 22 months of age of mice of the indicated genotypes. Note that diffuse FUS cytoplasmic staining, obvious in *Fus* $^{\Delta NLS/+}$ mice is rescued by the hFUS transgene.

D: Double immunostaining for the motoneuronal marker ChAT and FUS (N-terminal part) in the spinal cord ventral horn at 22 months of age. Note the cytoplasmic redistribution of truncated FUS in *Fus* $^{\Delta NLS/+}$ mice and its rescue by hFUS transgene.

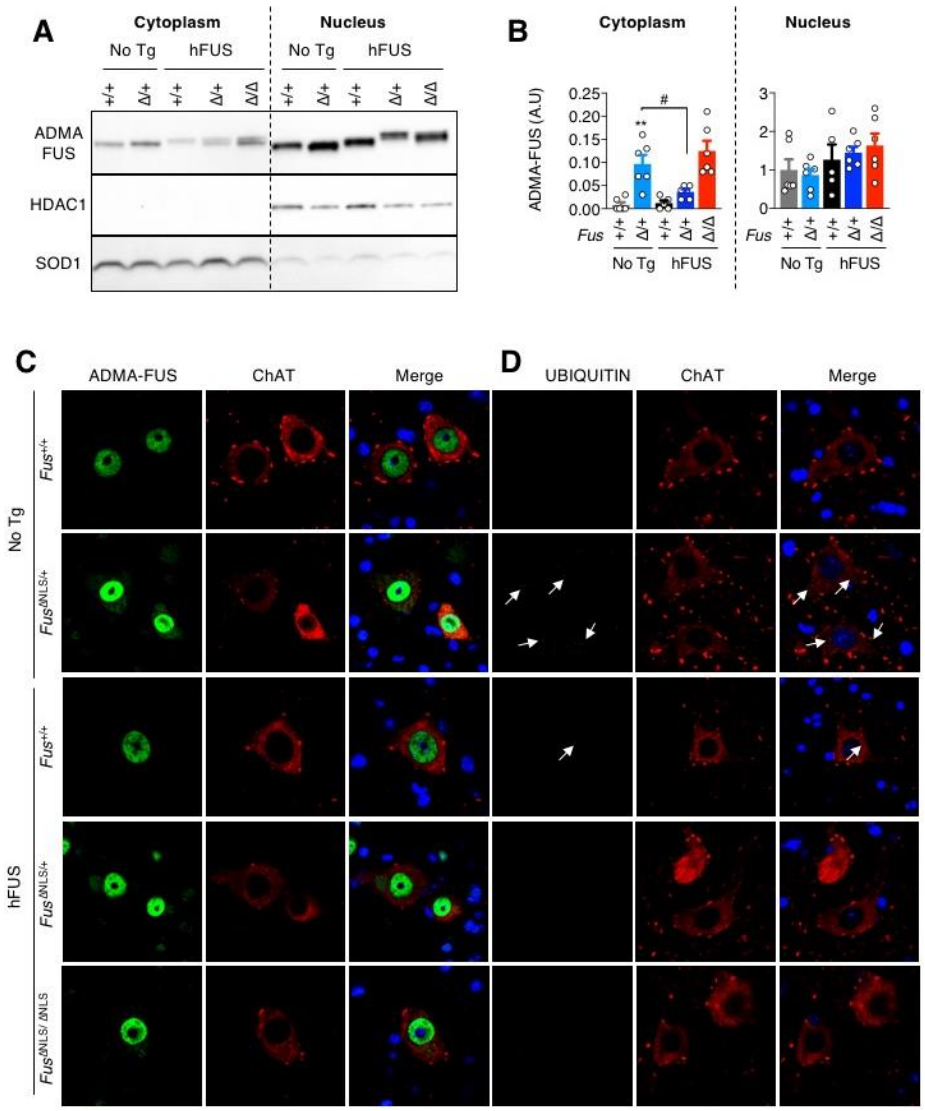

Figure 4: hFUS transgene corrects pathological features in *Fus*$^{\Delta NLS/+}$ mice.

A: Immunoblot analysis of asymmetrically arginine dimethylated FUS on cytoplasmic and nuclear fractions of cortex of *Fus* $^{+/+}$ (+/+) and *Fus* $^{\Delta NLS/+}$ (Δ/+) mice with or without hFUS transgene and of *Fus* $^{\Delta NLS/\Delta NLS}$ mice with hFUS transgene at 1 month of age. Representative results using an antibody recognizing asymmetrically arginine dimethylated FUS (ADMA-FUS). HDAC1 is used as a loading control for nuclear fractions and SOD1 for cytoplasmic fractions. Please note that HDAC1 and SOD1 immunoblots are identical to Figure 3 as these experiments have been performed in parallel. Note that these immunoblots were performed on different membranes to avoid cross reaction between different antibodies. Uncropped western blots and corresponding stain free gels are provided in supplementary data.

B: Quantification of ADMA-FUS protein levels in cytoplasmic and nuclear fractions of the indicated genotypes. *N* = 4-8. ***p* < 0.01 vs *Fus*$^{+/+}$, #, p<0.05 vs indicated genotype by ANOVA followed by Tukey.

C-D: double immunostaining for the motoneuronal marker ChAT (*red*), and either ADMA-FUS (C, *green*), or ubiquitin (D, green) in the spinal cord ventral horn.

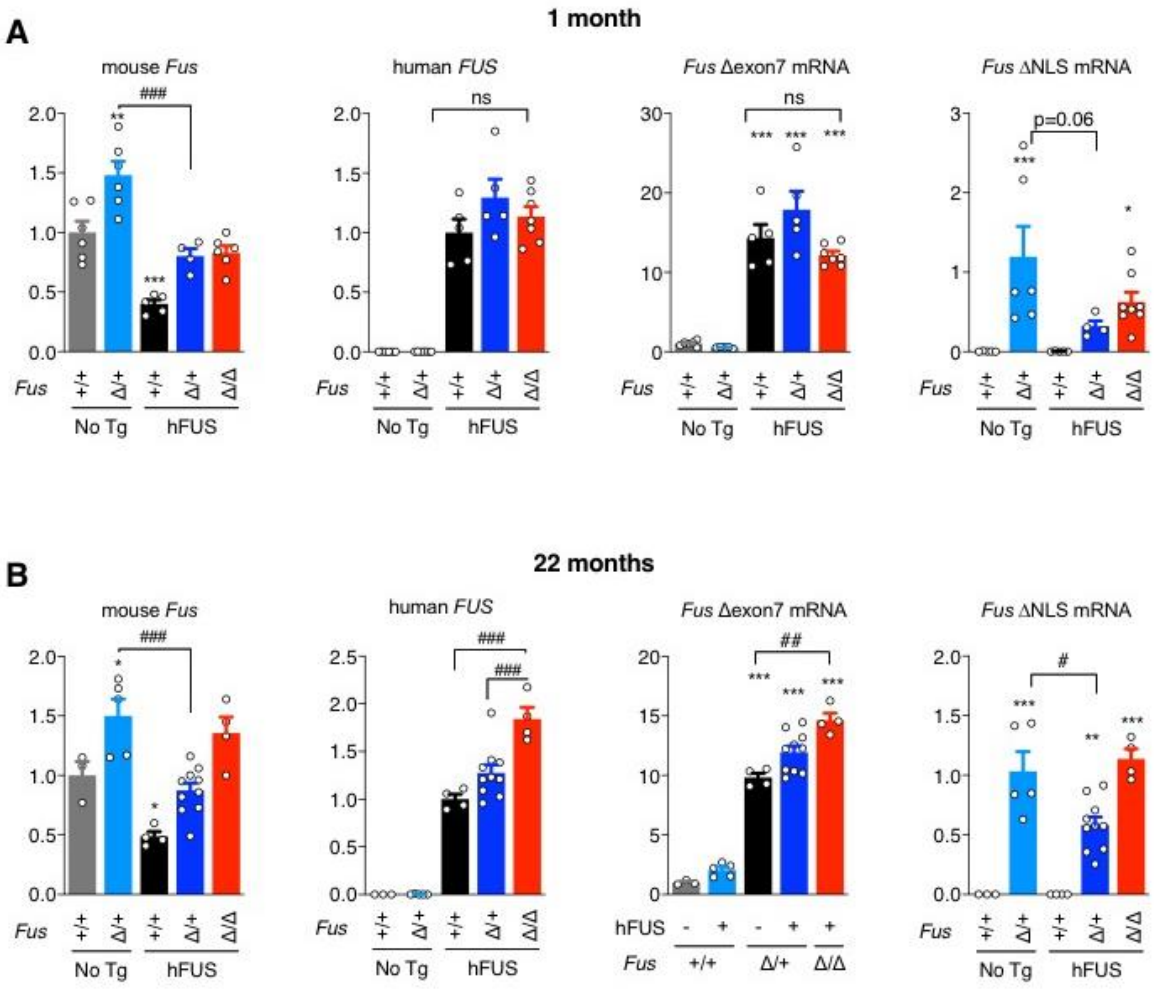

Figure 5: hFUS transgene activates autoregulatory splicing in Fus$^{\Delta NLS/+}$ spinal cord.

RT-qPCR results for endogenous mouse Fus mRNA (left), human FUS transgene (middle left) endogenous Fus mRNA deleted of exon 7 (middle right) and mutant *Fus* mRNA carrying the ΔNLS mutation in spinal cord at 1 month of age (A) or 22 months of age (B).

Note that the hFUS transgene decreases expression of endogenous *Fus* gene, activates autoregulatory *Fus* splicing and leads to decreased expression of mutant *Fus* mRNA at 1 and 22 months of age.

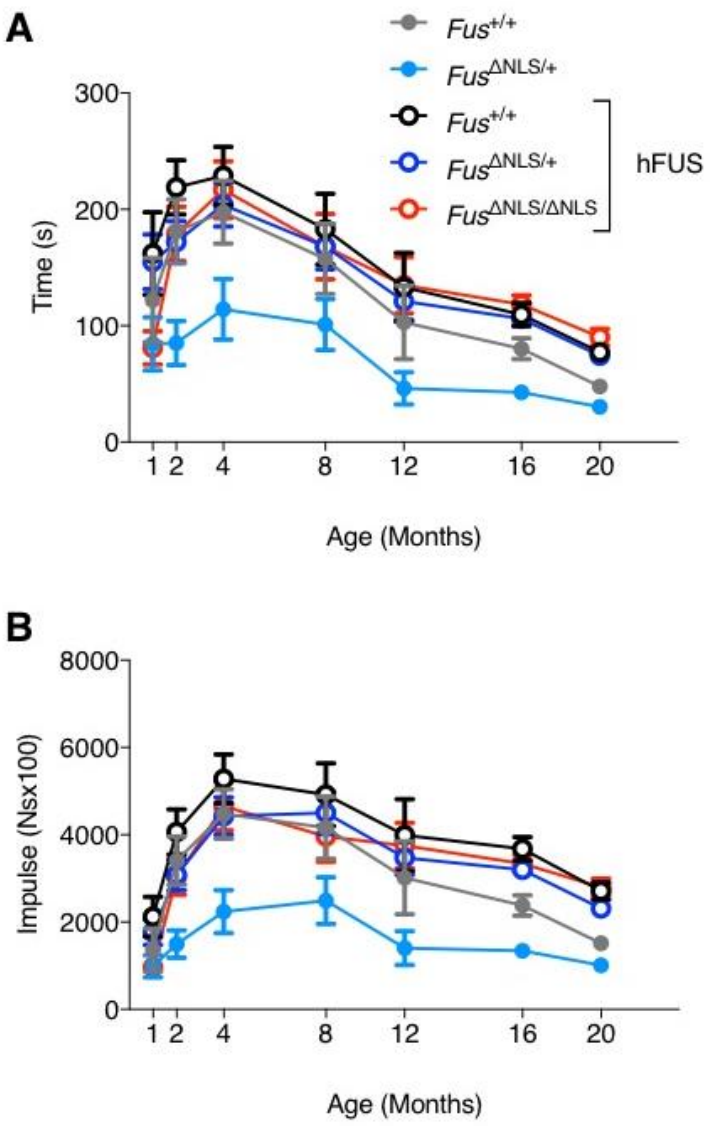

Supplementary figure 1: hFUS transgene rescues homozygous ΔNLS *Fus* mice.

A-B: age-dependent changes in the mean hanging time (s) (A) and holding impulse (N s) (B) in the four-limb wire inverted grid test in *Fus* $^{+/+}$, and *Fus* $^{\Delta NLS/+}$ mice with or without hFUS transgene. *N* =10-28 per group. *P = 0.0002 for genotype effect between Fus* $^{+/+}$, and *Fus* $^{\Delta NLS/+}$ mice, and p<0,0001 for genotype effect between *Fus* $^{\Delta NLS/+}$ and *Fus* $^{\Delta NLS/+}$ hFUS mice. 2 way anova with age and genotype as two factors.

Experimental data are identical to Figure 2, and includes other genotypes that were omitted from the main figure for clarity.

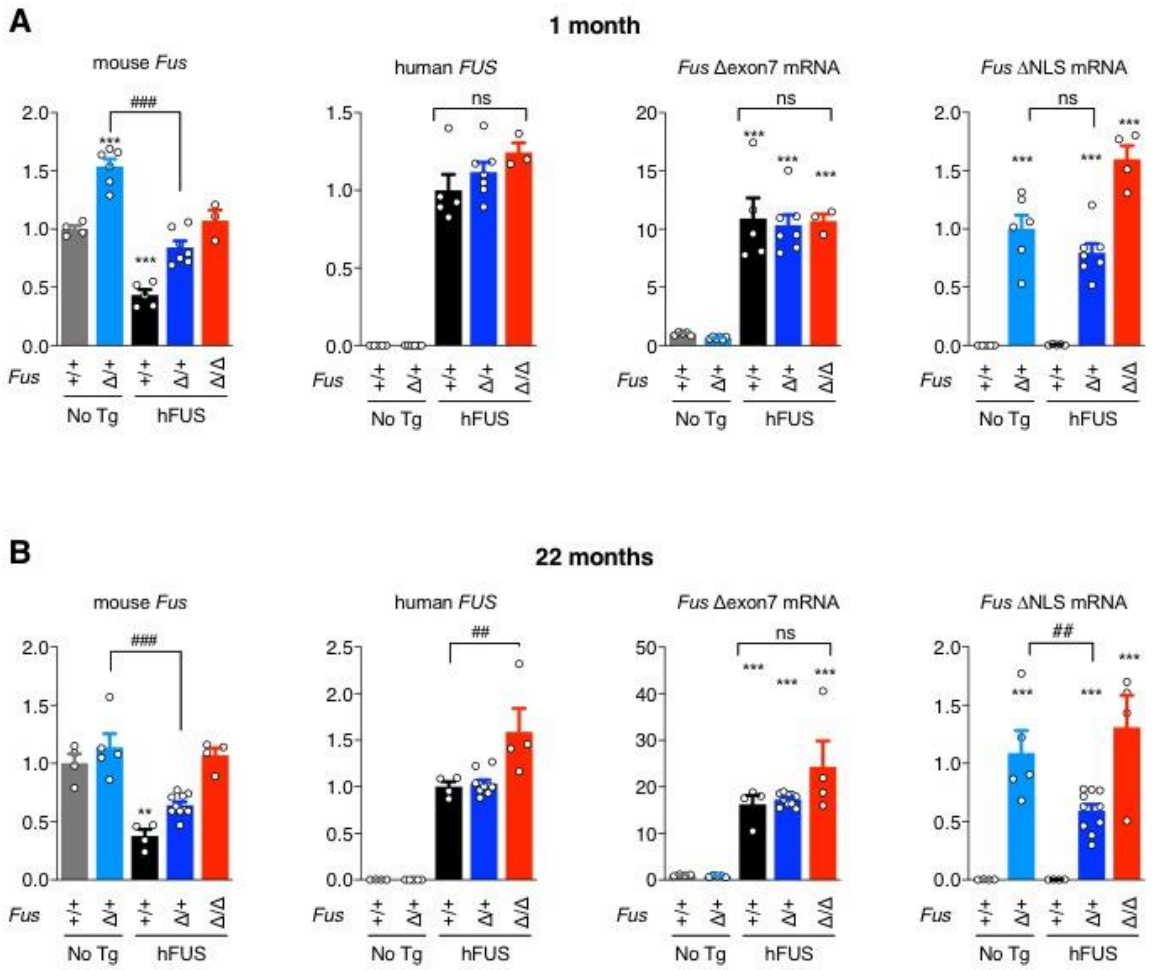

Supplementary Figure 2: hFUS transgene activates autoregulatory splicing in *Fus*$^{\Delta NLS/+}$ frontal cortex.
RT-qPCR results for endogenous mouse Fus mRNA (left), human FUS transgene (middle left) endogenous Fus mRNA deleted of exon 7 (middle right) and mutant *Fus* mRNA carrying the ΔNLS mutation in frontal cortex at 1 month of age (A) or 22 months of age (B).
Note that the hFUS transgene decreases expression of endogenous *Fus* gene, activates autoregulatory *Fus* splicing and leads to decreased expression of mutant *Fus* mRNA at 22 months of age.

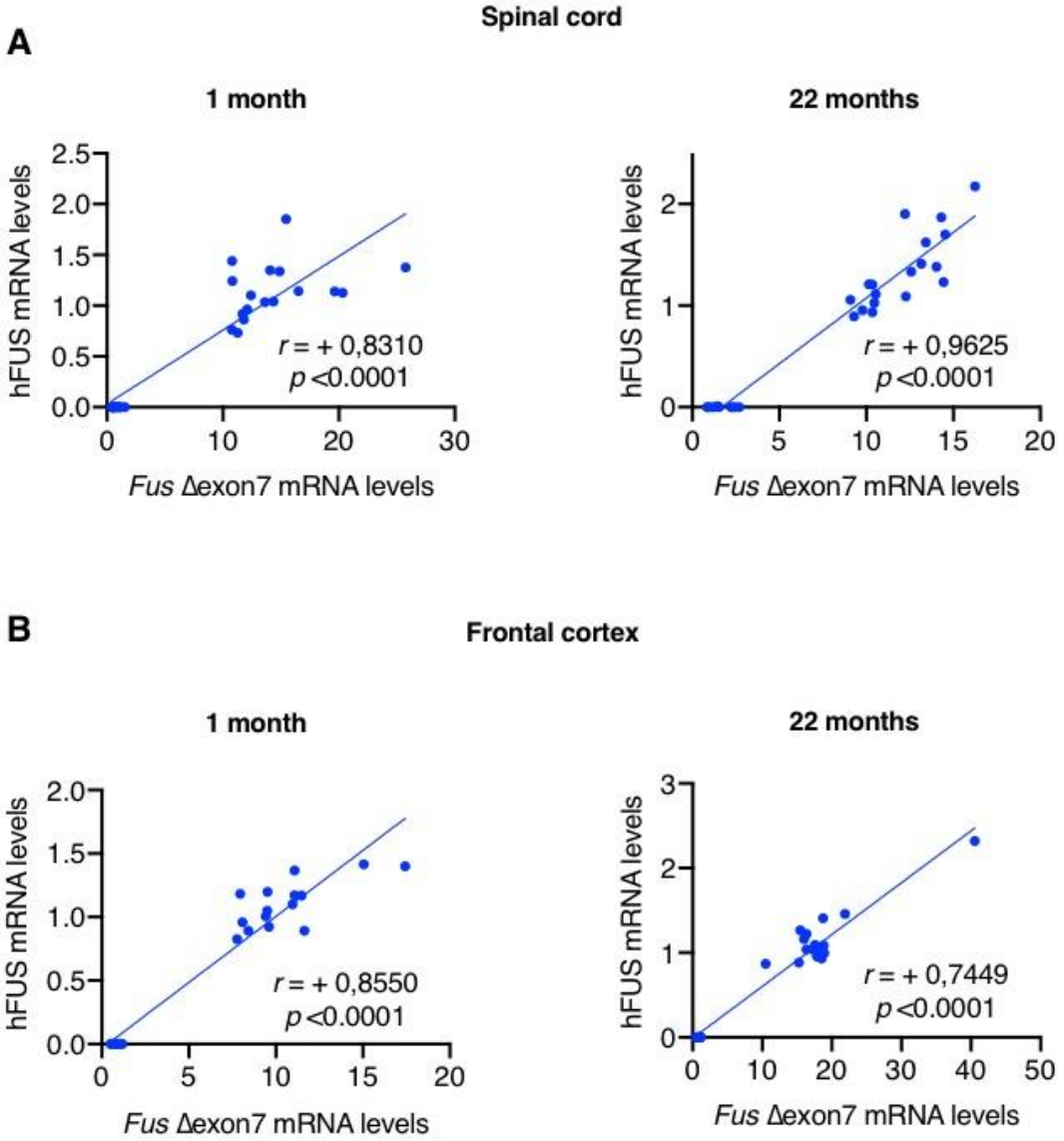

Supplementary Figure 3: expression of hFUS transgene correlates with activation of endogenous mouse exon 7 splicing.
hFUS mRNA levels were plotted against mRNA levels of mouse *Fus* mRNA deleted of exon 7 (data from Figures 5 and S2). A strong correlation between expression of both mRNAs was observed.
Spearman correlation.

References

1. van Es MA, Hardiman O, Chio A, et al. Amyotrophic lateral sclerosis. Lancet 2017;390:2084-98.
2. Brown RH, Jr., Al-Chalabi A. Amyotrophic Lateral Sclerosis. N Engl J Med 2017;377:162-72.
3. Taylor JP, Brown RH, Jr., Cleveland DW. Decoding ALS: from genes to mechanism. Nature 2016;539:197-206.
4. Vance C, Rogelj B, Hortobagyi T, et al. Mutations in FUS, an RNA processing protein, cause familial amyotrophic lateral sclerosis type 6. Science 2009;323:1208-11.
5. Kwiatkowski TJ, Jr., Bosco DA, Leclerc AL, et al. Mutations in the FUS/TLS gene on chromosome 16 cause familial amyotrophic lateral sclerosis. Science 2009;323:1205-8.
6. Kabashi E, Valdmanis PN, Dion P, et al. TARDBP mutations in individuals with sporadic and familial amyotrophic lateral sclerosis. Nat Genet 2008;40:572-4.
7. Sreedharan J, Blair IP, Tripathi VB, et al. TDP-43 mutations in familial and sporadic amyotrophic lateral sclerosis. Science 2008;319:1668-72.
8. Waibel S, Neumann M, Rabe M, Meyer T, Ludolph AC. Novel missense and truncating mutations in FUS/TLS in familial ALS. Neurology 2010;75:815-7.
9. Waibel S, Neumann M, Rosenbohm A, et al. Truncating mutations in FUS/TLS give rise to a more aggressive ALS-phenotype than missense mutations: a clinico-genetic study in Germany. Eur J Neurol 2013;20:540-6.
10. Dormann D, Rodde R, Edbauer D, et al. ALS-associated fused in sarcoma (FUS) mutations disrupt Transportin-mediated nuclear import. EMBO J 2010;29:2841-57.
11. Dormann D, Madl T, Valori CF, et al. Arginine methylation next to the PY-NLS modulates Transportin binding and nuclear import of FUS. EMBO J 2012;31:4258-75.
12. Suarez-Calvet M, Neumann M, Arzberger T, et al. Monomethylated and unmethylated FUS exhibit increased binding to Transportin and distinguish FTLD-FUS from ALS-FUS. Acta Neuropathol 2016;131:587-604.
13. Sun S, Ling SC, Qiu J, et al. ALS-causative mutations in FUS/TLS confer gain- and loss-of-function by altered association with SMN and U1-snRNP. Nat Commun 2015.
14. Sun S, Ling SC, Qiu J, et al. ALS-causative mutations in FUS/TLS confer gain and loss of function by altered association with SMN and U1-snRNP. Nat Commun 2015;6:6171.
15. Lopez-Erauskin J, Tadokoro T, Baughn MW, et al. ALS/FTD-Linked Mutation in FUS Suppresses Intra-axonal Protein Synthesis and Drives Disease Without Nuclear Loss-of-Function of FUS. Neuron 2018;100:816-30 e7.
16. Ling SC, Dastidar SG, Tokunaga S, et al. Overriding FUS autoregulation in mice triggers gain-of-toxic dysfunctions in RNA metabolism and autophagy-lysosome axis. eLife 2019;8.
17. Devoy A, Kalmar B, Stewart M, et al. Humanized mutant FUS drives progressive motor neuron degeneration without aggregation in 'FUSDelta14' knockin mice. Brain 2017;140:2797-805.
18. Scekic-Zahirovic J, Sendscheid O, El Oussini H, et al. Toxic gain of function from mutant FUS protein is crucial to trigger cell autonomous motor neuron loss. EMBO J 2016;35:1077-97.
19. Scekic-Zahirovic J, Oussini HE, Mersmann S, et al. Motor neuron intrinsic and extrinsic mechanisms contribute to the pathogenesis of FUS-associated amyotrophic lateral sclerosis. Acta Neuropathol 2017;133:887-906.

20. Colombrita C, Onesto E, Megiorni F, et al. TDP-43 and FUS RNA-binding proteins bind distinct sets of cytoplasmic messenger RNAs and differently regulate their post-transcriptional fate in motoneuron-like cells. J Biol Chem 2012;287:15635-47.
21. Morlando M, Dini Modigliani S, Torrelli G, et al. FUS stimulates microRNA biogenesis by facilitating co-transcriptional Drosha recruitment. EMBO J 2012;31:4502-10.
22. Polymenidou M, Lagier-Tourenne C, Hutt KR, et al. Long pre-mRNA depletion and RNA missplicing contribute to neuronal vulnerability from loss of TDP-43. Nat Neurosci 2011;14:459-68.
23. Ishigaki S, Masuda A, Fujioka Y, et al. Position-dependent FUS-RNA interactions regulate alternative splicing events and transcriptions. Sci Rep 2012;2:529.
24. Orozco D, Tahirovic S, Rentzsch K, Schwenk BM, Haass C, Edbauer D. Loss of fused in sarcoma (FUS) promotes pathological Tau splicing. EMBO Rep 2012;13:759-64.
25. Rogelj B, Easton LE, Bogu GK, et al. Widespread binding of FUS along nascent RNA regulates alternative splicing in the brain. Sci Rep 2012;2:603.
26. Zhou Y, Liu S, Liu G, Ozturk A, Hicks GG. ALS-associated FUS mutations result in compromised FUS alternative splicing and autoregulation. PLoS Genet 2013;9:e1003895.
27. Mastrocola AS, Kim SH, Trinh AT, Rodenkirch LA, Tibbetts RS. The RNA-binding Protein Fused in Sarcoma (FUS) Functions Downstream of Poly(ADP-ribose) Polymerase (PARP) in Response to DNA Damage. J Biol Chem 2013;288:24731-41.
28. Rulten SL, Rotheray A, Green RL, et al. PARP-1 dependent recruitment of the amyotrophic lateral sclerosis-associated protein FUS/TLS to sites of oxidative DNA damage. Nucleic Acids Res 2013.
29. Wang WY, Pan L, Su SC, et al. Interaction of FUS and HDAC1 regulates DNA damage response and repair in neurons. Nat Neurosci 2013;16:1383-91.
30. Lagier-Tourenne C, Polymenidou M, Hutt KR, et al. Divergent roles of ALS-linked proteins FUS/TLS and TDP-43 intersect in processing long pre-mRNAs. Nat Neurosci 2012;15:1488-97.
31. Dini Modigliani S, Morlando M, Errichelli L, Sabatelli M, Bozzoni I. An ALS-associated mutation in the FUS 3'-UTR disrupts a microRNA-FUS regulatory circuitry. Nat Commun 2014;5:4335.
32. Mitchell JC, McGoldrick P, Vance C, et al. Overexpression of human wild-type FUS causes progressive motor neuron degeneration in an age- and dose-dependent fashion. Acta Neuropathol 2013;125:273-88.
33. Vandesompele J, De Preter K, Pattyn F, et al. Accurate normalization of real-time quantitative RT-PCR data by geometric averaging of multiple internal control genes. Genome Biol 2002;3:research0034.1–.11.

2. PART 2: CYTOPLASMIC FUS ACCUMULATION TRIGGERS CORTICAL NEURONAL HYPEREXCITABILITY AND ALTERED BEHAVIOUR RELEVANT TO FRONTO-TEMPORAL DEMENTIA.

Résumé

Les patients atteints de DFT présentent des troubles cognitifs et comportementaux ainsi qu'une atrophie des lobes frontaux et latéraux. Une proportion importante des patients DFT présente des agrégats de FUS cytoplasmique, mais la contribution de FUS dans le cytoplasme à la DFT reste inconnue. Nous avons voulu déterminer si une accumulation de FUS dans le cytoplasme était suffisante pour provoquer des symptômes typiques de la DFT et avons caractérisé le comportement de notre modèle knock-in hétérozygote. Dans un premier temps, des études de comportement ont révélé une hyperactivité à des âges très jeunes (à partir de 3 mois) ainsi que des défauts cognitifs et de comportement social tels qu'une perte de mémoire et une désinhibition respectivement. De plus, nous avons retrouvé une pathologie corticale liée spécifiquement à la présence de FUS délocalisé dans le cytoplasme dans les neurones corticaux ainsi que l'absence de TAF15 et/ou EWSR1. Nous avons détecté également des agrégats dans les neurones pyramidaux du cortex mais de façon surprenante, nous n'avons pas observé de perte neuronale. Néanmoins, notre modèle knock-in hétérozygote présente des anomalies des synapses corticales aux niveaux moléculaires et structurels, ainsi que des altérations d'excitabilité. Ces résultats mettent en évidence des altérations physiopathologiques liés à la DFT dans notre modèle murin *Fus* knock-in hétérozygote, comme des altérations moléculaires de FUS au sein de la synapse, des altérations structurelles des synapses, de la balance inhibitrice-excitatrice corticale ainsi que des défauts de comportement. Ces résultats sont rassemblés dans un manuscrit collaboratif dont je suis co-premier auteur.

Cytoplasmic FUS accumulation triggers cortical neuronal hyperexcitability and altered behaviour relevant to fronto-temporal dementia

Jelena Scekic-Zahirovic*, Inmaculada Sanjuan-Ruiz* et al.

Involved labs with major contributions: Dupuis, Dormann, Lagier-Tourenne, Liebscher

Contributing labs: Ludolph, Boutillier/Cassel

* shared first authors

Abstract

Cytoplasmic aggregates of methylated FUS, a RNA binding protein involved in many steps of RNA metabolism, are characteristic of amyotrophic lateral sclerosis with mutations in the FUS gene (ALS-FUS). Cytoplasmic FUS positive aggregates are also found in a subset of patients with fronto-temporal dementia (FTD), generally in the absence of FUS mutations (FTD-FUS patients). In FTD-FUS patients, however, cytoplasmic FUS is not methylated and is co-deposited with related proteins such as TAF15 and EWSR1. While the causal role of cytoplasmic FUS in FUS-ALS is well established, its driving role in FTD remains unclear. Here, we show that a partial cytoplasmic mislocalization of FUS in heterozygous Fus knock-in mice is sufficient to drive profound FTD related behavioural deficits. Spontaneous neuronal activity was strongly increased in the frontal cortex of Fus knock-in mice in vivo. This was accompanied by electron dense aggregates in pyramidal neurons of the frontal cortex, in the absence of neuronal cell loss. Partial cytoplasmic FUS mislocalization impaired expression of multiple genes related to neuronal function in the frontal cortex and led to synaptic ultrastructural defects. Thus, FUS cytoplasmic enrichment is sufficient to trigger synaptic defects, increased spontaneous neuronal activity and FTD-related phenotypes. These findings suggest that FUS mislocalization is driving the neurological symptoms in FTD-FUS patients through impairment of synaptic cortical structure and function.

Introduction

Two major neurodegenerative diseases, Amyotrophic lateral sclerosis (ALS) and fronto-temporal dementia (FTD) are the extreme clinical phenotypes of a pathophysiological continuum[1-3]. ALS is the major adult onset motor neuron diseases, with onset usually in the 6th decade of life and death of respiratory insufficiency and progressive paralysis 3 to 5 years after onset of motor symptoms [1-3]. FTD, the second most common form of dementia after Alzheimer's disease, mostly affects social and executive functions. ALS and FTD clinically overlap, with a subset of ALS patients later developing cardinal features of FTD, and vice versa[4-6]. Moreover, TDP-43 pathology, observed in 95% of ALS patients, is typically found in about half of FTD patients[7,8]. Last, mutations in a number of genes, such as *C9ORF72, TARDBP* or *TBK1*, are associated to either ALS, FTD or both, in the same families[1-3].

The involvement of FUS in both ALS and FTD is a striking example of the continuum between ALS and FTD. FUS is a mostly nuclear RNA-binding protein involved in most steps of RNA metabolism, from transcription, splicing, transport to translation[9,10]. Mutations in the *FUS* gene have been associated with the most severe forms of ALS[11,12], with young onset and rapid disease progression[13,14], but were only rarely observed in FTD patients. In *FUS*-ALS cases, the FUS protein is found methylated in characteristic cytoplasmic inclusions, with nuclear clearance of the protein[15]. Mutations in the *FUS* gene are clustered in the C-terminal region of the FUS protein that includes the atypical PY nuclear localization sequence, and the severity of the disease correlates with the degree of impairment of FUS nuclear import[15,16]. Indeed, the most severe cases of ALS known to date lead to the complete truncation of the PY-NLS[13,14]. FUS is also involved in FTD, although in most cases, this occurs in the absence of germline mutations in *FUS*. In about 10% of FTD cases with prominent atrophy of the caudate putamen[17-19], FUS is also found in cytoplasmic aggregates in the absence of TDP-43 or TAU pathology. These FTD-FUS aggregates are however distinct from ALS-*FUS* aggregates since FUS is there mostly unmethylated[15,20-23], and multiple other proteins, in particular the FUS related proteins TAF15 and EWSR1, are co-deposited with FUS in FTD-FUS aggregates [15,20-23].

Two major mechanisms have been postulated to participate in FUS-related neurodegeneration. First, FUS cytoplasmic accumulation, as a consequence of *FUS* mutations, might trigger adverse events leading to neuronal death, as a result of a so-called cytoplasmic gain of function. Second, clearance of FUS from the nucleus might lead to alterations in the many nuclear FUS functions, including transcription, splicing or DNA damage repair[9]. Multiple studies in mouse models converge at showing that accumulation of cytoplasmic FUS is necessary to lead to motor neuron degeneration in *FUS*-ALS[24-30]. For instance, heterozygous *Fus* knock-in mouse models with truncating mutations develop mild, late onset muscle weakness and motor neuron degeneration, but not haploinsufficient *Fus* knock-out mice, demonstrating that the presence of the protein in the cytoplasm is necessary to trigger motor neuron toxicity [28-30]. Contrastingly, most studies related to the

role of FUS in FTD focused on the role of nuclear loss of function. Loss of FUS alters splicing of multiple mRNAs relevant to neuronal function, such as *MAPT,* encoding the TAU protein, and alters stability of mRNAs encoding relevant synaptic proteins such as GluA1 and SynGAP1 [31-35] . Thus complete loss of FUS function is able to lead to synaptic alterations. However, such loss is only expected to occur in the very end stage of neuronal degeneration as nuclear FUS levels are very efficiently buffered by autoregulatory mechanisms. Indeed, heterozygous *Fus* knock-in mice, while bearing one allele leading to cytoplasmic, and not nuclear, FUS, only show limited loss of nuclear FUS as a consequence of compensatory overexpression[29,30]. To date, there are few studies investigating whether accumulation of cytoplasmic FUS might participate in FTD pathogenesis. Thus, while the causal role of FUS in FUS-ALS is well established, the driving role of FUS mislocalization in FTD remains unclear. Here, using knock-in mice, we show that partial cytoplasmic FUS mislocalization is sufficient to drive abnormal, FTD-relevant, behaviour. Moreover, cytoplasmic FUS leads to defects in synaptic structure and function, and identify a number of potential downstream mRNAs altered by the presence of cytoplasmic FUS and relevant to synaptic function.

Materials and methods

Mouse models and genotyping

Wild-type and heterozygous Fus$^{\Delta NLS}$ mice were generated as previously described [29]. All mice were bred and housed in the animal facility of the faculty of Medicine of the University of Strasbourg (France). Mice were kept on a regular 12h light/dark cycle starting at 7 am under constant conditions (21 ± 1ºC and 60% humidity). They were provided with standard laboratory rodent food and water *ad libitum*. Genotyping was performed from tail biopsies by PCR of genomic DNA as previously described [29]. Mice aged of 10 and 22 months were subjected to behavioral and molecular tests.

All mice experiments were approved by local ethical committee from Strasbourg University (CREMEAS) under reference number AL/27/34/02/13.

Mouse behavior

Actimetry

Mice locomotion and spontaneous activity was assessed in one session for 3 consecutive days. All mice were individually placed in transparent Makroton cages (42 x 26 x 15 cm) containing two infrared beams targeting on two photocells 2,5 cm above the cage floor level and 28 cm apart from each other. Mice activity was automatically recorded by a computer, starting at 5 pm followed by 2h of habituation, then 3 days of recording. The number of cage crossings was individually measured for each mouse [36].

Open field

This test was used to assess mice anxiety and locomotor activity. Mice were subjected to one session of 15 minutes in an open field arena of white plywood (72 x 72 x 36 cm), divided into 16 18x18 cm squares. The room was illuminated with a 600 lux light and the apparatus was cleaned between tests with ethanol 70º. Mice were placed in the center of the arena and recorded with a camera place above the apparatus, connected to a computer where the behavior was automatically analyzed with a tracking system (Ethovision, Noldus). Exploratory and anxiety behaviors were analyzed from the time spent in the center *vs*. the perimeter of the open field arena, whereas locomotor activity was measured from total distance traveled and velocity.

Dark/light box test

All mice were tested in during morning periods, for a total duration of 5 minutes. The apparatus used consisted in two PVC compartments of equal size (18,5 x 18,5 x 15 cm), one illuminated with 400 lux and the other opaque. Mice were first placed in the dark compartment and recorded during the test by a video camera situated 150 cm above the center of the cage. Post-hoc video analysis allowed to measure the latency before the first transition to the light compartment, the number of transitions between compartments and the time spent in each one of them[37].

Resident-intruder test

This test examines exploratory behavior directed at a new/unknown "stranger" mouse. Wild-type "stranger" mice were non-littermate to test mice. All mice were isolated between 5 to 7 days before the test. Mice were placed in the behavior room 30 min prior test for habituation. Resident test mice were placed in their home cage under a video camera recording system and were allowed to habituate for 1 min. A novel "stranger" mouse was placed in the opposite corner of the home cage and allowed to roam for 5 min. All mice interactions were recorded and analyzed post-hoc in a double-blinded manner.

3 chamber test

The 3 chamber test apparatus consists in a box (59 x 39,5 x 21,5 cm) with three compartments made of plexiglass, each one of 18,5 x 39,5 cm with a 7 x 7 cm square opening. Each two chamber sides contain a cylinder of 20 x 10 cm of diameter with 18 transparent plexiglass bars of 6mm apart from each other and an upper end black lid. Test mice and stranger mice were from the same background, age, gender and weight. All test mice were individually housed one week before tests and were allowed to habituate to the test room prior tests. Sessions were video recorded and analyzed post-hoc to measure the time spent in each compartment and the time spent interacting with the stranger mouse or the empty cylinder. The test consisted in five different trials of 5 minutes each one in three consecutive parts. The first part included trial 1, placing the mouse in the middle compartment allowing them to habituate and explore compartments with empty wire cages. The second part included trials 2 to 4, were sociability and social learning acquisition behaviors are observed by placing a stranger mouse (stranger 1) in a wire cage on one side. Increased time in the compartment with stranger 1 reveals preference for social stimulus. The third and last part of the test included trial 5, were social novelty, discrimination and recognition memory can be evaluated, and a novel stranger mouse (stranger 2) along with the stranger 1 are placed in wire cylinders, one on each side of the apparatus. Social novelty behavior can be measured by the discrimination of the test mouse between the familial stranger 1 and the novel stranger 2 mice. It is more expected that test mice spend more time with stranger 2, indicating working memory functions. Sociability is measured by the interactions of the test mouse during trials 2 to 5.

Olfactory test

This test allows the detection of odor scents deficiencies. Mice were individually habituated in an empty cage without bedding and confronted to two filter papers embedded with substances for 3 minutes. On one side they were exposed to one filter embedded with vanilla and water, on the other side with 2-methyl butyrate and water, where water was considered as a neutral scent. If mice spent more time exploring the filter embedded with scent than with water it was considered to be “attractive”, whereas if mice spent less time exploring the filter embedded with scent it was considered to be “repulsive”. Total exploratory behavior was video recorded and analyzed post-hoc.

Morris water maze

A circular pool of 160 cm of diameter and 60 cm of height filled with water at 21 ± 1ºC rendered opaque by adding powdered milk (1,5 g/L) was used to perform this test. The first day consisted in one 4 trial session of 60 seconds with a visible black platform of 11cm of diameter protruding 1 cm above water surface. The pool was surrounded by a curtain to avoid any spatial clue. The following days the curtain was removed and a 5 days training period started consisting in 4 consecutive trials per day with a maximum duration of 60 seconds and inter-trail intervals of 10-15 seconds, where the platform was hidden in a different quadrant as the first day and mice started the tests at different random localization points at the pool edge. Mice were then tested for retention in an 18 days delay probe trial and two extinction tests, the first being 2h after the probe trial and the second 2 hours after the first extinction test. During probe trial the platform was removed, and mice were set to start the test from a different localization point of the pool edge they were never placed before for 60 seconds. The analysis was performed with a computer video tracking system (SMART; PanLab), where distance travelled, latency before reaching the platform and average speed were measured in the visible platform and trials, whereas time in % in the target quadrant was measured in probe trial and extinction trials.

Electrophysiological recordings

Animals

Both male and female *Fus*$^{+/+}$ and *Fus*$^{\Delta NLS/+}$ mice[30] were either housed alone or with siblings in groups of two. Mice were in standard cages with bedding and nesting material, under a 12h light/dark cycle. In total, 3 *Fus*$^{+/+}$and 6 *Fus*$^{\Delta NLS/+}$ mice were included in the study. All experimental procedures were conducted in accordance with a protocol approved by the local authorities (Regierung von Oberbayern).

Cranial window implantation and virus injection

At 9 months of age (+/- 10 days), AAV2/1.Syn.GCaMP6m.WPRE.SV40 (addgene, diluted 1:6 with saline) was slowly injected into the primary motor cortex (M1) of both *Fus*$^{+/+}$ and *Fus*$^{\Delta NLS/+}$ mice, followed by the implantation of a cranial window, as described previously [38]. In brief, mice were first anesthetized with Fentanyl (0.05mg/kg), Midazolam (5.0mg/kg) and Metedomidin (0.5mg/kg). A circular craniotomy with a 2mm radius, centered on M1 (1.7mm lateral and 0.8mm anterior to bregma), was performed, followed by the injection of a total of ~1ul of the calcium indicator into three sites (~300nl per site at 600µm depth). A 4mm glass cover slip was placed over the cortex and sealed with UV durable dental acrylic (Venus Diamond Flow, Heraeus Kulzer GmbH). A metal head bar was attached to the skull with dental acrylic (Paladur, Heraeus Kulzer GmbH), allowing stable access for the two-photon microscopy during imaging.

Two-photon imaging in anesthetized mice

Four weeks following the cranial window implantation, *in vivo* two-photon imaging was performed within layer 2/3 of M1 using a two-photon microscope (Hyperscope, Scientifica), equipped with an 8kHz resonant scanner, at frame rates of 30Hz and a resolution of 512x512 pixels. Using a 16x water-immersion objective (Nikon), stacks of 15,000 frames (equivalent to ~8 minutes) were acquired covering a field of view of 300x300 µm. Light source was a Ti:Sapphire laser with a DeepSee pre-chirp unit (Spectra Physics MaiTai eHP), as described previously (Liebscher et al., 2016). GCaMP6m was excited at 910nm, with a laser power not exceeding 40mW (typically 10 to 40mW), and a photomultiplier tubes (Hyperscope, Scentifica) were used to detect the emitted light using a 525/50nm band-pass filter. In each mouse, two regions at depths of 140 to 310 µm were imaged, yielding 350 cells in FUS$^{+/+}$ (n = 6 experiments) and 855 cells in FUS$^{dNLS/+}$ mice (n = 14 experiments). During imaging, mice were anesthetized with 1.5% isoflurane in pure O_2 at a flow rate at ~0.5L/min, to maintain a respiratory rate in the range of 110 to 130 breaths per minute. Body temperature was maintained at 37 degrees using a physiological monitoring system (Harvard Apparatus).

Image processing and data analysis

All image analyses were performed in Matlab (Math Works) using custom-written routines [38]. In brief, full frame images were motion corrected, and regions of interests (ROIs) were semi-automatically selected based on the maximum and mean projections of all frames. Fluorescence signals of all pixels within a selected ROI were averaged and the intensity traces were low pass filtered at 10Hz. Contamination from neuropil signals was accounted for, as described previously (Liebscher et al., 2016), using the following equation:

$F_{ROI\_comp} = F_{ROI} – 0.7 \times F_{neuropil} + 0.7 \times \text{median}(F_{neuropil})$

F_{ROI_comp} stands for neuropil-compensated fluorescence of the ROI, F_{ROI} and $F_{neuropil}$ represent the initial fluorescence signal of the ROI and the signal from the neuropil, respectively. A neuron was defined as 'active' if it displayed at least one prominent calcium transient over 20 frames (corresponding to ~0.7 seconds).

Statistics

The student's t-test was employed to compare the fraction of active cells, and the Kolmogorov-Smirnov (KS) test was used to analyze the distributions of transient frequency and amplitude.

Histological techniques

Mice were anesthetized with intraperitoneal injection of 100 mg/kg ketamine chlorhydrate and 5mg/kg xylazine then perfused with PFA 4%. After dissection, brain was included in agar 4% and serial cuts of 40µm thick were made with vibratome.

Peroxydase immunohistochemistry

For peroxidase immunohistochemistry, endogenous peroxidases were inactivated 10min with H2O2 3% then slides were washed with PBS 1x and incubated overnight with rabbit anti-FUS antibody (ProteinTech, 11570-1-AP, 1:100) at room temperature. After rinsing in PBS, anti-rabbit biotinylated (Jackson, 711-067-003, 1/500) was incubated 2h at room temperature. The staining was revealed using the ABC kit (Vectastain ABC kit, PK-6100, Vector Laboratories Inc.) during 1h. After 3 washes with PBS, slides were rinse in water and mounted in DPX (Sigma, O6522) and observed with ZEISS Apotome.

Electron microscopy

Mice were anesthetized with intraperitoneal injection of 100 mg/kg ketamine chlorhydrate and 5mg/kg xylazine and transcardiacally perfused with glutaraldehyde (2.5% in 0.1M cacodylate buffer at pH 7.4). Brains were dissected and immersed in the same fixative overnight. After 3 rinses in Cacodylate buffer (EMS, 11650), muscles were post fixed in 0.5% osmium and 0.8% potassium ferrocyanide in Cacodylate buffer 1h at room temperature. Finally, tissus were dehydrated in graded ethanol series and embedded in Embed 812 (EMS, 13940). The ultrathin sections (50 nm) were cut with an ultramicrotome (Leica, EM UC7), counterstained with uranyl acetate (1% (w/v) in 50% ethanol) and observed with a Hitachi 7500 transmission electron microscope (Hitachi High Technologies Corporation, Tokyo, Japan) equipped with an AMT Hamamatsu digital camera (Hamamatsu Photonics, Hamamatsu City, Japan).

RNAseq

RNAseq on frontal cortex was performed as previously described29,30. Briefly, RNA from cortex of 22 months old Fus ΔNLS/+ mice and their control littermates were extracted with TRIzol (Invitrogen). RNA quality was measured using the Agilent Bioanalyzer system or RNA screenTape (Agilent technologies) according to the manufacturer's recommendations. Samples were processed using the Illumina TruSeq single Stranded mRNA Sample Preparation Kit according to manufacturer's protocol. Generated cDNA libraries were sequenced using an Illumina HiSeq 2000 sequencer with 4–5 biological replicates sequenced per condition using single read, 50 cycle runs.

Quality of sequencing reads was assessed using FastQC (Babraham Bioinformatics) and then aligned to a mouse reference genome (mm9, UCSC Genome Browser) using Transcripts Alignment to a Reference (STAR) (v2.4.01). Sequencing yielded, on average, 40 million non-redundant reads per sample with a 70% mapping rate. FeatureCounts was used to assign reads to genes, and then the Deseq v2.1.1 package was used was used to generate transcript abundance for each annotated protein-coding gene as fragments per kilobase of transcript per million mapped reads (FPKM), and statistical analysis and comparison of FPKM values were calculated.

Genomewide unsupervised clustering analysis and heat maps with significant changes between different groups were generated using R (Bioconductor).

Gene set enrichment in up and down regulated genes over background annotated genes covering library of gene ontologies, databases and pathways was analyzed by using DAVID.

Statistics

All results from analysis are presented as mean ± standard error of the mean (SEM) and differences were considered significant when $p < 0.05$. Significance is presented as follows: * $p<0.05$, ** $p<0.01$, and *** $p<0.001$. For comparison of two groups, two-tailed unpaired Student's t –test was used in combination with F-test to confirm that the variances between groups were not significantly different. Data were analyzed by using the GraphPad Prism version 6.0.

Results

Spontaneous hyperactivity in Fus$^{\Delta NLS/+}$ mice.

Since FUS mislocalization and aggregation are also observed in a subset of FTD patients, we hypothesized that partial FUS cytoplasmic mislocalization in Fus$^{\Delta NLS/+}$ mice could be sufficient to lead to FTD-like phenotypes. Indeed, in the cortex of Fus$^{\Delta NLS/+}$ mice, FUS, but not TAF15, showed cytoplasmic mislocalization (**Supplementary figure 1A, B**). To examine FTD phenotypes in our mice, we performed behavioral analyses at 4 and 10 months old mice, before the appearance of motor impairment[30]. We first assessed spontaneous locomotor activity in the home cage as FTD patients can present disinhibitions and restlessness. Evaluation of basal motor activity in a familiar environment showed significantly increased locomotor activity in Fus$^{\Delta NLS/+}$ mice over the 3 consecutive days of observation (**Figure 1A, B**). Interestingly, this hyperactivity was observed through the entire night in 4 months old Fus$^{\Delta NLS/+}$ mice (**Figure 1A**), but only at late night in older Fus$^{\Delta NLS/+}$ mice (**Figure 1B**). Hyperactivity was not caused by reduced anxiety since Fus$^{\Delta NLS/+}$ mice showed similar preference for peripheral quadrants over central quadrants as Fus$^{+/+}$ mice in the open field test. Moreover, Fus$^{\Delta NLS/+}$ mice showed similar movement distances, durations, and speed compared to wild type littermates indicating absence of hyperactivity in the novel environment and during the day light period (**Supplementary figure 2A, B, C, D**). To further confirm the lack of anxiety related phenotype in Fus$^{\Delta NLS/+}$ mice we used the dark/light box, a test based on the preference of mice for dark compartments over illuminated places. In this test, Fus$^{\Delta NLS/+}$ mice and Fus$^{+/+}$ mice showed similar latency to enter, similar frequency of transitions and similar time duration to explore illuminated compartment (**Supplementary figure 2E, F, G**). Thus, Fus$^{\Delta NLS/+}$ mice are hyperactive but not anxious.

Social disinhibition in Fus$^{\Delta NLS/+}$ mice.

Marked changes in personality and social behavior such as social withdrawal or social disinhibition, obsessive-compulsive behaviors, euphoria or apathy are common in subjects with bvFTD[6,36,37]. Social deficits were also reported in progranulin haploinsufficient mice, an independent mouse model of FTD[4]. To determine whether our mice have disease-relevant social behavioral deficits, we first performed the resident-intruder test specific for evaluating sociability in mice. Interestingly, 10 months old Fus$^{\Delta NLS/+}$ mice interacted significantly longer with the intruder mouse as compared with Fus$^{+/+}$ mice and a trend towards a similar phenotype was observed at 4 months of age (p= 0.07) (**Figure 1C, D E, F**). To further characterize the social behavioral impairment, we used a modified version of the three-chamber social paradigm. After a first trial of habituation using an empty set up, a novel mouse is introduced in a side compartment. The interactions initiated by the test mouse with either the novel mouse or the empty cage were quantified. Of most relevance, across the three consecutive

trials (Trial 2, 3 and 4), we observed that 10 months $Fus^{\Delta NLS/+}$ mice consistently interacted more with the novel mouse than Fus+/+ mice, further confirming social disinhibition (**Figure 1G**). This was not observed at 4 months of age (**Figure 1I**). Importantly, mice of both genotypes spent more time interacting with the novel mouse than with the empty cage mice, indicating that mice could recognize its conspecific. The interaction time gradually decreased in later trials, suggesting progressive loss of social interest in the novel mouse while it becomes a familiar mouse (**Figure 1G**). In a Trial 5, both a familiar mouse (that was used in previous trials) and a second novel mouse were introduced in the two side compartments. While 10 months old $Fus^{+/+}$ mice spent more time interacting with the novel mouse than with the familiar mouse, $Fus^{\Delta NLS/+}$ mice spent almost the same amount of time with the novel mouse as with that of the familiar mouse suggesting decreased social memory (**Figure 1J**). Younger 4 months old mice failed to distinguish novel and familiar mice (**Figure 1H**). Yet, exploration pattern, defined as time spent in each chamber during trials, was similar between genotypes (**Supplementary figure 2H, I**). Furthermore, the olfactory function of $Fus^{\Delta NLS/+}$ mice was preserved, since results showed no differences between genotypes at 10 months of age in the time spent sniffing filter paper covered with either attractive scent (vanilla) or an aversive scent (2-methyl butyrate) (**Supplementary figure 2J**). These findings together with absence of major motor phenotype at that age (**Supplementary figure 2B, C**) indicated that social behavior is selectively affected in $Fus^{\Delta NLS/+}$ mice.

Executive dysfunction in $Fus^{\Delta NLS/+}$ mice.

To further explore the possibility that a subset of phenotypes of $Fus^{\Delta NLS/+}$ mice is associated with frontal lobe dysfunction, we tested spatial reference memory in the Morris water maze. This task requires the hippocampal function, at least during acquisition and to form a recent memory, but relies on a proper (fronto)cortico-hippocampal dialog for longer retention times or remote memory[38]. As shown in $Fus^{\Delta NLS/+}$ mice displayed a significant acquisition regarding distance travel and latency to find hidden platform over training days similar to their $Fus^{+/+}$ littermates (**Supplementary figure 2K, L, M**). We then performed a probe trial 18 days after the last training followed by two extinction tests and observed that $Fus^{\Delta NLS/+}$ mice displayed a significantly decreased performance at this retention time point (**Figure 1K**). Furthermore, $Fus^{\Delta NLS/+}$ mice extinguished their previous memory much faster than wild type mice as an extinction test performed 2 hours after the probe trial showed a weaker memory trace in wild type mice, while $Fus^{\Delta NLS/+}$ mice did not show a performance superior to chance (**Figure 1L**), and this was maintained in a second extinction test (**Figure 1M**). Altogether, these data show that $Fus^{\Delta NLS/+}$ mice are able to learn, but display alterations in the persistence of remote memory consolidation in agreement with a dysfunction in the fronto-cortical regions.

In summary, behavioral analyses in $Fus^{\Delta NLS/+}$ mice unraveled hyperactivity, selective impairment in sociability (or social interactional deficits), social memory dysfunction, cognitive defect and altered memory consolidation thus recapitulating several of the key clinical symptoms FTD. This suggests that the partial cytoplasmic mislocalization of FUS is sufficient to trigger behavioral FTD phenotypes.

Increased spontaneous neuronal activity in $Fus^{\Delta NLS/+}$ mice in vivo.

As the behavioral changes we observed are highly reminiscent of frontal lobe dysfunction, we next asked whether neuronal activity indeed is altered within that brain area. We thus examined spontaneous neuronal activity by means of in vivo two-photon calcium imaging (**Figure 2A-C**). In particular, we studied neurons in cortical layer 2/3 of the frontal cortex expressing the genetically encoded calcium indicator GCaMP6m, in mice at the age of 10 months (**Figure 2B**). Indeed, we observed a massive increase in spontaneous activity levels as seen in a larger fraction of active cells in $Fus^{\Delta NLS/+}$ (**Figure 2D**, p = 0.003, student's t-test, n = 14 experiments in $Fus^{\Delta NLS/+}$ mice and n = 6 experiments in $Fus^{+/+}$ mice). Moreover, we observed a right shift in the distribution of the transient amplitudes (**Figure 2E**, p = 0.005, KS test) and also in the transient frequency (**Figure 2F**, p = 8.4x10-11, KS test) in $Fus^{\Delta NLS/+}$ mice compared to their $Fus^{+/+}$ littermates (n = 350 neurons in $FUS^{+/+}$, n = 855 neurons in $Fus^{\Delta NLS/+}$ mice). Taken together, our data demonstrate a strong increase in neuronal activity in vivo within the frontal cortex of $Fus^{\Delta NLS/+}$ mice.

$Fus^{\Delta NLS/+}$ mice lack obvious loss of neurons.

In order to determine whether the observed phenotypes could be linked to neurodegeneration in the frontal cortex, we then performed brain histology in $Fus^{\Delta NLS/+}$ mice at both 10 and 22 months of age. Cortical histology appeared preserved in $Fus^{\Delta NLS/+}$ mice, with normal lamination and no cortical thinning. The density of NeuN positive, of VGlut2 positive or of GABA positive neurons in the frontal cortex were similar between $Fus^{\Delta NLS/+}$ mice and their wild type littermates at 22 months of age (**Figure 3**). Electron microscopy in pyramidal neurons of the frontal cortex however revealed that $Fus^{\Delta NLS/+}$ pyramidal neurons accumulated proteinaceous electron dense aggregates, that were not observed in wild type littermates (**Figure 4**). These data suggest that the behavioral phenotypes observed in $Fus^{\Delta NLS/+}$ mice result primarily from neuronal dysfunction rather than from neuronal loss.

Transcriptome of $Fus^{\Delta NLS/+}$ cortex and ultrastructural analysis points to defects in inhibitory synapses.

To understand the molecular basis of neuronal dysfunction, we then performed RNAseq on frontal cortex of 22 months old FusΔNLS/+ mice and their wild type littermates. Principal component analysis showed a clear separation between the 4 FusΔNLS/+ mice and their wild type littermates (**Figure 5A**), supporting the existence of RNA expression dysregulation. Statistical comparison identified 75 genes upregulated and 322 genes downregulated in FusΔNLS/+ mice (**Figure 5B, C, D**). Several axonal and dendritic protein coding genes were identified among significantly upregulated genes including the ionotropic glutamate receptor subunit Grin2a, as well as mRNAs encoding synaptic vesicle proteins such as synaptotagmin 2 (Syt2) or Vamp1 (**Figure 5E**). Gene ontology analysis of downregulated genes revealed significant enrichment for glycoproteins (FDR=1.04 10-19), signal peptides (FDR=2.15 10-12), plasma membrane (FDR=4.26 10-6) and extracellular matrix proteins (FDR=1.74 10-8). Downregulated genes included numerous genes encoding for proteins from the solute carriers family (**Figure 5F**). Notably, the Gad1 transcript encoding the GABA synthetizing enzyme Glutamate decarboxylase was downregulated in cortex of FusΔNLS/+ mice (**Figure 5D**). Thus, gene expression of multiple genes related to neuronal function, and in particular of inhibitory interneurons, was altered in the frontal cortex of 22 months old FusΔNLS/+ mice. In order to independently confirm the existence of an inhibitory synaptic defect in FusΔNLS/+ frontal cortex, we performed ultrastructural analysis of inhibitory synapses in layers II/III of the frontal cortex identified by the presence of mitochondria on both synaptic compartments (**Figure 6**). Wild type inhibitory synapses displayed densely packed synaptic vesicles close to the active zone. Contrastingly, FusΔNLS/+ inhibitory synapses showed disorganized synaptic vesicles, distant from the active zone. In all, our data point to defects in inhibitory synapses, that might cause the increased spontaneous neuronal activity and subsequent FTD-related behavioural abnormalities in FusΔNLS/+ mice.

Figures and legends

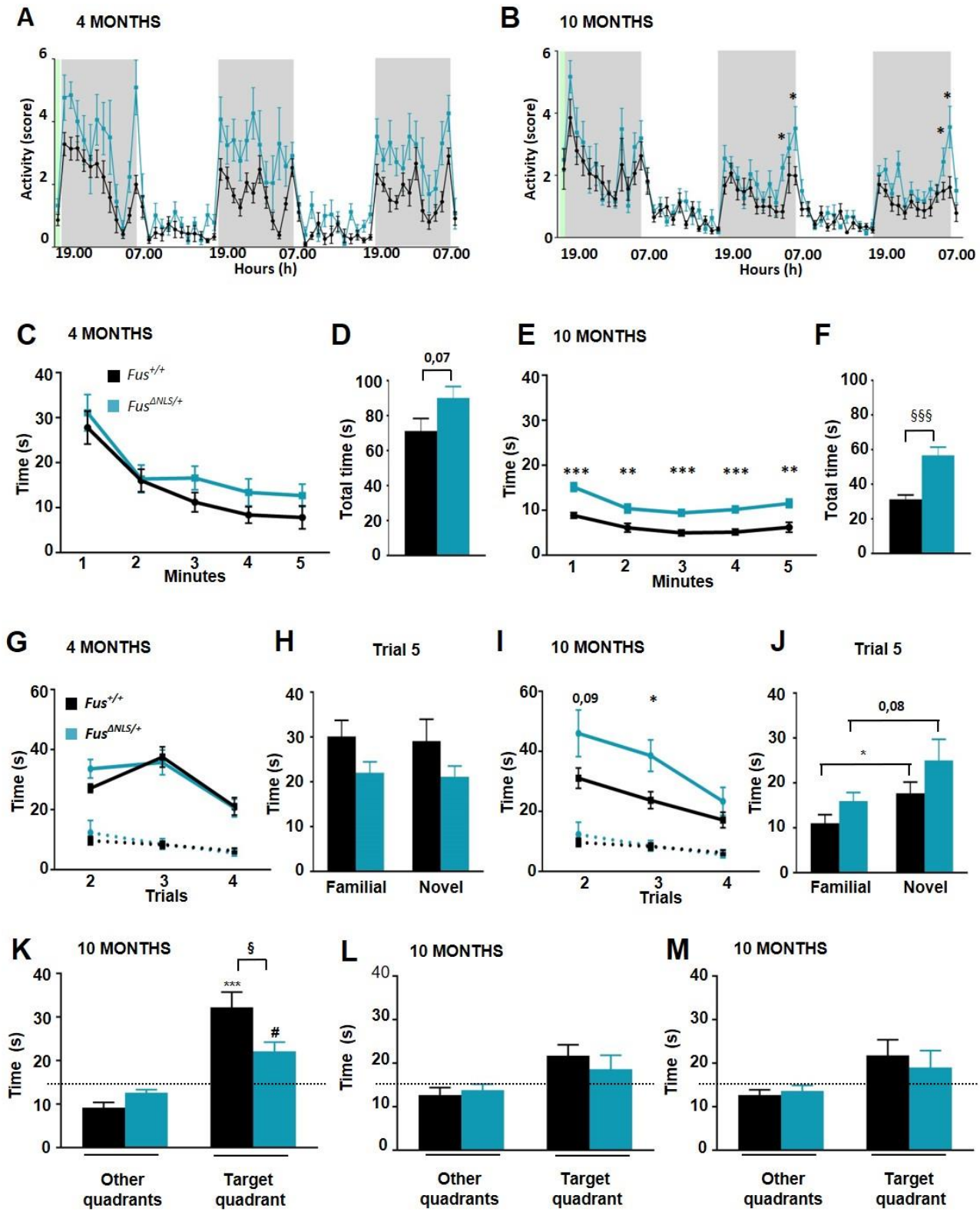

Figure 1: FTD-like behavioural abnormalities in $Fus^{\Delta NLS/+}$ mice.

A-B: Spontaneous home cage activity – actimetry at 4 months (A) and 10 months (B) of old $Fus^{+/+}$(black lines) and $Fus^{\Delta NLS/+}$ (blue lines) mice. N=11 for 4 months; N=15 for 10 months

C-F: Interaction time between mice during resident intruder test in home cage task at 4 (C, D) and 10 (E, F) months old. The difference in interaction time shows age-dependent impaired social behavior. N=9 for 4 months; N=14 for 10 months; (*) $p<0.05$, (***) $p<0.01$ with respect to Fus+/+; Two-way ANOVA followed by Tukey post hoc test.

G-J: Three chamber test at 4 months (G) and 10 months (I). Time exploring empty wired cage across trials is represented as dashed lines. N=9 for 4 months; N=14 for 10 months; Two-way ANOVA. Interaction time spent with Familial or Novel mice in Trial 5 at 4 months (H) and 10 months (J) mice. N=15 for 10 months; N=10 for 22 months. All values are mean and standard errors. N=9 for 4 months; N=14 for 10 months; Two-way ANOVA.

(K) Cognitive defect in FusΔNLS/+mice at months of age. The time spent in the target quadrant (target) is represented and compared with the average of the time spent in the three other quadrants (others). Chance is shown as a dashed line (15s per quadrant; i.e.25%). N=10. (§) One-way ANOVA genotype effect F(1,19)=6,33, p=0,02 ; Student t test comparison to chance level (*)Target quadrant: $Fus^{+/+}$=0,0008 Mean 3 others: . $Fus^{+/+}$=0,0008 Target quadrant: $Fus^{\Delta NLS/+}$ =0,006 Mean 3 others: $Fus^{\Delta NLS/+}$ =0,005

(L-M) Two extinction test: the first 2 hours after completing probe trial and the second 2 hours after the first.

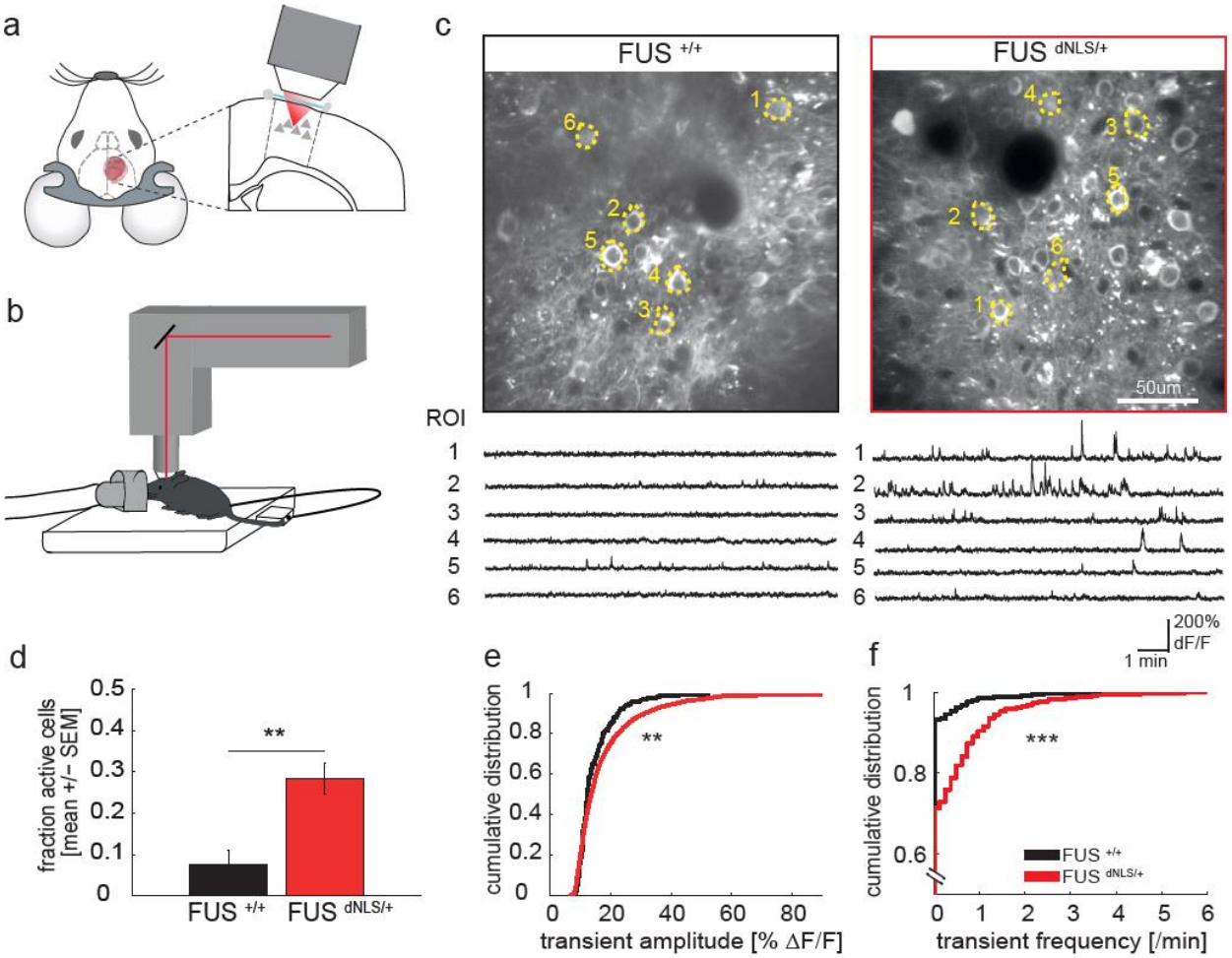

Figure 2: Assessment of neuronal activity in Fus$^{\Delta NLS/+}$ mice in vivo.

a: Scheme of the cranial window above motor cortex along with head bar implantation.

b: Two-photon imaging setup for anesthetized mice. A head-fixed mouse under a two-photon microscope receiving isoflurane, while resting on a physiological monitoring system including body temperature regulation

c: Top: Representative examples of field of views recorded in layer 2/3 of motor cortex in Fus$^{+/+}$ (left) and Fus$^{\Delta NLS/+}$ (right) mice. Bottom: Activity traces of selected neurons outlined in dashed yellow lines in the images above are shown.

d: The fraction of active cells is shown (black - Fus$^{+/+}$, red - Fus$^{\Delta NLS/+}$).

e: Cumulative distributions of calcium transient amplitudes in both genotypes.

f: Cumulative distributions of transient frequencies is shown. Data in (d) are mean +/- SEM, **P < 0.01, *** P < 0.001.

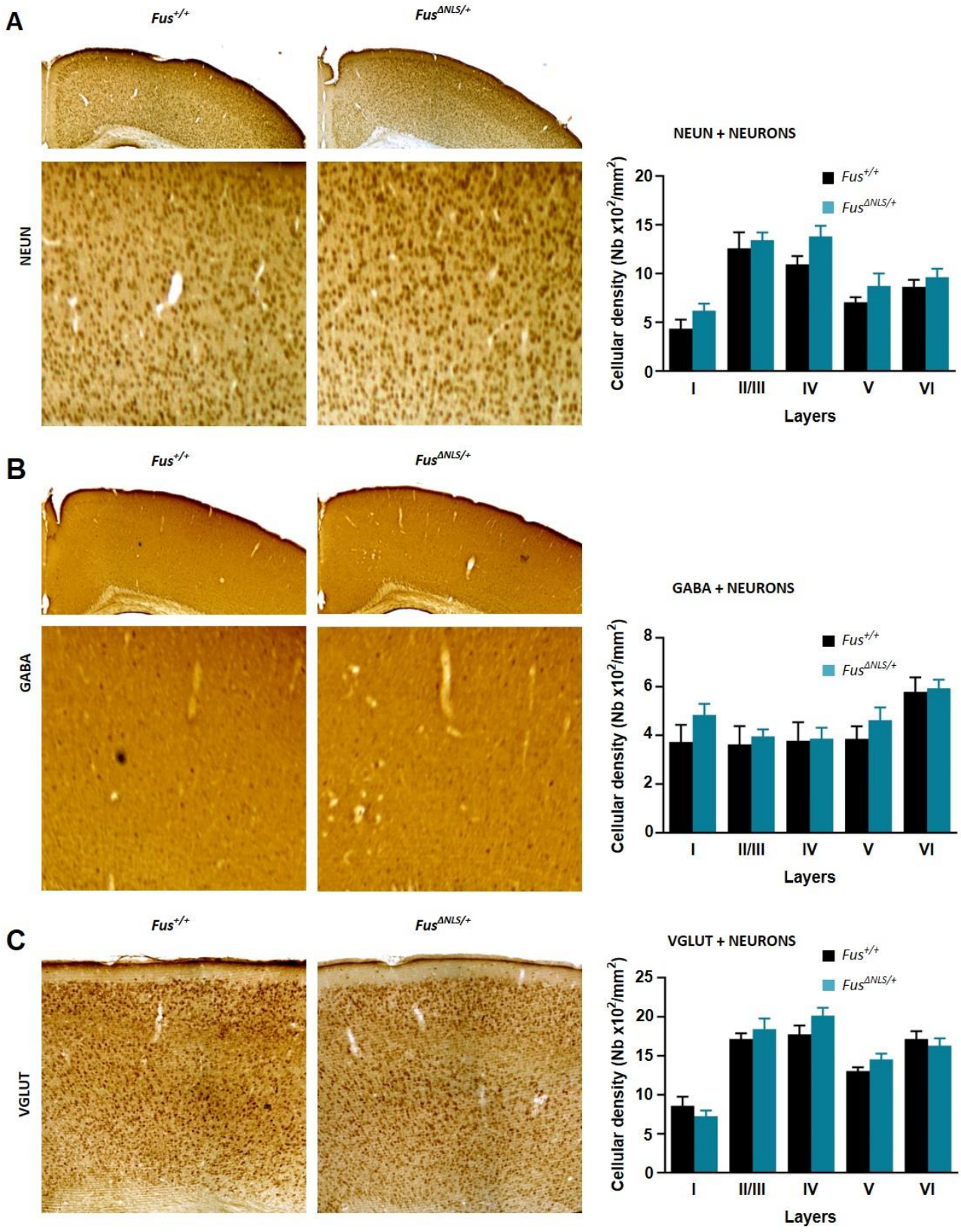

Figure 3: Fus$^{\Delta NLS/+}$ mice lack obvious loss of neurons.
Immunohistochemistry quantification of cortical neurons in Fus$^{+/+}$ (left images; black histogram bars) and Fus$^{\Delta NLS/+}$ (right images; blue histogram bars) mice of 22 months of age for: A: NeuN+ neurons; B: GABA+ neurons; and C: VGluT+ neurons.

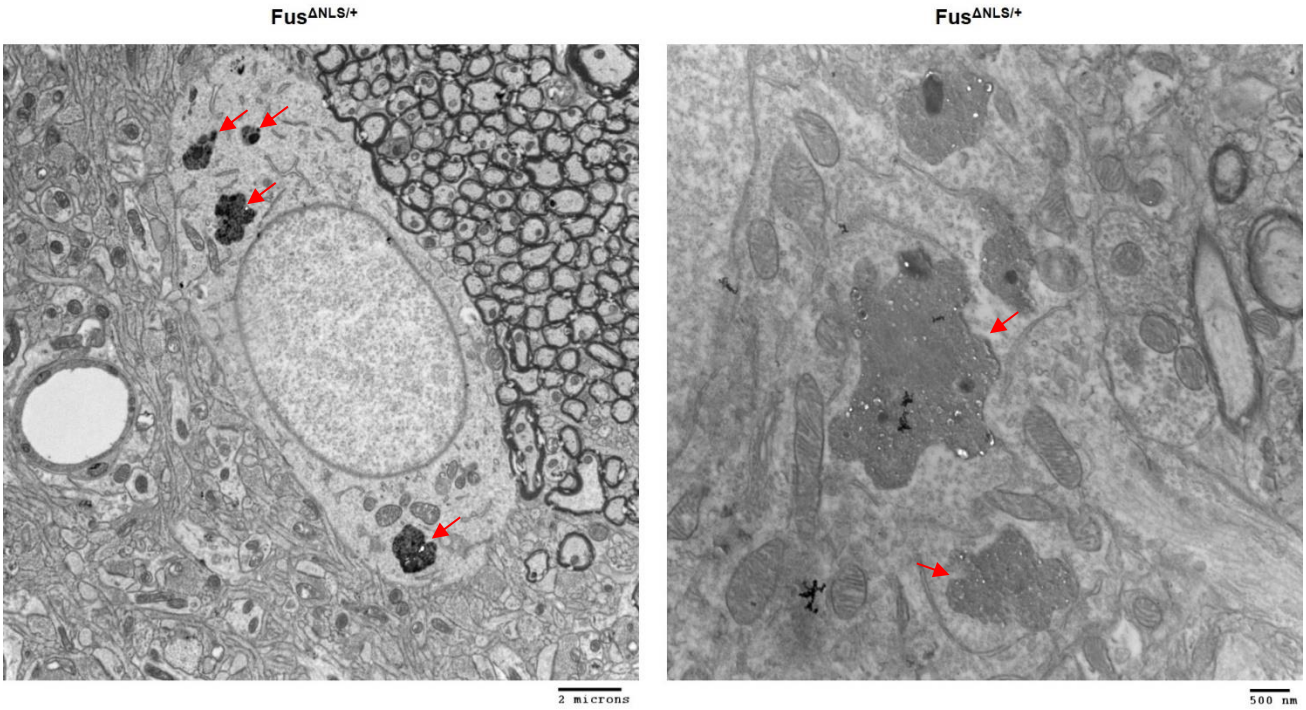

Figure 4: Protein aggregates in Fus$^{\Delta NLS/+}$ pyramidal neurons of the frontal cortex.
Pyramidal neurons of Fus$^{\Delta NLS/+}$ mice in the frontal cortex present protein aggregates in their cytosol (red arrows; left image). These aggregates appear to be dense membraneless structures (red arrows; right image).

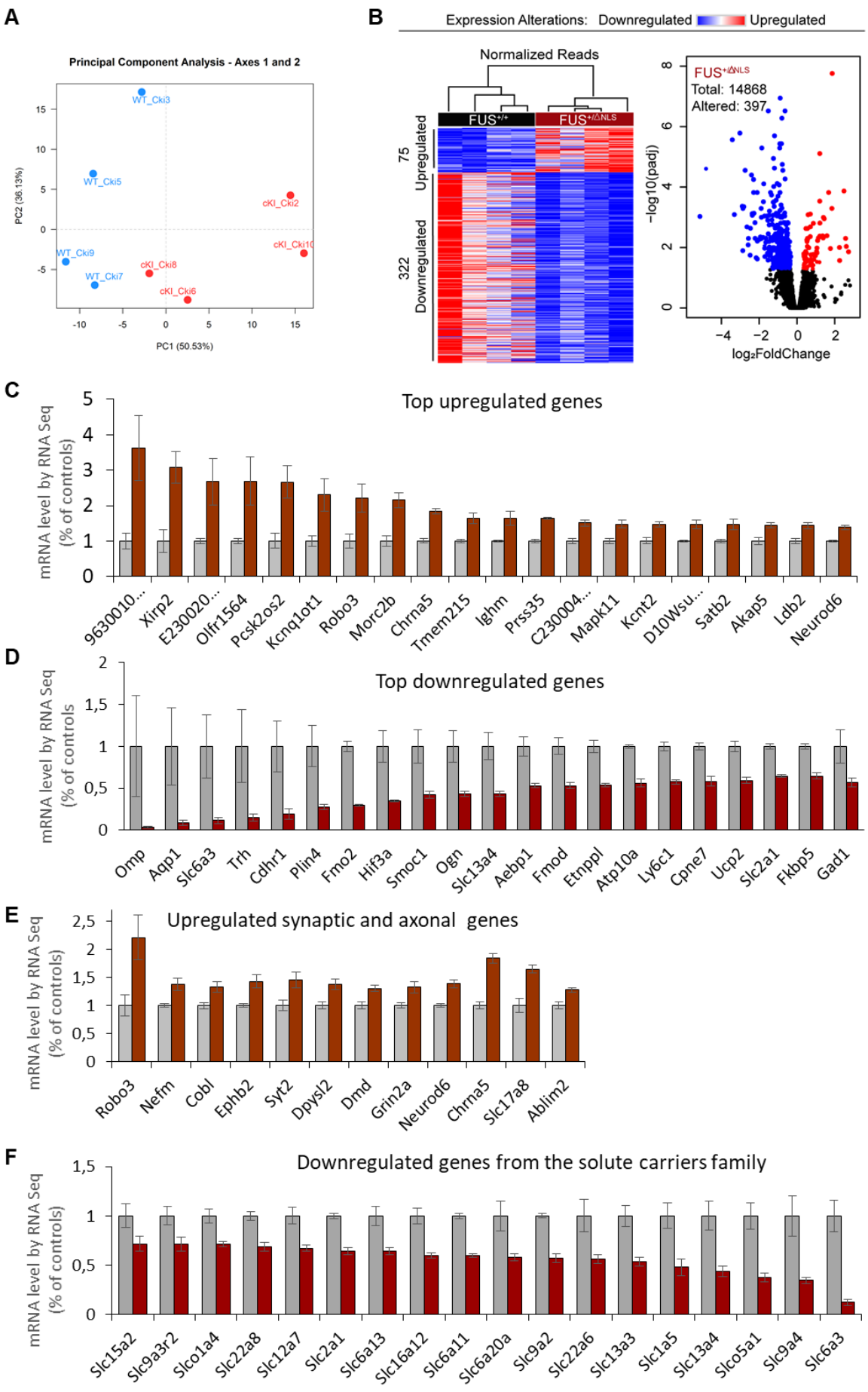
A
Principal Component Analysis - Axes 1 and 2
WT_Cki3
WT_Cki5
WT_Cki9
WT_Cki7
cKI_Cki2
cKI_Cki10
cKI_Cki8
cKI_Cki6
PC2 (36.13%)
PC1 (50.53%)
B
Expression Alterations: Downregulated Upregulated
Normalized Reads
FUS+/+
FUS+/ΔNLS
75 Upregulated
322 Downregulated
FUS+/ΔNLS
Total: 14868
Altered: 397
−log10(padj)
log2FoldChange
C
Top upregulated genes
mRNA level by RNA Seq (% of controls)
9630010...
Xirp2
E230020...
Olfr1564
Pcsk2os2
Kcnq1ot1
Robo3
Morc2b
Chrna5
Tmem215
Ighm
Prss35
C230004...
Mapk11
Kcnt2
D10Wsu...
Satb2
Akap5
Ldb2
Neurod6
D
Top downregulated genes
mRNA level by RNA Seq (% of controls
Omp
Aqp1
Slc6a3
Trh
Cdhr1
Plin4
Fmo2
Hif3a
Smoc1
Ogn
Slc13a4
Aebp1
Fmod
Etnppl
Atp10a
Ly6c1
Cpne7
Ucp2
Slc2a1
Fkbp5
Gad1
E
Upregulated synaptic and axonal genes
mRNA level by RNA Seq (% of controls)
Robo3
Nefm
Cobl
Ephb2
Syt2
Dpysl2
Dmd
Grin2a
Neurod6
Chrna5
Slc17a8
Ablim2
F
Downregulated genes from the solute carriers family
mRNA level by RNA Seq (% of controls)
Slc15a2
Slc9a3r2
Slco1a4
Slc22a8
Slc12a7
Slc2a1
Slc6a13
Slc16a12
Slc6a11
Slc6a20a
Slc9a2
Slc22a6
Slc13a3
Slc1a5
Slc13a4
Slco5a1
Slc9a4
Slc6a3

Figure 5: Transcriptome alterations in $Fus^{\Delta NLS/+}$ mice.
A: Principal component analysis of $Fus^{+/+}$ and $Fus^{\Delta NLS/+}$
B: Heatmap of upregulated and downregulated genes
C: Top upregulated mRNA genes
D: Top downregulated mRNA genes
E: Upregulated mRNAs of synaptic and axonal genes
F: Downregulated mRNAs from solute carriers family genes

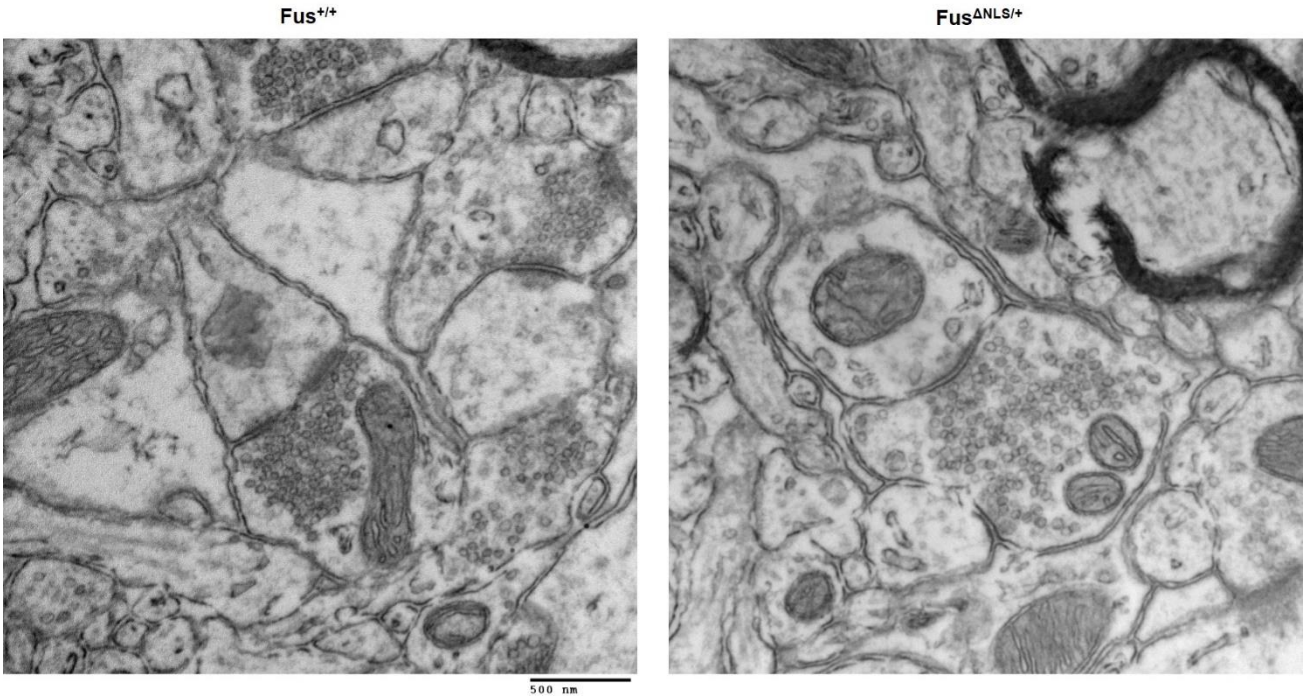

Figure 6: Ultrastructural defects in inhibitory synapses of $Fus^{\Delta NLS/+}$ mice.
Inhibitory synapses in $Fus^{+/+}$ mice aged of 22 months present a defined synaptic pool of vesicles near the active zone of the synaptic cleft (left image). $Fus^{\Delta NLS/+}$ mice inhibitory synapses present a more dispersed disposition of synaptic vesicles with a less defined pool near the active zone of the synaptic cleft (right image).

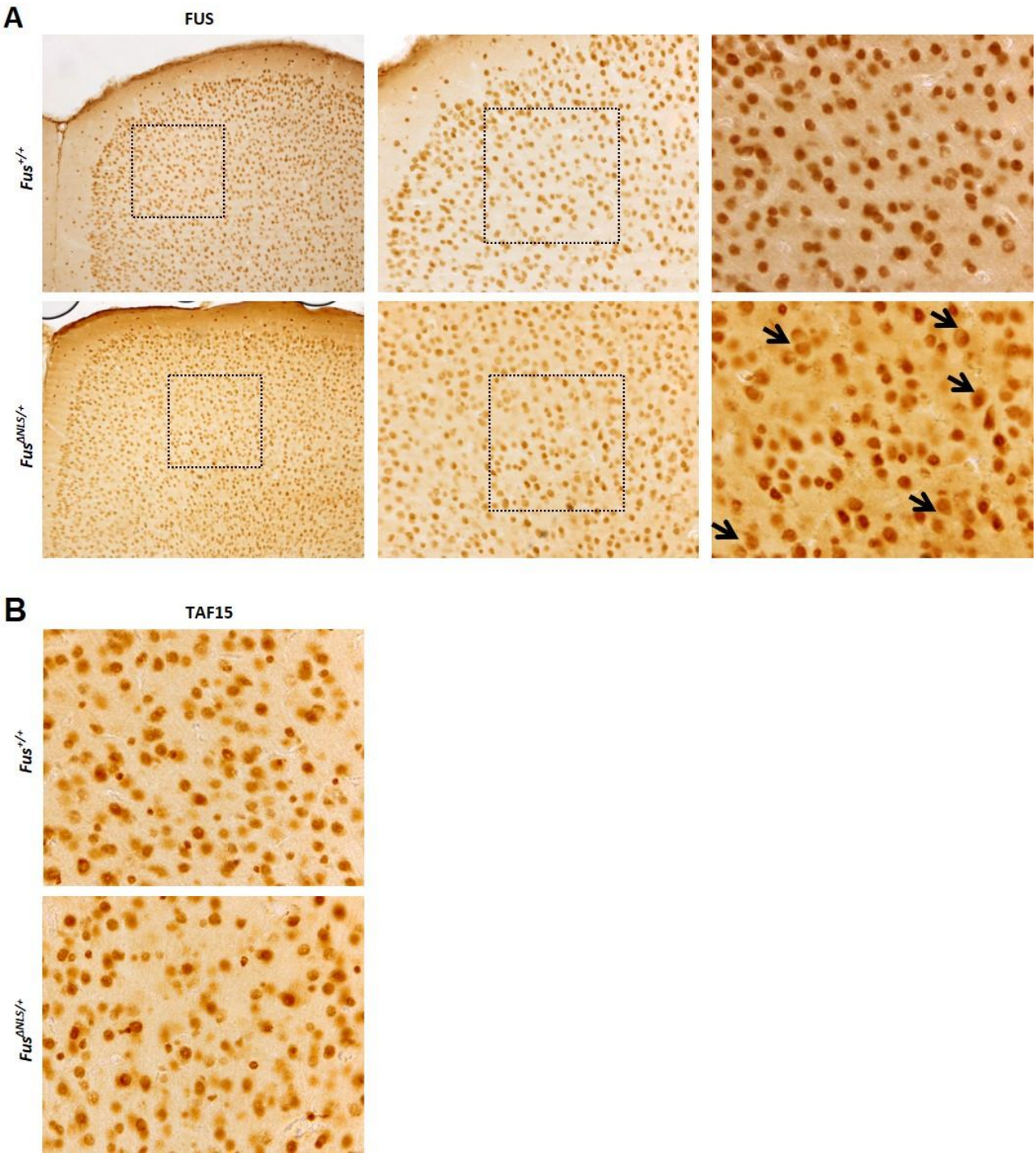

Supplementary figure 1: FET proteins immunoreactivity in Fus$^{\Delta NLS/+}$ frontal cortex.
Representative images of cortex showing mislocalization of FUS (A) (arrowheads) but not TAF15 (B) into the cytoplasm in neuronal cells in FusΔNLS/+ mice.

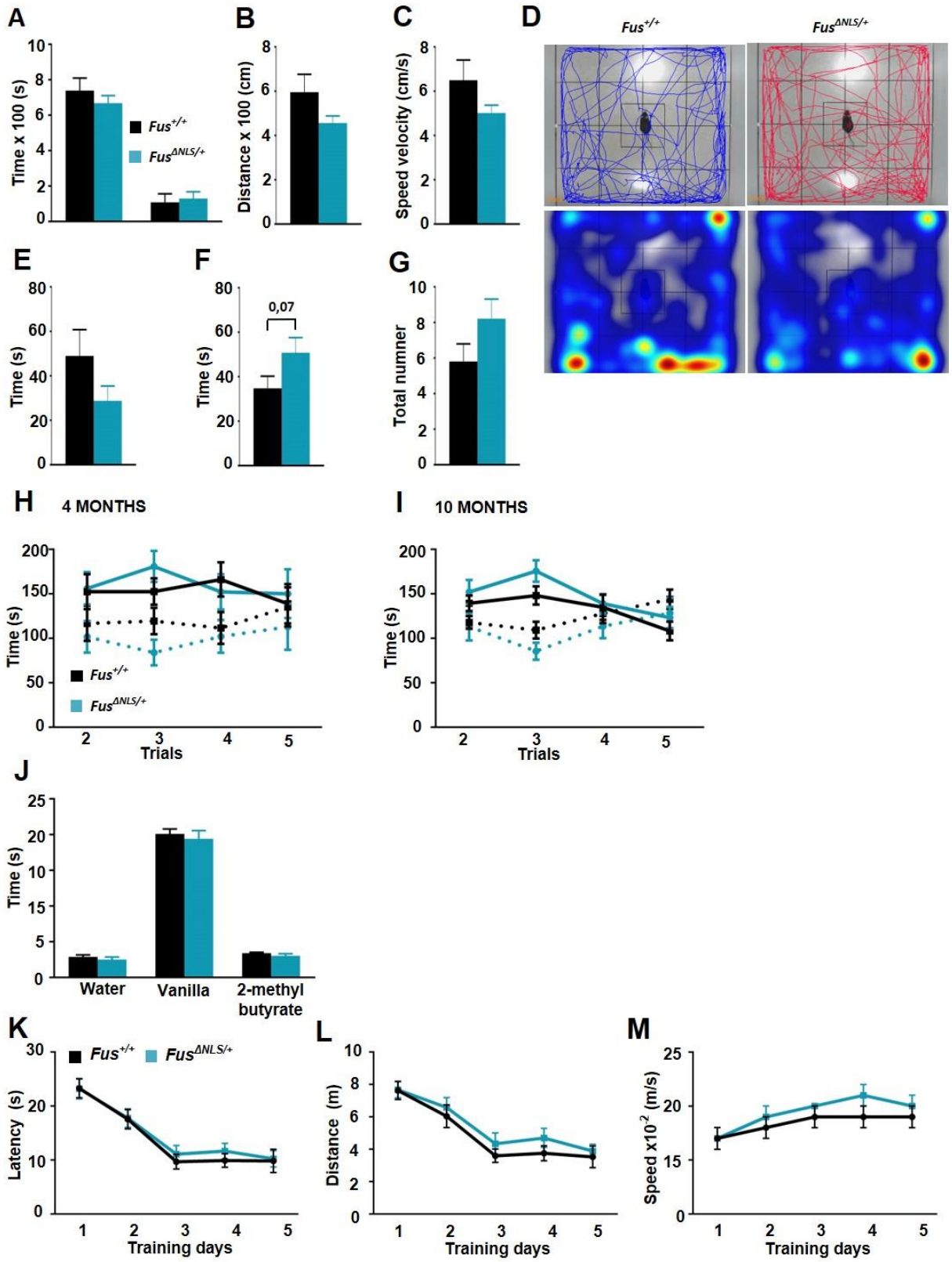
A
Time x 100 (s)
Fus+/+
FusΔNLS/+
B
Distance x 100 (cm)
C
Speed velocity (cm/s)
D
Fus+/+
FusΔNLS/+
E
Time (s)
F
Time (s)
0,07
G
Total numner
H
4 MONTHS
Time (s)
Trials
I
10 MONTHS
Time (s)
Trials
J
Time (s)
Water
Vanilla
2-methyl butyrate
K
Latency (s)
Training days
L
Distance (m)
Training days
M
Speed x10-2 (m/s)
Training days

Supplementary figure 2: FTD-like behavioural abnormalities in $Fus^{\Delta NLS/+}$ mice.

A: Bar chart showing mean sand standard errors of time spent in peripheral quadrants (left bars) and central quadrants (right bars) of the open field at 10.

B-C: Total distance traveled and avarage speed velocity. (*) p<0.05, (***) p<0.01 with respect to $Fus^{+/+}$; N=3; One-way ANOVA followed by Tukey post hoc test.

D: Representative images of trajectory trackings (upper pannels) and heat maps (lower pannels) and in the open field.

E-G: Bar charts showing means and standard errors of latency time to enter the illuminated compartment (E), absolute time spent in the spent in the illuminated compartment (F); number of transitions between dark and the illuminated compartments (G) in the dark-light box at 10. (*) p<0.05, (***) p<0.01 with respect to $Fus^{+/+}$; N=14-15 for 10 months; Student t-test.

H-I: Time spent exploring either chamber with Novel mice or empty wired cage across trials of 4 months (H) and 10 months (I) old mice. N=9 for 4 months; N=14 for 10 months; Two-way ANOVA

J: Analysis of olfactory preference at 10 months. N=6; All values are means and standard errors.

K-M: Latency (in seconds) (K); Distance swimmed (in meters) (L) and speed velocity (in meters per seconds) (M) to find the platform in the Morris water maze at 10 months of age. N=10 ; Two-way ANOVA (K)« days »: F(4,76)=24,35; p=0,00000 « genotype »: F(1,19)=1,10; p=0,64 (L)« days »: F(4,76)=35,62; p=0,00000 « genotype »: F(1,19)=0,21; p=0,64(M) « days »: F(4,76)=16,41; p=0,00000 « genotype »: F(1,19)=1,13; p=0,29

References

1. Taylor JP, Brown RH, Jr., Cleveland DW. Decoding ALS: from genes to mechanism. Nature 2016;539:197-206.
2. Brown RH, Jr., Al-Chalabi A. Amyotrophic Lateral Sclerosis. N Engl J Med 2017;377:162-72.
3. van Es MA, Hardiman O, Chio A, et al. Amyotrophic lateral sclerosis. Lancet 2017;390:2084-98.
4. Roberson ED. Mouse models of frontotemporal dementia. Ann Neurol 2012;72:837-49.
5. Burrell JR, Halliday GM, Kril JJ, et al. The frontotemporal dementia-motor neuron disease continuum. Lancet 2016;388:919-31.
6. Bang J, Spina S, Miller BL. Frontotemporal dementia. Lancet 2015;386:1672-82.
7. Mackenzie IR, Rademakers R, Neumann M. TDP-43 and FUS in amyotrophic lateral sclerosis and frontotemporal dementia. Lancet Neurol 2010;9:995-1007.
8. Neumann M. Frontotemporal lobar degeneration and amyotrophic lateral sclerosis: molecular similarities and differences. Rev Neurol (Paris) 2013;169:793-8.
9. Dormann D, Haass C. TDP-43 and FUS: a nuclear affair. Trends Neurosci 2011;34:339-48.
10. Dormann D, Haass C. Fused in sarcoma (FUS): an oncogene goes awry in neurodegeneration. Mol Cell Neurosci 2013;56:475-86.
11. Kwiatkowski TJ, Jr., Bosco DA, Leclerc AL, et al. Mutations in the FUS/TLS gene on chromosome 16 cause familial amyotrophic lateral sclerosis. Science 2009;323:1205-8.
12. Vance C, Rogelj B, Hortobagyi T, et al. Mutations in FUS, an RNA processing protein, cause familial amyotrophic lateral sclerosis type 6. Science 2009;323:1208-11.
13. Waibel S, Neumann M, Rabe M, Meyer T, Ludolph AC. Novel missense and truncating mutations in FUS/TLS in familial ALS. Neurology 2010;75:815-7.
14. Waibel S, Neumann M, Rosenbohm A, et al. Truncating mutations in FUS/TLS give rise to a more aggressive ALS-phenotype than missense mutations: a clinico-genetic study in Germany. Eur J Neurol 2013;20:540-6.
15. Dormann D, Madl T, Valori CF, et al. Arginine methylation next to the PY-NLS modulates Transportin binding and nuclear import of FUS. EMBO J 2012;31:4258-75.
16. Dormann D, Rodde R, Edbauer D, et al. ALS-associated fused in sarcoma (FUS) mutations disrupt Transportin-mediated nuclear import. EMBO J 2010;29:2841-57.
17. Snowden JS, Hu Q, Rollinson S, et al. The most common type of FTLD-FUS (aFTLD-U) is associated with a distinct clinical form of frontotemporal dementia but is not related to mutations in the FUS gene. Acta Neuropathol 2011;122:99-110.
18. Seelaar H, Klijnsma KY, de Koning I, et al. Frequency of ubiquitin and FUS-positive, TDP-43-negative frontotemporal lobar degeneration. J Neurol 2010;257:747-53.
19. Josephs KA, Whitwell JL, Parisi JE, et al. Caudate atrophy on MRI is a characteristic feature of FTLD-FUS. Eur J Neurol 2010;17:969-75.
20. Suarez-Calvet M, Neumann M, Arzberger T, et al. Monomethylated and unmethylated FUS exhibit increased binding to Transportin and distinguish FTLD-FUS from ALS-FUS. Acta Neuropathol 2016;131:587-604.
21. Urwin H, Josephs KA, Rohrer JD, et al. FUS pathology defines the majority of tau- and TDP-43-negative frontotemporal lobar degeneration. Acta Neuropathol 2010;120:33-41.
22. Mackenzie IR, Ansorge O, Strong M, et al. Pathological heterogeneity in amyotrophic lateral sclerosis with FUS mutations: two distinct patterns correlating with disease severity and mutation. Acta Neuropathol 2011;122:87-98.

23. Neumann M, Bentmann E, Dormann D, et al. FET proteins TAF15 and EWS are selective markers that distinguish FTLD with FUS pathology from amyotrophic lateral sclerosis with FUS mutations. Brain 2011;134:2595-609.
24. Sun S, Ling SC, Qiu J, et al. ALS-causative mutations in FUS/TLS confer gain- and loss-of-function by altered association with SMN and U1-snRNP. Nat Commun 2015.
25. Sun S, Ling SC, Qiu J, et al. ALS-causative mutations in FUS/TLS confer gain and loss of function by altered association with SMN and U1-snRNP. Nat Commun 2015;6:6171.
26. Lopez-Erauskin J, Tadokoro T, Baughn MW, et al. ALS/FTD-Linked Mutation in FUS Suppresses Intra-axonal Protein Synthesis and Drives Disease Without Nuclear Loss-of-Function of FUS. Neuron 2018;100:816-30 e7.
27. Ling SC, Dastidar SG, Tokunaga S, et al. Overriding FUS autoregulation in mice triggers gain-of-toxic dysfunctions in RNA metabolism and autophagy-lysosome axis. eLife 2019;8.
28. Devoy A, Kalmar B, Stewart M, et al. Humanized mutant FUS drives progressive motor neuron degeneration without aggregation in 'FUSDelta14' knockin mice. Brain 2017;140:2797-805.
29. Scekic-Zahirovic J, Sendscheid O, El Oussini H, et al. Toxic gain of function from mutant FUS protein is crucial to trigger cell autonomous motor neuron loss. EMBO J 2016;35:1077-97.
30. Scekic-Zahirovic J, Oussini HE, Mersmann S, et al. Motor neuron intrinsic and extrinsic mechanisms contribute to the pathogenesis of FUS-associated amyotrophic lateral sclerosis. Acta Neuropathol 2017;133:887-906.
31. Kino Y, Washizu C, Kurosawa M, et al. FUS/TLS deficiency causes behavioral and pathological abnormalities distinct from amyotrophic lateral sclerosis. Acta neuropathologica communications 2015;3:24.
32. Orozco D, Tahirovic S, Rentzsch K, Schwenk BM, Haass C, Edbauer D. Loss of fused in sarcoma (FUS) promotes pathological Tau splicing. EMBO Rep 2012;13:759-64.
33. Ishigaki S, Fujioka Y, Okada Y, et al. Altered Tau Isoform Ratio Caused by Loss of FUS and SFPQ Function Leads to FTLD-like Phenotypes. Cell Rep 2017;18:1118-31.
34. Yokoi S, Udagawa T, Fujioka Y, et al. 3'UTR Length-Dependent Control of SynGAP Isoform alpha2 mRNA by FUS and ELAV-like Proteins Promotes Dendritic Spine Maturation and Cognitive Function. Cell Rep 2017;20:3071-84.
35. Ishigaki S, Sobue G. Importance of Functional Loss of FUS in FTLD/ALS. Front Mol Biosci 2018;5:44.
36. Moreau PH, Cosquer B, Jeltsch H, Cassel JC, Mathis C. Neuroanatomical and behavioral effects of a novel version of the cholinergic immunotoxin mu p75-saporin in mice. Hippocampus 2008;18:610-22.
37. Hascoet M, Bourin M, Nic Dhonnchadha BA. The mouse light-dark paradigm: a review. Prog Neuropsychopharmacol Biol Psychiatry 2001;25:141-66.
38. Liebscher S, Keller GB, Goltstein PM, Bonhoeffer T, Hubener M. Selective Persistence of Sensorimotor Mismatch Signals in Visual Cortex of Behaving Alzheimer's Disease Mice. Curr Biol 2016;26:956-64.

3. PART 3: DEGENERATION OF CENTRAL CHOLINERGIC NEURONS CONTRIBUTE TO SOCIAL DISINHIBITION IN A MOUSE MODEL OF FUS ALS/FTD

Résumé

Nos travaux précédents avaient montré l'importance de l'expression de la mutation dans les motoneurones pour provoquer les symptômes moteurs. Pour cela, nous avions utilisé un modèle d'expression de la recombinase CRE dans les neurones cholinergiques, et avions montré que le sauvetage spécifique dans les neurones cholinergiques permettait de retarder l'installation du phénotype moteur. Etant donné le rôle de l'acétylcholine dans les syndrômes démentiels, dont la maladie d'Alzheimer, nous nous sommes intéressés à l'implication du système cholinergique et aux effets de sa modulation dans la pathologie. Notre modèle murin présente une perte de neurones cholinergiques du noyau basal de Meynert (NbM), aussi affecté dans la maladie d'Alzheimer, ainsi qu'une perte de projections ascendantes cholinergiques jusqu'au cortex, où une diminution d'innervation de fibres cholinergiques des couches internes est aussi retrouvée. De plus, les neurones cholinergiques du NbM présentent des marqueurs moléculaires de dommage à l'ADN. Comme le modèle knock-in hétérozygote présente des altérations de type DFT, nous avons étudié si ces phénotypes dépendaient de l'expression de la mutation dans les neurones cholinergiques. De fait, le sauvetage de la mutation dans les neurones cholinergiques atténue partiellement ces phénotypes. Ces résultats indiquent que l'expression de Fus muté altère le système cholinergique de façon globale, autant au niveau central que périphérique, et que celui-ci est directement lié aux symptômes comportementaux décrits dans notre modèle murin.

Ces données doivent être complétées d'expériences pharmacologiques et moléculaires actuellement en cours pour permettre la soumission d'un article complet.

Degeneration of central cholinergic neurons contribute to social disinhibition in a mouse model of FUS ALS/FTD

Current authors:

Inmaculada Sanjuan-Ruiz*, Jelena Scekic-Zahirovic* et al.

* shared first authorship

Summary

Deficits in acetylcholine are widespread in Alzheimer's disease (AD) and acetylcholinesterase inhibitors are widely used symptomatic treatments in AD. Cholinergic involvement has also been repeatedly observed in fronto-temporal dementia (FTD), and cholinergic neurons of the Nucleus basalis Meynert, the major source of cortical acetycholine, are affected. However, acetylcholinesterase inhibitors do not appear to relieve symptoms in FTD. It remains unknown whether central cholinergic neurons are selectively involved in subtypes of FTD, such as FTD-FUS characterized by cytoplasmic inclusions of the RNA binding protein FUS. Here, we show that partial FUS mislocalization in mice is sufficient to trigger non cell autonomous degeneration of cholinergic neurons in the basal forebrain, along with partial loss of cholinergic terminals in the cerebral cortex, similar to what observed in FTD-FUS patients. Indeed, rescue of FUS mislocalization in cholinergic neurons partially rescued the FTD-related social disinhibition in these animals showing the importance of cholinergic dysfunction in the effects of FUS mislocalization. These encouraging preliminary results call for further on the cholinergic system in FTD-FUS.

Introduction

Fronto-temporal dementia (FTD) and amyotrophic lateral sclerosis (ALS) and are two fatal neurodegenerative diseases that share clinical, genetic and pathological features, suggesting that they constitute a pathophysiological continuum[1-3]. ALS is the major adult onset motor neuron disease, with symptoms usually beginning around 60 years of age, and death within 3 to 5 years after onset. ALS is genetically heterogenous and mutations in 5 major genes, *C9ORF72, SOD1, FUS, TARDBP* and *TBK1* are causing a large proportion of familial cases. Mutations in the *FUS* gene cause the most severe forms of ALS, with early onset and rapid disease progression[4,5]. FTD is characterized by defects in social and executive functions. A large subset of FTD cases with prominent atrophy of the caudate putamen[6-8] develop FUS pathology, yet in the absence of germline *FUS* mutations. A number of other proteins, including other closely related TAF15 and EWSR1, as well as transportin 1, are also found in FUS inclusions of FTD FUS patients. However, mislocalization of FUS to the cytoplasm is, on its own, sufficient to lead to social disinhibition, executive dysfunction and hyperactivity that are relevant phenotypes for the behavioural variant of FTD (Scekic-Zahirovic, Sanjuan-Ruiz et al, in preparation). This suggests that the gain of a toxic function in the cytoplasm by mislocalized FUS participates to the clinical picture of FTD-FUS patients, along with loss of nuclear FUS function[9-13].

Acetylcholine is an essential neuromodulator involved in multiple behaviours [14], Indeed, deficits in cholinergic transmission are associated with most neurodegenerative disorders. Cholinergic neurons of the nucleus basalis Meynert (NBM), the primary source of acetylcholine of the cerebral cortex, degenerate in Parkinson's disease[15] and Alzheimer's disease[16], and cognitive deficits of AD or PD patients can be alleviated by cholinesterase inhibitors [17,18]. In FTD, cholinergic deficits appear less pronounced than in AD or PD [19], with cholinergic neurons reduced in NBM, but preserved in the cortex[20]. Surprisingly, and despite these evidence of cholinergic involvement, FTD patients appear to be resistant to cholinergic stimulation, as memantine does not alleviate symptoms of FTD patients[21]. However, the underlying mechanisms of resistance of FTD patients to cholinergic stimulation remain unknown. Also, the different pathological subtypes of FTD have not been studied independently, and it remains possible that a subset of FTD cases could respond to cholinergic stimulation.

Here, we show that partial cytoplasmic mislocalization of FUS is sufficient to trigger degeneration of NBM cholinergic neurons in mice. Importantly, behavioural abnormalities developed by these mice are partially rescued by the rescue of the mutation in cholinergic neurons themselves.

These encouraging preliminary results call for further on the cholinergic system in FTD-FUS.

Materials and methods

Animal housing and genotyping

All mice were pure C57/Bl6 genetic background, housed under controlled conditions (21 ± 1°C; 60% humidity) at the animal facility of the Faculty of Medicine of Strasbourg, France. Animals were maintained on a 12h light/dark cycle (lights on at 7 am) with ad libitum access to food and water. Wild-type, heterozygous $Fus^{\Delta NLS/+}$ and heterozygous ChAT-CRE mice were generated and genotyped by PCR of genomic DNA from tail biopsies as described [22]. 10- to 22- month-old male littermates each genotype underwent behavioural tests and molecular analyses. Behavioural tests were done during the light phase of mice light/dark cycle.

All experimental procedures were approved by the local ethical committee (CREMEAS in Strasbourg) under the references AL/27/34/02/13 and #17136-2018101514425048.

Behaviour

Resident intruder test

This test examines exploratory behavior directed at a new/unknown "stranger" mouse. Wild-type "stranger" mice were non-littermate to test mice. All mice were isolated between 5 to 7 days before the test. Mice were placed in the behavior room 30 min prior test for habituation. Resident test mice were placed in their home cage under a video camera recording system and were allowed to habituate for 1 min. A novel "stranger" mouse was placed in the opposite corner of the home cage and allowed to roam for 5 min. All mice interactions were recorded and analyzed post-hoc in a double-blinded manner.

Brain histology

Animals were anesthetized with an intraperitoneal injection of ketamine (Imalgene 80 mg/kg; Merial, Lyon, France) and xylazine (Rompun 20 mg/kg; Bayer, Lyon, France) and were perfused transcardially with 4% paraformaldehyde (PFA) in 0.1 M phosphate buffer pH 7.4. Brains were dissected and fixed by immersion in 4% PFA in 0.1 M phosphate buffer pH 7.4 overnight, then washed 3 times in PBS 1X and stored at 4°C in PBS 1X – 0.02% Thimerosal (Ref: , Sigma). Brains were embedded in agar 4% and 40 µm sections were obtained with vibratome (Leica …) and stored at 4°C in PBS 1X – 0.02% Thimerosal.

For peroxidase immunohistochemistry, brain sections were incubated 10 min with H2O2 3%, rinsed 3 times with PBS 1X and incubated with goat anti-ChAT antibody (Millipore AB144P; diluted 1:50) overnight at room temperature. The second day, sections were rinsed and incubated for 2h at room temperature with donkey anti-goat biotinylated antibody (Jackson 705-066-147; diluted 1:500). After sections were rinsed, they were incubated for 1h in horseradish peroxidase ABC kit (Vectastain ABC kit, PK-6100, Vector Laboratories Inc.), rinsed and incubated with DAB (Sigma, D5905). The enzymatic reaction was stop by adding PBS 1X and sections were mounted with DPX mounting medium (Sigma, O6522) and observed with ZEISS Apotome.

Statistics

All results from analysis are presented as mean ± standard error of the mean (SEM) and differences were considered significant when $p < 0.05$. Significance is presented as follows: * $p<0.05$, ** $p<0.01$, and *** $p<0.001$. Comparison for the three groups was performed using one-way ANOVA and Tukey or Bonferroni's multiple comparison post hoc tests. Data were analyzed using the GraphPad Prism version 6.0.

Results

Fus$^{\Delta NLS/+}$ mice develop non-cell autonomous degeneration of basal forebrain cholinergic neurons

In AD and PD cholinergic neurons of the basal forebrain degenerate, resulting in cognitive and behavioural deficits. Since we previously showed that *Fus$^{\Delta NLS/+}$* develop a number of behavioural deficits, we hypothesized that the cholinergic system in the basal forebrain could be affected. We found a trend towards a loss of ChAT+ neurons in the basal forebrain of 22 months old *Fus$^{\Delta NLS/+}$* mice. (**Figure 1A**). Furthermore, we observed that neurons in this brain region, including ChAT+ neurons present intense staining for γH2AX, a DNA damage marker, indicating that neurons in the basal forebrain are affected in *Fus$^{\Delta NLS/+}$* mice (**Figure 1B**). Cholinergic neurons in the basal forebrain project to varied brain regions and contribute to the maintenance of several functions such as attention or memory among others. In fact, basal forebrain cholinergic neurons project to cortical regions via different tracts where, particularly ascending cholinergic fibers embedded in the capsula interna project to medial prefrontal cortex and hippocampus [23,24]. Therefore, we assessed the integrity of this cholinergic fibers in our *Fus$^{\Delta NLS/+}$* mice and observed a significant loss of cholinergic fibers in the capsula interna as well as in cortical layers V and VI (**Figure 1C, 1D**). Mice carrying the *Fus$^{\Delta NLS/+}$* and a ChAT Cre transgene, allowing the specific rescue of mislocalized FUS in cholinergic neurons by Cre recombinase[22,25] were analysed in paralle and, surprisingly, we observed that the degeneration of cholinergic neurons was similar in *Fus$^{\Delta NLS/+}$* ; ChAT Cre and *Fus$^{\Delta NLS/+}$* mice (**Figure 1A, C, D**). Thus, the degeneration of basal forebrain cholinergic neurons and their ascending projections occur in a non-cell autonomous manner in *Fus$^{\Delta NLS/+}$* mice.

Fus$^{\Delta NLS/+}$ mice behavioural abnormalities are partially dependent upon cholinergic expression of the mutation

In view of the relevance of the cholinergic system in behavioural and cognitive functions, we then questioned whether the observed behaviour deficits in our mouse model (Scekic-Zahirovic, Sanjuan-Ruiz et al, in preparation) could arise from the observed cholinergic deficits. Therefore, we evaluated *Fus$^{\Delta NLS/+}$* and *Fus$^{\Delta NLS/+}$*-ChAT Cre mice at 10 months of age using the resident-intruder test. As previously observed, *Fus$^{\Delta NLS/+}$* mice showed increased social interest (or social disinhibition). Interestingly, *Fus$^{\Delta NLS/+}$*-ChAT Cre mice displayed attenuated social disinhibition (**Figure 2**). Thus, social disinhibition phenotype of *Fus$^{\Delta NLS/+}$* mice are partially rescued upon deletion of the expression of the mutation in cholinergic neurons, suggesting a contribution of cholinergic neurons dysfunction in this phenotype.

Figures and legends

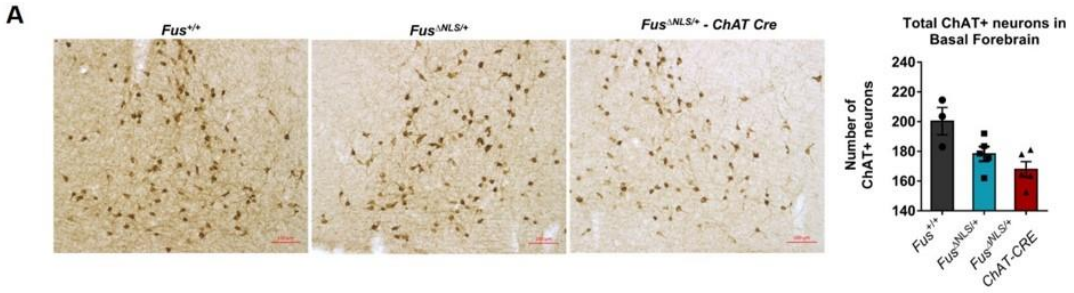

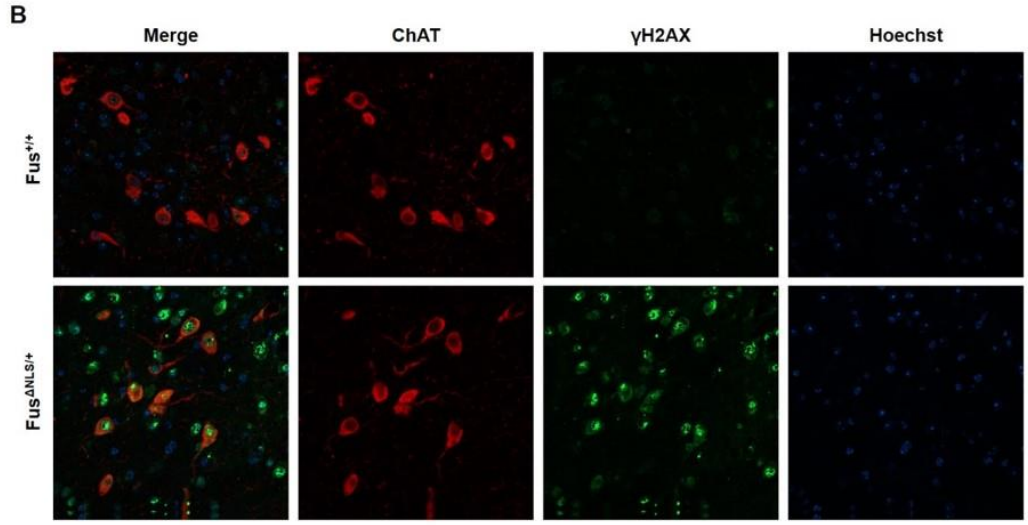

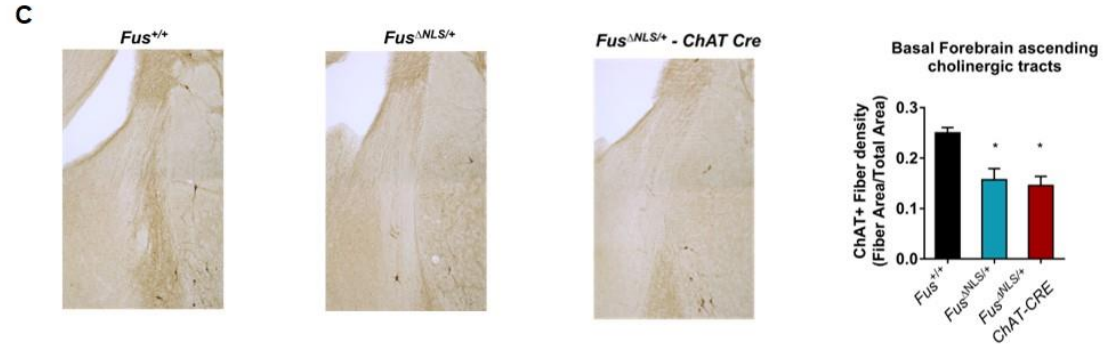

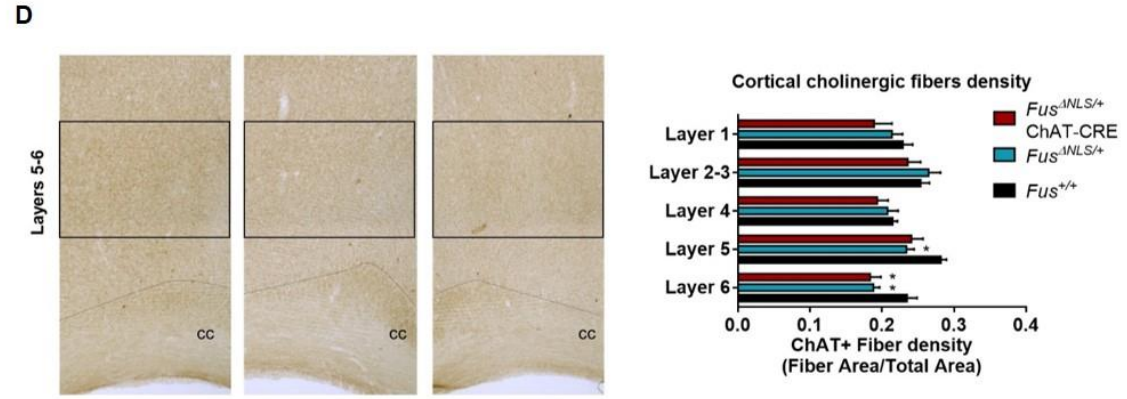

Figure 1: Fus$^{\Delta NLS/+}$ mice develop non-cell autonomous degeneration of basal forebrain cholinergic neurons.
A: Immunohistochemistry of ChAT+ neurons in the basal forebrain of Fus$^{+/+}$ (left), Fus$^{\Delta NLS/+}$ (middle) and Fus$^{\Delta NLS/+}$-ChAT Cre (right) mice with their corresponding quantification.
B: Immunofluorescence of ChAT+ and DNA damage marker γH2AX in basal forebrain of Fus$^{+/+}$ (upper) and Fus$^{\Delta NLS/+}$ (lower) mice.
C: Immunohistochemistry of ChAT+ ascending fibers from the basal forebrain, embedded in the capsula interna of Fus$^{+/+}$ (left), Fus$^{\Delta NLS/+}$ (middle) and Fus$^{\Delta NLS/+}$-ChAT Cre (right) mice with their corresponding quantification.
D: Immunohistochemistry of cortical ChAT+ fibers (image of layers V and VI) of Fus$^{+/+}$ (left), Fus$^{\Delta NLS/+}$ (middle) and Fus$^{\Delta NLS/+}$-ChAT Cre (right) mice and their corresponding quantification from layers I to VI.

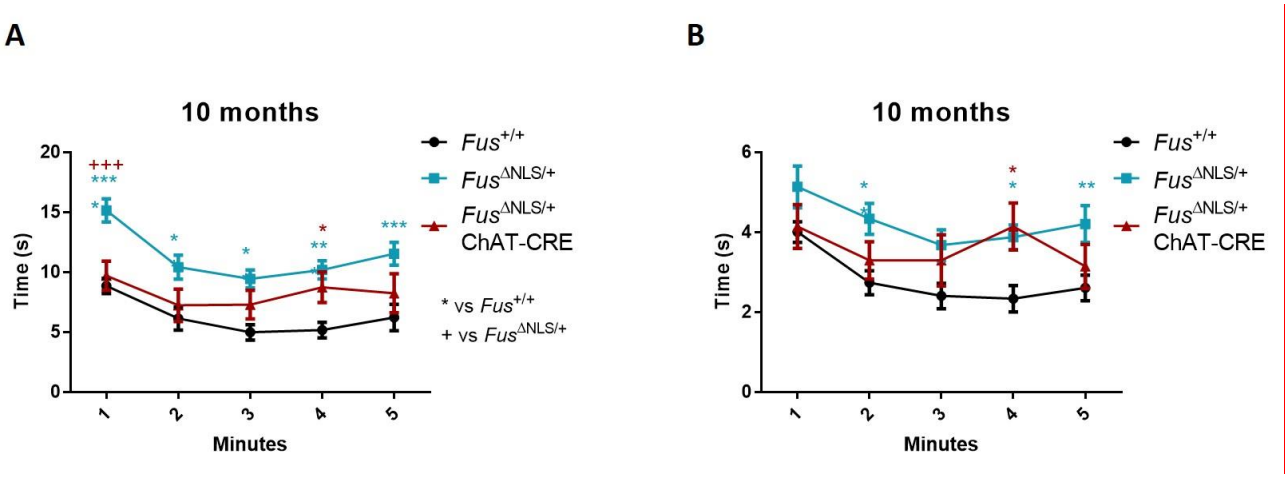

Figure 2: Social abnormalities of Fus deltaNLS/+ are partially dependent upon cholinergic expression of the mutation.
Resident intruder test of $Fus^{+/+}$ (black), $Fus^{\Delta NLS/+}$ (blue) and $Fus^{\Delta NLS/+}$-ChAT Cre (red) mice at 10 months of age.
A: Time of contact of the test mouse with the intruder mouse over time.
B: Number of contacts of the test mouse with the intruder mouse over time.

References

1. Taylor JP, Brown RH, Jr., Cleveland DW. Decoding ALS: from genes to mechanism. Nature 2016;539:197-206.
2. Brown RH, Jr., Al-Chalabi A. Amyotrophic Lateral Sclerosis. N Engl J Med 2017;377:162-72.
3. van Es MA, Hardiman O, Chio A, et al. Amyotrophic lateral sclerosis. Lancet 2017;390:2084-98.
4. Waibel S, Neumann M, Rabe M, Meyer T, Ludolph AC. Novel missense and truncating mutations in FUS/TLS in familial ALS. Neurology 2010;75:815-7.
5. Waibel S, Neumann M, Rosenbohm A, et al. Truncating mutations in FUS/TLS give rise to a more aggressive ALS-phenotype than missense mutations: a clinico-genetic study in Germany. Eur J Neurol 2013;20:540-6.
6. Snowden JS, Hu Q, Rollinson S, et al. The most common type of FTLD-FUS (aFTLD-U) is associated with a distinct clinical form of frontotemporal dementia but is not related to mutations in the FUS gene. Acta Neuropathol 2011;122:99-110.
7. Seelaar H, Klijnsma KY, de Koning I, et al. Frequency of ubiquitin and FUS-positive, TDP-43-negative frontotemporal lobar degeneration. J Neurol 2010;257:747-53.
8. Josephs KA, Whitwell JL, Parisi JE, et al. Caudate atrophy on MRI is a characteristic feature of FTLD-FUS. Eur J Neurol 2010;17:969-75.
9. Kino Y, Washizu C, Kurosawa M, et al. FUS/TLS deficiency causes behavioral and pathological abnormalities distinct from amyotrophic lateral sclerosis. Acta neuropathologica communications 2015;3:24.
10. Orozco D, Tahirovic S, Rentzsch K, Schwenk BM, Haass C, Edbauer D. Loss of fused in sarcoma (FUS) promotes pathological Tau splicing. EMBO Rep 2012;13:759-64.
11. Ishigaki S, Fujioka Y, Okada Y, et al. Altered Tau Isoform Ratio Caused by Loss of FUS and SFPQ Function Leads to FTLD-like Phenotypes. Cell Rep 2017;18:1118-31.
12. Yokoi S, Udagawa T, Fujioka Y, et al. 3'UTR Length-Dependent Control of SynGAP Isoform alpha2 mRNA by FUS and ELAV-like Proteins Promotes Dendritic Spine Maturation and Cognitive Function. Cell Rep 2017;20:3071-84.
13. Ishigaki S, Sobue G. Importance of Functional Loss of FUS in FTLD/ALS. Front Mol Biosci 2018;5:44.
14. Picciotto MR, Higley MJ, Mineur YS. Acetylcholine as a neuromodulator: cholinergic signaling shapes nervous system function and behavior. Neuron 2012;76:116-29.
15. Braak H, Ghebremedhin E, Rub U, Bratzke H, Del Tredici K. Stages in the development of Parkinson's disease-related pathology. Cell Tissue Res 2004;318:121-34.
16. Hampel H, Mesulam MM, Cuello AC, et al. The cholinergic system in the pathophysiology and treatment of Alzheimer's disease. Brain 2018;141:1917-33.
17. Summers WK, Majovski LV, Marsh GM, Tachiki K, Kling A. Oral tetrahydroaminoacridine in long-term treatment of senile dementia, Alzheimer type. N Engl J Med 1986;315:1241-5.
18. Emre M, Aarsland D, Albanese A, et al. Rivastigmine for dementia associated with Parkinson's disease. N Engl J Med 2004;351:2509-18.
19. Murley AG, Rowe JB. Neurotransmitter deficits from frontotemporal lobar degeneration. Brain 2018;141:1263-85.
20. Sparks DL, Markesbery WR. Altered serotonergic and cholinergic synaptic markers in Pick's disease. Arch Neurol 1991;48:796-9.
21. Boxer AL, Knopman DS, Kaufer DI, et al. Memantine in patients with frontotemporal lobar degeneration: a multicentre, randomised, double-blind, placebo-controlled trial. Lancet Neurol 2013;12:149-56.

22. Scekic-Zahirovic J, Sendscheid O, El Oussini H, et al. Toxic gain of function from mutant FUS protein is crucial to trigger cell autonomous motor neuron loss. EMBO J 2016;35:1077-97.
23. Bloem B, Poorthuis RB, Mansvelder HD. Cholinergic modulation of the medial prefrontal cortex: the role of nicotinic receptors in attention and regulation of neuronal activity. Front Neural Circuits 2014;8:17.
24. Bloem B, Schoppink L, Rotaru DC, et al. Topographic mapping between basal forebrain cholinergic neurons and the medial prefrontal cortex in mice. J Neurosci 2014;34:16234-46.
25. Scekic-Zahirovic J, Oussini HE, Mersmann S, et al. Motor neuron intrinsic and extrinsic mechanisms contribute to the pathogenesis of FUS-associated amyotrophic lateral sclerosis. Acta Neuropathol 2017;133:887-906.

Discussion

Discussion

The results of this thesis are three-fold. First, we rescued the phenotype of $Fus^{\Delta NLS}$ mice by crossbreeding them with human FUS transgenic mice. This has consequences for our understanding of FUS autoregulation, and opens up potential therapeutic strategies. Second, we document the existence of FTD relevant phenotypes in $Fus^{\Delta NLS}$ mice, and this has relevance to understand FUS-FTD pathophysiology. Third, we provide preliminary evidence of cholinergic dysfunction in $Fus^{\Delta NLS}$ mice, which could also be relevant for FTD understanding.

In the first study, the insertion of a human wild-type FUS transgene (hFUS) in our $Fus^{\Delta NLS}$ mouse model allowed us to rescue lethality of homozygous newborns carrying the mutation. Thus, by reintroducing wild-type nuclear FUS therefore compensating the nuclear loss of function, we have shown that FUS nuclear functions are indispensable for proper adulthood development. Furthermore, hFUS transgene was able to rescue muscular force defects in heterozygous and homozygous mice scoring values similar to their wild-type littermates. We asked ourselves whether hFUS expression could have an impact on the localization of FUS. As expected, FUS cytoplasmic levels were increased in $Fus^{\Delta NLS/+}$ mice due to the presence of the mutant allele, that produces a protein devoid of NLS. To our surprise, the addition of the wild-type transgene revealed a normalization of cytoplasmic protein levels, thus reverting FUS mislocalization in heterozygous and homozygous mice carrying the mutation, whereas nuclear levels remained at physiological levels in all genotypes showing hFUS has an effect specifically on mislocalized mutant protein. We corroborated these results with immunostaining techniques, where we observed restored levels of FUS from the cytoplasm to the nucleus. Moreover, the addition of hFUS prevented the detection of typical hallmarks such as methylated FUS and/or ubiquitin depositions that we observed in $Fus^{\Delta NLS/+}$ mice. To better understand the underlying mechanisms behind our observations as a result of the insertion of hFUS, we investigated the potential effects of the human transgene to FUS autoregulation functions. We found that the addition of hFUS downregulates endogenous mRNA levels as expected by its own autoregulation in wild-type mice and a decrease of mutant $Fus^{\Delta NLS}$ mRNA expression in heterozygous and homozygous mice carrying the mutation. This decrease was associated with activation of the alternative splicing skipping exon7 of FUS mRNA, resulting in the degradation of this aberrant mRNA by non-mediated decay. In all, our data suggests that the expression of mutant FUS leads to accumulated cytoplasmic FUS, disrupts nuclear FUS autoregulation and creates a vicious cycle leading to further production of cytoplasmic FUS. The introduction of the wild type allele allows to re-equilibrate the autoregulation towards the production of functional FUS, at the expense of cytoplasmic FUS.

ALS patients can also develop FTD symptoms and a fraction of FTD patients display FUS aggregates. Therefore, we asked ourselves if our $Fus^{\Delta NLS}$ mouse model could present FTD-like symptoms. Behaviour and cognitive

tests revealed that $Fus^{\Delta NLS/+}$ mice are hyperactive at early ages, and develop disinhibition, social memory disfunction and altered memory consolidation at later stages. Furthermore, cortical neurons of upper layers in frontal cortex appear to hyperexcitable. Thus, behavioural and electrophysiological data indicate that FUS mislocalization lead to frontal cortex neuronal activity alterations, behaviour deficits and cognitive dysfunctions *via* disruption of frontal cortex - hippocampus dialog. FTD patients are characterized by the development of a progressive atrophy of frontal and temporal lobes with subsequent neuronal degeneration. We did not observe any neuronal loss in our mouse model at advanced ages although we found cytoplasmic aggregates in layer V pyramidal neurons of the frontal cortex, similar to those found in post-mortem FTD patient's brains. The analysis we performed on the RNA expression of $Fus^{\Delta NLS/+}$ mice showed significant transcriptional deregulation compared to their wild-type littermates. In particular, we found upregulation of genes encoding for axonal, dendritic and synaptic proteins such as ionotropic glutamate subunit receptors (Grin2a, Grin2b), Pvalb, or synaptic vesicle components namely, Syt2 and Vamp1. Contrarily, we found a deregulation of genes encoding for the immune system, neurotransmitters transport and GABAergic synapses, where in particular we observed downregulation of GABA metabolism encoding genes such as Gad1 and Slc32a1, responsible of GABA synthesis and transport respectively. Moreover, we found that cortical inhibitory synapses of layers II//III in $Fus^{\Delta NLS/+}$ mice present structural alterations, with dispersed synaptic vesicles distant from the active zone of the synaptic cleft and less visible synaptic pools. Therefore, our data indicate that $Fus^{\Delta NLS/+}$ mice have a defective GABAergic metabolism, with altered inhibitory synaptic structures that could originate an impairment of the excitatory/inhibitory balance of the cortex, which could lead to the observed altered neuronal activity and generate subsequent cognitive and behavioural deficits (Figure 17) . Thus, we demonstrate that FUS cytoplasmic mislocalization is sufficient to induce FTD-like symptoms.

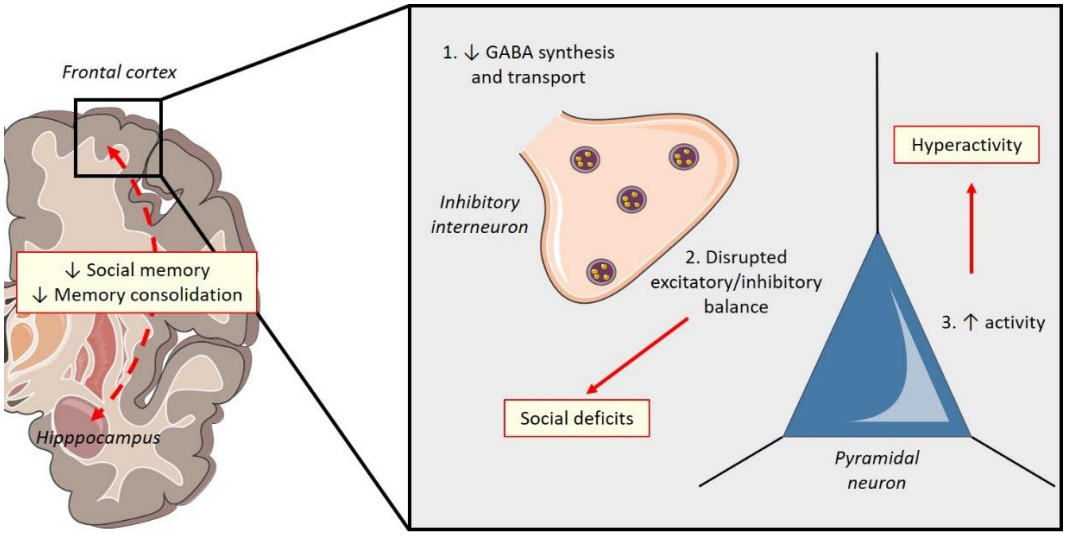

Figure 17: A working model to explain our results in the $Fus^{\Delta NLS}$ model.
It is possible that mutant FUS impairs GABA metabolism, development or stability of GABAergic synapses in the cortex leading to defects in inhibition that could result in increased activity of pyramidal neurons. These underlying defects could originate hyperactivity, social deficits and memory impairments.

In view of the specific vulnerability of cholinergic motor neurons in ALS and the relevant implications of the cholinergic system in other neurodegenerative diseases such as Alzheimer's or Parkinson's disease, we investigated whether there were cholinergic alterations at the central nervous system in our $Fus^{\Delta NLS/+}$ mouse model that could explain the behaviour and cognitive defects observed. In fact, we observed a degeneration at late ages of basal forebrain cholinergic neurons, brain structure largely studied in Alzheimer's or Parkinson's disease, with important implications in cognitive decline. Furthermore, we observed a degeneration of basal forebrain cholinergic ascending projections through the *internal capsula*, which target medial prefrontal cortex and the hippocampus. Similarly, we found a decrease in cholinergic fibers in frontal cortex but only in deeper layers V and VI. However, specific reversion of the mutation in cholinergic neurons by Cre recombination showed no beneficial effects in cholinergic neurons survival nor cholinergic projections, suggesting they degenerate via non-autonomous cellular mechanisms. In regards of the observed cholinergic alterations, we aimed to reassess $Fus^{\Delta NLS/+}$ mice behaviour deficits in $Fus^{\Delta NLS/+}$ - ChAT Cre mice. Interestingly, we observed that the previously characterized social disinhibition was partially rescued, suggesting that behaviour deficits are partially dependent upon FUS mislocalization in cholinergic neurons. Therefore, we demonstrated that $Fus^{\Delta NLS/+}$ mice present an alteration of the central nervous cholinergic system, with the degeneration of cholinergic neurons of the basal forebrain induced by other mechanisms than FUS cytoplasmic mislocalization and that the behavioural deficits of these mice are partially dependent of FUS mislocalization.

These three major results will be discussed below, sequentially in the context of the existing literature.

1. IS GENE THERAPY THE ANSWER FOR BETTER THERAPEUTIC APPROACHES IN FUS ALS-FTD?

Recent studies independently show that the addition of an exogenous FUS transgene leads to downregulation of endogenous murine *Fus.* This is particularly the case of two studies that added human FUS to their mouse animal models of *FUS*-ALS. Lopez-Euraskin and collaborators inserted a human wild-type floxed sequence and observed a reduction of more than 50% of endogenous *Fus* mRNA and protein, resulting in total Fus levels similar to those of their wild-type littermates (Lopez-Erauskin *et al.*, 2018). Likewise, Ling ang collaborators used a similar mouse model, where they inserted a human wild-type floxed transgene and observed the same effect. Similarly, in our $Fus^{\Delta NLS}$ mouse model, we observe the same effect upon the addition of the human transgene, where endogenous levels of murine *Fus* are diminished, although Fus total levels remain at physiological conditions (Ling *et al.*, 2019). Therefore, the addition of a human wild-type transgene activates *Fus* autoregulation mechanisms, allowing a tight control of mRNA and protein levels by decreasing the endogenous expression allowing to maintain homeostatic physiological conditions. Furthermore, both studies showed that the human FUS transgene is capable of rescuing lethality in mutant homozygous models of Fus, as we could observe in our study. Nevertheless, hFUS also showed to cause a decrease in NMJ innervation in both studies and age-dependent motor deficits, motor neuron loss and astrogliosis in Ling and collaborators study. Contrastingly, hFUS in our $Fus^{\Delta NLS}$ mouse model seem to rescue motor deficits although mice develop hindlimb clasping at very early ages, suggesting there are underlying motor functions altered.

In all, our study together with Lopez-Euraskin et al and Ling et al demonstrate that the addition of a human transgene activates Fus autoregulation mechanisms and that hFUS can compensate for some nuclear functions lost by FUS cytoplasmic mislocalization of great relevance for development. FUS autoregulation mechanisms are still not totally understood, however we propose three different mechanisms through which FUS could activate its autoregulatory loop and lead to the phenotype alleviation we observed in our $Fus^{\Delta NLS}$ mouse model. First, Zhou and collaborators described Fus autoregulation mechanisms *via* the activation of an alternative splicing pathway of its own mRNA, resulting in the skipping of the exon7 which is automatically degraded by nonsense-mediate decay. Furthermore, mutations in Fus resulted in a disruption of this autoregulatory mechanism, leading to increased synthesis of mutant protein subsequently cumulating in the cytoplasm (Zhou, Y. *et al.*, 2013). In our study we have indeed demonstrated that the addition of hFUS results in the activation of this alternative splicing pathway, leading to an increase of exon7 skipped variants that will undergo degradation, thus decreasing mutant mRNA and protein levels resulting in decreased levels of mutant cytoplasmic FUS. Second, Dini Modigliani and collaborators elucidated another mechanism pathway through which FUS is regulated by miRNAs. More precisely, FUS participates in the biogenesis of miR-141 and miR-200a, which in turn bind to the 3'UTR of FUS mRNA, thus regulating its expression levels and resulting in a feed-forward regulatory loop. In this model, Zeb1 is a target of miR141 and miR200a but at the same time acts

as their transcriptional repressor, contributing to this regulatory loop (Dini Modigliani *et al.*, 2014). Importantly, Dini Modigliani and collaborators showed that mutations affecting the 3'UTR of FUS result in the dysregulation of this feed-forward regulatory loop as miR141 and miR200a interaction with Fus mRNA is impaired resulting in an accumulation of wild-type FUS that has been shown to induce ALS in humans as well as in animal models (Mitchell *et al.*, 2013; Sabatelli *et al.*, 2013; Ling *et al.*, 2019). Defects in this microRNA regulatory loop and the potential effects of hFUS are currently being investigated in our $Fus^{\Delta NLS}$ mouse model. Finally, Ling SC and collaborators highlighted transcriptional deregulations in the RNA expression of autophagy mechanisms in mice overexpressing wild-type human FUS as well as in transgenic mice a human mutation, both of them identifying a decrease of autophagic pathways. Indeed, our unpublished results suggest accumulation of autophagosomes in $Fus^{\Delta NLS}$ mice rescued with hFUS transgene. Interestingly, a recent study published by Chitiprolu and collaborators observed that cytoplasmic FUS can be degraded by autophagy through a pathway involving its symetrical arginine methylation by PRTM5 on its Arg218, leading to p62 binding and subsequent re-routing to the autophagy pathway (Chitiprolu *et al.*, 2018). Preliminary results in our $Fus^{\Delta NLS}$ mouse model are indeed consistent with such a degradative pathway of cytoplasmic FUS excess, and its activation by hFUS transgene (Figure 18). Further analysis of the key players in the autophagy pathway are ongoing to confirm its involvement.

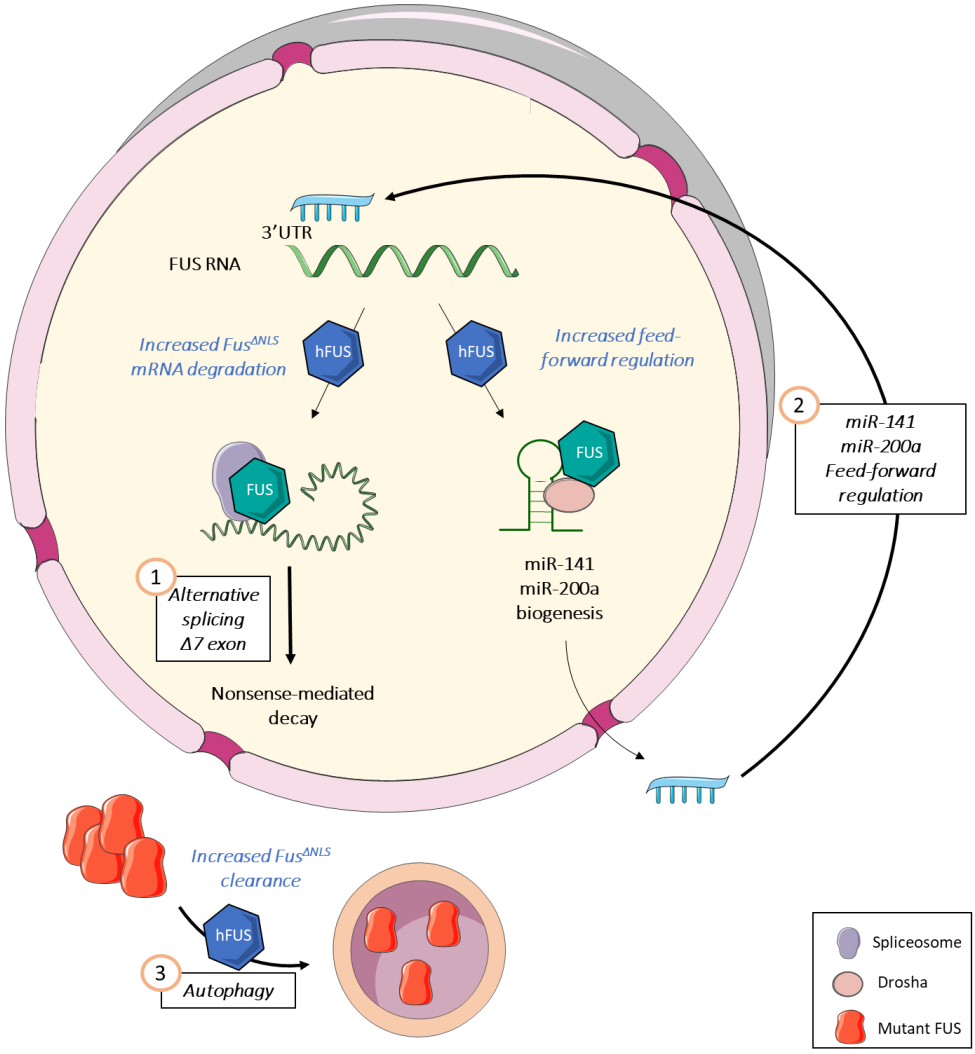

Figure 18: Working model of protection by activation of FUS autoregulation mechanisms.
hFUS can lead to degradation of mutant FUS through the activation of three potential mechanisms of autoregulation: (1) the activation of an alternative splicing pathway resulting in the skipping of the exon7 of its own mRNA, leading to degradation by nonsense-mediated decay (2) FUS participates in the biogenesis of miR141 and miR-200a, which in turn bind to FUS 3'UTR mRNA and repress its expression in a feed-forward loop (3) excessive cytoplasmic levels of FUS undergo degradation by the autophagy pathway.

A better understanding of FUS autoregulation and degradation mechanisms could bring the possibility to find specific therapeutic approaches. Zhou and collaborators suggested the application of ASOs as a tool to regulate the alternative splicing exon7 skipping pathway, where they designed an ASO targeting the junction of intron 6 and exon 7 and demonstrated in vitro it restored FUS autoregulation in a dose-dependent manner (Zhou, Y. *et al.*, 2013). However, Bailey and collaborators demonstrated that depending on the ASOs structure, these can have increased affinity for RBPs such as FUS and be recruited to stress granules or RNPs thus, limiting their distribution in the adequate cellular compartments (Bailey *et al.*, 2017). Furthermore, ASOs will be difficult to set up in a mutation specific manner, and will likely lead to general FUS downregulation, with expected side effects on synaptic plasticity and behaviour (Ishigaki e Sobue, 2018). An alternative would be to

design mutation specific ASOs, yet this will not be doable for all mutations, and will need highly personalized medicine not necessarily economically viable.

Our results of a therapeutic effect of a human transgene on the $Fus^{\Delta NLS}$ phenotype suggesting that therapeutic approaches using gene therapy could be of great interest in the frame of ALS-FTD, by adding an exogenous gene to compensate the loss of function of the endogenous mutated proteins and restore cellular homeostasis. The principal advantage of this gene therapy approach is that unlike ASOs strategies, it might work in a mutation independent manner, by restoring levels of wild type FUS and decreasing levels of mutant FUS irrespective of the mutation. Furthermore, if the transgene used remains competent for autoregulation, it would avoid most of the toxic effects linked to FUS overexpression (Mitchell *et al.*, 2013). In principle, such approach of overexpression of an autoregulatory competent mRNA could be applied to a number of ALS related genes that also show similar autoregulation. This is the case for instance of mutations in other RBPs such as *TARDBP* or *MATR3*. White and collaborators demonstrated that mutant TDP-43 leads to splicing alterations of its mRNA, in which variants containing the exon7 increase, thus increasing TDP-43 levels which become toxic to cells (White *et al.*, 2018). A similar gene strategy as the one we have used in our $Fus^{\Delta NLS}$ mouse model could be of aimed in TDP-43 mutations, since the addition of human TDP-43 could lead promote the exon 7 skipping pathway, thus activating its autoregulation mechanism and normalizing TDP-43 protein levels. Such an approach could also improve the gene therapy approach in the frame of other MNDs such as spinal muscular atrophy (SMA), where *SMN* mutations result in the degeneration of lower motor neurons (Lefebvre *et al.*, 1995). Interestingly, *SMN* undergoes similar alternative splicing with exon7 skipping resulting in nonsense-mediated decay of the product (Naryshkin *et al.*, 2014). Two clinical trials have shown beneficial effects in SMA patients, the first one using ASO leading to increased levels of SMN protein containing the exon7, and the second one by the administration of human SMN via an AAV9, compensating the loss of endogenous SMN protein (Chiriboga *et al.*, 2016; Mendell *et al.*, 2017). However, both therapeutic approaches present their limitations since the administration of ASOs was intrathecally performed, which is invasive, and the administration of AAV9 can lead to immune responses against the viral vector (Pattali *et al.*, 2019) . Long term toxic effects of SMN overexpression are also not well characterized. In view of our results with the activation of *Fus* autoregulation *via* this alternative splicing pathway, it would be of great interest to investigate whether such gene therapy approach could be applied in the frame of SMA, by introducing human SMN mRNA competent for autoregulation, which would limit overexpression and remain in a more physiological concentration range.

2. THE FUS$^{\Delta NLS}$ MOUSE MODEL IN THE FRAME OF FTD.

The characterization of our Fus$^{\Delta NLS}$ mouse model has allowed us to demonstrate for the first time that the mislocalization of FUS is sufficient to induce FTD-like phenotypes. Importantly, we have recapitulated many behavioural and cognitive aspects where mice show to be hyperactive, disinhibited, with social memory and consolidation memory deficits. All of these symptoms are also present in FTD patients', particularly in bvFTD individuals, showing agitated and disinhibited behaviours as well as memory impairments (Lanata e Miller, 2016). Other mouse models have shown to present similar behavioural and cognitive deficits such as disinhibition in in C9orf72, GRN, CHMP2B and Tau mice models; social disinterest in C9orf72, GRN and CHMP2B mice models; and memory deficits in GRN, TDP-43, Tau and VCP mice models. Nevertheless, FTD patients progress towards behavioural changes that we did not observe in our mouse model but have been identified in others such as apathy in Tau mice models or stereotypies in Tau and CHMP2B mice models (Vernay *et al.*, 2016).

Atrophy of frontal and temporal lobes in FTD is another hallmark of the disease, whereas specifically in bvFTD patients an atrophy of the striatum has been observed, being the most severe in FUS-FTD patients' (Halabi *et al.*, 2013). Preliminary results of 7T MRI scans of our Fus$^{\Delta NLS}$ mice seem to indicate a global atrophy of the brain, with marked striatal atrophy and ventriculomegaly. Striatal atrophy has been linked in FTD with the development of disinhibition and motor symptoms (Josephs *et al.*, 2010; Garibotto *et al.*, 2011; Halabi *et al.*, 2013). Thus, FUS alterations could lead to atrophy of brain structures, in particular cortical, striatal and hippocampal in bvFTD disrupting the proper communication between these regions and contributing to the observed behavioural, motor and cognitive defects in FUS-FTD patients. The respective importance of the different structures involved in the developed phenotypes is a matter of future research.

Besides brain atrophy, FTD is also characterized by the concomitant loss of synaptic density in the frontal cortex upper layers (Brun *et al.*, 1995; Liu *et al.*, 1996), accompanied by the loss of synaptic markers such as synaptophysin (Clare *et al.*, 2010), Rab3A, synaptotagmin and SNAP-25 among others (Ferrer, 1999). Moreover, FTD patients' have been clinically characterized by a decrease in short-interval intracortical inhibition and facilitation (Benussi *et al.*, 2017), thus showing dysfunctional cortical inhibitory circuits. GABAergic synapses are involved in many cortical circuits participating in the control of varied functions such as motor control with cortico-striatal circuits or cognitive functions in cortico-hippocampic circuits among others (Maffei *et al.*, 2017). Importantly, their proper functioning is essential to maintain homeostatic levels of neurons activation with the excitatory/inhibitory balance (Maffei *et al.*, 2017). In accordance, our results seem to indicate that FUS mislocalization leads to alterations in the expression of synaptic proteins and synaptic vesicles in the frontal cortex, but more importantly of inhibitory synapses, which further present

structural abnormalities. Furthermore, $Fus^{\Delta NLS}$ mice present altered neuronal activity patterns, overall suggesting dysfunctions in the excitatory/inhibitory balance. However, not only alterations in FUS result in defects in synapses, since loss of synaptic density has also been observed in mouse models of Tau-FTD (Roberson, 2012).

Interestingly, several studies have shown similar behaviour and cognitive defects in mice models carrying *MAPT* mutations resulting in Tau protein depositions (Jul *et al.*, 2016; Przybyla *et al.*, 2016). FUS is known to participate in the splicing of many mRNAs, where mutations in FUS lead to defective spliced products. Tau is a FUS target and its splicing is controlled by FUS. Mutations in FUS have been described to increase levels of the variant 4R-Tau, prone to form aggregates (Orozco *et al.*, 2012; Ishigaki *et al.*, 2017). Furthermore, FUS participates in the mRNA splicing of Nrxn, SynGAP and GluA1 and stabilizes their mRNA. Alterations in FUS have shown to alter synaptic mRNA levels of these RNA targets, leading to defects in dendrites and synapses, resulting in behaviour and cognitive functions (Lagier-Tourenne *et al.*, 2012; Udagawa *et al.*, 2015; Yokoi *et al.*, 2017). Therefore, defects in FUS localization could alter splicing variants of many of its mRNA targets having important roles in the development and maintenance of synapses and synaptic functions, which contribute to the development of behavioural and cognitive symptoms in FTD.

We did not observe some typical FTD histopathological hallmarks such as, cytoplasmic FUS aggregates colocalizing with other proteins such as TNPO as it has been described in FTD patients (Neumann, Rademakers, *et al.*, 2009; Neumann *et al.*, 2012). Likewise, other FUS mouse models expressing mutant forms of the protein have been unable to observe FUS aggregates (Lopez-Erauskin *et al.*, 2018). TDP-43, GRN and VCP mice models have been characterized with the presence of neuronal ubiquitinated TDP-43 inclusions. In particular, TDP-43 mice models have shown to present TDP-43 inclusions in interneurons and cortical pyramidal neurons in layer V, which are particularly vulnerable in FTD (Roberson, 2012). Furthermore, FUS-FTD patients present post-translational modifications of FUS with decreased levels of arginine-methylation and FUS is found in unmethylated or monomethylated forms, whereas in healthy conditions it is found dimethylated. Our mice model did not show such decrease in methylation, thus differing from FUS-FTD physiopathology. Besides, FTD patients also present markers of neuroinflammation since increased levels of cytokines have been found in their CSF. Our $Fus^{\Delta NLS}$ mouse model showed no reactive astrocytes nor microglial cells. Several studies have been able to observe astocytosis and microgliosis in their animal models, presenting TDP-43, GRN, VCP or FUS mutations (Roberson, 2012; Lopez-Erauskin *et al.*, 2018). The lack of certain pathophysiological hallmarks in our ALS-FTD mouse model suggest the intervention of other underlying molecular mechanisms of FUS in the frame of FTD. Further investigations are required to elucidate the mechanisms of action of FUS in pathological conditions leading to full FUS-FTD phenotypes.

In all, our $Fus^{\Delta NLS}$ mouse model represents a reliable model for FUS-FTD as we recapitulate a series of behavioural (disinhibition), cognitive (memory impairment), anatomical (atrophy) and cellular (synapses) deficits found in FTD patients by mislocalizing FUS to the cytoplasm. However, our study has raised several questions such as with which molecular targets mislocalized FUS may interact at the synapses leading to the alterations we have observed. For that, in collaboration with Dr Dormann laboratory, we have immunoprecipitated cortical cytosolic FUS and characterized interacting RNAs. We found that FUS interacts with a series of components in our preliminary results that could be responsible of these alterations. Interestingly, we found that mutant cytoplasmic FUS interacts less than wild-type FUS with Chrnb2 and Ric3 mRNAs, where Chrnb2 is a subunit of nicotinic receptors and *Ric3* acts as a nicotinic receptor assembly chaperone. *CHRNB2* encodes for the β2 subunit of nicotinic ACh receptors and their activation has been shown to play a role in the formation of dendritic spines in neurons (Lozada *et al.*, 2012). The β2 subunit is most commonly found in the CNS forming the heteromeric α4β2 nicotinic receptor which has been linked to improve working memory (Buccafusco *et al.*, 2007). Furthermore, mutations in *CHRNB2* have been linked to a subtype of epilepsy, indicating it is involved in the excitatory/inhibitory balance and its depletion leads to attention deficits (Phillips *et al.*, 2001; Guillem *et al.*, 2011). Therefore, FUS decreased interaction with Chrnb2 mRNA could lead to decreased expression of β2 subunit, which could contribute to neuronal hyperexcitability, dendritic spines defects and cognitive impairments. Importantly, Ric3 is a chaperone involved in the assembly of subunit nicotinic receptor such as the homomeric α7 nicotinic receptor, whereas it increases the expression of α4 and β2 subunits (Dau *et al.*, 2013). Mutations in RIC3 have been linked to Parkinson's disease, particularly to patients without motor-symptoms but showing extrapyramidal symptoms such as hallucinations or depression (Sudhaman *et al.*, 2016). Thus, decreased interaction of FUS with Ric3 mRNA could impact the expression levels of α4 and β2 subunits, contributing to the aforementioned symptoms. Moreover, we found that the interaction of mutant cytoplasmic FUS with other nicotinic receptor assembly components such as *Apc*, *Macf1* and *Nrxn1* results in altered spliced variants of their mRNAs. APC participates in the assembly of neuronal nicotinic synapses (Temburni *et al.*, 2004) by retrograde signals via neurogilin, neurexin's post-synaptic clustering partner, thus indicating neurexin's localization at the pre-synaptic neuronal nicotinic synapses (Rosenberg *et al.*, 2010). Neurexin mediates the assembly of presynaptic terminals, where α-neurexin couples calcium channels to the exocytotic machinery and β-neurexin assembles the pre-synaptic active zone (Dean *et al.*, 2003). Mutations in APC have been linked to mental retardation or autism, whereas defects in neurexin have been linked to also been linked to schizophrenia and epilepsy. Finally, Macf1 has been found to regulate the migration and position of GABAergic cortical interneurons in the mouse cortex (Ka *et al.*, 2017) and mutations have been linked to Parkinson's disease (Wang *et al.*, 2017). Overall, alterations in the splicing of these mRNAs could lead to defects in cortical interneurons, impairment of the excitatory/inhibitory balance and defects in synapses maturation and transmission. Therefore, we are

currently investigating if cytoplasmic FUS impairs the transport or translation of these mRNAs on synaptosomes extractions and aim to determine FUS localization in pre-/post-synapses in the cortex along with other relevant target proteins with immunohistochemical techniques.

3. THE CHOLINERGIC SYSTEM: CAUSE OR CONSEQUENCE?

In the CNS the cholinergic system is involved in the modulation of many different functions. It is characterized by two major pools of cholinergic nuclei in the basal forebrain and the brainstem. The basal forebrain (BF) is the cholinergic pool which projections reach most cortical and subcortical regions of the brain and is composed of several nuclei namely, the medial septal nucleus (MSN), the diagonal band of Broca (DBB), the nucleus basalis of Meynert (NBM) and the substantia innominate (SI). The MSN and the vertical limb of the DBB send projections to the hippocampus, enthorinal cortex and parahippocampus, whereas the horizontal limb of the DBB, the NMB and the SI send their projections to the neocortex and the amygadala (Ballinger *et al.*, 2016). Therefore, the BF is actively involved in the modulation of attention with projections targeting the frontal and sensory cortex, spatial memory with projections emanating from the MSN and DBB to the hippocampus and retention of emotional memory with projection to the amygdala (Ballinger *et al.*, 2016). The modulation of these cholinergic functions is mainly performed by enhancing the cholinergic tone via the activation of cholinergic receptors. Two types of cholinergic receptors exist, muscarinic metabotropic cholinergic receptors and nicotinic ionotropic cholinergic receptors, where both of them are widely expressed in the brain (Thiele, 2013). A great variety of cholinergic receptors composition and functions have been characterized, but particularly nicotinic β2 and α7 receptors have been involved in the modulation of attention (Guillem *et al.*, 2011) and memory (Ballinger *et al.*, 2016). At the cortical level, they can induce cholinergic currents in interneurons of all layers and pyramidal neurons in layers II/III and V, where pre-synaptic β2 can also activate pyramidal neurons in layer VI (Poorthuis *et al.*, 2013). Memory modulation in the hippocampus as well as in the amygdala seems to be dependent upon the expression and activation of the nicotinic α7 receptor, which has been also found to strengthen hippocampal synapses by the stabilization of GluA1 receptors in hippocampal dendritic spines (Halff *et al.*, 2014; Ballinger *et al.*, 2016). Therefore, alterations in the cholinergic system can result in defects in the modulation of such cognitive functions.

Alzheimer's disease was the first neurodegenerative disease characterized by the degeneration of the cholinergic system, accompanied by the formation of amyloid-β (Aβ) deposition plaques and neurofibrillary tangles due to protein Tau phosphorylation. Patients' generally present a loss of 75% of BF cholinergic neurons (BFCN), decreased cortical and hippocampal ChAT activity and reduction of cholinergic fibers network density (Geula e Mesulam, 1989; Pepeu e Grazia Giovannini, 2017). Thus, BFCN dysfunction and loss result in cognitive dysfunction in AD patients (Ballinger *et al.*, 2016). Moreover, the atrophy of the BF precedes and predicts the cortical pathology and further correlates with Aβ burden (Kerbler *et al.*, 2015; Schmitz *et al.*, 2016). Parkinson's disease is characterized by the loss of dopaminergic neurons in the substantia nigra, motor symptoms and in some cases the presence of α-synuclein depositions also known as Lewy bodies (Bernheimer *et al.*, 1973; Spillantini, 1999). Nevertheless, Parkinson's disease has also been characterized by the loss of BFCN

(Whitehouse *et al.*, 1983), decreased cholinergic innervation of cortex and thalamus and attention and memory deficits. α-synuclein animal models have shown to present cognitive deficits, loss of cholinergic neurons in MSN and DBB along with reduced cholinergic fibers in cortex and hippocampus. Furthermore, the deposition of α-synuclein in cholinergic neurons disrupts the synthesis of Ach, its trafficking and release (Magen *et al.*, 2012). Interestingly, Quik and collaborators demonstrated that the administration of nicotine in a mouse model of Parkinson's disease had neuroprotective effects preserving dopaminergic neurons degeneration and modulating neuroinflammation (Quik *et al.*, 2012). Therefore, enhancement of the cholinergic tone seems to have neuroprotective properties. However, Ziegler and collaborators found that the degeneration of the dopaminergic system would precede the degeneration of the cholinergic system in Parkinson's disease (Ziegler *et al.*, 2013), where the cholinergic system would compensate the deficits of the dopaminergic system, delaying the appearance of symptoms which would become visible when the cholinergic system would be profoundly affected (Ballinger *et al.*, 2016). Moreover, the cholinergic dysfunction in Parkinson's disease could be at the origin of Parkinson's disease with dementia, since reduced BF volume has been linked to cognitive decline in Parkinson's disease patients (Barrett *et al.*, 2019). Conversely, studies in FTD patients have not observed major alterations of the BFCN nor cortical cholinergic innervation (Pepeu e Grazia Giovannini, 2017), therefore suggesting deficits in FTD patients would arise from the other underlying dysfunctions.

The vulnerability of BFCN has been widely studied, in particular in the case of Alzheimer's disease where novel hypotheses have been proposed. While BFCN degenerate in Alzheimer's disease, cholinergic neurons in the brainstem are spared (Giovannelli *et al.*, 1995). The main difference between these two cholinergic populations is that BFCN bind and express nerve growth factor (NGF) receptors, a neurotrophic factor, whereas brainstem cholinergic neurons do not (Richardson *et al.*, 1986). NGF has been shown to play crucial roles in the modulation of BFCN where its mRNA and protein expression have been found in BFCN, hippocampus, cortex and cholinergic interneurons. In the BFCN, NGF has shown to increase ChAT activity allowing the differentiation of BFCN and the modulation of synaptic functions in the hippocampus and cortical circuits. Furthermore, it can be internalized and retrogradely transported along BFCN axons, which have the particularity of being extremely long. Thus, BFCN require of important metabolic energy for their proper functioning. Conversely, alterations in NGF expression or NGF sequestration have shown to decrease ChAT expression and subsequently reduced number and size of BFCN. Moreover, hippocampal cholinergic denervation has shown to lead to the accumulation of NGF in the hippocampus, suggesting a disruption in the NGF-BFCN axis (Chen e Mobley, 2019). Therefore, NGF seems to be a crucial neurotrophic factor for the homeostasis of BFCN and alterations in its transport or signalling could lead to dysfunctions in the BFCN. NGF signalling pathway occurs via its binding to two different receptors, TrKA and p75NTR, with higher affinity for the first one. TrKA activation leads to activation of MAPK, Pi3K and PLC-γ pathways, involved in cellular

homeostasis and proliferation, whereas the activation of p75NTR has been linked in regulating BFCN axons pruning and further can lead to the activation of cell death signalling pathways (Bothwell, 2016; Boskovic *et al.*, 2018). Furthermore, the knock-out of TrKA in a mouse model showed degeneration of BFCN and reduced hippocampal cholinergic fibers (Fagan *et al.*, 1997). NGF preferentially binds to TrKA and the complex ligand-activated receptor can be internalized in endocytes and retrogradely transported via dynein transport (Howe e Mobley, 2005). In Alzheimer's disease patients' decreased levels of NGF and TrKA have been found in the BFCN and cortex, accompanied of increased levels of NGF in the hippocampus, indicating a disruption of the NGF-BFCN axis. Furthermore, increased levels of the immature form of NGF (pro-NGF) have been found in patient's cortex, suggesting alterations in NGF maturation processes (Pepeu e Grazia Giovannini, 2017; Chen e Mobley, 2019). However, p75NTR levels remain the same and studies suggest that Aβ would induce the activation of cell death signalling pathways *via* p75NTR, thus resulting toxic for cholinergic neurons by decreasing trophic factors and promoting apoptotic molecules (Perini *et al.*, 2002; Pákáski e Kálmán, 2008). Interestingly, pre-tangle Tau depositions have been observed in BFCN and correlate with early changes in cognition in Alzheimer's disease patients. Moreover, the degeneration of other neurodegenerative diseases such as ALS have observed alterations in the BFCN, where a study using the $SOD1^{G93A}$, known to present toxic aggregates in motor neurons, observed significant loss of BFCN (Crochemore *et al.*, 2005). Thus, Alzheimer's, Parkinson's and ALS share a common feature that could lead to the degeneration of BFCN, which because of their morphological and functional properties require constant trophic support, which is the formation of aberrant toxic intracellular protein depositions.

In regards to aforementioned hypothesis of BFCN neurodegeneration and subsequent cognitive deficits, we could hypothesize that similar mechanisms could be involved in our $Fus^{\Delta NLS}$ mouse model. $Fus^{\Delta NLS}$ mice show cognitive deficits and behavioural impairments. It is well known that FUS is responsible for the transport of GluA1 mRNA to dendrites and that Ric3 is necessary for the assembly of nicotinic α7 receptors. Our preliminary results suggest that mutant cytoplasmic FUS interacts less with Ric3 and GluA1 mRNA transport could also be altered as previous studies have suggested (Udagawa *et al.*, 2015). Therefore, decreased interactions of FUS with Ric3 could lead to impaired assembly of nicotinic α7 receptors, important for the stabilization of GluA1 in synapses, and decreased levels of GluA1 in dendrites due to defects in transport could lead to defects in dendrites resulting in cognitive impairments. Furthermore, β2 nicotinic receptors have been shown to induce cholinergic currents in cortical interneurons and pyramidal neurons. Similarly, our preliminary results suggest decreased interactions of FUS with CHRNB2, which could originate defects in cortical the excitatory/inhibitory balance, resulting in the observed neuronal hyperexcitability of $Fus^{\Delta NLS}$ mice. The degeneration of BFCN accompanied by reduced cortical cholinergic innervation and the fact that $Fus^{\Delta NLS}$-ChAT Cre mice present alleviation in behavioural impairments, clearly indicate an active involvement of the cholinergic system. Therefore, aiming to modulate the cholinergic tone could be considered as therapeutic approach. Two

different treatments could be considered, first like Quik and collaborators did with the administration of nicotine (Quik *et al.*, 2012), which we are currently testing in acute and chronic treatments, which we could expect to improve cognitive deficits and behavioural impairments. Second, by administrating NGF as Figuereido and collaborators did, where they administered intracerebroventricularly NGF in a lesioned mouse model and prevented the degeneration of BFCN (Figueiredo *et al.*, 1996). Notably, clinical trials in Alzheimer's and FTD patients with NGF have shown promising results (Eyjolfsdottir *et al.*, 2016; De Bellis *et al.*, 2018). Nevertheless, preliminary studies should be performed in order to identify potential alterations of the NGF-BFCN axis in our $Fus^{\Delta NLS}$ mouse model, with measurements of NGF, pro-NGF, TrKA levels in BFCN, cortex and hippocampus and molecular indicators of the activation of cell death pathways in BFCN. Moreover, we could speculate several hypothesis where mutant FUS could alter the NGF-BFCN axis at different levels such as interfering with the endocytosis process of NGF-active TrKA, sequestering NGF in aggregates, therefore decreasing the availability of trophic factors, rendering BFCN vulnerable and leading to their degeneration by enhancing the activation of apoptotic pathways *via* p75NTR activation (Figure 19).

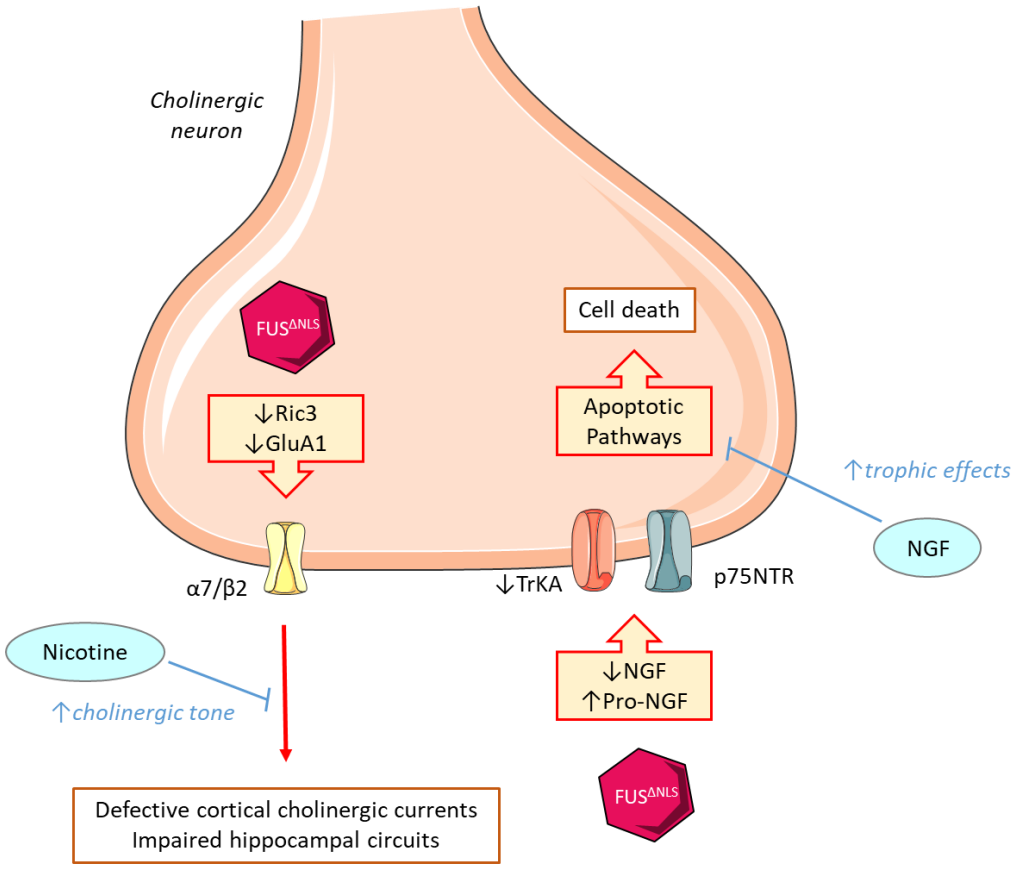

Figure 19: Working model of BFCN degeneration.
$Fus^{\Delta NLS}$ interacts less with mRNAs of nicotinic subunits (β2) and molecules involved in nicotinic receptors assembly (Ric3) and synaptic functions (GluA1). This could lead to cortical defects in cholinergic currents transmission and disruption of hippocampal circuits. Moreover, $Fus^{\Delta NLS}$ could interfere with the maturation of NGF or its receptor TrkA expression, leading to the activation of apoptotic pathways via p75NTR stimulation. Therapeutic treatments enhancing the cholinergic tone by nicotine administration or promoting cell survival increasing the availability of trophic factor NGF could prevent BFCN degeneration and preserve proper cholinergic transmission.

Conclusion

Conclusion

ALS and FTD are two neurodegenerative diseases with no current effective treatments. Even though they are two distinctive diseases where ALS is characterized by the progressive degeneration of upper and lower motor neurons with the subsequent appearance of motor functions deterioration and FTD is characterized by the progressive atrophy of frontal and temporal lobes with subsequent neurodegeneration and development of cognitive and behavioural deficits, they share a series of genetic mutations and pathophysiological hallmarks that define a continuum between them. Interestingly, about 15% of ALS patients clinically develop FTD and vice versa, endorsing even more the existence of an ALS-FTD continuum.

Mutations in FUS are linked mainly with familial cases of ALS, affecting young patients and leading to a rapid progression of the disease. Most FUS mutations lead to alterations in its NLS resulting in cytoplasmic mislocalization of the protein, gaining toxic functions that contribute to motor neurons degeneration. FTD patients, although not carrying FUS mutations, present cytoplasmic FUS aggregates, thus alterations in FUS are linked to both diseases seemingly by different molecular mechanisms.

Our findings have allowed to highlight in a $Fus^{\Delta NLS}$ mouse model a potential gene therapy therapeutic approach by the addition of a human wild-type FUS gene, showing a rescue in homozygous mutation lethality, muscular weakness and cytoplasmic levels of mislocalized mutant FUS. We have demonstrated that these effects are regulated by the activation of the alternative splicing pathway of its own mRNA leading to the skipping of the exon7, which results in an unstable form that is degraded by nonsense-mediated decay. Importantly, similar gene therapy approaches can be considered for other mutations linked to ALS such as TDP-43 or MATR3.

Furthermore, we have shown that solely the mislocalization of FUS in our $Fus^{\Delta NLS}$ mouse model is sufficient to induce FTD-like symptoms, accompanied by transcriptomic and structural synaptic defects. In particular, behavioural and cognitive deficits such as disinhibition, impaired social interactions and memory deficits which are also found in FTD patients. Moreover, we have identified alterations of cortical inhibitory synapses that could contribute to an imbalance of the excitatory and inhibitory systems resulting in cortical neurons hyperexcitability, which could underly the development of the observed FTD-like symptoms.

Finally, we have found that the cholinergic system is profoundly affected in our mouse model, with the degeneration of BFCN and their projections to cortical regions and hippocampus, crucial for the proper sustaining of behavioural and cognitive functions. The selective restoration of FUS mutation in cholinergic neurons showed no beneficial effects in the degeneration of cholinergic neurons even though behavioural phenotypes were partially rescued. Therefore, the cholinergic system in our $Fus^{\Delta NLS}$ mouse model degenerates in a non-autonomous manner and behaviour impairments are partially dependent upon cholinergic expression

of the mutation. Thus, novel therapeutic approaches targeting the cholinergic system could be of great interest to modulate or alleviate symptoms in FTD patients.

In all, these studies have allowed a better understanding of FUS autoregulation mechanism and how important the modulation of the protein levels are in terms of aiming new genetic therapeutic approaches. Moreover, we have elucidated molecular and structural abnormalities due to FUS mislocalization that mimic FTD patients' symptoms and novel implications of the cholinergic system in the disease. Further investigations are required to develop efficient therapies regulating FUS homeostatic levels and its molecular mechanisms involved in the frame of ALS-FTD.

Annex

FUS-mediated transcriptional regulation of acetylcholine receptor at neuromuscular junctions is compromised in amyotrophic lateral sclerosis

Gina Picchiarelli[1,*], Maria Demestre[2,*], Amila Zuko[3], Marije Been[3], Julia Higelin[2], Stéphane Dieterlé[1], Marc-Antoine Goy[1], Moushami Mallik[3,4,5], Chantal Sellier[6], Jelena Scekic-Zahirovic[1], Li Zhang[4,5], Angela Rosenbohm[7], Céline Sijlmans[3], Amr Aly[2], Sina Mersmann[4,5], Inmaculada Sanjuan-Ruiz[1], Annemarie Hübers[7], Nadia Messaddeq[6], Marina Wagner[4,5], Nick van Bakel[3], Anne-Laurence Boutillier[8], Albert Ludolph[7], Clotilde Lagier-Tourenne[9,10], Tobias M. Boeckers[2,11,#], Luc Dupuis[1,#], Erik Storkebaum[3,4,5,#]

[1]Université de Strasbourg, Inserm, UMR-S1118, F-67085, Strasbourg, France
[2]Institute of Anatomy and Cell Biology, Ulm University, 89081 Ulm, Germany
[3]Department of Molecular Neurobiology, Donders Institute for Brain, Cognition and Behaviour, Radboud University, Nijmegen, The Netherlands
[4]Molecular Neurogenetics Laboratory, Max Planck Institute for Molecular Biomedicine, Muenster, Germany
[5]Faculty of Medicine, University of Muenster, Muenster, Germany
[6]IGBMC, INSERM U964, CNRS UMR7104, University of Strasbourg, 67404, Illkirch, France.
[7]Department of Neurology, Oberer Eselsberg 45, 89081 Ulm Germany
[8]Université de Strasbourg, Centre National de la Recherche Scientifique, UMR 7364, Laboratoire de Neurosciences Cognitives et Adaptatives, F-67000 Strasbourg, France
[9]Department of Neurology, Massachusetts General Hospital, Harvard Medical School, Charlestown, MA 02129, USA
[10]Broad Institute of Harvard University and MIT, Cambridge, MA 02142, USA
[11]DZNE, Ulm site, 89081 Ulm, Germany

*these authors contributed equally

[#]corresponding authors:

Erik Storkebaum: e.storkebaum@donders.ru.nl
Phone: +31 6 25 76 60 73
Luc Dupuis: ldupuis@unistra.fr
Phone: +33 3 68 85 34 57
Tobias Boeckers: tobias.boeckers@uni-ulm.de
Phone:+ 49-731-5023220/1

Abstract

Acetylcholine receptor (AChR) subunit genes are selectively expressed in subsynaptic nuclei of innervated muscle fibers. This is mediated by binding of neural agrin to its postsynaptic receptor Lrp4, leading to activation of MuSK and the ETS transcription factor ERM. Neuromuscular junction (NMJ) disruption is considered an early event in the pathogenesis of the motor neurodegenerative disorder amyotrophic lateral sclerosis (ALS). Yet, there is currently no direct link between NMJ establishing pathways and ALS-causing gene mutations. The most severe forms of ALS are associated with heterozygous mutations in *FUS*, encoding a DNA/RNA-binding protein involved in gene expression regulation. Here, we report NMJ morphology defects in a knock-in *Fus*-ALS mouse model. Newborn homozygous *Fus* knock-in mice displayed predominantly postsynaptic NMJ defects that could be attributed to intrinsic toxicity of mutant *Fus* in muscle. Adult heterozygous *Fus* knock-in mice displayed smaller neuromuscular endplates, that denervated long before motor neuron cell body loss, consistent with a 'dying-back' mechanism of motor neurodegeneration. Importantly, FUS was enriched in subsynaptic nuclei in wild type mice and this enrichment depended on innervation and was perturbed in heterozygous *Fus* knock-in mice. Mechanistically, FUS bound to the promoter region of AChR subunit genes and stimulated their transcription. Moreover, FUS physically interacted with ERM, was required for ERM-dependent induction of AChR expression, and *vice versa*, ERM was required for FUS to stimulate AChR expression. In iPSC-derived myotube cultures and motor neuron-myotube co-cultures from *FUS*-ALS patients, endplate maturation was impaired and AChR expression reduced. Co-cultures showed intrinsic toxicity of ALS-mutant FUS in both motor neurons and myotubes. Finally, electromyographic examination and muscle biopsies of *FUS*-ALS patients revealed myogenic changes, muscle atrophy and impaired enrichment of FUS in subsynaptic nuclei, underscoring the potential relevance of our findings for human *FUS*-ALS. Together, our findings reveal a key role for FUS in regulating selective expression of AChR genes in subsynaptic nuclei and suggest that intrinsic toxicity of ALS-mutant FUS in muscle may contribute to dying-back motor neuronopathy in *FUS*-ALS.

Introduction

The neuromuscular junction (NMJ) is the chemical synapse between motor neurons and skeletal muscle fibers. In mammals, neuromuscular transmission is mediated by release of acetylcholine (ACh) from presynaptic terminals, which binds and activates the postsynaptic nicotinic acetylcholine receptor (AChR), a ligand-gated ion channel. During development, even before innervation, AChR clusters are already present in the center of the muscle – the region of future innervation – in a nerve-independent process called prepatterning [1, 2]. Muscle innervation by motor neurons induces AChR aggregation in postjunctional membranes and dispersion of nonsynaptic AChR clusters. Interestingly, upon innervation, transcription of AChR subunit genes and other synapse-specific genes becomes confined to myonuclei underlying the neuromuscular contact, referred to as 'fundamental' or 'subsynaptic' nuclei [2, 3]. On the one hand, this process involves suppression of synapse-specific genes in nonsynaptic nuclei by nerve-evoked muscle activity. On the other hand, synapse-specific gene expression is stimulated in subsynaptic nuclei by agrin secreted from motor nerve terminals. Agrin binding to its postsynaptic receptor Lrp4 (lipoprotein receptor-related protein 4) leads to activation of MuSK (muscle-specific kinase) and the downstream Rac/MKK7/JNK pathway [2, 3]. This results in phosphorylation and activation of the ETS transcription factor ERM, also known as ETV5, which binds to N-box elements in the promoters of synapse-specific genes, including those encoding AChR subunits, utrophin and acetylcholinesterase [4], and is associated with specific chromatin modifications in these subsynaptic nuclei [5].

Proper NMJ function is essential for posture, movement and respiration, and structural and functional NMJ defects have been implicated in a plethora of diseases [2], including the motor neurodegenerative disease amyotrophic lateral sclerosis (ALS) [6]. ALS is considered a 'dying-back' motor neuronopathy, as at least in mutant SOD1 mouse models and a sporadic ALS patient, denervation of neuromuscular endplates is an early pathological event that precedes axonal degeneration and loss of motor neuron cell bodies [7-9]. The most severe forms of ALS, with early onset and rapid disease progression, are caused by heterozygous mutations in *FUS*, which encodes a DNA/RNA binding protein that is involved in several steps of gene expression regulation, including regulation of transcription, chromatin remodeling, mRNA splicing and mRNA subcellular localization [10]. FUS is one of the protagonists of a group of

RNA-binding proteins that have all been linked to ALS, including TDP-43, TAF15, EWSR1, hnRNPA2B1, hnRNPA1 and Matrin-3, thus implicating defects in RNA metabolism in ALS pathogenesis [6, 11]. Beyond ALS, cytoplasmic inclusions containing FUS or TDP-43 are pathological hallmarks in respectively ~10% and ~45% of patients with frontotemporal dementia, the most common form of dementia before the age of 60 [11]. The vast majority of ALS-causing *FUS* mutations cluster in the extreme C-terminus of FUS, either missense mutations in the nuclear localization signal (NLS) or frameshift or nonsense (truncating) mutations in or before the NLS [12]. These mutations result in cytoplasmic mislocalization of FUS and concomitant reduction of nuclear FUS levels, and this subcellular mislocalization is likely an important event in ALS pathogenesis [11, 13].

We have previously generated a knock-in *Fus*-ALS mouse model, which expresses a truncated FUS protein that lacks the 20 C-terminal amino acids which constitute the NLS ($Fus^{\Delta NLS}$ mice) [14]. Reminiscent of *FUS*-ALS, in motor neurons the $Fus^{\Delta NLS}$ mutation results in FUS cytoplasmic mislocalization with concomitant reduction of nuclear FUS levels. In order to discriminate between phenotypes induced by loss of nuclear FUS function versus toxicity induced by cytoplasmic mislocalization of the mutant FUS protein, we also generated *Fus* knockout mice ($Fus^{-/-}$ mice)[14]. Overall, homozygous $Fus^{\Delta NLS/\Delta NLS}$ and $Fus^{-/-}$ mice displayed similar phenotypes, most prominently perinatal lethality due to respiratory insufficiency, likely attributable to loss of nuclear FUS function. However, loss of ~30% of motor neuron cell bodies was found in $Fus^{\Delta NLS/\Delta NLS}$ but not $Fus^{-/-}$ mice, suggesting a gain-of-toxic-function mechanism [14]. Heterozygous $Fus^{\Delta NLS/+}$ mice provide a mouse model for *FUS*-ALS, as they recapitulate several pathological hallmarks of ALS and they display adult-onset progressive motor neurodegeneration associated with motor deficits [15].

Here, we investigated the possible contribution of NMJ defects to *FUS*-ALS. In *Fus* mutant mouse models, we identified predominantly postsynaptic defects: the endplate surface area and the total number of endplates in hind limb muscles was significantly reduced in newborn $Fus^{\Delta NLS/\Delta NLS}$ mice. In adult $Fus^{\Delta NLS/+}$ mice, endplate surface area was reduced and progressive endplate denervation preceding motor neuron loss was found. Selective reversal of the $Fus^{\Delta NLS}$ allele to wild type in skeletal muscle revealed that postsynaptic defects in $Fus^{\Delta NLS/\Delta NLS}$ mice are attributable to intrinsic toxicity of the cytoplasmically mislocalized FUS protein in muscle.

Furthermore, we found that FUS is enriched in subsynaptic nuclei and that FUS stimulates transcription of AChR subunit genes through ERM. These findings may be relevant for human *FUS*-ALS, as studies in iPSC-derived myotubes and motor neurons of *FUS*-ALS patients demonstrated an intrinsic toxicity of ALS-mutant FUS in both motor neurons and myotubes. In addition, electromyography (EMG) and muscle biopsies from *FUS*-ALS patients revealed myogenic pathological activity and impaired enrichment of FUS in subsynaptic nuclei. Together, our data indicate that FUS regulates the synapse-specific expression of AChR subunit genes, that NMJ pathology is likely an early event in *FUS*-ALS, and that ALS-mutant FUS is not only toxic in motor neurons but also in muscle fibers.

Results

Neuromuscular junction morphology defects in newborn *Fus* mutant mice

Complete loss of the FUS protein in *Fus*$^{-/-}$ mice, as well as its mislocalization in the cytoplasm in *Fus*$^{\Delta NLS/\Delta NLS}$ mice, leads to death at birth [14]. Since possible defects in NMJs could underlie premature death of both mouse models, we evaluated NMJ morphology in newborn *Fus*$^{\Delta NLS/\Delta NLS}$ and *Fus*$^{-/-}$ mice. Thick longitudinal sections through the tibialis anterior muscle were stained for neurofilament to visualize motor axons and SV2 to visualize synaptic vesicles in nerve terminals. Fluorescently labeled bungarotoxin (BTX) was used to simultaneously visualize AChR clusters in muscle endplates (**Figure 1a-d**). As endplate morphology and size is rather heterogeneous, even in wild type pups, we analyzed ~100 to 150 NMJs per muscle, in order to obtain representative average values.

Surprisingly, in the tibialis anterior, endplate innervation - evaluated by scoring whether endplates are apposed by a presynaptic nerve terminal - was not different between *Fus*$^{\Delta NLS/\Delta NLS}$ and wild type littermate controls, with almost all endplates innervated (**Figure 1a,b,e**). However, the endplate surface area was significantly reduced in *Fus*$^{\Delta NLS/\Delta NLS}$ muscles, by ~27% as compared to control (**Figure 1f**). We further quantified the total number of endplates in the tibialis anterior by counting all endplates in the different focal planes of each section (see methods for details). Remarkably, the total number of endplates was significantly reduced (~19%) in *Fus*$^{\Delta NLS/\Delta NLS}$ muscles (**Figure 1g**). In *Fus*$^{-/-}$ muscles, endplates were normally innervated (**Figure 1c,d,h**), and the endplate area was not altered (**Figure 1i**). However, similar to *Fus*$^{\Delta NLS/\Delta NLS}$ mice, the total number of endplates in the tibialis anterior was reduced by ~25% (**Figure 1j**). To evaluate whether the findings in the tibialis anterior can be generalized to other muscles, we performed a similar analysis in the gastrocnemius and obtained similar results. The innervation status was not changed in either *Fus*$^{\Delta NLS/\Delta NLS}$ or *Fus*$^{-/-}$, the endplate area was significantly reduced in *Fus*$^{\Delta NLS/\Delta NLS}$ (~17%), but not *Fus*$^{-/-}$, and the total number of endplates was significantly reduced in both *Fus*$^{\Delta NLS/\Delta NLS}$ (~33%) and *Fus*$^{-/-}$ (~44%) (**Supplementary Figure 1a-f**). Together, these findings point towards a postsynaptic defect in NMJs of *Fus* mutant mice, with a reduced endplate number (both models) and size (only *Fus*$^{\Delta NLS/\Delta NLS}$).

Ultrastructural (TEM) analysis of E18.5 gastrocnemius revealed morphological defects in *Fus* mutant NMJs that appeared slightly more pronounced in $Fus^{\Delta NLS/\Delta NLS}$ than in $Fus^{-/-}$ mice (**Figure 1k-n**). This was confirmed by semi-quantitative analysis of TEM images (**Supplementary Figure 1g-k**). Pre- and postjunctional membranes were frequently not apposed in *Fus* mutant mice (**Supplementary Figure 1g**) and the characteristic invaginations of the postsynaptic muscle membrane (postjunctional folds) were often missing (**Supplementary Figure 1h**). In contrast, in wild type littermate controls, muscle membranes were properly apposed to neuronal membranes, with characteristic junctional folds (arrows in **Figure 1k,m**). In addition, the continuity of both the neuronal and muscle membrane was frequently disrupted (**Supplementary Figure 1i,j**), presynaptic terminals often lacked visible synaptic vesicles and mitochondria (**Figure 1l, Supplementary Figure 1k**), and some $Fus^{\Delta NLS/\Delta NLS}$ neuromuscular junctions showed signs of presynaptic degeneration (**Figure 1l**).

To exclude the possibility that the reduced number of endplates in FUS mutant muscles is simply due to a reduced number of muscle fibers, we quantified the total number of muscle fibers in the extensor digitorum longus (EDL) and tibialis anterior muscles of mutant *Fus* and control newborn pups. Muscle fiber membranes were visualized by dystrophin staining (**Supplementary Figure 2a,b**), and quantification revealed no significant differences in the total number of muscle fibers in the EDL of $Fus^{\Delta NLS/\Delta NLS}$ or $Fus^{-/-}$ versus control (**Supplementary Figure 2c,d**). Also in the tibialis anterior of $Fus^{-/-}$ pups, the total number of muscle fibers was not changed (**Supplementary Figure 2e**).

Cytoplasmic mislocalized $Fus^{\Delta NLS}$ protein is intrinsically toxic to muscle

As morphological analysis of NMJs in newborn $Fus^{\Delta NLS/\Delta NLS}$ and $Fus^{-/-}$ mice revealed predominantly postsynaptic defects, we decided to evaluate whether the $FUS^{\Delta NLS}$ protein is intrinsically toxic to muscle, by selectively reverting the $Fus^{\Delta NLS}$ allele to wild type in skeletal muscle. $MyoD^{iCre}$ mice were selected for this purpose, as they selectively express iCre in committed myogenic progenitor cells from E10.5 onwards, resulting in excision of loxP-flanked genomic sequences in skeletal muscles [16, 17]. To quantify the efficiency of excision of loxP-flanked sequences in skeletal muscles, $MyoD^{iCre/+}$ mice were crossed to $ROSA^{mT/mG}$ reporter mice [18]. These mice express

membrane-targeted tandem dimer Tomato (mT) prior to Cre-mediated excision and membrane-targeted EGFP (mG) after excision (**Supplementary Figure 3a**). In contrast to *ROSA*$^{mT/mG}$/+ (control) mice, in which all cells were mT labeled, ≥99.5% of muscle fibers in the tibialis anterior of adult *MyoD*$^{iCre/+}$*; ROSA*$^{mT/mG}$/+ mice were mG labeled (**Supplementary Figure 3b,c**). Thus, *MyoD*^{iCre} mediates highly efficient recombination in skeletal muscle fibers.

We next crossed the *MyoD*^{iCre} mice to *Fus*$^{\Delta NLS}$ mice, with the purpose of selectively reverting the *Fus*$^{\Delta NLS}$ allele to wild type in skeletal muscle. Immunostaining revealed that in the tibialis anterior of newborn *MyoD*$^{iCre/+}$*; Fus*$^{+/+}$ (control) mice, FUS was predominantly localized to the nucleus (**Figure 2a**). In contrast, in *MyoD*$^{+/+}$*; Fus*$^{\Delta NLS/\Delta NLS}$ muscle, FUS displayed a diffuse cytoplasmic localization and was no longer enriched in nuclei (**Figure 2a**). Consistent with successful reversal of *Fus*$^{\Delta NLS}$, FUS nuclear localization was restored in *MyoD*$^{iCre/+}$*; Fus*$^{\Delta NLS/\Delta NLS}$ myofibers (**Figure 2a**). These observations were confirmed by quantitative analysis of the cytoplasmic:nuclear ratio of FUS localization (**Figure 2b**). To assess whether the selective restoration of FUS subcellular localization in muscle fibers would rescue the NMJ morphology defects, we quantified the endplate surface area in the tibialis anterior of these mice. As expected, the endplate area was significantly reduced in *MyoD*$^{+/+}$*; Fus*$^{\Delta NLS/\Delta NLS}$ mice as compared to *MyoD*$^{iCre/+}$*; Fus*$^{+/+}$ and wild type control mice (**Figure 2c**). Strikingly, in the tibialis anterior of *MyoD*$^{iCre/+}$*; Fus*$^{\Delta NLS/\Delta NLS}$ mice, the endplate area was significantly rescued as compared to *MyoD*$^{+/+}$*; Fus*$^{\Delta NLS/\Delta NLS}$, to a level that was not significantly different from control genotypes (**Figure 2c**). These data are consistent with cell-autonomous toxicity of the FUS$^{\Delta NLS}$ protein in skeletal muscle. Of note, in spite of rescuing postsynaptic defects, the presence of *MyoD*^{iCre} did not rescue the early postnatal lethality of *Fus*$^{\Delta NLS/\Delta NLS}$ mice, indicating that FUS$^{\Delta NLS}$ toxicity in other cell types is sufficient to cause neonatal lethality.

Neuromuscular junction defects in adult heterozygous *Fus*$^{\Delta NLS/+}$ mice

Whereas homozygous *Fus*$^{\Delta NLS/\Delta NLS}$ and *Fus*$^{-/-}$ mice die shortly after birth [14], heterozygous *Fus*$^{\Delta NLS/+}$ mice develop adult-onset motor neurodegeneration after 10 months of age with associated defects in motor behavior, thus constituting a *FUS*-ALS mouse model [15]. We evaluated NMJ morphology in *Fus*$^{\Delta NLS/+}$ mice at 1 and 10 months of age. Motor axons and presynaptic terminals were visualized by immunostaining with antibodies against neurofilament and synaptophysin, and

endplates were labeled by fluorescent BTX (**Figure 3a,b**). Already at 1 month of age, we observed significant denervation of NMJs in tibialis anterior muscle that worsened with age (**Figure 3c,d**). Importantly, the endplate surface area was significantly reduced in *Fus*$^{\Delta NLS/+}$ mice at both ages (**Figure 3f,g**). In contrast to newborn homozygous *Fus*$^{\Delta NLS/\Delta NLS}$ mice, the total number of endplates in the tibialis anterior of 1-month-old *Fus*$^{\Delta NLS/+}$ mice was similar to wild type controls (**Supplementary Figure 2f**). Consistent with the reduced endplate area which presumably corresponds to a reduced AChR number, we found that repetitive stimulation of the sciatic nerve at 20 Hz and 50 Hz resulted in a successive decrease in compound muscle action potential (CMAP) amplitude between first and tenth stimulus in *Fus*$^{\Delta NLS/+}$ but not in *Fus*$^{+/+}$ mice (**Figure 3i**), indicating that the 'safety factor' of neuromuscular transmission is reduced in *Fus*$^{\Delta NLS/+}$ mice. Together, these data show chronic endplate denervation, progressing with age, accompanied with an early and sustained reduction of endplate size in *Fus*$^{\Delta NLS/+}$ mice. Since loss of motor neuron cell bodies occurs after 18 months of age in this *FUS*-ALS model, our results are consistent with a 'dying-back' mechanism of motor neurodegeneration. Importantly, in 28-month-old heterozygous *Fus*$^{+/-}$ mice, endplate innervation status and endplate surface area was not significantly different from wild type control littermates (**Figure 3e,h**). Thus, heterozygous loss of *Fus* function is not sufficient to induce NMJ defects. Rather, a gain-of-toxic function is required to induce the NMJ defects observed in adult heterozygous *Fus*$^{\Delta NLS/+}$ mice.

FUS is enriched in subsynaptic nuclei dependent on innervation

Our findings that the endplate surface area is significantly reduced in *Fus*$^{\Delta NLS/\Delta NLS}$ and *Fus*$^{\Delta NLS/+}$ mice through effects of the mutation in muscle cells suggested that FUS may regulate the expression of AChR genes and possibly other genes encoding endplate components. It is well known that upon innervation, synapse-specific genes, including AChR subunit genes, become exclusively expressed in subsynaptic nuclei [2, 3]. This prompted us to investigate the subcellular localization of FUS in adult gastrocnemius muscle, in relation to endplate localization. Intriguingly, we found that FUS was significantly enriched in subsynaptic nuclei, defined as nuclei located directly underneath BTX-stained endplates. (**Figure 4a,b**). In contrast, FUS subsynaptic enrichment was lost in muscle of 10-month-old *Fus*$^{\Delta NLS/+}$ mice (**Figure 4a,b**).

To investigate whether FUS enrichment in subsynaptic nuclei is dependent on innervation, unilateral axotomy of the sciatic nerve was performed in adult wild type mice, and FUS subsynaptic enrichment was evaluated in ipsilateral and contralateral gastrocnemius muscles. This experiment revealed that 5 days after injury, subsynaptic FUS enrichment was lost in ipsilateral as compared to contralateral muscles (**Figure 4c,d**). Together, these data indicate that muscle innervation maintains enrichment of FUS in subsynaptic nuclei, and that this process is disrupted in the presence of *Fus*$^{\Delta NLS}$ protein.

FUS regulates expression of AChR subunit genes through ERM

It is tempting to speculate that the innervation-dependent FUS enrichment in subsynaptic nuclei regulates the selective expression of genes encoding endplate components in these nuclei. To investigate this possibility, we turned to C2C12 mouse myoblast cells, a simplified cellular model standardly used in the NMJ field [19, 20]. C2C12 cells were treated with siRNA targeting FUS (si*Fus*) or control siRNA (siCt), and differentiated for 2 days. si*Fus* induced a strong knock-down of FUS expression, both at the transcript (**Figure 5a**) and the protein level (**Figure 5b**). Interestingly, FUS knock-down substantially reduced expression of each of the five AChR subunit genes, by >50% (**Figure 5c**). Consistently, also in muscles of E18.5 *Fus*$^{\Delta NLS/\Delta NLS}$ mice, transcript levels of several AChR subunits were significantly reduced as compared to wild type littermate controls (**Supplementary Figure 4a**), and a similar decrease in expression was observed in the tibialis anterior muscle of 1-month-old *Fus*$^{\Delta NLS/+}$ mice (**Supplementary Figure 4b**).

To determine whether FUS might directly activate transcription of AChR encoding genes, we performed chromatin immunoprecipitation in C2C12 cells. Two different anti-FUS antibodies were able to robustly immunoprecipitate chromatin at the promoters of *Chrna1, Chrnd* and *Chrne* genes (encoding the AChR alpha1, delta and epsilon subunits, respectively), while there was no observable binding at the histone 2ac (*H2ac*) promoter. Importantly, FUS binding at AChR gene promoters was similar to its binding at the *Mecp2* promoter, a known FUS target [21] (**Figure 5d**). These data are consistent with the presence of predicted FUS binding sites in the promoter regions of murine and human AChR subunit genes (**Supplementary Data 1**).To evaluate a direct promoter-dependent transcriptional mechanism, we transfected

C2C12 cells with reporter constructs in which the *Chrnd* or *Chrne* promoters drive luciferase expression. FUS knock-down significantly reduced luciferase expression driven by either the *Chrnd* (**Figure 5e**) or the *Chrne* (**Figure 5f**) promoters [5], but not when luciferase expression was driven by the CMV promoter (**Figure 5g**). Conversely, overexpression of wild type human FUS significantly induced *Chrnd* and *Chrne* promoter activity (**Figure 5h**). Thus, FUS induces transcription of the *Chrnd* and *Chrne* genes by a promoter-dependent mechanism. Importantly, overexpression of FUS carrying the ALS-causing R495X mutation did not induce *Chrnd* or *Chrne* promoter activity (**Figure 5h**). This correlated with subcellular mislocalization of FUS_R495X, which was localized to the cytoplasm, in contrast to the predominant nuclear localization of wild type FUS (**Supplementary Figure 5**). In addition, when co-expressed with wild type FUS, FUS_R495X dose-dependently inhibited the induction of *Chrne* promoter activity by wild type FUS (**Figure 5i**), suggesting that FUS_R495X exerts a dominant negative effect on FUS-induced *Chrne* promoter activity. Co-transfection of C2C12 cells with differentially tagged wild type and R495X FUS proteins indicated that this dominant negative effect may be attributable to (i) increased localization of wild type FUS to the cytoplasm in the presence of FUS_R495X, and in addition (ii) a more granular localization pattern of wild type FUS in the nucleus, together resulting in reduced levels of diffusely distributed wild type FUS in the nucleus (**Supplementary Figure 5**).

Treatment of C2C12 cells with agrin, a secreted factor known to stimulate synapse-specific gene expression [2, 3], induced luciferase expression driven by the *Chrne* promoter (**Supplementary Figure 6a**). Strikingly, knock-down of FUS prevented induction of *Chrne*-luciferase expression by agrin, indicating that FUS is required for induction of *Chrne* transcription in response to agrin (**Supplementary Figure 6a**). Selective *Chrne* expression in subsynaptic nuclei is mediated by the ETS transcription factor ERM [4]. Importantly, *Erm* knockdown largely decreased FUS-induced *Chrne* promoter activity (**Figure 5j**), while conversely, activation of *Chrne* promoter activity by ERM overexpression was severely blunted by FUS knock-down (**Figure 5k**). Since EWSR1, a protein of the FET family to which also FUS belongs, has been shown to physically interact with ERM [22], we postulated that these effects may be mediated by direct physical interaction. Indeed, immunoprecipitation in HEK293 cells transfected with tagged versions of FUS and ERM revealed a direct

interaction between both proteins (**Supplementary Figure 6b**), and such interaction was also detected using immunoprecipitation of endogenous proteins in mouse (C2C12) and human (HSkMC) myoblast cell lines (**Figure 5l,m**), as well as in HEK293 cells (**Supplementary Figure 6c**). Importantly, the interaction between FUS and ERM proteins was not affected by RNase treatment (**Figure 5l,m; Supplementary Figure 5b,c**), indicating that it did not depend on RNA. Altogether, our results indicate that subsynaptic gene expression is mediated by the synergistic action of FUS and ERM on AChR-encoding gene promoters.

Impaired endplate maturation in iPSC-derived myotubes from *FUS*-ALS patients

To explore the potential relevance of our findings in mutant *Fus* mouse models for human *FUS*-ALS, we studied endplate maturation and NMJ formation in cultured myotubes and motor neuron-myotube co-cultures derived from *FUS*-ALS patients and neurologically healthy control subjects. Induced pluripotent stem cell (iPSC) lines derived from juvenile ALS patients carrying a c.1483delC deletion leading to a R495QfsX527 frameshift mutation (FUS1) or a c.1504delG deletion leading to an D502Tfs*27 frameshift mutation (FUS2) have been previously described [23]. Two control lines (CNTL1 and CNTL2) were generated from neurologically healthy volunteers, and an additional control line (CNTL3) was obtained by correcting the c.1483delC deletion in the R495QfsX527 iPSCs by CRISPR/Cas9 technology, thus providing an isogenic control [23] (**Figure 6a**).

As a first paradigm to test the effect of ALS-mutant FUS on AChR clustering and endplate maturation, patient and control iPSCs were differentiated in myogenic cells and subsequently in myotubes. Myogenic cells were grown in spheres for 6 weeks and then plated to form multinucleated myotubes (**Supplementary Figure 7a**; see methods for details) [24]. Extensive characterization of expression levels and localization of myogenic markers confirmed appropriate myogenic proliferation and differentiation in mature myotubes, with no significant differences between *FUS*-ALS and control. Indeed, transcript levels of the myogenic markers *PAX7* and *MYOG* were not significantly different between *FUS*-ALS and control at different time points during myoblast proliferation and myotube differentiation (**Supplementary Figure 7b**). Furthermore, MYOG protein displayed the expected nuclear localization, and the contractile filament myosin heavy chain (MHC) and the muscle-specific intermediate

filament desmin were characteristically localized to the cytoplasm (**Supplementary Figure 7c**). In addition, the microfilament protein α-actinin, which is necessary for attachment of actin filaments to the sarcomeric Z-disks, was indeed localized to Z-disks (**Figure 6b, Supplementary Figure 7d**). Finally, the muscle cells stained positive for the skeletal muscle ryanodine receptor isoform RyR1 and the voltage-dependent dihydropyridine receptor alpha subunit (**Supplementary Figure 7c**, arrowheads), both intracellular calcium channels that mediate calcium release from the sarcoplasmic reticulum, an essential step in muscle contraction. Surprisingly, FUS predominantly localized to the nucleus in both control and *FUS*-ALS myotubes (**Supplementary Figure 7d**), in contrast to the previously reported cytoplasmic mislocalization of ALS-mutant FUS in motor neurons [23].

To characterize endplate morphology in *FUS*-ALS and control myotubes, endplates were visualized by fluorescently labeled BTX and categorized in three groups based on AChR clustering: (i) diffuse puncta, (ii) aligned puncta, and (iii) dense cluster (**Figure 6b**), reflecting subsequent steps in endplate maturation. Quantitative analysis revealed impaired endplate maturation in *FUS*-ALS myotubes as compared to control (**Figure 6c**).

Finally, expression of AChR subunit genes was evaluated at different time points during myoblast proliferation and myotube differentiation. While transcript levels of the AChR gamma (*CHNRG*) and epsilon (*CHNRE*) subunits were not significantly different between *FUS*-ALS and control (data not shown), transcript levels of the AChR alpha1 subunit were substantially reduced in *FUS*-ALS myotubes (**Supplementary Figure 7b**), consistent with the observed endplate maturation defect and the data in mutant *Fus* mouse models and C2C12 cells.

ALS-mutant FUS is intrinsically toxic to motor neurons and myotubes

During development, before motor axons reach their muscle targets, clusters of AChRs are already ‘pre-patterned’ on muscle fibers. However, innervation of muscle fibers by motor axons induces a major rearrangement of the postsynaptic compartment, including increases in number, stability, density and clustering of AChRs [1, 2]. To evaluate the effect of motor innervation on endplate maturation, we co-cultured motor neurons and myotubes, following our previously established protocol [25]. Wild type (CNTL1) or *FUS*-ALS (FUS1 or FUS2) motor neurons and myotubes were differentiated separately and subsequently co-cultured for three

weeks in all possible CNTL/FUS combinations. Similar to myotube monocultures, endplate maturation was evaluated by categorizing endplate morphology, but a fourth category of 'pretzel'-shaped endplates (most mature) was added and only endplates innervated by neurofilament-positive motor axons were included (**Figure 6d**).

Consistent with the above-described endplate maturation defect in myotube monocultures, *FUS*-ALS myotubes co-cultured with CNTL1 motor neurons displayed significantly less mature endplates as compared to CNTL1-CNTL1 co-cultures (**Figure 6e**). Co-culturing of *FUS*_R495QfsX527 (FUS1) motor neurons and myotubes significantly aggravated the endplate maturation defect (**Figure 6e**), suggesting that at least for this *FUS* mutation, mutant motor neurons have a detrimental effect on endplate maturation. Consistent with this notion, co-culturing of *FUS*-ALS motor neurons with CNTL myotubes was sufficient to induce an endplate maturation defect (**Figure 6e**). To solidify these data, we measured the average size of single puncta within endplates. This analysis revealed that, as compared to CNTL1-CNTL1 co-cultures, combinations containing *FUS*-ALS motor neurons and/or myotubes displayed significantly reduced single particle size (**Supplementary Figure 8a**), again indicative of defective AChR clustering in the presence of *FUS*-ALS cells.

To exclude potential confounding effects of the genetic background of *FUS*-ALS patients and CNTL, we performed motor neuron-myotube co-cultures derived from FUS1 and its isogenic CNTL3. This experiment revealed an even more striking defect in endplate maturation in co-cultures in which either myotubes or motor neurons carried the FUS_R495QfsX527 mutation, and the most severe maturation defect was observed when both myotubes and motor neurons were FUS mutant (**Figure 6f**, **Supplementary Figure 8b**).

Immunostaining for FUS, AChR, neurofilament heavy chain (NF-H) and DAPI (**Supplementary Figure 8c**) revealed that in cultures derived from CNTL motor neurons and myotubes, FUS was strongly expressed in motor neuron nuclei (indicated by red arrowheads) and in myotube nuclei (indicated by white arrowheads). In cultures from CNTL myotubes and FUS mutant motor neurons, FUS localized to both nucleus and cytoplasm of motor neurons (red arrowheads). FUS predominantly localized to nuclei in myotubes, even in co-cultures of FUS mutant motor neurons and myotubes (white arrowheads in **Supplementary Figure 8c**).

We further analyzed expression of myogenic differentiation markers and AChR

subunits in motor neuron-myotube co-cultures. Since myotube differentiation was induced by PAX7 overexpression, we first assessed PAX7 levels. No significant differences in PAX7 expression were found across the different genotypic combinations (**Supplementary Figure 8d**), indicating that similar differentiation efficacies could be expected for the various combinations. However, in D502Tfs*27 (FUS2) 'full' mutant co-cultures, *MYOD* and *MYOG* transcript levels were significantly reduced, suggesting impaired myogenic differentiation (**Supplementary Figure 8d**). Furthermore, *MYOG* expression levels were also significantly reduced when either motor neurons or myotubes were FUS2 mutant. In addition, transcript levels of AChR alpha 1 and gamma subunits were substantially reduced in FUS2 full mutant co-cultures, while transcript levels of the AChR epsilon subunit were not significantly different across combinations (**Supplementary Figure 8d**). These data are consistent with the most pronounced endplate differentiation defect in *FUS*-ALS full mutant co-cultures.

Muscle biopsies from *FUS*-ALS patients show muscle atrophy, endplate denervation, FUS mislocalization and loss of FUS enrichment in subsynaptic nuclei

To further investigate the potential clinical relevance of our findings for *FUS*-ALS, we analyzed muscle biopsies from three controls and three *FUS*-ALS patients with R495QfsX527 (FUS1, obtained from the same patient as our FUS1 iPSC cell line) and K510R (FUS4 and FUS5) mutations. The controls were not affected by neurodegenerative disease, but presented with chronic pain syndrome and muscle biopsies were taken to exclude myositis. FUS1 and FUS4 had juvenile spinal and bulbar onset, respectively, and FUS5 presented at the age of 39 with spinal onset (**Figure 7a**). EMG was performed in all FUS patients and surprisingly revealed myopathic changes. Specifically, small and polyphasic motor unit action potentials (MUAPs) were detected in FUS1 and FUS5. In FUS1, myopathic changes were seen alongside neurogenic changes, but in FUS5, only myopathic changes were found. All patients showed pathological spontaneous activity (PSA) in the body regions studied, according to the electrophysiological Awaji Criteria [26] (**Figure 7a**). H&E staining on muscle biopsy sections revealed neurogenic muscle atrophy in each of the three *FUS*-ALS patients, with groups of small angulated fibers, increased density of muscle

nuclei and increased presence of connective tissue, in particular in patients FUS4 and FUS5 (**Figure 7b**). Quantitative analysis confirmed the abundant presence of very small muscle fibers (surface area <500μm^2) in each of the three FUS-ALS patients, which were never found in control muscle biopsies (**Figure 7c and Supplementary Figure 9a**). Furthermore, muscle fiber size was highly heterogeneous in FUS1, with a small fraction of abnormally large fibers. Consistently, the average muscle fiber surface area was significantly reduced in FUS1 (as compared to CNTL4 and CNTL5), FUS4 and FUS5 biopsies (as compared to all controls) (**Figure 7c**), and the density of nuclei was significantly increased in FUS4 and FUS5 (**Supplementary Figure 9b**). Immunostaining for synaptophysin (SYN), AChR, FUS and DAPI revealed endplate denervation in *FUS*-ALS muscle biopsies (**Figure 7d**), and endplate surface area was significantly reduced in *FUS*-ALS biopsies as compared to CNTL6, but not as compared to CNTL4 and CNTL5 (**Supplementary Figure 9d**). In *FUS*-ALS biopsies, nuclear FUS staining often displayed a granular pattern, in contrast to diffuse staining in controls (white arrowheads in **Figure 7d**), and cytoplasmic FUS mislocalization was occasionally observed in *FUS*-ALS biopsies (red arrowheads). Quantification of FUS staining intensity showed that on average, FUS nuclear staining was not significantly changed in *FUS*-ALS muscle biopsies, and cytoplasmic FUS staining was significantly increased in FUS1 but not FUS4 and FUS5 patients (**Supplementary Figure 9c**). However, importantly, FUS was found to be enriched in subsynaptic nuclei in control muscle biopsies by about 2-fold, but this enrichment was completely lost in FUS1 and substantially reduced in FUS4 (**Figure 7e**). Thus, similar to muscles of *Fus*$^{\Delta NLS/+}$ mice, FUS enrichment in subsynaptic nuclei is affected in *FUS*-ALS patients.

Discussion

Motor neuron degeneration in ALS is thought to occur in a retrograde fashion: NMJs are affected first, followed by motor axonal degeneration and finally degeneration of motor neuron cell bodies. This 'dying-back' pattern of motor neuron degeneration has been reported in a single sporadic ALS (sALS) patient [8] and in mouse models of familial ALS (fALS) caused by mutations in SOD1 [7-9]. It is however unclear whether this is also the case for other forms of fALS, and for the broad population of sALS patients. In this study, we investigated NMJ morphology in mouse models of *FUS*-ALS that carry a homozygous or heterozygous *Fus* mutation that results in deletion of the last 20 amino acids of the endogenous FUS protein, similar to mutations found in human *FUS*-ALS patients [12], affecting the NLS and thus impairing FUS nuclear import [13] and being associated with early disease onset and fast disease progression [27-29]. Although the innervation of muscle endplates in hind limb muscles of newborn $Fus^{\Delta NLS/\Delta NLS}$ pups was not affected, the endplate surface area and the total number of endplates in an entire hind limb muscle were significantly reduced, while the total number of muscle fibers was not altered. The total number of endplates was also reduced in $Fus^{-/-}$ newborn pups, indicating that this postsynaptic defect is likely attributable to loss of FUS function. However, the average endplate surface area was not changed in $Fus^{-/-}$ pups, indicating that a gain-of-toxic-function mechanism underlies the reduced endplate area in $Fus^{\Delta NLS/\Delta NLS}$ muscles. Ultrastructural analysis confirmed the presence of structural NMJ defects in both $Fus^{\Delta NLS/\Delta NLS}$ and $Fus^{-/-}$ pups. Consistently, in iPSC-derived myotube cultures and in motor neuron-myotube co-cultures from *FUS*-ALS patients, endplate maturation was significantly impaired, underscoring the potential relevance of our findings in mouse models for human *FUS*-ALS. Importantly, also in adult $Fus^{\Delta NLS/+}$ mice, which recapitulate the genetic situation in the vast majority of *FUS*-ALS patients, endplate surface area was significantly reduced, and endplate denervation was already detected at one month of age, and progressively worsened. Given the fact that loss of motor neuron cell bodies only occurs after the age of 10 months [15], these data clearly indicate that in this *FUS*-ALS mouse model motor neuron degeneration occurs in a dying-back pattern, consistent with what others observed recently in transgenic mice overexpressing wild type or ALS-mutant human FUS [30, 31], and in human iPSC-derived *FUS*-ALS motor neuron models [32].

An unresolved question in the ALS field is whether skeletal muscle fibers are merely bystanders or rather actively contribute to motor neuron degeneration in ALS. This conundrum has been investigated in mutant SOD1 mouse models of ALS, with conflicting results. Indeed, on the one hand, two studies reported that reducing mutant SOD1 expression in skeletal muscle of mutant SOD1 mice does not affect disease course, neither did increasing muscle fiber number and diameter by follistatin expression [33, 34]. On the other hand, selective expression of ALS-mutant SOD1 G93A in skeletal muscle was reported to result in progressive muscle atrophy, significant reduction in muscle strength, alteration in the contractile apparatus and mitochondrial dysfunction [35]. Strikingly, another study reported that skeletal muscle-restricted expression of wild type, G37R and G93A SOD1 resulted in limb weakness, paresis and motor defects, associated not only with severe skeletal muscle pathology, but also with marked NMJ abnormalities and spinal motor neuron pathology [36]. Furthermore, loss of skeletal muscle-specific microRNA miR-206 accelerates NMJ denervation and disease progression in SOD1 G93A mice [37]. In this study, we show that selective reversal of the $Fus^{\Delta NLS}$ allele to wild type in skeletal muscle restored the subcellular localization of FUS (from cytoplasmic mislocalization to appropriate nuclear localization) and rescued the reduced endplate surface area in $Fus^{\Delta NLS/\Delta NLS}$ newborn pups, showing that this postsynaptic defect is attributable to intrinsic toxicity of the $FUS^{\Delta NLS}$ protein in skeletal muscle. Consistently, myotubes derived from *FUS*-ALS patients displayed impaired endplate maturation, not only when co-cultured with *FUS*-ALS motor neurons, but also when co-cultured with control motor neurons. These findings call for future research to investigate a possible non-cell-autonomous contribution of skeletal muscle to the dying-back neuronopathy in *FUS*-ALS.

Besides toxicity in skeletal muscle, intrinsic toxicity of mutant FUS in motor neurons is likely a key event in triggering motor neuron degeneration in *FUS*-ALS. Indeed, ultrastructural analysis of motor terminals in $Fus^{\Delta NLS/\Delta NLS}$ muscles, as well as in transgenic mice overexpressing wild type or P525L mutant FUS revealed presynaptic defects [30, 31]. Furthermore, selective overexpression of FUS P525L in motor neurons was sufficient to induce progressive motor neuron loss and NMJ denervation [31], and reversal of the $Fus^{\Delta NLS}$ allele to wild type in both $Fus^{\Delta NLS/\Delta NLS}$ and $Fus^{\Delta NLS/+}$ mice prevented progressive motor neuron loss [14, 15], indicating that expression of ALS-mutant FUS in motor neurons is both necessary and sufficient to induce motor

neuron loss. Similarly, in our human motor neuron-myotube co-cultures, motor neurons derived from *FUS*-ALS patients induced defective maturation of neuromuscular endplates, even when myotubes were derived from control subjects. Intriguingly, however, in spite of preventing loss of motor neuron cell bodies in adult heterozygous $Fus^{\Delta NLS/+}$ mice, ChAT-cre delayed, but did not prevent the development of motor deficits in these mice [15], suggesting the involvement of cell types other than motor neurons. Our findings that toxicity of the $FUS^{\Delta NLS}$ protein in myotubes induces NMJ morphological defects suggests that skeletal muscle fibers may contribute to the development of motor deficits in adult $Fus^{\Delta NLS/+}$ mice, although this remains to be experimentally proven.

The reduced neuromuscular endplate size in hind limb muscles of both newborn $Fus^{\Delta NLS/\Delta NLS}$ and adult $Fus^{\Delta NLS/+}$ mice, as well as the reduced total number of endplates in $Fus^{\Delta NLS/\Delta NLS}$ and $Fus^{-/-}$ muscles prompted us to investigate a possible role of FUS in regulation of AChR subunit (*Chrn*) gene expression. Indeed, downregulation of subsynaptic gene expression, as is the case in *Erm* mutant mice, was associated with a substantial reduction in endplate surface area [4]. Consistent with a role for FUS in *Chrn* gene regulation, knock-down of FUS in C2C12 mouse myoblast cells substantially reduced expression of each of the AChR subunits (α1, β1, γ, δ and ε). Furthermore, in $Fus^{\Delta NLS/\Delta NLS}$ muscles, transcript levels of the β1, γ and δ subunits were significantly reduced, and in adult $Fus^{\Delta NLS/+}$ muscles, expression of the α1, γ and ε subunits were significantly reduced. In addition, AChRα1 subunit expression was significantly reduced in *FUS*-ALS myotube cultures, and in *FUS*-ALS motor neuron-myotube co-cultures, expression of AChRα1 and AChRγ was diminished. Together, these findings indicate that FUS stimulates expression of *Chrn* genes, and this function is compromised in *FUS*-ALS mouse and cell culture models.

After innervation of skeletal muscles during development, expression of AChR subunits and other 'synaptic' genes becomes restricted to subsynaptic nuclei [1, 2]. At the molecular level, agrin, secreted from motor nerve terminals, binds to Lrp4 on the postsynaptic membrane, resulting in MuSK activation and subsequent activation of Rac and JNK, further activating ERM/ETV5 and other ETS transcription factors, which drives expression of *Chrn* genes, *Musk*, and other synaptic genes. The transcription factor ERM is highly enriched in subsynaptic nuclei, and when mutated in mice, many genes highly expressed in subsynaptic nuclei are downregulated [4]. In

addition, muscle denervation results in re-expression of *Chrn* genes in nonsynaptic nuclei and thus loss of selective expression of *Chrn* genes in subsynaptic nuclei. Interestingly, consistent with a role for FUS in stimulating synaptic gene expression, we found FUS enrichment in subsynaptic nuclei, and this enrichment was lost upon denervation. Furthermore, in $Fus^{\Delta NLS/+}$ mice, FUS enrichment in subsynaptic nuclei is disrupted (independent of denervation) and expression of AChR subunit genes is reduced. Experiments in C2C12 cells revealed that FUS modulates expression of AChR subunit genes through regulation of transcription, as knock-down of FUS reduced and FUS overexpression increased the promoter activity of both the *Chrnd* and *Chrne* genes. Importantly, FUS was required to mediate induction of *Chrne* promoter activity by neural agrin, suggesting that FUS is required for ERM function. Consistently, ChIP experiments showed that FUS binds to the promoter region of *Chrn* genes, and co-IP showed that FUS and ERM proteins interact with each other in an RNA-independent manner. Last, FUS-mediated induction of *Chrne* promoter activity was ERM-dependent, and ERM-mediated induction of the *Chrne* promoter was FUS-dependent. Of note, it was recently reported that ERM also directly interacts with EWS (Ewing's sarcoma breakpoint protein) [22], a protein which, together with FUS and TAF-15, constitutes the FET protein family. FUS and EWS are highly homologous, and both proteins contain a low complexity (LC) domain, three RGG domains, an RNA recognition motif (RRM) and a C4 Znf domain [10]. The domains in FUS and EWS that mediate ERM interaction remain to be identified. Together, these findings suggests that FET proteins may be critical regulators of multiple ETS transcription factor activities. Besides NMJ development and maintenance, the synergistic action of ETS transcription factors and FET proteins may play a role in development of malignant diseases [22]. Taken together, our data suggest a model in which agrin-Lrp4-MuSK signaling results in recruitment of FUS and ERM to promoter regions of subsynaptic genes, increasing their expression (**Figure 8**).

To the best of our knowledge, this is the first time that an ALS gene is directly implicated in NMJ maintenance and stability. Given the fact that NMJ pathology is considered an early event in ALS pathogenesis, this may constitute an important novel insight. Furthermore, a possible contribution of FUS to the pathogenesis of other neuromuscular diseases with prominent NMJ pathology, including myasthenic syndromes, peripheral neuropathy and spinal muscular atrophy is conceivable. EMG

analysis in *Fus*$^{\Delta NLS/+}$ mice revealed a successive decrease in CMAP amplitude in response to repetitive stimulation, indicating that the 'safety factor' of neuromuscular transmission is decreased in these mice. In mouse models for myasthenic syndrome, a similar decremental response to repetitive stimulation can be detected, but at substantially lower frequencies. Therefore, *Fus*$^{\Delta NLS/+}$ mice constitute a mouse model for *FUS*-ALS rather than for myasthenic syndrome. Our data further indicate that ALS-mutant FUS is intrinsically toxic to both motor neurons and skeletal muscle, implying that therapeutic approaches for *FUS*-ALS – and possibly all forms of ALS – should ideally target both cell types. In conclusion, in this study we uncovered that FUS and ERM collaborate to promote the transcription of AChR subunit genes in subsynaptic nuclei. Impairment of this novel FUS function in *FUS*-ALS mouse and cell models suggests that possibly, intrinsic toxicity of mutant FUS in skeletal muscle may contribute to the dying-back motor neuronopathy in *FUS*-ALS patients.

Materials and methods

Compliance with ethical standards

Mouse experiments were approved by the local ethical committee from Strasbourg University (CREMEAS) under reference numbers 2015070711529814 and 2016021114497517, and by the LANUV-NRW under reference numbers 84-02.04.2011.A100 and 84-02.04.2016.A166. Human hair and skeletal muscle biopsy donors gave informed consent for the study prior to sampling. All studies with human material were in accordance with the ethical committee of Ulm University (Nr. 0148/2009 and 265/12 for hairs and 12/09 for muscle biopsies) and in compliance with the guidelines of the Federal Government of Germany (Nr. O.103). Experiments were in accordance with the Declaration of Helsinki concerning Principles for Medical Research containing Human Subjects.

Animals

Transgenic mice were housed in the Faculty of medicine from Strasbourg University and in the animal facility of the Max Planck Institute for Molecular Biomedicine, with 12/12 hours of light/dark cycle and unrestricted access to food and water.
Fus knock-in, *Fus* knock-out mice and *MyoD*^{iCre} were previously described [14, 15 16, 17]. *Fus* knock-in mice express a truncated FUS protein that lacks the PY-NLS, which is encoded by exon 15 of the *Fus* gene. This mutation can be reverted to a wild type FUS protein upon CRE-mediated recombination [14, 15]. Mice heterozygous and homozygous for the targeted allele will hereafter be referred to as *Fus*$^{\Delta NLS/+}$ and *Fus*$^{\Delta NLS/\Delta NLS}$, respectively. The genetic background of all mice used in this study is C57Bl6/J.

Histology, immunohistochemistry and morphometric analysis

NMJ morphology in newborn mice

After sacrifice and removal of the skin, the body of the pups was fixed in 4% paraformaldehyde (PFA) in PBS on ice, washed in PBS and stored at 4°C. After genotyping, gastrocnemius and tibialis anterior muscles were embedded in 3% agarose in PBS and cut in 100 µm longitudinal sections using vibratome.

Immunostainings were done free-floating. Sections were permeabilized for 30 min in PTT (PBS + 0.5% Triton X-100, 0.1% Tween 20), washed in PBS (3x 15 min) and

blocked for 1 h in 10% normal goat serum in PBT (1% BSA, 0.5% Triton X-100 in PBS). Sections were incubated with mouse anti-SV2 (DSHB, 1/10), mouse anti-synaptophysin (Millipore, 1/250) and/or mouse anti-NF (2H3, DSHB, 1/100) primary antibodies in PBT at 4°C overnight. Sections were washed in PBS (10 x 30 min) and incubated with goat-anti-mouse-Alexa-488 (Invitrogen, 1/500) and α-bungarotoxin (BTX) Alexa Fluor 594 conjugate (BTX-Alexa-555, Life Technologies, 1/1000) in PBT at 4°C overnight. Sections were washed in PBT (2 x 30 min) and PBS (8 x 30 min), and mounted on microscopy slides in Vectashield mounting medium.

For quantification of the total number of endplates, BTX-labeled endplates were identified using an epifluorescence microscope (Zeiss Axio Imager Z2, 20x magnification) and a manual counter was used to count all endplates in the different focal planes of each section. Endplate numbers in all sections of the same muscle were added up to obtain the total number of endplates per muscle.

For quantification of endplate area and innervation status, sections stained with anti-SV2 and BTX-Alexa-568 were imaged at a 63x magnification on a Zeiss LSM700 confocal microscope. For each muscle, two sections were imaged, and for each section, images of 5 distinct fields were obtained. Fiji software was used to obtain maximum intensity projections of a limited number of confocal sections (5 to 10), in order to generate images of a select number of individual, non-overlapping endplates. This allowed for analysis of ~100 to 150 endplates per muscle. The surface area of each of these endplates was determined using the “freehand selection” tool in Fiji to delineate endplates. To quantify innervation status, composite images of the red and green channels were generated. Endplates that were apposed by at least three SV2-positive ‘dots’ were scored as innervated, and the percentage of innervated endplates per muscle was calculated and used for statistical analysis.

The tissue preparation for one-month old mice was similar as described before. For quantification of total number of endplates, immunostaining on free-floating 100 µm longitudinal sections was performed. Sections were permeabilized for 30 min in PTT, washed in PBS (3x 15 min) and blocked for 1 h in 10% normal goat serum, 1% BSA, 0.5% Triton X-100 in PBS. Sections were incubated with Alexa-555-conjugated BTX (Sigma, T0195, 1/1000) for 2 hrs, washed in PBS (3 x 15 min) and mounted on microscopy slides in Fluorsave mounting medium (Vector, H-1000).

Muscle fiber number in newborn mice

The extensor digitorum longus (EDL) and tibialis anterior (TA) muscles were used for quantification of the total number of muscle fibers, as this muscle is smaller than the tibialis anterior or the gastrocnemius, with a lower number of muscle fibers, what makes the quantification of the total number of muscle fibers practically feasible. Furthermore, all fibers of the EDL muscle run from tendon to tendon, so that a cross section through the middle part of the muscle allows for quantification of the total number of muscle fibers. EDL muscles were freshly dissected and directly embedded in OCT compound (Sakura) following a 'cryo-no-fix' procedure. 16 µm transverse sections were made using a cryostat and stored at -80°C or immediately used for immunostaining using anti-dystrophin antibodies to selectively label muscle plasma membranes.

For immunostaining, sections were incubated at room temperature and hydrated with PBS (2 x 10 min). Sections were briefly fixed (15 min) in 4% PFA in 0.1 mM sucrose, washed with PBS (2 x 10 min), and incubated with mouse anti-dystrophin (MANDRA1, DSHB, 1/20) primary antibody in PBS with 2% donkey serum and 0.1% Triton X-100 at 4°C overnight. Sections were subsequently washed with PBS (2 x 10 min), followed by Alexa-568-conjugated anti-mouse secondary antibody in PBS with 2% donkey serum and 0.1% Triton X-100 for 2h at room temperature. Sections were washed in PBS (3 x 10 min) and mounted in mounting medium with DAPI.

For quantification of the total number of muscle fibers, dystrophin-stained sections were imaged at a 10x magnification on a Zeiss LSM700 or Leica SP8 (Leica Microsystems) confocal microscope. Fiji software was used to count the total number of muscle fibers per section (multi-point selection tool). For quantifying the size of muscle fibers, a line grid was superimposed on a maximum intensity projection of the muscle fiber. Dystrophin-stained membranes of approximately 100 representative individual fibers were marked (polygon selection tool) and surface area was measured.

NMJ morphology in adult mice

Mice were anesthetized with intraperitoneal injection of 100 mg/kg ketamine chlorhydrate and 5mg/kg xylazine and transcardially perfused with 4% PFA in 0.1 M phosphate buffer pH 7.4. Gastrocnemius and tibialis anterior muscles were

dissected, post-fixed overnight in 4% PFA at 4°C, and washed three times with PBS. Muscles were ‘teased’ into muscle fiber bundles and stained overnight at room temperature with antibodies against neurofilament (custom made, 1/100) and synaptophysin (custom made, 1/100) in PBS-0.1% Triton X-100. After three washes with PBS-0.1% Triton X-100, muscles were stained with Alexa-488-conjugated anti-rabbit secondary antibody (Jackson, 711-547-003, 1/500), BTX-Alexa-594 (Sigma, T195; 1/500) and hoechst (Sigma, B2261, 1/1000). Finally, muscles were washed and mounted in aquapolymount (Polysciences, 18606-5). Z-stack images (2µm optical section, objective x63) were acquired under a confocal microscope (Leica SP5, Leica Microsystems). Excitation rays were sequential argon laser 488nm, diode 561nm, Helium Neon laser 633nm. Emission bandwidths were 500-550nm for Alexa488, 570-620nm for Alexa594, and 460nm for Hoechst. Endplate area of 100 - 150 NMJ was quantified using Image J software and innervation status was evaluated based on the alignment of juxtaposed pre- and postsynapses. NMJs with >80% of innervation were classified as innervated, <80% as partially denervated and <1% as denervated.

NMJ innervation status and endplate surface area in 28-month old mice

Mice were anesthetized with intraperitoneal injection of 100 mg/kg ketamine chlorhydrate and 5mg/kg xylazine and transcardially perfused with 4% PFA in 0.1 M phosphate buffer pH 7.4. Gastrocnemius and tibialis anterior muscles were dissected, post-fixed overnight in 4% PFA at 4°C, and washed three times with PBS. Muscles were ‘teased’ into muscle fiber bundles, incubated in blocking buffer (10% normal goat serum, 1% BSA, and 0.5% Triton X-100 in PBS) prior to staining overnight at 4°C with antibodies against neurofilament (2H3, DSHB, 1/100) and synaptic vesicle glycoprotein 2A (SV2, DSHB, 1/20) in blocking buffer. After three washes with PBS, muscles were stained with Alexa-405-conjugated anti-mouse secondary antibody (Thermo, A31553, Jackson, 1/300) and Alexa-555-conjugated BTX (Sigma, T0195, 1/500). Finally, muscles were washed and mounted in Fluorsave (Vector, H-1000). Z-stack images (0.6µm optical section, zoom 3.5, objective x40) were acquired under a confocal microscope (Leica SP8, Leica Microsystems). Excitation rays were sequential HyD lasers at 405nm and 552nm. Emission bandwidths were 410-480nm for Alexa-405, and 555-660nm for Alexa-555. 50 images were acquired per sample. Endplate area was quantified using Image J

software and innervation status was evaluated based on the alignment of juxtaposed pre- and postsynapses. NMJs with >80% of innervation were classified as innervated, <80% as partially denervated and <1% as denervated.

MyoD-Cre efficiency in newborn mice

To evaluate the efficiency of MyoD^{iCre} mice [16, 17] to excise loxP-flanked genomic sequences, *MyoD$^{iCre/+}$* mice were crossed to *ROSA$^{mT/mG}$* reporter mice [18]. Adult *MyoD$^{iCre/+}$; ROSA$^{mT/mG}$*/+ (experimental) and *ROSA$^{mT/mG}$*/+ (control) mice were anesthetized by i.p. injection of a mixture of ketamin (100mg/kg) and xylazin (10mg/kg). Tibialis anterior muscles were dissected and fixed for 2h in 4% PFA in PBS on ice. Muscles were washed in PBS (3 x 15 min), cryoprotected in 30% sucrose in PBS and embedded in OCT compound (Sakura) before cryostat sectioning (20µm).

For immunostaining, slides were incubated for 20 minutes in antigen retrieval buffer (2.94 g Tri-Sodium citrate and 0.5 ml Tween 20 in 1 L distilled water, pH 6) that had been heated in a microwave till boiling. Slides were washed in PBS (2 x 10 min) and incubated with chicken anti-GFP (Aves Labs, GFP-1020, 1/300) and rabbit anti-RFP (MBL Life Science, PM005, 1/250) primary antibodies in 2% donkey serum /0.1% Triton X-100 in PBS at 4°C overnight. Next, slides were washed in PBS (2 x 10 min) and incubated with Alexa-488-conjugated anti-chicken and Alexa-568-conjugated anti-rabbit secondary antibodies (1/300) in PBS with 2% donkey serum and 0.1% Triton X-100 for 2h at room temperature. Finally, slides were washed in PBS (2 x 10 min) and incubated with Alexa Fluor 647 phalloidin (Thermo Fisher Scientific, 1/20) at room temperature for 15 min, rinsed in PBS (5 min) and mounted in DAPI-containing mounting medium (Vectashield).

FUS/phalloidin/DAPI staining on newborn muscles

To evaluate the efficiency of MyoD^{iCre} mice to revert the *Fus$^{\Delta NLS}$* allele to wild type, *MyoD$^{iCre/+}$* males were crossed to *Fus$^{\Delta NLS/+}$* females, and timed matings were set up between *MyoD$^{iCre/+}$; Fus$^{\Delta NLS/+}$* males in the offspring and *Fus$^{\Delta NLS/+}$* females. Fixed tibialis anterior muscles were dissected from *MyoD$^{iCre/+}$; Fus$^{\Delta NLS/\Delta NLS}$ (experimental), Fus$^{\Delta NLS/\Delta NLS}$ and MyoD$^{iCre/+}$* (control) pups, washed in PBS and incubated overnight in 30% sucrose in PBS at 4°C. Muscles were embedded in OTC and 16 µm thick cryosections were made with a cryostat.

For immunostaining, sections were incubated at room temperature and hydrated with PBS (2 x 10 min). Sections were incubated with rabbit anti-FUS (Sigma, HPA008784, 1/150) primary antibody in PBS with 2% donkey serum and 0.1% Triton X-100 at 4°C overnight. Sections were subsequently washed with PBS (2 x 10 min), followed by Alexa-488-conjugated anti-rabbit secondary antibody in PBS with 2% donkey serum and 0.1% Triton X-100 for 2h at room temperature. Sections were washed in PBS (3 x 10 min) and incubated with Alexa Fluor 647-conjugated phalloidin (Cell Signaling, 8940, 1/20) for 30 min at room temperature. Sections were washed in PBS (3 x 10 min) and mounted in mounting medium with DAPI (VectaShield) for confocal imaging.

FUS immunostaining in adult muscles

Unfixed muscles embedded in OCT (Tissue-Tek® O.C.T. Compound, Sakura, 4583) were frozen in melting isopentane. Serial cuts of 14µm thick were made with cryostat (Leica CM 3050S) and deposited on Superfrost® slides (Superfrost, VWR, 631-0448). Slides were dried 20min then fixed with 4% PFA in 0.1mM sucrose 15min at room temperature. After washes with PBS, AChR clusters were stained with Alexa Fluor 594-conjugated α-Bungarotoxin (Sigma, T195; 1/500) during 1h at room temperature. Unspecific binding sites were blocked with 0,1% TritonX100 and 3% BSA in PBS, 2h at room temperature. Rabbit anti FUS antibody (Bethyl, A300-294A, 1:1000) was incubated overnight at 4°C. After rinsing in PBS, anti-rabbit Alexa Fluor 488 (Jackson, 711-547-003, 1/500) was incubated 2h at room temperature. Finally, sections were washed with PBS followed by water and mounted in aquapolymount (Polysciences, 18606-5).

Fus extrasynaptic and subsynaptic nuclei intensity was measured using Image J software. Subsynaptic nuclei were defined as nuclei directly underneath alpha-bungarotoxin staining (labeling AChR) (i.e. overlapping in a confocal stack), while other nuclei were considered as extrasynaptic. The criteria for inclusion of synapses for analysis were that an endplate was clearly visible on confocal images, and that subsynaptic nuclei were present. FUS staining intensity was determined in all nuclei present in a confocal image stack. Mean FUS staining intensity in subsynaptic nuclei was then divided by FUS staining intensity in nonsynaptic nuclei, resulting in a ratio of FUS enrichment in synaptic nuclei. The resulting ratio (enrichment score) reflects the relative enrichment of FUS in subsynaptic nuclei: a ratio of 1 means no

enrichment (FUS staining similar in subsynaptic and extrasynaptic nuclei), while a ratio of e.g. 3 indicates a 3-fold enrichment of FUS in subsynaptic nuclei.

Axotomy experiments

For axotomy, intraperitoneal injection of 100 mg/kg ketamine chlorhydrate and 5mg/kg xylazine was performed on wild type C57Bl6/J mice. 1-2 mm of sciatic nerve was removed and lidocaine was deposited on surgical wound. Skin was sutured and mice were daily surveyed until sacrifice 5 days after surgery.

Electron microscopy

Gastrocnemius muscles of newborn mice were fixed by immersion in 2.5% glutaraldehyde and 2.5% PFA in cacodylate buffer (0.1M, pH 7.4), postfixed in 1% osmium tetroxide in 0.1M cacodylate buffer for 1 hour at 4°C and dehydrated through graded alcohol (50, 70, 90, 100%) and propylene oxide for 30 minutes each. Samples were embedded in Epon 812. Ultrathin sections were cut at 70nm, contrasted with uranyl acetate and lead citrate and examined at 70kv with a Morgagni 268D electron microscope. Images were captured digitally by Mega View III camera (Soft Imaging System).

Electromyography with repetitive nerve stimulation

12-month-old mice were anesthetized with intraperitoneal injection of 100 mg/kg ketamine chlorhydrate and 5mg/kg xylazine. Repetitive nerve stimulation was performed by supramaximally stimulating the sciatic nerve and detecting responses in the gastrocnemius. 3 trains of 10 stimuli were delivered at different frequency: 3, 10, 20 and 50 Hz. The maximal amplitude (negative + positive peak) of the CMAP was measured using image J software and the percentage decrement between first and tenth stimulus of each train was calculated.

C2C12 myoblast culture experiments

C2C12 myoblast cells were purchased from ATCC (ATCC® CRL-1772™). Cells were cultured in Dulbecco's modified Eagle's medium containing 10% Fetal Bovine Serum (Fisher scientific, 11531831) and 1% Penicillin-Streptomycin (Sigma, P4333) at 37 °C in an incubator with 5% CO_2. Between 60 and 80% of confluency, myoblasts were differentiated in myotubes with differentiation medium (identical medium, with

0.1% Fetal Bovine Serum). Culture medium was changed every day and transfections were performed between passages 5 and 15.

siRNA Transfection

C2C12 were cultured in 6-well plates until 60% of confluency. Cells were transfected with siRNA in differentiation medium using Lipofectamine RNA iMAX (Fischer scientific sas, 13778150) according to the manufacturer's instructions. siRNA against FUS and negative control siRNA were provided by Dharmacon (respectively D-001810-10-20 and L-051741-00-0050). Cells were harvested 48h after transfection.

Plasmid Transfection and luciferase assay

C2C12 were cultured in 24 well-plates until 80% of confluency. Transfection was performed in differentiation medium with expression and reporter plasmids using TransIT-X2 (MIR6000, Myrus) according to the manufacturer's instructions. Expression vectors used for transfections were: pCMV empty plasmid, pCMV-Myc-FUS (expressing N-terminal myc-tagged human wild type FUS) and pCMV-Myc-FUS-R495X. Reporter plasmids were pcDNA3.1-Chrne-luc, pcDNA3.1-chrnd-luc and pcDNA3.1-CMV-luc obtained from L. Schaeffer (Lyon, France) [5]. After 24h of transfection, proteins were extracted and luciferase activity was measured (Promega, E4550) and normalized by total proteins measured with BCA assay (Interchim, UP95424A, UP95425A).

Plasmid Transfection and immunostaining

C2C12 were cultured in 24 well-plates until 80% of confluency. Transfection was performed in differentiation medium with expression vectors using TransIT-X2 (MIR6000, Myrus) according to the manufacturer's instructions. Expression vectors used for transfections were: pCMV-Myc-FUS (expressing N-terminal myc-tagged human wild type FUS), pCMV-GFP-FUS and pCMV-Myc-FUS-R495X obtained from L. Schaeffer (Lyon, France) and N. Charlet Berguerand (Strasbourg, France). 24h after transfection, cells were fixed in 4% PFA during 10min and then washed with PBS 1X. Transfected cells were incubated with anti-Myc antibody (sigma, M4437, 1/250) overnight. After three washes with PBS-0.1% Triton X-100, cells were incubated with Alexa-596-conjugated anti-mouse secondary antibody (Molecular probes, A21203, 1/500) and hoechst (Sigma, B2261, 1/1000) for 2h at room temperature. Finally, cells were washed with PBS followed by water and mounted in

aquapolymount (Polysciences, 18606-5). For analysis, 10 images per condition (condition 1: pCMV-GFP-FUS + pCMV-Myc-FUS; condition 2: pCMV-GFP-FUS + pCMV-Myc-FUS-R495X) were used to quantify the percentage of cytoplasmic pCMV-GFP-FUS and the percentage of granular pCMV-GFP-FUS using Image J software.

RNA extraction and quantitative reverse transcription-polymerase chain reaction

Total RNA was extracted from C2C12 or muscles (tibialis or gastrocnemius) of mice using TRIzol® reagent (Life Technologies). 1 µg of RNA was reverse transcribed with iScript™ reverse transcription (Biorad, 1708841). Quantitative polymerase chain reaction was performed using Sso Advanced Universal SYBR Green Supermix (Bio-Rad) and quantified with Bio-Rad software. Gene expression was normalized by calculating a normalization factor using H2A Histone Family Member X (H2AX), Histone Cluster 1 H2A Family Member C (H2AC), Histone Cluster 1 H2B Family Member C (H1H2BC) genes according to GeNorm software [38].

Primer sequences were as follows:

H2AX: F-TCCTGCCCAACATCCAGG, R-TCAGTACTCCTGAGAGGCCTGC

H2AC: F-CAACGACGAGGAGCTCAACAAG, R-GAAGTTTCCGCAGATTCTGTTGC

H1H2BC: F-AACAAGCGCTCGACCATCA, R-GAATTCGCTACGGAGGCTTACT

Chrna1: F-CCACAGACTCAGGGGAGAAG, R-AACGGTGGTGTGTGTTGATG

Chrnb1: F-GGCAAGTTCCTGCTTTTCGG, R-CGTCCGGAAGTGGATGTTCA

Chrng: F-GAGAGCCACCTCGAAGACAC, R-GACCAACCTCATCTCCCTGA

Chrnd: F-CGC-TGC-TTC-TGC-TTC-TAG-GG, R-ATCAGTTGGCCTTCGGCTT

Chrne: F-CAATGCCAATCCAGACACTG, R-CCCTGCTTCTCCTGACACTC

Chromatin immunoprecipitation

1.08x 10^7 of C2C12 cells differentiated during 48h, were washed with PBS and fixed in 1% PFA during 10 minutes. Glycine (0.125M) was added to stop the crosslinking reaction. After washes in PBS, cells were detached, centrifuged and resuspended in nuclei buffer (50mM Tris HCL pH8, 2mM EDTA pH8, 0.1%NP40, 10% glycerol, 1M Na butyrate, protease inhibitor 1x). After centrifugation, nuclei were resuspended in sonication buffer (50mM TrisHCL pH8, 10mM EDTA, 0.3% SDS, 1M Na butyrate, protease inhibitor 1x) and sonicated with Diagenode Bioruptor (B0102001 - 3 Cycles of 5 minutes - 30s on / 30s off). A fraction of sonicated chromatin was reverse cross linked and fragment size was checked. We used chromatin with fragment size 200-500 bp, and saved 0.3µg as 1% input. 30µg of chromatin was used for

immunoprecipitation. Sonicated chromatin was incubated overnight at 4°C with 10µg of primary antibodies against FUS (FUS-1: A300-294A - Bethyl, FUS-2: A300-293A - Bethyl), or without antibody (WAB) as negative control. Addition of 50µL of protein A/G beads (53133- Thermo Scientific) during 2h, followed by centrifugation and washes allowed chromatin immunoprecipitation. Beads were then resuspended in elution buffer (10mM Tris pH8, 1mM EDTA pH8), and chromatin was reverse cross linked (0.2M NaCl, 50µg.mL of RNase, proteinase K 0.15%) during 3h at 65°C. DNA purification was performed with QIAquick ® PCR Purification Kit (28106 – Qiagen). qPCR was performed with following primers :

Chnra F-GACAAGCCTCTGACTCATGATCTATGT, R-GCTGCCGGTCCTACTCCACCCTGGCT,

Chnrd F-TCCTGCCTGGGATCTTTTCGTTCTGCCCTTGG, R-GGTTTGTCTTCCCTTCAGCCTGTTGCTGTGGA,

Chnre F-GATGACAGGCCTTGTGGATT, R-GACAAGCTTGAGGGAACAGG,

Mecp2 (positive control for Fus) F- AGTATGACTCTTCCTTACCAGGAG, R-CTGATTCAAATTTGGCTCCCCT,

H2AC (negative control for Fus) F-CGCGAAACTTGCGTTTTCAG, R-TTGGTGGTTATTTGGCCCCT.

Data were presented normalized to 1% input.

Western blotting

Cells were washed in PBS1x and lysed in RIPA buffer (Tris 50mM, NaCl 150mM, EDTA 1mM, SDS 0.1%, Deoxycholate 0.5%,Triton 100X) containing protease inhibitor (Sigma P8340) and phosphatase inhibitor cocktail (Sigma 8345). After centrifugation at 10 000rpm, 4°C during 10min,supernatant was saved and used to dose protein extract by using a BCA Assay (Interchim, UP95424A, UP95425A). Protein were denatured and SDS page were performed with 25µg of protein on criterion TGX stain free gel 4-20% (Biorad, 5678094).Proteins were blotted on nitrocellulose membrane using semi-dry Transblot Turbo system (BioRad, France) and blocked with 10% non-fat milk during 1h. Anti-FUS antibody (Proteintech, 18592-1-AP, 1:1000) was incubated overnight at 4°C in 3% non-fat milk. Washing were proceeded with washing buffer (Tris pH 7.4 1 M, NaCl 5M, Tween 20 100 %) and anti-rabbit HRP (PARIS, BI2407) was incubated 1h30 at room temperature. After successive washes, proteins were visualized with chemiluminescence using ECL

Lumina Forte (Millipore, France) and chemiluminescence detector (Bio-Rad, France). Total proteins were detected with stain free gel capacity (Biorad, 5678094) and used to normalized.

Experiments on human iPSC- derived motor neurons and myotubes or human skeletal muscle biopsies

Patients from which a hair sample was obtained

FUS1 (male, 26) harbored a novel 1bp deletion (c.1483delC) leading to a frameshift [39-41] and the modification of the protein transcript before the stop codon (R495QfsX527) within a highly conserved RGG-rich region. FUS2 (male, 19) carried the frameshift mutation c.1504delG, leading to an extended translation into the 3'-UTR of the protein (D502TfS∗27). Mutations in FUS1 and FUS2 displayed a juvenile ALS onset. All FUS-ALS patients showed a spinal disease onset with a bulbar progression for FUS2. ALS-related mutations within the *FUS* gene were localized at the C-terminus of the transcript, affecting the NLS of the protein. This information is included in the table shown in Figure 6a.

Reprogramming of human keratinocytes and cultivation of hiPSCs

Generation of human iPS cells from reprogrammed human keratinocytes was performed as previously described [42, 43], using a lentiviral multicistronic vector [44]. All cell lines used were already characterized and previously published [23, 45].

Plucked human hair samples were cultivated in conditioned MEF medium supplemented with 50µg/ml ascorbic acid (Sigma-Aldrich, A4403), 10ng/ml FGF2 (Cell Guidance Systems, GFH146-50) and 10 µM Rho-associated kinase (ROCK) inhibitor (Ascent Scientific, Asc-129). After outgrow of keratinocytes, medium was changed to Epilife (Gibco, M-EPICF, S0015) supplemented with 10 µM ROCK inhibitor. To obtain high reprogramming efficiency, cells were not passaged more than two times with k-dispase (BD Bioscience 354235). Viral infection was performed using polybrene (sigma-Aldrich, TR-1003-G) on two consecutive days. Subsequently, cells were seeded on irradiated rat embryonic feeder cells and cultivated in hiPSC medium (Knockout DMEM, 20% Knockout Serum Replacement (Thermo Fisher Scientific, 10828028), 1% NEAA (Gibco, 11140), 1% GlutaMax^{TM}, 35050-038, 100µM ß-mercaptoethanol (Millipore, ES-007-E), 1% Antibiotic Antimycotic (Thermo Fisher Scientific, 15240062) supplemented with 50µg/ml ascorbic acid, 10ng/ml FGF2,

10µM ROCK inhibitor). Colonies displaying iPSC morphology were mechanically lifted and cultivated under feeder free conditions with mTeSR1 medium (Stem Cell technologies, 05850) at 37°C, 5% CO_2 and 5% O_2. HiPSCs were kept in culture maximally up to 35 passages.

All pluripotency tests and the spontaneous germ layer differentiation were performed as previously published [45, 46] or carried out according to manufacturer`s protocol.

Differentiation of motor neurons

Differentiation of hiPSCs into motor neurons was performed according to published protocols [45, 47].

For embryoid bodies (EBs) formation, hiPSCs were cultured in suspension in EB medium (DMEM/F12 (Gibco, 31331), 20% Knockout Serum Replacement, 1% NEAA, 1% β-Mercaptoethanol, 1% Antibiotic-Antimycotic) in ultra low attachment flasks (Corning Costar, 734-4140). 10µM ROCK inhibitor was supplemented for the first 24 hours. Neuronal differentiation was induced by changing the medium to Differentiation medium 1 (DMEM/F12, 1% NEAA, 2µg/ml heparin (Sigma, H3149), 1% Antibiotic Antimycotic, 2% Hormone mix (24 nM Sodium Selenite (Sigma, S9133-1MG) + 16 nM Progesterone (Sigma, P6149-1MG) + 0.08 mg/ml Apotransferrin (Sigma, T2036-1G) + 0.02 mg/ml Insulin (SAFC, 91077C-1G) + 7.72 µg/ml Putrescin (Sigma, P7505-25MG)) supplemented with 10ng/ml GDNF (Peprotech, 450-10), 10ng/ml BDNF (Peprotech, 540-02), 10ng/ml IGF-1 (Peprotech, 100-11), 0.1µM cAMP (Sigma, D0260), 20µg/ml ascorbic acid) on day 4. EBs were seeded in Differentiation medium 1 on laminin-coated (Sigma-Aldrich, 11243217001) plates on day 7. On day 10, medium was replaced with Differentiation medium 2 (Differentiation medium 1, containing 0.1µM of retinoid acid (Sigma-Aldrich, R2625-100MG)). On day 15, neurospheres were transferred into T75 low-attachment flasks containing Differentiation medium 3 (Differentiation medium1, containing 1µM pumorphamine (Calbiochem, 540220), 0.1µM retinoid acid and 2% B27 (Gibco, 12587)). At day 28, up to 3 neurospheres were seeded on 35mm µ-dishes (Ibidi, 86694) pre-coated with Poly-L-Ornithin (Sigma, P4957) and coated with laminin. Medium was changed to Differentiation medium 4 (Differentiation medium 1, containing 0.05 µM retinoid acid, 0.5 µM pumorphamine and 2% B27).

Differentiation of myotubes

Differentiation of myogenic cells from human iPSCs was performed basically as previously published using a spheres-based culture [24].

Briefly, hiPSCs were cultured in suspension using ultra low attachment flasks in Stemline medium (Sigma, SA3194) containing 100ng/ml FGF-2, 100ng/ml EGF and 5ng/ml heparan sulfate (Sigma, H7640-1mg). Cells were split weekly using a 2 min accutase (Sigma, A6964) digestion and media were exchanged every second day. After 6 weeks of cultivation, cells were transferred into single cells using accutase digestion and filtration through a 30μm pre-separation filter (Miltenyi Biotec, 130-041-407). 200,000 Cells per well were seeded on glass coverslips in 24 well plates, coated with PLO and laminin. Medium was changed to DMEM (Gibco, 41965) containing 2% B27 and 1% Antibiotic-Antimycotic with a media exchange twice per week. After 8 weeks of final differentiation mature myotubes were obtained and fixed or lysed for analysis.

To perform co-cultivation of iPSC-derived muscle cells with iPSC-derived motor neurons, myogenic cells were differentiated using Pax7-induced stem cell-derived progenitors, as described [25, 48].

Generation of isogenic control cell line

An isogenic control cell line (CNTL3) was generated by inserting a cytosine in position 1483 and consequently correcting the mutation, using Clustered Regularly Interspaced Short Palindromic Repeats (CRISPR) technology. This cell line was previously characterized and published [23].

The C-nucleotide was inserted using a customized guide RNA (TATGATCGAGGCGGCTACCGGG) and a sequence specific donor vector purchased from Genewiz, containing the respective template with the C-nucleotide insertion. DNA transfection into patient-derived iPSCs was performed using Amaxa nucleofection (Lonza, VPH-5012). Subsequently, single cell-derived colonies were screened by a PCR-based approach. Total DNA was isolated using QIAamp DNA Mini Kit (Qiagen, 51306). The region of interest was amplified by PCR using sequence-specific primers (TCTAGGTCTTGCCTATTCCCC, GTGATCAGGAATTGGAAGGTTAC) and the Phusion High-Fidelity DNA Polymerase (Thermo Scientific, F-530L).

Quantitative Real-time PCR

Total RNA was isolated using the RNeasy Mini Kit (Qiagen, 74106) according to the manufacturers' protocol and eluted in 40 µl RNAse-free water.

First strand synthesis and quantitative real-time-PCR amplification were performed in a one-step, single-tube reaction using the QuantiFast SYBR Green RT-PCR kit (Qiagen, 204174) and the Rotor-Gene-Q real-time PCR machine model 2-Plex HRM (Qiagen) in a total reaction volume of 20 µl. Reactions were performed in 0.1 ml strip tubes and were composed of 1 µl of RNA, 10 µl QuantiFast SYBR Green RT-PCR Master Mix, 0.2 µl RT Enzyme, 6.8 µl RNAse-free water and 2 µl of QuantiTect primer (0.5 µmol).

qRT-PCR cycling conditions were as follows: 1 cycle Reverse Transcription of 10 min at 50°C, 1 cycle Denaturation of 5 min at 95°C, 40 cycles of 5 sec at 95°C for denaturation, 10 sec at 60°C for annealing and elongation. The cycle threshold (C_T) for fluorescence detection were calculated and set by the Rotor-Gene Q Software version 2.0.2 (Qiagen) at 10^{-2} norm. fluorescence. All results are shown relative to the reference-housekeeping gene hydroxymethylbilane synthase (*HMBS)* to obtain values for relative quantification. QuantiTect Primer pairs were purchased from Qiagen.

Immunocytochemistry

For immunocytochemistry, cultures were fixed using 4% paraformaldehyde (Merck) and 10% sucrose (Roth, 4621.1) in phosphate buffered saline (DPBS, Gibco, H15-001) for 15 min. After washing, samples were permeabilized with 0.2% Triton X-100 (Roche, 10789704001) for 10 min. After blocking with 5% FBS (Gibco, 10500) and 10% goat serum (Millipore, S26-100mL) in DPBS for 1 hour, primary antibodies rabbit anti-FUS (Bethyl Labs, Montgomery, A300-294A, 1;1000), rabbit anti-FUS (Sigma, HPA008784, 1:1000) chicken anti-NF-H (Antibodies online, ABIN1842223, 1:10.000), mouse anti-actinin (Sigma, A7811, 1:500), mouse anti-Desmin (Dako, M0760, 1;500), rabbit anti-Myosin heavy chain (R&D Systems, MAB4470, 1:500), mouse anti-MyoG (Millipore, MAB3876), anti-Dihydropyridine Receptor alpha (Millipore, MAB427. 1:500), anti-Ryanodine receptor (Millipore, AB9078. 1:500), α-Bungarotoxin conjugated with TRITC (Sigma, T0195, 1:1000) were incubated for 48 hours at 4°C. After subsequent washing, secondary antibodies were incubated for 1 hour at RT:

Alexa Fluor^{R} 488 goat anti-rabbit (A-11034), Alexa Fluor^{R} 647 goat anti-chicken (A-21449), Alexa Fluor^{R} 568 goat anti-mouse (A-110049) (all 1:500, Invitrogen). Samples were mounted with ProLong Gold Antifade reagent with DAPI (Invitrogen, P36935).

Image acquisition and analysis

Fluorescence images were obtained using an Axioscope microscope (Zeiss) equipped with a CCD camera (16bits, 1280 x 1024pixels) and the Axiovision software (Zeiss). Quantification analysis and analysis of BT positive structures were performed using Image J Fiji software (www.imageJ.nih.gov) [49]. To investigate the structures forming an individual endplate, the Image J Fiji plugin "Analyze Particles" was used.

Human skeletal muscle biopsies

Muscle specimens were extracted in open biopsy of vastus lateralis (FUS3, CTRL), deltoid (FUS2), triceps (FUS1) and biceps (CNTRL4,5,6). Control patients presented at our Center with chronic pain syndrome, which was the reason for muscular biopsy, showing no myopathic changes in the biopsy results. FUS1 and FUS 4 had juvenile onset of the disease and clinically the disease onset for FUS1 and FUS5 was spinal and for FUS4 bulbar.

Samples were frozen with chilled isopentane and stored at -80 °C. Serial cuts of 10 µm thick were made with cryostat (Leica CM 3050S) and deposited on Superfrost® slides (Superfrost, VWR, 631-0448). Slides were dried 20min then fixed with 4% PFA in 0.1mM sucrose 15min at room temperature. Sections were stained with Hematoxylin and Eosin or used for immunohistochemistry. After washing with PBS, AChR clusters were stained with TRITC-conjugated α-BTX (Sigma, T0195; 1:500) during 1h at room temperature. Sections were then permeabilized with 0.1% Triton and nonspecific binding sites were blocked with 10% goat serum and 5% FBS in PBS, 2h at room temperature. Rabbit anti-FUS (Sigma, HPA008784, 1:1000), guinea pig anti- Synaptophysin (synaptic systems, 101004, 1:500) were incubated overnight at 4°C. After rinsing in PBS and goat anti-rabbit Alexa Fluor 488, (Invitrogen, A-11034, 1/500) and goat anti-guinea pig Alexa Fluor 6472 (Invitrogen, A-21450) were incubated 2h at room temperature. Finally, sections were washed with PBS followed by water and mounted with ProLong Gold Antifade reagent with DAPI (Invitrogen, P36935). Confocal images were acquired with a laser scanning microscope (Leica

DMi8) equipped with a ACS APO 20x, 40x or 63 x oil DIC immersion objective. Images were acquired with a resolution of 1024x1024 pixels.

Electromyography

Needle electromyography (EMG) was performed in all FUS patients and controls using concentric needle electrodes (38 x 0.45 mm). EMG was performed on a 4 channel SIGMA EMG machine by Neurowerk (Neurowerk Medizintechnik, Gelenau, Germany). In each patient and muscle, manual single potential analysis with 20 single potentials minimum per muscle was performed, it was checked whether abnormal spontaneous activity was present on at least 20 sites of the muscle and the maximal innervation pattern was recorded. The needle EMG was performed within the clinical diagnostic work-up at the University Hospital of Ulm, Germany, by an experienced neurologist.

Statistics

All results from analysis are presented as mean ± standard error of the mean (SEM) and differences were considered significant when $p < 0.05$.

Before analysis, all outliers were removed using a ROUT test and normality and homoscedasticity were assessed. For comparison of normally distributed data of two groups, two-tailed unpaired Student's *t*–test was used in combination with F-test to confirm that the variances between groups were not significantly different. Non-parametric Mann-Whitney was performed for data not distributed normally.

Comparisons of data consisting of more than two groups, varying in a single factor, were performed using (nested) one-way ANOVA or Kruskall-Wallis. Analysis of normally distributed data consisting of only biological replicates,was performed using one-way ANOVA followed byTukey's, Dunnett's or Bonferroni's multiple comparisons *post hoc* test. Normally distributed data consisting of both biological and technical replicates were analyzed using nested one-way ANOVA and subsequent Tukey's multiple comparisons test. For not normally distributed data, a non-parametric Kruskall-Wallis followed by Dunn's multiple comparisons test was used.

Comparisons of data consisting of more than two groups, varying in two factors, was performed using two-way ANOVA and subsequent Tukey's or Bonferroni's multiple comparisons test.

For human cell culture experiments, Fisher's Exact Test followed by Bonferroni correction for multiple comparisons was used. Data were analyzed by using GraphPad Prism version 8.0 and R.

Acknowledgements

We thank Drs. L. Schaeffer, A. Verger, J. Weishaupt and R. Perlingeiro for the kind gift of plasmids, and Dr. Nicolas Charlet Berguerand for advice in siRNA treatment. We would like to thank the General Instruments Facility of the Science faculty of Radboud University, and Ioannis Alexopoulos in particular for advise on image acquisition and analysis. The authors would like to thank Sabine Seltenheim, Lilli Dietz and Renate Zienecker for excellent technical support. Antje Knehr, Department of Neurology, Ulm University, for collecting human material. Benjamin Mayer, Institute for Epimediology and Medical Biometrics, Ulm University, for advice in statistical analysis. We are grateful to all the participants for willingly providing us with hair and muscle samples. This work was directly supported by ALS Association Investigator Initiated Awards (grants 2235, 3209 and 8075; to LD and CLT); the Frick Foundation (award 2013 to LD and CLT); Association Française contre les Myopathies (grant #18280; to LD, CLT and ES); Virtual Helmholtz Institute “RNA dysmetabolism in ALS and FTD” (WP2, to LD, ACL and TMB), the DZNE (Ulm site) and agence nationale de la recherche (ToFU, EpiFUS, to LD) and the Bundesministerium für Bildung und Forschung (BMBF01EK1611C to TMB and MD).

Work in our laboratories is supported by ARSla (call 2014 and 2016 to LD), the fondation “recherche sur le cerveau” (call 2015, to LD), Axa Banque Patrimoniale (Bourse recherche maladies rares, to LD), Fondation pour la recherche médicale (Equipe FRM, to LD), the Max Planck Society (to ES), the Muscular Dystrophy Association (MDA, to ES), the EU Joint Programme – Neurodegenerative Disease Research (JPND; grant numbers ZonMW 733051075 (TransNeuro) and ZonMW 733051073 (LocalNMD) to ES) and an ERC consolidator grant (ERC-2017-COG 770244 to ES).

Author contributions

GP performed most of the experiments in heterozygous knock-in mice and in C2C12 cells, with the help of SD, MAG, JSZ and ISR. MD, JH and AA performed most of the

experiments in human derived cells and tissues. AZ, MB, MM, LZ, CZ, SM, MW and NvB performed and analyzed the experiments in homozygous knock-in, MyoD-CRE rescued knock-in, and knock-out mice. CS performed immunoprecipitation experiments. NM performed electron microscopy. ALB supervised ChIP experiments. AR provided human muscle biopsies. AMH performed and analyzed EMGs. ACL provided patient and clinical material. MD, CLT, TB, LD and ES initiated, conceived and supervised the project. GP, MD, LD and ES wrote the manuscript. All authors contributed to the experimental design and interpretation and commented on the manuscript.

Competing interest statement

The authors declare no competing interests.

Data availability

All data reported in this paper are shown in the main or supplementary figures and data. Raw data are available upon request.

References

1. Darabid, H., Perez-Gonzalez, A.P. & Robitaille, R. Neuromuscular synaptogenesis: coordinating partners with multiple functions. *Nat Rev Neurosci* **15**, 703-718 (2014).
2. Tintignac, L.A., Brenner, H.R. & Ruegg, M.A. Mechanisms Regulating Neuromuscular Junction Development and Function and Causes of Muscle Wasting. *Physiol Rev* **95**, 809-852 (2015).
3. Shi, L., Fu, A.K. & Ip, N.Y. Molecular mechanisms underlying maturation and maintenance of the vertebrate neuromuscular junction. *Trends Neurosci* **35**, 441-453 (2012).
4. Hippenmeyer, S., Huber, R.M., Ladle, D.R., Murphy, K. & Arber, S. ETS transcription factor Erm controls subsynaptic gene expression in skeletal muscles. *Neuron* **55**, 726-740 (2007).
5. Ravel-Chapuis, A., Vandromme, M., Thomas, J.L. & Schaeffer, L. Postsynaptic chromatin is under neural control at the neuromuscular junction. *EMBO J* **26**, 1117-1128 (2007).
6. Taylor, J.P., Brown, R.H., Jr. & Cleveland, D.W. Decoding ALS: from genes to mechanism. *Nature* **539**, 197-206 (2016).
7. Pun, S., Santos, A.F., Saxena, S., Xu, L. & Caroni, P. Selective vulnerability and pruning of phasic motoneuron axons in motoneuron disease alleviated by CNTF. *Nat Neurosci* **9**, 408-419 (2006).
8. Fischer, L.R.*, et al.* Amyotrophic lateral sclerosis is a distal axonopathy: evidence in mice and man. *Exp Neurol* **185**, 232-240 (2004).
9. Dadon-Nachum, M., Melamed, E. & Offen, D. The "dying-back" phenomenon of motor neurons in ALS. *J Mol Neurosci* **43**, 470-477 (2011).
10. Schwartz, J.C., Cech, T.R. & Parker, R.R. Biochemical Properties and Biological Functions of FET Proteins. *Annu Rev Biochem* **84**, 355-379 (2015).
11. Ling, S.C., Polymenidou, M. & Cleveland, D.W. Converging mechanisms in ALS and FTD: disrupted RNA and protein homeostasis. *Neuron* **79**, 416-438 (2013).
12. Deng, H., Gao, K. & Jankovic, J. The role of FUS gene variants in neurodegenerative diseases. *Nature Reviews Neurology* **10**, 337-348 (2014).
13. Dormann, D.*, et al.* ALS-associated fused in sarcoma (FUS) mutations disrupt Transportin-mediated nuclear import. *EMBO J* **29**, 2841-2857 (2010).
14. Scekic-Zahirovic, J.*, et al.* Toxic gain of function from mutant FUS protein is crucial to trigger cell autonomous motor neuron loss. *EMBO J* **35**, 1077-1097 (2016).
15. Scekic-Zahirovic, J.*, et al.* Motor neuron intrinsic and extrinsic mechanisms contribute to the pathogenesis of FUS-associated amyotrophic lateral sclerosis. *Acta Neuropathol* **133**, 887-906 (2017).
16. Kanisicak, O., Mendez, J.J., Yamamoto, S., Yamamoto, M. & Goldhamer, D.J. Progenitors of skeletal muscle satellite cells express the muscle determination gene, MyoD. *Dev Biol* **332**, 131-141 (2009).
17. Yamamoto, M.*, et al.* A multifunctional reporter mouse line for Cre- and FLP-dependent lineage analysis. *Genesis* **47**, 107-114 (2009).
18. Muzumdar, M.D., Tasic, B., Miyamichi, K., Li, L. & Luo, L. A global double-fluorescent Cre reporter mouse. *Genesis* **45**, 593-605 (2007).
19. Angus, L.M.*, et al.* Calcineurin-NFAT signaling, together with GABP and peroxisome PGC-1{alpha}, drives utrophin gene expression at the neuromuscular junction. *Am J Physiol Cell Physiol* **289**, C908-917 (2005).

20. Handschin, C.*, et al.* PGC-1alpha regulates the neuromuscular junction program and ameliorates Duchenne muscular dystrophy. *Genes Dev* **21**, 770-783 (2007).
21. Tan, A.Y., Riley, T.R., Coady, T., Bussemaker, H.J. & Manley, J.L. TLS/FUS (translocated in liposarcoma/fused in sarcoma) regulates target gene transcription via single-stranded DNA response elements. *Proc Natl Acad Sci U S A* **109**, 6030-6035 (2012).
22. Kedage, V.*, et al.* An Interaction with Ewing's Sarcoma Breakpoint Protein EWS Defines a Specific Oncogenic Mechanism of ETS Factors Rearranged in Prostate Cancer. *Cell Rep* **17**, 1289-1301 (2016).
23. Higelin, J.*, et al.* FUS Mislocalization and Vulnerability to DNA Damage in ALS Patients Derived hiPSCs and Aging Motoneurons. *Front Cell Neurosci* **10**, 290 (2016).
24. Hosoyama, T., McGivern, J.V., Van Dyke, J.M., Ebert, A.D. & Suzuki, M. Derivation of myogenic progenitors directly from human pluripotent stem cells using a sphere-based culture. *Stem Cells Transl Med* **3**, 564-574 (2014).
25. Demestre, M.*, et al.* Formation and characterisation of neuromuscular junctions between hiPSC derived motoneurons and myotubes. *Stem Cell Res* **15**, 328-336 (2015).
26. de Carvalho, M.*, et al.* Electrodiagnostic criteria for diagnosis of ALS. *Clin Neurophysiol* **119**, 497-503 (2008).
27. Baumer, D.*, et al.* Juvenile ALS with basophilic inclusions is a FUS proteinopathy with FUS mutations. *Neurology* **75**, 611-618 (2010).
28. Waibel, S.*, et al.* Truncating mutations in FUS/TLS give rise to a more aggressive ALS-phenotype than missense mutations: a clinico-genetic study in Germany. *European journal of neurology* **20**, 540-546 (2013).
29. Zou, Z.Y., Liu, M.S., Li, X.G. & Cui, L.Y. Mutations in FUS are the most frequent genetic cause in juvenile sporadic ALS patients of Chinese origin. *Amyotroph Lateral Scler Frontotemporal Degener* **17**, 249-252 (2016).
30. So, E.*, et al.* Mitochondrial abnormalities and disruption of the neuromuscular junction precede the clinical phenotype and motor neuron loss in hFUSWT transgenic mice. *Hum Mol Genet* **27**, 463-474 (2018).
31. Sharma, A.*, et al.* ALS-associated mutant FUS induces selective motor neuron degeneration through toxic gain of function. *Nature communications* **7**, 10465 (2016).
32. Naumann, M.*, et al.* Impaired DNA damage response signaling by FUS-NLS mutations leads to neurodegeneration and FUS aggregate formation. *Nature communications* **9**, 335 (2018).
33. Miller, T.M.*, et al.* Gene transfer demonstrates that muscle is not a primary target for non-cell-autonomous toxicity in familial amyotrophic lateral sclerosis. *Proc Natl Acad Sci U S A* **103**, 19546-19551 (2006).
34. Towne, C., Raoul, C., Schneider, B.L. & Aebischer, P. Systemic AAV6 delivery mediating RNA interference against SOD1: neuromuscular transduction does not alter disease progression in fALS mice. *Mol Ther* **16**, 1018-1025 (2008).
35. Dobrowolny, G.*, et al.* Skeletal muscle is a primary target of SOD1G93A-mediated toxicity. *Cell Metab* **8**, 425-436 (2008).
36. Wong, M. & Martin, L.J. Skeletal muscle-restricted expression of human SOD1 causes motor neuron degeneration in transgenic mice. *Hum Mol Genet* **19**, 2284-2302 (2010).
37. Williams, A.H.*, et al.* MicroRNA-206 delays ALS progression and promotes regeneration of neuromuscular synapses in mice. *Science* **326**, 1549-1554 (2009).

38. Vandesompele, J.*, et al.* Accurate normalization of real-time quantitative RT-PCR data by geometric averaging of multiple internal control genes. *Genome Biol* **3**, RESEARCH0034 (2002).
39. Belzil, V.V.*, et al.* Novel FUS deletion in a patient with juvenile amyotrophic lateral sclerosis. *Arch Neurol* **69**, 653-656 (2012).
40. Japtok, J.*, et al.* Stepwise acquirement of hallmark neuropathology in FUS-ALS iPSC models depends on mutation type and neuronal aging. *Neurobiol Dis* **82**, 420-429 (2015).
41. Lenzi, J.*, et al.* ALS mutant FUS proteins are recruited into stress granules in induced pluripotent stem cell-derived motoneurons. *Dis Model Mech* **8**, 755-766 (2015).
42. Aasen, T.*, et al.* Efficient and rapid generation of induced pluripotent stem cells from human keratinocytes. *Nat Biotechnol* **26**, 1276-1284 (2008).
43. Takahashi, K. & Yamanaka, S. Induction of pluripotent stem cells from mouse embryonic and adult fibroblast cultures by defined factors. *Cell* **126**, 663-676 (2006).
44. Warlich, E.*, et al.* Lentiviral vector design and imaging approaches to visualize the early stages of cellular reprogramming. *Mol Ther* **19**, 782-789 (2011).
45. Stockmann, M.*, et al.* Developmental and functional nature of human iPSC derived motoneurons. *Stem Cell Rev* **9**, 475-492 (2013).
46. Linta, L.*, et al.* Rat embryonic fibroblasts improve reprogramming of human keratinocytes into induced pluripotent stem cells. *Stem Cells Dev* **21**, 965-976 (2012).
47. Hu, B.Y. & Zhang, S.C. Differentiation of spinal motor neurons from pluripotent human stem cells. *Nat Protoc* **4**, 1295-1304 (2009).
48. Darabi, R.*, et al.* Human ES- and iPS-derived myogenic progenitors restore DYSTROPHIN and improve contractility upon transplantation in dystrophic mice. *Cell Stem Cell* **10**, 610-619 (2012).
49. Schindelin, J.*, et al.* Fiji: an open-source platform for biological-image analysis. *Nat Methods* **9**, 676-682 (2012).
50. Kikin, O., D'Antonio, L. & Bagga, P.S. QGRS Mapper: a web-based server for predicting G-quadruplexes in nucleotide sequences. *Nucleic acids research* **34**, W676-682 (2006).

Figure legends

Figure 1: Neuromuscular junction (NMJ) defects in newborn *Fus* mutant mice. **a-d,** Representative images showing NMJs in tibialis anterior muscles of newborn $Fus^{+/+}$ (a) versus $Fus^{\Delta NLS/\Delta NLS}$ (b) and $Fus^{+/+}$ (c) versus $Fus^{-/-}$ mice (d). Axons and presynaptic terminals were visualized by immunostaining with antibodies against neurofilament and SV2 (green). AChRs in muscle endplates were visualized using fluorescently labeled BTX (red). Scale bar: 10µm. **e-j,** Dot plots showing the percentage (%) of innervated endplates (e, h), the average endplate area (as % of $Fus^{+/+}$) (f, i) and the total number of endplates (g, j) in the tibialis anterior muscle of newborn $Fus^{+/+}$ versus $Fus^{\Delta NLS/\Delta NLS}$ (e-g) and $Fus^{+/+}$ versus $Fus^{-/-}$ mice (h-j). Mann-Whitney (e,h) or two-tailed unpaired t-test (f,g,i,j); *p<0.05, **p<0.005, ***p<0.0001; N= 12 $Fus^{+/+}$ versus 13 $Fus^{\Delta NLS/\Delta NLS}$ (e), 16 $Fus^{+/+}$ versus 15 $Fus^{\Delta NLS/\Delta NLS}$ (f), 11 $Fus^{+/+}$ versus 11 $Fus^{\Delta NLS/\Delta NLS}$ (g), 8 $Fus^{+/+}$ versus 8 $Fus^{-/-}$ (h,i,j). Average ± SEM. **k-n,** TEM images of NMJs in E18.5 gastrocnemius muscle of $Fus^{+/+}$ (k) versus $Fus^{\Delta NLS/\Delta NLS}$ (l) and $Fus^{+/+}$ (m) versus $Fus^{-/-}$ (n) mice. Arrows indicate junctional folds; * indicates membrane disruption. Nt: nerve terminal; M: muscle; Mc: mitochondria; Sv: synaptic vesicles. Scale bar: 0.5µm (k,l) and 1µm (m,n).

Figure 2: Cytoplasmic mislocalized $Fus^{\Delta NLS}$ protein is intrinsically toxic to muscle. **a,** immunostaining of FUS in the tibialis anterior of newborn $MyoD^{iCre/+}; Fus^{+/+}$ (upper row), $MyoD^{+/+}; Fus^{\Delta NLS/\Delta NLS}$ (middle row), and $MyoD^{iCre/+}; Fus^{\Delta NLS/\Delta NLS}$ (lower row) mice. Nuclei were labeled with DAPI and myofibers with the filamentous actin probe phalloidin. Merged images are shown in the right column. **b,** Ratio of cytoplasmic:nuclear FUS distribution, relative to $MyoD^{iCre/+}; Fus^{+/+}$ (= control set at 1). One-way ANOVA with Dunn's multiple comparisons test; ***p<0.0001; N= 81-103 muscle cells from 3 tibialis anterior sections per genotype. Average ± SEM. **c,** Endplate surface area as % of wild type littermate controls in tibialis anterior of newborn offspring from $MyoD^{iCre/+}$; $Fus^{\Delta NLS/+}$ x $Fus^{\Delta NLS/+}$ crosses. Two-way ANOVA with Tukey's multiple comparisons test; *p<0.05, **p<0.005, ***p<0.0001; N=8 $MyoD^{+/+}; Fus^{+/+}$, 14 $MyoD^{iCre/+}; Fus^{+/+}$, 11 $MyoD^{+/+}; Fus^{\Delta NLS/\Delta NLS}$, 8 $MyoD^{iCre/+}; Fus^{\Delta NLS/\Delta NLS}$. Average ± SEM.

Figure 3: Neuromuscular junction (NMJ) defects in heterozygous $Fus^{\Delta NLS/+}$ mice. **a, b,** Representative images showing NMJs in tibialis anterior muscles of 1-month-old and 10-month-old $Fus^{+/+}$ versus $Fus^{\Delta NLS/+}$ mice. Panel b shows magnifications of

individual NMJs (1 to 4) delineated in panel a. Axons and presynaptic terminals were visualized by immunostaining with antibodies against neurofilament and synaptophysin (green). AChRs in muscle endplates were visualized using fluorescently labeled BTX (red). Nuclei were labeled with DAPI (blue). Scale bars: 50µm (a), 15µm (b). **c-e,** Bar graphs showing the percentage of innervated, partially denervated and fully denervated endplates in the tibialis anterior muscle of 1-month-old (c) and 10-month-old (d) *Fus*$^{+/+}$ versus *Fus*$^{\Delta NLS/+}$ mice, and 28-month-old *Fus*$^{+/+}$ versus *Fus*$^{+/-}$ mice (e). Two-tailed unpaired t-test; **p<0.005, ***p<0.001; N= 6 vs 8 mice (c); 6 vs 7 (d); 7 vs 9 (e), with ~150 NMJs analyzed per mouse. Average ± SEM. **f-h,** Average endplate area (as % of *Fus*$^{+/+}$) in the tibialis anterior muscle of 1-month-old (f) and 10-month-old (g) *Fus*$^{+/+}$ versus *Fus*$^{\Delta NLS/+}$ mice, and 28-month-old *Fus*$^{+/+}$ versus *Fus*$^{+/-}$ mice (h). Two-tailed unpaired t-test; *p<0.05, **p<0.01; N= 6 vs 8 mice (f); 9 vs 9 (g); 7 vs 9 (h), with ~150 NMJs analyzed per mouse. Average ± SEM. **i,** Percentage decrement in maximal CMAP amplitude between the first and tenth stimulus administered at frequencies of 3, 10, 20 or 50 Hz. CMAP amplitude was recorded in gastrocnemius in response to repetitive stimulation (10x) of the sciatic nerve of 12-month-old *Fus*$^{+/+}$ versus *Fus*$^{\Delta NLS/+}$ mice. Two-tailed unpaired t-test; *p<0.05; N= 6 vs 6 mice. Average ± SEM.

Figure 4: Innervation-dependent enrichment of FUS in subsynaptic nuclei. **a,** Representative images showing FUS immunoreactivity (cyan) in the gastrocnemius muscle of 10-month-old *Fus*$^{+/+}$ versus *Fus*$^{\Delta NLS/+}$ mice. Axons and presynaptic terminals were visualized by immunostaining of neurofilament and synaptophysin (green). AChRs in muscle endplates were visualized using fluorescently labeled BTX (red). **b,** Relative enrichment of FUS immunoreactivity in subsynaptic versus nonsynaptic nuclei in gastrocnemius muscle of 10-month-old *Fus*$^{+/+}$ versus *Fus*$^{\Delta NLS/+}$ mice. Subsynaptic nuclei were defined as nuclei apposed to BTX-positive endplates. Two-tailed unpaired t-test; **p<0.005; N= 4 versus 4 mice. Average ± SEM. **c,** Representative images showing FUS immunoreactivity (cyan) in the contralateral (upper panels) or ipsilateral (lower panels) gastrocnemius muscle of mice, 5 days after sciatic nerve axotomy. **d,** Quantification of subsynaptic enrichment of FUS in ipsilateral and contralateral gastrocnemius. Two-tailed unpaired t-test; **p<0.005; N= 8 mice. Average ± SEM.

Figure 5: FUS regulates subsynaptic expression of AChR subunit genes. **a, b,** *Fus* relative mRNA (a) and protein (b) levels in C2C12 cells 48 hours after transfection with control siRNA (*siCt*, 100 nM) or siRNA targeting *Fus* (*siFus*, 100 nM). In b, lower panel: total protein stain of the corresponding western blot. (a) Two-tailed unpaired t-test; ***p<0.0001; N=13 wells per condition. Average ± SEM. **c,** Relative mRNA levels of AChR subunit genes in C2C12 cells processed as in a. Two-tailed unpaired t-test; ***p<0.0001, **p<0.005, *p<0.05; N=8-13 wells per condition. Average ± SEM. **d,** Fraction of chromatin immunoprecipitated (% input) with buffer, or with two different anti-FUS antibodies (anti-FUS-1 and anti-FUS-2) as detected using qPCR with primers located in the promoter regions of corresponding genes. One-way ANOVA with Dunnett's multiple comparisons test; ***p<0.001, **p<0.005, *p<0.05; N=3 per condition. Average ± SEM. **e-g,** Light units (RLU) relative to siCt in C2C12 cells 24 hours after transfection with *siCt* (25 nM) or *siFus* (25 nM) and luciferase reporter plasmids carrying promoters of *Chrnd* (e), *Chrne* (f) genes or CMV (g). Two-tailed nested t-test; **p<0.005, *p<0.05; N= 4 *(e, g)* and 8 *(f)* biological replicates, each representing the average of 6 technical replicates. Average ± SEM. **h,** Light units relative to the empty control in C2C12 cells transfected with the same reporter plasmids and plasmids expressing hFUS_WT, hFUS_R495X or empty control plasmid. Nested one-way ANOVA with Tukey's multiple comparisons test; ***p<0.0005, *p<0.05; N= 5 *(Chrnd-luc)*, 12 *(Chrne-luc)*, 3 *(CMV-luc)* biological replicates, each representing the average of 4 (8 for *CMV-luc*) technical replicates. Average ± SEM. **i,** Light units relative to empty control plasmid in C2C12 cells transfected with indicated reporter plasmids, hFUS_WT expression plasmid and increasing doses of hFUS_R495X. Nested one-way ANOVA with Tukey's multiple comparisons test; ***p<0.0005, **p<0.005; N= 5 *(Chrne-luc)*, 3 *(CMV-luc)* biological replicates, each representing the average of 5 *(Chrne-luc)* or 4 *(CMV-luc)* technical replicates. Average ± SEM. **j-k,** Light units relative to siCt in C2C12 cells 24h after transfection of *Chrne*-luciferase plasmid and either siCt (25nM) or siErm (25nM, j) or siFus (25nM, k), and an expression plasmid for either hFUS_WT (j) or ERM (k) or empty control. Nested one-way ANOVA with Tukey's multiple comparisons test **p<0.005, *p<0.05; N= 4 *(j)*, 3 *(k)* biological replicates, each representing the average of 6 *(j)* or 4 *(k)* technical replicates. Average ± SEM. **l, m,** Endogenous FUS was immunoprecipitated from C2C12 *(l)* and HSkMC *(m)* cells using a specific antibody (IP) or beads only, in the presence or absence of RNase. Native lysates

(input) and immunoprecipitates were analyzed by Western blotting with anti-FUS or anti-ERM antibodies.

Figure 6: Impaired endplate maturation in iPSC-derived myotubes from *FUS*-ALS patients. **a,** Table listing hiPS cell lines with respective FUS mutations, gender, age of onset and age at biopsy. In addition to two control cell lines (CNTL1 and 2), one isogenic control cell line was generated via CRISPR/Cas9 technology (CNTL3). Two different FUS mutations (FUS1 and 2), both frameshift mutations, were analyzed. **b,** Structure of AChR clusters on hiPSC-derived myotubes was visualized with BTX (green) and assorted based on their morphology in three categories with increasing maturity (diffuse puncta, aligned puncta, dense/cluster). Myotubes were immunolabeled with actinin (red) and nuclei with DAPI (blue). Scale bar: 10µm. **c,** Quantification of maturation state revealed less mature endplate structures in both patient-derived cell lines compared to CNTL1 and CNTL2. Fisher's Exact Test with Bonferroni correction for multiple testing; ***$p<0.0005$; N (number of endplates)= 127 (CNTL1), 116 (CNTL2), 71 (CNTL3), 88 (FUS1), 94 (FUS2). **d,** Structure of AChR clusters in hiPSC-derived motor neuron-myotube co-cultures was visualized with BTX (green) and assorted based on their morphology in four categories with increasing maturity (diffuse puncta, aligned puncta, dense/cluster or complex). Myotubes were immunolabeled with actinin (red) and nuclei with DAPI (blue). Scale bar: 10µm. **e,** Quantification of maturation state is shown in the bar graph, revealing less mature endplate-like structures in co-cultures in which myotubes and/or motor neurons were derived from *FUS*-ALS patients. Fisher's Exact Test with Bonferroni correction for multiple testing; ***$p<0.00005$; N (number of endplates)= 99 (CNTL1 MT + CNTL 1 MN), 74 (CNTL1 MT + FUS1 MN), 226 (FUS1 MT + CNTL1 MN), 52 (FUS1 MT + FUS1 MN), 35 (CNTL1 MT + FUS2 MN), 19 (FUS2 MT + CNTL1 MN), 93 (FUS2 MT + FUS2 MT). **f,** Quantification of maturation state in motor-neuron myotube co-cultures derived from FUS1 and its isogenic CNTL3. Fisher's Exact Test with Bonferroni correction for multiple testing; ***$p<5x10^{-8}$; N (number of endplates)= 273 (CNTL3 MT + CNTL3 MN), 73 (CNTL3 MT + FUS1 MN), 381 (FUS1 MN + CNTL3 MT), 285 (FUS1 MT + FUS1 MN). N=3 biological replicates.

Figure 7: Skeletal muscle of *FUS*-ALS patients displays muscle atrophy, FUS mislocalization, and impaired FUS enrichment in subsynaptic nuclei. **a,** Table listing the six human skeletal muscle biopsies, including gender, age of onset, age of

biopsy, *FUS* mutation, and findings of electromyographic (EMG) examination of *FUS*-ALS patients. For EMG, the degree of pathological spontaneous activity (PSA) was semi-quantitatively scored on a scale ranging from 0 (no PSA) over + and ++ to +++ (substantial PSA). Pathological changes in motor unit action potential (MUAP) were classified as neurogenic or myogenic. **b,** H&E staining on muscle biopsies revealed muscle atrophy in *FUS*-ALS patients, with angular and shrunken myofibers, increased density of nuclei and connective tissue. **c,** Quantification of muscle fiber size in muscle biopsies. **p<0.005; ***p<0.0001 by Kruskal-Wallis test with Dunn's multiple comparisons test. Number of muscle fibers=66 (CNTL4), 72 (CNTL5), 73 (CNTL6), 91 (FUS1), 349 (FUS4), 415 (FUS5). **d,** Staining of skeletal muscle biopsies for FUS (green), synaptophysin (SYN, magenta, labels presynaptic terminals), AChR (BTX, red) and DAPI (blue). White arrowheads indicate FUS localization in the nucleus, which was diffuse in CNTL biopsies, whereas in *FUS*-ALS patients staining was often either lost, reduced, or showed a granular pattern. Red arrowheads indicate cytoplasmic FUS localization in *FUS*-ALS patients. Scale Bar: 20 µm. **e,** Quantification of FUS staining intensity in either all nuclei or selectively in subsynaptic nuclei. Two-tailed unpaired t-test; *p<0.05, ***p<0.0001; N (all nuclei-subsynaptic nuclei)= 218-8 (CNTL4), 416-16 (CNTL5), 232-12 (CNTL6), 493-12 (FUS1), 910-11 (FUS4), 3397-39 (FUS5). Average ± SEM.

Figure 8: Working model illustrating how FUS may regulate transcription of AChR subunit genes in subsynaptic myonuclei. Agrin secreted from motor nerve endings binds to LRP4 on postsynaptic membranes, resulting in MuSK activation and subsequent activation of ERM through Rac1 and JNK pathways. FUS is enriched in subsynaptic nuclei, interacts with ERM, binds to AChR gene promoters and cooperates with ERM to stimulate transcription of AChR subunit genes.

Supplementary Figure legends

Supplementary Figure 1: NMJ morphology defects in the gastrocnemius of newborn *Fus*$^{\Delta NLS/\Delta NLS}$ and *Fus*$^{-/-}$ mice. **a-f** Dot plots showing the percentage (%) of innervated endplates (a, d), endplate surface area as % of *Fus*$^{+/+}$ littermate controls (b, e) and the total number of endplates in the gastrocnemius (c, f) of newborn *Fus*$^{\Delta NLS/\Delta NLS}$ (a-c) and *Fus*$^{-/-}$ (d-f) mice. Two-tailed unpaired t-test; **p<0.01, ***p<0.0005; N=12 vs 11 (a), 17 vs 14 (b), 4 vs 5 (c), 8 vs 8 (d), 15 vs 13 (e), 9 vs 10 (f). Average ± SEM. **g-k,** Quantification of ultrastructural NMJ defects in gastrocnemius of E18.5 *Fus*$^{+/+}$, *Fus*$^{-/-}$ and *Fus*$^{\Delta NLS/\Delta NLS}$ mice. **g,** The neuromuscular contact was scored as intact (1) when pre- and postsynaptic membranes were closely apposed and the synaptic cleft was filled with electron dense material. A widened synaptic cleft was scored as 0, and intermediate morphology as 0.5. **h,** The presence or absence of postsynaptic membrane foldings was scored as 1 or 0, respectively. **i,j,** Presynaptic (i) and postsynaptic (j) membrane integrity was scored as intact (1), thin (0.5) or disrupted (0). **k,** The abundance of synaptic vesicles was scored as abundant (1), rare (0.5) or absent (0). For g-k: Kruskal-Wallis test with Dunn's multiple comparisons test; *p<0.05, **p<0.01; N=4-5 animals per genotype; for each parameter, the average value per animal was used as a data point. Average ± SEM.

Supplementary Figure 2: Quantification of fiber number in hind limb muscles of *Fus*$^{+/+}$, *Fus*$^{-/-}$, *Fus*$^{\Delta NLS/\Delta NLS}$, and *Fus*$^{\Delta NLS/+}$ mice. **a,b,** Dystrophin staining to visualize individual muscle fibers in extensor digitorum longus (EDL) muscle of newborn *Fus*$^{+/+}$ versus *Fus*$^{\Delta NLS/\Delta NLS}$ mice. **c,d,** Dot plots showing the total number of muscle fibers in EDL muscle of newborn *Fus*$^{+/+}$ versus *Fus*$^{\Delta NLS/\Delta NLS}$ *(c)* or *Fus*$^{-/-}$ *(d)* mice. p=NS by two-tailed unpaired t-test; N= 5 vs 4 (c) and 2 vs 2 (d). Average ± SEM. **e,** Dot plot showing the total number of muscle fibers in tibialis anterior of newborn *Fus*$^{+/+}$ versus *Fus*$^{-/-}$ mice. p=NS by two-tailed unpaired t-test; N= 7 vs 4. Average ± SEM. **f,** Dot plot showing the total number of endplates in tibialis anterior of 1-month-old *Fus*$^{+/+}$ versus *Fus*$^{\Delta NLS/+}$ mice. p=NS by two-tailed unpaired t-test; N=3 vs 7. Average ± SEM.

Supplementary Figure 3: MyoD^{iCre} mediates highly efficient recombination between LoxP sites. **a,** Schematic illustrating the working principle of the ROSA$^{mT/mG}$ reporter mice. The chicken β-actin core promoter with a CMV enhancer (pCA) drives expression of the loxP-flanked (triangles) coding sequence of membrane-targeted tandem dimer Tomato (mT). After Cre-mediated excision of the mT sequence, the

pCA promoter drives expression of membrane-targeted EGFP (mG). pA: polyadenylation sequence. **b,** Transverse sections through the tibialis anterior of adult *ROSA*$^{mT/mG}$/+ (control, upper panels) and *MyoD*$^{iCre/+}$; *ROSA*$^{mT/mG}$/+ (experimental, lower panels) mice were labeled with phalloidin (to visualize muscle fibers), antibodies against tdTomato and GFP, and DAPI. **c,** Bar graph showing the percentage (%) or GFP-positive muscle fibers in *MyoD*$^{iCre/+}$; *ROSA*$^{mT/mG}$/+ and *ROSA*$^{mT/mG}$/+ mice. Mann Whitney test; **p<0.01; N= 6 versus 6 mice.

Supplementary Figure 4: Reduced expression of AChR subunit genes in *Fus*-ALS mouse models. **a, b,** Relative mRNA levels of AChR subunit genes, including *Chrna1, Chrnb1, Chrng, Chrnd,* and *Chrne,* in gastrocnemius muscle of E18.5 *Fus*$^{+/+}$ versus *Fus*$^{\Delta NLS/\Delta NLS}$ mice (a) and tibialis anterior muscle of 1-month-old *Fus*$^{+/+}$ versus *Fus*$^{\Delta NLS/+}$ mice (b). Note that *Chrne* is not expressed at E18.5, and *Chrng* is not expressed at 1 month of age. Two-tailed unpaired t-test; *p<0.05, **p<0.01; N=4-6 mice per genotype. Average ± SEM.

Supplementary Figure 5: R495X mutant FUS mislocalizes to the cytoplasm and induces cytoplasmic mislocalization and granular nuclear staining of wild type FUS in C2C12 cells. **a,** Representative images of C2C12 cells co-transfected with plasmids expressing N-terminal GFP-tagged wild type human FUS (FUS_WT::GFP) and N-terminal Myc-tagged human FUS, either wild type (FUS_WT::Myc) or R495X mutant (FUS_R495X::Myc). 24 hours later, cells were immunostained for Myc and Hoechst was used to label nuclei. Scale bar: 25 µm. **b,c,** Quantification of the percentage of cytoplasmic relative to total (nuclear + cytoplasmic) FUS_WT::GFP (b) and the percentage of granular relative to total nuclear FUS_WT::GFP (c) in C2C12 cells co-transfected with either FUS_WT::Myc or FUS_R495X::Myc. Two-tailed unpaired t-test; ***p<0.0001; N= 34 vs 33 cells. Average ± SEM.

Supplementary Figure 6: FUS and ERM collaborate to promote transcription of AChR subunit genes in subsynaptic nuclei. **a,** FUS is required for Agrin induced transcriptional activation of *Chrne* promoter. Luminescence intensity (in RLU) measured in C2C12 cells 24 hours after transfection with *siCt* (25 nM) or *siFus* (25 nM) and a luciferase reporter plasmid carrying the promoter of *Chrne* gene, and further treated for 24 hours with agrin (10 ng/mL) or its vehicle. Data of 10 biological replicates (independent transfections) are shown. Each biological replicate included 3 to 6 technical replicates per condition. For each biological replicate, luminescence

intensity was normalized to siCt without agrin treatment after removal of statistical outliers, and the median value of the technical replicates was determined per condition and plotted in the graph. Lines and error bars indicate median ± interquartile range. Two-way ANOVA with Tukey post-hoc test for multiple comparisons was used. **p<0.01; ***p<0.001; ns: not significant. **b,** HEK293 cells were transfected with FLAG-ERM and Myc-Fus expression plasmids and lysates were immunoblotted before (input) and after (IP) immunoprecipitation with anti-Myc, in the presence or absence of RNase. **c,** Endogenous FUS was immunoprecipitated from HEK293 cells using a specific antibody (IP) or beads only, in the presence or absence of RNase. Native lysates (input) and immunoprecipitates were analyzed by Western blotting with anti-FUS or anti-ERM antibodies.

Supplementary Figure 7: Characterization of hiPSC-derived myotubes. **a,** Time course of the spheres-based protocol for myogenic differentiation, including progenitor and final myotube differentiation steps. **b,** Relative mRNA levels of *MYOG, PAX7 and CHRNA1* as determined by quantitative real time PCR (qPCR) on hiPSC-derived myocytes from two control and two *FUS*-ALS patients at different time points during differentiation (4, 5, 6, 7 and 8 weeks). The *HMBS* gene (encoding hydroxymethylbilane synthase) was used as housekeeping gene for normalization. Transcript levels of AChR subunit gene *CHNRA1* were significantly reduced in *FUS*-ALS myotubes after 8 weeks of differentiation. ***p<0.001 by two-way ANOVA with Bonferroni post-test. N= 3 biological replicates per genotype, with each biological replicate representing the average of two technical replicates. Average ± SEM. **c,** Differentiated muscle cells stained positive for desmin, myosin heavy chain (MHC), MYOG, ryanodine receptor isoform RyR1 and voltage-dependent dihydropyridine receptor alpha subunit (DHPRα). Staining for FUS and DAPI revealed FUS localization in nuclei. Scale bar: 10µm. **d,** hiPSC-derived myotubes were labeled with BTX (AChR, yellow), FUS (green), actinin (red) and DAPI (blue). FUS predominantly localized to nuclei in both CNTL and FUS myotubes. Scale bar: 10µm.

Supplementary Figure 8: Characterization hiPSC-derived motor neuron-myotube co-cultures. **a,b,** Average size of single BTX positive puncta within endplates in motor neuron-myotube co-cultures. Compared to CNTL-CNTL co-cultures, combinations containing *FUS*-ALS myotubes showed reduced single particle size. Panel a shows co-cultures derived from CNTL1 and FUS1 or FUS2, panel b shows co-cultures

derived from FUS1 and its isogenic control CNTL3. **p<0.01; ***p<0.001 by Kruskal-Wallis test with multiple comparisons. N= 759 (CNTL1 MT + CNTL1 MN), 846 (CNTL1 MT + FUS1 MN), 3467 (FUS1 MT + CNTL1 MN), 1872 (FUS1 MT + FUS1 MN), 307 (CNTL1 MT + FUS2 MN), 364 (FUS2 MT + CNTL1 MN), 841 (FUS2 MT + FUS2 MN), 978 (CNTL3 MT + CNTL3 MN), 1842 (CNTL3 MT + FUS1MN), 1799 (FUS1 MT + CNTL3 MN), 1116 (FUS1 MT + FUS1 MN). N=3 biological replicates. **c,** Motor neuron-myotube co-cultures were labeled for FUS (green), AChR (BTX, yellow), neurofilament heavy chain (NF-H, red, labels axons) and DAPI (blue). FUS localized to nuclei of both CNTL and FUS myotubes (white arrowheads), but in FUS-mutant motor neurons, FUS localized to both nucleus and cytoplasm, in contrast to nuclear FUS localization in CNTL motor neurons (red arrowheads). Scale bar: 10µm. **d,** Relative mRNA levels of myogenic differentiation markers and AChR subunits in motor neuron-myotube co-cultures as determined by qPCR. The *HMBS* gene was used as housekeeping gene for normalization. *p<0.05, **p<0.01, ***p<0.001 by one-way ANOVA with Bonferroni post-test. N= 3 biological replicates per genotype, with each biological replicate representing the average of two technical replicates. Average ± SEM.

Supplementary Figure 9: Characterization of muscle biopsies from *FUS*-ALS patients and controls. **a,** Distribution of muscle fiber size in muscle biopsies. Muscle fibers were assorted in the indicated size categories based on their surface area (in μm^2) and the percentage of fibers in each category is shown in the bar graph. **b,** Density of nuclei in muscle biopsies as a proxy for muscle atrophy. The number of nuclei per field of 13,547 μm^2 is shown in the dot plot. One-way ANOVA with Tukey's multiple comparisons test; **p<0.01, ***p<0.001; N= 4 fields. Average ± SEM. **c,** Dot plot showing cytoplasmic FUS staining intensity in muscle biopsies. Kruskal-Wallis test with Dunn's multiple comparisons test; *p<0.05, ***p<0.0001. Number of fields in which the average cytoplasmic FUS staining intensity is measured=3 (CNTL4), 5 (CNTL5), 2 (CNTL6), 4 (FUS1), 5 (FUS4), 10 (FUS5). Average ± SEM. **d,** Dot plot showing BTX-positive endplate area in muscle biopsies. One-way ANOVA with Tukey's multiple comparisons test; *p<0.05, ***p<0.0001. Number of endplates=3 (CNTL4), 6 (CNTL5), 4 (CNTL6), 5 (FUS1), 7 (FUS4), 24 (FUS5). Average ± SEM.

Supplementary Data legends

Supplementary Data 1: Predicted FUS DNA-binding sites in promoters of human and mouse muscle nicotinic AChR subunit genes. The presence of FUS DNA-binding sequences reported by Tan et al [21] was evaluated in the promoter regions of muscle nicotinic AChR subunit genes: CHRNA1, CHRNB1, CHRND, CHRNE (adult) and CHRNG (fetal). Additionally, QGRS mapper [50] was used to identify possible G-quadruplex sites in the complementary strand. Combination of the results of both analyses allowed identification of possible single strands (ss) DNA-binding sites of FUS.

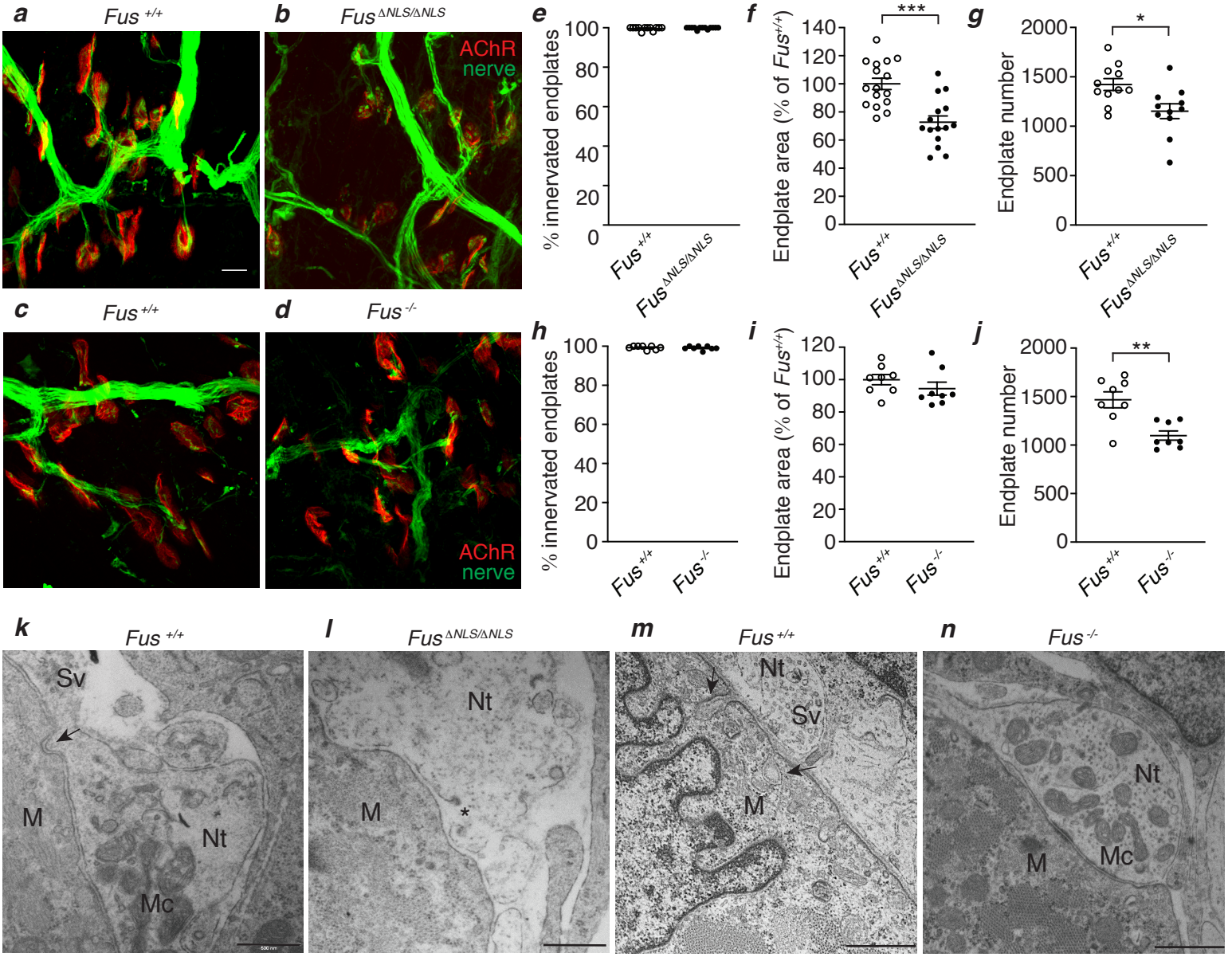
a
Fus +/+
b
Fus ΔNLS/ΔNLS
AChR
nerve
c
Fus +/+
d
Fus -/-
AChR
nerve
e
% innervated endplates
Fus +/+
Fus ΔNLS/ΔNLS
f
Endplate area (% of Fus+/+)
***
Fus +/+
Fus ΔNLS/ΔNLS
g
Endplate number
*
Fus +/+
Fus ΔNLS/ΔNLS
h
% innervated endplates
Fus +/+
Fus -/-
i
Endplate area (% of Fus+/+)
Fus +/+
Fus -/-
j
Endplate number
**
Fus +/+
Fus -/-
k
Fus +/+
Sv
M
Nt
Mc
l
Fus ΔNLS/ΔNLS
Nt
M
*
m
Fus +/+
Nt
Sv
M
n
Fus -/-
Nt
M
Mc

Figure 1

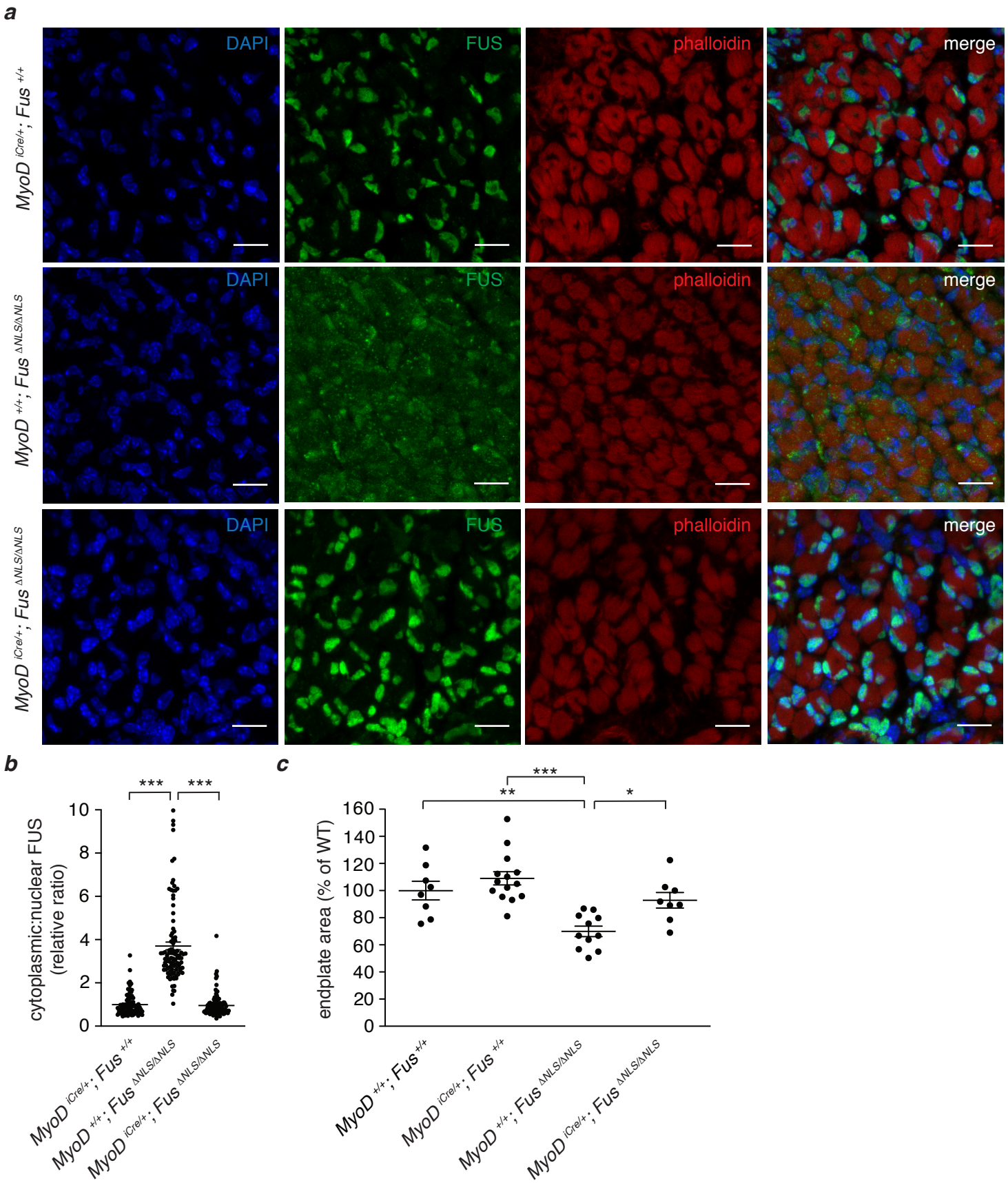
a
MyoD iCre/+; Fus +/+
MyoD +/+; Fus ΔNLS/ΔNLS
MyoD iCre/+; Fus ΔNLS/ΔNLS
DAPI
FUS
phalloidin
merge
b
cytoplasmic:nuclear FUS (relative ratio)
***
***
MyoD iCre/+; Fus +/+
MyoD +/+; Fus ΔNLS/ΔNLS
MyoD iCre/+; Fus ΔNLS/ΔNLS
c
endplate area (% of WT)
***
**
*
MyoD +/+; Fus +/+
MyoD iCre/+; Fus +/+
MyoD +/+; Fus ΔNLS/ΔNLS
MyoD iCre/+; Fus ΔNLS/ΔNLS

Figure 2

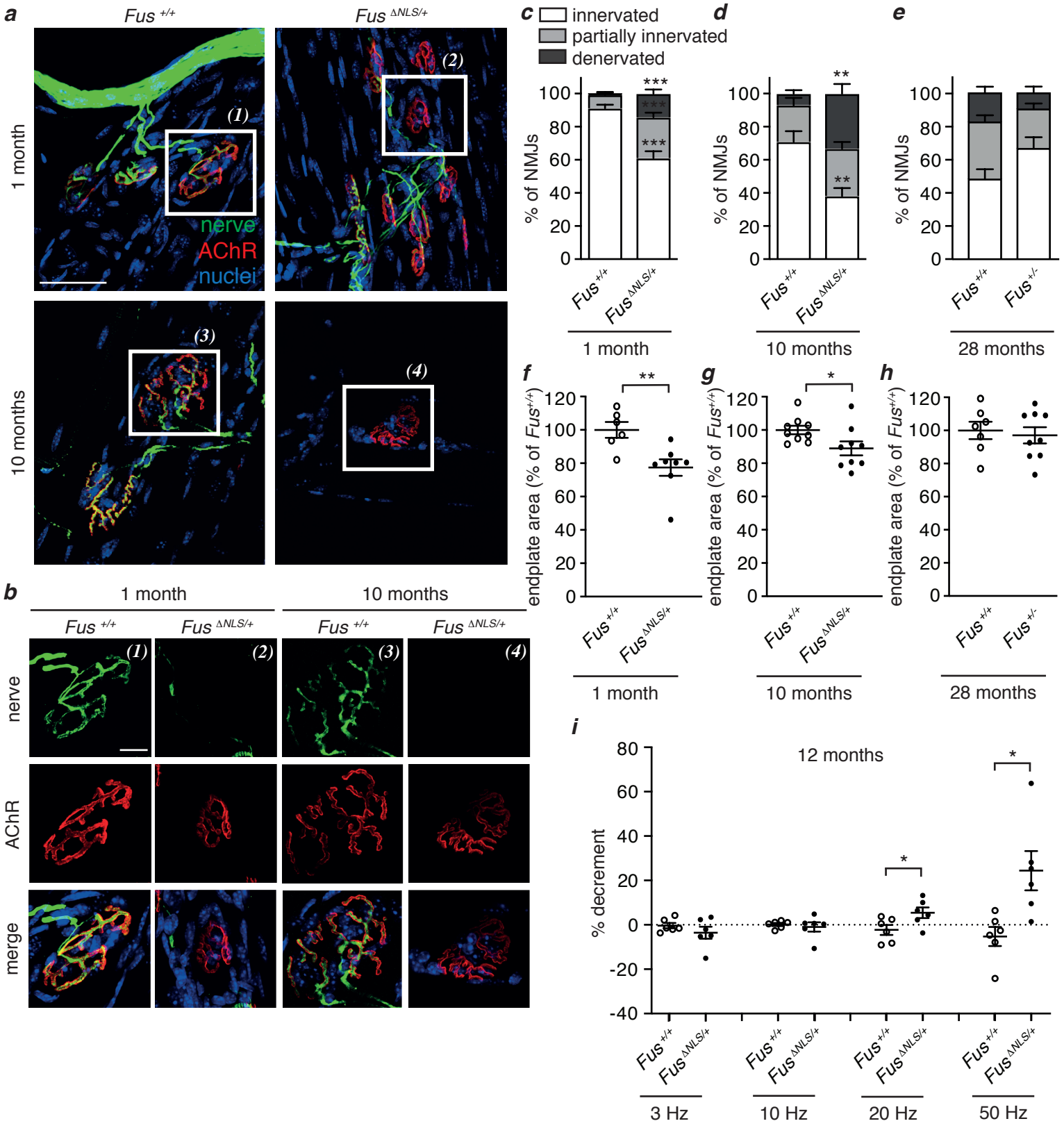
a
Fus +/+
Fus ΔNLS/+
1 month
10 months
(1)
(2)
(3)
(4)
nerve
AChR
nuclei
b
1 month
10 months
Fus +/+
Fus ΔNLS/+
Fus +/+
Fus ΔNLS/+
nerve
AChR
merge
c
innervated
partially innervated
denervated
% of NMJs
Fus +/+
Fus ΔNLS/+
1 month
d
% of NMJs
Fus +/+
Fus ΔNLS/+
10 months
e
% of NMJs
Fus +/+
Fus +/-
28 months
f
endplate area (% of Fus+/+)
Fus +/+
Fus ΔNLS/+
1 month
g
endplate area (% of Fus+/+)
Fus +/+
Fus ΔNLS/+
10 months
h
endplate area (% of Fus+/+)
Fus +/+
Fus +/-
28 months
i
12 months
% decrement
Fus +/+
Fus ΔNLS/+
3 Hz
10 Hz
20 Hz
50 Hz

Figure 3

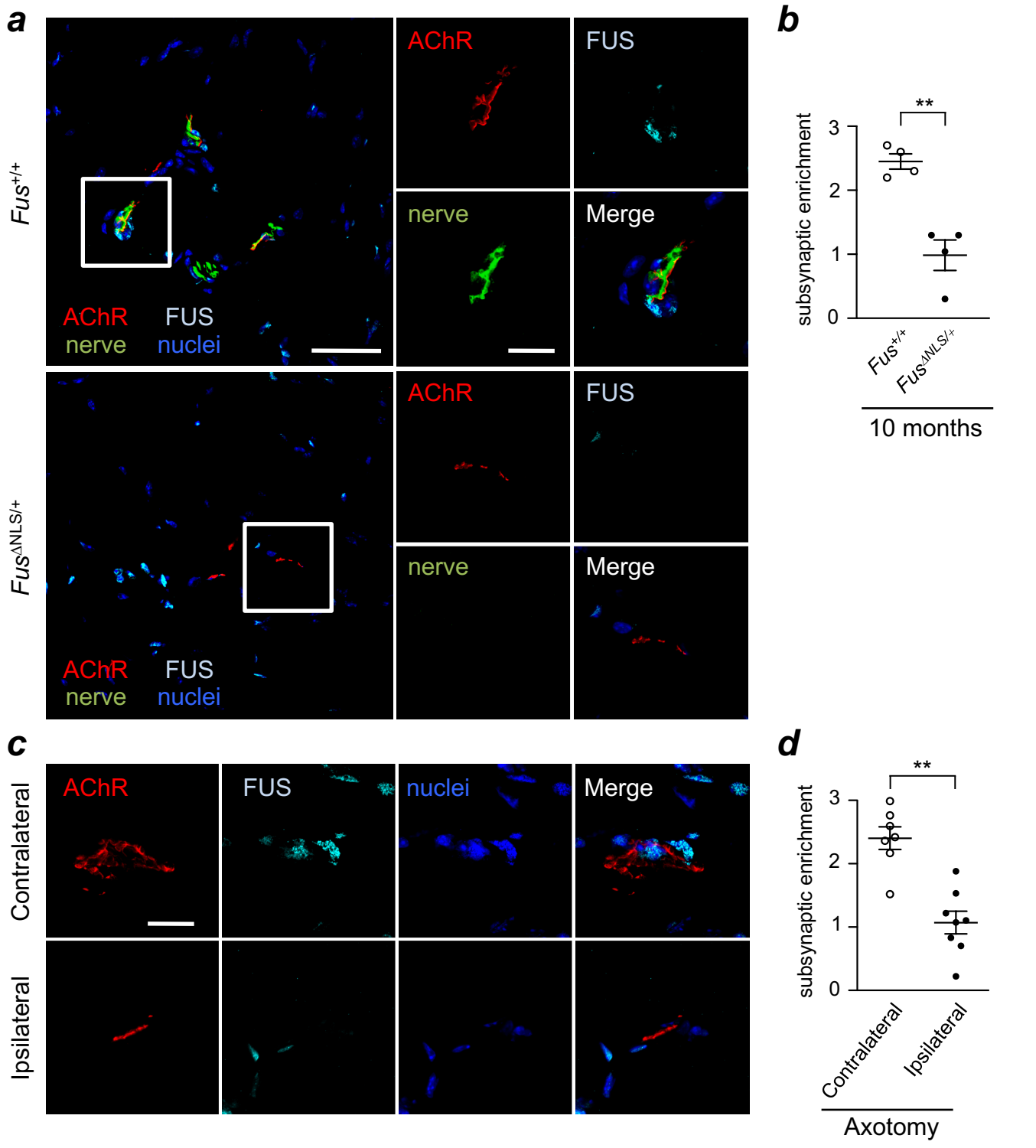
a
Fus+/+
AChR
FUS
nerve
Merge
AChR
nerve
FUS
nuclei
FusΔNLS/+
AChR
FUS
nerve
Merge
AChR
nerve
FUS
nuclei
b
subsynaptic enrichment
0
1
2
3
**
Fus+/+
FusΔNLS/+
10 months
c
Contralateral
Ipsilateral
AChR
FUS
nuclei
Merge
d
subsynaptic enrichment
0
1
2
3
**
Contralateral
Ipsilateral
Axotomy

Figure 4

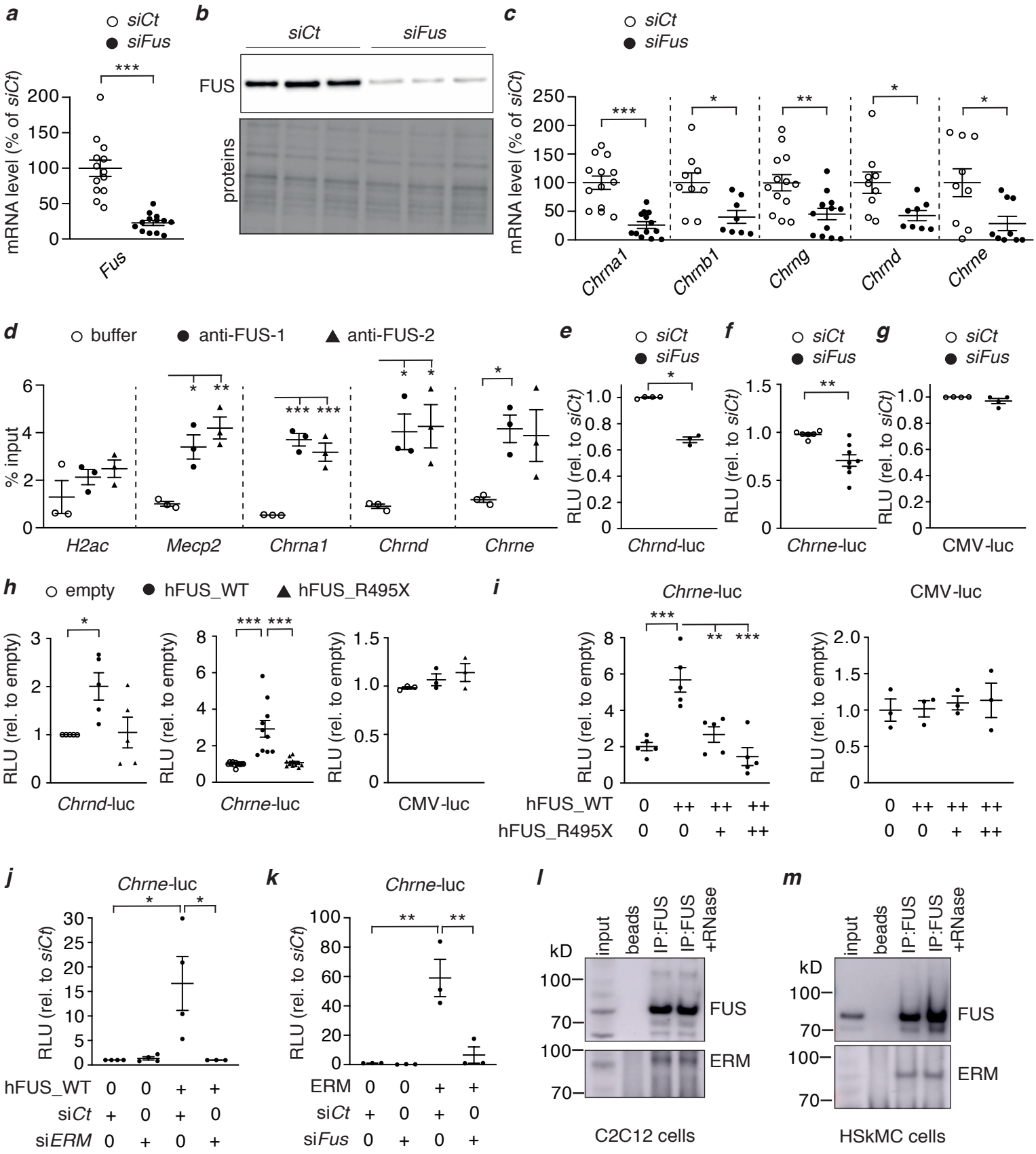
a
siCt
siFus
mRNA level (% of siCt)
Fus
b
siCt
siFus
FUS
proteins
c
siCt
siFus
mRNA level (% of siCt)
Chrna1
Chrnb1
Chrng
Chrnd
Chrne
d
buffer
anti-FUS-1
anti-FUS-2
% input
H2ac
Mecp2
Chrna1
Chrnd
Chrne
e
siCt
siFus
RLU (rel. to siCt)
Chrnd-luc
f
siCt
siFus
RLU (rel. to siCt)
Chrne-luc
g
siCt
siFus
RLU (rel. to siCt)
CMV-luc
h
empty
hFUS_WT
hFUS_R495X
RLU (rel. to empty)
Chrnd-luc
Chrne-luc
CMV-luc
i
Chrne-luc
CMV-luc
RLU (rel. to empty)
hFUS_WT 0 ++ ++ ++
hFUS_R495X 0 0 + ++
j
Chrne-luc
RLU (rel. to siCt)
hFUS_WT 0 0 + +
siCt + 0 + 0
siERM 0 + 0 +
k
Chrne-luc
RLU (rel. to siCt)
ERM 0 0 + +
siCt + 0 + 0
siFus 0 + 0 +
l
kD
input
beads
IP:FUS
IP:FUS +RNase
100
70
FUS
ERM
C2C12 cells
m
kD
input
beads
IP:FUS
IP:FUS +RNase
100
70
FUS
ERM
HSkMC cells

Figure 5

a

Cell line	gender	age*	mutation
CNTL1	female	(45)	-
CNTL2	male	(29)	-
CNTL3	male	26 (28)	isogenic control for FUS1
FUS1	male	26 (28)	R495QfsX527
FUS2	male	19 (20)	D502Tfs*27

*Age of onset (age of biopsy)

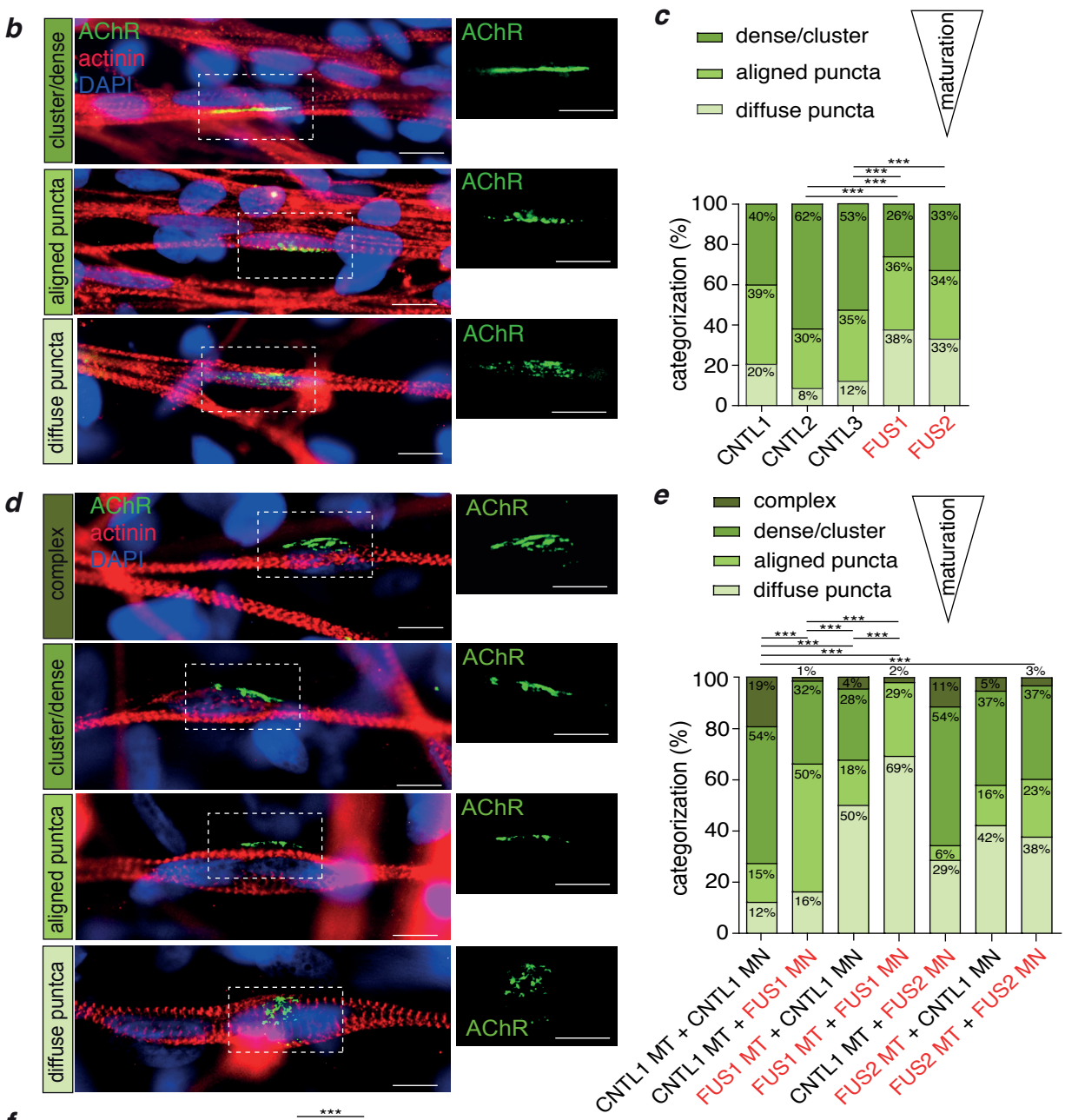

Figure 6

a

biopsy	gender	age*	mutation	electromyography
CNTL4	male	(52)	-	
CNTL5	female	(33)	-	
CNTL6	male	(30)	-	
FUS1	male	26 (26)	R495QfsX527	PSA: 3, chronic neurogenic and myogenic MUAP
FUS4	female	24 (27)	K510R	PSA: 3, chronic neurogenic MUAP
FUS5	male	39 (42)	K510R	PSA: 2, myogenic MUAP

*Age of onset (age of biopsy); PSA: pathological spontaneous activity; MUAP: motor unit action potential

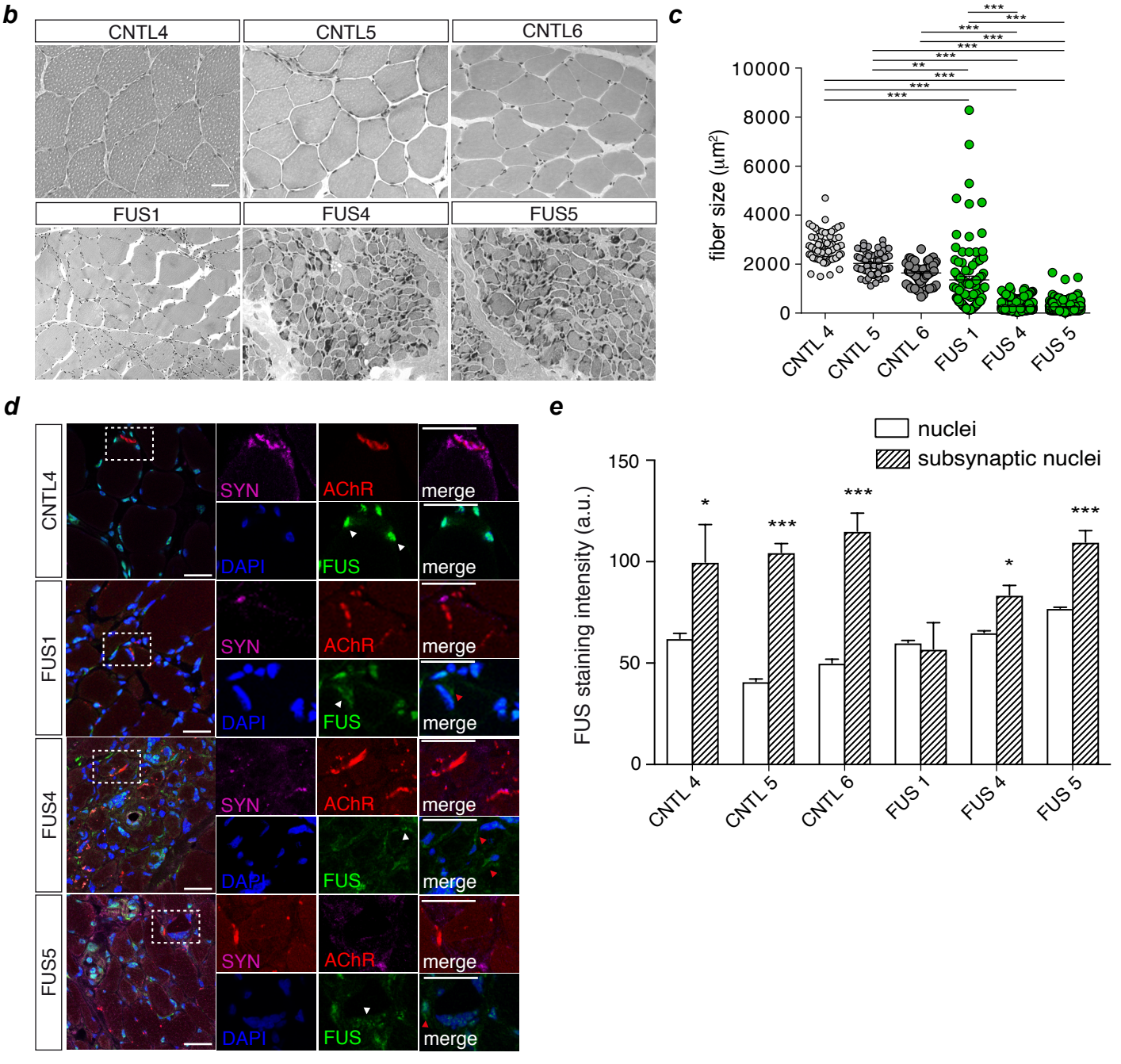

Figure 7

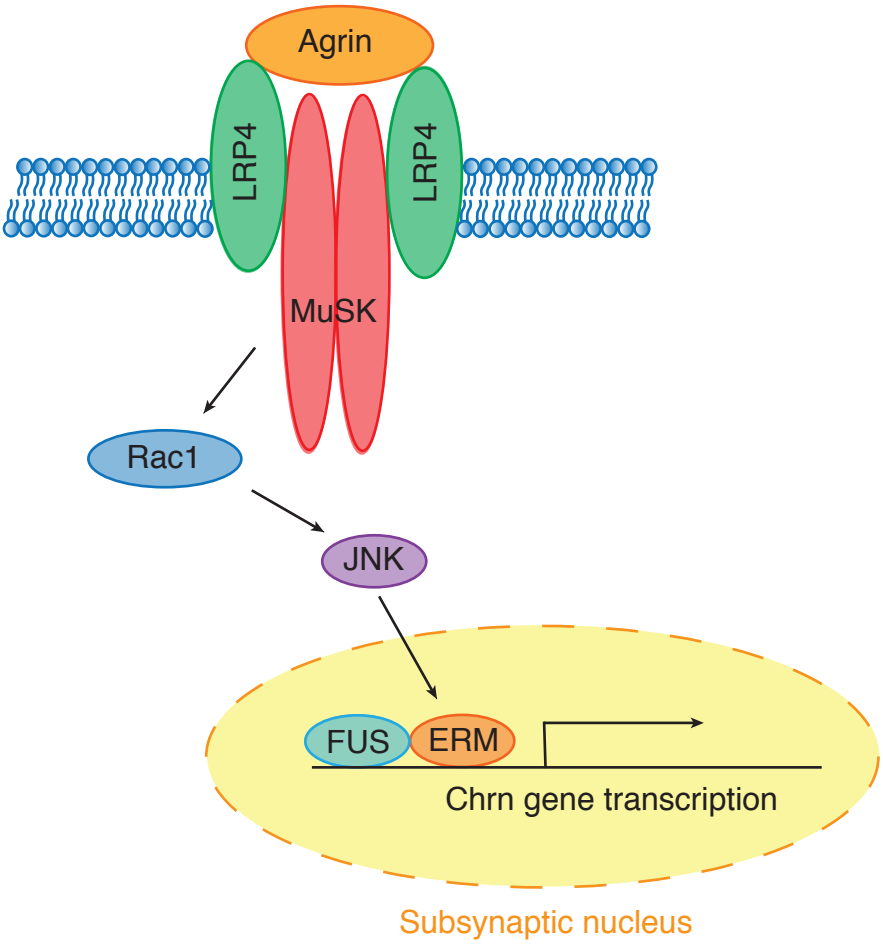
Agrin
LRP4
LRP4
MuSK
Rac1
JNK
FUS
ERM
Chrn gene transcription
Subsynaptic nucleus

Figure 8

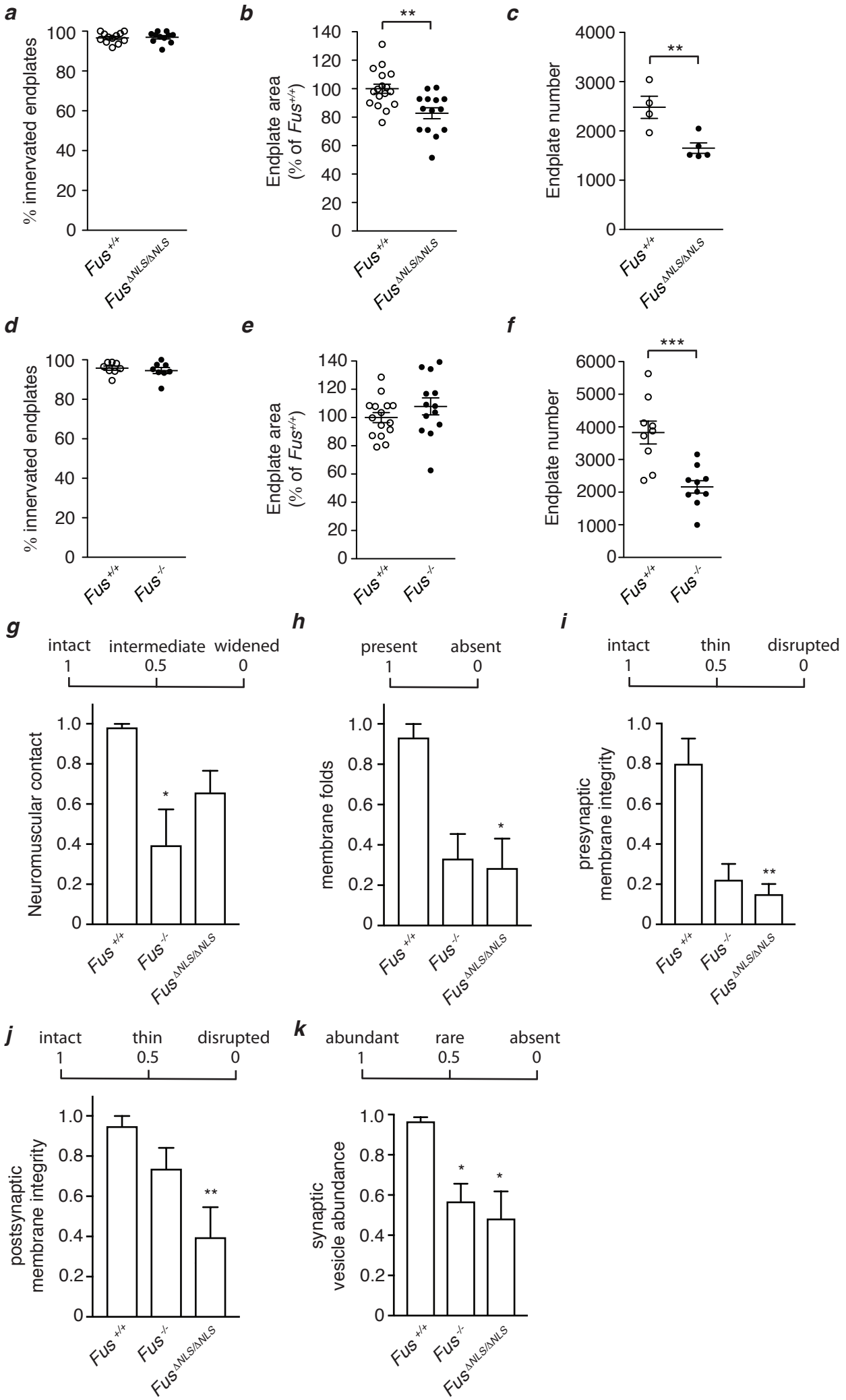

Supplementary Figure 1

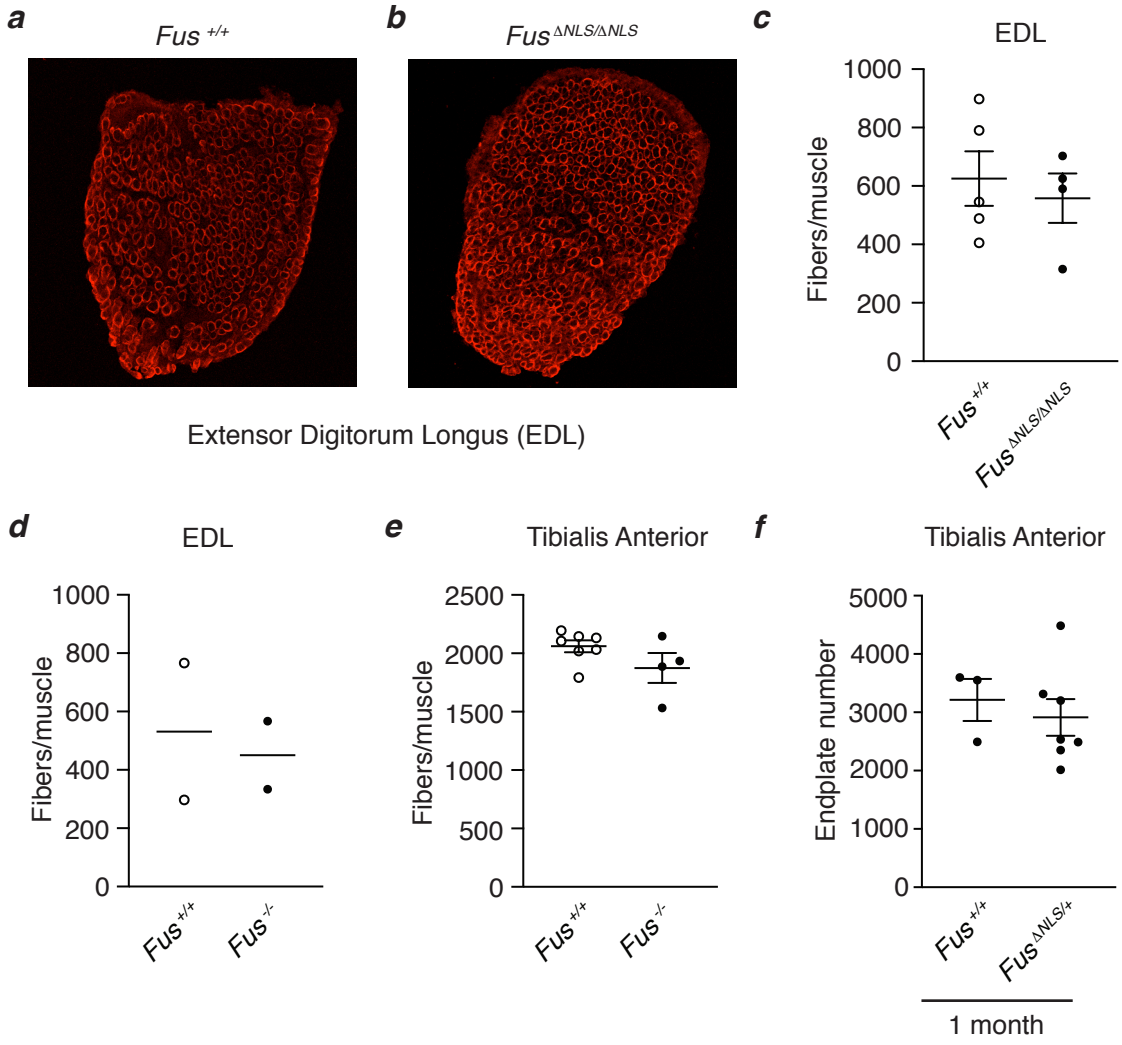

Supplementary Figure 2

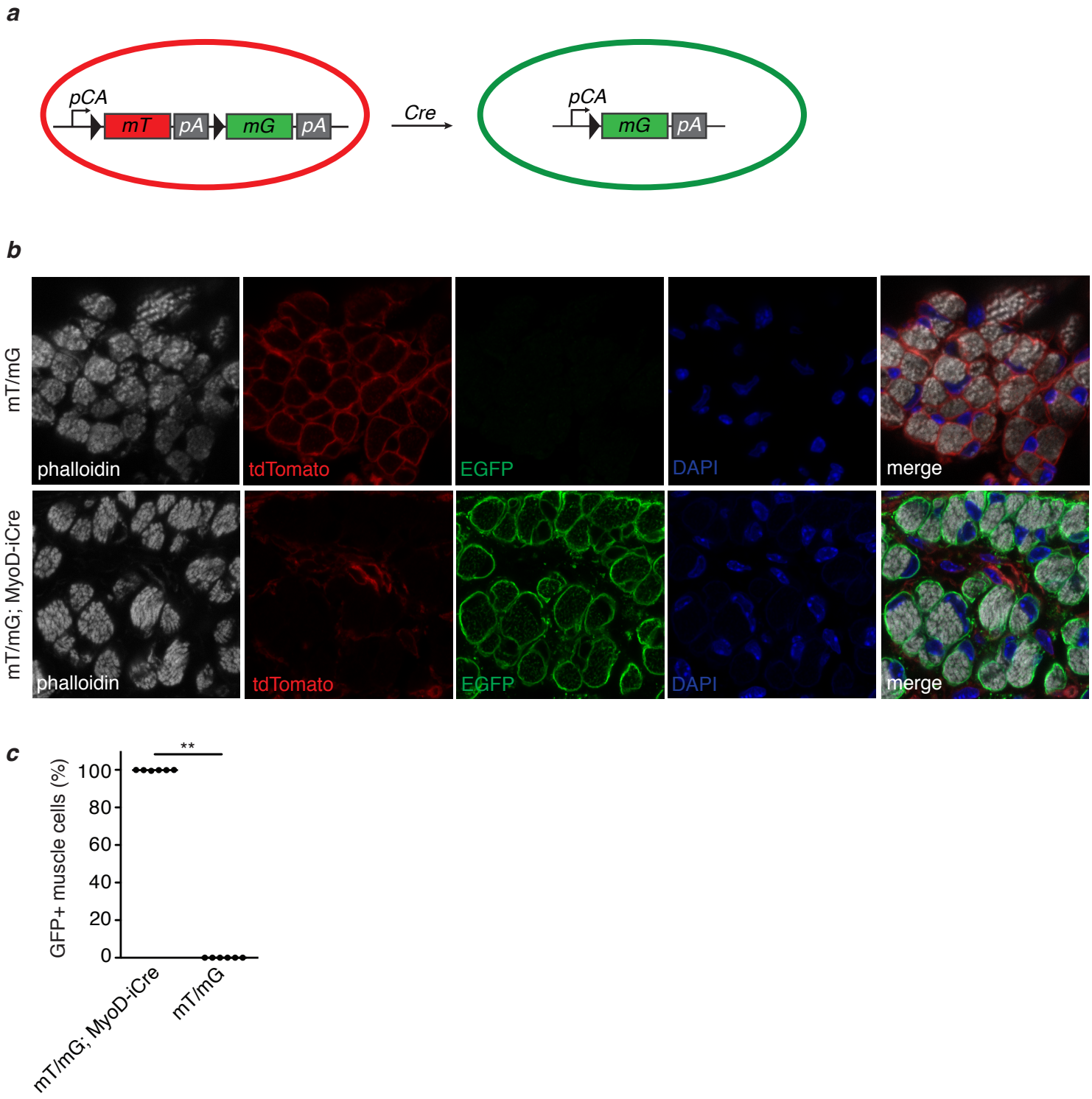

Supplementary Figure 3

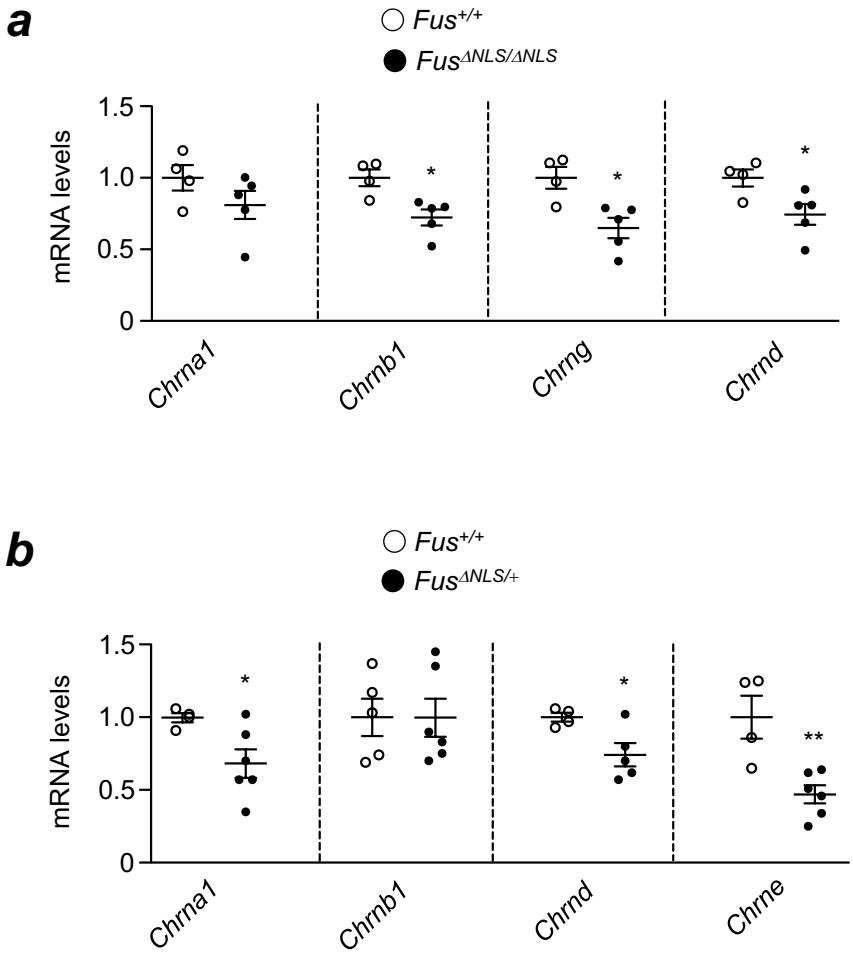

Supplementary Figure 4

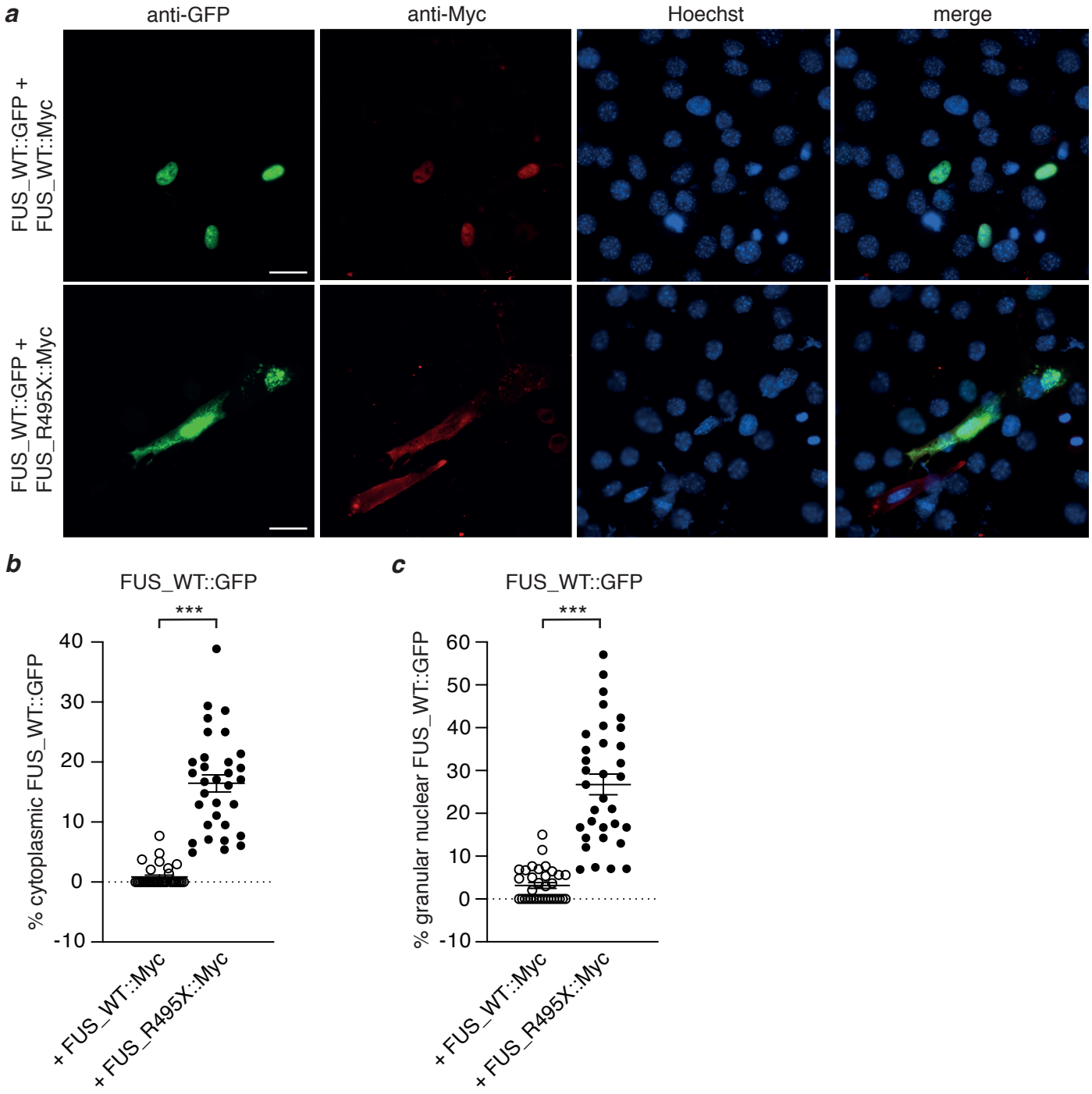

Supplementary Figure 5

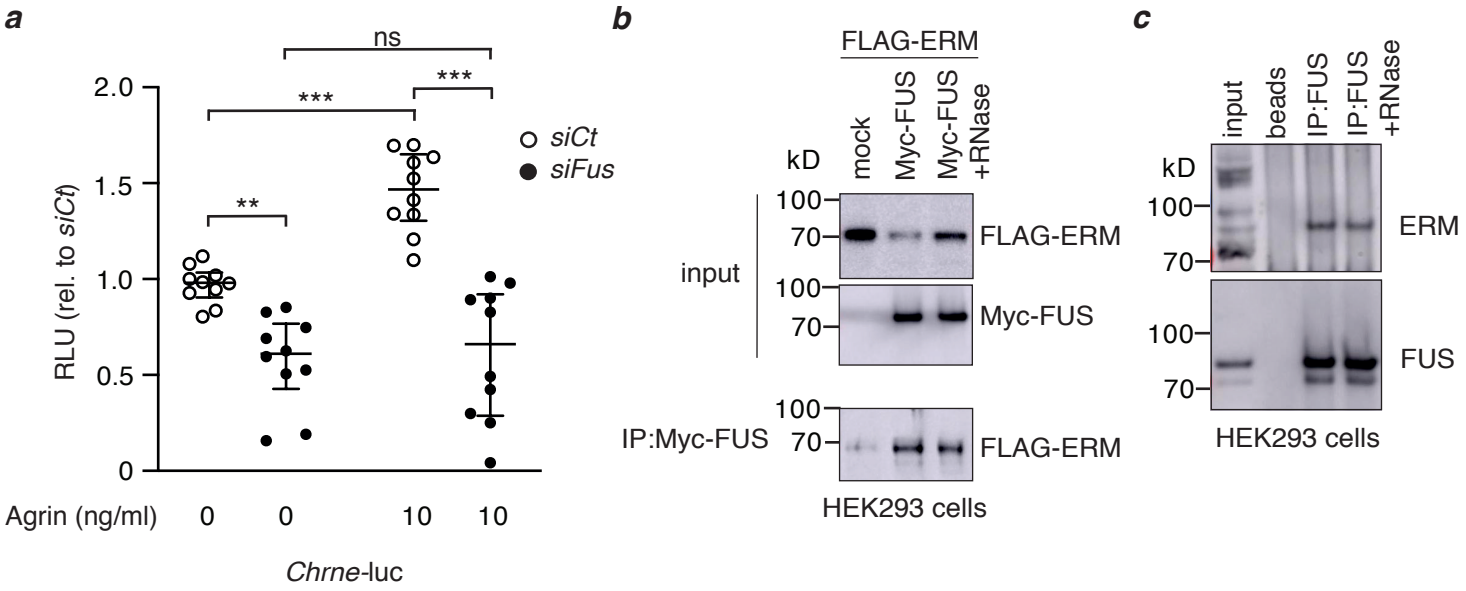

Supplementary Figure 6

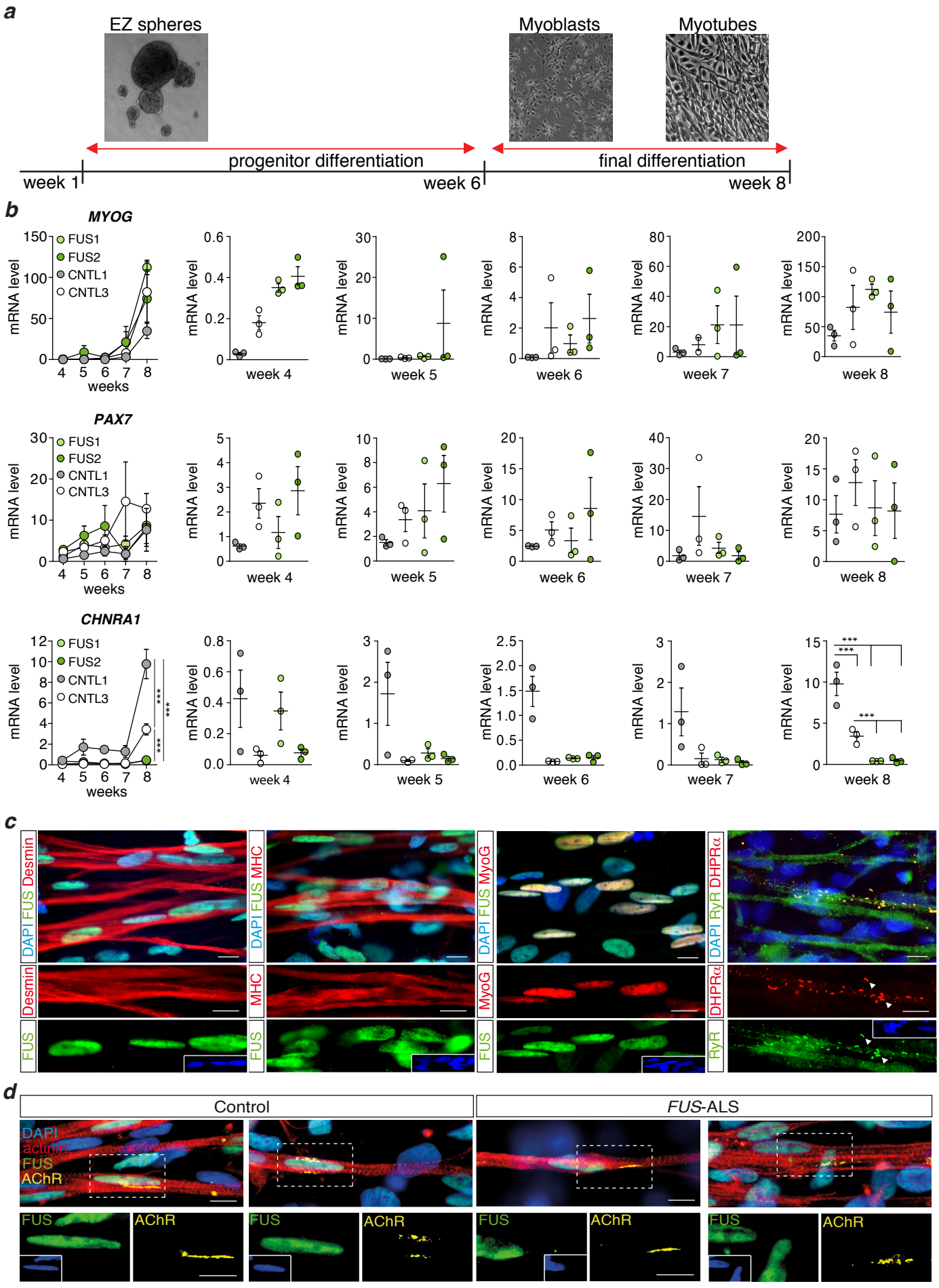

Supplementary Figure 7

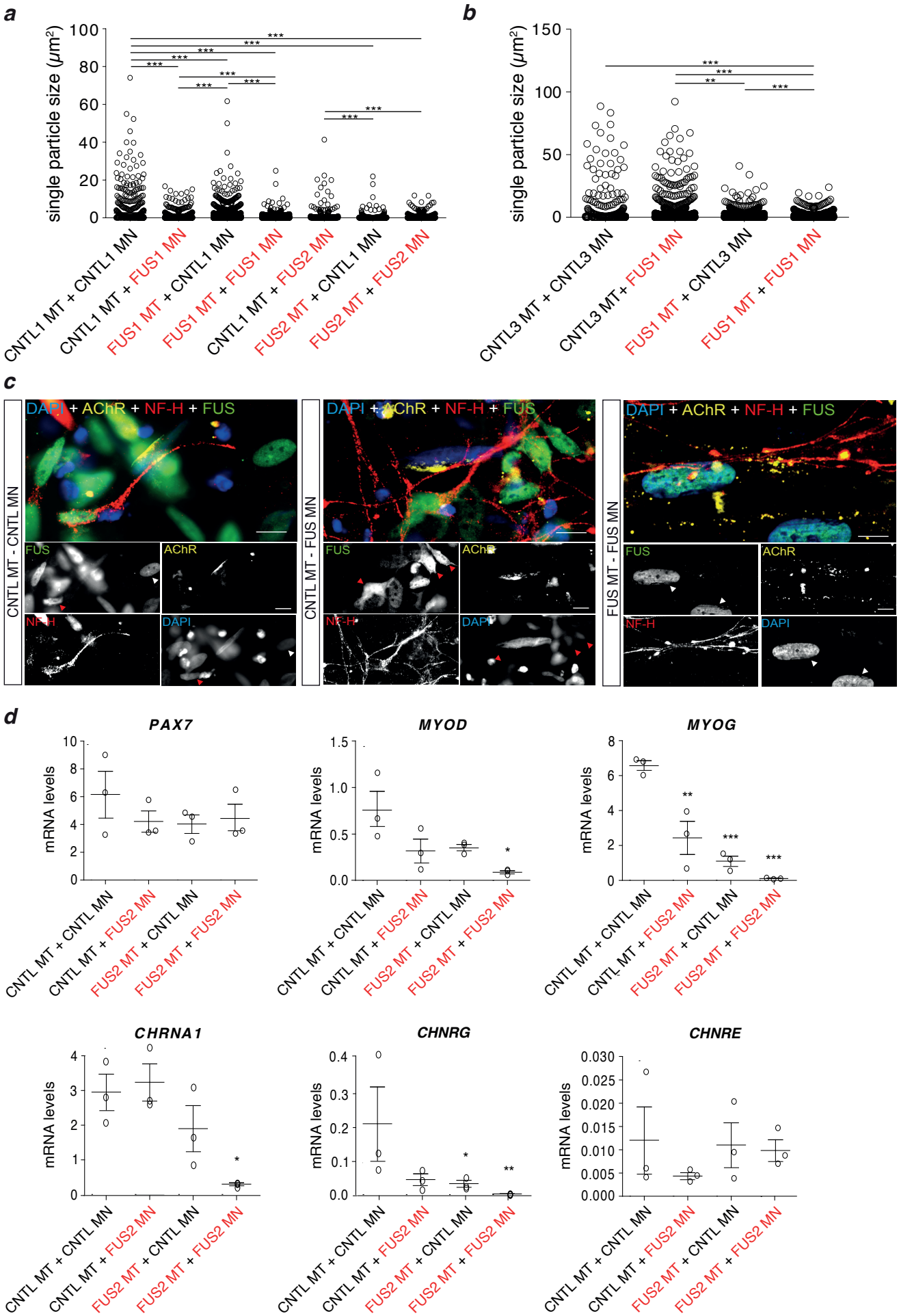

Supplementary Figure 8

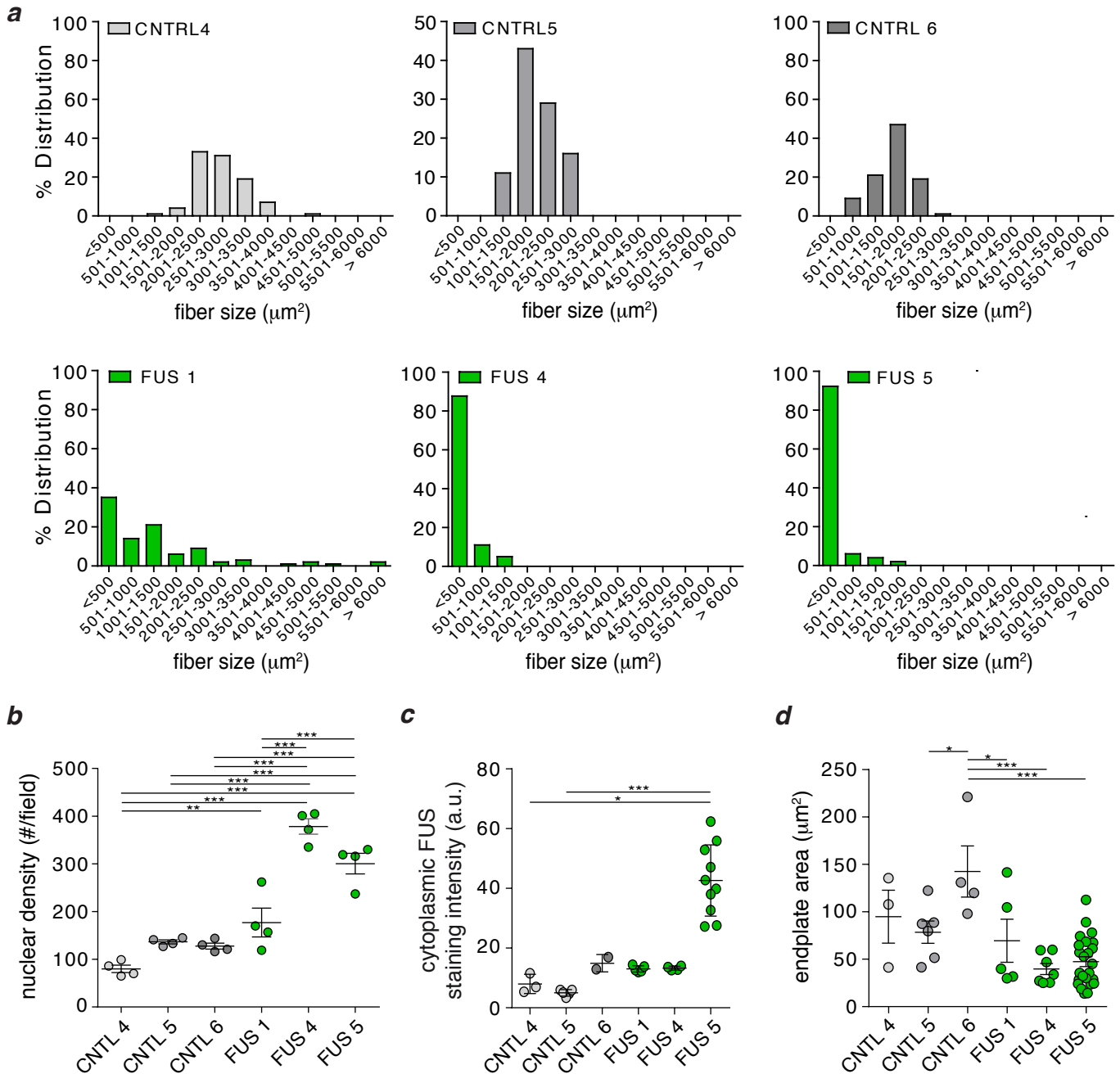

Supplementary Figure 9

Supplementary Data 1: Predicted FUS binding sites in the promoter regions of muscle nicotinic acetylcholine receptor

The presence of predicted FUS DNA-binding sequences reported by Tan et al [1] was analyzed in the promoter regions of muscle nicotinic AChR subunit genes: CHRNA1, CHRNB1, CHRND, CHRNE (adult) and CHRNG (fetal). Furthermore, we used QGRS mapper [2] to identify possible G-quadruplex sites in the complementary strand. Combination of the results of both analyses thus allowed us to identify possible single strands (ss) DNA-binding sites of FUS. This analysis was performed on both human and mouse CHRN genes.

Methods:
-promoter sequences of muscle CHRN genes were obtained from the ENSEMBL database (confirmed via BLAT tool). 1000 bp upstream of exon 1 were used, unless the coding region of another gene was present in this region.
-Predicted sequences by Tan et al [1] were identified in the relative forward direction of each promoter (marked in yellow). Only sequences that are allowed according to Figure 4 in Tan et al [1] were included.

Deviations of one or two nucleotides from these most optimal affinity sequences were allowed, and the number of mismatches (mm) is indicated.
-Reverse complementary sequences of each promoter were analysed by QGRS mapper [2] to locate possible G-quadruplex sites (marked in yellow).
-Possible ssDNA binding sites of FUS (G-quaduplex predicted in complementary strand) are marked in green.

Human CHRN genes:

CHRNA1 (Chromosome 2: 174,747,592-174,787,935 reverse strand)

AAGGTGATGGAGTGGGAAGGCTTCCCCCCTGGAGTCGACAGCTCAGCGGCCT
GGGCTCTCATCCGACTGCCACAGCATCATTCTGCTTCTGCCGGTCAGTGGCCT
AGTTCCTCCGCCATTGTGCTCCTCTCCACGTCCTGCCATCTGTGTGTCTGCCTG
CTAGGGCCTCAGGATTTTTATAGGCACAGGATGGGGGCGTGGCAGGCCAGGG
TGGTCTTGGGAAATGCAGCATTTGAGCAGGAAAACAAAAATGCCTGTCCTCATC
TAGGCTCGTAGGGGTGGAGCCCTAGCCAGGGGCCACGCCCTTCCCTCCCCCC
CCCCCCCCGCCCCCGCTTCCGTATCACTTAAAGGGACCACGCTCTTCCCTTCG
GTATCATTAGGAAGCTCAACAGGAAGGGAGGTGGGGTTATCATAGGCTAGCCA
TTCCAAAATACTATTTGAAAATGGGACTGAGACCGTAGTTTGGAAAGAAGTACTT
GTTCTGAATGATCAAAGGGGAAGATGATCAAAGGGGAAGATGACACAAACTCTA
TAAAAGGGTCAGATGTCTGTTCAAGGAAATGAAGCATTAAGGATCTGATTATTCT
TTAGGTTTTTAACTGATCAGGACTTGCAGTTCTTGTGTTACCAAGGGCCTGGTTT
TCTGGTCAGCAGCACACAATTGTTTTAAATCCCAACCACTCATCCTAGTAATCCA
AGCCCCTGAGTAGCCACAGGGGTCTTGCATTTCCCCGGGGCAATGGCTTGAGG
GAGAGTCTCCTGCCCCTCTATGATTTTCAGGAAGAACTGATTCCCTGTCCCAGG
TTAGATGGGTCTCCAGGAATATCCCTTAGTGACTAGAACAGAGCCCTCAGCCAG
CCATCCTGGAGCTTCAAGCACCCTACTGCAGTGGGTGGTACATCTGGGCCCCA
TATGTTCGCAGGGAGGGGCTGAAGAGCCCAGGCCTACATTGCCAGGTCACCCA
CCCATTTGATGTGTGGTCACAGTGGAATCTGGTTGC

Contains predicted FUS-binding sequences:

- TCCACGT
- TCACAGT
- TCCCAGG
- AAAGGGTC
- AAAGGGAC

Reverse complement (forward strand):

GCAACCAGATTCCACTGTGACCACACATCAAATGGGTGGGTGACCTGGCAATG
TAGGCCTGGCTCTTCAGCCCCTCCCTGCGAACATATGGGGCCCAGATGTACC
ACCCACTGCAGTAGGGTGCTTGAAGCTCCAGGATGGCTGGCTGAGGGCTCTGT
TCTAGTCACTAAGGGATATTCCTGGAGACCCATCTAACCTGGGACAGGGAATCA
GTTCTTCCTGAAAATCATAGAGGGGCAGGAGACTCTCCCTCAAGCCATTGCCC
CGGGGAAATGCAAGACCCCTGTGGCTACTCAGGGGCTTGGATTACTAGGATGA
GTGGTTGGGATTTAAAACAATTGTGTGCTGCTGACCAGAAAACCAGGCCCTTGG
TAACACAAGAACTGCAAGTCCTGATCAGTTAAAAACCTAAAGAATAATCAGATCC
TTAATGCTTCATTTCCTTGAACAGACATCTGACCCTTTTATAGAGTTTGTGTCAT
CTTCCCCTTTGATCATCTTCCCCTTTGATCATTCAGAACAAGTACTTCTTTCCAA
ACTACGGTCTCAGTCCCATTTTCAAATAGTATTTTGGAATGGCTAGCCTATGATA
ACCCCACCTCCCTTCCTGTTGAGCTTCCTAATGATACCGAAGGGAAGAGCGTG
GTCCCTTTAAGTGATACGGAAGCGGGGGCGGGGGGGGGGGGGGGAGGGAAGG
GCGTGGCCCCTGGCTAGGGCTCCACCCCTACGAGCCTAGATGAGGACAGGCA
TTTTTGTTTTCCTGCTCAAATGCTGCATTTCCCAAGACCACCCTGGCCTGCCAC
GCCCCCATCCTGTGCCTATAAAAATCCTGAGGCCCTAGCAGGCAGACACACAG
ATGGCAGGACGTGGAGAGGAGCACAATGGCGGAGGAACTAGGCCACTGACCG
GCAGAAGCAGAATGATGCTGTGGCAGTCGGATGAGAGCCCAGGCCGCTGAGC
TGTCGACTCCAGGGGGGAAGCCTTCCCACTCCATCACCTT

Contains predicted G-quadruplexes:

Position	Length	QGRS	G-Score
38	26	GGGTGACCTGGCAATGTAGGCCTGGG	18
137	16	GGATGGCTGGCTGAGG	19
289	27	GGCTACTCAGGGGCTTGGATTACTAGG	19
671	19	GGGGCGGGGGGGGGGGGGG	63
696	21	GGGCGTGGCCCCTGGCTAGGG	20
859	17	GGCAGGACGTGGAGAGG	19
884	15	GGCGGAGGAACTAGG	17

Possible ssDNA FUS-binding sites:

- TCCACGT

CHRNB1 (Chromosome 17: 7,445,061-7,457,707 forward strand)

GGCACTGCTCCCAGGGGATCGGGTCTCCACTCCAGCTTTCTCAATTAAAGACG
ATTTATACAACTGAAGTGCTGTCTGTCATCTGTCGGTGGCGGGCTTGGCAGTTG
CTCGAGGCAGGATCAAGTCCCGGGGGCGGGGCGGGTGGGCTGGCGGCTGTC
CTCCAGCAACAGGTGCACATTCCCGGGCTCCTC

Contains predicted FUS-binding sequences:

- TTCCCGG

Reverse complement (reverse strand):

GAGGAGCCCGGGAATGTGCACCTGTTGCTGGAGGACAGCCGCCAGCCCACCC
GCCCCGCCCCCGGGACTTGATCCTGCCTCGAGCAACTGCCAAGCCCGCCACC
GACAGATGACAGACAGCACTTCAGTTGTATAAATCGTCTTTAATTGAGAAAGCT
GGAGTGGAGACCCGATCCCCTGGGAGCAGTGCC

Contains predicted g-quadruplexes:

-none

Possible ssDNA FUS-binding sites:

-none

CHRND (Chromosome 2: 232,525,993-232,536,667 forward strand)

CAACTCTGGAGCTTTCTTGGGATGGGACCTGGTGGGTGGACATTCAGTCTCAG
GGGTGGGGCCCAGGCAGGGCTGCCTCTGGAAGCAGTTGGCAAGGGTAACAGA
TGCTGGAAAGGGGCTGTAAGGCCCCTATCTGAGCCTATCTCCTGCCTCCTGAG
AAGCAGCAGCAGCTGGCCTGCCTGTTGCCCCGCCCCCGTGCATGGCTGCCCA
GCGCTGGCCCCAGTGCCCAGCGTCTCCGCCCAGCACCCCCCCGGCCCTCCCT
CCCCACCCCCCGCCTCCGAGCTGCGGGGAGTCCCAGCCTGGGATCTTTGCCT
CATGTCCTTGGGCTCCTGCCCTGGCTGGCCCGTCCCCCACCGCCATGAGGTGT
CAGATTGTGTTTCCGGCTGCCTCTTCCCGTTGACCCCCTCCTCCCCCAACACCT
GTCCCCTCTCCCGCCCACCCTC

Contains predicted FUS-binding sequence:

- TTCCCGT
- AAAGGGGC

Reverse complement (reverse strand):

GA**GGG**T**GGG**C**GGG**AGA**GGG**GACAGGTGTT**GG**G**GG**A**GG**A**GG**G**GG**TCAAC**GG**
GAAGA**GG**CAGCC**GG**AAACACAATCTGACACCTCAT**GG**C**GG**T**GG**G**GG**ACGGGC
CAGCCA**GG**GCA**GG**AGCCCAA**GG**ACATGA**GG**CAAAGATCCCAGGCTGGGACTC
CCCGCAGCTC**GG**A**GG**C**GG**G**GG**GTGGGGAGGGAGGGCCGGGGGGGTGCTGG

GCGGAGACGCTGGGCACTGGGGCCAGCGCTGGGCAGCCATGCACGGGGGCG
GGGCAACAGGCAGGCCAGCTGCTGCTGCTTCTCAGGAGGCAGGAGATAGGCT
CAGATAGGGGCCTTACAGCCCCTTTCCAGCATCTGTTACCCTTGCCAACTGCTT
CCAGAGGCAGCCCTGCCTGGGCCCCACCCCTGAGACTGAATGTCCACCCACC
AGGTCCCATCCCAAGAAAGCTCCAGAGTTG

Contains predicted g-quadruplexes:

Position	Length	QGRS	G-Score
3	17	GGGTGGGCGGGAGAGGG	40
30	11	GGGGGAGGAGG	21
42	23	GGTCAACGGGAAGAGGCAGCCGG	21
86	11	GGCGGTGGGGG	21
109	24	GGGCAGGAGCCCAAGGACATGAGG	17
165	11	GGAGGCGGGGG	21
179	27	GGGAGGGAGGGCCGGGGGGGTGCTGGG	42
207	30	GGAGACGCTGGGCACTGGGGCCAGCGCTGG	20
249	10	GGGGGCGGGG	20
290	26	GGAGGCAGGAGATAGGCTCAGATAGG	18

Possible ssDNA FUS-binding sites:

- TTCCCGT

CHRNE/ ACHRE (17p13.2 reverse strand)

ACAGAAAAACAAAAAACATCGAGGCTGGGCGCGGTGGCTCACGCCTATAATCC
CAGCACTTTGGGAGGCCCAGGTAGGTGGCTCACGAGGTCAGGAGATCGAGAC
CATCCTGGCTAACATGGTGAAACCCCATCTCTACTAAAAAATACAAAAATTAGCC
GGGCATGGTGGCATGCGCCTGTAGTCCCAGCTACTCCAGAGGTTGAGGCAGG
AGAATCGCTTGAACCCGGGAGGCGGAGGTTGCAGTGAGCCGAGATCATGCCA
CTGCACTCCAGTCTGGGCGCCAGAGCGAGACTTGGTCTCAAAAAAATTTTTTTT
AAAAAGGAACATCAAAAGGATCTATTAAGGTGTCATCAGGTGTGTGTGTATGTG
TGCACGTGTGTGTTTAGGAGAGTAGGATGGGAAGACGGTACTATCATCTGTGA
CCACAAGGTGGCAGCAGGGATAGACAAGGAGAAACAAGTCTCCCACCCAGAG
GGGCTGGGCATGGGCAAACCTGGCGATCAGGTTGTGGAAGGAGGTGGGTCCT
TTACATGATCTCCTTTGCTAGATGGAATCTCTGTACCGCAGGGCTAATCCCCTG
TGACCACCTGTCTCTTTATCAGGTCTTTATGGAGACTGTTTTTTGCCACTCTGTC
GGCAAGAAAGGCATTGTGAGCTTGGGTGGTGATAGTGTGTGTTCCACATGGGT
GAGAATGGGAGGCAAGGGGTGTGTCACATCCCCAGATGTGTTCATCAGTCAGG
GTCACCTACACAGGGCAGCTTACTCAAAGGACAACAGTGCCTGCTGAAAGCAG
TGTCTCCCACCCCCTGCTACTAGAATTGTGGTTGCAGGTGCCTCTCAGGAGAC
GCCCACATCTGTGGCTGGGGAGTTGGCCAAATACCAGGCAAAGGACGCTGGG
CTGGGGCGGGGCAGGGGCAGGAAACACAGGATGGGGCAGCTGCCTCTGGAA
GCAGCCAAAATGTCCCCAGCTGCAGCAGGGGTGAGCAGAGGATTAGGTGACA

GTCCCCTAACAGCCCGGAACTAACACCCTCCTCCCCCTCACACAGGCACCCTG
GCATGCCCCCTCCAAGCCTGCCAGAGCTC

Contains predicted FUS-binding sequence:

- None

Reverse complement (forward strand):

GAGCTCTGGCAGGCTTGGAGGGGCATGCCAGGGTGCCTGTGTGAGGGGGGA
GGAGGGTGTTAGTTCCGGGCTGTTAGGGGACTGTCACCTAATCCTCTGCTCAC
CCCTGCTGCAGCTGGGGGACATTTTGGCTGCTTCCAGAGGCAGCTGCCCCATCC
TGTGTTTCCTGCCCCTGCCCCGCCCCAGCCCAGCGTCCTTTGCCTGGTATTTG
GCCAACTCCCCAGCCACAGATGTGGGCGTCTCCTGAGAGGCACCTGCAACCAC
AATTCTAGTAGCAGGGGGGTGGGAGACACTGCTTTCAGCAGGCACTGTTGTCCT
TTGAGTAAGCTGCCCTGTGTAGGTGACCCTGACTGATGAACACATCTGGGGAT
GTGACACACCCCTTGCCTCCCATTCTCACCCATGTGGAACACACACTATCACCA
CCCAAGCTCACAATGCCTTTCTTGCCGACAGAGTGGCAAAAAACAGTCTCCATA
AAGACCTGATAAAGAGACAGGTGGTCACAGGGGGATTAGCCCTGCGGTACAGAG
ATTCCATCTAGCAAAGGAGATCATGTAAAGGACCCACCTCCTTCCACAACCTGA
TCGCCAGGTTTGCCCATGCCCAGCCCCTCTGGGTGGGAGACTTGTTTCTCCTT
GTCTATCCCTGCTGCCACCTTGTGGTCACAGATGATAGTACCGTCTTCCCATCC
TACTCTCCTAAACACACACGTGCACACATACACACACACCTGATGACACCTTAA
TAGATCCTTTTGATGTTCCTTTTTAAAAAAAATTTTTTTGAGACCAAGTCTCGCTC
TGGCGCCCAGACTGGAGTGCAGTGGCATGATCTCGGCTCACTGCAACCTCCGC
CTCCCGGGTTCAAGCGATTCTCCTGCCTCAACCTCTGGAGTAGCTGGGACTAC
AGGCGCATGCCACCATGCCCGGCTAATTTTTGTATTTTTTAGTAGAGATGGGGT
TTCACCATGTTAGCCAGGATGGTCTCGATCTCCTGACCTCGTGAGCCACCTACC
TGGGCCTCCCAAAGTGCTGGGATTATAGGCGTGAGCCACCGCGCCCAGCCTC
GATGTTTTTTGTTTTTCTGT

Contains predicted g-quadruplexes:

Position	Length	QGRS	G-Score
8	15	GGCAGGCTTGGAGGG	20
46	11	GGGGGAGGAGG	21
118	26	GGGGACATTTTGGCTGCTTCCAGAGG	10
277	28	GGGGGTGGGAGACACTGCTTTCAGCAGG	5
497	14	GGTGGTCACAGGGG	16
957	27	GGGGTTTCACCATGTTAGCCAGGATGG	4

CHRNG (Chromosome 2: 232,539,727-232,546,403 forward strand)

GGGATGCCCAGGGAGGGGGAAGCTCAGGAAGGGGGAAGCTCAGGGAGGAGG
AAGCTCAGAGAGGAGGAAGCTCAGGGAAAGGGAAGCCCAGTGAGGGGGAAGC
TTAGGGAGGGAGAAGCTCAGGGAGGGGGAAGCTCTGGGAGGAGGAAGCTCAG
GGAAAGGGAAGCCCAGTGAGGGGGAAGGTCAGCGAGGGGGAAGTTCAGGGA
GAGGGATGCTGAGTGAGGGGGATGCCGAGTGAGGGGGAGGCCGAGTGAGGG
GGATGCCCAGTGAGGGGGATGCCCAGTGGCAGGCCAAGATGGGTGGATCACT
TGAGTTCAGGAGTTCCAAGACTGGCCTGGCCAACATGGTGAAACCCCGTCTCT
ACTAAAAATACAAAAAAGAAAAAAGAAGAAGAAGAAGAAAAATTAGCCAGGCGT
GTTGGCGCATGCCAGTAGTCCCAGCTACTCAGAAGGCTGAAGTAGAAGAATCA
AGGTGGAGGTTGTAGTGAGCCAAGATCGCACCACTGCACTCCAGCAAAAAACA
AACAAACAAACAAACACAAAAACCCTCACATGCCTACCCAACAGCCTTCACACC
CACCCAAATCCTGACTCCCTGGAGGGAGTAGGAGGCAGTCCACCTCAGCCCTC
TCTGGAGCCGCTGTCAGGTTCCTCGGCGACCTGCCTTCCCTACCACACCCAGC
TGGCCCTGGCTGTCCTTGCCCCCCATGTGGAACATGGAGGTGAGGCTGGGAC
AACTGAGCCCGAGTTGGGGCTGGAAGGTGGATGTCTCTTTTGGGGCAGACGG
GGCCCCTGTCTCCCCTCTCCAGCCCAGGTAACCTGAGCCCAGCATTGTGTCCA
TCCTGGAACAGCTGACAACGCTGTGGTCAGACAGCTGGTGGGGCTGGGCCAG
GCTGGCCGGGCTGGCTGGGCTGGCTGGGGTGGGAGTGTAGGCTGTTATATGA
CACCCAGAGCCCATCTCTCTCTGCCCCAGACCTTGGAGCTGTTGTCCCACCCC
TGTC

Contains predicted FUS-binding sequences:

- AGGTTGTA

Reverse complement (reverse strand):

GACAGGGGTGGGACAACAGCTCCAA**GG**TCTGG**GG**CAGAGAGAGAT**GG**GCTCT
G**GG**TGTCATATAACAGCCTACACTCCCACCCCAGCCAGCCCAGCCAGCCCGGC
CAGCCTGGCCCAGCCCCACCAGCTGTCTGACCACAGCGTTGTCAGCTGTTCCA
GGATGGACACAATGCTGGGCTCA**GG**TTACCTG**GG**CTGGAGA**GG**GGAGACA**GG**
GGCCCCGTCTGCCCCAAAAGAGACATCCACCTTCCAGCCCCAACTCGGGCTCA
GTTGTCCCAGCCTCACCTCCATGTTCCACAT**GGGGGG**CAAGGACAGCCA**GGG**
CCAGCT**GGG**TGT**GG**TA**GG**GAA**GG**CA**GG**TCGCCGAGGAACCTGACAGC**GG**CTC
CAGAGA**GG**GCTGA**GG**T**GG**ACTGCCTCCTACTCCCTCCAGGGAGTCA**GG**ATTTG
GGT**GG**GTGTGAA**GG**CTGTTG**GG**TAGGCATGTGAGGGTTTTTGTGTTTGTTTGTT
TGTTTGTTTTTTGCTGGAGTGCAGTGGTGCGATCTTGGCTCACTACAACCTCCA
CCTTGATTCTTCTACTTCAGCCTTCTGAGTAGCTGGGACTACTGGCATGCGCCA
ACACGCCTGGCTAATTTTTCTTCTTCTTCTTCTTTTTTCTTTTTTGTATTTTTAGTA
GAGAC**GGGG**TTTCACCATGTT**GG**CCA**GG**CCAGTCTTGGAACTCCTGAACTCAA
GTGATCCACCCATCTTGGCCTGCCACTGGGCATCCCCCTCACTGGGCATCCCC
CTCACTCGGCCTCCCCCTCACTCGGCATCCCCCTCACTCAGCATCCCTCTCCC
TGAACTTCCCCCTCGCTGACCTTCCCCCTCACTGGGCTTCCCTTTCCCTGAGCT
TCCTCCTCCCAGAGCTTCCCCCTCCCTGAGCTTCTCCCTCCCTAAGCTTCCCCC
TCACTGGGCTTCCCTTTCCCTGAGCTTCCTCCTCTCTGAGCTTCCTCCTCCCTG
AGCTTCCCCCTTCCTGAGCTTCCCCCTCCCTGGGCATCCC

Contains predicted g-quadruplexes:

Position	Length	QGRS	G-Score
26	30	**GG**TCTGG**GG**CAGAGAGAGAT**GG**GCTCTG**GG**	15
182	29	**GG**TTACCTG**GG**CTGGAGA**GG**GGAGACA**GG**	21
295	30	**GGGGGG**CAAGGACAGCCA**GGG**CCAGCT**GGG**	30
328	15	**GG**TA**GG**GAA**GG**CA**GG**	20
363	23	**GG**CTCCAGAGA**GG**GCTGA**GG**T**GG**	13
414	29	**GG**ATTTGGGT**GG**GTGTGAA**GG**CTGTTG**GG**	19
645	23	**GGGG**TTTCACCATGTT**GG**CCA**GG**	9

Possible ssDNA FUS-binding sites:

-none

Mouse Chrn genes

Chrna1 (Chromosome 2: 73,563,215-73,580,338 reverse strand)

TGAGGGAGAGTGGGTTGAGGGAGGCAGCAGGAAACAGGACTCTGGAACAAAT
GCCACTGGGGTGGAAGACTTCCCACGAAGTGCTGCGCTGTAATAACAGGACAC
AGGAGGCTGCAGTGGGCCCAGCTAAGCTCTGGGTGGGCTTGGTACTGCCTGA
CAGAGATGAGGGGAGGGAATTGCTGCCTAGGGCCCTGGGGGAAAACCAGTTC
ACAGAAGGGAAAAAAAAAAACCAACTATCTTTGTTAAAAGCTGCATATGATCGTA
TATGGAATTCTCCAGCATCCAATTCAACACTGGCTACTTCTTTCAAACTCATGCA
GGCACAAAAGATGTCACAGGCCTATGACACAGAATTTCATTCCATGTCTAGGGA
GAGTACACTTGCGTGGTTAAGGACAGTTGCACAGTGGTGTCTACTCAAATCCGT
AGCCTCCACTGAAATCATGCTCAAAGTATTTTGCTAATAATTGATTCATGGGCCT
GCGAGATGACTCAGCGGGTGAAGGAACTTGCCACCAAGTCTGATAACCTGAGT
TTGATCCCCAGGGCACACACAGTAGGAGAACCAACTTCTGAAGACTCTCTCTAT
TCTACATAGGCACCATGGCATACCACCACCACCCTCACATAAAGCAAATTAATT
AATTAATTAAAACCCCTATATACAAGACTAGGGGTTCAGTACACTGGTAGAGTTG
TGATAGCCATTTCTATTTAACCCATTTATATTTAGCTAGCACGTGTGAAGTCAGG
GTTTGATCTTCAACACCAAACACAATGACAAGCCTCTGACTCATGATCTATGTAG
ACTCTCAGACACTTTACATCTAGTAAGAGTATAGCGATCATGTTAAGCAAGGCA
CGTCTGTGGCCACAGAAGGCCCCAAGCTTTGAGGCTGTGGGCAGCTCAGCTGT
CATGCGGGCACACAGGTGATGTAAGACAATAGCTGTGGAGTCAGCTGGCTTCC
AAGGCCAGCAGCCAAGCTCCCTAAGCCAGGGT

Contains predicted FUS-binding sequence:

- None

Reverse complement (forward strand):

ACCCT**GG**CTTAG**GG**AGCTT**GG**CTGCT**GG**CCTTGGAAGCCAGCTGACTCCACAG
CTATTGTCTTACATCACCTGTGTGCCCGCATGACAGCTGAGCTGCCCACAGCCT

CAAAGCTTGGGGCCTTCTGTGGCCACAGACGTGCCTTGCTTAACATGATCGCT
ATACTCTTACTAGATGTAAAGTGTCTGAGAGTCTACATAGATCATGAGTCAGAG
GCTTGTCATTGTGTTTGGTGTTGAAGATCAAACCCTGACTTCACACGTGCTAGC
TAAATATAAATGGGTTAAATAGAAATGGCTATCACAACTCTACCAGTGTACTGAA
CCCCTAGTCTTGTATATAGGGGTTTTAATTAATTAATTAATTTGCTTTATGTGAG**G**
GT**GG**T**GG**T**GG**TATGCCATGGTGCCTATGTAGAATAGAGAGAGTCTTCAGAAGTT
GGTTCTCCTACTGTGTGTGCCCTGG**GG**ATCAAACTCA**GG**TTATCAGACTT**GG**T**G**
GCAAGTTCCTTCACCCGCTGAGTCATCTCGCAGGCCCATGAATCAATTATTAGC
AAAATACTTTGAGCATGATTTCAGTGGAGGCTACGGATTTGAGTAGACACCACT
GTGCAACTGTCCTTAACCACGCAAGTGTACTCTCCCTAGACATGGAATGAAATT
CTGTGTCATAGGCCTGTGACATCTTTTGTGCCTGCATGAGTTTGAAAGAAGTAG
CCAGTGTTGAATTGGATGCTGGAGAATTCCATATACGATCATATGCAGCTTTTAA
CAAAGATAGTTGGTTTTTTTTTTCCCTTCTGTGAACTGGTTTTCCCCCAGGGCC
CTAGGCAGCAATTCCCTCCCCTCATCTCTGTCAGGCAGTACCAAGCCCACCCA
GAGCTTAGCTGGGCCCACTGCAGCCTCCTGTGTCCTGTTATTACAGCGCAGCA
CTTCGTGGGAAGTCTTCCACCCCAGTGGCATTTGTTCCAGAGTCCTGTTTCCTG
CTGCCTCCCTCAACCCACTCTCCCTCA

Contains predicted g-quadruplexes:

Position	Length	QGRS	G-Score
6	23	**GG**CTTAG**GG**AGCTT**GG**CTGCT**GG**	21
379	11	**GG**T**GG**T**GG**T**GG**	21
459	30	**GG**ATCAAACTCA**GG**TTATCAGACTT**GG**T**GG**	11

Possible ssDNA FUS-binding sites:

-none

Chrnb1 (Chromosome 11: 69,784,036-69,795,943 reverse strand)

GTGTTATCTGACATTTGTGAGTGGAGGGCGACTGCAGTTGCTCCGGGCGGGAC
CAAGTCCCGAGGGCGGGGCGGGTGGGCTGGCGTCTGGTCCCCCGACAACAG
GTGCACATTCCTGGGCGCCT

Contains predicted FUS binding sequence:

- none

Reverse complement (forward strand):

AGGCGCCCAGGAATGTGCACCTGTTGTCGGGGGACCAGACGCCAGCCCACCC
GCCCCGCCCTCGGGACTTGGTCCCGCCCGGAGCAACTGCAGTCGCCCTCCAC
TCACAAATGTCAGATAACAC

Contains predicted g-quadruplexes:

- None

Possible ssDNA FUS-binding sites:

- none

Chrnd (Chromosome 1: 87,190,607-87,200,070 forward strand)

GCCTGACGGTTCTGGCTTTCTGATTCCTATTAGATAGAAGCAGATCACGGTGCC
CAGGCACCTTTGAGGGTTGTATTCTCTTAAGCATACTCTTAGTGCCATCTATCCC
GACCACTGACTTCTAGCCACAGTCATTACAACGGACAGGCCTGACTCTGTGTG
GAAACGACCCTCCTTGCCCCAGTGGATCCCCTTTTCTTTCCCTTTGGTTTTGGC
TACTCATAGATGCAGGAACGGTGAGGAGACTTCAGTTCAAATTAAAGAAAGAAA
AGAAATGGGCCAGTAAGGTGGCTTAGCAAATAAAGGTACCTGCTGCCGAGCCA
TGTGAAAGGAAAAAAAAATTTAACTCCTTCAAGTTTCCTCTGACTTCCACACATG
CCACAAACTGCGCAGAAACACACTGAGTGGATGGGTGGATGGATGGATGGATG
GATGGATTTTATTTATTTACTTATTTATTTATTTATAAATCTTTGGGGTTTTTTGGA
GACATGGCTTCTCTGTGTAACAACCTGGCAGTCCTGGAACTCATTCTGTAGACC
AGGCTGGCCTTGAACTCAGAGATCCTTCCTCTCTTCCCAAGTGCTGGGATTAAA
AGCATACACTGCCACACCCAGCTTAGAGGTAATATTTTTAAAGATGGGGGAAAA
AATACACAAGTACAGGTGGAGCACTAGCAAGATGGCTCAACAGGTAACAGTTG
CCTGCTGTACAAGAAGTTTCACCTCAGAACCCTCTGTAGAAAGAGAGAAGCAAT
TGTGACAGGTGTACACACACACACACACACACACACACACACACACACACAGA
GGATTCGCCCCCCACCCTCTGCCACCCTACCCCACCAGGCCCCACCCTACCAA
CAATCTGTGACAATCCCTGCCTGGGATCTTTTCGTTCTGCCCTTGGCTCCTGCC
CTAACTGGCAAACCCCACCCCCTCATCACCAGCTTTCAAGTATCAGATTGCGTT
TCCGGCCTCTTCTTTCCAAACCCCTAAAC

Contains predicted FUS binding sequence:

- GGGTTGTA
- CAAGTTTC

Reverse complement (reverse strand):

GTTTAGG**GG**TTT**GG**AAAGAAGA**GG**CC**GG**AAACGCAATCTGATACTTGAAAGCT
GGTGATGA**GG**G**GG**T**GGGG**TTTGCCAGTTAGGGCAGGAGCCAAGGGCAGAACG
AAAAGATCCCA**GG**CAG**GG**ATTGTCACAGATTGTT**GG**TAG**GG**T**GGG**GCCTGGT**G**
GGGTA**GGG**TGGCAGA**GGG**TGGGGGGCGAATCCTCTGTGTGTGTGTGTGTG
TGTGTGTGTGTGTGTGTGTGTACACCTGTCACAATTGCTTCTCTCTTTCTACAGA
GGGTTCTGAGGTGAAACTTCTTGTACAGCAGGCAACTGTTACCTGTTGAGCCAT
CTTGCTAGTGCTCCACCTGTACTTGTGTATTTTTTCCCCCATCTTTAAAAATATTA
CCTCTAAGCTGGGTGTGGCAGTGTATGCTTTTAATCCCAGCACTTG**GG**AAGAGA
GGAA**GG**ATCTCTGAGTTCAA**GG**CCAGCCTGGTCTACAGAATGAGTTCCAGGAC
TGCCAGGTTGTTACACAGAGAAGCCATGTCTCCAAAAAACCCCAAAGATTTATA
AATAAATAAATAAGTAAATAAATAAAATCCATCCATCCATCCATCCATCCACCCAT
CCACTCAGTGTGTTTCTGCGCAGTTTGTGGCATGTGTGGAAGTCAGAGGAAACT
TGAAGGAGTTAAATTTTTTTTTCCTTTCACATGGCTCGGCAGCAGGTACCTTTAT
TTGCTAAGCCACCTTACTGGCCCATTTCTTTTCTTTCTTTAATTTGAACTGAAGTC
TCCTCACCGTTCCTGCATCTATGAGTAGCCAAAACCAAAGGGAAAGAAAAGGG
GATCCACT**GGGG**CAA**GG**AG**GG**TCGTTTCCACACAGAGTCAGGCCTGTCCGTTG

TAATGACTGTGGCTAGAAGTCAGTGGTCGGGATAGATGGCACTAAGAGTATGC
TTAAGAGAATACAACCCTCAAAGGTGCCTGGGCACCGTGATCTGCTTCTATCTA
ATAGGAATCAGAAAGCCAGAACCGTCAGGC

Contains predicted g-quadruplexes:

Position	Length	QGRS	G-Score
8	21	GGTTTGGAAAGAAGAGGCCGG	15
62	10	GGGGGTGGGG	20
117	30	GGCAGGGATTGTCACAGATTGTTGGTAGGG	8
148	29	GGGGCCTGGTGGGGTAGGGTGGCAGAGGG	38
422	30	GGAAGAGAGGAAGGATCTCTGAGTTCAAGG	9
819	13	GGGGCAAGGAGGG	18
874	29	GGCTAGAAGTCAGTGGTCGGGATAGATGG	12

Possible ssDNA FUS-binding sites:

-none

Chrne (Chromosome 11: 70,614,883-70,619,216 reverse strand)

AAAAAAAGCCAACAACAAAAATCAAAATGTTTATTCCTCTACCTCTTAGCCAGTG
AGGAAGACCTAGCGAGCTTTTTAGGAGCTCATGCCTGCAGGCCAAGGCCCCAG
ACGGCCTGCAACATCAGGAGTCCCTGCAGACTAATTCTGTACAGTGACCTGTCT
TATTGCTAGGTCTTTATGGAGACTTTTTGTGTAACTGTAATAGTGTGAATTGGCC
CCTGTCAGGGTATAATAGCATGTACTGCACAGGGAGGTTGTGGTGGTTTGAAT
GAGAAACCCCATGACACACACACACACACACACACACACACACACACACACAAA
GGACCAAGGCTCATGTTTGAATGCTTGGTCCTTAGTTGGTGGAACTGTATGGGA
AGGATTAAATGTGGCCTTATTGGAGGAGGTGTGACATTGGGGTTGGCCTTTGA
GGTTTCAAGACTATTGCCAGTTCTCTACTTCATGGCTGTCATCTGAAGATGTGG
GCTCTCAGCTTTTGCTCCAGCACCGTGCCTGCGACCGTGCTCCCCACCGTGAT
GATTCTGAATCTCACTCTCAGCAGCCACGACCTTCAAAGGTTTTCTATGTTGCCT
TGGATATGGGGTCTTAGGATGGCAATAGAAAAGAGTCTAACCAGGGGTAATATG
GGAGGTGCGGGATGTTACTCCCTTGGATGCATCCATTAGAATAACCAATACAGG
GCAGCAGTACAGAAGATAGCAGTATGTGTTGAGAATGGGGTCTACAGCCTAAT
GGCTTGTGGTTTCAAGTGTTATTAGAGGCCTGCTTCTCTCCTGAGATGACAGGC
CTTGTGGATTACAGAACTGGCTGAAACCCAGGCAAAGGATGCTGGGATGAGGT
GGGGCAAGGGACACAGGATGGGGCAGCTGCCTCCCCCACCCCCACAGCAGG
GGCAGAGGATTAGGTGACAGTCCCCAAACCTAGCCCGGAACTAACACCCTCCT
CCCCTTCACACAGGCACCTTGGCCTGTTCCCTCAA

Contains predicted FUS-binding sequence:

- ACAGTGAC
- AAAGAGTC

- AGGGTATA
- GGGGTCTA

Reverse complement (forward strand):

TTGAGGGAACAGGCCAAGGTGCCTGTGTGAA**GGGG**A**GG**A**GG**GTGTTAGTTCC
G**GG**CTA**GG**TTT**GGGG**ACTGTCACCTAATCCTCTGCCCCTGCTGTGGG**GG**T**GG**
G**GG**A**GG**CAGCTGCCCCATCCTGTGTCCCTTGCCCCACCTCATCCCAGCATCCT
TTGCCTGGGTTTCAGCCAGTTCTGTAATCCACAAGGCCTGTCATCTCAGGAGAG
AAGCAGGCCTCTAATAACACTTGAAACCACAAGCCATTAGGCTGTAGACCCCAT
TCTCAACACATACTGCTATCTTCTGTACTGCTGCCCTGTATTGGTTATTCTAATG
GATGCATCCAAGGGAGTAACATCCCGCACCTCCCATATTACCCCTGGTTAGACT
CTTTTCTATTGCCATCCTAAGACCCCATATCCAAGGCAACATAGAAAACCTTTGA
AGGTCGTGGCTGCTGAGAGTGAGATTCAGAATCATCAC**GG**TGG**GG**AGCAC**GG**T
CGCA**GG**CACGGTGCTGGAGCAAAAGCTGAGAGCCCACATCTTCAGATGACAGC
CATGAAGTAGAGAACTGGCAATAGTCTTGAAACCTCAAAGGCCAACCCCAATGT
CACACCTCCTCCAATAAGGCCACATTTAATCCTTCCCATACAGTTCCACCAACTA
AGGACCAAGCATTCAAACATGAGCCTTGGTCCTTTGTGTGTGTGTGTGTGTGTG
TGTGTGTGTGTGTGTGTGTCATGGGGTTTCTCATTCAAACCACCACAACCTCCC
TGTGCAGTACATGCTATTATACCCTGACAGGGGCCAATTCACACTATTACAGTT
ACACAAAAAGTCTCCATAAAGACCTAGCAATAAGACAGGTCACTGTACAGAATT
AGTCTGCAGGGACTCCTGATGTTGCA**GG**CCGTCT**GG**GGCCTT**GG**CCTGCA**GG**
CATGAGCTCCTAAAAAGCTCGCTA**GG**TCTTCCTCACT**GG**CTAAGA**GG**TAGA**GG**
AATAAACATTTTGATTTTTGTTGTTGGCTTTTTTT

Contains predicted g-quadruplexes:

Position	Length	QGRS	G-Score
32	10	**GGGGAGGAGG**	20
54	14	**GGCTAGGTTTGGGG**	18
100	11	**GGTGGGGGAGG**	21
468	21	**GGTGGGGAGCACGGTCGCAGG**	19
887	26	**GGCCGTCTGGGGCCTTGGCCTGCAGG**	21
937	29	**GGTCTTCCTCACTGGCTAAGAGGTAGAGG**	14

Possible ssDNA FUS-binding sites:

- none

Chrng (Chromosome 1: 87,204,657-87,212,694 forward strand)

ACAAGCCTAGAAGTAGACGGGCTTCCTTTCACTGTAGTTCTCCTTCGATGGCTC
TGGGGGATGCATCCTCAAGTCTGGCCCATCTGCCTCAGCGGACCATGAGTCCT
CCTAAGCGGCTTGATGCATCCCCGAGTCTCCCCAGCTTTGCAGAGGACCTGAC
ATTATCTGTCTGATGATTTTATGAACTGCAGCCCCACTGACAAGCCACCGTTCA
CAGCTGACCTAGTCACAAGAACCACCCACACACACACACACACACACACAAATA

CACATTCCAGACTCTTCTCAGCCCTCCTAAAGCTTAGTACATCTGTGTCCCTTGT
CTCAGGGCACAGGAGAAGCTGCTGTGGTCCCCCGATCGTCAATACCACAGTCT
TTACACATACAGCCACCTTCGACCTGTGGCCTATGGGTCACAGGCCTCCCAAG
ATGCAACCCTTACCCACTTGTAAATAAAAACAGGATATGACACTGTCAACAATTA
GACGCCCTGCAGGCACTTCCTTCCTGTGTCCCAGTCCACTGGAGTGACTACAG
AGCCACCAGGCTAGTGGTGGCAGGGGATTGAAGTACTAAGGCACAGTCACCAA
GACTCTCATGTGTAAATCATACCCCTACCCCCCTGCCGGGTACAGAATGAAGGT
TCTTGATCAGTCACCACCAACCGCTGCAGCACCACTGCTGTCCCCACACCCAT
CTGTCCTTGGCCATTTGCTGAGTCTCCTAGCTGGAAAAAGAGGTGTAGGACCG
AAGCAACTAAGTTTGAGGGTGTCCAGTCTCTGTTGAGACACTTTTGAGGGTGTC
CTGTCTCTGGTGGGACTATTCCATCTTTCGTCCCCTGGCTGGCCCATGTAATCT
GAGCCCAGCATTGTACATATCCTGGGAACAGCTGACAATGCAGTGGTCAGACA
GCTGGTGGGGCCAGCTAGAGCTGGCAGGGTTGGCTGGGAGGGGAGTGTAGG
CTGACACATGACACTCCGACCCCCCTCTGCAACCCCCCCCCCCAGGCCTGTAG
AGCTACTGTCCTGCTCTTCACTGGG

Contains predicted FUS-binding sequence:

- TCCCAGT
- AGGTTCTT

Reverse complement (reverse strand):

CCCAGTGAAGAGCAGGACAGTAGCTCTACAGGCCT**GGG**G**GGG**G**GGG**TTGCAG
A**GGG**GGGTCGGAGTGTCATGTGTCAGCCTACACTCCCCTCCCAGCCAACCCTG
CCAGCTCTAGCTGGCCCCACCAGCTGTCTGACCACTGCATTGTCAGCTGTTCC
CAGGATATGTACAATGCTGGGCTCAGATTACAT**GG**GCCAGCCA**GGGG**ACGAAA
GAT**GG**AATAGTCCCACCAGAGACAGGACACCCTCAAAAGTGTCTCAACAGAGA
CTGGACACCCTCAAACTTAGTTGCTTCGGTCCTACACCTCTTTTTCCAGCTAGG
AGACTCAGCAAAT**GG**CCAA**GG**ACAGAT**GG**GTGT**GGGG**ACAGCAGT**GG**TGCTG
CAGC**GG**TTGGT**GG**TGACTGATCAAGAACCTTCATTCTGTACCC**GG**CA**GG**GG**GG**
TA**GG**GGTATGATTTACACATGAGAGTCTTGGTGACTGTGCCTTAGTACTTCAAT
CCCCTGCCACCACTAGCCTGGTGGCTCTGTAGTCACTCCAGT**GG**ACTG**GG**ACA
CA**GG**AA**GG**AAGTGCCTGCAGGGCGTCTAATTGTTGACAGTGTCATATCCTGTTT
TTATTTACAAGT**GG**GTAAG**GG**TTGCATCTT**GG**GA**GG**CCTGTGACCCATA**GG**CC
ACA**GG**TCGAA**GG**T**GG**CTGTATGTGTAAAGACTGTGGTATTGACGATCGGGGGA
CCACAGCAGCTTCTCCTGTGCCCTGAGACAAGGGACACAGATGTACTAAGCTTT
AGGAGGGCTGAGAAGAGTCTGGAATGTGTATTTGTGTGTGTGTGTGTGTGTGT
GTGGGTGGTTCTTGTGACTAGGTCAGCTGTGAAC**GG**T**GG**CTTGTCAGT**GGGG**C
TGCAGTTCATAAAATCATCAGACAGATAATGTCA**GG**TCCTCTGCAAAGCT**GG**GG
AGACTC**GGGG**ATGCATCAAGCCGCTTAGGA**GG**ACTCAT**GG**TCCGCTGA**GG**CA
GATG**GG**CCAGACTTGAGGATGCATCCCCCAGAGCCATCGAAGGAGAACTACAG
TGAAAGGAAGCCCGTCTACTTCTAGGCTTGT

Contains predicted g-quadruplexes:

Position	Length	QGRS	G-Score
36	21	**GGG**G**GGG**G**GGG**TTGCAGA**GGG**	36

192	25	**GGGCCAGCCAGGGGACGAAAGATGG**	12
332	22	**GGCCAAGGACAGATGGGTGTGG**	19
354	30	**GGACAGCAGTGGTGCTGCAGCGGTTGGTGG**	17
414	14	**GGCAGGGGGGTAGG**	21
520	19	**GGACTGGGACACAGGAAGG**	18
597	24	**GGGTAAGGGTTGCATCTTGGGAGG**	14
634	19	**GGCCACAGGTCGAAGGTGG**	17
832	18	**GGTGGCTTGTCAGTGGGG**	12
885	30	**GGTCCTCTGCAAAGCTGGGGAGACTCGGGG**	7
935	28	**GGACTCATGGTCCGCTGAGGCAGATGGG**	19

Possible ssDNA FUS-binding sites:

- TCCCAGT

Summary table:

Species	gene	# predicted FUS binding sites	ssDNA binding sites
human	CHRNA1	5	1
	CHRNB1	5	0
	CHRND	2	1
	CHRNE	0	0
	CHRNG	1	0
mouse	Chrna1	0	0
	Chrnb1	0	0
	Chrnd	1	0
	Chrne	4	0
	Chrng	2	1

References:

1. Tan, A.Y., Riley, T.R., Coady, T., Bussemaker, H.J. & Manley, J.L. TLS/FUS (translocated in liposarcoma/fused in sarcoma) regulates target gene transcription via single-stranded DNA response elements. *Proc Natl Acad Sci U S A* **109**, 6030-6035 (2012).
2. Kikin, O., D'Antonio, L. & Bagga, P.S. QGRS Mapper: a web-based server for predicting G-quadruplexes in nucleotide sequences. *Nucleic acids research* **34**, W676-682 (2006).

Bibliography

ABELLA, V. et al. Progranulin as a biomarker and potential therapeutic agent. **Drug Discov Today,** v. 22, n. 10, p. 1557-1564, 10 2017. ISSN 1878-5832. Disponível em: < https://www.ncbi.nlm.nih.gov/pubmed/28651064 >.

ABU-RAYA, S. et al. Rasagiline, a monoamine oxidase-B inhibitor, protects NGF-differentiated PC12 cells against oxygen-glucose deprivation. **J Neurosci Res,** v. 58, n. 3, p. 456-63, Nov 1999. ISSN 0360-4012. Disponível em: < https://www.ncbi.nlm.nih.gov/pubmed/10518120 >.

AGOSTA, F. et al. The present and the future of neuroimaging in amyotrophic lateral sclerosis. **AJNR Am J Neuroradiol,** v. 31, n. 10, p. 1769-77, Nov 2010. ISSN 1936-959X. Disponível em: < https://www.ncbi.nlm.nih.gov/pubmed/20360339 >.

AGOSTA, F. et al. MRI signatures of the frontotemporal lobar degeneration continuum. **Hum Brain Mapp,** v. 36, n. 7, p. 2602-14, Jul 2015. ISSN 1097-0193. Disponível em: < https://www.ncbi.nlm.nih.gov/pubmed/25821176 >.

AGOSTA, F. et al. Voxel-based morphometry study of brain volumetry and diffusivity in amyotrophic lateral sclerosis patients with mild disability. **Hum Brain Mapp,** v. 28, n. 12, p. 1430-8, Dec 2007. ISSN 1065-9471. Disponível em: < https://www.ncbi.nlm.nih.gov/pubmed/17370339 >.

AHMED, R. M. et al. Autonomic dysregulation in frontotemporal dementia. **J Neurol Neurosurg Psychiatry,** v. 86, n. 9, p. 1048-9, Sep 2015. ISSN 1468-330X. Disponível em: < https://www.ncbi.nlm.nih.gov/pubmed/25550415 >.

AHMED, R. M. et al. Amyotrophic lateral sclerosis and frontotemporal dementia: distinct and overlapping changes in eating behaviour and metabolism. **Lancet Neurol,** v. 15, n. 3, p. 332-42, Mar 2016. ISSN 1474-4465. Disponível em: < https://www.ncbi.nlm.nih.gov/pubmed/26822748 >.

AHMED, R. M. et al. Energy expenditure in frontotemporal dementia: a behavioural and imaging study. **Brain,** v. 140, n. 1, p. 171-183, 01 2017. ISSN 1460-2156. Disponível em: < https://www.ncbi.nlm.nih.gov/pubmed/27789521 >.

AHMED, R. M. et al. Eating behavior in frontotemporal dementia: Peripheral hormones vs hypothalamic pathology. **Neurology,** v. 85, n. 15, p. 1310-7, Oct 2015. ISSN 1526-632X. Disponível em: < https://www.ncbi.nlm.nih.gov/pubmed/26377252 >.

AHMED, R. M. et al. Body mass index delineates ALS from FTD: implications for metabolic health. **J Neurol,** v. 261, n. 9, p. 1774-80, Sep 2014. ISSN 1432-1459. Disponível em: < https://www.ncbi.nlm.nih.gov/pubmed/24957296 >.

AHN, S. W. et al. Reproducibility of the motor unit number index (MUNIX) in normal controls and amyotrophic lateral sclerosis patients. **Muscle Nerve,** v. 42, n. 5, p. 808-13, Nov 2010. ISSN 1097-4598. Disponível em: < https://www.ncbi.nlm.nih.gov/pubmed/20976784 >.

AL-CHALABI, A.; HARDIMAN, O. The epidemiology of ALS: a conspiracy of genes, environment and time. **Nat Rev Neurol,** v. 9, n. 11, p. 617-28, Nov 2013. ISSN 1759-4766. Disponível em: < https://www.ncbi.nlm.nih.gov/pubmed/24126629 >.

AL-CHALABI, A. et al. Amyotrophic lateral sclerosis: moving towards a new classification system. **Lancet Neurol,** v. 15, n. 11, p. 1182-94, 10 2016. ISSN 1474-4465. Disponível em: < https://www.ncbi.nlm.nih.gov/pubmed/27647646 >.

ALAMI, N. H. et al. Axonal transport of TDP-43 mRNA granules is impaired by ALS-causing mutations. **Neuron,** v. 81, n. 3, p. 536-543, Feb 2014. ISSN 1097-4199. Disponível em: < https://www.ncbi.nlm.nih.gov/pubmed/24507191 >.

ALARCÓN, C. R. et al. HNRNPA2B1 Is a Mediator of m(6)A-Dependent Nuclear RNA Processing Events. **Cell,** v. 162, n. 6, p. 1299-308, Sep 2015. ISSN 1097-4172. Disponível em: < https://www.ncbi.nlm.nih.gov/pubmed/26321680 >.

ALBERTI, S. Phase separation in biology. **Curr Biol,** v. 27, n. 20, p. R1097-R1102, Oct 2017. ISSN 1879-0445. Disponível em: < https://www.ncbi.nlm.nih.gov/pubmed/29065286 >.

ALLADI, S. et al. Subtypes of dementia: a study from a memory clinic in India. **Dement Geriatr Cogn Disord,** v. 32, n. 1, p. 32-8, 2011. ISSN 1421-9824. Disponível em: < https://www.ncbi.nlm.nih.gov/pubmed/21832829 >.

ALMAD, A. A. et al. Connexin 43 in astrocytes contributes to motor neuron toxicity in amyotrophic lateral sclerosis. **Glia,** v. 64, n. 7, p. 1154-69, 07 2016. ISSN 1098-1136. Disponível em: < https://www.ncbi.nlm.nih.gov/pubmed/27083773 >.

ALVAREZ, F. J.; FYFFE, R. E. The continuing case for the Renshaw cell. **J Physiol,** v. 584, n. Pt 1, p. 31-45, Oct 2007. ISSN 0022-3751. Disponível em: < https://www.ncbi.nlm.nih.gov/pubmed/17640932 >.

AMICK, J.; ROCZNIAK-FERGUSON, A.; FERGUSON, S. M. C9orf72 binds SMCR8, localizes to lysosomes, and regulates mTORC1 signaling. **Mol Biol Cell,** v. 27, n. 20, p. 3040-3051, 10 2016. ISSN 1939-4586. Disponível em: < https://www.ncbi.nlm.nih.gov/pubmed/27559131 >.

ANDERSEN, P. M. Amyotrophic lateral sclerosis associated with mutations in the CuZn superoxide dismutase gene. **Curr Neurol Neurosci Rep,** v. 6, n. 1, p. 37-46, Jan 2006. ISSN 1528-4042. Disponível em: < https://www.ncbi.nlm.nih.gov/pubmed/16469270 >.

ANDERSEN, P. M. et al. EFNS guidelines on the clinical management of amyotrophic lateral sclerosis (MALS)--revised report of an EFNS task force. **Eur J Neurol,** v. 19, n. 3, p. 360-75, Mar 2012. ISSN 1468-1331. Disponível em: < https://www.ncbi.nlm.nih.gov/pubmed/21914052 >.

ANDERSEN, P. M.; AL-CHALABI, A. Clinical genetics of amyotrophic lateral sclerosis: what do we really know? **Nat Rev Neurol,** v. 7, n. 11, p. 603-15, Oct 2011. ISSN 1759-4766. Disponível em: < https://www.ncbi.nlm.nih.gov/pubmed/21989245 >.

ANDERSON, P.; KEDERSHA, N. Stress granules: the Tao of RNA triage. **Trends Biochem Sci,** v. 33, n. 3, p. 141-50, Mar 2008. ISSN 0968-0004. Disponível em: < https://www.ncbi.nlm.nih.gov/pubmed/18291657 >.

ANDERSON, P.; KEDERSHA, N. Stress granules. **Curr Biol,** v. 19, n. 10, p. R397-8, May 2009. ISSN 1879-0445. Disponível em: < https://www.ncbi.nlm.nih.gov/pubmed/19467203 >.

AOKI, Y. et al. C9orf72 and RAB7L1 regulate vesicle trafficking in amyotrophic lateral sclerosis and frontotemporal dementia. **Brain,** v. 140, n. 4, p. 887-897, 04 2017. ISSN 1460-2156. Disponível em: < https://www.ncbi.nlm.nih.gov/pubmed/28334866 >.

ARBOUR, D.; VANDE VELDE, C.; ROBITAILLE, R. New perspectives on amyotrophic lateral sclerosis: the role of glial cells at the neuromuscular junction. **J Physiol,** v. 595, n. 3, p. 647-661, 02 2017. ISSN 1469-7793. Disponível em: < https://www.ncbi.nlm.nih.gov/pubmed/27633977 >.

ARIMOTO, K. et al. Formation of stress granules inhibits apoptosis by suppressing stress-responsive MAPK pathways. **Nat Cell Biol,** v. 10, n. 11, p. 1324-32, Nov 2008. ISSN 1476-4679. Disponível em: < https://www.ncbi.nlm.nih.gov/pubmed/18836437 >.

ARNOLD, A.; EDGREN, D. C.; PALLADINO, V. S. Amyotrophic lateral sclerosis; fifty cases observed on Guam. **J Nerv Ment Dis,** v. 117, n. 2, p. 135-9, Feb 1953. ISSN 0022-3018. Disponível em: < https://www.ncbi.nlm.nih.gov/pubmed/13061952 >.

ARUMUGAM, S. et al. Regulation of Survival Motor Neuron Protein by the Nuclear Factor-Kappa B Pathway in Mouse Spinal Cord Motoneurons. **Mol Neurobiol,** v. 55, n. 6, p. 5019-5030, Jun 2018. ISSN 1559-1182. Disponível em: < https://www.ncbi.nlm.nih.gov/pubmed/28808928 >.

ASH, P. E. et al. Neurotoxic effects of TDP-43 overexpression in C. elegans. **Hum Mol Genet,** v. 19, n. 16, p. 3206-18, Aug 2010. ISSN 1460-2083. Disponível em: < https://www.ncbi.nlm.nih.gov/pubmed/20530643 >.

ASKANAS, V.; WOJCIK, S.; ENGEL, W. K. Expression of Nogo-A in human muscle fibers is not specific for amyotrophic lateral sclerosis. **Ann Neurol,** v. 62, n. 6, p. 676-7; author reply 677, Dec 2007. ISSN 1531-8249. Disponível em: < https://www.ncbi.nlm.nih.gov/pubmed/17894379 >.

ATAGI, Y. et al. Apolipoprotein E Is a Ligand for Triggering Receptor Expressed on Myeloid Cells 2 (TREM2). **J Biol Chem,** v. 290, n. 43, p. 26043-50, Oct 2015. ISSN 1083-351X. Disponível em: < https://www.ncbi.nlm.nih.gov/pubmed/26374899 >.

ATKIN, J. D. et al. Mutant SOD1 inhibits ER-Golgi transport in amyotrophic lateral sclerosis. **J Neurochem,** v. 129, n. 1, p. 190-204, Apr 2014. ISSN 1471-4159. Disponível em: < https://www.ncbi.nlm.nih.gov/pubmed/24134191 >.

AYALA, V. et al. Cell stress induces TDP-43 pathological changes associated with ERK1/2 dysfunction: implications in ALS. **Acta Neuropathol,** v. 122, n. 3, p. 259-70, Sep 2011. ISSN 1432-0533. Disponível em: < https://www.ncbi.nlm.nih.gov/pubmed/21706176 >.

AYERS, J. I. et al. Experimental transmissibility of mutant SOD1 motor neuron disease. **Acta Neuropathol,** v. 128, n. 6, p. 791-803, Dec 2014. ISSN 1432-0533. Disponível em: < https://www.ncbi.nlm.nih.gov/pubmed/25262000 >.

BAE, J. S. et al. The puzzling case of hyperexcitability in amyotrophic lateral sclerosis. **J Clin Neurol,** v. 9, n. 2, p. 65-74, Apr 2013. ISSN 1738-6586. Disponível em: < https://www.ncbi.nlm.nih.gov/pubmed/23626643 >.

BAECHTOLD, H. et al. Human 75-kDa DNA-pairing protein is identical to the pro-oncoprotein TLS/FUS and is able to promote D-loop formation. **J Biol Chem,** v. 274, n. 48, p. 34337-42, Nov 1999. ISSN 0021-9258. Disponível em: < https://www.ncbi.nlm.nih.gov/pubmed/10567410 >.

BAILEY, J. K. et al. Nucleic acid binding proteins affect the subcellular distribution of phosphorothioate antisense oligonucleotides. **Nucleic Acids Res,** v. 45, n. 18, p. 10649-10671, Oct 2017. ISSN 1362-4962. Disponível em: < https://www.ncbi.nlm.nih.gov/pubmed/28977508 >.

BAKER, M. et al. Mutations in progranulin cause tau-negative frontotemporal dementia linked to chromosome 17. **Nature,** v. 442, n. 7105, p. 916-9, Aug 2006. ISSN 1476-4687. Disponível em: < https://www.ncbi.nlm.nih.gov/pubmed/16862116 >.

BAKKAR, N.; BOEHRINGER, A.; BOWSER, R. Use of biomarkers in ALS drug development and clinical trials. **Brain Res,** v. 1607, p. 94-107, May 2015. ISSN 1872-6240. Disponível em: < https://www.ncbi.nlm.nih.gov/pubmed/25452025 >.

BALLINGER, E. C. et al. Basal Forebrain Cholinergic Circuits and Signaling in Cognition and Cognitive Decline. **Neuron,** v. 91, n. 6, p. 1199-1218, Sep 2016. ISSN 1097-4199. Disponível em: < https://www.ncbi.nlm.nih.gov/pubmed/27657448 >.

BARMADA, S. J. et al. Cytoplasmic mislocalization of TDP-43 is toxic to neurons and enhanced by a mutation associated with familial amyotrophic lateral sclerosis. **J Neurosci,** v. 30, n. 2, p. 639-49, Jan 2010. ISSN 1529-2401. Disponível em: < https://www.ncbi.nlm.nih.gov/pubmed/20071528 >.

BARON, D. M. et al. Amyotrophic lateral sclerosis-linked FUS/TLS alters stress granule assembly and dynamics. **Mol Neurodegener,** v. 8, p. 30, Aug 2013. ISSN 1750-1326. Disponível em: < https://www.ncbi.nlm.nih.gov/pubmed/24090136 >.

BARRETT, M. J. et al. Lower volume, more impairment: reduced cholinergic basal forebrain grey matter density is associated with impaired cognition in Parkinson disease. **J Neurol Neurosurg Psychiatry**, Jun 2019. ISSN 1468-330X. Disponível em: < https://www.ncbi.nlm.nih.gov/pubmed/31175168 >.

BEDFORD, M. T.; CLARKE, S. G. Protein arginine methylation in mammals: who, what, and why. **Mol Cell,** v. 33, n. 1, p. 1-13, Jan 2009. ISSN 1097-4164. Disponível em: < https://www.ncbi.nlm.nih.gov/pubmed/19150423 >.

BELLY, A. et al. Delocalization of the multifunctional RNA splicing factor TLS/FUS in hippocampal neurones: exclusion from the nucleus and accumulation in dendritic granules and spine heads. **Neurosci Lett,** v. 379, n. 3, p. 152-7, May 2005. ISSN 0304-3940. Disponível em: < https://www.ncbi.nlm.nih.gov/pubmed/15843054 >.

BELZIL, V. V. et al. Novel FUS deletion in a patient with juvenile amyotrophic lateral sclerosis. **Arch Neurol,** v. 69, n. 5, p. 653-6, May 2012. ISSN 1538-3687. Disponível em: < https://www.ncbi.nlm.nih.gov/pubmed/22248478 >.

BENSIMON, G.; LACOMBLEZ, L.; MEININGER, V. A controlled trial of riluzole in amyotrophic lateral sclerosis. ALS/Riluzole Study Group. **N Engl J Med,** v. 330, n. 9, p. 585-91, Mar 1994. ISSN 0028-4793. Disponível em: < https://www.ncbi.nlm.nih.gov/pubmed/8302340 >.

BENTMANN, E. et al. Requirements for stress granule recruitment of fused in sarcoma (FUS) and TAR DNA-binding protein of 43 kDa (TDP-43). **J Biol Chem,** v. 287, n. 27, p. 23079-94, Jun 2012. ISSN 1083-351X. Disponível em: < https://www.ncbi.nlm.nih.gov/pubmed/22563080 >.

BENUSSI, A. et al. Transcranial magnetic stimulation distinguishes Alzheimer disease from frontotemporal dementia. **Neurology,** v. 89, n. 7, p. 665-672, Aug 2017. ISSN 1526-632X. Disponível em: < https://www.ncbi.nlm.nih.gov/pubmed/28747446 >.

BERLOWITZ, D. J. et al. Identifying who will benefit from non-invasive ventilation in amyotrophic lateral sclerosis/motor neurone disease in a clinical cohort. **J Neurol Neurosurg Psychiatry,** v. 87, n. 3, p. 280-6, Mar 2016. ISSN 1468-330X. Disponível em: < https://www.ncbi.nlm.nih.gov/pubmed/25857659 >.

BERNHEIMER, H. et al. Brain dopamine and the syndromes of Parkinson and Huntington. Clinical, morphological and neurochemical correlations. **J Neurol Sci,** v. 20, n. 4, p. 415-55, Dec 1973. ISSN 0022-510X. Disponível em: < https://www.ncbi.nlm.nih.gov/pubmed/4272516 >.

BERTEL, O. et al. Amyotrophic lateral sclerosis: changes of noradrenergic and serotonergic transmitter systems in the spinal cord. **Brain Res,** v. 566, n. 1-2, p. 54-60, Dec 1991. ISSN 0006-8993. Disponível em: < https://www.ncbi.nlm.nih.gov/pubmed/1726065 >.

BERTOLOTTI, A. et al. hTAF(II)68, a novel RNA/ssDNA-binding protein with homology to the pro-oncoproteins TLS/FUS and EWS is associated with both TFIID and RNA polymerase II. **EMBO J,** v. 15, n. 18, p. 5022-31, Sep 1996. ISSN 0261-4189. Disponível em: < https://www.ncbi.nlm.nih.gov/pubmed/8890175 >.

BHATTACHARYA, A. et al. Neuronal cells but not muscle cells are resistant to oxidative stress mediated protein misfolding and cell death: role of molecular chaperones. **Biochem Biophys Res Commun,** v. 446, n. 4, p. 1250-4, Apr 2014. ISSN 1090-2104. Disponível em: < https://www.ncbi.nlm.nih.gov/pubmed/24685484 >.

BOILLÉE, S.; VANDE VELDE, C.; CLEVELAND, D. W. ALS: a disease of motor neurons and their nonneuronal neighbors. **Neuron,** v. 52, n. 1, p. 39-59, Oct 2006. ISSN 0896-6273. Disponível em: < https://www.ncbi.nlm.nih.gov/pubmed/17015226 >.

BOSCO, D. A.; LANDERS, J. E. Genetic determinants of amyotrophic lateral sclerosis as therapeutic targets. **CNS Neurol Disord Drug Targets,** v. 9, n. 6, p. 779-90, Dec 2010. ISSN 1996-3181. Disponível em: < https://www.ncbi.nlm.nih.gov/pubmed/20942785 >.

BOSKOVIC, Z. et al. Cholinergic basal forebrain neurons regulate fear extinction consolidation through p75 neurotrophin receptor signaling. **Transl Psychiatry,** v. 8, n. 1, p. 199, 09 2018. ISSN 2158-3188. Disponível em: < https://www.ncbi.nlm.nih.gov/pubmed/30242146 >.

BOTHWELL, M. Recent advances in understanding neurotrophin signaling. **F1000Res,** v. 5, 2016. ISSN 2046-1402. Disponível em: < https://www.ncbi.nlm.nih.gov/pubmed/27540475 >.

BOUTELOUP, C. et al. Hypermetabolism in ALS patients: an early and persistent phenomenon. **J Neurol,** v. 256, n. 8, p. 1236-42, Aug 2009. ISSN 1432-1459. Disponível em: < https://www.ncbi.nlm.nih.gov/pubmed/19306035 >.

BOWEN, D. M. et al. Imbalance of a serotonergic system in frontotemporal dementia: implication for pharmacotherapy. **Psychopharmacology (Berl),** v. 196, n. 4, p. 603-10, Mar 2008. ISSN 0033-3158. Disponível em: < https://www.ncbi.nlm.nih.gov/pubmed/18026720 >.

BOXER, A. L. et al. Memantine in patients with frontotemporal lobar degeneration: a multicentre, randomised, double-blind, placebo-controlled trial. **Lancet Neurol,** v. 12, n. 2, p. 149-56, Feb 2013. ISSN 1474-4465. Disponível em: < https://www.ncbi.nlm.nih.gov/pubmed/23290598 >.

BOXER, A. L. et al. An open-label study of memantine treatment in 3 subtypes of frontotemporal lobar degeneration. **Alzheimer Dis Assoc Disord,** v. 23, n. 3, p. 211-7, 2009 Jul-Sep 2009. ISSN 1546-4156. Disponível em: < https://www.ncbi.nlm.nih.gov/pubmed/19812461 >.

BRAAK, H. et al. Amyotrophic lateral sclerosis--a model of corticofugal axonal spread. **Nat Rev Neurol,** v. 9, n. 12, p. 708-14, 12 2013. ISSN 1759-4766. Disponível em: < https://www.ncbi.nlm.nih.gov/pubmed/24217521 >.

BRAMBILLA, L. et al. Disruption of the astrocytic TNFR1-GDNF axis accelerates motor neuron degeneration and disease progression in amyotrophic lateral sclerosis. **Hum Mol Genet,** v. 25, n. 14, p. 3080-3095, 07 2016. ISSN 1460-2083. Disponível em: < https://www.ncbi.nlm.nih.gov/pubmed/27288458 >.

BRENNER, D. et al. Hot-spot KIF5A mutations cause familial ALS. **Brain,** v. 141, n. 3, p. 688-697, 03 2018. ISSN 1460-2156. Disponível em: < https://www.ncbi.nlm.nih.gov/pubmed/29342275 >.

BROOKS, B. R. The role of axonal transport in neurodegenerative disease spread: a meta-analysis of experimental and clinical poliomyelitis compares with amyotrophic lateral sclerosis. **Can J Neurol Sci,** v. 18, n. 3 Suppl, p. 435-8, Aug 1991. ISSN 0317-1671. Disponível em: < https://www.ncbi.nlm.nih.gov/pubmed/1718581 >.

BROOKS, B. R. El Escorial World Federation of Neurology criteria for the diagnosis of amyotrophic lateral sclerosis. Subcommittee on Motor Neuron Diseases/Amyotrophic Lateral Sclerosis of the World Federation of Neurology Research Group on Neuromuscular Diseases and the El Escorial "Clinical limits of amyotrophic lateral sclerosis" workshop contributors. **J Neurol Sci,** v. 124 Suppl, p. 96-107, Jul 1994. ISSN 0022-510X. Disponível em: < https://www.ncbi.nlm.nih.gov/pubmed/7807156 >.

BROOKS, B. R. et al. El Escorial revisited: revised criteria for the diagnosis of amyotrophic lateral sclerosis. **Amyotroph Lateral Scler Other Motor Neuron Disord,** v. 1, n. 5, p. 293-9, Dec 2000. ISSN 1466-0822. Disponível em: < https://www.ncbi.nlm.nih.gov/pubmed/11464847 >.

BRUIJN, L. I. et al. ALS-linked SOD1 mutant G85R mediates damage to astrocytes and promotes rapidly progressive disease with SOD1-containing inclusions. **Neuron,** v. 18, n. 2, p. 327-38, Feb 1997. ISSN 0896-6273. Disponível em: < https://www.ncbi.nlm.nih.gov/pubmed/9052802 >.

BRUN, A.; LIU, X.; ERIKSON, C. Synapse loss and gliosis in the molecular layer of the cerebral cortex in Alzheimer's disease and in frontal lobe degeneration. **Neurodegeneration,** v. 4, n. 2, p. 171-7, Jun 1995. ISSN 1055-8330. Disponível em: < https://www.ncbi.nlm.nih.gov/pubmed/7583681 >.

BUCCAFUSCO, J. J. et al. Profile of nicotinic acetylcholine receptor agonists ABT-594 and A-582941, with differential subtype selectivity, on delayed matching accuracy by young monkeys. **Biochem Pharmacol,** v. 74, n. 8, p. 1202-11, Oct 2007. ISSN 0006-2952. Disponível em: < https://www.ncbi.nlm.nih.gov/pubmed/17706609 >.

BUCHAN, J. R. et al. Eukaryotic stress granules are cleared by autophagy and Cdc48/VCP function. **Cell,** v. 153, n. 7, p. 1461-74, Jun 2013. ISSN 1097-4172. Disponível em: < https://www.ncbi.nlm.nih.gov/pubmed/23791177 >.

BURATTI, E.; BARALLE, F. E. Multiple roles of TDP-43 in gene expression, splicing regulation, and human disease. **Front Biosci,** v. 13, p. 867-78, Jan 2008. ISSN 1093-9946. Disponível em: < https://www.ncbi.nlm.nih.gov/pubmed/17981595 >.

BURD, C. G.; DREYFUSS, G. Conserved structures and diversity of functions of RNA-binding proteins. **Science,** v. 265, n. 5172, p. 615-21, Jul 1994. ISSN 0036-8075. Disponível em: < https://www.ncbi.nlm.nih.gov/pubmed/8036511 >.

BURDA, J. E.; BERNSTEIN, A. M.; SOFRONIEW, M. V. Astrocyte roles in traumatic brain injury. **Exp Neurol,** v. 275 Pt 3, p. 305-315, Jan 2016. ISSN 1090-2430. Disponível em: < https://www.ncbi.nlm.nih.gov/pubmed/25828533 >.

BURKE, D.; SKUSE, N. F.; LETHLEAN, A. K. Cutaneous and muscle afferent components of the cerebral potential evoked by electrical stimulation of human peripheral nerves. **Electroencephalogr Clin Neurophysiol,** v. 51, n. 6, p. 579-88, Jun 1981. ISSN 0013-4694. Disponível em: < https://www.ncbi.nlm.nih.gov/pubmed/6165559 >.

BURKE, K. A. et al. Residue-by-Residue View of In Vitro FUS Granules that Bind the C-Terminal Domain of RNA Polymerase II. **Mol Cell,** v. 60, n. 2, p. 231-41, Oct 2015. ISSN 1097-4164. Disponível em: < https://www.ncbi.nlm.nih.gov/pubmed/26455390 >.

BUTOVSKY, O. et al. Targeting miR-155 restores abnormal microglia and attenuates disease in SOD1 mice. **Ann Neurol,** v. 77, n. 1, p. 75-99, Jan 2015. ISSN 1531-8249. Disponível em: < https://www.ncbi.nlm.nih.gov/pubmed/25381879 >.

BUTOVSKY, O. et al. Identification of a unique TGF-β-dependent molecular and functional signature in microglia. **Nat Neurosci,** v. 17, n. 1, p. 131-43, Jan 2014. ISSN 1546-1726. Disponível em: < https://www.ncbi.nlm.nih.gov/pubmed/24316888 >.

BUTOVSKY, O.; WEINER, H. L. Microglial signatures and their role in health and disease. **Nat Rev Neurosci,** v. 19, n. 10, p. 622-635, Oct 2018. ISSN 1471-0048. Disponível em: < https://www.ncbi.nlm.nih.gov/pubmed/30206328 >.

BYRNE, S. et al. Cognitive and clinical characteristics of patients with amyotrophic lateral sclerosis carrying a C9orf72 repeat expansion: a population-based cohort study. **Lancet Neurol,** v. 11, n. 3, p. 232-40, Mar 2012. ISSN 1474-4465. Disponível em: < https://www.ncbi.nlm.nih.gov/pubmed/22305801 >.

BÄUMER, D. et al. Juvenile ALS with basophilic inclusions is a FUS proteinopathy with FUS mutations. **Neurology,** v. 75, n. 7, p. 611-8, Aug 2010. ISSN 1526-632X. Disponível em: < https://www.ncbi.nlm.nih.gov/pubmed/20668261 >.

CADY, J. et al. TREM2 variant p.R47H as a risk factor for sporadic amyotrophic lateral sclerosis. **JAMA Neurol,** v. 71, n. 4, p. 449-53, Apr 2014. ISSN 2168-6157. Disponível em: < https://www.ncbi.nlm.nih.gov/pubmed/24535663 >.

CAMPANARI, M. L. et al. Neuromuscular Junction Impairment in Amyotrophic Lateral Sclerosis: Reassessing the Role of Acetylcholinesterase. **Front Mol Neurosci,** v. 9, p. 160, 2016. ISSN 1662-5099. Disponível em: < https://www.ncbi.nlm.nih.gov/pubmed/28082868 >.

CAPPELLO, V. et al. Analysis of neuromuscular junctions and effects of anabolic steroid administration in the SOD1G93A mouse model of ALS. **Mol Cell Neurosci,** v. 51, n. 1-2, p. 12-21, Aug 2012. ISSN 1095-9327. Disponível em: < https://www.ncbi.nlm.nih.gov/pubmed/22800606 >.

CAREW, J. D. et al. Presymptomatic spinal cord neurometabolic findings in SOD1-positive people at risk for familial ALS. **Neurology,** v. 77, n. 14, p. 1370-5, Oct 2011. ISSN 1526-632X. Disponível em: < https://www.ncbi.nlm.nih.gov/pubmed/21940617 >.

CASSINA, P. et al. Mitochondrial dysfunction in SOD1G93A-bearing astrocytes promotes motor neuron degeneration: prevention by mitochondrial-targeted antioxidants. **J Neurosci,** v. 28, n. 16, p. 4115-22, Apr 2008. ISSN 1529-2401. Disponível em: < https://www.ncbi.nlm.nih.gov/pubmed/18417691 >.

CASTELLANO, J. M. et al. Human apoE isoforms differentially regulate brain amyloid-β peptide clearance. **Sci Transl Med,** v. 3, n. 89, p. 89ra57, Jun 2011. ISSN 1946-6242. Disponível em: < https://www.ncbi.nlm.nih.gov/pubmed/21715678 >.

CEDARBAUM, J. M. et al. The ALSFRS-R: a revised ALS functional rating scale that incorporates assessments of respiratory function. BDNF ALS Study Group (Phase III). **J Neurol Sci,** v. 169, n. 1-2, p. 13-21, Oct 1999. ISSN 0022-510X. Disponível em: < https://www.ncbi.nlm.nih.gov/pubmed/10540002 >.

CERAMI, C. et al. The Role of Single-Subject Brain Metabolic Patterns in the Early Differential Diagnosis of Primary Progressive Aphasias and in Prediction of Progression to Dementia. **J Alzheimers Dis,** v. 55, n. 1, p. 183-197, 2017. ISSN 1875-8908. Disponível em: < https://www.ncbi.nlm.nih.gov/pubmed/27662315 >.

CHANDRAN, J.; DING, J.; CAI, H. Alsin and the molecular pathways of amyotrophic lateral sclerosis. **Mol Neurobiol,** v. 36, n. 3, p. 224-31, Dec 2007. ISSN 0893-7648. Disponível em: < https://www.ncbi.nlm.nih.gov/pubmed/17955197 >.

CHANG, L.; MONTEIRO, M. J. Defective Proteasome Delivery of Polyubiquitinated Proteins by Ubiquilin-2 Proteins Containing ALS Mutations. **PLoS One,** v. 10, n. 6, p. e0130162, 2015. ISSN 1932-6203. Disponível em: < https://www.ncbi.nlm.nih.gov/pubmed/26075709 >.

CHANG, Q.; MARTIN, L. J. Glycinergic innervation of motoneurons is deficient in amyotrophic lateral sclerosis mice: a quantitative confocal analysis. **Am J Pathol,** v. 174, n. 2, p. 574-85, Feb 2009. ISSN 1525-2191. Disponível em: < https://www.ncbi.nlm.nih.gov/pubmed/19116365 >.

CHEN, C. et al. Fused in Sarcoma: Properties, Self-Assembly and Correlation with Neurodegenerative Diseases. **Molecules,** v. 24, n. 8, Apr 2019. ISSN 1420-3049. Disponível em: < https://www.ncbi.nlm.nih.gov/pubmed/31022909 >.

CHEN, X. et al. Saccharomyces cerevisiae Sen1 as a model for the study of mutations in human Senataxin that elicit cerebellar ataxia. **Genetics,** v. 198, n. 2, p. 577-90, Oct 2014. ISSN 1943-2631. Disponível em: < https://www.ncbi.nlm.nih.gov/pubmed/25116135 >.

CHEN, X. Q.; MOBLEY, W. C. Exploring the Pathogenesis of Alzheimer Disease in Basal Forebrain Cholinergic Neurons: Converging Insights From Alternative Hypotheses. **Front Neurosci,** v. 13, p. 446, 2019. ISSN 1662-4548. Disponível em: < https://www.ncbi.nlm.nih.gov/pubmed/31133787 >.

CHENG, A. J. et al. Intact single muscle fibres from SOD1. **J Physiol,** v. 597, n. 12, p. 3133-3146, Jun 2019. ISSN 1469-7793. Disponível em: < https://www.ncbi.nlm.nih.gov/pubmed/31074054 >.

CHENG, S. T. et al. Mental and physical activities delay cognitive decline in older persons with dementia. **Am J Geriatr Psychiatry,** v. 22, n. 1, p. 63-74, Jan 2014. ISSN 1545-7214. Disponível em: < https://www.ncbi.nlm.nih.gov/pubmed/23582750 >.

CHERRY, J. D.; OLSCHOWKA, J. A.; O'BANION, M. K. Neuroinflammation and M2 microglia: the good, the bad, and the inflamed. **J Neuroinflammation,** v. 11, p. 98, Jun 2014. ISSN 1742-2094. Disponível em: < https://www.ncbi.nlm.nih.gov/pubmed/24889886 >.

CHIRIBOGA, C. A. et al. Results from a phase 1 study of nusinersen (ISIS-SMN(Rx)) in children with spinal muscular atrophy. **Neurology,** v. 86, n. 10, p. 890-7, Mar 2016. ISSN 1526-632X. Disponível em: < https://www.ncbi.nlm.nih.gov/pubmed/26865511 >.

CHITIPROLU, M. et al. A complex of C9ORF72 and p62 uses arginine methylation to eliminate stress granules by autophagy. **Nat Commun,** v. 9, n. 1, p. 2794, 07 2018. ISSN 2041-1723. Disponível em: < https://www.ncbi.nlm.nih.gov/pubmed/30022074 >.

CHIU, A. Y. et al. Age-dependent penetrance of disease in a transgenic mouse model of familial amyotrophic lateral sclerosis. **Mol Cell Neurosci,** v. 6, n. 4, p. 349-62, Aug 1995. ISSN 1044-7431. Disponível em: < https://www.ncbi.nlm.nih.gov/pubmed/8846004 >.

CHIÒ, A. et al. Lower serum lipid levels are related to respiratory impairment in patients with ALS. **Neurology,** v. 73, n. 20, p. 1681-5, Nov 2009. ISSN 1526-632X. Disponível em: < https://www.ncbi.nlm.nih.gov/pubmed/19917991 >.

CHIÒ, A. et al. Phenotypic heterogeneity of amyotrophic lateral sclerosis: a population based study. **J Neurol Neurosurg Psychiatry,** v. 82, n. 7, p. 740-6, Jul 2011. ISSN 1468-330X. Disponível em: < https://www.ncbi.nlm.nih.gov/pubmed/21402743 >.

CHOW, T. W.; MENDEZ, M. F. Goals in symptomatic pharmacologic management of frontotemporal lobar degeneration. **Am J Alzheimers Dis Other Demen,** v. 17, n. 5, p. 267-72, 2002 Sep-Oct 2002. ISSN 1533-3175. Disponível em: < https://www.ncbi.nlm.nih.gov/pubmed/12392261 >.

CHRISTIDI, F. et al. The Clinical and Radiological Spectrum of Hippocampal Pathology in Amyotrophic Lateral Sclerosis. **Front Neurol,** v. 9, p. 523, 2018. ISSN 1664-2295. Disponível em: < https://www.ncbi.nlm.nih.gov/pubmed/30018591 >.

CIRULLI, E. T. et al. Exome sequencing in amyotrophic lateral sclerosis identifies risk genes and pathways. **Science,** v. 347, n. 6229, p. 1436-41, Mar 2015. ISSN 1095-9203. Disponível em: < https://www.ncbi.nlm.nih.gov/pubmed/25700176 >.

CLARE, R. et al. Synapse loss in dementias. **J Neurosci Res,** v. 88, n. 10, p. 2083-90, Aug 2010. ISSN 1097-4547. Disponível em: < https://www.ncbi.nlm.nih.gov/pubmed/20533377 >.

CLARK, J. A. et al. Axonal degeneration, distal collateral branching and neuromuscular junction architecture alterations occur prior to symptom onset in the SOD1(G93A) mouse model of amyotrophic lateral sclerosis. **J Chem Neuroanat,** v. 76, n. Pt A, p. 35-47, 10 2016. ISSN 1873-6300. Disponível em: < https://www.ncbi.nlm.nih.gov/pubmed/27038603 >.

CLARK, R. M. et al. Calretinin and Neuropeptide Y interneurons are differentially altered in the motor cortex of the SOD1. **Sci Rep,** v. 7, p. 44461, 03 2017. ISSN 2045-2322. Disponível em: < https://www.ncbi.nlm.nih.gov/pubmed/28294153 >.

CLARK, R. M. et al. Reduced Excitability and Increased Neurite Complexity of Cortical Interneurons in a Familial Mouse Model of Amyotrophic Lateral Sclerosis. **Front Cell Neurosci,** v. 12, p. 328, 2018. ISSN 1662-5102. Disponível em: < https://www.ncbi.nlm.nih.gov/pubmed/30323744 >.

CLAYTON, E. L. et al. Early microgliosis precedes neuronal loss and behavioural impairment in mice with a frontotemporal dementia-causing CHMP2B mutation. **Hum Mol Genet,** v. 26, n. 5, p. 873-887, 03 2017. ISSN 1460-2083. Disponível em: < https://www.ncbi.nlm.nih.gov/pubmed/28093491 >.

CLAYTON, E. L. et al. Frontotemporal dementia caused by CHMP2B mutation is characterised by neuronal lysosomal storage pathology. **Acta Neuropathol,** v. 130, n. 4, p. 511-23, Oct 2015. ISSN 1432-0533. Disponível em: < https://www.ncbi.nlm.nih.gov/pubmed/26358247 >.

CLÉMENT, J. F.; MELOCHE, S.; SERVANT, M. J. The IKK-related kinases: from innate immunity to oncogenesis. **Cell Res,** v. 18, n. 9, p. 889-99, Sep 2008. ISSN 1001-0602. Disponível em: < https://www.ncbi.nlm.nih.gov/pubmed/19160540 >.

COHEN-ADAD, J. et al. Involvement of spinal sensory pathway in ALS and specificity of cord atrophy to lower motor neuron degeneration. **Amyotroph Lateral Scler Frontotemporal Degener,** v. 14, n. 1, p. 30-8, Jan 2013. ISSN 2167-9223. Disponível em: < https://www.ncbi.nlm.nih.gov/pubmed/22881412 >.

COHEN-ADAD, J. et al. 7-T MRI of the spinal cord can detect lateral corticospinal tract abnormality in amyotrophic lateral sclerosis. **Muscle Nerve,** v. 47, n. 5, p. 760-2, May 2013. ISSN 1097-4598. Disponível em: < https://www.ncbi.nlm.nih.gov/pubmed/23553571 >.

COLOMBRITA, C. et al. TDP-43 and FUS RNA-binding proteins bind distinct sets of cytoplasmic messenger RNAs and differently regulate their post-transcriptional fate in motoneuron-like cells. **J Biol Chem,** v. 287, n. 19, p. 15635-47, May 2012. ISSN 1083-351X. Disponível em: < https://www.ncbi.nlm.nih.gov/pubmed/22427648 >.

COLONNA, M.; WANG, Y. TREM2 variants: new keys to decipher Alzheimer disease pathogenesis. **Nat Rev Neurosci,** v. 17, n. 4, p. 201-7, Apr 2016. ISSN 1471-0048. Disponível em: < https://www.ncbi.nlm.nih.gov/pubmed/26911435 >.

COMBS, B.; GAMBLIN, T. C. FTDP-17 tau mutations induce distinct effects on aggregation and microtubule interactions. **Biochemistry,** v. 51, n. 43, p. 8597-607, Oct 2012. ISSN 1520-4995. Disponível em: < https://www.ncbi.nlm.nih.gov/pubmed/23043292 >.

COMMITTEE, D. W.; COLLABORATORS, D. S. G. Safety and efficacy of diaphragm pacing in patients with respiratory insufficiency due to amyotrophic lateral sclerosis (DiPALS): a multicentre, open-label, randomised controlled trial. **Lancet Neurol,** v. 14, n. 9, p. 883-892, 09 2015. ISSN 1474-4465. Disponível em: < https://www.ncbi.nlm.nih.gov/pubmed/26234554 >.

CONICELLA, A. E. et al. ALS Mutations Disrupt Phase Separation Mediated by α-Helical Structure in the TDP-43 Low-Complexity C-Terminal Domain. **Structure,** v. 24, n. 9, p. 1537-49, 09 2016. ISSN 1878-4186. Disponível em: < https://www.ncbi.nlm.nih.gov/pubmed/27545621 >.

COOPER-KNOCK, J. et al. Clinico-pathological features in amyotrophic lateral sclerosis with expansions in C9ORF72. **Brain,** v. 135, n. Pt 3, p. 751-64, Mar 2012. ISSN 1460-2156. Disponível em: < https://www.ncbi.nlm.nih.gov/pubmed/22366792 >.

COOPER-KNOCK, J. et al. The Spectrum of C9orf72-mediated Neurodegeneration and Amyotrophic Lateral Sclerosis. **Neurotherapeutics,** v. 12, n. 2, p. 326-39, Apr 2015. ISSN 1878-7479. Disponível em: < https://www.ncbi.nlm.nih.gov/pubmed/25731823 >.

CORCIA, P. et al. Staging amyotrophic lateral sclerosis: A new focus on progression. **Rev Neurol (Paris),** v. 175, n. 5, p. 277-282, May 2019. ISSN 0035-3787. Disponível em: < https://www.ncbi.nlm.nih.gov/pubmed/30606512 >.

COSOTTINI, M. et al. Structural and functional evaluation of cortical motor areas in Amyotrophic Lateral Sclerosis. **Exp Neurol,** v. 234, n. 1, p. 169-80, Mar 2012. ISSN 1090-2430. Disponível em: < https://www.ncbi.nlm.nih.gov/pubmed/22226599 >.

COURATIER, P. et al. Epidemiology of amyotrophic lateral sclerosis: A review of literature. **Rev Neurol (Paris),** v. 172, n. 1, p. 37-45, Jan 2016. ISSN 0035-3787. Disponível em: < https://www.ncbi.nlm.nih.gov/pubmed/26727307 >.

COUTHOUIS, J. et al. Evaluating the role of the FUS/TLS-related gene EWSR1 in amyotrophic lateral sclerosis. **Hum Mol Genet,** v. 21, n. 13, p. 2899-911, Jul 2012. ISSN 1460-2083. Disponível em: < https://www.ncbi.nlm.nih.gov/pubmed/22454397 >.

COX, L. E. et al. Mutations in CHMP2B in lower motor neuron predominant amyotrophic lateral sclerosis (ALS). **PLoS One,** v. 5, n. 3, p. e9872, Mar 2010. ISSN 1932-6203. Disponível em: < https://www.ncbi.nlm.nih.gov/pubmed/20352044 >.

CROCHEMORE, C. et al. Disease-related regressive alterations of forebrain cholinergic system in SOD1 mutant transgenic mice. **Neurochem Int,** v. 46, n. 5, p. 357-68, Apr 2005. ISSN 0197-0186. Disponível em: < https://www.ncbi.nlm.nih.gov/pubmed/15737434 >.

CRUTS, M. et al. Null mutations in progranulin cause ubiquitin-positive frontotemporal dementia linked to chromosome 17q21. **Nature,** v. 442, n. 7105, p. 920-4, Aug 2006. ISSN 1476-4687. Disponível em: < https://www.ncbi.nlm.nih.gov/pubmed/16862115 >.

CRUTS, M.; VAN BROECKHOVEN, C. Loss of progranulin function in frontotemporal lobar degeneration. **Trends Genet,** v. 24, n. 4, p. 186-94, Apr 2008. ISSN 0168-9525. Disponível em: < https://www.ncbi.nlm.nih.gov/pubmed/18328591 >.

CUDKOWICZ, M. E. et al. Epidemiology of mutations in superoxide dismutase in amyotrophic lateral sclerosis. **Ann Neurol,** v. 41, n. 2, p. 210-21, Feb 1997. ISSN 0364-5134. Disponível em: < https://www.ncbi.nlm.nih.gov/pubmed/9029070 >.

CUSHMAN, M. et al. Prion-like disorders: blurring the divide between transmissibility and infectivity. **J Cell Sci,** v. 123, n. Pt 8, p. 1191-201, Apr 2010. ISSN 1477-9137. Disponível em: < https://www.ncbi.nlm.nih.gov/pubmed/20356930 >.

DADON-NACHUM, M.; MELAMED, E.; OFFEN, D. The "dying-back" phenomenon of motor neurons in ALS. **J Mol Neurosci,** v. 43, n. 3, p. 470-7, Mar 2011. ISSN 1559-1166. Disponível em: < https://www.ncbi.nlm.nih.gov/pubmed/21057983 >.

DAU, A. et al. RIC-3 differentially modulates α4β2 and α7 nicotinic receptor assembly, expression, and nicotine-induced receptor upregulation. **BMC Neurosci,** v. 14, p. 47, Apr 2013. ISSN 1471-2202. Disponível em: < https://www.ncbi.nlm.nih.gov/pubmed/23586521 >.

DE ALBUQUERQUE, M. et al. Longitudinal evaluation of cerebral and spinal cord damage in Amyotrophic Lateral Sclerosis. **Neuroimage Clin,** v. 14, p. 269-276, 2017. ISSN 2213-1582. Disponível em: < https://www.ncbi.nlm.nih.gov/pubmed/28203530 >.

DE BELLIS, A.; DE BELLIS, M.; ALOE, L. Long-Term Non-Invasive Treatment via Intranasal Administration of Nerve Growth Factor Protects the Human Brain in Frontotemporal Dementia associated with Corticobasal Syndrome: A Pilot Study. **J Alzheimers Dis Rep,** v. 2, n. 1, p. 67-77, Mar 2018. ISSN 2542-4823. Disponível em: < https://www.ncbi.nlm.nih.gov/pubmed/30480250 >.

DEAKIN, J. B. et al. Paroxetine does not improve symptoms and impairs cognition in frontotemporal dementia: a double-blind randomized controlled trial. **Psychopharmacology (Berl),** v. 172, n. 4, p. 400-8, Apr 2004. ISSN 0033-3158. Disponível em: < https://www.ncbi.nlm.nih.gov/pubmed/14666399 >.

DEAN, C. et al. Neurexin mediates the assembly of presynaptic terminals. **Nat Neurosci,** v. 6, n. 7, p. 708-16, Jul 2003. ISSN 1097-6256. Disponível em: < https://www.ncbi.nlm.nih.gov/pubmed/12796785 >.

DEJESUS-HERNANDEZ, M. et al. De novo truncating FUS gene mutation as a cause of sporadic amyotrophic lateral sclerosis. **Hum Mutat,** v. 31, n. 5, p. E1377-89, May 2010. ISSN 1098-1004. Disponível em: < https://www.ncbi.nlm.nih.gov/pubmed/20232451 >.

DEJESUS-HERNANDEZ, M. et al. Expanded GGGGCC hexanucleotide repeat in noncoding region of C9ORF72 causes chromosome 9p-linked FTD and ALS. **Neuron,** v. 72, n. 2, p. 245-56, Oct 2011. ISSN 1097-4199. Disponível em: < https://www.ncbi.nlm.nih.gov/pubmed/21944778 >.

DENG, Q. et al. FUS is phosphorylated by DNA-PK and accumulates in the cytoplasm after DNA damage. **J Neurosci,** v. 34, n. 23, p. 7802-13, Jun 2014. ISSN 1529-2401. Disponível em: < https://www.ncbi.nlm.nih.gov/pubmed/24899704 >.

DENTEL, C. et al. Degeneration of serotonergic neurons in amyotrophic lateral sclerosis: a link to spasticity. **Brain,** v. 136, n. Pt 2, p. 483-93, Feb 2013. ISSN 1460-2156. Disponível em: < https://www.ncbi.nlm.nih.gov/pubmed/23114367 >.

DERVISHI, I.; OZDINLER, P. H. Incorporating upper motor neuron health in ALS drug discovery. **Drug Discov Today,** v. 23, n. 3, p. 696-703, Mar 2018. ISSN 1878-5832. Disponível em: < https://www.ncbi.nlm.nih.gov/pubmed/29331501 >.

DESHPANDE, D. et al. Synaptic FUS Localization During Motoneuron Development and Its Accumulation in Human ALS Synapses. **Front Cell Neurosci,** v. 13, p. 256, 2019. ISSN 1662-5102. Disponível em: < https://www.ncbi.nlm.nih.gov/pubmed/31244613 >.

DESPORT, J. C.; COURATIER, P.; PREUX, P. M. What can we do for ALS patients with low vital capacity needing a digestive access for enteral nutrition? **Clin Nutr,** v. 25, n. 4, p. 705, Aug 2006. ISSN 0261-5614. Disponível em: < https://www.ncbi.nlm.nih.gov/pubmed/16769158 >.

DEVINE, M. S. et al. Exposing asymmetric gray matter vulnerability in amyotrophic lateral sclerosis. **Neuroimage Clin,** v. 7, p. 782-7, 2015. ISSN 2213-1582. Disponível em: < https://www.ncbi.nlm.nih.gov/pubmed/25844330 >.

DEVOY, A. et al. Humanized mutant FUS drives progressive motor neuron degeneration without aggregation in 'FUSDelta14' knockin mice. **Brain,** v. 140, n. 11, p. 2797-2805, Nov 2017. ISSN 1460-2156. Disponível em: < https://www.ncbi.nlm.nih.gov/pubmed/29053787 >.

DIAPER, D. C. et al. Drosophila TDP-43 dysfunction in glia and muscle cells cause cytological and behavioural phenotypes that characterize ALS and FTLD. **Hum Mol Genet,** v. 22, n. 19, p. 3883-93, Oct 2013. ISSN 1460-2083. Disponível em: < https://www.ncbi.nlm.nih.gov/pubmed/23727833 >.

DINI MODIGLIANI, S. et al. An ALS-associated mutation in the FUS 3'-UTR disrupts a microRNA-FUS regulatory circuitry. **Nat Commun,** v. 5, p. 4335, Jul 2014. ISSN 2041-1723. Disponível em: < https://www.ncbi.nlm.nih.gov/pubmed/25004804 >.

DOBROWOLNY, G.; AUCELLO, M.; MUSARÒ, A. Muscle atrophy induced by SOD1G93A expression does not involve the activation of caspase in the absence of denervation. **Skelet Muscle,** v. 1, n. 1, p. 3, Jan 2011. ISSN 2044-5040. Disponível em: < https://www.ncbi.nlm.nih.gov/pubmed/21798081 >.

DOI, H. et al. The RNA-binding protein FUS/TLS is a common aggregate-interacting protein in polyglutamine diseases. **Neurosci Res,** v. 66, n. 1, p. 131-3, Jan 2010. ISSN 1872-8111. Disponível em: < https://www.ncbi.nlm.nih.gov/pubmed/19833157 >.

DORMANN, D.; HAASS, C. TDP-43 and FUS: a nuclear affair. **Trends Neurosci,** v. 34, n. 7, p. 339-48, Jul 2011. ISSN 1878-108X. Disponível em: < https://www.ncbi.nlm.nih.gov/pubmed/21700347 >.

DORMANN, D. et al. Arginine methylation next to the PY-NLS modulates Transportin binding and nuclear import of FUS. **EMBO J,** v. 31, n. 22, p. 4258-75, Nov 2012. ISSN 1460-2075. Disponível em: < https://www.ncbi.nlm.nih.gov/pubmed/22968170 >.

DORMANN, D. et al. ALS-associated fused in sarcoma (FUS) mutations disrupt Transportin-mediated nuclear import. **EMBO J,** v. 29, n. 16, p. 2841-57, Aug 2010. ISSN 1460-2075. Disponível em: < https://www.ncbi.nlm.nih.gov/pubmed/20606625 >.

DORST, J.; CYPIONKA, J.; LUDOLPH, A. C. High-caloric food supplements in the treatment of amyotrophic lateral sclerosis: a prospective interventional study. **Amyotroph Lateral Scler Frontotemporal Degener,** v. 14, n. 7-8, p. 533-6, Dec 2013. ISSN 2167-9223. Disponível em: < https://www.ncbi.nlm.nih.gov/pubmed/23944684 >.

DORST, J. et al. Patients with elevated triglyceride and cholesterol serum levels have a prolonged survival in amyotrophic lateral sclerosis. **J Neurol,** v. 258, n. 4, p. 613-7, Apr 2011. ISSN 1432-1459. Disponível em: < https://www.ncbi.nlm.nih.gov/pubmed/21128082 >.

DORST, J.; LUDOLPH, A. C.; HUEBERS, A. Disease-modifying and symptomatic treatment of amyotrophic lateral sclerosis. **Ther Adv Neurol Disord,** v. 11, p. 1756285617734734, 2018. ISSN 1756-2856. Disponível em: < https://www.ncbi.nlm.nih.gov/pubmed/29399045 >.

DU, K. et al. TLS and PRMT1 synergistically coactivate transcription at the survivin promoter through TLS arginine methylation. **Biochem Biophys Res Commun,** v. 404, n. 4, p. 991-6, Jan 2011. ISSN 1090-2104. Disponível em: < https://www.ncbi.nlm.nih.gov/pubmed/21187067 >.

DUPUIS, L. et al. Dyslipidemia is a protective factor in amyotrophic lateral sclerosis. **Neurology,** v. 70, n. 13, p. 1004-9, Mar 2008. ISSN 1526-632X. Disponível em: < https://www.ncbi.nlm.nih.gov/pubmed/18199832 >.

DUPUIS, L. et al. Nogo provides a molecular marker for diagnosis of amyotrophic lateral sclerosis. **Neurobiol Dis,** v. 10, n. 3, p. 358-65, Aug 2002. ISSN 0969-9961. Disponível em: < https://www.ncbi.nlm.nih.gov/pubmed/12270696 >.

DUPUIS, L. et al. Evidence for defective energy homeostasis in amyotrophic lateral sclerosis: benefit of a high-energy diet in a transgenic mouse model. **Proc Natl Acad Sci U S A,** v. 101, n. 30, p. 11159-64, Jul 2004. ISSN 0027-8424. Disponível em: < https://www.ncbi.nlm.nih.gov/pubmed/15263088 >.

DUPUIS, L. et al. Energy metabolism in amyotrophic lateral sclerosis. **Lancet Neurol,** v. 10, n. 1, p. 75-82, Jan 2011. ISSN 1474-4465. Disponível em: < https://www.ncbi.nlm.nih.gov/pubmed/21035400 >.

DUPUIS, L. et al. Platelet serotonin level predicts survival in amyotrophic lateral sclerosis. **PLoS One,** v. 5, n. 10, p. e13346, Oct 2010. ISSN 1932-6203. Disponível em: < https://www.ncbi.nlm.nih.gov/pubmed/20967129 >.

DUREGOTTI, E. et al. Mitochondrial alarmins released by degenerating motor axon terminals activate perisynaptic Schwann cells. **Proc Natl Acad Sci U S A,** v. 112, n. 5, p. E497-505, Feb 2015. ISSN 1091-6490. Disponível em: < https://www.ncbi.nlm.nih.gov/pubmed/25605902 >.

DUTERTRE, M. et al. DNA damage: RNA-binding proteins protect from near and far. **Trends Biochem Sci,** v. 39, n. 3, p. 141-9, Mar 2014. ISSN 0968-0004. Disponível em: < https://www.ncbi.nlm.nih.gov/pubmed/24534650 >.

EDBAUER, D.; HAASS, C. An amyloid-like cascade hypothesis for C9orf72 ALS/FTD. **Curr Opin Neurobiol,** v. 36, p. 99-106, Feb 2016. ISSN 1873-6882. Disponível em: < https://www.ncbi.nlm.nih.gov/pubmed/26555807 >.

EDENS, B. M.; MILLER, N.; MA, Y. C. Impaired Autophagy and Defective Mitochondrial Function: Converging Paths on the Road to Motor Neuron Degeneration. **Front Cell Neurosci,** v. 10, p. 44, 2016. ISSN 1662-5102. Disponível em: < https://www.ncbi.nlm.nih.gov/pubmed/26973461 >.

EDERLE, H.; DORMANN, D. TDP-43 and FUS en route from the nucleus to the cytoplasm. **FEBS Lett,** v. 591, n. 11, p. 1489-1507, 06 2017. ISSN 1873-3468. Disponível em: < https://www.ncbi.nlm.nih.gov/pubmed/28380257 >.

EITAN, C.; HORNSTEIN, E. Vulnerability of microRNA biogenesis in FTD-ALS. **Brain Res,** v. 1647, p. 105-111, 09 2016. ISSN 1872-6240. Disponível em: < https://www.ncbi.nlm.nih.gov/pubmed/26778173 >.

EL MENDILI, M. M. et al. Multi-parametric spinal cord MRI as potential progression marker in amyotrophic lateral sclerosis. **PLoS One,** v. 9, n. 4, p. e95516, 2014. ISSN 1932-6203. Disponível em: < https://www.ncbi.nlm.nih.gov/pubmed/24755826 >.

EL OUSSINI, H. et al. Serotonin 2B receptor slows disease progression and prevents degeneration of spinal cord mononuclear phagocytes in amyotrophic lateral sclerosis. **Acta Neuropathol,** v. 131, n. 3, p. 465-80, Mar 2016. ISSN 1432-0533. Disponível em: < https://www.ncbi.nlm.nih.gov/pubmed/26744351 >.

EL OUSSINI, H. et al. Degeneration of serotonin neurons triggers spasticity in amyotrophic lateral sclerosis. **Ann Neurol,** v. 82, n. 3, p. 444-456, Sep 2017. ISSN 1531-8249. Disponível em: < https://www.ncbi.nlm.nih.gov/pubmed/28856708 >.

ERICKSON, S. L.; LYKKE-ANDERSEN, J. Cytoplasmic mRNP granules at a glance. **J Cell Sci,** v. 124, n. Pt 3, p. 293-7, Feb 2011. ISSN 1477-9137. Disponível em: < https://www.ncbi.nlm.nih.gov/pubmed/21242308 >.

ERKKINEN, M. G.; KIM, M. O.; GESCHWIND, M. D. Clinical Neurology and Epidemiology of the Major Neurodegenerative Diseases. **Cold Spring Harb Perspect Biol,** v. 10, n. 4, 04 2018. ISSN 1943-0264. Disponível em: < https://www.ncbi.nlm.nih.gov/pubmed/28716886 >.

EVERS, M. M.; TOONEN, L. J.; VAN ROON-MOM, W. M. Antisense oligonucleotides in therapy for neurodegenerative disorders. **Adv Drug Deliv Rev,** v. 87, p. 90-103, Jun 2015. ISSN 1872-8294. Disponível em: < https://www.ncbi.nlm.nih.gov/pubmed/25797014 >.

EYJOLFSDOTTIR, H. et al. Targeted delivery of nerve growth factor to the cholinergic basal forebrain of Alzheimer's disease patients: application of a second-generation encapsulated cell biodelivery device. **Alzheimers Res Ther,** v. 8, n. 1, p. 30, 07 2016. ISSN 1758-9193. Disponível em: < https://www.ncbi.nlm.nih.gov/pubmed/27389402 >.

FABBRINI, G. et al. Donepezil in the treatment of progressive supranuclear palsy. **Acta Neurol Scand,** v. 103, n. 2, p. 123-5, Feb 2001. ISSN 0001-6314. Disponível em: < https://www.ncbi.nlm.nih.gov/pubmed/11227131 >.

FAGAN, A. M. et al. A role for TrkA during maturation of striatal and basal forebrain cholinergic neurons in vivo. **J Neurosci,** v. 17, n. 20, p. 7644-54, Oct 1997. ISSN 0270-6474. Disponível em: < https://www.ncbi.nlm.nih.gov/pubmed/9315886 >.

FANG, T. et al. Stage at which riluzole treatment prolongs survival in patients with amyotrophic lateral sclerosis: a retrospective analysis of data from a dose-ranging study. **Lancet Neurol,** v. 17, n. 5, p. 416-422, 05 2018. ISSN 1474-4465. Disponível em: < https://www.ncbi.nlm.nih.gov/pubmed/29525492 >.

FARB, N. A. et al. Abnormal network connectivity in frontotemporal dementia: evidence for prefrontal isolation. **Cortex,** v. 49, n. 7, p. 1856-73, 2013 Jul-Aug 2013. ISSN 1973-8102. Disponível em: < https://www.ncbi.nlm.nih.gov/pubmed/23092697 >.

FARG, M. A. et al. C9ORF72, implicated in amytrophic lateral sclerosis and frontotemporal dementia, regulates endosomal trafficking. **Hum Mol Genet,** v. 23, n. 13, p. 3579-95, Jul 2014. ISSN 1460-2083. Disponível em: < https://www.ncbi.nlm.nih.gov/pubmed/24549040 >.

FERRER, I. Neurons and their dendrites in frontotemporal dementia. **Dement Geriatr Cogn Disord,** v. 10 Suppl 1, p. 55-60, 1999. ISSN 1420-8008. Disponível em: < https://www.ncbi.nlm.nih.gov/pubmed/10436342 >.

FERRI, A.; COCCURELLO, R. What is "Hyper" in the ALS Hypermetabolism? **Mediators Inflamm,** v. 2017, p. 7821672, 2017. ISSN 1466-1861. Disponível em: < https://www.ncbi.nlm.nih.gov/pubmed/29081604 >.

FIGUEIREDO, B. C. et al. NGF prevents further atrophy of cholinergic cells of the nucleus basalis due to cortical infarction in adult post-hypothyroid rats but does not restore cell size compared to euthyroid [correction of euthroid] rats. **J Chem Neuroanat,** v. 12, n. 1, p. 15-27, Nov 1996. ISSN 0891-0618. Disponível em: < https://www.ncbi.nlm.nih.gov/pubmed/9001945 >.

FIL, D. et al. Mutant Profilin1 transgenic mice recapitulate cardinal features of motor neuron disease. **Hum Mol Genet,** v. 26, n. 4, p. 686-701, 02 2017. ISSN 1460-2083. Disponível em: < https://www.ncbi.nlm.nih.gov/pubmed/28040732 >.

FILIPPI, M. et al. Functional network connectivity in the behavioral variant of frontotemporal dementia. **Cortex,** v. 49, n. 9, p. 2389-401, Oct 2013. ISSN 1973-8102. Disponível em: < https://www.ncbi.nlm.nih.gov/pubmed/23164495 >.

FILLINGHAM, J.; KEOGH, M. C.; KROGAN, N. J. GammaH2AX and its role in DNA double-strand break repair. **Biochem Cell Biol,** v. 84, n. 4, p. 568-77, Aug 2006. ISSN 0829-8211. Disponível em: < https://www.ncbi.nlm.nih.gov/pubmed/16936829 >.

FLOYD, A. G. et al. Transcranial magnetic stimulation in ALS: utility of central motor conduction tests. **Neurology,** v. 72, n. 6, p. 498-504, Feb 2009. ISSN 1526-632X. Disponível em: < https://www.ncbi.nlm.nih.gov/pubmed/19204259 >.

FOGARTY, M. J. et al. Cortical synaptic and dendritic spine abnormalities in a presymptomatic TDP-43 model of amyotrophic lateral sclerosis. **Sci Rep,** v. 6, p. 37968, 11 2016. ISSN 2045-2322. Disponível em: < https://www.ncbi.nlm.nih.gov/pubmed/27897242 >.

FOGARTY, M. J.; NOAKES, P. G.; BELLINGHAM, M. C. Motor cortex layer V pyramidal neurons exhibit dendritic regression, spine loss, and increased synaptic excitation in the presymptomatic hSOD1(G93A) mouse model of amyotrophic lateral sclerosis. **J Neurosci,** v. 35, n. 2, p. 643-7, Jan 2015. ISSN 1529-2401. Disponível em: < https://www.ncbi.nlm.nih.gov/pubmed/25589758 >.

FRANZMANN, T. M.; ALBERTI, S. Protein Phase Separation as a Stress Survival Strategy. **Cold Spring Harb Perspect Biol,** v. 11, n. 6, Jun 2019. ISSN 1943-0264. Disponível em: < https://www.ncbi.nlm.nih.gov/pubmed/30617047 >.

FRATTA, P. et al. Mice with endogenous TDP-43 mutations exhibit gain of splicing function and characteristics of amyotrophic lateral sclerosis. **EMBO J,** v. 37, n. 11, 06 2018. ISSN 1460-2075. Disponível em: < https://www.ncbi.nlm.nih.gov/pubmed/29764981 >.

FUENTEALBA, R. A. et al. Interaction with polyglutamine aggregates reveals a Q/N-rich domain in TDP-43. **J Biol Chem,** v. 285, n. 34, p. 26304-14, Aug 2010. ISSN 1083-351X. Disponível em: < https://www.ncbi.nlm.nih.gov/pubmed/20554523 >.

FUJII, R. et al. The RNA binding protein TLS is translocated to dendritic spines by mGluR5 activation and regulates spine morphology. **Curr Biol,** v. 15, n. 6, p. 587-93, Mar 2005. ISSN 0960-9822. Disponível em: < https://www.ncbi.nlm.nih.gov/pubmed/15797031 >.

FUJII, R.; TAKUMI, T. TLS facilitates transport of mRNA encoding an actin-stabilizing protein to dendritic spines. **J Cell Sci,** v. 118, n. Pt 24, p. 5755-65, Dec 2005. ISSN 0021-9533. Disponível em: < https://www.ncbi.nlm.nih.gov/pubmed/16317045 >.

GANASSI, M. et al. A Surveillance Function of the HSPB8-BAG3-HSP70 Chaperone Complex Ensures Stress Granule Integrity and Dynamism. **Mol Cell,** v. 63, n. 5, p. 796-810, 09 2016. ISSN 1097-4164. Disponível em: < https://www.ncbi.nlm.nih.gov/pubmed/27570075 >.

GANESALINGAM, J. et al. Combination of neurofilament heavy chain and complement C3 as CSF biomarkers for ALS. **J Neurochem,** v. 117, n. 3, p. 528-37, May 2011. ISSN 1471-4159. Disponível em: < https://www.ncbi.nlm.nih.gov/pubmed/21418221 >.

GARIBOTTO, V. et al. Subcortical and deep cortical atrophy in Frontotemporal Lobar Degeneration. **Neurobiol Aging,** v. 32, n. 5, p. 875-84, May 2011. ISSN 1558-1497. Disponível em: < https://www.ncbi.nlm.nih.gov/pubmed/19501427 >.

GASCON, E.; GAO, F. B. The emerging roles of microRNAs in the pathogenesis of frontotemporal dementia-amyotrophic lateral sclerosis (FTD-ALS) spectrum disorders. **J Neurogenet,** v. 28, n. 1-2, p. 30-40, 2014 Mar-Jun 2014. ISSN 1563-5260. Disponível em: < https://www.ncbi.nlm.nih.gov/pubmed/24506814 >.

GASCON, E. et al. Alterations in microRNA-124 and AMPA receptors contribute to social behavioral deficits in frontotemporal dementia. **Nat Med,** v. 20, n. 12, p. 1444-51, Dec 2014. ISSN 1546-170X. Disponível em: < https://www.ncbi.nlm.nih.gov/pubmed/25401692 >.

GAUTAM, M. et al. Absence of alsin function leads to corticospinal motor neuron vulnerability via novel disease mechanisms. **Hum Mol Genet,** v. 25, n. 6, p. 1074-87, Mar 2016. ISSN 1460-2083. Disponível em: < https://www.ncbi.nlm.nih.gov/pubmed/26755825 >.

GEEVASINGA, N. et al. Riluzole exerts transient modulating effects on cortical and axonal hyperexcitability in ALS. **Amyotroph Lateral Scler Frontotemporal Degener,** v. 17, n. 7-8, p. 580-588, 2016 Oct - Nov 2016. ISSN 2167-9223. Disponível em: < https://www.ncbi.nlm.nih.gov/pubmed/27249331 >.

GENDRON, T. F. et al. Antisense transcripts of the expanded C9ORF72 hexanucleotide repeat form nuclear RNA foci and undergo repeat-associated non-ATG translation in c9FTD/ALS. **Acta Neuropathol,** v. 126, n. 6, p. 829-44, Dec 2013. ISSN 1432-0533. Disponível em: < https://www.ncbi.nlm.nih.gov/pubmed/24129584 >.

GENÇ, B. et al. Apical dendrite degeneration, a novel cellular pathology for Betz cells in ALS. **Sci Rep,** v. 7, p. 41765, 02 2017. ISSN 2045-2322. Disponível em: < https://www.ncbi.nlm.nih.gov/pubmed/28165465 >.

GERBINO, V. et al. Mislocalised FUS mutants stall spliceosomal snRNPs in the cytoplasm. **Neurobiol Dis,** v. 55, p. 120-8, Jul 2013. ISSN 1095-953X. Disponível em: < https://www.ncbi.nlm.nih.gov/pubmed/23523636 >.

GEULA, C.; MESULAM, M. M. Cortical cholinergic fibers in aging and Alzheimer's disease: a morphometric study. **Neuroscience,** v. 33, n. 3, p. 469-81, 1989. ISSN 0306-4522. Disponível em: < https://www.ncbi.nlm.nih.gov/pubmed/2636703 >.

GHATAK, N. R. et al. Anterior horn changes of motor neuron disease associated with demyelinating radiculopathy. **J Neuropathol Exp Neurol,** v. 45, n. 4, p. 385-95, Jul 1986. ISSN 0022-3069. Disponível em: < https://www.ncbi.nlm.nih.gov/pubmed/3014067 >.

GIJSELINCK, I. et al. Loss of TBK1 is a frequent cause of frontotemporal dementia in a Belgian cohort. **Neurology,** v. 85, n. 24, p. 2116-25, Dec 2015. ISSN 1526-632X. Disponível em: < https://www.ncbi.nlm.nih.gov/pubmed/26581300 >.

GIL, J. et al. Causes of death amongst French patients with amyotrophic lateral sclerosis: a prospective study. **Eur J Neurol,** v. 15, n. 11, p. 1245-51, Nov 2008. ISSN 1468-1331. Disponível em: < https://www.ncbi.nlm.nih.gov/pubmed/18973614 >.

GIL-NAVARRO, S. et al. Decreased striatal dopamine transporter uptake in the non-fluent/agrammatic variant of primary progressive aphasia. **Eur J Neurol,** v. 20, n. 11, p. 1459-e126, Nov 2013. ISSN 1468-1331. Disponível em: < https://www.ncbi.nlm.nih.gov/pubmed/23679075 >.

GILKS, N. et al. Stress granule assembly is mediated by prion-like aggregation of TIA-1. **Mol Biol Cell,** v. 15, n. 12, p. 5383-98, Dec 2004. ISSN 1059-1524. Disponível em: < https://www.ncbi.nlm.nih.gov/pubmed/15371533 >.

GILL, C. et al. SOD1-positive aggregate accumulation in the CNS predicts slower disease progression and increased longevity in a mutant SOD1 mouse model of ALS. **Sci Rep,** v. 9, n. 1, p. 6724, Apr 2019. ISSN 2045-2322. Disponível em: < https://www.ncbi.nlm.nih.gov/pubmed/31040321 >.

GIOVANNELLI, L. et al. Differential effects of amyloid peptides beta-(1-40) and beta-(25-35) injections into the rat nucleus basalis. **Neuroscience,** v. 66, n. 4, p. 781-92, Jun 1995. ISSN 0306-4522. Disponível em: < https://www.ncbi.nlm.nih.gov/pubmed/7651609 >.

GIRALDO, M. et al. Variants in triggering receptor expressed on myeloid cells 2 are associated with both behavioral variant frontotemporal lobar degeneration and Alzheimer's disease. **Neurobiol**

Aging, v. 34, n. 8, p. 2077.e11-8, Aug 2013. ISSN 1558-1497. Disponível em: < https://www.ncbi.nlm.nih.gov/pubmed/23582655 >.

GITLER, A. D.; SHORTER, J. RNA-binding proteins with prion-like domains in ALS and FTLD-U. **Prion,** v. 5, n. 3, p. 179-87, 2011 Jul-Sep 2011. ISSN 1933-690X. Disponível em: < https://www.ncbi.nlm.nih.gov/pubmed/21847013 >.

GONZALEZ-BERMEJO, J. et al. Early diaphragm pacing in patients with amyotrophic lateral sclerosis (RespiStimALS): a randomised controlled triple-blind trial. **Lancet Neurol,** v. 15, n. 12, p. 1217-1227, Nov 2016. ISSN 1474-4465. Disponível em: < https://www.ncbi.nlm.nih.gov/pubmed/27751553 >.

GOODE, A. et al. ALS-FTLD associated mutations of SQSTM1 impact on Keap1-Nrf2 signalling. **Mol Cell Neurosci,** v. 76, p. 52-58, 10 2016. ISSN 1095-9327. Disponível em: < https://www.ncbi.nlm.nih.gov/pubmed/27554286 >.

GORDON, P. H. et al. Clinical features that distinguish PLS, upper motor neuron-dominant ALS, and typical ALS. **Neurology,** v. 72, n. 22, p. 1948-52, Jun 2009. ISSN 1526-632X. Disponível em: < https://www.ncbi.nlm.nih.gov/pubmed/19487653 >.

GORDON, P. H. et al. The natural history of primary lateral sclerosis. **Neurology,** v. 66, n. 5, p. 647-53, Mar 2006. ISSN 1526-632X. Disponível em: < https://www.ncbi.nlm.nih.gov/pubmed/16534101 >.

GORGES, M. et al. Hypothalamic atrophy is related to body mass index and age at onset in amyotrophic lateral sclerosis. **J Neurol Neurosurg Psychiatry,** v. 88, n. 12, p. 1033-1041, 12 2017. ISSN 1468-330X. Disponível em: < https://www.ncbi.nlm.nih.gov/pubmed/28596251 >.

GORNO-TEMPINI, M. L. et al. Cognition and anatomy in three variants of primary progressive aphasia. **Ann Neurol,** v. 55, n. 3, p. 335-46, Mar 2004. ISSN 0364-5134. Disponível em: < https://www.ncbi.nlm.nih.gov/pubmed/14991811 >.

GORNO-TEMPINI, M. L. et al. Classification of primary progressive aphasia and its variants. **Neurology,** v. 76, n. 11, p. 1006-14, Mar 2011. ISSN 1526-632X. Disponível em: < https://www.ncbi.nlm.nih.gov/pubmed/21325651 >.

GRACE, G. M. et al. Neuropsychological functioning in PLS: a comparison with ALS. **Can J Neurol Sci,** v. 38, n. 1, p. 88-97, Jan 2011. ISSN 0317-1671. Disponível em: < https://www.ncbi.nlm.nih.gov/pubmed/21156436 >.

GREGORY, R. I. et al. The Microprocessor complex mediates the genesis of microRNAs. **Nature,** v. 432, n. 7014, p. 235-40, Nov 2004. ISSN 1476-4687. Disponível em: < https://www.ncbi.nlm.nih.gov/pubmed/15531877 >.

GROEN, E. J. et al. ALS-associated mutations in FUS disrupt the axonal distribution and function of SMN. **Hum Mol Genet,** v. 22, n. 18, p. 3690-704, Sep 2013. ISSN 1460-2083. Disponível em: < https://www.ncbi.nlm.nih.gov/pubmed/23681068 >.

GROLEZ, G. et al. MRI of the cervical spinal cord predicts respiratory dysfunction in ALS. **Sci Rep,** v. 8, n. 1, p. 1828, 01 2018. ISSN 2045-2322. Disponível em: < https://www.ncbi.nlm.nih.gov/pubmed/29379040 >.

GROS-LOUIS, F. et al. A frameshift deletion in peripherin gene associated with amyotrophic lateral sclerosis. **J Biol Chem,** v. 279, n. 44, p. 45951-6, Oct 2004. ISSN 0021-9258. Disponível em: < https://www.ncbi.nlm.nih.gov/pubmed/15322088 >.

GUILLEM, K. et al. Nicotinic acetylcholine receptor β2 subunits in the medial prefrontal cortex control attention. **Science,** v. 333, n. 6044, p. 888-91, Aug 2011. ISSN 1095-9203. Disponível em: < https://www.ncbi.nlm.nih.gov/pubmed/21836018 >.

GUO, W. et al. HDAC6 inhibition reverses axonal transport defects in motor neurons derived from FUS-ALS patients. **Nat Commun,** v. 8, n. 1, p. 861, 10 2017. ISSN 2041-1723. Disponível em: < https://www.ncbi.nlm.nih.gov/pubmed/29021520 >.

GURNEY, M. E. et al. Motor neuron degeneration in mice that express a human Cu,Zn superoxide dismutase mutation. **Science,** v. 264, n. 5166, p. 1772-5, Jun 1994. ISSN 0036-8075. Disponível em: < https://www.ncbi.nlm.nih.gov/pubmed/8209258 >.

HAEUSLER, A. R. et al. C9orf72 nucleotide repeat structures initiate molecular cascades of disease. **Nature,** v. 507, n. 7491, p. 195-200, Mar 2014. ISSN 1476-4687. Disponível em: < https://www.ncbi.nlm.nih.gov/pubmed/24598541 >.

HALABI, C. et al. Patterns of striatal degeneration in frontotemporal dementia. **Alzheimer Dis Assoc Disord,** v. 27, n. 1, p. 74-83, 2013 Jan-Mar 2013. ISSN 1546-4156. Disponível em: < https://www.ncbi.nlm.nih.gov/pubmed/22367382 >.

HALFF, A. W. et al. A novel mechanism for nicotinic potentiation of glutamatergic synapses. **J Neurosci,** v. 34, n. 6, p. 2051-64, Feb 2014. ISSN 1529-2401. Disponível em: < https://www.ncbi.nlm.nih.gov/pubmed/24501347 >.

HAMMER, R. P.; TOMIYASU, U.; SCHEIBEL, A. B. Degeneration of the human Betz cell due to amyotrophic lateral sclerosis. **Exp Neurol,** v. 63, n. 2, p. 336-46, Feb 1979. ISSN 0014-4886. Disponível em: < https://www.ncbi.nlm.nih.gov/pubmed/437007 >.

HAN, T. W. et al. Cell-free formation of RNA granules: bound RNAs identify features and components of cellular assemblies. **Cell,** v. 149, n. 4, p. 768-79, May 2012. ISSN 1097-4172. Disponível em: < https://www.ncbi.nlm.nih.gov/pubmed/22579282 >.

HANDLEY, E. E. et al. Synapse Dysfunction of Layer V Pyramidal Neurons Precedes Neurodegeneration in a Mouse Model of TDP-43 Proteinopathies. **Cereb Cortex,** v. 27, n. 7, p. 3630-3647, 07 2017. ISSN 1460-2199. Disponível em: < https://www.ncbi.nlm.nih.gov/pubmed/27496536 >.

HANDSCHIN, C.; SPIEGELMAN, B. M. Peroxisome proliferator-activated receptor gamma coactivator 1 coactivators, energy homeostasis, and metabolism. **Endocr Rev,** v. 27, n. 7, p. 728-35, Dec 2006. ISSN 0163-769X. Disponível em: < https://www.ncbi.nlm.nih.gov/pubmed/17018837 >.

HASEGAWA, M. et al. Phosphorylated TDP-43 in frontotemporal lobar degeneration and amyotrophic lateral sclerosis. **Ann Neurol,** v. 64, n. 1, p. 60-70, Jul 2008. ISSN 1531-8249. Disponível em: < https://www.ncbi.nlm.nih.gov/pubmed/18546284 >.

HELGASON, E.; PHUNG, Q. T.; DUEBER, E. C. Recent insights into the complexity of Tank-binding kinase 1 signaling networks: the emerging role of cellular localization in the activation and substrate specificity of TBK1. **FEBS Lett,** v. 587, n. 8, p. 1230-7, Apr 2013. ISSN 1873-3468. Disponível em: < https://www.ncbi.nlm.nih.gov/pubmed/23395801 >.

HENEKA, M. T. et al. Locus ceruleus controls Alzheimer's disease pathology by modulating microglial functions through norepinephrine. **Proc Natl Acad Sci U S A,** v. 107, n. 13, p. 6058-63, Mar 2010. ISSN 1091-6490. Disponível em: < http://www.ncbi.nlm.nih.gov/pubmed/20231476 >.

HEO, J. M. et al. The PINK1-PARKIN Mitochondrial Ubiquitylation Pathway Drives a Program of OPTN/NDP52 Recruitment and TBK1 Activation to Promote Mitophagy. **Mol Cell,** v. 60, n. 1, p. 7-20, Oct 2015. ISSN 1097-4164. Disponível em: < https://www.ncbi.nlm.nih.gov/pubmed/26365381 >.

HERRMANN, N. et al. Serotonergic function and treatment of behavioral and psychological symptoms of frontotemporal dementia. **Am J Geriatr Psychiatry,** v. 20, n. 9, p. 789-97, Sep 2012. ISSN 1545-7214. Disponível em: < https://www.ncbi.nlm.nih.gov/pubmed/21878805 >.

HICKS, G. G. et al. Fus deficiency in mice results in defective B-lymphocyte development and activation, high levels of chromosomal instability and perinatal death. **Nat Genet,** v. 24, n. 2, p. 175-9, Feb 2000. ISSN 1061-4036. Disponível em: < https://www.ncbi.nlm.nih.gov/pubmed/10655065 >.

HIGELIN, J. et al. FUS Mislocalization and Vulnerability to DNA Damage in ALS Patients Derived hiPSCs and Aging Motoneurons. **Front Cell Neurosci,** v. 10, p. 290, 2016. ISSN 1662-5102. Disponível em: < https://www.ncbi.nlm.nih.gov/pubmed/28082870 >.

HIJI, M. et al. White matter lesions in the brain with frontotemporal lobar degeneration with motor neuron disease: TDP-43-immunopositive inclusions co-localize with p62, but not ubiquitin. **Acta Neuropathol,** v. 116, n. 2, p. 183-91, Aug 2008. ISSN 0001-6322. Disponível em: < https://www.ncbi.nlm.nih.gov/pubmed/18584184 >.

HILL, S. J. et al. Two familial ALS proteins function in prevention/repair of transcription-associated DNA damage. **Proc Natl Acad Sci U S A,** v. 113, n. 48, p. E7701-E7709, 11 2016. ISSN 1091-6490. Disponível em: < https://www.ncbi.nlm.nih.gov/pubmed/27849576 >.

HOELL, J. I. et al. RNA targets of wild-type and mutant FET family proteins. **Nat Struct Mol Biol,** v. 18, n. 12, p. 1428-31, Nov 2011. ISSN 1545-9985. Disponível em: < https://www.ncbi.nlm.nih.gov/pubmed/22081015 >.

HOFWEBER, M. et al. Phase Separation of FUS Is Suppressed by Its Nuclear Import Receptor and Arginine Methylation. **Cell,** v. 173, n. 3, p. 706-719.e13, 04 2018. ISSN 1097-4172. Disponível em: < https://www.ncbi.nlm.nih.gov/pubmed/29677514 >.

HOGAN, D. B. et al. The Prevalence and Incidence of Frontotemporal Dementia: a Systematic Review. **Can J Neurol Sci,** v. 43 Suppl 1, p. S96-S109, Apr 2016. ISSN 0317-1671. Disponível em: < https://www.ncbi.nlm.nih.gov/pubmed/27307130 >.

HOWE, C. L.; MOBLEY, W. C. Long-distance retrograde neurotrophic signaling. **Curr Opin Neurobiol,** v. 15, n. 1, p. 40-8, Feb 2005. ISSN 0959-4388. Disponível em: < https://www.ncbi.nlm.nih.gov/pubmed/15721743 >.

HUANG, E. J. et al. Extensive FUS-immunoreactive pathology in juvenile amyotrophic lateral sclerosis with basophilic inclusions. **Brain Pathol,** v. 20, n. 6, p. 1069-76, Nov 2010. ISSN 1750-3639. Disponível em: < https://www.ncbi.nlm.nih.gov/pubmed/20579074 >.

HUEY, E. D.; PUTNAM, K. T.; GRAFMAN, J. A systematic review of neurotransmitter deficits and treatments in frontotemporal dementia. **Neurology,** v. 66, n. 1, p. 17-22, Jan 2006. ISSN 1526-632X. Disponível em: < https://www.ncbi.nlm.nih.gov/pubmed/16401839 >.

HUGHES, J. T. Pathology of amyotrophic lateral sclerosis. **Adv Neurol,** v. 36, p. 61-74, 1982. ISSN 0091-3952. Disponível em: < https://www.ncbi.nlm.nih.gov/pubmed/7180695 >.

HUGHES, L. E. et al. Improving response inhibition systems in frontotemporal dementia with citalopram. **Brain,** v. 138, n. Pt 7, p. 1961-75, Jul 2015. ISSN 1460-2156. Disponível em: < https://www.ncbi.nlm.nih.gov/pubmed/26001387 >.

HUISMAN, M. H. et al. Population based epidemiology of amyotrophic lateral sclerosis using capture-recapture methodology. **J Neurol Neurosurg Psychiatry,** v. 82, n. 10, p. 1165-70, Oct 2011. ISSN 1468-330X. Disponível em: < https://www.ncbi.nlm.nih.gov/pubmed/21622937 >.

HUTTON, M. et al. Association of missense and 5'-splice-site mutations in tau with the inherited dementia FTDP-17. **Nature,** v. 393, n. 6686, p. 702-5, Jun 1998. ISSN 0028-0836. Disponível em: < https://www.ncbi.nlm.nih.gov/pubmed/9641683 >.

IGAZ, L. M. et al. Enrichment of C-terminal fragments in TAR DNA-binding protein-43 cytoplasmic inclusions in brain but not in spinal cord of frontotemporal lobar degeneration and amyotrophic lateral sclerosis. **Am J Pathol,** v. 173, n. 1, p. 182-94, Jul 2008. ISSN 1525-2191. Disponível em: < https://www.ncbi.nlm.nih.gov/pubmed/18535185 >.

IGLESIAS, C. et al. Electrophysiological and spinal imaging evidences for sensory dysfunction in amyotrophic lateral sclerosis. **BMJ Open,** v. 5, n. 2, p. e007659, Feb 2015. ISSN 2044-6055. Disponível em: < https://www.ncbi.nlm.nih.gov/pubmed/25712823 >.

IKENAKA, K. et al. Disruption of axonal transport in motor neuron diseases. **Int J Mol Sci,** v. 13, n. 1, p. 1225-38, 2012. ISSN 1422-0067. Disponível em: < https://www.ncbi.nlm.nih.gov/pubmed/22312314 >.

ILIEVA, H.; POLYMENIDOU, M.; CLEVELAND, D. W. Non-cell autonomous toxicity in neurodegenerative disorders: ALS and beyond. **J Cell Biol,** v. 187, n. 6, p. 761-72, Dec 2009. ISSN 1540-8140. Disponível em: < https://www.ncbi.nlm.nih.gov/pubmed/19951898 >.

IRWIN, D. J. et al. Deep clinical and neuropathological phenotyping of Pick disease. **Ann Neurol,** v. 79, n. 2, p. 272-87, Feb 2016. ISSN 1531-8249. Disponível em: < https://www.ncbi.nlm.nih.gov/pubmed/26583316 >.

ISHIGAKI, S. et al. Altered Tau Isoform Ratio Caused by Loss of FUS and SFPQ Function Leads to FTLD-like Phenotypes. **Cell Rep,** v. 18, n. 5, p. 1118-1131, 01 2017. ISSN 2211-1247. Disponível em: < https://www.ncbi.nlm.nih.gov/pubmed/28147269 >.

ISHIGAKI, S.; SOBUE, G. Importance of Functional Loss of FUS in FTLD/ALS. **Front Mol Biosci,** v. 5, p. 44, 2018. ISSN 2296-889X. Disponível em: < https://www.ncbi.nlm.nih.gov/pubmed/29774215 >.

ISHIURA, H. et al. C9ORF72 repeat expansion in amyotrophic lateral sclerosis in the Kii peninsula of Japan. **Arch Neurol,** v. 69, n. 9, p. 1154-8, Sep 2012. ISSN 1538-3687. Disponível em: < https://www.ncbi.nlm.nih.gov/pubmed/22637429 >.

ISRAELSON, A. et al. Misfolded mutant SOD1 directly inhibits VDAC1 conductance in a mouse model of inherited ALS. **Neuron,** v. 67, n. 4, p. 575-87, Aug 2010. ISSN 1097-4199. Disponível em: < https://www.ncbi.nlm.nih.gov/pubmed/20797535 >.

JARA, J. H. et al. AAV2 mediated retrograde transduction of corticospinal motor neurons reveals initial and selective apical dendrite degeneration in ALS. **Neurobiol Dis,** v. 47, n. 2, p. 174-83, Aug 2012. ISSN 1095-953X. Disponível em: < https://www.ncbi.nlm.nih.gov/pubmed/22521461 >.

JOHNSON, B. S. et al. TDP-43 is intrinsically aggregation-prone, and amyotrophic lateral sclerosis-linked mutations accelerate aggregation and increase toxicity. **J Biol Chem,** v. 284, n. 30, p. 20329-39, Jul 2009. ISSN 0021-9258. Disponível em: < https://www.ncbi.nlm.nih.gov/pubmed/19465477 >.

JOHNSTON, C. A. et al. Amyotrophic lateral sclerosis in an urban setting: a population based study of inner city London. **J Neurol,** v. 253, n. 12, p. 1642-3, Dec 2006. ISSN 0340-5354. Disponível em: < https://www.ncbi.nlm.nih.gov/pubmed/17219036 >.

JOKIC, N. et al. The neurite outgrowth inhibitor Nogo-A promotes denervation in an amyotrophic lateral sclerosis model. **EMBO Rep,** v. 7, n. 11, p. 1162-7, Nov 2006. ISSN 1469-221X. Disponível em: < https://www.ncbi.nlm.nih.gov/pubmed/17039253 >.

JOKIC, N. et al. Nogo expression in muscle correlates with amyotrophic lateral sclerosis severity. **Ann Neurol,** v. 57, n. 4, p. 553-6, Apr 2005. ISSN 0364-5134. Disponível em: < https://www.ncbi.nlm.nih.gov/pubmed/15786457 >.

JOSEPHS, K. A. et al. Neuropathological background of phenotypical variability in frontotemporal dementia. **Acta Neuropathol,** v. 122, n. 2, p. 137-53, Aug 2011. ISSN 1432-0533. Disponível em: < https://www.ncbi.nlm.nih.gov/pubmed/21614463 >.

JOSEPHS, K. A. et al. Caudate atrophy on MRI is a characteristic feature of FTLD-FUS. **Eur J Neurol,** v. 17, n. 7, p. 969-75, Jul 2010. ISSN 1468-1331. Disponível em: < https://www.ncbi.nlm.nih.gov/pubmed/20236174 >.

JUL, P. et al. Hyperactivity with Agitative-Like Behavior in a Mouse Tauopathy Model. **J Alzheimers Dis,** v. 49, n. 3, p. 783-95, 2016. ISSN 1875-8908. Disponível em: < https://www.ncbi.nlm.nih.gov/pubmed/26519432 >.

JÄCKEL, S. et al. Nuclear import factor transportin and arginine methyltransferase 1 modify FUS neurotoxicity in Drosophila. **Neurobiol Dis,** v. 74, p. 76-88, Feb 2015. ISSN 1095-953X. Disponível em: < https://www.ncbi.nlm.nih.gov/pubmed/25447237 >.

KA, M.; MOFFAT, J. J.; KIM, W. Y. MACF1 Controls Migration and Positioning of Cortical GABAergic Interneurons in Mice. **Cereb Cortex,** v. 27, n. 12, p. 5525-5538, 12 2017. ISSN 1460-2199. Disponível em: < https://www.ncbi.nlm.nih.gov/pubmed/27756764 >.

KABASHI, E. et al. Gain and loss of function of ALS-related mutations of TARDBP (TDP-43) cause motor deficits in vivo. **Hum Mol Genet,** v. 19, n. 4, p. 671-83, Feb 2010. ISSN 1460-2083. Disponível em: < https://www.ncbi.nlm.nih.gov/pubmed/19959528 >.

KABASHI, E. et al. TARDBP mutations in individuals with sporadic and familial amyotrophic lateral sclerosis. **Nat Genet,** v. 40, n. 5, p. 572-4, May 2008. ISSN 1546-1718. Disponível em: < https://www.ncbi.nlm.nih.gov/pubmed/18372902 >.

KANAI, Y.; DOHMAE, N.; HIROKAWA, N. Kinesin transports RNA: isolation and characterization of an RNA-transporting granule. **Neuron,** v. 43, n. 4, p. 513-25, Aug 2004. ISSN 0896-6273. Disponível em: < https://www.ncbi.nlm.nih.gov/pubmed/15312650 >.

KANAZAWA, I. et al. Studies on neurotransmitter markers of the basal ganglia in Pick's disease, with special reference to dopamine reduction. **J Neurol Sci,** v. 83, n. 1, p. 63-74, Jan 1988. ISSN 0022-510X. Disponível em: < https://www.ncbi.nlm.nih.gov/pubmed/2450180 >.

KANG, H.; TIAN, L.; THOMPSON, W. Terminal Schwann cells guide the reinnervation of muscle after nerve injury. **J Neurocytol,** v. 32, n. 5-8, p. 975-85, 2003 Jun-Sep 2003. ISSN 0300-4864. Disponível em: < https://www.ncbi.nlm.nih.gov/pubmed/15034280 >.

KANG, S. H. et al. Degeneration and impaired regeneration of gray matter oligodendrocytes in amyotrophic lateral sclerosis. **Nat Neurosci,** v. 16, n. 5, p. 571-9, May 2013. ISSN 1546-1726. Disponível em: < https://www.ncbi.nlm.nih.gov/pubmed/23542689 >.

KANNING, K. C.; KAPLAN, A.; HENDERSON, C. E. Motor neuron diversity in development and disease. **Annu Rev Neurosci,** v. 33, p. 409-40, 2010. ISSN 1545-4126. Disponível em: < https://www.ncbi.nlm.nih.gov/pubmed/20367447 >.

KAO, A. W. et al. Progranulin, lysosomal regulation and neurodegenerative disease. **Nat Rev Neurosci,** v. 18, n. 6, p. 325-333, 06 2017. ISSN 1471-0048. Disponível em: < https://www.ncbi.nlm.nih.gov/pubmed/28435163 >.

KASSUBEK, J. et al. Global brain atrophy and corticospinal tract alterations in ALS, as investigated by voxel-based morphometry of 3-D MRI. **Amyotroph Lateral Scler Other Motor Neuron Disord,** v. 6, n. 4, p. 213-20, Dec 2005. ISSN 1466-0822. Disponível em: < https://www.ncbi.nlm.nih.gov/pubmed/16319024 >.

KATO, M. et al. Cell-free formation of RNA granules: low complexity sequence domains form dynamic fibers within hydrogels. **Cell,** v. 149, n. 4, p. 753-67, May 2012. ISSN 1097-4172. Disponível em: < https://www.ncbi.nlm.nih.gov/pubmed/22579281 >.

KAUFMANN, P. et al. Objective tests for upper motor neuron involvement in amyotrophic lateral sclerosis (ALS). **Neurology,** v. 62, n. 10, p. 1753-7, May 2004. ISSN 1526-632X. Disponível em: < https://www.ncbi.nlm.nih.gov/pubmed/15159473 >.

KAWAMATA, H. et al. Abnormal intracellular calcium signaling and SNARE-dependent exocytosis contributes to SOD1G93A astrocyte-mediated toxicity in amyotrophic lateral sclerosis. **J Neurosci,** v. 34, n. 6, p. 2331-48, Feb 2014. ISSN 1529-2401. Disponível em: < https://www.ncbi.nlm.nih.gov/pubmed/24501372 >.

KAWAMATA, T. et al. Immunologic reactions in amyotrophic lateral sclerosis brain and spinal cord tissue. **Am J Pathol,** v. 140, n. 3, p. 691-707, Mar 1992. ISSN 0002-9440. Disponível em: < https://www.ncbi.nlm.nih.gov/pubmed/1347673 >.

KEIZMAN, D. et al. Low-grade systemic inflammation in patients with amyotrophic lateral sclerosis. **Acta Neurol Scand,** v. 119, n. 6, p. 383-9, Jun 2009. ISSN 1600-0404. Disponível em: < https://www.ncbi.nlm.nih.gov/pubmed/18976328 >.

KERBLER, G. M. et al. Basal forebrain atrophy correlates with amyloid β burden in Alzheimer's disease. **Neuroimage Clin,** v. 7, p. 105-13, 2015. ISSN 2213-1582. Disponível em: < https://www.ncbi.nlm.nih.gov/pubmed/25610772 >.

KEREN-SHAUL, H. et al. A Unique Microglia Type Associated with Restricting Development of Alzheimer's Disease. **Cell,** v. 169, n. 7, p. 1276-1290.e17, Jun 2017. ISSN 1097-4172. Disponível em: < https://www.ncbi.nlm.nih.gov/pubmed/28602351 >.

KERTESZ, A. et al. Galantamine in frontotemporal dementia and primary progressive aphasia. **Dement Geriatr Cogn Disord,** v. 25, n. 2, p. 178-85, 2008. ISSN 1421-9824. Disponível em: < https://www.ncbi.nlm.nih.gov/pubmed/18196898 >.

KIM, N. C. et al. VCP is essential for mitochondrial quality control by PINK1/Parkin and this function is impaired by VCP mutations. **Neuron,** v. 78, n. 1, p. 65-80, Apr 2013. ISSN 1097-4199. Disponível em: < https://www.ncbi.nlm.nih.gov/pubmed/23498974 >.

KIM, W. J. et al. Sequestration of TRAF2 into stress granules interrupts tumor necrosis factor signaling under stress conditions. **Mol Cell Biol,** v. 25, n. 6, p. 2450-62, Mar 2005. ISSN 0270-7306. Disponível em: < https://www.ncbi.nlm.nih.gov/pubmed/15743837 >.

KIM, W. K. et al. Study of 962 patients indicates progressive muscular atrophy is a form of ALS. **Neurology,** v. 73, n. 20, p. 1686-92, Nov 2009. ISSN 1526-632X. Disponível em: < https://www.ncbi.nlm.nih.gov/pubmed/19917992 >.

KING, O. D.; GITLER, A. D.; SHORTER, J. The tip of the iceberg: RNA-binding proteins with prion-like domains in neurodegenerative disease. **Brain Res,** v. 1462, p. 61-80, Jun 2012. ISSN 1872-6240. Disponível em: < https://www.ncbi.nlm.nih.gov/pubmed/22445064 >.

KINO, Y. et al. FUS/TLS deficiency causes behavioral and pathological abnormalities distinct from amyotrophic lateral sclerosis. **Acta Neuropathol Commun,** v. 3, p. 24, Apr 2015. ISSN 2051-5960. Disponível em: < https://www.ncbi.nlm.nih.gov/pubmed/25907258 >.

KINOSHITA, Y. et al. Nuclear contour irregularity and abnormal transporter protein distribution in anterior horn cells in amyotrophic lateral sclerosis. **J Neuropathol Exp Neurol,** v. 68, n. 11, p. 1184-92, Nov 2009. ISSN 1554-6578. Disponível em: < https://www.ncbi.nlm.nih.gov/pubmed/19816199 >.

KLEINBERGER, G. et al. Mechanisms of granulin deficiency: lessons from cellular and animal models. **Mol Neurobiol,** v. 47, n. 1, p. 337-60, Feb 2013. ISSN 1559-1182. Disponível em: < https://www.ncbi.nlm.nih.gov/pubmed/23239020 >.

KOERNER, D. R. Amyotrophic lateral sclerosis on Guam. **Ann Intern Med,** v. 37, n. 6, p. 1204-20, Dec 1952. ISSN 0003-4819. Disponível em: < https://www.ncbi.nlm.nih.gov/pubmed/13008298 >.

KORAC, J. et al. Ubiquitin-independent function of optineurin in autophagic clearance of protein aggregates. **J Cell Sci,** v. 126, n. Pt 2, p. 580-92, Jan 2013. ISSN 1477-9137. Disponível em: < https://www.ncbi.nlm.nih.gov/pubmed/23178947 >.

KORTTE, K. B.; ROGALSKI, E. J. Behavioural interventions for enhancing life participation in behavioural variant frontotemporal dementia and primary progressive aphasia. **Int Rev Psychiatry,** v. 25, n. 2, p. 237-45, Apr 2013. ISSN 1369-1627. Disponível em: < https://www.ncbi.nlm.nih.gov/pubmed/23611353 >.

KRASEMANN, S. et al. The TREM2-APOE Pathway Drives the Transcriptional Phenotype of Dysfunctional Microglia in Neurodegenerative Diseases. **Immunity,** v. 47, n. 3, p. 566-581.e9, 09 2017. ISSN 1097-4180. Disponível em: < https://www.ncbi.nlm.nih.gov/pubmed/28930663 >.

KRASNIANSKI, A. et al. Mitochondrial changes in skeletal muscle in amyotrophic lateral sclerosis and other neurogenic atrophies. **Brain,** v. 128, n. Pt 8, p. 1870-6, Aug 2005. ISSN 1460-2156. Disponível em: < https://www.ncbi.nlm.nih.gov/pubmed/15901649 >.

KUIJPERS, M. et al. Amyotrophic lateral sclerosis (ALS)-associated VAPB-P56S inclusions represent an ER quality control compartment. **Acta Neuropathol Commun,** v. 1, p. 24, Jun 2013. ISSN 2051-5960. Disponível em: < https://www.ncbi.nlm.nih.gov/pubmed/24252306 >.

KURODA, M. et al. Male sterility and enhanced radiation sensitivity in TLS(-/-) mice. **EMBO J,** v. 19, n. 3, p. 453-62, Feb 2000. ISSN 0261-4189. Disponível em: < https://www.ncbi.nlm.nih.gov/pubmed/10654943 >.

KWIATKOWSKI, T. J. et al. Mutations in the FUS/TLS gene on chromosome 16 cause familial amyotrophic lateral sclerosis. **Science,** v. 323, n. 5918, p. 1205-8, Feb 2009. ISSN 1095-9203. Disponível em: < https://www.ncbi.nlm.nih.gov/pubmed/19251627 >.

KWONG, L. K. et al. TDP-43 proteinopathy: the neuropathology underlying major forms of sporadic and familial frontotemporal lobar degeneration and motor neuron disease. **Acta Neuropathol,** v. 114, n. 1, p. 63-70, Jul 2007. ISSN 0001-6322. Disponível em: < https://www.ncbi.nlm.nih.gov/pubmed/17492294 >.

LACOMBLEZ, L. et al. Dose-ranging study of riluzole in amyotrophic lateral sclerosis. Amyotrophic Lateral Sclerosis/Riluzole Study Group II. **Lancet,** v. 347, n. 9013, p. 1425-31, May 1996. ISSN 0140-6736. Disponível em: < https://www.ncbi.nlm.nih.gov/pubmed/8676624 >.

LAGIER-TOURENNE, C. et al. Targeted degradation of sense and antisense C9orf72 RNA foci as therapy for ALS and frontotemporal degeneration. **Proc Natl Acad Sci U S A,** v. 110, n. 47, p. E4530-9, Nov 2013. ISSN 1091-6490. Disponível em: < https://www.ncbi.nlm.nih.gov/pubmed/24170860 >.

LAGIER-TOURENNE, C.; POLYMENIDOU, M.; CLEVELAND, D. W. TDP-43 and FUS/TLS: emerging roles in RNA processing and neurodegeneration. **Hum Mol Genet,** v. 19, n. R1, p. R46-64, Apr 2010. ISSN 1460-2083. Disponível em: < https://www.ncbi.nlm.nih.gov/pubmed/20400460 >.

LAGIER-TOURENNE, C. et al. Divergent roles of ALS-linked proteins FUS/TLS and TDP-43 intersect in processing long pre-mRNAs. **Nat Neurosci,** v. 15, n. 11, p. 1488-97, Nov 2012. ISSN 1546-1726. Disponível em: < https://www.ncbi.nlm.nih.gov/pubmed/23023293 >.

LANATA, S. C.; MILLER, B. L. The behavioural variant frontotemporal dementia (bvFTD) syndrome in psychiatry. **J Neurol Neurosurg Psychiatry,** v. 87, n. 5, p. 501-11, May 2016. ISSN 1468-330X. Disponível em: < https://www.ncbi.nlm.nih.gov/pubmed/26216940 >.

LEBERT, F. et al. Frontotemporal dementia: a randomised, controlled trial with trazodone. **Dement Geriatr Cogn Disord,** v. 17, n. 4, p. 355-9, 2004. ISSN 1420-8008. Disponível em: < https://www.ncbi.nlm.nih.gov/pubmed/15178953 >.

LECLERC, N. et al. Selective changes in mitochondria respiratory properties in oxidative or glycolytic muscle fibers isolated from G93AhumanSOD1 transgenic mice. **Neuromuscul Disord,** v. 11, n. 8, p. 722-7, Nov 2001. ISSN 0960-8966. Disponível em: < https://www.ncbi.nlm.nih.gov/pubmed/11595514 >.

LEE, B. J. et al. Rules for nuclear localization sequence recognition by karyopherin beta 2. **Cell,** v. 126, n. 3, p. 543-58, Aug 2006. ISSN 0092-8674. Disponível em: < https://www.ncbi.nlm.nih.gov/pubmed/16901787 >.

LEE, J. A. et al. ESCRT-III dysfunction causes autophagosome accumulation and neurodegeneration. **Curr Biol,** v. 17, n. 18, p. 1561-7, Sep 2007. ISSN 0960-9822. Disponível em: < https://www.ncbi.nlm.nih.gov/pubmed/17683935 >.

LEE, J. K. et al. Role of autophagy in the pathogenesis of amyotrophic lateral sclerosis. **Biochim Biophys Acta,** v. 1852, n. 11, p. 2517-24, Nov 2015. ISSN 0006-3002. Disponível em: < https://www.ncbi.nlm.nih.gov/pubmed/26264610 >.

LEFEBVRE, S. et al. Identification and characterization of a spinal muscular atrophy-determining gene. **Cell,** v. 80, n. 1, p. 155-65, Jan 1995. ISSN 0092-8674. Disponível em: < https://www.ncbi.nlm.nih.gov/pubmed/7813012 >.

LEHNERT, S. et al. Multicentre quality control evaluation of different biomarker candidates for amyotrophic lateral sclerosis. **Amyotroph Lateral Scler Frontotemporal Degener,** v. 15, n. 5-6, p. 344-50, Sep 2014. ISSN 2167-9223. Disponível em: < https://www.ncbi.nlm.nih.gov/pubmed/24575871 >.

LEMON, R. N. Descending pathways in motor control. **Annu Rev Neurosci,** v. 31, p. 195-218, 2008. ISSN 0147-006X. Disponível em: < https://www.ncbi.nlm.nih.gov/pubmed/18558853 >.

LENZI, J. et al. ALS mutant FUS proteins are recruited into stress granules in induced pluripotent stem cell-derived motoneurons. **Dis Model Mech,** v. 8, n. 7, p. 755-66, Jul 2015. ISSN 1754-8411. Disponível em: < https://www.ncbi.nlm.nih.gov/pubmed/26035390 >.

LERGA, A. et al. Identification of an RNA binding specificity for the potential splicing factor TLS. **J Biol Chem,** v. 276, n. 9, p. 6807-16, Mar 2001. ISSN 0021-9258. Disponível em: < https://www.ncbi.nlm.nih.gov/pubmed/11098054 >.

LI, F. et al. Structural insights into the interaction and disease mechanism of neurodegenerative disease-associated optineurin and TBK1 proteins. **Nat Commun,** v. 7, p. 12708, 09 2016. ISSN 2041-1723. Disponível em: < https://www.ncbi.nlm.nih.gov/pubmed/27620379 >.

LI, Y. et al. A Drosophila model for TDP-43 proteinopathy. **Proc Natl Acad Sci U S A,** v. 107, n. 7, p. 3169-74, Feb 2010. ISSN 1091-6490. Disponível em: < https://www.ncbi.nlm.nih.gov/pubmed/20133767 >.

LIEPELT, I. et al. Rivastigmine for the treatment of dementia in patients with progressive supranuclear palsy: Clinical observations as a basis for power calculations and safety analysis. **Alzheimers Dement,** v. 6, n. 1, p. 70-4, Jan 2010. ISSN 1552-5279. Disponível em: < https://www.ncbi.nlm.nih.gov/pubmed/20129321 >.

LING, S. C. et al. Overriding FUS autoregulation in mice triggers gain-of-toxic dysfunctions in RNA metabolism and autophagy-lysosome axis. **Elife,** v. 8, Feb 2019. ISSN 2050-084X. Disponível em: < https://www.ncbi.nlm.nih.gov/pubmed/30747709 >.

LING, S. C.; POLYMENIDOU, M.; CLEVELAND, D. W. Converging mechanisms in ALS and FTD: disrupted RNA and protein homeostasis. **Neuron,** v. 79, n. 3, p. 416-38, Aug 2013. ISSN 1097-4199. Disponível em: < https://www.ncbi.nlm.nih.gov/pubmed/23931993 >.

LIU, X.; ERIKSON, C.; BRUN, A. Cortical synaptic changes and gliosis in normal aging, Alzheimer's disease and frontal lobe degeneration. **Dementia,** v. 7, n. 3, p. 128-34, 1996 May-Jun 1996. ISSN 1013-7424. Disponível em: < https://www.ncbi.nlm.nih.gov/pubmed/8740626 >.

LIU, Y. J. et al. Aberrant activation of AMP-activated protein kinase contributes to the abnormal distribution of HuR in amyotrophic lateral sclerosis. **FEBS Lett,** v. 589, n. 4, p. 432-9, Feb 2015. ISSN 1873-3468. Disponível em: < https://www.ncbi.nlm.nih.gov/pubmed/25592834 >.

LOEFFLER, J. P. et al. The Role of Skeletal Muscle in Amyotrophic Lateral Sclerosis. **Brain Pathol,** v. 26, n. 2, p. 227-36, Mar 2016. ISSN 1750-3639. Disponível em: < https://www.ncbi.nlm.nih.gov/pubmed/26780251 >.

LOGROSCINO, G. et al. Incidence of amyotrophic lateral sclerosis in Europe. **J Neurol Neurosurg Psychiatry,** v. 81, n. 4, p. 385-90, Apr 2010. ISSN 1468-330X. Disponível em: < https://www.ncbi.nlm.nih.gov/pubmed/19710046 >.

LOMEN-HOERTH, C. Clinical phenomenology and neuroimaging correlates in ALS-FTD. **J Mol Neurosci,** v. 45, n. 3, p. 656-62, Nov 2011. ISSN 1559-1166. Disponível em: < https://www.ncbi.nlm.nih.gov/pubmed/21971978 >.

LOPEZ-ERAUSKIN, J. et al. ALS/FTD-Linked Mutation in FUS Suppresses Intra-axonal Protein Synthesis and Drives Disease Without Nuclear Loss-of-Function of FUS. **Neuron,** v. 100, n. 4, p. 816-830 e7, Nov 21 2018. ISSN 1097-4199 (Electronic)
0896-6273 (Linking). Disponível em: < https://www.ncbi.nlm.nih.gov/pubmed/30344044 >.

LORENZO-BETANCOR, O. et al. Analysis of nuclear export sequence regions of FUS-Related RNA-binding proteins in essential tremor. **PLoS One,** v. 9, n. 11, p. e111989, 2014. ISSN 1932-6203. Disponível em: < https://www.ncbi.nlm.nih.gov/pubmed/25375143 >.

LOZADA, A. F. et al. Induction of dendritic spines by β2-containing nicotinic receptors. **J Neurosci,** v. 32, n. 24, p. 8391-400, Jun 2012. ISSN 1529-2401. Disponível em: < https://www.ncbi.nlm.nih.gov/pubmed/22699919 >.

LU, P. H. et al. Regional differences in white matter breakdown between frontotemporal dementia and early-onset Alzheimer's disease. **J Alzheimers Dis,** v. 39, n. 2, p. 261-9, 2014. ISSN 1875-8908. Disponível em: < https://www.ncbi.nlm.nih.gov/pubmed/24150110 >.

LUDOLPH, A. C. et al. Safety and efficacy of rasagiline as an add-on therapy to riluzole in patients with amyotrophic lateral sclerosis: a randomised, double-blind, parallel-group, placebo-controlled,

phase 2 trial. **Lancet Neurol,** v. 17, n. 8, p. 681-688, 08 2018. ISSN 1474-4465. Disponível em: < https://www.ncbi.nlm.nih.gov/pubmed/29934198 >.

MACCHI, Z. et al. A multi-center screening trial of rasagiline in patients with amyotrophic lateral sclerosis: Possible mitochondrial biomarker target engagement. **Amyotroph Lateral Scler Frontotemporal Degener,** v. 16, n. 5-6, p. 345-52, 2015. ISSN 2167-9223. Disponível em: < https://www.ncbi.nlm.nih.gov/pubmed/25832828 >.

MACHAMER, J. B. et al. FUS causes synaptic hyperexcitability in Drosophila dendritic arborization neurons. **Brain Res,** v. 1693, n. Pt A, p. 55-66, 08 2018. ISSN 1872-6240. Disponível em: < https://www.ncbi.nlm.nih.gov/pubmed/29625118 >.

MACKENZIE, I. R. et al. Pathological heterogeneity in amyotrophic lateral sclerosis with FUS mutations: two distinct patterns correlating with disease severity and mutation. **Acta Neuropathol,** v. 122, n. 1, p. 87-98, Jul 2011. ISSN 1432-0533. Disponível em: < https://www.ncbi.nlm.nih.gov/pubmed/21604077 >.

MACKENZIE, I. R. et al. Dipeptide repeat protein pathology in C9ORF72 mutation cases: clinico-pathological correlations. **Acta Neuropathol,** v. 126, n. 6, p. 859-79, Dec 2013. ISSN 1432-0533. Disponível em: < https://www.ncbi.nlm.nih.gov/pubmed/24096617 >.

MACKENZIE, I. R. et al. Heterogeneity of ubiquitin pathology in frontotemporal lobar degeneration: classification and relation to clinical phenotype. **Acta Neuropathol,** v. 112, n. 5, p. 539-49, Nov 2006. ISSN 0001-6322. Disponível em: < https://www.ncbi.nlm.nih.gov/pubmed/17021754 >.

MACKENZIE, I. R. et al. Quantitative analysis and clinico-pathological correlations of different dipeptide repeat protein pathologies in C9ORF72 mutation carriers. **Acta Neuropathol,** v. 130, n. 6, p. 845-61, Dec 2015. ISSN 1432-0533. Disponível em: < https://www.ncbi.nlm.nih.gov/pubmed/26374446 >.

MACKENZIE, I. R. et al. Distinct pathological subtypes of FTLD-FUS. **Acta Neuropathol,** v. 121, n. 2, p. 207-18, Feb 2011. ISSN 1432-0533. Disponível em: < https://www.ncbi.nlm.nih.gov/pubmed/21052700 >.

MADABHUSHI, R.; PAN, L.; TSAI, L. H. DNA damage and its links to neurodegeneration. **Neuron,** v. 83, n. 2, p. 266-282, Jul 2014. ISSN 1097-4199. Disponível em: < https://www.ncbi.nlm.nih.gov/pubmed/25033177 >.

MADJI HOUNOUM, B. et al. Wildtype motoneurons, ALS-Linked SOD1 mutation and glutamate profoundly modify astrocyte metabolism and lactate shuttling. **Glia,** v. 65, n. 4, p. 592-605, 04 2017. ISSN 1098-1136. Disponível em: < https://www.ncbi.nlm.nih.gov/pubmed/28139855 >.

MAEKAWA, S. et al. Cortical selective vulnerability in motor neuron disease: a morphometric study. **Brain,** v. 127, n. Pt 6, p. 1237-51, Jun 2004. ISSN 0006-8950. Disponível em: < https://www.ncbi.nlm.nih.gov/pubmed/15130949 >.

MAFFEI, A. et al. Emerging Mechanisms Underlying Dynamics of GABAergic Synapses. **J Neurosci,** v. 37, n. 45, p. 10792-10799, 11 2017. ISSN 1529-2401. Disponível em: < https://www.ncbi.nlm.nih.gov/pubmed/29118207 >.

MAGEN, I. et al. Cognitive deficits in a mouse model of pre-manifest Parkinson's disease. **Eur J Neurosci,** v. 35, n. 6, p. 870-82, Mar 2012. ISSN 1460-9568. Disponível em: < https://www.ncbi.nlm.nih.gov/pubmed/22356593 >.

MAHONEY, C. J. et al. Frontotemporal dementia with the C9ORF72 hexanucleotide repeat expansion: clinical, neuroanatomical and neuropathological features. **Brain,** v. 135, n. Pt 3, p. 736-50, Mar 2012. ISSN 1460-2156. Disponível em: < https://www.ncbi.nlm.nih.gov/pubmed/22366791 >.

MAHONEY, C. J. et al. Profiles of white matter tract pathology in frontotemporal dementia. **Hum Brain Mapp,** v. 35, n. 8, p. 4163-79, Aug 2014. ISSN 1097-0193. Disponível em: < https://www.ncbi.nlm.nih.gov/pubmed/24510641 >.

MARAGAKIS, N. J.; ROTHSTEIN, J. D. Mechanisms of Disease: astrocytes in neurodegenerative disease. **Nat Clin Pract Neurol,** v. 2, n. 12, p. 679-89, Dec 2006. ISSN 1745-834X. Disponível em: < https://www.ncbi.nlm.nih.gov/pubmed/17117171 >.

MARUYAMA, W.; YOUDIM, M. B.; NAOI, M. Antiapoptotic properties of rasagiline, N-propargylamine-1(R)-aminoindan, and its optical (S)-isomer, TV1022. **Ann N Y Acad Sci,** v. 939, p. 320-9, Jun 2001. ISSN 0077-8923. Disponível em: < https://www.ncbi.nlm.nih.gov/pubmed/11462787 >.

MASTROCOLA, A. S. et al. The RNA-binding protein fused in sarcoma (FUS) functions downstream of poly(ADP-ribose) polymerase (PARP) in response to DNA damage. **J Biol Chem,** v. 288, n. 34, p. 24731-41, Aug 2013. ISSN 1083-351X. Disponível em: < https://www.ncbi.nlm.nih.gov/pubmed/23833192 >.

MASUDA, A. et al. Position-specific binding of FUS to nascent RNA regulates mRNA length. **Genes Dev,** v. 29, n. 10, p. 1045-57, May 2015. ISSN 1549-5477. Disponível em: < https://www.ncbi.nlm.nih.gov/pubmed/25995189 >.

MATSUMOTO, G. et al. TBK1 controls autophagosomal engulfment of polyubiquitinated mitochondria through p62/SQSTM1 phosphorylation. **Hum Mol Genet,** v. 24, n. 15, p. 4429-42, Aug 2015. ISSN 1460-2083. Disponível em: < https://www.ncbi.nlm.nih.gov/pubmed/25972374 >.

MAZZOCCHIO, R.; ROSSI, A.; ROTHWELL, J. C. Depression of Renshaw recurrent inhibition by activation of corticospinal fibres in human upper and lower limb. **J Physiol,** v. 481 (Pt 2), p. 487-98, Dec 1994. ISSN 0022-3751. Disponível em: < https://www.ncbi.nlm.nih.gov/pubmed/7738840 >.

MCGOWN, A. et al. Early interneuron dysfunction in ALS: insights from a mutant sod1 zebrafish model. **Ann Neurol,** v. 73, n. 2, p. 246-58, Feb 2013. ISSN 1531-8249. Disponível em: < https://www.ncbi.nlm.nih.gov/pubmed/23281025 >.

MCMILLAN, C. T. et al. White matter imaging helps dissociate tau from TDP-43 in frontotemporal lobar degeneration. **J Neurol Neurosurg Psychiatry,** v. 84, n. 9, p. 949-55, Sep 2013. ISSN 1468-330X. Disponível em: < https://www.ncbi.nlm.nih.gov/pubmed/23475817 >.

MEETER, L. H. et al. Imaging and fluid biomarkers in frontotemporal dementia. **Nat Rev Neurol,** v. 13, n. 7, p. 406-419, Jul 2017. ISSN 1759-4766. Disponível em: < https://www.ncbi.nlm.nih.gov/pubmed/28621768 >.

MEININGER, V. et al. Safety, pharmacokinetic, and functional effects of the nogo-a monoclonal antibody in amyotrophic lateral sclerosis: a randomized, first-in-human clinical trial. **PLoS One,** v. 9, n. 5, p. e97803, 2014. ISSN 1932-6203. Disponível em: < https://www.ncbi.nlm.nih.gov/pubmed/24841795 >.

MELAMED, Z. et al. Premature polyadenylation-mediated loss of stathmin-2 is a hallmark of TDP-43-dependent neurodegeneration. **Nat Neurosci,** v. 22, n. 2, p. 180-190, 02 2019. ISSN 1546-1726. Disponível em: < https://www.ncbi.nlm.nih.gov/pubmed/30643298 >.

MENDELL, J. R. et al. Single-Dose Gene-Replacement Therapy for Spinal Muscular Atrophy. **N Engl J Med,** v. 377, n. 18, p. 1713-1722, 11 2017. ISSN 1533-4406. Disponível em: < https://www.ncbi.nlm.nih.gov/pubmed/29091557 >.

MENDEZ, M. F. et al. Preliminary findings: behavioral worsening on donepezil in patients with frontotemporal dementia. **Am J Geriatr Psychiatry,** v. 15, n. 1, p. 84-7, Jan 2007. ISSN 1064-7481. Disponível em: < https://www.ncbi.nlm.nih.gov/pubmed/17194818 >.

MEYER, H.; BUG, M.; BREMER, S. Emerging functions of the VCP/p97 AAA-ATPase in the ubiquitin system. **Nat Cell Biol,** v. 14, n. 2, p. 117-23, Feb 2012. ISSN 1476-4679. Disponível em: < https://www.ncbi.nlm.nih.gov/pubmed/22298039 >.

MILLER, R. G.; MITCHELL, J. D.; MOORE, D. H. Riluzole for amyotrophic lateral sclerosis (ALS)/motor neuron disease (MND). **Cochrane Database Syst Rev**, n. 3, p. CD001447, Mar 2012. ISSN 1469-493X. Disponível em: < https://www.ncbi.nlm.nih.gov/pubmed/22419278 >.

MILLER, T. M. et al. An antisense oligonucleotide against SOD1 delivered intrathecally for patients with SOD1 familial amyotrophic lateral sclerosis: a phase 1, randomised, first-in-man study. **Lancet Neurol,** v. 12, n. 5, p. 435-42, May 2013. ISSN 1474-4465. Disponível em: < https://www.ncbi.nlm.nih.gov/pubmed/23541756 >.

MITCHELL, J. C. et al. Overexpression of human wild-type FUS causes progressive motor neuron degeneration in an age- and dose-dependent fashion. **Acta Neuropathol,** v. 125, n. 2, p. 273-88, Feb 2013. ISSN 1432-0533. Disponível em: < https://www.ncbi.nlm.nih.gov/pubmed/22961620 >.

MITCHELL, R. M. et al. A CSF biomarker panel for identification of patients with amyotrophic lateral sclerosis. **Neurology,** v. 72, n. 1, p. 14-9, Jan 2009. ISSN 1526-632X. Disponível em: < https://www.ncbi.nlm.nih.gov/pubmed/18987350 >.

MIZIELINSKA, S. et al. C9orf72 repeat expansions cause neurodegeneration in Drosophila through arginine-rich proteins. **Science,** v. 345, n. 6201, p. 1192-1194, Sep 2014. ISSN 1095-9203. Disponível em: < https://www.ncbi.nlm.nih.gov/pubmed/25103406 >.

MIZIELINSKA, S. et al. C9orf72 frontotemporal lobar degeneration is characterised by frequent neuronal sense and antisense RNA foci. **Acta Neuropathol,** v. 126, n. 6, p. 845-57, Dec 2013. ISSN 1432-0533. Disponível em: < https://www.ncbi.nlm.nih.gov/pubmed/24170096 >.

MIZUSAWA, H. et al. Focal accumulation of phosphorylated neurofilaments within anterior horn cell in familial amyotrophic lateral sclerosis. **Acta Neuropathol,** v. 79, n. 1, p. 37-43, 1989. ISSN 0001-6322. Disponível em: < https://www.ncbi.nlm.nih.gov/pubmed/2511732 >.

MOHAMMADI, B. et al. Amyotrophic lateral sclerosis affects cortical and subcortical activity underlying motor inhibition and action monitoring. **Hum Brain Mapp,** v. 36, n. 8, p. 2878-89, Aug 2015. ISSN 1097-0193. Disponível em: < https://www.ncbi.nlm.nih.gov/pubmed/25913637 >.

MOLLIEX, A. et al. Phase separation by low complexity domains promotes stress granule assembly and drives pathological fibrillization. **Cell,** v. 163, n. 1, p. 123-33, Sep 2015. ISSN 1097-4172. Disponível em: < https://www.ncbi.nlm.nih.gov/pubmed/26406374 >.

MOLONEY, E. B.; DE WINTER, F.; VERHAAGEN, J. ALS as a distal axonopathy: molecular mechanisms affecting neuromuscular junction stability in the presymptomatic stages of the disease. **Front Neurosci,** v. 8, p. 252, 2014. ISSN 1662-4548. Disponível em: < https://www.ncbi.nlm.nih.gov/pubmed/25177267 >.

MONACO, F. et al. Plasma and cerebrospinal fluid tryptophan in multiple sclerosis and degenerative diseases. **J Neurol Neurosurg Psychiatry,** v. 42, n. 7, p. 640-1, Jul 1979. ISSN 0022-3050. Disponível em: < https://www.ncbi.nlm.nih.gov/pubmed/479903 >.

MONAHAN, Z. et al. Phosphorylation of the FUS low-complexity domain disrupts phase separation, aggregation, and toxicity. **EMBO J,** v. 36, n. 20, p. 2951-2967, 10 2017. ISSN 1460-2075. Disponível em: < https://www.ncbi.nlm.nih.gov/pubmed/28790177 >.

MORETTI, R. et al. Rivastigmine in frontotemporal dementia: an open-label study. **Drugs Aging,** v. 21, n. 14, p. 931-7, 2004. ISSN 1170-229X. Disponível em: < https://www.ncbi.nlm.nih.gov/pubmed/15554751 >.

MORETTI, R. et al. Frontotemporal dementia: paroxetine as a possible treatment of behavior symptoms. A randomized, controlled, open 14-month study. **Eur Neurol,** v. 49, n. 1, p. 13-9, 2003. ISSN 0014-3022. Disponível em: < https://www.ncbi.nlm.nih.gov/pubmed/12464713 >.

MORFINI, G. A. et al. Inhibition of fast axonal transport by pathogenic SOD1 involves activation of p38 MAP kinase. **PLoS One,** v. 8, n. 6, p. e65235, 2013. ISSN 1932-6203. Disponível em: < https://www.ncbi.nlm.nih.gov/pubmed/23776455 >.

MORI, K. et al. The C9orf72 GGGGCC repeat is translated into aggregating dipeptide-repeat proteins in FTLD/ALS. **Science,** v. 339, n. 6125, p. 1335-8, Mar 2013. ISSN 1095-9203. Disponível em: < https://www.ncbi.nlm.nih.gov/pubmed/23393093 >.

MORLANDO, M. et al. FUS stimulates microRNA biogenesis by facilitating co-transcriptional Drosha recruitment. **EMBO J,** v. 31, n. 24, p. 4502-10, Dec 2012. ISSN 1460-2075. Disponível em: < https://www.ncbi.nlm.nih.gov/pubmed/23232809 >.

MOROHOSHI, F. et al. Genomic structure of the human RBP56/hTAFII68 and FUS/TLS genes. **Gene,** v. 221, n. 2, p. 191-8, Oct 1998. ISSN 0378-1119. Disponível em: < https://www.ncbi.nlm.nih.gov/pubmed/9795213 >.

MOSER, J. M.; BIGINI, P.; SCHMITT-JOHN, T. The wobbler mouse, an ALS animal model. **Mol Genet Genomics,** v. 288, n. 5-6, p. 207-29, Jun 2013. ISSN 1617-4623. Disponível em: < https://www.ncbi.nlm.nih.gov/pubmed/23539154 >.

MULDER, D. W.; KURLAND, L. T.; IRIARTE, L. L. Neurologic diseases on the island of Guam. **U S Armed Forces Med J,** v. 5, n. 12, p. 1724-39, Dec 1954. ISSN 0566-0777. Disponível em: < https://www.ncbi.nlm.nih.gov/pubmed/13217119 >.

MUNOZ, D. G. et al. Accumulation of phosphorylated neurofilaments in anterior horn motoneurons of amyotrophic lateral sclerosis patients. **J Neuropathol Exp Neurol,** v. 47, n. 1, p. 9-18, Jan 1988. ISSN 0022-3069. Disponível em: < https://www.ncbi.nlm.nih.gov/pubmed/3334727 >.

MUNOZ, D. G. et al. FUS pathology in basophilic inclusion body disease. **Acta Neuropathol,** v. 118, n. 5, p. 617-27, Nov 2009. ISSN 1432-0533. Disponível em: < https://www.ncbi.nlm.nih.gov/pubmed/19830439 >.

MURAKAMI, T. et al. ALS/FTD Mutation-Induced Phase Transition of FUS Liquid Droplets and Reversible Hydrogels into Irreversible Hydrogels Impairs RNP Granule Function. **Neuron,** v. 88, n. 4, p. 678-90, Nov 2015. ISSN 1097-4199. Disponível em: < https://www.ncbi.nlm.nih.gov/pubmed/26526393 >.

MURESAN, V.; LADESCU MURESAN, Z. Shared Molecular Mechanisms in Alzheimer's Disease and Amyotrophic Lateral Sclerosis: Neurofilament-Dependent Transport of sAPP, FUS, TDP-43 and SOD1, with Endoplasmic Reticulum-Like Tubules. **Neurodegener Dis,** v. 16, n. 1-2, p. 55-61, 2016. ISSN 1660-2862. Disponível em: < https://www.ncbi.nlm.nih.gov/pubmed/26605911 >.

MURLEY, A. G.; ROWE, J. B. Neurotransmitter deficits from frontotemporal lobar degeneration. **Brain,** v. 141, n. 5, p. 1263-1285, 05 2018. ISSN 1460-2156. Disponível em: < https://www.ncbi.nlm.nih.gov/pubmed/29373632 >.

MURRAY, D. T. et al. Structure of FUS Protein Fibrils and Its Relevance to Self-Assembly and Phase Separation of Low-Complexity Domains. **Cell,** v. 171, n. 3, p. 615-627.e16, Oct 2017. ISSN 1097-4172. Disponível em: < https://www.ncbi.nlm.nih.gov/pubmed/28942918 >.

MÜNCH, C. et al. The p150 subunit of dynactin (DCTN1) gene in multiple sclerosis. **Acta Neurol Scand,** v. 116, n. 4, p. 231-4, Oct 2007. ISSN 0001-6314. Disponível em: < https://www.ncbi.nlm.nih.gov/pubmed/17824900 >.

MÜNCH, C.; O'BRIEN, J.; BERTOLOTTI, A. Prion-like propagation of mutant superoxide dismutase-1 misfolding in neuronal cells. **Proc Natl Acad Sci U S A,** v. 108, n. 9, p. 3548-53, Mar 2011. ISSN 1091-6490. Disponível em: < https://www.ncbi.nlm.nih.gov/pubmed/21321227 >.

NAGAOKA, S. et al. A juvenile case of frontotemporal dementia: neurochemical and neuropathological investigations. **Prog Neuropsychopharmacol Biol Psychiatry,** v. 19, n. 8, p. 1251-61, Dec 1995. ISSN 0278-5846. Disponível em: < https://www.ncbi.nlm.nih.gov/pubmed/8868207 >.

NAKAJIMA, K. et al. Molecular motor KIF5A is essential for GABA(A) receptor transport, and KIF5A deletion causes epilepsy. **Neuron,** v. 76, n. 5, p. 945-61, Dec 2012. ISSN 1097-4199. Disponível em: < https://www.ncbi.nlm.nih.gov/pubmed/23217743 >.

NARYSHKIN, N. A. et al. Motor neuron disease. SMN2 splicing modifiers improve motor function and longevity in mice with spinal muscular atrophy. **Science,** v. 345, n. 6197, p. 688-93, Aug 2014. ISSN 1095-9203. Disponível em: < https://www.ncbi.nlm.nih.gov/pubmed/25104390 >.

NAUMANN, M. et al. Impaired DNA damage response signaling by FUS-NLS mutations leads to neurodegeneration and FUS aggregate formation. **Nat Commun,** v. 9, n. 1, p. 335, 01 2018. ISSN 2041-1723. Disponível em: < https://www.ncbi.nlm.nih.gov/pubmed/29362359 >.

NAVE, K. A. Myelination and support of axonal integrity by glia. **Nature,** v. 468, n. 7321, p. 244-52, Nov 2010. ISSN 1476-4687. Disponível em: < https://www.ncbi.nlm.nih.gov/pubmed/21068833 >.

NEUMANN, M. et al. Phosphorylation of S409/410 of TDP-43 is a consistent feature in all sporadic and familial forms of TDP-43 proteinopathies. **Acta Neuropathol,** v. 117, n. 2, p. 137-49, Feb 2009. ISSN 1432-0533. Disponível em: < https://www.ncbi.nlm.nih.gov/pubmed/19125255 >.

NEUMANN, M. et al. A new subtype of frontotemporal lobar degeneration with FUS pathology. **Brain,** v. 132, n. Pt 11, p. 2922-31, Nov 2009. ISSN 1460-2156. Disponível em: < https://www.ncbi.nlm.nih.gov/pubmed/19674978 >.

NEUMANN, M. et al. Abundant FUS-immunoreactive pathology in neuronal intermediate filament inclusion disease. **Acta Neuropathol,** v. 118, n. 5, p. 605-16, Nov 2009. ISSN 1432-0533. Disponível em: < https://www.ncbi.nlm.nih.gov/pubmed/19669651 >.

NEUMANN, M. et al. Ubiquitinated TDP-43 in frontotemporal lobar degeneration and amyotrophic lateral sclerosis. **Science,** v. 314, n. 5796, p. 130-3, Oct 2006. ISSN 1095-9203. Disponível em: < https://www.ncbi.nlm.nih.gov/pubmed/17023659 >.

NEUMANN, M. et al. Transportin 1 accumulates specifically with FET proteins but no other transportin cargos in FTLD-FUS and is absent in FUS inclusions in ALS with FUS mutations. **Acta Neuropathol,** v. 124, n. 5, p. 705-16, Nov 2012. ISSN 1432-0533. Disponível em: < https://www.ncbi.nlm.nih.gov/pubmed/22842875 >.

NIHEI, K.; KOWALL, N. W. Involvement of NPY-immunoreactive neurons in the cerebral cortex of amyotrophic lateral sclerosis patients. **Neurosci Lett,** v. 159, n. 1-2, p. 67-70, Sep 1993. ISSN 0304-3940. Disponível em: < https://www.ncbi.nlm.nih.gov/pubmed/8264981 >.

NISHIMURA, A. L. et al. A mutation in the vesicle-trafficking protein VAPB causes late-onset spinal muscular atrophy and amyotrophic lateral sclerosis. **Am J Hum Genet,** v. 75, n. 5, p. 822-31, Nov 2004. ISSN 0002-9297. Disponível em: < https://www.ncbi.nlm.nih.gov/pubmed/15372378 >.

NISHIMURA, A. L. et al. Nuclear import impairment causes cytoplasmic trans-activation response DNA-binding protein accumulation and is associated with frontotemporal lobar degeneration. **Brain,** v. 133, n. Pt 6, p. 1763-71, Jun 2010. ISSN 1460-2156. Disponível em: < https://www.ncbi.nlm.nih.gov/pubmed/20472655 >.

NISHITOH, H. et al. ALS-linked mutant SOD1 induces ER stress- and ASK1-dependent motor neuron death by targeting Derlin-1. **Genes Dev,** v. 22, n. 11, p. 1451-64, Jun 2008. ISSN 0890-9369. Disponível em: < https://www.ncbi.nlm.nih.gov/pubmed/18519638 >.

NONNEMAN, A.; ROBBERECHT, W.; VAN DEN BOSCH, L. The role of oligodendroglial dysfunction in amyotrophic lateral sclerosis. **Neurodegener Dis Manag,** v. 4, n. 3, p. 223-39, 2014. ISSN 1758-2032. Disponível em: < https://www.ncbi.nlm.nih.gov/pubmed/25095817 >.

NORDLUND, A.; OLIVEBERG, M. SOD1-associated ALS: a promising system for elucidating the origin of protein-misfolding disease. **HFSP J,** v. 2, n. 6, p. 354-64, Dec 2008. ISSN 1955-2068. Disponível em: < https://www.ncbi.nlm.nih.gov/pubmed/19436494 >.

NOTO, Y. et al. Elevated CSF TDP-43 levels in amyotrophic lateral sclerosis: specificity, sensitivity, and a possible prognostic value. **Amyotroph Lateral Scler,** v. 12, n. 2, p. 140-3, Mar 2011. ISSN 1471-180X. Disponível em: < https://www.ncbi.nlm.nih.gov/pubmed/21126161 >.

O'CONNELL, R. M. et al. MicroRNA-155 promotes autoimmune inflammation by enhancing inflammatory T cell development. **Immunity,** v. 33, n. 4, p. 607-19, Oct 2010. ISSN 1097-4180. Disponível em: < https://www.ncbi.nlm.nih.gov/pubmed/20888269 >.

O'REILLY, É. et al. Premorbid body mass index and risk of amyotrophic lateral sclerosis. **Amyotroph Lateral Scler Frontotemporal Degener,** v. 14, n. 3, p. 205-11, Apr 2013. ISSN 2167-9223. Disponível em: < https://www.ncbi.nlm.nih.gov/pubmed/23134505 >.

OHSUGI, K. et al. Lack of change in indoleamine metabolism in spinal cord of patients with amyotrophic lateral sclerosis. **Neurosci Lett,** v. 79, n. 3, p. 351-4, Aug 1987. ISSN 0304-3940. Disponível em: < https://www.ncbi.nlm.nih.gov/pubmed/2443876 >.

ONYIKE, C. U.; DIEHL-SCHMID, J. The epidemiology of frontotemporal dementia. **Int Rev Psychiatry,** v. 25, n. 2, p. 130-7, Apr 2013. ISSN 1369-1627. Disponível em: < https://www.ncbi.nlm.nih.gov/pubmed/23611343 >.

OROZCO, D. et al. Loss of fused in sarcoma (FUS) promotes pathological Tau splicing. **EMBO Rep,** v. 13, n. 8, p. 759-64, Aug 2012. ISSN 1469-3178. Disponível em: < https://www.ncbi.nlm.nih.gov/pubmed/22710833 >.

OU, Y. H. et al. TBK1 directly engages Akt/PKB survival signaling to support oncogenic transformation. **Mol Cell,** v. 41, n. 4, p. 458-70, Feb 2011. ISSN 1097-4164. Disponível em: < https://www.ncbi.nlm.nih.gov/pubmed/21329883 >.

PAGANONI, S. et al. Body mass index, not dyslipidemia, is an independent predictor of survival in amyotrophic lateral sclerosis. **Muscle Nerve,** v. 44, n. 1, p. 20-4, Jul 2011. ISSN 1097-4598. Disponível em: < https://www.ncbi.nlm.nih.gov/pubmed/21607987 >.

PAN, P. L. et al. Gray matter atrophy in behavioral variant frontotemporal dementia: a meta-analysis of voxel-based morphometry studies. **Dement Geriatr Cogn Disord,** v. 33, n. 2-3, p. 141-8, 2012. ISSN 1421-9824. Disponível em: < https://www.ncbi.nlm.nih.gov/pubmed/22722668 >.

PAPADOPOULOS, C. et al. VCP/p97 cooperates with YOD1, UBXD1 and PLAA to drive clearance of ruptured lysosomes by autophagy. **EMBO J,** v. 36, n. 2, p. 135-150, 01 2017. ISSN 1460-2075. Disponível em: < https://www.ncbi.nlm.nih.gov/pubmed/27753622 >.

PAPIANI, G. et al. Restructured endoplasmic reticulum generated by mutant amyotrophic lateral sclerosis-linked VAPB is cleared by the proteasome. **J Cell Sci,** v. 125, n. Pt 15, p. 3601-11, Aug 2012. ISSN 1477-9137. Disponível em: < https://www.ncbi.nlm.nih.gov/pubmed/22611258 >.

PAQUIN, M. et al. Spinal Cord Gray Matter Atrophy in Amyotrophic Lateral Sclerosis. **AJNR Am J Neuroradiol,** v. 39, n. 1, p. 184-192, Jan 2018. ISSN 1936-959X. Disponível em: < https://www.ncbi.nlm.nih.gov/pubmed/29122760 >.

PARKINSON, N. et al. ALS phenotypes with mutations in CHMP2B (charged multivesicular body protein 2B). **Neurology,** v. 67, n. 6, p. 1074-7, Sep 2006. ISSN 1526-632X. Disponível em: < https://www.ncbi.nlm.nih.gov/pubmed/16807408 >.

PASQUALI, L. et al. Autophagy, lithium, and amyotrophic lateral sclerosis. **Muscle Nerve,** v. 40, n. 2, p. 173-94, Aug 2009. ISSN 0148-639X. Disponível em: < https://www.ncbi.nlm.nih.gov/pubmed/19609902 >.

PATEL, A. et al. A Liquid-to-Solid Phase Transition of the ALS Protein FUS Accelerated by Disease Mutation. **Cell,** v. 162, n. 5, p. 1066-77, Aug 2015. ISSN 1097-4172. Disponível em: < https://www.ncbi.nlm.nih.gov/pubmed/26317470 >.

PATTALI, R.; MOU, Y.; LI, X. J. AAV9 Vector: a Novel modality in gene therapy for spinal muscular atrophy. **Gene Ther**, Jun 2019. ISSN 1476-5462. Disponível em: < https://www.ncbi.nlm.nih.gov/pubmed/31243392 >.

PEHAR, M. et al. Role and Therapeutic Potential of Astrocytes in Amyotrophic Lateral Sclerosis. **Curr Pharm Des,** v. 23, n. 33, p. 5010-5021, 2017. ISSN 1873-4286. Disponível em: < https://www.ncbi.nlm.nih.gov/pubmed/28641533 >.

PEPEU, G.; GRAZIA GIOVANNINI, M. The fate of the brain cholinergic neurons in neurodegenerative diseases. **Brain Res,** v. 1670, p. 173-184, Sep 2017. ISSN 1872-6240. Disponível em: < https://www.ncbi.nlm.nih.gov/pubmed/28652219 >.

PERERA, N. D. et al. Mutant TDP-43 deregulates AMPK activation by PP2A in ALS models. **PLoS One,** v. 9, n. 4, p. e95549, 2014. ISSN 1932-6203. Disponível em: < https://www.ncbi.nlm.nih.gov/pubmed/24740287 >.

PERINI, G. et al. Role of p75 neurotrophin receptor in the neurotoxicity by beta-amyloid peptides and synergistic effect of inflammatory cytokines. **J Exp Med,** v. 195, n. 7, p. 907-18, Apr 2002. ISSN 0022-1007. Disponível em: < https://www.ncbi.nlm.nih.gov/pubmed/11927634 >.

PETRI, S.; KÖRNER, S.; KIAEI, M. Nrf2/ARE Signaling Pathway: Key Mediator in Oxidative Stress and Potential Therapeutic Target in ALS. **Neurol Res Int,** v. 2012, p. 878030, 2012. ISSN 2090-1860. Disponível em: < https://www.ncbi.nlm.nih.gov/pubmed/23050144 >.

PHILIPS, T. et al. Oligodendrocyte dysfunction in the pathogenesis of amyotrophic lateral sclerosis. **Brain,** v. 136, n. Pt 2, p. 471-82, Feb 2013. ISSN 1460-2156. Disponível em: < https://www.ncbi.nlm.nih.gov/pubmed/23378219 >.

PHILLIPS, H. A. et al. CHRNB2 is the second acetylcholine receptor subunit associated with autosomal dominant nocturnal frontal lobe epilepsy. **Am J Hum Genet,** v. 68, n. 1, p. 225-31, Jan 2001. ISSN 0002-9297. Disponível em: < https://www.ncbi.nlm.nih.gov/pubmed/11104662 >.

PIERROT-DESEILLIGNY, C. et al. The role of the human dorsolateral prefrontal cortex in ocular motor behavior. **Ann N Y Acad Sci,** v. 1039, p. 239-51, Apr 2005. ISSN 0077-8923. Disponível em: < https://www.ncbi.nlm.nih.gov/pubmed/15826978 >.

PIGUET, O. Eating disturbance in behavioural-variant frontotemporal dementia. **J Mol Neurosci,** v. 45, n. 3, p. 589-93, Nov 2011. ISSN 1559-1166. Disponível em: < https://www.ncbi.nlm.nih.gov/pubmed/21584651 >.

PIJNENBURG, Y. A. et al. Discriminative and prognostic potential of cerebrospinal fluid phosphoTau/tau ratio and neurofilaments for frontotemporal dementia subtypes. **Alzheimers Dement (Amst),** v. 1, n. 4, p. 505-12, Dec 2015. ISSN 2352-8729. Disponível em: < https://www.ncbi.nlm.nih.gov/pubmed/27239528 >.

PILLI, M. et al. TBK-1 promotes autophagy-mediated antimicrobial defense by controlling autophagosome maturation. **Immunity,** v. 37, n. 2, p. 223-34, Aug 2012. ISSN 1097-4180. Disponível em: < https://www.ncbi.nlm.nih.gov/pubmed/22921120 >.

POLLARI, E. et al. The role of oxidative stress in degeneration of the neuromuscular junction in amyotrophic lateral sclerosis. **Front Cell Neurosci,** v. 8, p. 131, 2014. ISSN 1662-5102. Disponível em: < https://www.ncbi.nlm.nih.gov/pubmed/24860432 >.

POLYMENIDOU, M. et al. Long pre-mRNA depletion and RNA missplicing contribute to neuronal vulnerability from loss of TDP-43. **Nat Neurosci,** v. 14, n. 4, p. 459-68, Apr 2011. ISSN 1546-1726. Disponível em: < https://www.ncbi.nlm.nih.gov/pubmed/21358643 >.

POORTHUIS, R. B. et al. Layer-specific modulation of the prefrontal cortex by nicotinic acetylcholine receptors. **Cereb Cortex,** v. 23, n. 1, p. 148-61, Jan 2013. ISSN 1460-2199. Disponível em: < https://www.ncbi.nlm.nih.gov/pubmed/22291029 >.

POTTIER, C. et al. Whole-genome sequencing reveals important role for TBK1 and OPTN mutations in frontotemporal lobar degeneration without motor neuron disease. **Acta Neuropathol,** v. 130, n. 1, p. 77-92, Jul 2015. ISSN 1432-0533. Disponível em: < https://www.ncbi.nlm.nih.gov/pubmed/25943890 >.

PRADAT, P. F. et al. Muscle Nogo-A expression is a prognostic marker in lower motor neuron syndromes. **Ann Neurol,** v. 62, n. 1, p. 15-20, Jul 2007. ISSN 0364-5134. Disponível em: < https://www.ncbi.nlm.nih.gov/pubmed/17455292 >.

PRASAD, D. D. et al. TLS/FUS fusion domain of TLS/FUS-erg chimeric protein resulting from the t(16;21) chromosomal translocation in human myeloid leukemia functions as a transcriptional activation domain. **Oncogene,** v. 9, n. 12, p. 3717-29, Dec 1994. ISSN 0950-9232. Disponível em: < https://www.ncbi.nlm.nih.gov/pubmed/7970732 >.

PREMI, E. et al. Functional genetic variation in the serotonin 5-HTTLPR modulates brain damage in frontotemporal dementia. **Neurobiol Aging,** v. 36, n. 1, p. 446-51, Jan 2015. ISSN 1558-1497. Disponível em: < https://www.ncbi.nlm.nih.gov/pubmed/25128279 >.

PROCTER, A. W.; QURNE, M.; FRANCIS, P. T. Neurochemical features of frontotemporal dementia. **Dement Geriatr Cogn Disord,** v. 10 Suppl 1, p. 80-4, 1999. ISSN 1420-8008. Disponível em: < https://www.ncbi.nlm.nih.gov/pubmed/10436347 >.

PRODAN, C. I.; MONNOT, M.; ROSS, E. D. Behavioural abnormalities associated with rapid deterioration of language functions in semantic dementia respond to sertraline. **J Neurol Neurosurg Psychiatry,** v. 80, n. 12, p. 1416-7, Dec 2009. ISSN 1468-330X. Disponível em: < https://www.ncbi.nlm.nih.gov/pubmed/19917830 >.

PRZYBYLA, M. et al. Disinhibition-like behavior in a P301S mutant tau transgenic mouse model of frontotemporal dementia. **Neurosci Lett,** v. 631, p. 24-9, Sep 2016. ISSN 1872-7972. Disponível em: < https://www.ncbi.nlm.nih.gov/pubmed/27521751 >.

PUN, S. et al. Selective vulnerability and pruning of phasic motoneuron axons in motoneuron disease alleviated by CNTF. **Nat Neurosci,** v. 9, n. 3, p. 408-19, Mar 2006. ISSN 1097-6256. Disponível em: < https://www.ncbi.nlm.nih.gov/pubmed/16474388 >.

PUPILLO, E. et al. Long-term survival in amyotrophic lateral sclerosis: a population-based study. **Ann Neurol,** v. 75, n. 2, p. 287-97, Feb 2014. ISSN 1531-8249. Disponível em: < https://www.ncbi.nlm.nih.gov/pubmed/24382602 >.

PÁKÁSKI, M.; KÁLMÁN, J. Interactions between the amyloid and cholinergic mechanisms in Alzheimer's disease. **Neurochem Int,** v. 53, n. 5, p. 103-11, Nov 2008. ISSN 0197-0186. Disponível em: < https://www.ncbi.nlm.nih.gov/pubmed/18602955 >.

QAMAR, S. et al. FUS Phase Separation Is Modulated by a Molecular Chaperone and Methylation of Arginine Cation-π Interactions. **Cell,** v. 173, n. 3, p. 720-734.e15, 04 2018. ISSN 1097-4172. Disponível em: < https://www.ncbi.nlm.nih.gov/pubmed/29677515 >.

QIU, H. et al. ALS-associated mutation FUS-R521C causes DNA damage and RNA splicing defects. **J Clin Invest,** v. 124, n. 3, p. 981-99, Mar 2014. ISSN 1558-8238. Disponível em: < https://www.ncbi.nlm.nih.gov/pubmed/24509083 >.

QUIK, M.; PEREZ, X. A.; BORDIA, T. Nicotine as a potential neuroprotective agent for Parkinson's disease. **Mov Disord,** v. 27, n. 8, p. 947-57, Jul 2012. ISSN 1531-8257. Disponível em: < https://www.ncbi.nlm.nih.gov/pubmed/22693036 >.

RAAPHORST, J. et al. Cognitive dysfunction in lower motor neuron disease: executive and memory deficits in progressive muscular atrophy. **J Neurol Neurosurg Psychiatry,** v. 82, n. 2, p. 170-5, Feb 2011. ISSN 1468-330X. Disponível em: < https://www.ncbi.nlm.nih.gov/pubmed/20562407 >.

RABBITTS, T. H. et al. Fusion of the dominant negative transcription regulator CHOP with a novel gene FUS by translocation t(12;16) in malignant liposarcoma. **Nat Genet,** v. 4, n. 2, p. 175-80, Jun 1993. ISSN 1061-4036. Disponível em: < https://www.ncbi.nlm.nih.gov/pubmed/7503811 >.

RACZYNSKA, K. D. et al. FUS/TLS contributes to replication-dependent histone gene expression by interaction with U7 snRNPs and histone-specific transcription factors. **Nucleic Acids Res,** v. 43, n. 20, p. 9711-28, Nov 2015. ISSN 1362-4962. Disponível em: < https://www.ncbi.nlm.nih.gov/pubmed/26250115 >.

RAJPUT, A. et al. Identification of FUS p.R377W in essential tremor. **Eur J Neurol,** v. 21, n. 2, p. 361-3, Feb 2014. ISSN 1468-1331. Disponível em: < https://www.ncbi.nlm.nih.gov/pubmed/23834483 >.

RASCOVSKY, K. et al. Sensitivity of revised diagnostic criteria for the behavioural variant of frontotemporal dementia. **Brain,** v. 134, n. Pt 9, p. 2456-77, Sep 2011. ISSN 1460-2156. Disponível em: < https://www.ncbi.nlm.nih.gov/pubmed/21810890 >.

RASOANANDRIANINA, H. et al. Region-specific impairment of the cervical spinal cord (SC) in amyotrophic lateral sclerosis: A preliminary study using SC templates and quantitative MRI (diffusion tensor imaging/inhomogeneous magnetization transfer). **NMR Biomed,** v. 30, n. 12, Dec 2017. ISSN 1099-1492. Disponível em: < https://www.ncbi.nlm.nih.gov/pubmed/28926131 >.

RAVITS, J. Focality, stochasticity and neuroanatomic propagation in ALS pathogenesis. **Exp Neurol,** v. 262 Pt B, p. 121-6, Dec 2014. ISSN 1090-2430. Disponível em: < https://www.ncbi.nlm.nih.gov/pubmed/25108067 >.

RAVITS, J. M.; LA SPADA, A. R. ALS motor phenotype heterogeneity, focality, and spread: deconstructing motor neuron degeneration. **Neurology,** v. 73, n. 10, p. 805-11, Sep 2009. ISSN 1526-632X. Disponível em: < https://www.ncbi.nlm.nih.gov/pubmed/19738176 >.

RAYNOR, E. M.; SHEFNER, J. M. Recurrent inhibition is decreased in patients with amyotrophic lateral sclerosis. **Neurology,** v. 44, n. 11, p. 2148-53, Nov 1994. ISSN 0028-3878. Disponível em: < https://www.ncbi.nlm.nih.gov/pubmed/7969975 >.

REAUME, A. G. et al. Motor neurons in Cu/Zn superoxide dismutase-deficient mice develop normally but exhibit enhanced cell death after axonal injury. **Nat Genet,** v. 13, n. 1, p. 43-7, May 1996. ISSN 1061-4036. Disponível em: < https://www.ncbi.nlm.nih.gov/pubmed/8673102 >.

REN, R. J. et al. History, present, and progress of frontotemporal dementia in china: a systematic review. **Int J Alzheimers Dis,** v. 2012, p. 587215, 2012. ISSN 2090-0252. Disponível em: < https://www.ncbi.nlm.nih.gov/pubmed/22536536 >.

RENTON, A. E.; CHIÒ, A.; TRAYNOR, B. J. State of play in amyotrophic lateral sclerosis genetics. **Nat Neurosci,** v. 17, n. 1, p. 17-23, Jan 2014. ISSN 1546-1726. Disponível em: < https://www.ncbi.nlm.nih.gov/pubmed/24369373 >.

RICHARDSON, P. M.; ISSA, V. M.; RIOPELLE, R. J. Distribution of neuronal receptors for nerve growth factor in the rat. **J Neurosci,** v. 6, n. 8, p. 2312-21, Aug 1986. ISSN 0270-6474. Disponível em: < https://www.ncbi.nlm.nih.gov/pubmed/3018191 >.

RINNE, J. O. et al. Striatal dopamine transporter and extrapyramidal symptoms in frontotemporal dementia. **Neurology,** v. 58, n. 10, p. 1489-93, May 2002. ISSN 0028-3878. Disponível em: < https://www.ncbi.nlm.nih.gov/pubmed/12034784 >.

ROBBERECHT, W.; PHILIPS, T. The changing scene of amyotrophic lateral sclerosis. **Nat Rev Neurosci,** v. 14, n. 4, p. 248-64, Apr 2013. ISSN 1471-0048. Disponível em: < https://www.ncbi.nlm.nih.gov/pubmed/23463272 >.

ROBELIN, L.; GONZALEZ DE AGUILAR, J. L. Blood biomarkers for amyotrophic lateral sclerosis: myth or reality? **Biomed Res Int,** v. 2014, p. 525097, 2014. ISSN 2314-6141. Disponível em: < https://www.ncbi.nlm.nih.gov/pubmed/24991560 >.

ROBERSON, E. D. Mouse models of frontotemporal dementia. **Ann Neurol,** v. 72, n. 6, p. 837-49, Dec 2012. ISSN 1531-8249. Disponível em: < https://www.ncbi.nlm.nih.gov/pubmed/23280835 >.

ROBINSON, H. K. et al. Early lethality and neuronal proteinopathy in mice expressing cytoplasm-targeted FUS that lacks the RNA recognition motif. **Amyotroph Lateral Scler Frontotemporal Degener,** v. 16, n. 5-6, p. 402-9, 2015. ISSN 2167-9223. Disponível em: < https://www.ncbi.nlm.nih.gov/pubmed/25991062 >.

ROCHA, A. J.; MAIA JÚNIOR, A. C. Is magnetic resonance imaging a plausible biomarker for upper motor neuron degeneration in amyotrophic lateral sclerosis/primary lateral sclerosis or merely a useful paraclinical tool to exclude mimic syndromes? A critical review of imaging applicability in

clinical routine. **Arq Neuropsiquiatr,** v. 70, n. 7, p. 532-9, Jul 2012. ISSN 1678-4227. Disponível em: < https://www.ncbi.nlm.nih.gov/pubmed/22836461 >.

ROGELJ, B. et al. Widespread binding of FUS along nascent RNA regulates alternative splicing in the brain. **Sci Rep,** v. 2, p. 603, 2012. ISSN 2045-2322. Disponível em: < https://www.ncbi.nlm.nih.gov/pubmed/22934129 >.

ROHRER, J. D. et al. Serum neurofilament light chain protein is a measure of disease intensity in frontotemporal dementia. **Neurology,** v. 87, n. 13, p. 1329-36, Sep 2016. ISSN 1526-632X. Disponível em: < https://www.ncbi.nlm.nih.gov/pubmed/27581216 >.

ROSELLI, F.; CARONI, P. Modeling neuronal vulnerability in ALS. **Neuron,** v. 83, n. 4, p. 758-60, Aug 2014. ISSN 1097-4199. Disponível em: < https://www.ncbi.nlm.nih.gov/pubmed/25144872 >.

ROSEN, D. R. et al. Genetic linkage analysis of familial amyotrophic lateral sclerosis using human chromosome 21 microsatellite DNA markers. **Am J Med Genet,** v. 51, n. 1, p. 61-9, May 1994. ISSN 0148-7299. Disponível em: < https://www.ncbi.nlm.nih.gov/pubmed/7913294 >.

ROSENBERG, M. M. et al. The postsynaptic adenomatous polyposis coli (APC) multiprotein complex is required for localizing neuroligin and neurexin to neuronal nicotinic synapses in vivo. **J Neurosci,** v. 30, n. 33, p. 11073-85, Aug 2010. ISSN 1529-2401. Disponível em: < https://www.ncbi.nlm.nih.gov/pubmed/20720115 >.

ROSS, C. A.; POIRIER, M. A. Opinion: What is the role of protein aggregation in neurodegeneration? **Nat Rev Mol Cell Biol,** v. 6, n. 11, p. 891-8, Nov 2005. ISSN 1471-0072. Disponível em: < https://www.ncbi.nlm.nih.gov/pubmed/16167052 >.

ROSSKOPF, J. et al. Ex post facto assessment of diffusion tensor imaging metrics from different MRI protocols: preparing for multicentre studies in ALS. **Amyotroph Lateral Scler Frontotemporal Degener,** v. 16, n. 1-2, p. 92-101, Mar 2015. ISSN 2167-9223. Disponível em: < https://www.ncbi.nlm.nih.gov/pubmed/25574564 >.

ROSSO, S. M. et al. Frontotemporal dementia in The Netherlands: patient characteristics and prevalence estimates from a population-based study. **Brain,** v. 126, n. Pt 9, p. 2016-22, Sep 2003. ISSN 0006-8950. Disponível em: < https://www.ncbi.nlm.nih.gov/pubmed/12876142 >.

ROT, G. et al. High-Resolution RNA Maps Suggest Common Principles of Splicing and Polyadenylation Regulation by TDP-43. **Cell Rep,** v. 19, n. 5, p. 1056-1067, 05 2017. ISSN 2211-1247. Disponível em: < https://www.ncbi.nlm.nih.gov/pubmed/28467899 >.

ROTHSTEIN, J. D.; MARTIN, L. J.; KUNCL, R. W. Decreased glutamate transport by the brain and spinal cord in amyotrophic lateral sclerosis. **N Engl J Med,** v. 326, n. 22, p. 1464-8, May 1992. ISSN 0028-4793. Disponível em: < https://www.ncbi.nlm.nih.gov/pubmed/1349424 >.

ROTUNNO, M. S.; BOSCO, D. A. An emerging role for misfolded wild-type SOD1 in sporadic ALS pathogenesis. **Front Cell Neurosci,** v. 7, p. 253, Dec 2013. ISSN 1662-5102. Disponível em: < https://www.ncbi.nlm.nih.gov/pubmed/24379756 >.

ROWLAND, L. P.; SHNEIDER, N. A. Amyotrophic lateral sclerosis. **N Engl J Med,** v. 344, n. 22, p. 1688-700, May 2001. ISSN 0028-4793. Disponível em: < https://www.ncbi.nlm.nih.gov/pubmed/11386269 >.

RULTEN, S. L. et al. PARP-1 dependent recruitment of the amyotrophic lateral sclerosis-associated protein FUS/TLS to sites of oxidative DNA damage. **Nucleic Acids Res,** v. 42, n. 1, p. 307-14, Jan 2014. ISSN 1362-4962. Disponível em: < https://www.ncbi.nlm.nih.gov/pubmed/24049082 >.

RUTHERFORD, N. J. et al. Length of normal alleles of C9ORF72 GGGGCC repeat do not influence disease phenotype. **Neurobiol Aging,** v. 33, n. 12, p. 2950.e5-7, Dec 2012. ISSN 1558-1497. Disponível em: < https://www.ncbi.nlm.nih.gov/pubmed/22840558 >.

RUTKOVE, S. Electrical impedance myography as a biomarker for ALS. **Lancet Neurol,** v. 8, n. 3, p. 226; author reply 227, Mar 2009. ISSN 1474-4422. Disponível em: < https://www.ncbi.nlm.nih.gov/pubmed/19233030 >.

RUTKOVE, S. B. et al. Electrical impedance myography correlates with standard measures of ALS severity. **Muscle Nerve,** v. 49, n. 3, p. 441-3, Mar 2014. ISSN 1097-4598. Disponível em: < https://www.ncbi.nlm.nih.gov/pubmed/24273034 >.

RUTKOVE, S. B. et al. Electrical impedance myography as a biomarker to assess ALS progression. **Amyotroph Lateral Scler,** v. 13, n. 5, p. 439-45, Sep 2012. ISSN 1471-180X. Disponível em: < https://www.ncbi.nlm.nih.gov/pubmed/22670883 >.

RYU, H. H. et al. Autophagy regulates amyotrophic lateral sclerosis-linked fused in sarcoma-positive stress granules in neurons. **Neurobiol Aging,** v. 35, n. 12, p. 2822-2831, Dec 2014. ISSN 1558-1497. Disponível em: < https://www.ncbi.nlm.nih.gov/pubmed/25216585 >.

SABATELLI, M. et al. Mutations in the 3' untranslated region of FUS causing FUS overexpression are associated with amyotrophic lateral sclerosis. **Hum Mol Genet,** v. 22, n. 23, p. 4748-55, Dec 2013. ISSN 1460-2083. Disponível em: < https://www.ncbi.nlm.nih.gov/pubmed/23847048 >.

SABATELLI, M. et al. Uncovering amyotrophic lateral sclerosis phenotypes: clinical features and long-term follow-up of upper motor neuron-dominant ALS. **Amyotroph Lateral Scler,** v. 12, n. 4, p. 278-82, Jul 2011. ISSN 1471-180X. Disponível em: < https://www.ncbi.nlm.nih.gov/pubmed/21702734 >.

SABERI, S. et al. Sense-encoded poly-GR dipeptide repeat proteins correlate to neurodegeneration and uniquely co-localize with TDP-43 in dendrites of repeat-expanded C9orf72 amyotrophic lateral sclerosis. **Acta Neuropathol,** v. 135, n. 3, p. 459-474, 03 2018. ISSN 1432-0533. Disponível em: < https://www.ncbi.nlm.nih.gov/pubmed/29196813 >.

SABERI, S. et al. Neuropathology of Amyotrophic Lateral Sclerosis and Its Variants. **Neurol Clin,** v. 33, n. 4, p. 855-76, Nov 2015. ISSN 1557-9875. Disponível em: < https://www.ncbi.nlm.nih.gov/pubmed/26515626 >.

SAMA, R. R. et al. ALS-linked FUS exerts a gain of toxic function involving aberrant p38 MAPK activation. **Sci Rep,** v. 7, n. 1, p. 115, 03 2017. ISSN 2045-2322. Disponível em: < https://www.ncbi.nlm.nih.gov/pubmed/28273913 >.

SASABE, J. et al. D-amino acid oxidase controls motoneuron degeneration through D-serine. **Proc Natl Acad Sci U S A,** v. 109, n. 2, p. 627-32, Jan 2012. ISSN 1091-6490. Disponível em: < https://www.ncbi.nlm.nih.gov/pubmed/22203986 >.

SAU, D. et al. Mutation of SOD1 in ALS: a gain of a loss of function. **Hum Mol Genet,** v. 16, n. 13, p. 1604-18, Jul 2007. ISSN 0964-6906. Disponível em: < https://www.ncbi.nlm.nih.gov/pubmed/17504823 >.

SCEKIC-ZAHIROVIC, J. et al. Motor neuron intrinsic and extrinsic mechanisms contribute to the pathogenesis of FUS-associated amyotrophic lateral sclerosis. **Acta Neuropathol,** v. 133, n. 6, p. 887-906, 06 2017. ISSN 1432-0533. Disponível em: < https://www.ncbi.nlm.nih.gov/pubmed/28243725 >.

SCEKIC-ZAHIROVIC, J. et al. Toxic gain of function from mutant FUS protein is crucial to trigger cell autonomous motor neuron loss. **EMBO J,** v. 35, n. 10, p. 1077-97, 05 2016. ISSN 1460-2075. Disponível em: < https://www.ncbi.nlm.nih.gov/pubmed/26951610 >.

SCHAFER, D. P.; LEHRMAN, E. K.; STEVENS, B. The "quad-partite" synapse: microglia-synapse interactions in the developing and mature CNS. **Glia,** v. 61, n. 1, p. 24-36, Jan 2013. ISSN 1098-1136. Disponível em: < https://www.ncbi.nlm.nih.gov/pubmed/22829357 >.

SCHERLING, C. S. et al. Cerebrospinal fluid neurofilament concentration reflects disease severity in frontotemporal degeneration. **Ann Neurol,** v. 75, n. 1, p. 116-26, Jan 2014. ISSN 1531-8249. Disponível em: < https://www.ncbi.nlm.nih.gov/pubmed/24242746 >.

SCHIFFER, D. et al. Reactive astrogliosis of the spinal cord in amyotrophic lateral sclerosis. **J Neurol Sci,** v. 139 Suppl, p. 27-33, Aug 1996. ISSN 0022-510X. Disponível em: < https://www.ncbi.nlm.nih.gov/pubmed/8899654 >.

SCHMITZ, T. W.; NATHAN SPRENG, R.; INITIATIVE, A. S. D. N. Basal forebrain degeneration precedes and predicts the cortical spread of Alzheimer's pathology. **Nat Commun,** v. 7, p. 13249, 11 2016. ISSN 2041-1723. Disponível em: < https://www.ncbi.nlm.nih.gov/pubmed/27811848 >.

SCHOEN, M. et al. Super-Resolution Microscopy Reveals Presynaptic Localization of the ALS/FTD Related Protein FUS in Hippocampal Neurons. **Front Cell Neurosci,** v. 9, p. 496, 2015. ISSN 1662-5102. Disponível em: < https://www.ncbi.nlm.nih.gov/pubmed/26834559 >.

SCHROETER, M. L. et al. Frontomedian cortex is central for moral deficits in behavioural variant frontotemporal dementia. **J Neurol Neurosurg Psychiatry,** v. 86, n. 6, p. 700-1, Jun 2015. ISSN 1468-330X. Disponível em: < https://www.ncbi.nlm.nih.gov/pubmed/25248367 >.

SCHROETER, M. L. et al. Towards a nosology for frontotemporal lobar degenerations-a meta-analysis involving 267 subjects. **Neuroimage,** v. 36, n. 3, p. 497-510, Jul 2007. ISSN 1053-8119. Disponível em: < https://www.ncbi.nlm.nih.gov/pubmed/17478101 >.

SCHWARTZ, J. C. et al. FUS binds the CTD of RNA polymerase II and regulates its phosphorylation at Ser2. **Genes Dev,** v. 26, n. 24, p. 2690-5, Dec 2012. ISSN 1549-5477. Disponível em: < https://www.ncbi.nlm.nih.gov/pubmed/23249733 >.

SCHWARTZ, J. C. et al. FUS is sequestered in nuclear aggregates in ALS patient fibroblasts. **Mol Biol Cell,** v. 25, n. 17, p. 2571-8, Sep 2014. ISSN 1939-4586. Disponível em: < https://www.ncbi.nlm.nih.gov/pubmed/25009283 >.

SEELAAR, H. et al. Frequency of ubiquitin and FUS-positive, TDP-43-negative frontotemporal lobar degeneration. **J Neurol,** v. 257, n. 5, p. 747-53, May 2010. ISSN 1432-1459. Disponível em: < https://www.ncbi.nlm.nih.gov/pubmed/19946779 >.

SEELEY, W. W. et al. Neurodegenerative diseases target large-scale human brain networks. **Neuron,** v. 62, n. 1, p. 42-52, Apr 2009. ISSN 1097-4199. Disponível em: < https://www.ncbi.nlm.nih.gov/pubmed/19376066 >.

SEPHTON, C. F. et al. Identification of neuronal RNA targets of TDP-43-containing ribonucleoprotein complexes. **J Biol Chem,** v. 286, n. 2, p. 1204-15, Jan 2011. ISSN 1083-351X. Disponível em: < https://www.ncbi.nlm.nih.gov/pubmed/21051541 >.

SEPHTON, C. F. et al. TDP-43 is a developmentally regulated protein essential for early embryonic development. **J Biol Chem,** v. 285, n. 9, p. 6826-34, Feb 2010. ISSN 1083-351X. Disponível em: < https://www.ncbi.nlm.nih.gov/pubmed/20040602 >.

SHANG, Y.; HUANG, E. J. Mechanisms of FUS mutations in familial amyotrophic lateral sclerosis. **Brain Res,** v. 1647, p. 65-78, 09 2016. ISSN 1872-6240. Disponível em: < https://www.ncbi.nlm.nih.gov/pubmed/27033831 >.

SHARMA, A. et al. ALS-associated mutant FUS induces selective motor neuron degeneration through toxic gain of function. **Nat Commun,** v. 7, p. 10465, Feb 2016. ISSN 2041-1723. Disponível em: < https://www.ncbi.nlm.nih.gov/pubmed/26842965 >.

SHEFNER, J. M.; LOGIGIAN, E. L. The mixed nerve silent period in normal subjects and patients with amyotrophic lateral sclerosis. **Electromyogr Clin Neurophysiol,** v. 38, n. 8, p. 505-10, Dec 1998. ISSN 0301-150X. Disponível em: < https://www.ncbi.nlm.nih.gov/pubmed/9842486 >.

SHEFNER, J. M. et al. Multipoint incremental motor unit number estimation as an outcome measure in ALS. **Neurology,** v. 77, n. 3, p. 235-41, Jul 2011. ISSN 1526-632X. Disponível em: < https://www.ncbi.nlm.nih.gov/pubmed/21676915 >.

SHEN, W. C. et al. Mutations in the ubiquitin-binding domain of OPTN/optineurin interfere with autophagy-mediated degradation of misfolded proteins by a dominant-negative mechanism.

Autophagy, v. 11, n. 4, p. 685-700, Apr 2015. ISSN 1554-8635. Disponível em: < https://www.ncbi.nlm.nih.gov/pubmed/25484089 >.

SHI, K. Y. et al. Toxic PR. **Proc Natl Acad Sci U S A,** v. 114, n. 7, p. E1111-E1117, 02 2017. ISSN 1091-6490. Disponível em: < https://www.ncbi.nlm.nih.gov/pubmed/28069952 >.

SHI, S. H.; JAN, L. Y.; JAN, Y. N. Hippocampal neuronal polarity specified by spatially localized mPar3/mPar6 and PI 3-kinase activity. **Cell,** v. 112, n. 1, p. 63-75, Jan 2003. ISSN 0092-8674. Disponível em: < https://www.ncbi.nlm.nih.gov/pubmed/12526794 >.

SHI, Y. et al. Haploinsufficiency leads to neurodegeneration in C9ORF72 ALS/FTD human induced motor neurons. **Nat Med,** v. 24, n. 3, p. 313-325, 03 2018. ISSN 1546-170X. Disponível em: < https://www.ncbi.nlm.nih.gov/pubmed/29400714 >.

SHIIHASHI, G. et al. Dendritic Homeostasis Disruption in a Novel Frontotemporal Dementia Mouse Model Expressing Cytoplasmic Fused in Sarcoma. **EBioMedicine,** v. 24, p. 102-115, Oct 2017. ISSN 2352-3964. Disponível em: < https://www.ncbi.nlm.nih.gov/pubmed/28928015 >.

SHIIHASHI, G. et al. Mislocated FUS is sufficient for gain-of-toxic-function amyotrophic lateral sclerosis phenotypes in mice. **Brain,** v. 139, n. Pt 9, p. 2380-94, 09 2016. ISSN 1460-2156. Disponível em: < https://www.ncbi.nlm.nih.gov/pubmed/27368346 >.

SHOESMITH, C. L. et al. Prognosis of amyotrophic lateral sclerosis with respiratory onset. **J Neurol Neurosurg Psychiatry,** v. 78, n. 6, p. 629-31, Jun 2007. ISSN 1468-330X. Disponível em: < https://www.ncbi.nlm.nih.gov/pubmed/17088331 >.

SIMÓN-SÁNCHEZ, J. et al. The clinical and pathological phenotype of C9ORF72 hexanucleotide repeat expansions. **Brain,** v. 135, n. Pt 3, p. 723-35, Mar 2012. ISSN 1460-2156. Disponível em: < https://www.ncbi.nlm.nih.gov/pubmed/22300876 >.

SINGH, G. et al. The Clothes Make the mRNA: Past and Present Trends in mRNP Fashion. **Annu Rev Biochem,** v. 84, p. 325-54, 2015. ISSN 1545-4509. Disponível em: < https://www.ncbi.nlm.nih.gov/pubmed/25784054 >.

SIVADASAN, R. et al. C9ORF72 interaction with cofilin modulates actin dynamics in motor neurons. **Nat Neurosci,** v. 19, n. 12, p. 1610-1618, 12 2016. ISSN 1546-1726. Disponível em: < https://www.ncbi.nlm.nih.gov/pubmed/27723745 >.

SKIBINSKI, G. et al. Mutations in the endosomal ESCRTIII-complex subunit CHMP2B in frontotemporal dementia. **Nat Genet,** v. 37, n. 8, p. 806-8, Aug 2005. ISSN 1061-4036. Disponível em: < https://www.ncbi.nlm.nih.gov/pubmed/16041373 >.

SKILLBÄCK, T. et al. CSF neurofilament light differs in neurodegenerative diseases and predicts severity and survival. **Neurology,** v. 83, n. 21, p. 1945-53, Nov 2014. ISSN 1526-632X. Disponível em: < https://www.ncbi.nlm.nih.gov/pubmed/25339208 >.

SKOURTI-STATHAKI, K.; PROUDFOOT, N. J.; GROMAK, N. Human senataxin resolves RNA/DNA hybrids formed at transcriptional pause sites to promote Xrn2-dependent termination. **Mol Cell,** v. 42, n. 6, p. 794-805, Jun 2011. ISSN 1097-4164. Disponível em: < https://www.ncbi.nlm.nih.gov/pubmed/21700224 >.

SMITH, B. N. et al. Exome-wide rare variant analysis identifies TUBA4A mutations associated with familial ALS. **Neuron,** v. 84, n. 2, p. 324-31, Oct 2014. ISSN 1097-4199. Disponível em: < https://www.ncbi.nlm.nih.gov/pubmed/25374358 >.

SOFIC, E. et al. Biogenic amines and metabolites in spinal cord of patients with Parkinson's disease and amyotrophic lateral sclerosis. **J Neural Transm Park Dis Dement Sect,** v. 3, n. 2, p. 133-42, 1991. ISSN 0936-3076. Disponível em: < https://www.ncbi.nlm.nih.gov/pubmed/1716905 >.

SOFRONIEW, M. V. Astrocyte barriers to neurotoxic inflammation. **Nat Rev Neurosci,** v. 16, n. 5, p. 249-63, May 2015. ISSN 1471-0048. Disponível em: < https://www.ncbi.nlm.nih.gov/pubmed/25891508 >.

SPARKS, D. L.; MARKESBERY, W. R. Altered serotonergic and cholinergic synaptic markers in Pick's disease. **Arch Neurol,** v. 48, n. 8, p. 796-9, Aug 1991. ISSN 0003-9942. Disponível em: < https://www.ncbi.nlm.nih.gov/pubmed/1898253 >.

SPATARO, R. et al. Tracheostomy mechanical ventilation in patients with amyotrophic lateral sclerosis: clinical features and survival analysis. **J Neurol Sci,** v. 323, n. 1-2, p. 66-70, Dec 2012. ISSN 1878-5883. Disponível em: < https://www.ncbi.nlm.nih.gov/pubmed/22989611 >.

SPILLANTINI, M. G. Parkinson's disease, dementia with Lewy bodies and multiple system atrophy are alpha-synucleinopathies. **Parkinsonism Relat Disord,** v. 5, n. 4, p. 157-62, Dec 1999. ISSN 1353-8020. Disponível em: < https://www.ncbi.nlm.nih.gov/pubmed/18591134 >.

SREEDHARAN, J. et al. TDP-43 mutations in familial and sporadic amyotrophic lateral sclerosis. **Science,** v. 319, n. 5870, p. 1668-72, Mar 2008. ISSN 1095-9203. Disponível em: < https://www.ncbi.nlm.nih.gov/pubmed/18309045 >.

STATLAND, J. M. et al. Rasagiline for amyotrophic lateral sclerosis: A randomized, controlled trial. **Muscle Nerve,** v. 59, n. 2, p. 201-207, 02 2019. ISSN 1097-4598. Disponível em: < https://www.ncbi.nlm.nih.gov/pubmed/30192007 >.

STAUNTON, L.; JOCKUSCH, H.; OHLENDIECK, K. Proteomic analysis of muscle affected by motor neuron degeneration: the wobbler mouse model of amyotrophic lateral sclerosis. **Biochem Biophys Res Commun,** v. 406, n. 4, p. 595-600, Mar 2011. ISSN 1090-2104. Disponível em: < https://www.ncbi.nlm.nih.gov/pubmed/21354103 >.

STIEBER, A.; GONATAS, J. O.; GONATAS, N. K. Aggregates of mutant protein appear progressively in dendrites, in periaxonal processes of oligodendrocytes, and in neuronal and astrocytic perikarya of mice expressing the SOD1(G93A) mutation of familial amyotrophic lateral sclerosis. **J Neurol Sci,** v. 177, n. 2, p. 114-23, Aug 2000. ISSN 0022-510X. Disponível em: < https://www.ncbi.nlm.nih.gov/pubmed/10980307 >.

STONE, J. et al. Non-Picks frontotemporal dementia imitating schizophrenia in a 22-year-old man. **J Neurol,** v. 250, n. 3, p. 369-70, Mar 2003. ISSN 0340-5354. Disponível em: < https://www.ncbi.nlm.nih.gov/pubmed/12749325 >.

SU, X. W. et al. Biomarker-based predictive models for prognosis in amyotrophic lateral sclerosis. **JAMA Neurol,** v. 70, n. 12, p. 1505-11, Dec 2013. ISSN 2168-6157. Disponível em: < https://www.ncbi.nlm.nih.gov/pubmed/24145899 >.

SUAREZ-CALVET, M. et al. Monomethylated and unmethylated FUS exhibit increased binding to Transportin and distinguish FTLD-FUS from ALS-FUS. **Acta Neuropathol,** v. 131, n. 4, p. 587-604, Apr 2016. ISSN 1432-0533 (Electronic)
0001-6322 (Linking). Disponível em: < http://www.ncbi.nlm.nih.gov/pubmed/26895297 >.

SUDHAMAN, S. et al. Evidence of mutations in RIC3 acetylcholine receptor chaperone as a novel cause of autosomal-dominant Parkinson's disease with non-motor phenotypes. **J Med Genet,** v. 53, n. 8, p. 559-66, 08 2016. ISSN 1468-6244. Disponível em: < https://www.ncbi.nlm.nih.gov/pubmed/27055476 >.

SUGIURA, T.; SAKURAI, K.; NAGANO, Y. Intracellular characterization of DDX39, a novel growth-associated RNA helicase. **Exp Cell Res,** v. 313, n. 4, p. 782-90, Feb 2007. ISSN 0014-4827. Disponível em: < https://www.ncbi.nlm.nih.gov/pubmed/17196963 >.

SUN, Z. et al. Molecular determinants and genetic modifiers of aggregation and toxicity for the ALS disease protein FUS/TLS. **PLoS Biol,** v. 9, n. 4, p. e1000614, Apr 2011. ISSN 1545-7885. Disponível em: < https://www.ncbi.nlm.nih.gov/pubmed/21541367 >.

SUNIL, N.; LEE, S.; SHEA, T. B. Interference with kinesin-based anterograde neurofilament axonal transport increases neurofilament-neurofilament bundling. **Cytoskeleton (Hoboken),** v. 69, n. 6, p. 371-9, Jun 2012. ISSN 1949-3592. Disponível em: < https://www.ncbi.nlm.nih.gov/pubmed/22434685 >.

SWANBERG, M. M. Memantine for behavioral disturbances in frontotemporal dementia: a case series. **Alzheimer Dis Assoc Disord,** v. 21, n. 2, p. 164-6, 2007 Apr-Jun 2007. ISSN 0893-0341. Disponível em: < https://www.ncbi.nlm.nih.gov/pubmed/17545743 >.

SWINNEN, B.; ROBBERECHT, W. The phenotypic variability of amyotrophic lateral sclerosis. **Nat Rev Neurol,** v. 10, n. 11, p. 661-70, Nov 2014. ISSN 1759-4766. Disponível em: < https://www.ncbi.nlm.nih.gov/pubmed/25311585 >.

SÜSSMUTH, S. D. et al. CSF glial markers correlate with survival in amyotrophic lateral sclerosis. **Neurology,** v. 74, n. 12, p. 982-7, Mar 2010. ISSN 1526-632X. Disponível em: < https://www.ncbi.nlm.nih.gov/pubmed/20308682 >.

TAN, A. Y. et al. TLS/FUS (translocated in liposarcoma/fused in sarcoma) regulates target gene transcription via single-stranded DNA response elements. **Proc Natl Acad Sci U S A,** v. 109, n. 16, p.

6030-5, Apr 2012. ISSN 1091-6490. Disponível em: < https://www.ncbi.nlm.nih.gov/pubmed/22460799 >.

TANG, J. et al. PRMT1 is the predominant type I protein arginine methyltransferase in mammalian cells. **J Biol Chem,** v. 275, n. 11, p. 7723-30, Mar 2000. ISSN 0021-9258. Disponível em: < https://www.ncbi.nlm.nih.gov/pubmed/10713084 >.

TARIOT, P. N. et al. Memantine treatment in patients with moderate to severe Alzheimer disease already receiving donepezil: a randomized controlled trial. **JAMA,** v. 291, n. 3, p. 317-24, Jan 2004. ISSN 1538-3598. Disponível em: < https://www.ncbi.nlm.nih.gov/pubmed/14734594 >.

TARTAGLIA, M. C. et al. Differentiation between primary lateral sclerosis and amyotrophic lateral sclerosis: examination of symptoms and signs at disease onset and during follow-up. **Arch Neurol,** v. 64, n. 2, p. 232-6, Feb 2007. ISSN 0003-9942. Disponível em: < https://www.ncbi.nlm.nih.gov/pubmed/17296839 >.

TEMBURNI, M. K. et al. Neuronal nicotinic synapse assembly requires the adenomatous polyposis coli tumor suppressor protein. **J Neurosci,** v. 24, n. 30, p. 6776-84, Jul 2004. ISSN 1529-2401. Disponível em: < https://www.ncbi.nlm.nih.gov/pubmed/15282282 >.

TEULING, E. et al. Motor neuron disease-associated mutant vesicle-associated membrane protein-associated protein (VAP) B recruits wild-type VAPs into endoplasmic reticulum-derived tubular aggregates. **J Neurosci,** v. 27, n. 36, p. 9801-15, Sep 2007. ISSN 1529-2401. Disponível em: < https://www.ncbi.nlm.nih.gov/pubmed/17804640 >.

THIELE, A. Muscarinic signaling in the brain. **Annu Rev Neurosci,** v. 36, p. 271-94, Jul 2013. ISSN 1545-4126. Disponível em: < https://www.ncbi.nlm.nih.gov/pubmed/23841840 >.

TIPPETT, D. C.; HILLIS, A. E.; TSAPKINI, K. Treatment of Primary Progressive Aphasia. **Curr Treat Options Neurol,** v. 17, n. 8, p. 362, Aug 2015. ISSN 1092-8480. Disponível em: < https://www.ncbi.nlm.nih.gov/pubmed/26062526 >.

TIWARI, A.; XU, Z.; HAYWARD, L. J. Aberrantly increased hydrophobicity shared by mutants of Cu,Zn-superoxide dismutase in familial amyotrophic lateral sclerosis. **J Biol Chem,** v. 280, n. 33, p. 29771-9, Aug 2005. ISSN 0021-9258. Disponível em: < https://www.ncbi.nlm.nih.gov/pubmed/15958382 >.

TODD, P. K.; PAULSON, H. L. C9orf72-associated FTD/ALS: when less is more. **Neuron,** v. 80, n. 2, p. 257-8, Oct 2013. ISSN 1097-4199. Disponível em: < https://www.ncbi.nlm.nih.gov/pubmed/24139028 >.

TOLLERVEY, J. R. et al. Characterizing the RNA targets and position-dependent splicing regulation by TDP-43. **Nat Neurosci,** v. 14, n. 4, p. 452-8, Apr 2011. ISSN 1546-1726. Disponível em: < https://www.ncbi.nlm.nih.gov/pubmed/21358640 >.

TORTELLI, R. et al. Elevated cerebrospinal fluid neurofilament light levels in patients with amyotrophic lateral sclerosis: a possible marker of disease severity and progression. **Eur J Neurol,** v.

19, n. 12, p. 1561-7, Dec 2012. ISSN 1468-1331. Disponível em: < https://www.ncbi.nlm.nih.gov/pubmed/22680408 >.

TOURRIÈRE, H. et al. The RasGAP-associated endoribonuclease G3BP assembles stress granules. **J Cell Biol,** v. 160, n. 6, p. 823-31, Mar 2003. ISSN 0021-9525. Disponível em: < https://www.ncbi.nlm.nih.gov/pubmed/12642610 >.

TRADEWELL, M. L. et al. Arginine methylation by PRMT1 regulates nuclear-cytoplasmic localization and toxicity of FUS/TLS harbouring ALS-linked mutations. **Hum Mol Genet,** v. 21, n. 1, p. 136-49, Jan 2012. ISSN 1460-2083. Disponível em: < https://www.ncbi.nlm.nih.gov/pubmed/21965298 >.

TRESSE, E. et al. VCP/p97 is essential for maturation of ubiquitin-containing autophagosomes and this function is impaired by mutations that cause IBMPFD. **Autophagy,** v. 6, n. 2, p. 217-27, Feb 2010. ISSN 1554-8635. Disponível em: < https://www.ncbi.nlm.nih.gov/pubmed/20104022 >.

TSAI, R. M.; BOXER, A. L. Therapy and clinical trials in frontotemporal dementia: past, present, and future. **J Neurochem,** v. 138 Suppl 1, p. 211-21, 08 2016. ISSN 1471-4159. Disponível em: < https://www.ncbi.nlm.nih.gov/pubmed/27306957 >.

TSUJIHATA, M. et al. The motor end-plate fine structure and ultrastructural localization of acetylcholine receptors in amyotrophic lateral sclerosis. **Muscle Nerve,** v. 7, n. 3, p. 243-9, 1984 Mar-Apr 1984. ISSN 0148-639X. Disponível em: < https://www.ncbi.nlm.nih.gov/pubmed/6708970 >.

TURNBULL, J. Is edaravone harmful? (A placebo is not a control). **Amyotroph Lateral Scler Frontotemporal Degener,** v. 19, n. 7-8, p. 477-482, 11 2018. ISSN 2167-9223. Disponível em: < https://www.ncbi.nlm.nih.gov/pubmed/30373406 >.

TURNER, B. J.; LOPES, E. C.; CHEEMA, S. S. Neuromuscular accumulation of mutant superoxide dismutase 1 aggregates in a transgenic mouse model of familial amyotrophic lateral sclerosis. **Neurosci Lett,** v. 350, n. 2, p. 132-6, Oct 2003. ISSN 0304-3940. Disponível em: < https://www.ncbi.nlm.nih.gov/pubmed/12972170 >.

TURNER, M. R. et al. [11C]-WAY100635 PET demonstrates marked 5-HT1A receptor changes in sporadic ALS. **Brain,** v. 128, n. Pt 4, p. 896-905, Apr 2005. ISSN 1460-2156. Disponível em: < https://www.ncbi.nlm.nih.gov/pubmed/15689356 >.

UDAGAWA, T. et al. FUS regulates AMPA receptor function and FTLD/ALS-associated behaviour via GluA1 mRNA stabilization. **Nat Commun,** v. 6, p. 7098, May 2015. ISSN 2041-1723. Disponível em: < https://www.ncbi.nlm.nih.gov/pubmed/25968143 >.

UDAKA, F.; KAMEYAMA, M.; TOMONAGA, M. Degeneration of Betz cells in motor neuron disease. A Golgi study. **Acta Neuropathol,** v. 70, n. 3-4, p. 289-95, 1986. ISSN 0001-6322. Disponível em: < https://www.ncbi.nlm.nih.gov/pubmed/2429495 >.

VAISMAN, N. et al. Do patients with amyotrophic lateral sclerosis (ALS) have increased energy needs? **J Neurol Sci,** v. 279, n. 1-2, p. 26-9, Apr 2009. ISSN 1878-5883. Disponível em: < https://www.ncbi.nlm.nih.gov/pubmed/19185883 >.

VALENTINE, J. S.; DOUCETTE, P. A.; ZITTIN POTTER, S. Copper-zinc superoxide dismutase and amyotrophic lateral sclerosis. **Annu Rev Biochem,** v. 74, p. 563-93, 2005. ISSN 0066-4154. Disponível em: < https://www.ncbi.nlm.nih.gov/pubmed/15952898 >.

VAN BLITTERSWIJK, M.; RADEMAKERS, R. Neurodegenerative disease: C9orf72 repeats compromise nucleocytoplasmic transport. **Nat Rev Neurol,** v. 11, n. 12, p. 670-2, Dec 2015. ISSN 1759-4766. Disponível em: < https://www.ncbi.nlm.nih.gov/pubmed/26526532 >.

VAN DAMME, P. et al. Astrocytes regulate GluR2 expression in motor neurons and their vulnerability to excitotoxicity. **Proc Natl Acad Sci U S A,** v. 104, n. 37, p. 14825-30, Sep 2007. ISSN 0027-8424. Disponível em: < https://www.ncbi.nlm.nih.gov/pubmed/17804792 >.

VAN HOECKE, A. et al. EPHA4 is a disease modifier of amyotrophic lateral sclerosis in animal models and in humans. **Nat Med,** v. 18, n. 9, p. 1418-22, Sep 2012. ISSN 1546-170X. Disponível em: < https://www.ncbi.nlm.nih.gov/pubmed/22922411 >.

VAN SWIETEN, J.; SPILLANTINI, M. G. Hereditary frontotemporal dementia caused by Tau gene mutations. **Brain Pathol,** v. 17, n. 1, p. 63-73, Jan 2007. ISSN 1015-6305. Disponível em: < https://www.ncbi.nlm.nih.gov/pubmed/17493040 >.

VANCE, C. et al. Mutations in FUS, an RNA processing protein, cause familial amyotrophic lateral sclerosis type 6. **Science,** v. 323, n. 5918, p. 1208-1211, Feb 2009. ISSN 1095-9203. Disponível em: < https://www.ncbi.nlm.nih.gov/pubmed/19251628 >.

VANCE, C. et al. ALS mutant FUS disrupts nuclear localization and sequesters wild-type FUS within cytoplasmic stress granules. **Hum Mol Genet,** v. 22, n. 13, p. 2676-88, Jul 2013. ISSN 1460-2083. Disponível em: < https://www.ncbi.nlm.nih.gov/pubmed/23474818 >.

VERBEECK, C. et al. Expression of Fused in sarcoma mutations in mice recapitulates the neuropathology of FUS proteinopathies and provides insight into disease pathogenesis. **Mol Neurodegener,** v. 7, p. 53, Oct 2012. ISSN 1750-1326. Disponível em: < https://www.ncbi.nlm.nih.gov/pubmed/23046583 >.

VERCELLETTO, M. et al. Memantine in behavioral variant frontotemporal dementia: negative results. **J Alzheimers Dis,** v. 23, n. 4, p. 749-59, 2011. ISSN 1875-8908. Disponível em: < https://www.ncbi.nlm.nih.gov/pubmed/21157021 >.

VERCRUYSSE, P. et al. Alterations in the hypothalamic melanocortin pathway in amyotrophic lateral sclerosis. **Brain,** v. 139, n. Pt 4, p. 1106-22, Apr 2016. ISSN 1460-2156. Disponível em: < https://www.ncbi.nlm.nih.gov/pubmed/26984187 >.

VERNAY, A. et al. A transgenic mouse expressing CHMP2Bintron5 mutant in neurons develops histological and behavioural features of amyotrophic lateral sclerosis and frontotemporal dementia. **Hum Mol Genet,** v. 25, n. 15, p. 3341-3360, 08 2016. ISSN 1460-2083. Disponível em: < https://www.ncbi.nlm.nih.gov/pubmed/27329763 >.

VERSTRAETE, E. et al. TDP-43 plasma levels are higher in amyotrophic lateral sclerosis. **Amyotroph Lateral Scler,** v. 13, n. 5, p. 446-51, Sep 2012. ISSN 1471-180X. Disponível em: < https://www.ncbi.nlm.nih.gov/pubmed/22873561 >.

VERSTRAETE, E. et al. Structural MRI reveals cortical thinning in amyotrophic lateral sclerosis. **J Neurol Neurosurg Psychiatry,** v. 83, n. 4, p. 383-8, Apr 2012. ISSN 1468-330X. Disponível em: < https://www.ncbi.nlm.nih.gov/pubmed/21965521 >.

VISSER, J. et al. Disease course and prognostic factors of progressive muscular atrophy. **Arch Neurol,** v. 64, n. 4, p. 522-8, Apr 2007. ISSN 0003-9942. Disponível em: < https://www.ncbi.nlm.nih.gov/pubmed/17420313 >.

VOLK, A. E. et al. Current knowledge and recent insights into the genetic basis of amyotrophic lateral sclerosis. **Med Genet,** v. 30, n. 2, p. 252-258, 2018. ISSN 0936-5931. Disponível em: < https://www.ncbi.nlm.nih.gov/pubmed/30220791 >.

VOLKENING, K. et al. Tar DNA binding protein of 43 kDa (TDP-43), 14-3-3 proteins and copper/zinc superoxide dismutase (SOD1) interact to modulate NFL mRNA stability. Implications for altered RNA processing in amyotrophic lateral sclerosis (ALS). **Brain Res,** v. 1305, p. 168-82, Dec 2009. ISSN 1872-6240. Disponível em: < https://www.ncbi.nlm.nih.gov/pubmed/19815002 >.

VUCIC, S.; NICHOLSON, G. A.; KIERNAN, M. C. Cortical hyperexcitability may precede the onset of familial amyotrophic lateral sclerosis. **Brain,** v. 131, n. Pt 6, p. 1540-50, Jun 2008. ISSN 1460-2156. Disponível em: < https://www.ncbi.nlm.nih.gov/pubmed/18469020 >.

VUCIC, S.; ROTHSTEIN, J. D.; KIERNAN, M. C. Advances in treating amyotrophic lateral sclerosis: insights from pathophysiological studies. **Trends Neurosci,** v. 37, n. 8, p. 433-42, Aug 2014. ISSN 1878-108X. Disponível em: < https://www.ncbi.nlm.nih.gov/pubmed/24927875 >.

VÁZQUEZ-COSTA, J. F. et al. Brain signal intensity changes as biomarkers in amyotrophic lateral sclerosis. **Acta Neurol Scand,** v. 137, n. 2, p. 262-271, Feb 2018. ISSN 1600-0404. Disponível em: < https://www.ncbi.nlm.nih.gov/pubmed/29082510 >.

WAIBEL, S. et al. Truncating mutations in FUS/TLS give rise to a more aggressive ALS-phenotype than missense mutations: a clinico-genetic study in Germany. **Eur J Neurol,** v. 20, n. 3, p. 540-6, Mar 2013. ISSN 1468-1331. Disponível em: < https://www.ncbi.nlm.nih.gov/pubmed/23217123 >.

WAIBEL, S. et al. Rasagiline alone and in combination with riluzole prolongs survival in an ALS mouse model. **J Neurol,** v. 251, n. 9, p. 1080-4, Sep 2004. ISSN 0340-5354. Disponível em: < https://www.ncbi.nlm.nih.gov/pubmed/15372249 >.

WALHOUT, R. et al. Cortical thickness in ALS: towards a marker for upper motor neuron involvement. **J Neurol Neurosurg Psychiatry,** v. 86, n. 3, p. 288-94, Mar 2015. ISSN 1468-330X. Disponível em: < https://www.ncbi.nlm.nih.gov/pubmed/25121571 >.

WANG, A. et al. A single N-terminal phosphomimic disrupts TDP-43 polymerization, phase separation, and RNA splicing. **EMBO J,** v. 37, n. 5, 03 2018. ISSN 1460-2075. Disponível em: < https://www.ncbi.nlm.nih.gov/pubmed/29438978 >.

WANG, I. F.; WU, L. S.; SHEN, C. K. TDP-43: an emerging new player in neurodegenerative diseases. **Trends Mol Med,** v. 14, n. 11, p. 479-85, Nov 2008. ISSN 1471-4914. Disponível em: < https://www.ncbi.nlm.nih.gov/pubmed/18929508 >.

WANG, J. et al. An ALS-linked mutant SOD1 produces a locomotor defect associated with aggregation and synaptic dysfunction when expressed in neurons of Caenorhabditis elegans. **PLoS Genet,** v. 5, n. 1, p. e1000350, Jan 2009. ISSN 1553-7404. Disponível em: < https://www.ncbi.nlm.nih.gov/pubmed/19165329 >.

WANG, W. Y. et al. Interaction of FUS and HDAC1 regulates DNA damage response and repair in neurons. **Nat Neurosci,** v. 16, n. 10, p. 1383-91, Oct 2013. ISSN 1546-1726. Disponível em: < https://www.ncbi.nlm.nih.gov/pubmed/24036913 >.

WANG, X. et al. Genetic Variants of Microtubule Actin Cross-linking Factor 1 (MACF1) Confer Risk for Parkinson's Disease. **Mol Neurobiol,** v. 54, n. 4, p. 2878-2888, 05 2017. ISSN 1559-1182. Disponível em: < https://www.ncbi.nlm.nih.gov/pubmed/27021023 >.

WANG, X. et al. Activation of ER Stress and Autophagy Induced by TDP-43 A315T as Pathogenic Mechanism and the Corresponding Histological Changes in Skin as Potential Biomarker for ALS with the Mutation. **Int J Biol Sci,** v. 11, n. 10, p. 1140-9, 2015. ISSN 1449-2288. Disponível em: < https://www.ncbi.nlm.nih.gov/pubmed/26327808 >.

WEINBERGER, D. R. et al. The distribution of cerebral muscarinic acetylcholine receptors in vivo in patients with dementia. A controlled study with 123IQNB and single photon emission computed tomography. **Arch Neurol,** v. 48, n. 2, p. 169-76, Feb 1991. ISSN 0003-9942. Disponível em: < https://www.ncbi.nlm.nih.gov/pubmed/1993008 >.

WHITE, M. A. et al. TDP-43 gains function due to perturbed autoregulation in a Tardbp knock-in mouse model of ALS-FTD. **Nat Neurosci,** v. 21, n. 4, p. 552-563, 04 2018. ISSN 1546-1726. Disponível em: < https://www.ncbi.nlm.nih.gov/pubmed/29556029 >.

WHITEHOUSE, P. J. et al. Basal forebrain neurons in the dementia of Parkinson disease. **Ann Neurol,** v. 13, n. 3, p. 243-8, Mar 1983. ISSN 0364-5134. Disponível em: < https://www.ncbi.nlm.nih.gov/pubmed/6847136 >.

WHITWELL, J. L.; JOSEPHS, K. A. Neuroimaging in frontotemporal lobar degeneration--predicting molecular pathology. **Nat Rev Neurol,** v. 8, n. 3, p. 131-42, Jan 2012. ISSN 1759-4766. Disponível em: < https://www.ncbi.nlm.nih.gov/pubmed/22290573 >.

WILD, P. et al. Phosphorylation of the autophagy receptor optineurin restricts Salmonella growth. **Science,** v. 333, n. 6039, p. 228-33, Jul 2011. ISSN 1095-9203. Disponível em: < https://www.ncbi.nlm.nih.gov/pubmed/21617041 >.

WILLIAMS, K. L. et al. Pathophysiological insights into ALS with C9ORF72 expansions. **J Neurol Neurosurg Psychiatry,** v. 84, n. 8, p. 931-5, Aug 2013. ISSN 1468-330X. Disponível em: < https://www.ncbi.nlm.nih.gov/pubmed/23463871 >.

WILLIAMSON, T. L. et al. Absence of neurofilaments reduces the selective vulnerability of motor neurons and slows disease caused by a familial amyotrophic lateral sclerosis-linked superoxide dismutase 1 mutant. **Proc Natl Acad Sci U S A,** v. 95, n. 16, p. 9631-6, Aug 1998. ISSN 0027-8424. Disponível em: < https://www.ncbi.nlm.nih.gov/pubmed/9689132 >.

WILLS, A. M. et al. Hypercaloric enteral nutrition in patients with amyotrophic lateral sclerosis: a randomised, double-blind, placebo-controlled phase 2 trial. **Lancet,** v. 383, n. 9934, p. 2065-2072, Jun 2014. ISSN 1474-547X. Disponível em: < https://www.ncbi.nlm.nih.gov/pubmed/24582471 >.

WILS, H. et al. TDP-43 transgenic mice develop spastic paralysis and neuronal inclusions characteristic of ALS and frontotemporal lobar degeneration. **Proc Natl Acad Sci U S A,** v. 107, n. 8, p. 3858-63, Feb 2010. ISSN 1091-6490. Disponível em: < https://www.ncbi.nlm.nih.gov/pubmed/20133711 >.

WINER, L. et al. SOD1 in cerebral spinal fluid as a pharmacodynamic marker for antisense oligonucleotide therapy. **JAMA Neurol,** v. 70, n. 2, p. 201-7, Feb 2013. ISSN 2168-6157. Disponível em: < https://www.ncbi.nlm.nih.gov/pubmed/23147550 >.

WINTON, M. J. et al. Disturbance of nuclear and cytoplasmic TAR DNA-binding protein (TDP-43) induces disease-like redistribution, sequestration, and aggregate formation. **J Biol Chem,** v. 283, n. 19, p. 13302-9, May 2008. ISSN 0021-9258. Disponível em: < https://www.ncbi.nlm.nih.gov/pubmed/18305110 >.

WITTIE, M. et al. Utility of capture-recapture methodology to assess completeness of amyotrophic lateral sclerosis case ascertainment. **Neuroepidemiology,** v. 40, n. 2, p. 133-41, 2013. ISSN 1423-0208. Disponível em: < https://www.ncbi.nlm.nih.gov/pubmed/23095852 >.

WOERNER, A. C. et al. Cytoplasmic protein aggregates interfere with nucleocytoplasmic transport of protein and RNA. **Science,** v. 351, n. 6269, p. 173-6, Jan 2016. ISSN 1095-9203. Disponível em: < https://www.ncbi.nlm.nih.gov/pubmed/26634439 >.

WOLOZIN, B. Regulated protein aggregation: stress granules and neurodegeneration. **Mol Neurodegener,** v. 7, p. 56, Nov 2012. ISSN 1750-1326. Disponível em: < https://www.ncbi.nlm.nih.gov/pubmed/23164372 >.

WONG, M.; MARTIN, L. J. Skeletal muscle-restricted expression of human SOD1 causes motor neuron degeneration in transgenic mice. **Hum Mol Genet,** v. 19, n. 11, p. 2284-302, Jun 2010. ISSN 1460-2083. Disponível em: < https://www.ncbi.nlm.nih.gov/pubmed/20223753 >.

WONG, Y. C.; HOLZBAUR, E. L. Optineurin is an autophagy receptor for damaged mitochondria in parkin-mediated mitophagy that is disrupted by an ALS-linked mutation. **Proc Natl Acad Sci U S A,** v. 111, n. 42, p. E4439-48, Oct 2014. ISSN 1091-6490. Disponível em: < https://www.ncbi.nlm.nih.gov/pubmed/25294927 >.

WOOD, P. L. et al. A post-mortem comparison of the cortical cholinergic system in Alzheimer's disease and Pick's disease. **J Neurol Sci,** v. 62, n. 1-3, p. 211-7, Dec 1983. ISSN 0022-510X. Disponível em: < https://www.ncbi.nlm.nih.gov/pubmed/6142096 >.

WU, C. H. et al. Mutations in the profilin 1 gene cause familial amyotrophic lateral sclerosis. **Nature,** v. 488, n. 7412, p. 499-503, Aug 2012. ISSN 1476-4687. Disponível em: < https://www.ncbi.nlm.nih.gov/pubmed/22801503 >.

WU, D. et al. Angiogenin loss-of-function mutations in amyotrophic lateral sclerosis. **Ann Neurol,** v. 62, n. 6, p. 609-17, Dec 2007. ISSN 1531-8249. Disponível em: < https://www.ncbi.nlm.nih.gov/pubmed/17886298 >.

WU, L. S.; CHENG, W. C.; SHEN, C. K. Targeted depletion of TDP-43 expression in the spinal cord motor neurons leads to the development of amyotrophic lateral sclerosis-like phenotypes in mice. **J Biol Chem,** v. 287, n. 33, p. 27335-44, Aug 2012. ISSN 1083-351X. Disponível em: < https://www.ncbi.nlm.nih.gov/pubmed/22718760 >.

YAMANAKA, K. et al. Astrocytes as determinants of disease progression in inherited amyotrophic lateral sclerosis. **Nat Neurosci,** v. 11, n. 3, p. 251-3, Mar 2008. ISSN 1097-6256. Disponível em: < https://www.ncbi.nlm.nih.gov/pubmed/18246065 >.

YAMASHITA, S. et al. Sporadic juvenile amyotrophic lateral sclerosis caused by mutant FUS/TLS: possible association of mental retardation with this mutation. **J Neurol,** v. 259, n. 6, p. 1039-44, Jun 2012. ISSN 1432-1459. Disponível em: < https://www.ncbi.nlm.nih.gov/pubmed/22057404 >.

YAMAZAKI, T. et al. FUS-SMN protein interactions link the motor neuron diseases ALS and SMA. **Cell Rep,** v. 2, n. 4, p. 799-806, Oct 2012. ISSN 2211-1247. Disponível em: < https://www.ncbi.nlm.nih.gov/pubmed/23022481 >.

YANG, C. et al. Partial loss of TDP-43 function causes phenotypes of amyotrophic lateral sclerosis. **Proc Natl Acad Sci U S A,** v. 111, n. 12, p. E1121-9, Mar 2014. ISSN 1091-6490. Disponível em: < https://www.ncbi.nlm.nih.gov/pubmed/24616503 >.

YANG, L. et al. Self-assembled FUS binds active chromatin and regulates gene transcription. **Proc Natl Acad Sci U S A,** v. 111, n. 50, p. 17809-14, Dec 2014. ISSN 1091-6490. Disponível em: < https://www.ncbi.nlm.nih.gov/pubmed/25453086 >.

YASUDA, K. et al. The RNA-binding protein Fus directs translation of localized mRNAs in APC-RNP granules. **J Cell Biol,** v. 203, n. 5, p. 737-46, Dec 2013. ISSN 1540-8140. Disponível em: < https://www.ncbi.nlm.nih.gov/pubmed/24297750 >.

YOKOI, S. et al. 3'UTR Length-Dependent Control of SynGAP Isoform alpha2 mRNA by FUS and ELAV-like Proteins Promotes Dendritic Spine Maturation and Cognitive Function. **Cell Rep,** v. 20, n. 13, p. 3071-3084, Sep 26 2017. ISSN 2211-1247 (Electronic). Disponível em: < https://www.ncbi.nlm.nih.gov/pubmed/28954225 >.

YOSHIMURA, A. et al. Myosin-Va facilitates the accumulation of mRNA/protein complex in dendritic spines. **Curr Biol,** v. 16, n. 23, p. 2345-51, Dec 2006. ISSN 0960-9822. Disponível em: < https://www.ncbi.nlm.nih.gov/pubmed/17141617 >.

YU, T. et al. The pivotal role of TBK1 in inflammatory responses mediated by macrophages. **Mediators Inflamm,** v. 2012, p. 979105, 2012. ISSN 1466-1861. Disponível em: < https://www.ncbi.nlm.nih.gov/pubmed/23304064 >.

YU, Y.; REED, R. FUS functions in coupling transcription to splicing by mediating an interaction between RNAP II and U1 snRNP. **Proc Natl Acad Sci U S A,** v. 112, n. 28, p. 8608-13, Jul 2015. ISSN 1091-6490. Disponível em: < https://www.ncbi.nlm.nih.gov/pubmed/26124092 >.

ZALDIVAR, T. et al. Reduced frequency of ALS in an ethnically mixed population: a population-based mortality study. **Neurology,** v. 72, n. 19, p. 1640-5, May 2009. ISSN 1526-632X. Disponível em: < https://www.ncbi.nlm.nih.gov/pubmed/19433736 >.

ZHANG, F. et al. Interaction between familial amyotrophic lateral sclerosis (ALS)-linked SOD1 mutants and the dynein complex. **J Biol Chem,** v. 282, n. 22, p. 16691-9, Jun 2007. ISSN 0021-9258. Disponível em: < https://www.ncbi.nlm.nih.gov/pubmed/17403682 >.

ZHANG, H. et al. TDP-43-immunoreactive neuronal and glial inclusions in the neostriatum in amyotrophic lateral sclerosis with and without dementia. **Acta Neuropathol,** v. 115, n. 1, p. 115-22, Jan 2008. ISSN 0001-6322. Disponível em: < https://www.ncbi.nlm.nih.gov/pubmed/17786458 >.

ZHANG, J. et al. Altered distributions of nucleocytoplasmic transport-related proteins in the spinal cord of a mouse model of amyotrophic lateral sclerosis. **Acta Neuropathol,** v. 112, n. 6, p. 673-80, Dec 2006. ISSN 0001-6322. Disponível em: < https://www.ncbi.nlm.nih.gov/pubmed/16957927 >.

ZHANG, K. et al. The C9orf72 repeat expansion disrupts nucleocytoplasmic transport. **Nature,** v. 525, n. 7567, p. 56-61, Sep 2015. ISSN 1476-4687. Disponível em: < https://www.ncbi.nlm.nih.gov/pubmed/26308891 >.

ZHANG, Q. et al. Side of limb-onset predicts laterality of gray matter loss in amyotrophic lateral sclerosis. **Biomed Res Int,** v. 2014, p. 473250, 2014. ISSN 2314-6141. Disponível em: < https://www.ncbi.nlm.nih.gov/pubmed/25093168 >.

ZHANG, W. et al. Hyperactive somatostatin interneurons contribute to excitotoxicity in neurodegenerative disorders. **Nat Neurosci,** v. 19, n. 4, p. 557-559, Apr 2016. ISSN 1546-1726. Disponível em: < https://www.ncbi.nlm.nih.gov/pubmed/26900927 >.

ZHANG, Y. et al. MRI signatures of brain macrostructural atrophy and microstructural degradation in frontotemporal lobar degeneration subtypes. **J Alzheimers Dis,** v. 33, n. 2, p. 431-44, 2013. ISSN 1875-8908. Disponível em: < https://www.ncbi.nlm.nih.gov/pubmed/22976075 >.

ZHOU, F. et al. Altered motor network functional connectivity in amyotrophic lateral sclerosis: a resting-state functional magnetic resonance imaging study. **Neuroreport,** v. 24, n. 12, p. 657-62, Aug 2013. ISSN 1473-558X. Disponível em: < https://www.ncbi.nlm.nih.gov/pubmed/23839257 >.

ZHOU, Y. et al. ALS-associated FUS mutations result in compromised FUS alternative splicing and autoregulation. **PLoS Genet,** v. 9, n. 10, p. e1003895, Oct 2013. ISSN 1553-7404. Disponível em: < https://www.ncbi.nlm.nih.gov/pubmed/24204307 >.

ZIEGLER, D. A. et al. Substantia nigra volume loss before basal forebrain degeneration in early Parkinson disease. **JAMA Neurol,** v. 70, n. 2, p. 241-7, Feb 2013. ISSN 2168-6157. Disponível em: < https://www.ncbi.nlm.nih.gov/pubmed/23183921 >.

ZOCCOLELLA, S. et al. Riluzole and amyotrophic lateral sclerosis survival: a population-based study in southern Italy. **Eur J Neurol,** v. 14, n. 3, p. 262-8, Mar 2007. ISSN 1468-1331. Disponível em: < https://www.ncbi.nlm.nih.gov/pubmed/17355545 >.

ZU, T. et al. RAN proteins and RNA foci from antisense transcripts in C9ORF72 ALS and frontotemporal dementia. **Proc Natl Acad Sci U S A,** v. 110, n. 51, p. E4968-77, Dec 2013. ISSN 1091-6490. Disponível em: < https://www.ncbi.nlm.nih.gov/pubmed/24248382 >.

UNIVERSITE DE STRASBOURG

RESUME DE LA THESE DE DOCTORAT

Discipline : Neurosciences et Sciences de la Santé

Présentée par : Inmaculada SANJUAN RUIZ

Titre : Mécanismes physiopathologiques de la sclérose latérale amyotrophique causée par des mutations du gène *FUS*

Unité de Recherche : Inserm U-1118 Mécanismes centraux et périphériques de la neurodégénérescence

Directeur de Thèse : DUPUIS, Luc – Directeur de Recherche

Localisation : Strasbourg

ECOLES DOCTORALES :
(cocher la case)

☐ ED - Sciences de l'Homme et des sociétés ☐ ED 99 – Humanités ☐ ED 101 – Droit, sciences politique et histoire ☐ ED 182 – Physique et chimie physique ☐ ED 221 – Augustin Cournot ☐ ED 222 - Sciences chimiques	☐ ED 269 - Mathématiques, sciences de l'information et de l'ingénieur ☐ ED 270 – Théologie et sciences religieuses ☐ ED 413 – Sciences de la terre, de l'univers et de l'environnement ☒ ED 414 – Sciences de la vie et de la santé

Liste d'articles :

- *Soumis, actuellement en révision à Nature Neuroscience*
  FUS-mediated transcriptional regulation of acetylcholine receptor at neuromuscular junctions is compromised in amyotrophic lateral sclerosis

  G. Picchiarelli*, M Demestre*, A Zuko, M Been, J Higelin, Dieterle S, MA Goy, M Mallik, C. Sellier, J Scekic-Zahirovic L Zhang, A Rosenbohm, C Sijlmans, A Aly, S Mersmann, **I Sanjuan-Ruiz,** AM Hubers, N Messadeq, M Wagner, N van Bakel, AL Boutillier, AC Ludolph, C Lagier-Tourenne, TM Boeckers#, L Dupuis# & E. Storkebaum#

- *En préparation*
  - A mutation in *Fus* leads to defective central cholinergic signalling relevant to fronto-temporal dementia

  Sanjuan-Ruiz I*, Scekic-Zahirovic J*, et al.

  - Cytoplasmic FUS accumulation triggers synaptic dysfunction and altered behaviour relevant to fronto-temporal dementia

  Scekic-Zahirovic J*, **Sanjuan-Ruiz I***, et al.

  - Phenotypic rescue of a mouse model of *FUS*-ALS by addition of an autoregulatory competent wild-type *FUS* transgene.

  Sanjuan-Ruiz I, et al.

Liste de communications orales et posters :

- *Communications orales :* "Testing for synergy between loss and gain of function in causing motor neuron degeneration" par Inmaculada SANJUAN-RUIZ
  - 4ème Journées Recherche sur la SLA et les maladies du neurone moteur (JR4SLA) 16-17 Octobre 2018 – Paris, France (prix de la meilleure communication orale)
  - 1er French, German and Swiss Symposium on ALS and FTD
    28 Feb to 02 March 2019 – Gunzburg, Allemagne

- *Posters :* par Inmaculada SANJUAN-RUIZ
  - "FTD-like Behavior Is Accompanied With Loss Of Cortical Cholinergic Innervation In A Fus Knock-in Mouse Model Of ALS-FTD"
    4ème Journées Recherche sur la SLA et les maladies du neurone moteur (JR4SLA) – 16-17 Octobre 2018 – Paris, France
  - "Testing for synergy between loss and gain of function in causing motor neuron degeneration"
    ENCALS 20-22 Juin 2018 – Oxford, Angleterre
  - "Testing for synergy between loss and gain of function in causing motor neuron degeneration"
    Advances in neurodevelopmental and neurodegenerative disorders, 3ème Journées Thématiques IGBMC – 7-8 Juin 2018 – Strasbourg, France
  - "Testing for synergy between loss and gain of function in causing motor neuron degeneration"
    3ème Journées Recherche sur la SLA et les maladies du neurone moteur (JR3SLA) – 16-17 Octobre 2017 – Paris, France

Résumé de la thèse :

La sclérose latérale amyotrophique (SLA) est une maladie neurodégénérative affectant l'adulte avec une incidence de 3 nouveaux cas pour 100.000 individus par année et une prévalence de 1/1000. La SLA est caractérisée par une dégénérescence des neurones moteurs qui contrôlent la contraction des muscles squelettiques. La dégénérescence de ce type cellulaire entraîne une paralysie progressive, résultant en la mort du patient par insuffisance respiratoire, généralement en 2 à 5 années après le déclenchement des symptômes. Il n'y a aucun traitement actuellement capable de guérir cette maladie à l'exception du riluzole qui augmente l'espérance de vie de quelques mois. La SLA est un phénotype extrême d'un continuum pathophysiologique avec une autre maladie neurodégénérative, appelée démence fronto-temporale (DFT). La DFT est la démence la plus fréquente après la maladie d'Alzheimer, et est caractérisée par des anomalies du comportement social, du langage et des défauts exécutifs progressifs qui amènent au décès en 5 à 8 ans. La SLA et la DFT se superposent cliniquement, partagent les mêmes lésions anatomo-pathologiques et des mutations dans les mêmes gènes provoquent ces deux maladies.

La plupart des cas de SLA ne sont pas associés à une histoire familiale, et sont appelés cas « sporadiques » de SLA (sSLA). Cependant, 10 à 20% des cas de SLA et de démence fronto-temporale (DFT) sont d'origine héréditaire, et sont appelés cas « familiaux » de SLA (fSLA). Parmi ces cas, environ 5% sont dus à des mutations du gène *FUS*. Les cas de SLA associés à des mutations de FUS sont caractérisés par un déclenchement très jeune parfois dès l'âge de 20 ans et une progression très rapide et agressive résultant en la mort du patient au bout de quelques mois. De façon importante, des agrégats de FUS sont aussi retrouvés dans une partie importante de patients affectés par la DFT, sans que, dans la plupart de ces cas, des mutations germinales de *FUS* soient retrouvées. Ainsi, FUS est impliqué à la fois dans les cas les plus sévères de SLA, via des mutations du gène *FUS ;* mais la protéine FUS est anormale dans une proportion importante de patients atteints de DFT.

FUS est une protéine principalement localisée dans le noyau cellulaire. La plupart des mutations de *FUS* sont localisées dans la partie C-terminale de la protéine, où est située la séquence de localisation nucléaire (SLN) de la protéine. Les mutations de *FUS* entraînent ainsi une délocalisation de la protéine du noyau vers le cytoplasme. Généralement, chez le patient, les cellules contenant des agrégats cytoplasmiques de FUS présentent aussi une perte partielle ou totale de l'immunoréactivité de FUS dans le noyau. La maladie peut donc être potentiellement causée par la perte nucléaire de FUS, car FUS a de très nombreuses

fonctions au sein du noyau. Par ailleurs, l'accumulation de protéine FUS dans le cytoplasme pourrait participer à la toxicité des mutations. Pour déterminer si la perte nucléaire, l'accumulation cytoplasmique de FUS ou les deux événements participent à la toxicité des mutations de FUS, nous avons généré un modèle murin knock-in expressant *Fus* totalement délocalisée vers le cytoplasme et un modèle murin knock-out pour la protéine *Fus*. Les deux modèles présentent de façon similaire une mort périnatale par insuffisance respiratoire, une diminution de la taille corporelle et de poids ainsi qu'une multitude de similitudes en gènes altérés et ARNm altérés. Ces résultats indiquent que la délocalisation de FUS aboutit en une perte substantielle de ses fonctions en conditions physiologiques.

Par ailleurs, seules les souris Fus knock-in, mais pas les souris *Fus* knock-out, présentent une perte du nombre de motoneurones à la naissance, associée avec une augmentation de l'apoptose des neurones moteurs. Cette dégénérescence peut néanmoins être prévenue en renversant de façon spécifique la mutation grâce à la CRE recombinase dans les neurones ChAT+. L'ensemble de ces résultats indique que la délocalisation cytoplasmique de FUS non seulement entraîne une perte de fonction nucléaire de la protéine, mais aussi déclenche la dégénérescence de neurones moteurs à travers un processus toxique intrinsèque.

Les patients SLA porteurs de mutations *FUS* étant porteurs d'un seul allèle muté, nous avons caractérisé le phénotype des souris knock-in hétérozygotes. Ces souris présentent des problèmes moteurs légers liés à la symptomatologie SLA à un âge avancé (22 mois) ainsi que des altérations de gènes intrinsèques et extrinsèques aux neurones moteurs. (Scekic-Zahirovic et al. 2016, 2017)

Mon projet de thèse est issu de ces résultats précédents du laboratoire, et nous nous sommes posé deux questions complémentaires :

Tout d'abord nous nous sommes demandés s'il était possible de contrecarrer la perte de fonction nucléaire chez les souris *Fus* knock-in. Pour cela, nous avons utilisé notre modèle murin knock-in hétérozygote que nous avons croisé avec une souris sauvage contenant un transgène de *FUS* humain sauvage (hFUS) inséré dans un chromosome artificiel bactérien. A l'issue de ces croisements nous avons caractérisé l'effet du transgène humain sauvage sur notre modèle murin knock-in. Nous avons observé que le transgène hFUS permet de sauver la létalité de *Fus* muté en homozygote, et ce jusqu'à l'âge adulte. Par la suite, nous avons observé que les troubles moteurs présents dans le modèle knock-in hétérozygote sont reversés par l'ajout du transgène hFUS, atteignant des valeurs de force musculaire similaires à celles des souris sauvages. Ces résultats indiquent que hFUS est capable de compenser les altérations physiopathologiques liées à la toxicité de Fus

cytoplasmique. Pour comprendre le mécanisme à travers lequel cette compensation est réalisée, nous avons fait l'hypothèse que le transgène hFUS compensait la mutation par activation de l'autorégulation de FUS. De fait, il est connu que *FUS* à une forte capacité à s'autoréguler par activation d'une voie alternative d'épissage de l'exon 7, résultant en la dégradation de son propre ARNm (Zhou et al 2013). Nous avons montré que l'insertion du transgène hFUS active cette voie d'épissage alternatif résultant en une diminution d'expression d'ARNm, entraînant une diminution des niveaux de protéine mutée dans le cytoplasme. L'augmentation de la méthylation de FUS dans le cytoplasme est un autre indicatif physiopathologique de la maladie présent dans notre modèle knock-in qui est également diminué par l'ajout du transgène hFUS. De la même façon, nous avons confirmé ces données par des méthodes de marquage histologiques montrant une diminution de la protéine mutée dans le cytoplasme ainsi qu'une diminution des niveaux de méthylation. Ces résultats indiquent que le transgène hFUS contrôle et renverse les niveaux de traduction de Fus muté en s'autorégulant par une voie d'épissage alternative de l'exon 7, contribuant à une diminution des effets toxiques de la mutation.

Grâce à ces données, nous avons pu conclure que l'insertion d'un transgène hFUS est capable de compenser la perte de fonction nucléaire de Fus ainsi que son gain de fonction toxique dans le cytoplasme en activant une voie d'autorégulation, prévenant la neurodégénérescence et résultant en une préservation des capacités motrices. De ce fait, des approches thérapeutiques basées dans des techniques de thérapie génique seraient de grand intérêt, permettant un ciblage plus précis des voies altérées dans la pathologie. Ces résultats sont rassemblés dans un manuscrit en préparation dont je suis premier auteur.

Une deuxième partie de ma thèse s'est centrée à élucider le rôle potentiel de FUS cytoplasmique dans la DFT. Les patients atteints de DFT présentent des troubles cognitifs et comportementaux ainsi qu'une atrophie des lobes frontaux et latéraux. Une proportion importante des patients DFT présente des agrégats de FUS cytoplasmique, mais la contribution de FUS dans le cytoplasme à la DFT reste inconnue. Nous avons voulu déterminer si une accumulation de FUS dans le cytoplasme était suffisante pour provoquer des symptômes typiques de la DFT et avons caractérisé le comportement de notre modèle knock-in hétérozygote. Dans un premier temps, des études de comportement ont révélé une hyperactivité à des âges très jeunes (à partir de 3 mois) ainsi que des défauts cognitifs et de comportement social tels qu'une perte de mémoire et une désinhibition respectivement. De plus, nous avons retrouvé une pathologie corticale liée spécifiquement à la présence de FUS délocalisé dans le cytoplasme dans les neurones corticaux ainsi que l'absence de TAF15 et/ou EWSR1. Nous avons détecté également des agrégats dans les neurones pyramidaux du cortex ainsi qu'une atrophie fronto-temporale accompagnée d'une ventriculomégalie. De façon surprenante, nous n'avons pas observé de perte neuronale au niveau du cortex.

Néanmoins, notre modèle knock-in hétérozygote présente des anomalies des synapses corticales aux niveaux moléculaires et structurels, ainsi que des altérations d'excitabilité. D'un point de vue moléculaire, nous avons montré que FUS se lie de façon altérée à des ARNm d'importance cruciale dans la synapse. Ces résultats mettent en évidence des altérations pathophysiologiques liés à la DFT dans notre modèle murin Fus knock-in hétérozygote, comme des altérations moléculaires de FUS au sein de la synapse, des altérations structurelles des synapses, de la balance inhibitrice-excitatrice corticale ainsi que des défauts de comportement. Ces résultats sont rassemblés dans un manuscrit collaboratif dont je suis co-premier auteur.

Nos travaux précédents avaient montré l'importance de l'expression de la mutation dans les motoneurones pour provoquer les symptômes moteurs. Pour cela, nous avions utilisé un modèle d'expression de la recombinase CRE dans les neurones cholinergiques, et avions montré que le sauvetage spécifique dans les neurones cholinergiques permettait de retarder l'installation du phénotype moteur. Etant donné le rôle de l'acétylcholine dans les syndrômes démentiels, dont la maladie d'Alzheimer, nous nous sommes intéressés à l'implication du système cholinergique et aux effets de sa modulation dans la pathologie. Notre modèle murin présente une perte de neurones cholinergiques du noyau basal de Meynert (NbM), aussi affecté dans la maladie d'Alzheimer, ainsi qu'une perte de projections ascendantes cholinergiques jusqu'au cortex, où une diminution d'innervation de fibres cholinergiques des couches internes est aussi retrouvée. De plus, FUS se trouve délocalisé dans le cytoplasme dans les neurones cholinergiques du NbM et ces neurones présentent des marqueurs moléculaire de dommage à l'ADN. Comme le modèle knock-in hétérozygote présente des altérations de type DFT, nous avons étudié si ces phénotypes dépendaient de l'expression de la mutation dans les neurones cholinergiques. De fait, le sauvetage de la mutation dans les neurones cholinergiques atténue partiellement ces phénotypes. Ces résultats indiquent que l'expression de Fus muté altère le système cholinergique de façon globale, autant au niveau central que périphérique, et que celui-ci est directement lié aux symptômes comportementaux décrits dans notre modèle murin. Nous avons tenté une approche pharmacologique pour moduler le système cholinergique et les possibles effets sur le comportement des souris avec de la nicotine, un agent agoniste qui potentialise la transmission cholinergique. Les souris ont montré être résistantes au traitement et donc aucun effet sur leur comportement n'a été observé. Ces résultats sont cohérents avec les patients atteints de DFT, qui eux, présentent une résistance aux inhibiteurs d'acétylcholinestérase, qui potentialisent la transmission cholinergique. Ces résultats seront rassemblés dans un manuscrit dont je serai co-premier auteur.

Les résultats obtenus pendant ma thèse ont permis d'identifier d'un côté une stratégie génétique susceptible d'amener à une thérapie génique pour la SLA-FUS. De plus, mes

travaux montrent que la présence cytoplasmique de FUS est suffisante pour déclencher des symptômes pertinents pour la DFT tout en démontrant une contribution cholinergique à ces phénotypes.

Inmaculada SANJUAN RUIZ

Pathophysiological mechanisms involved in amyotrophic lateral sclerosis caused by mutations in the *FUS* gene

La sclérose latérale amyotrophique (SLA) et la démence frontotemporale (DTF) sont deux maladies neurodégénératives incurables. Même si ces deux maladies sont distinctes, elles sont liées par une série de facteurs cliniques, génétiques et histologiques donnant lieu à ce qu'on connaît comme le continuum SLA-DFT. Des mutations du gène FUS sont liées à la SLA, et des défauts de la protéine FUS sont retrouvés dans la DFT, les deux caractérisées par la formation d'agrégats de FUS.

Nous avons étudié les mécanismes d'autorégulation de FUS dans un modèle murin, par l'activation d'une voie alternative d'épissage en insérant un transgène FUS humain sauvage, ce qui nous a permis de potentiellement élucider de nouvelles pistes envisageant des thérapies géniques. De plus, nos souris développent des symptômes liés à la DFT. Nos résultats indiquent une altération des synapses corticales qui pourraient être à l'origine des défauts comportementaux que nous avons observés, ainsi que des défauts du système cholinergique.

Mots clés : sclérose latérale amyotrophique, démence frontotemporale, FUS, autorégulation, synapses, système cholinergique.

Amyotrophic lateral sclerosis (ALS) and frontotemporal dementia (FTD) are two untreatable neurodegenerative diseases. Even thought they are two distinctive diseases they share a series of clinical, genetic and histological hallmarks, thus defining the ALS-FTD continuum. Mutations in the FUS gene have been linked with ALS, whereas alterations in FUS proteins have been detected in FTD patients. Both diseases are characterized by the presence of cytosolic FUS aggregates.

We have studied the autoregulation mechanisms of FUS in a mouse model via the activation of an alternative splicing pathway by the insertion of a human wild-type FUS transgene, which has allowed us to potentially elucidate new therapeutic approaches by gene therapy. Furthermore, our mice develop FTD-like symptoms. Our results suggest an alteration in cortical synapses which could originate the observed cognitive and behavioural deficits, accompanied by alterations in the cholinergic system.

Key words: amyotrophic lateral sclerosis, frontotemporal dementia, FUS, autoregulation, synapses, cholinergic system